NASA TECHNICAL TRANSLATION

NASA TT F-494
c.1

NASA TT F-494

HELICOPTERS

CALCULATION AND DESIGN

Volume I. Aerodynamics

by M. L. Mil' et al.

"Mashinostroyeniye" Publishing House
Moscow, 1966

NATIONAL AERONAUTICS AND SPACE ADMINISTRATION • WASHINGTON, D. C. • SEPTEMBER 1967

NASA TT F-494

HELICOPTERS

CALCULATION AND DESIGN

Vol. I. Aerodynamics

By M. L. Mil', A. V. Nekrasov, A. S. Braverman,
L. N. Grodko, and M. A. Leykand

Translation of "Vertolety. Raschet i proyektirovaniye. 1. Aerodinamika."
Izdatel'stvo Mashinostroyeniye, Moscow, 1966.

NATIONAL AERONAUTICS AND SPACE ADMINISTRATION

For sale by the Clearinghouse for Federal Scientific and Technical Information
Springfield, Virginia 22151 – CFSTI price $3.00

ANNOTATION

/2*

The work "Helicopters (Calculation and Design)" is published in three volumes.

Vol.I - Aerodynamics;
Vol.II - Vibrations and Dynamic Strength;
Vol.III - Design.

The first volume is devoted to ways of developing helicopters, the basic principles of their design, and the position occupied by helicopters among other means of aviation not requiring airfields. Various theories of rotors and corresponding methods of determining their aerodynamic characteristics are presented: the classical theory of a rotor with hinged blades in the general case of curvilinear flight of the helicopter; the momentum theory of an ideal rotor and its application to the energy method of calculation; the classical theory when using methods of numerical quadrature; the vortex theory and methods of experimental determination of rotor performance in flight tests and in wind tunnels. Various methods of aerodynamic calculation of a helicopter and the theory of blade flutter are presented in detail. This volume gives an account of methods of calculating flutter in hovering and in forward flight. Particular attention is devoted to consideration of friction in the axial hinges of the hub and to the transfer of blade vibrations through the automatic pitch control mechanism. Experimental investigations of flutter are described.

The book is intended for engineers of design offices, scientific workers, graduate students, and teachers of higher institutes of learning. It might be useful to engineers of helicopter manufacturers and to students for furthering their knowledge of the aerodynamics and mechanical strength of helicopters. Many sections of the book will be a useful tool also to flight and technical staffs of helicopter flight units.

---

* Numbers in the margin indicate pagination in the original foreign text.

PREFACE

/3

The present book generalizes the experience of the scientific work and practical design activity of engineers of one of the Soviet teams working on the development of helicopters.

Twenty years ago, when the team had just set out on their work, everything in this field seemed to have been already long discovered and invented.

Those to whom belongs credit for the original ideas and designs of rotary-wing aircraft - Leonardo da Vinci, M.V.Lomonosov, N.Ye.Zhukovskiy (Joukowski), B.N.Yur'yev, and others - had long ago proposed almost all of the existing designs of helicopters. Designers, scientists, and inventors in various countries built dozens of helicopter models which successfully rose into the air. However, not one of these rotocraft was suitable for practical use, large-scale production, or regular service.

A very difficult problem that required considerable and tedious work remained unsolved, namely, the problem of developing helicopters which would find practical use in everyday life.

To solve this problem we had at our disposal an important scientific basis in the form of classical works, the studies of the Central Aero-Hydrodynamic Institute (TsAGI), and of foreign scientists. However, testing of each new aircraft confronted design engineers with new acute problems and forced them to work out many theoretical problems to find the proper method of solving specific design problems.

This volume discusses the basic problems of the theory, calculation, and design of helicopters worked out by the team and representing the vital interests of its design activity.

The fact that some of the authors had occasion to participate in applying the classical rotor theory to the calculation and design of the first autogiros, in the original experimental work on models and on full-scale rotors in wind tunnels, in developing methods of aerodynamic calculation of helicopters, and then - for more than 15 years - in designing an entire family of helicopters of the same configuration in all weight classes, offers an opportunity to elucidate the basic problems of the theory and calculation of helicopters that have been /4 checked out by practice.

As early as 1948 there was not a single helicopter in service in our country. Now thousands of such machines created by various design teams assist people in many areas of their life and activity.

Engineers and designers working on the design or construction of helicopters, pilots and technicians, students of air academies who are studying or are interested in helicopters will find useful information in this book.

Engineering, especially aircraft engineering, is rapidly becoming obsolete. However, it is hoped that the general methods of approach to the development of a new type of aircraft, as presented in this book, will outlive today's helicopter models.

M.Mil'

*

Chapter I of Vol.I, Sections 1 and 2 of Chapter II, and Section 2 of Chapter III were written by M.L.Mil'; Chapter IV and Section 5 of Chapter II were written by A.V.Nekrasov; the remaining Sections of Chapters II and III and also Subsections 19-28 of Section 2 of Chapter II were written by A.S.Braverman.

In preparing the manuscript, the authors were assisted by engineers F.L. Zarzhevskaya, R.L.Kreyer, and L.G.Rudnitskiy.

Reviewer R.A.Mikheyev made many valuable comments.

The authors express their sincere gratitude to these coworkers.

TABLE OF CONTENTS

Aerodynamic Characteristics

α = angle of attack of rotor;
α_r = angle of attack of blade section;
α_o = angle of zero lift of blade profile;
$\Delta\alpha$ = downwash angle of flow;

$a_\infty = \frac{dc_y}{d\alpha} = c_y^\alpha$ = tangent of angle of slope of the lift curve with respect to angle of attack of the profile;

$\Phi = \tan^{-1}\frac{U_x}{U_y}$ = inflow angle in blade section;

Γ = circulation in blade section;
M = Mach number of blade section;
M_o = average Mach number with respect to azimuth, in tip section of blade $\left(M_o = \frac{\omega R}{a}\right)$;

M_{fl} = flight Mach number $\left(M_{fl} = \frac{V}{a}\right)$;

$T,\ t = \frac{C_T}{\sigma}$ = thrust and coefficient of thrust of rotor $\left(t = \frac{T}{\frac{1}{2}\rho\sigma\pi R^2(\omega R)^2}\right)$;

$H,\ h = \frac{C_H}{\sigma}$ = longitudinal force and coefficient of longitudinal force of rotor $\left(h = \frac{H}{\frac{1}{2}\rho\sigma\pi R^2(\omega R)^2}\right)$;

$S,\ s = \frac{C_S}{\sigma}$ = lateral force and coefficient of lateral force of rotor $\left(s = \frac{S}{\frac{1}{2}\rho\sigma\pi R^2(\omega R)^2}\right)$;

$M_t,\ m_t = \frac{\bar{m}_t}{\sigma}$ = torque and torque coefficient of rotor $\left(m_t = \frac{M_t}{\frac{1}{2}\rho\sigma\pi R^3(\omega R)^2}\right)$;

N = power of motor (of rotor in Chapt.II);

$Y,\ t_y = \frac{C_Y}{\sigma}$ = lift and lift coefficient of rotor $\left(t_y = \frac{Y}{\frac{1}{2}\rho\sigma\pi R^2(\omega R)^2}\right)$;

X, $t_x = \frac{C_x}{\sigma}$ = propulsive force and coefficient of propulsive force of rotor $\left(t_x = \frac{X}{\frac{1}{2}\rho\sigma\pi R^2(\omega R)^2}\right)$; /6

c_y, c_{xp} = coefficients of lift and profile drag of blade section (airfoil) referred to dynamic pressure $\frac{1}{2}\rho V^2$;

B = coefficient of tip losses;

Velocities

ωR = angular velocity;

V, $\left(\overline{V} = \frac{V}{\omega R}\right)$ = path velocity of helicopter flight;

V_x, V_y, V_z = horizontal, vertical, and lateral components of flight velocity;

v, $\left(\overline{v} = \frac{v}{\omega R}\right)$ = induced velocity;

U, $\left(\overline{U} = \frac{U}{\omega R}\right)$ = relative velocity of flow past a blade element;

U_x, U_y, $\left(\overline{U}_x = \frac{U_x}{\omega R}, \overline{U}_y = \frac{U_y}{\omega R}\right)$ = horizontal and vertical components of relative velocity of flow past a blade element;

λ = coefficient of flow;

μ = characteristic (coefficient) of rotor performance.

Geometric Characteristics

D = diameter of rotor;

R = radius of rotor;

F = disk area;

r = radius of rotor blade section $\left(\overline{r} = \frac{r}{R}\right)$;

b = blade chord $\left(\overline{b} = \frac{b}{R}, \overline{\overline{b}} = \frac{b}{b_{0.7}}\right)$;

z_b = number of blades;

z_r = number of rotors;

$\sigma = \frac{z_b b_{0.7}}{\pi R}$ = load factor of rotor;

$l_{h.h}$, $l_{v.h}$ = distance from axis of rotation of rotor to the horizontal (flapping) and vertical (drag) hinges, respectively;

c = thickness of profile section, $\overline{c} = \frac{c}{b}$;

β = flapping angle of blade;

a_n, b_n = coefficients of flapping;
φ, φ_o = blade angle (pitch); angle between chord of blade profile and plane of rotation;
$\varkappa$, η = angles of deflection of automatic pitch control mechanism; $\varkappa$ with index = mutual influence coefficient of lifting elements;
θ_o = blade angle at $\bar{r} = 0.7$ for $\beta = \varkappa = \eta = 0$;
θ_1, θ_2 = components of change of blade angle relative to the plane of rotation, due to deflection of the automatic pitch control mechanism;
ν = change of blade angle due to elastic deformation of blade.

HELICOPTERS; CALCULATION AND DESIGN. VOL.I: AERODYNAMICS /7

M.L.Mil', Editor

ABSTRACT. A review of the historical development of Russian and Western helicopters, in size and lift capacity, for civil and military purposes is followed by detailed discussions on rotor aerodynamics for various angles of attack, blade setting, flapping angle, center-of-pressure position, blade vibration (natural, forced, harmonic, etc.), and other rotor parameters in their influence on rotor rpm and craft stability. Formulas are given for the forces and moments of rotor damping in hovering and forward flight; for the redistribution of aerodynamic forces over the rotor disk due to flapping; for cyclic pitch change of rotors with variable and constant pitch. The theory of an ideal helicopter is developed on the basis of optimum blade profile, prevention of rotor profile losses, and proper balancing. Flutter in hovering and forward flight is calculated, with emphasis on friction in the axial hub hinges and transfer of vibrations through the automatic pitch control.

CHAPTER I

EVOLUTIONAL HISTORY OF HELICOPTERS AND BASIC DESIGN PRINCIPLES (Selection of Parameters and Configuration)

Section 1. Evolution of the Helicopter Industry

Designing is always directed toward the future. However, for a better picture of the potentialities of the future development of helicopters it is useful to attempt to understand the basic trends of their evolution from past experience. Naturally, we are not interested here in the prehistory of helicopter construction, which we will only briefly mention, but in its history from the time when the helicopter as a new type of aircraft became useful for practical application.

The writings of Leonardo da Vinci going back to 1483 contained the first mention of an apparatus with a vertical rotor, a helicopter. The first stage of evolution ranges from the model of a helicopter developed by M.V.Lomonosov in 1754 through a long series of designs, models, and even full-scale apparatus which were not destined to rise into the air, to the construction of the world's first helicopter which, in 1907, was able to become airborne. This four-rotor helicopter was constructed by the French designers Breguet and Riche. In 1923, a passenger became airborne for the first time in the USA in a helicopter designed by de Bothezat. The first world altitude record of a helicopter of 18 m was set in 1930 on the Italian coaxial helicopter by d'Ascanio.

In Russia, a single-rotor helicopter was built in 1911, on the basis of the scientific research by N.Ye.Zhukovskiy devoted to helicopter rotors, by a group of his students headed by B.N.Yur'yev. The configurations of this machine represent the basic scheme of the single-rotor helicopters used widely at present. B.N.Yur'yev was able to resume this work only in 1925. In 1932, a group of engineers headed by A.M.Cheremukhin constructed the helicopter TsAGI 1-EA (Fig.1.1) which reached an altitude of 600 m and stayed in the air for 18 min, which - for that time - was an outstanding achievement. It suffices to say that the official altitude record established three years later on Breguet's new coaxial helicopter was only 180 m.

At this time there was a pause in the development of helicopters. A new branch of rotary-wing aircraft came to the forefront, known as autogiros. The idea of the autogiro, as an aircraft with a rotary wing (freely rotating airfoil) never losing speed, occurred to the young Spanish engineer Juan de la Cierva in the 1920s. At that time, conventional aircraft whose development had been vigorous during the years of World War I and which, by then, carried /8 armament and thus had greater wing loading were troubled by a new problem of spin, i.e., stalling. It appeared simpler to develop a safe and sufficiently perfected autogiro than to build a helicopter. The rotor, freely rotating due to the relative flow, eliminated the need for complex reduction gearing and transmissions. The hinged attachment of the rotor blades to the hub used on autogiros gave far greater strength to the blades and higher stability to the autogiro. Finally, engine failure ceased to be a threat, as had been the case in the first helicopters; the autogiro, with autorotating blades, had no difficulty in landing at low speed.

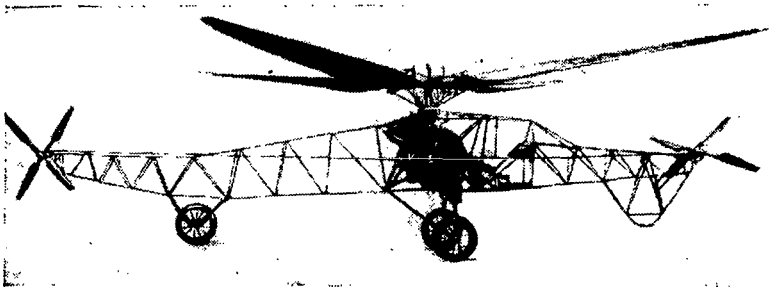

Fig.1.1 Helicopter TsAGI 1-EA.

Cierva, working in England, created several autogiro designs, the best known of which was the C-30 autogiro which was produced as a pilot series. Autogiros were also built in the USA by the Pitcairn and Kellett Companies and in the Soviet Union at TsAGI by the designers I.P.Bratukhin, V.A.Kuznetsov, N.I.Kamov, N.K.Skrzhinskiy, M.L.Mil', and others.

The flying speed of Soviet autogiros in 1937 reached 260 km/hr. The A-7 autogiros designed by N.I.Kamov were used at the front during the first year of World War II.

The great lift capacity of the rotating rotor gave the autogiro a short ground run. Even though, a mechanical drive from the engine, for spinning the rotor before takeoff, was used in this design to further shorten the takeoff run. In the design of the British C-40 autogiro the rotor was given a spin-up before flight to an rpm such that, at the instant of disengagement from the engine - which, in forward flight, rotated the propeller - the machine, due to the marked increase in pitch, took off without a run, rising vertically into the air.

Only one step remained for the development of a true helicopter. And this step, as is always the case in technology, was made almost simultaneously in various countries. This was the beginning of the present development stage of helicopters. It was started by flights of the FW-61 helicopter designed by Professor Focke in Germany (1937), the VS-300 helicopter designed by Sikorsky in the USA (1939), and the "Omega" helicopter designed by I.P.Bratukhin in the USSR (1940). All three of these helicopters used a hinged rotor capable of autorotation, which had already become standard for autogiros.

World War II somewhat delayed the development of helicopters. They were still unsuitable for practical use, and the ways and means for experimental studies were limited. After the end of the war (1946 and 1947), large numbers of designers and inventors invaded this new and promising area of development of aviation engineering. Within a short time, literally dozens of new helicopter /9 designs were created. This was a contest of the most diverse schemes and configurations, generally of the single- or two-seater type and used mainly for experimental purposes. Military agencies were the only users of this expensive and complex equipment. The first helicopters in various countries were used as liaison and reconnaissance military aircraft.

In the development of helicopters, just as in many other areas of technology, one can clearly distinguish two trends of development: the quantitative trend concerned with size of the machine and the almost simultaneous qualitative trend concerned with improvement of the craft within a certain size or weight class. The former trend represents development with respect to lift capacity and the second with respect to improvement of the tactical or economic features of helicopters.

1. Development of Helicopters in Size

A study of foreign helicopters indicates that the use of helicopters for landing Marines from ships was the determining factor in the further development of military helicopters as troop carriers. The American landing of troops in S-55 helicopters at Inchon during the Korean War (1951) was a typical example of this trend.

The size range of the assault helicopters was predicated on bulk and weight of ground transportation means used by the troops and to be dropped by air. It is a known fact that conventional weapons - mainly artillery - transported by prime movers are close in weight to the weight of the prime movers themselves. Thus, the lift capacity of the first transport helicopters in armies of other countries was 1200 - 1600 kg (the weight of a light military truck used as

prime mover together with the respective weapons). Subsequently, the required lift capacity of helicopters was increased to 6 - 8 tons which, in accordance with military technique, was based on automobile carriers with a lift capacity of 3 - 4 tons. Still later, for example in projects developed by Sikorsky Aircraft, the lift capacity of helicopters rose to 20 - 25 tons and finally to 36 - 40 tons. Such weights correspond to the weight of light and medium tanks or of self-propelled landing craft. Whether this development trend in size increase will ever come to an end depends on the constantly changing military planning. Artillery systems are being largely replaced by missiles, for which reason the foreign press often mentions the need to transport missiles or missile systems, the prime factor in determining the size of modern helicopters.

In the attempt to single out the main trend of future helicopter development, after successively outlining the creation of new types of machines in the few designer firms that have been successful in developing experimental models into practical prototypes and in starting pilot series, it will be found that the major development was toward an increase in the lift capacity of helicopters.

TABLE 1.1

Characteristics	Helicopters							
	USSR			USA				
	Mi-1	Mi-4	Mi-6	S-51	S-58	S-64	DS-103	—
Year of production	1948	1952	1957	1946	1956	1962	Projects	
Lift capacity, in ton-force	0.3	1.2—1.6	8—12	0.3	1.2	5—6	20	40
Increase over previous model		4	7		3	4	3	2
Flying weight, ton-force	2.3	7.2	39—41	2	6	17.0	—	—

Table 1.1 gives data characterizing the development of the lift capacity of single-rotor helicopters of the same configuration by two aircraft construction departments - helicopters Mi-1 (Fig.1.2), Mi-4 (Fig.1.3), Mi-6 (Fig.1.4), Mi-10 (Fig.1.5), S-51 (Fig.1.6), S-58 (Fig.1.7), and S-64 (Fig.1.8).

As we see from Table 1.1, the lift capacity increases severalfold with each prototype.

However, it is easy to show that an increase in size and weight of helicopters is impossible without a qualitative improvement of the engines used /10 (reduction in weight per unit horsepower and increase in economy, i.e., decrease in fuel consumption).

Actually, an increase in flying weight is possible either by increasing the rotor span or the installed power, or both factors

$$G = T = (k\eta ND)^{3/2}. \qquad (1.1)$$

The weight of the engine is proportional to the first power of its output, while the weight of the machine itself increases only in proportion to the 2/3 power.

Fig.1.2 Mi-1 Helicopter.

Thus, a helicopter with a larger power-to-weight ratio will have a relatively greater design weight, owing to the power plant.

In like manner the weight of the blade and, accordingly, the weight of the lifting system change in proportion to the third power of the diameter, whereas the weight of the helicopter again changes only in proportion to the 2/3 power. Here also, the weight of the lifting system of a larger helicopter proves to be relatively greater. Thus, on increasing the size of a helicopter its load ratio, i.e., the ratio of useful load to flying weight, should be decreased, if there is no weight improvement in engines, blade design, reduction gears, or transmissions. Actually, in the 1930s papers were published that demonstrated the uselessness of developing helicopters with a power greater than 500 hp, since an increase in power would not lead to an increase in useful load. /13 According to technical specifications of that time, the weight of rotors, reduction gears, and of the entire machine as a whole increased with increasing power more rapidly than the lift.

However, in developing a new military - and especially a new general-purpose - helicopter, the designer will not tolerate a lowering of the achieved level of load ratio.

Thus, a "quantitative" development with respect to size is impossible without a qualitative development; in fact, it always is concurrent with the qualitative advance of technology.

The development of helicopters larger than the first two- or three-place models took place in a comparatively short time, since the unit weight of piston engines always decreased with an increase in power. But in 1953, after development of the 13-ton Sikorsky S-56 helicopter (Fig.1.10) with two 2300-hp piston

/11

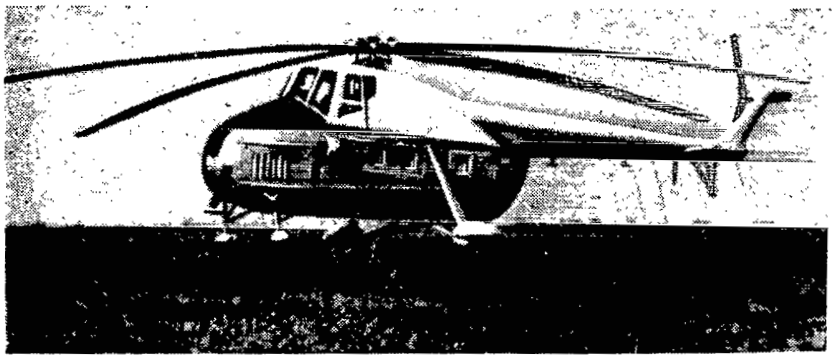

Fig.1.3 Mi-4 Helicopter.

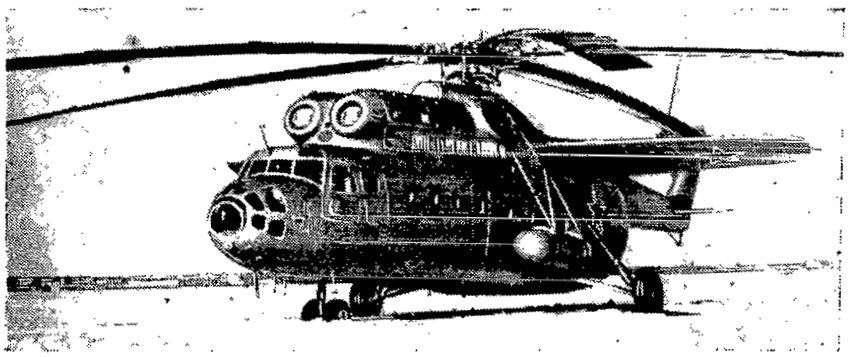

Fig.1.4 Mi-6 Helicopter.

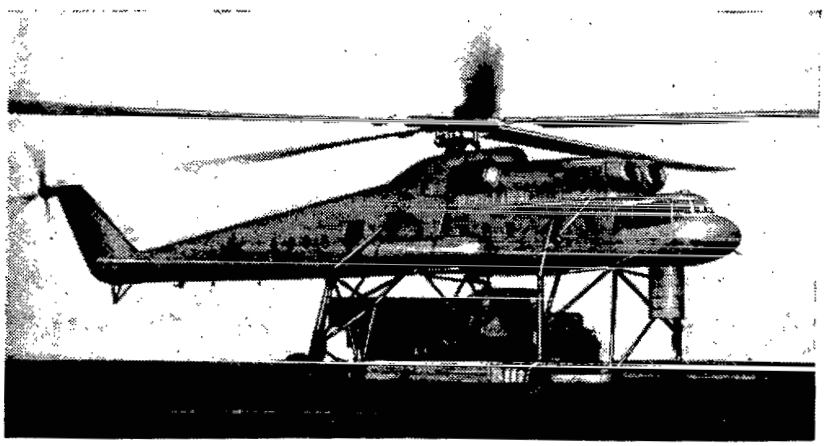

Fig.1.5 Mi-10 Helicopter.

Fig.1.6 S-51 Helicopter.

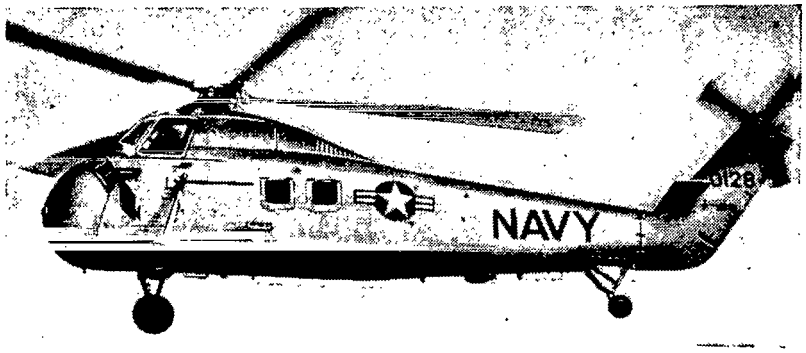

Fig.1.7 S-58 Helicopter.

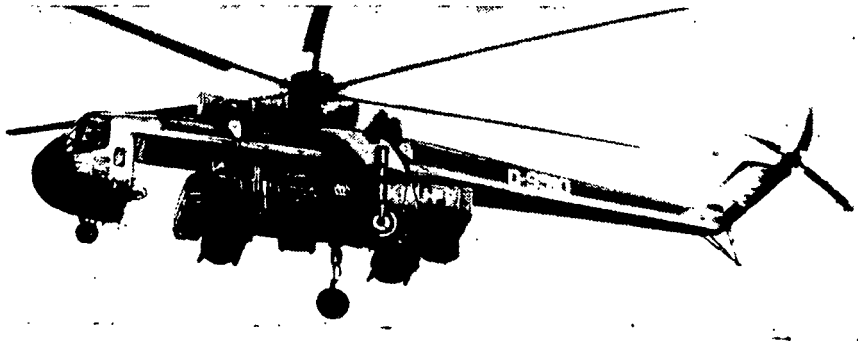

Fig.1.8 S-64 Helicopter.

engines, the size series of helicopters in the West was discontinued and only in the USSR was it possible, in 1957, to develop the Mi-6 helicopter with a flying weight of 40 tons by using turboprop engines.

2. Qualitative Development of Helicopters

In the middle of the 1950s, the reliability of helicopters became appreciably greater so that also their use potentialities for the national economy increased. This moved problems of economy into the foreground.

The operating cost per hour of a helicopter plays a decisive role in whether to use them for geological surveys, in agriculture, or for transporting passengers. Amortization, i.e., the price of a helicopter divided by its service life, constitutes a large portion of the cost. The service life of the helicopter is determined by the durability of its components. The problem of increasing the fatigue strength of blades, shafts, transmissions, rotor hubs, and other units of the helicopter became a prime problem, which helicopter designers are still studying at present. Today, a life of 1000 hours is no longer a rarity for series-produced helicopters and there are no grounds to doubt its further increase. When using helicopters in transportation, the concepts of cost per ton-mile of the transported load and the cost per passenger-mile become decisive. This is the hourly operating cost divided by hourly productivity, i.e., by the product of the weight of the payload and the cruising speed.

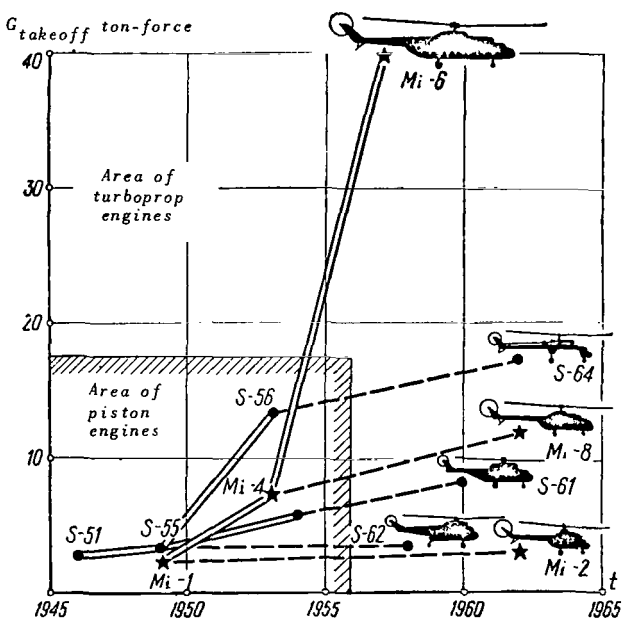

Fig.1.9 Size Evolution of Helicopters.

Since the construction weight largely determines the price of a helicopter, the direct relation between economy and load ratio of the helicopter is obvious. Flying speed also acquires a new role.

This automatically leads to the idea of developing helicopters with higher economic indexes. The development of turboprop engines with an appreciably smaller unit weight than piston engines made it possible to produce helicopters with a larger load ratio while retaining, in each weight category, the rotor dimensions.

Generally, replacement of piston engines by turboprop engines not only results in a decrease in relative weight of the power plant but also in some increase in power; produces a dual effect and also leads to an appreciable

increase in cruising speeds.

In the diagram (Fig.1.9) we traced these quantitative and qualitative development trends of the most common helicopters produced by the three design engineering departments. Given are the single-rotor helicopters designed by Sikorsky Aircraft (USA), the single-rotor Soviet helicopters, and the fore-and-aft helicopters of the Piasecki Aircraft Corporation, which subsequently became the Vertol Div. of Boeing. /14

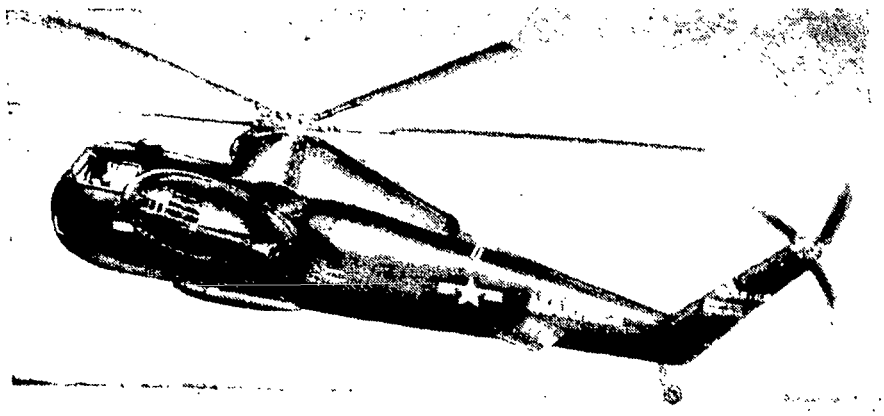

Fig.1.10 S-56 Helicopter.

Thus, the size development trend on the basis of piston engines (solid lines in Fig.1.9) was terminated as early as 1953. Then, as turboprop engines of the necessary size were developed over a period of five to ten years, second-generation helicopters appeared (points referring to these in the diagrams are connected with the original models by the broken line of qualitative development).

Thus, the helicopters S-55, S-58, and S-56 with piston engines served as prototypes, respectively, for the turboprop machines S-61 (Fig.1.11), S-62 and S-65 (Fig.1.12). The same holds for the fore-and-aft helicopters of the Vertol Div. of Boeing V-107 and VB-114 "Chinook" (Fig.1.13). /16

The Soviet turboprop helicopters Mi-2 (Fig.1.14) and Mi-8 (Fig.1.15) also constitute a further development of the well-known helicopters Mi-1 and Mi-4.

The unusually long service life of helicopters is striking in comparison with airplanes. Almost all piston helicopters shown in the diagram (with the exception of the experimental helicopters XH-16 and S-56) were in production and service before the appearance of their second turboprop generation, and the Mi-1 helicopter has managed to stay in production for 15 years and is approaching the record longevity of the Li-2 airplane.

We can assume that the weight categories of helicopters indicated in

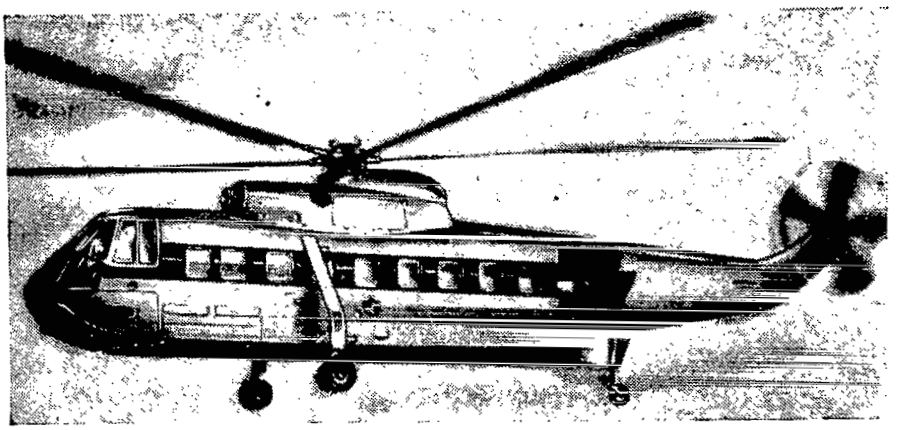

Fig.1.11 S-61 Helicopter.

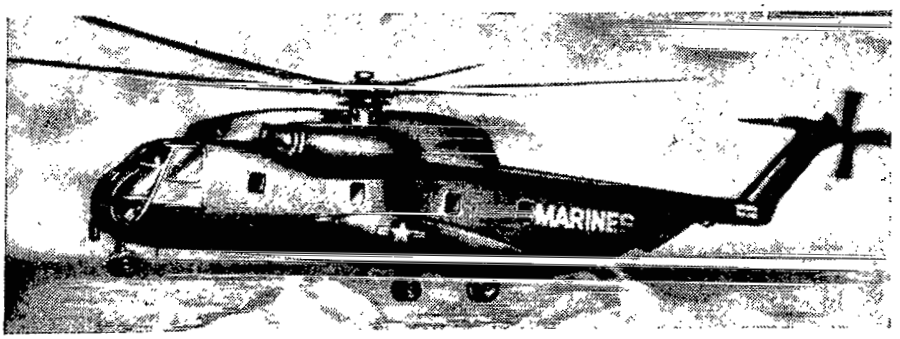

Fig.1.12 S-65 Helicopter.

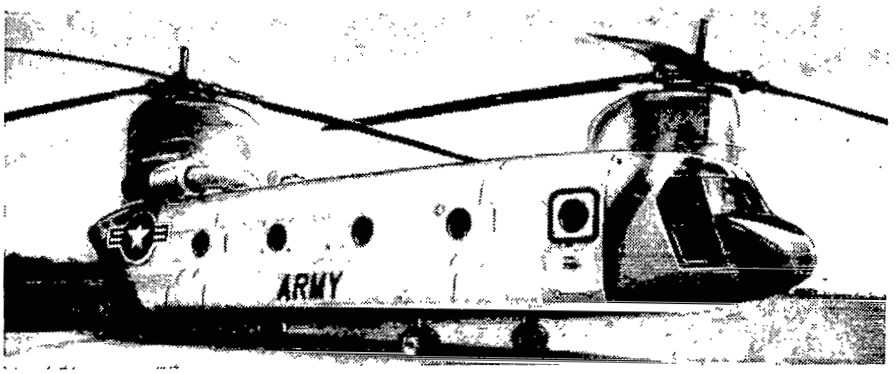

Fig.1.13 Chinook Helicopter.

Table 1.2 have become established by now.

What will be the future development of helicopters? /18

The process of developing a new generation of helicopters, on the basis of improved turboprop engines, is now being completed in the lightest category of helicopters. The lag in this weight category can be attributed to difficulties

Fig.1.14 Mi-2 Helicopter.

Fig.1.15 Mi-8 Helicopter.

in developing a lighter and simultaneously more economic low-power turboprop engine in comparison with piston engines. In the end, such an engine was developed in the USA by the Allison Company - this was the T-63 weighing only 174 lbs at a power of 315 hp and a consumption of 280 gm/hp-hr. The award in the competition for a light three- or four-place military helicopter in the USA was made to the Hughes Aircraft Company, which created the UH-6A helicopter (Fig.1.16) weighing only 2680 lbs at an empty weight of about 1340 lbs; this is

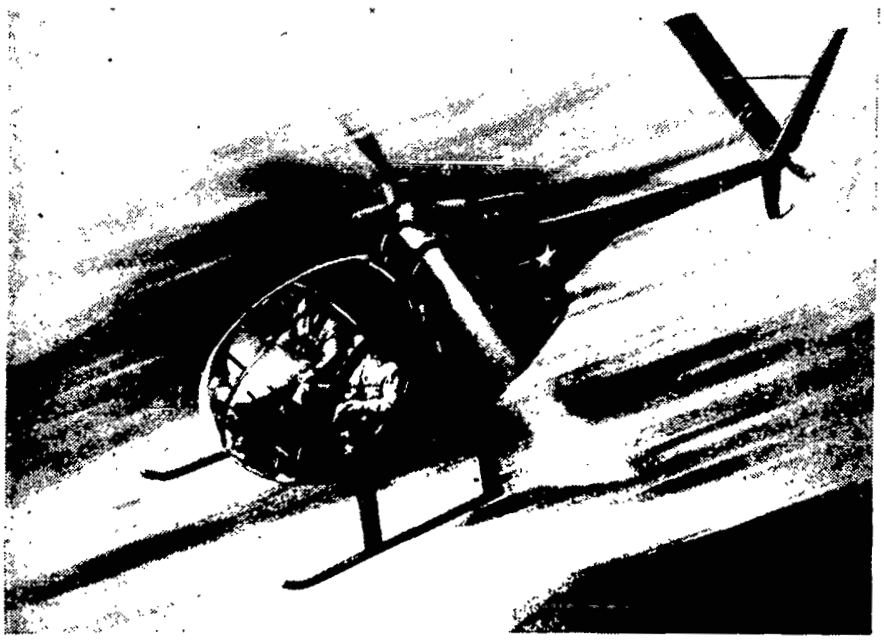

Fig.1.16 Hughes Helicopter UH-6A.

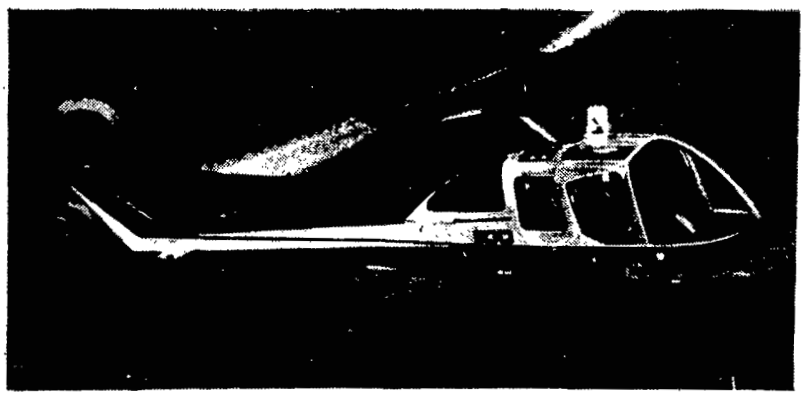

Fig.1.17 Fairchild Hiller Helicopter FH-1100.

an appreciable technical achievement which required a number of new design solutions, in particular the use of a rotor with an elastic spring retention of the blades instead of the conventional hinge attachment. This helicopter has a high load ratio (50%) combined with a high cruising speed (213 km/hr), for a light machine. The Fairchild Hiller FH-1100 is also in this class (Fig.1.17). It is obvious that these helicopters considerably outstrip the light liaison reconnaissance aircraft of World War II, both with respect to speed and lift capacity and, furthermore, have the great advantage of vertical takeoff and landing. Thus, the decision made in a number of countries to replace light reconnaissance aircraft by helicopters is not surprising.

TABLE 1.2

Characteristics	Type of Helicopter					
	Light Liaison	Light Multi-purpose	Light Transport	Medium Transport	Heavy Transport	Superheavy Transport
Lift capacity or number of places	2—4 persons	1 ton or 10—12 persons	3 ton or 25—30 persons	6—8 ton	20 ton	40 ton
Flight weight	1.5—2 ton	3.5—4 ton	10—12 ton	20—40 ton	—	—

Of course, a new generation of light helicopters will also be developed in other countries of the world. In France, this is being done on the basis of the 350-hp Turbomecca-Oredon-III engine. In West Germany, the Bölkow Company is working on such a machine.

Thus, in speaking of the qualitative development trend of helicopters, it is obvious from the foregoing that each new generation of engines gives rise to a new generation of helicopters in all weight categories, simultaneously having greater economy and better flight performance data. This line of development probably has no upper limit.

As regards the size evolution of helicopters, no machine with a lift capacity of 20 tons (see Table 1.2) has been developed as yet.

According to a request for proposals, announced in the USA, firms such as Kaman, Fairchild Hiller, and Sikorsky Aircraft are working on the development of a helicopter with a lift capacity of 20 tons. In West Germany, the Bölkow Company is working on a helicopter with a 40-ton lift capacity. Below, we will review the possible ways of developing heavy and superheavy helicopters.

3. Special-Purpose Helicopters /19

It is necessary to mention also the development of various models of special-purpose helicopters within the indicated weight categories. In this connection, let us make a brief remark on the new concept of using helicopters in the Army which has recently developed in the West - especially in the USA - namely, the creation of so-called airborne mobile troops.

In this instance, helicopters are used in place of motorized transport for all types of troop movement. The Bell "Iroquois" helicopter UH-1D (Fig.1.18) is particularly adapted for transporting troops by platoons (11-12 men).

Light reconnaissance three- or four-place armed helicopters (Hughes helicopters OH-6A), flying in front of battle formations, are also a necessity. Finally, regular troop-carrier helicopters of various classes, supplying the

means of ground fire support such as artillery, rockets, and tanks, take over the task of troop movements.

Also used in realization of this concept are helicopters for air support of infantry, constituting a unique type of assault helicopters. Ordinary helicopters armed with radio-controlled missiles and weapons are presently used for this purpose.

Fig.1.18 Bell "Iroquois" Helicopter UH-1D.

Such an airborne mobile division is supplied from the air by airplanes and helicopters of the Air Force Materiel Command.

It is not difficult to detect behind this concept past military experience, wherein any new type of transportation that became accessible engendered a new type of troops. Beginning with cavalry, we recall the bicycle and motorcycle units of World War I, and the motorized infantry, motorized divisions, and airborne troops of World War II.

It is clear by now that this concept is finding followers in many western countries.

Thus, the 12-place SA-330 (Fig.1.19) helicopter ordered by the French Army corresponds to the 11-place Iroquois helicopter (USA). A similar machine is being designed also in West Germany.

The need to retain the class of 10-to 12-place light transport helicopters is confirmed also by the practical experience with the 12-place Mi-4 helicopters in the national economy. It is obvious that the development of more economic (for airlines) 30-place Mi-8 helicopters does not interfere with the advantage of using the 10-place helicopters in the national economy for geology and other purposes.

4. Compound Helicopters with Additional Engines - Rotocraft /20

Of considerable interest was the appearance of compound helicopters which use propellers for forward flight, as autogiros did earlier. Such are the Rotodyne Ferry designed by Hislop and especially the rotocraft of the Soviet designer N.I.Kamov.

In 1964, world records for machines of this type were set on the rotocraft Ka-22: speed 360 km/hr, lift capacity 16 tons. N.I.Kamov's rotocraft again focused attention of the helicopter world, after 20 years, on the side-by-side configuration which had been successfully developed by Focke in Germany and by I.P.Bratukhin in the USSR. This machine recalled the great advantages of the side-by-side configuration in flying range and lift capacity with a running takeoff which must be accounted for in a successful design.

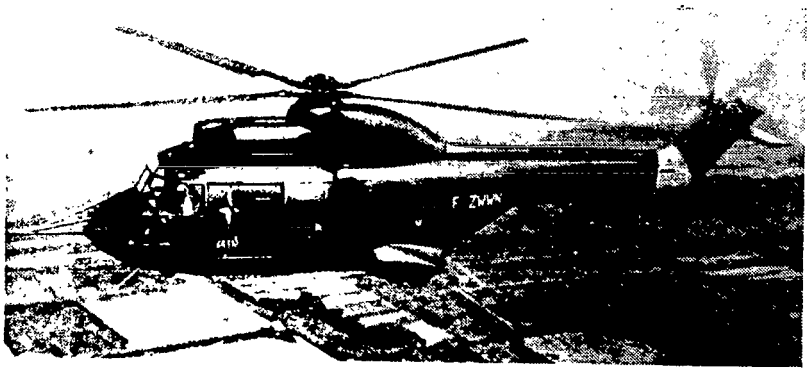

Fig.1.19 SA-330 Helicopter.

A further development of compound helicopters with propeller is represented by the helicopter prototype with additional turbojet engines now being proposed in the West for military purposes.

An interesting prototype of an assault helicopter is the Lockheed composite helicopter (Fig.1.20). This two-place experimental machine, in addition to the main 550-hp turboshaft engine driving a four-blade rotor with elastic blade retention, uses a turbofan engine mounted on a small wing and permitting rev-up to 426 km/hr when briefly cut in during flight.

The successful development of dual-flow turbofan engines, especially with a large bypass ratio, may lead to the development of models which, at cruising speed, would have a specific consumption of the order of C_R = 0.5 kg/kg • hr. Since

$$C_e = \frac{75\eta}{V} \cdot C_R,$$

it is not difficult to calculate that, in this case, the consumption per horsepower of an equivalent propeller engine at a propeller efficiency of 0.75 and a flying speed of 150 m/sec is only about 200 gm/(hp • hr).

If we also take into account the small weight of such a motor in comparison with the weight of a turboprop engine, it becomes clear that the use of turbofan engines of this type can be economically advantageous even at lower cruising /21 speeds and may lead to the development of compound helicopters with an auxiliary thrust engine and wing for passenger transport between urban centers at cruising speeds of the order of 350 - 450 km/hr. At the same time, such helicopters may find military use as fire-support craft for troops.

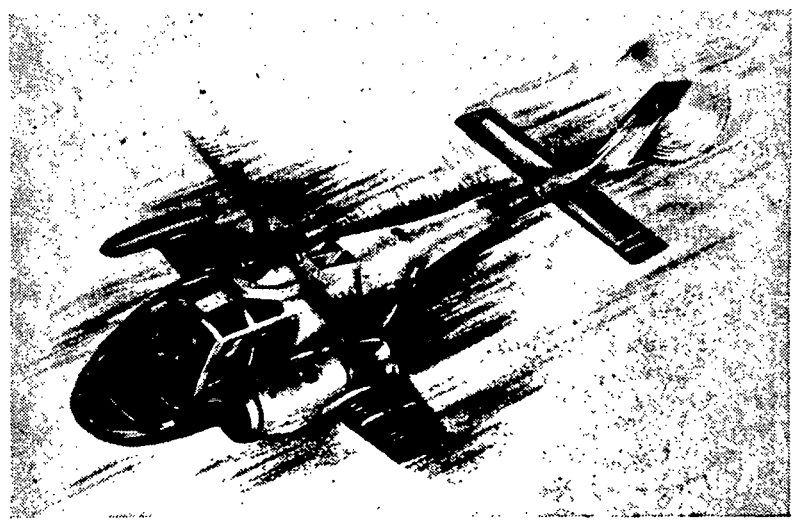

Fig.1.20 Lockheed Helicopter XH-51A.

In analyzing the ways and means of helicopter development, one cannot sidestep the question of vertical takeoff aircraft. Will the development trend and use of helicopters come to an abrupt end with the appearance of such craft, as had been the case with autogiros when helicopters came into being?

Section 2. The Helicopter Compared to Vertical Takeoff and Landing and Short Takeoff and Landing Aircraft

When talking of the prospects of helicopter engineering development, one must study the problem of the possibility of coexistence of helicopter and vertical takeoff aircraft. Do helicopters have a future? Or are the potentialities of the helicopter exhausted? Can the helicopter successfully compete with vertical takeoff aircraft? Will their development trend terminate, as was the case with autogiros which ceased to exist with the appearance, in 1940, of the first successful helicopters? A comparative investigation of helicopters and VTOL or STOL craft as means in transport aviation not requiring an airfield will enable us to answer these fundamental problems.

It is known that recently the matter of vertical takeoff aircraft (in English, VTOL) and short-run aircraft (in English, STOL) has become urgent*. (For footnote, see following page).

Actually, the present flying speed of fighters, reaching 2500 - 3000 km/hr, requires such high-power engines that very little remains to add for their vertical takeoff. Therefore, judging by the literature in other countries we can assume that fighters and fighter bombers will be developed mainly as /22
VTOL aircraft not requiring the use of an airfield. The direction of development of transport aircraft, whose power plant is limited by considerations of economics or quite simply by fuel consumption, tends toward STOL aircraft.

Some propose that the future development of helicopters will offer a better solution to transport problems for a range up to 600 km than do VTOL aircraft or special STOL transport aircraft.

In examining the possible development trend of aviation, we cannot limit the study to an analysis based on the present state of the art in science and technology.

By using such methods, many scientists have repeatedly arrived at erroneous conclusions concerning the "limits" in the development of various aircraft or helicopters, since they did not provide for the development of parameters characterizing the weight and economic perfection of engines or perfection of design and materials used. It is necessary to extrapolate their development somehow to the future.

Leaving room in the future for such an investigation, we will estimate the situation at hand. We will compare helicopters with VTOL and STOL aircraft, using data of the best helicopters that have been built as well as of aircraft being in the design or construction stage.

1. Tactical and Technical Requirements for VTOL and STOL Military Transport Aircraft of the West

The tactical and technical specifications for VTOL transport aircraft, worked out in the USA, call for a flying range of 550 - 700 km, a lift capacity of 3600 kg or 32 troops, and a cruising speed of 450 - 550 km/hr at a gross weight of not more than 16,000 kg. At the same time a very long delivery range, of the order of 4000 km, is required, which is probably intended for the possibility of ferrying aircraft from the USA over the ocean.

In studying STOL transport aircraft, one comes across ordinary classical propeller transport planes such as, for example, the British-Canadian De Havilland "Caribou" (Fig.1.21).

By STOL transport aircraft we mean aircraft that use engine power for /23
reducing the takeoff and landing runs. This is useful and necessary.

A study of STOL aircraft must include one of the first aircraft of this type, the French aircraft Breguet-941 (Fig.1.22). On this aircraft the entire wing area is in the zone of propeller slipstream. All propellers are inter-

* VTOL - vertical takeoff and landing; STOL - short takeoff and landing.

connected by a transmission which provides safe takeoff or landing if one or two of its four engines fail. The propeller slipstream, deflected downward by a double-slotted flap, produces additional lift, which reduces takeoff speed and shortens the run. However, these qualities are achieved at the expense of an increase in empty weight and shorten the range of this STOL aircraft. Helicopters can operate successfully at such a range.

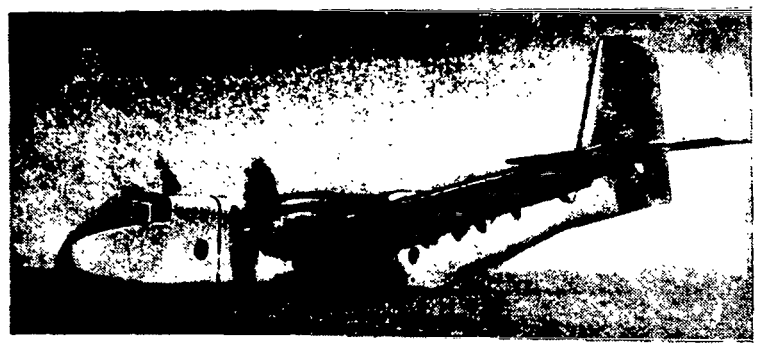

Fig.1.21 British-Canadian Transport Plane De Havilland "Caribou".

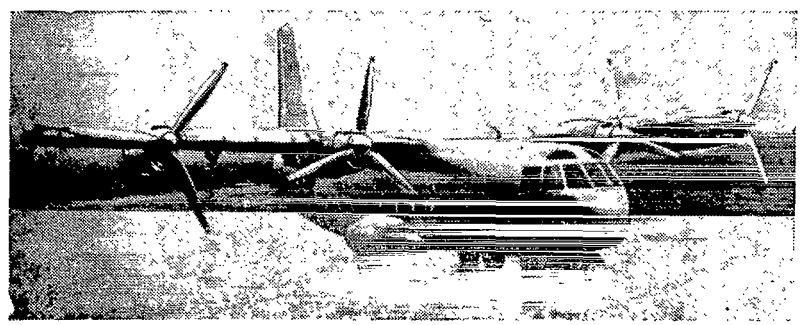

Fig.1.22 French STOL Aircraft Breguet-941.

Despite the great type diversity of VTOL and STOL aircraft, it is not difficult to arrange them logically in a general classification of aircraft. They should be placed between helicopters and airplanes.

It is commonly known that the larger the area over which air flows (it makes no difference whether it flows through a rotor or the nozzle of a jet engine) or, more precisely, the smaller the velocity imparted to the air mass for producing lift in aircraft or helicopter, the smaller will be the power required for this per unit weight of machine.

Thus, the ordinary helicopter and the aircraft taking off vertically by the thrust of jet engines are at opposite poles of this classification (Fig.1.23).

In the pursuit of greater range and probably higher speed, the helicopter was provided with a wing; as the wing area and hence the lift increased further (since the thrust of the rotor at maximum flying speed decreases so much that it is insufficient for forward flight), propellers appeared on the wing. Thus arose the British "Rotodyne" (Fig.1.24) and the Soviet rotocraft designed by N.I.Kamov (Fig.1.25) - aircraft which in place of one lifting and moving system have two, one being the rotor and wing for sustention and the other being a system of tractor propellers, inclined forward to the thrust vector of the rotor, to provide forward propulsion. During vertical takeoff, the wing and the propellers are useless, and in horizontal flight the rotor is superfluous. The attempt to avoid such superfluous units whose weight unavoidably reduces the useful load led to a configuration with a wing and pivoted rotor (Bell XV-3, Fig.1.26) in /24 which the rotor in horizontal flight becomes a propeller, and to a configuration with a pivoted wing whose propellers during takeoff - turning together with the wing - act as rotors as, for example, the XC-142 aircraft produced by Chance Vought - Ryan - Hiller (Fig.1.27).

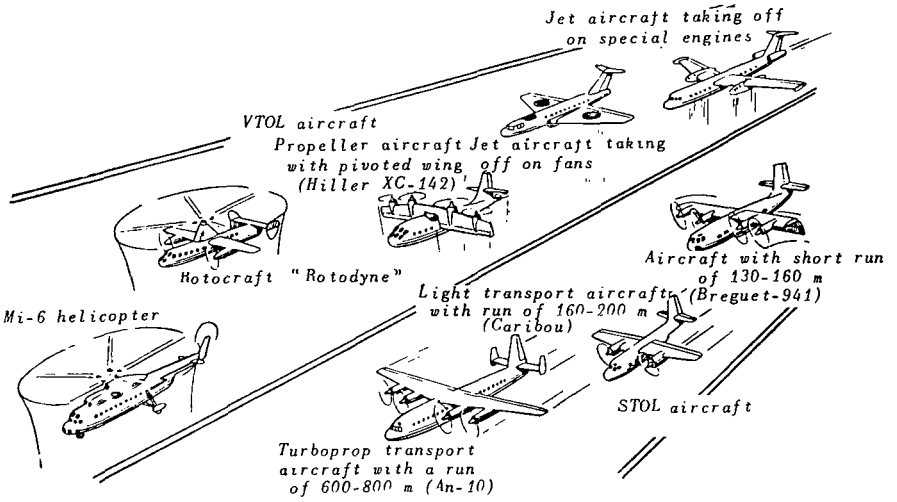

Fig.1.23 Classification Scheme for VTOL and STOL Aircraft.

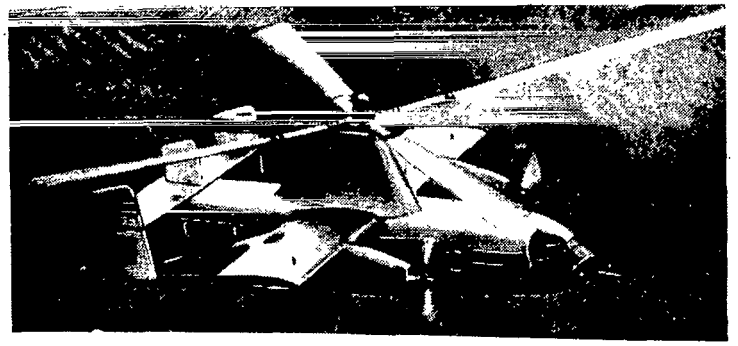

Fig.1.24 Rotodyne Rotocraft.

Passing now to aircraft with an engine more powerful than that of the above types of aircraft, the STOL jet aircraft is provided with means for downward deflection of the blast from the jet engines or from various types of auxiliary turbofan engines.

The configuration of the Breguet-941 aircraft (see Fig.1.22) can be regarded as a variant of an ordinary airplane which, to increase the lift coefficient, utilizes the airflow over the wing created by the propellers, or else as a variant of an aircraft with a pivoted wing where the thrust of the propellers is not literally turned but is deflected downward by means of the mechanized wing.

/25

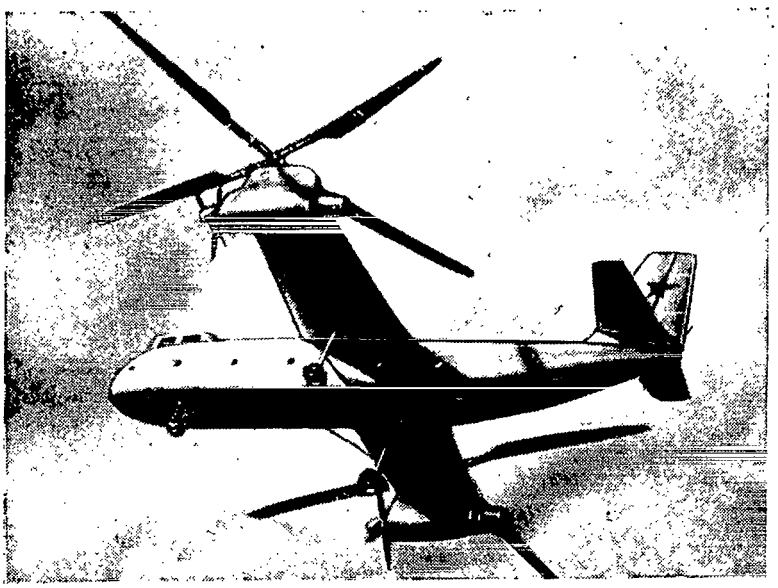

Fig.1.25 Rotocraft Designed by N.I.Kamov.

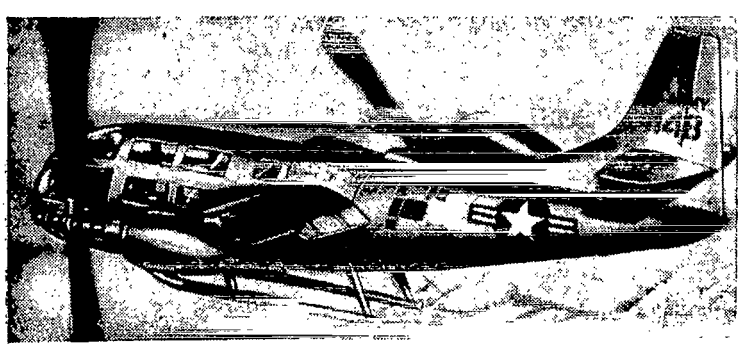

Fig.1.26 Bell XV-3 Convertiplane.

The diameter of the propellers of the VTOL aircraft shown in Fig.1.23 (from left to right) gradually decreases down to the VTOL jet aircraft which

has no propeller at all. With a reduction in propeller diameter, the engine power increases per unit takeoff weight from 0.25 - 0.3 hp/kg for helicopters to 3 - 4 hp/kg for jet aircraft (the values of the equivalent horsepower are taken here for the aircraft). /26

The cruising speed of these aircraft continuously increases along with the increase in installed horsepower. However, this is not a decisive factor for the problem of a transport aircraft with a range of 800 - 1000 km.

This defines the scope of VTOL and STOL transport aircraft to be compared and the flying range over which they are effective.

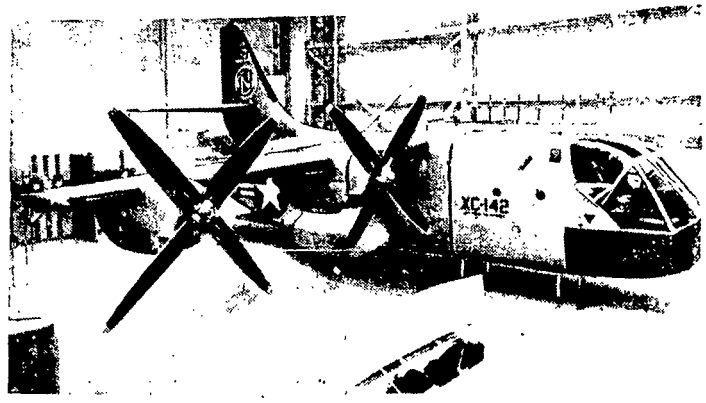

Fig.1.27 Chance Vought - Ryan - Hiller XC-142 VTOL Aircraft with Tilt Wing.

To which of these types of aircraft will belong the future in solving the formulated problem?

Before comparing the helicopter with its competitors with respect to economy, let us examine the problem of the flying range of the helicopter. In view of its comparatively short range, can the helicopter enter this competition at all?

Let us first examine and compare the best of the VTOL and STOL transport aircraft that have been or are being constructed: the tilt-wing VTOL aircraft of the type XC-142; the STOL aircraft of the type Breguet-941; the regular transport aircraft of the type "Caribou" HC-4; the rotocraft with turboprop engines of the "Rotodyne" type; and helicopters.

2. Means for Increasing the Flying Range of Helicopters

The helicopter has always been regarded as a short-range aircraft; a figure of 400 - 500 km is usually given as the maximum for its normal range. In order to treat the helicopter as a competitive aircraft in this new area of use, the

range should be almost doubled while retaining its lift capacity. How does one increase the flying range?

Let us turn to the well-known formula of flying range: /27

$$L = 270 \frac{G_T}{G} \frac{c_y}{c_x} \frac{\eta\xi}{C_e}, \qquad (2.1)$$

where

G = weight of the aircraft (average during flying time);
G_T = weight of the fuel;
c_y/c_x = aerodynamic efficiency of the aircraft (taken to be constant);
C_e = specific fuel consumption of the engine;
ξ = a coefficient taking into account power losses in the transmission due to cooling, etc.;
η = rotor efficiency.

Equation (2.1) shows that the range is greater, the larger the proportion of fuel in the all-up weight of the aircraft and the higher its aerodynamic efficiency, engine economy, and efficiency of engine and auxiliary units.

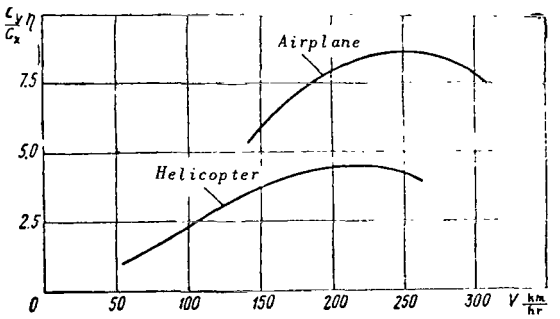

Fig.1.28 Product of Aerodynamic Efficiency and Rotor Efficiency as a Function of Flying Speed.

This formula holds for any heavier-than-air craft, including airplanes and helicopters. Specifically, it follows from this equation that the flying range of various flying machines, other conditions being equal, does not depend on their cruising speed.

Can a helicopter be given a range sufficient for competing with STOL aircraft?

As indicated in Fig.1.28, the product of aerodynamic efficiency c_y/c_x and rotor efficiency η for a helicopter with a fixed landing gear is lower than for a transport airplane by almost a factor of 2. Furthermore, the fuel consumption of the helicopter is somewhat greater than that of the airplane since the engine characteristics are inferior at low altitudes and flying speeds. Thus, a helicopter can be given a range equal to that of airplanes only by increasing the fuel supply, i.e., the quantity G_T/G. However, in so doing how does one maintain the useful load? This can be done only by increasing the takeoff weight, but the helicopter will then no longer be able to take off vertically.

What happens if we place these aircraft under equal conditions, i.e., allow the helicopter the same takeoff run as an STOL aircraft, namely 150 - 200 m or even less? At a relatively large value of c_y, will the helicopter then be able to lift - at low speed - a much greater weight than an airplane, accommodate

more fuel, and thus compensate for its lack in aerodynamic efficiency?

3. Helicopter with Takeoff Run

As shown in Fig.1.29 which gives the curves of the required and available horsepower of a "Caribou"-type transport airplane and of a modern helicopter, an airplane can be kept in the air at a speed not below 115 km/hr. A helicopter can hover in the air without moving. If the helicopter is overloaded by 15% above the normal takeoff weight G_0, it can no longer hover and, like the airplane, will only be able to fly without dropping if it has some speed - in this case, a speed of not less than 50 km/hr. At a greater speed than this, it will gain altitude and at a lower speed, lose altitude. The difference here in favor of the helicopter, in comparison with the conventional airplane, lies only in the fact that the helicopter retains full controllability at a speed below its minimal and that there is no danger of separation of flow and loss of controllability, both of which are possible in the airplane. /28

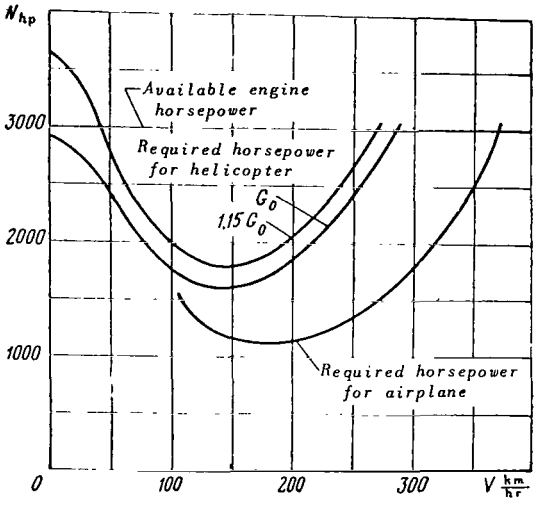

Fig.1.29 Required and Available Power as a Function of Flying Speed.

So far as the takeoff distance is concerned, assuming that the helicopter takes off at a speed of V_{min}, this distance at some average acceleration j, will be

$$L_{run} = \frac{jt^2}{2} = \frac{V_{min}^2}{2j} \qquad (2.2)$$

Thus, the takeoff run is shorter, the lower the minimum flying speed (close to takeoff speed) and the greater the acceleration.

The minimum speed is

$$V_{min} = \sqrt{\frac{2G}{\rho S_w c_{y_{max}}}},$$

where

S_w = wing area;
ρ = air density.

What values of $c_{y_{max}}$ are available to airplanes and helicopters?

For this, let us calculate the value of c_y that an airplane of the "Caribou" type should have at the same weight as the helicopter in order to fly without descending at speeds less than minimum. Figure 1.30 shows the values of c_y,

calculated from the formula

$$c_y = \frac{2G}{\varrho S_w V^2} \qquad (2.3)$$

of a helicopter referred to the wing area of an equivalent airplane, which characterizes the lift capacity of a helicopter in comparison with the airplane. The curve c_y of the helicopter in Fig.1.30 extends to infinity. This is natural since the helicopter has a rotor which in essence is a rotating wing with a power plant suspended from it and is capable of producing lift at zero forward speed of the entire machine. Here we see that at speeds of 50 - 60 km/hr the available values of c_y of the helicopter are several times greater than for an airplane of the "Caribou" type at a speed of 115 km/hr, which has a highly mechanized wing.

Thus, at equal power a greater weight can be lifted by the helicopter at low speeds than by an airplane. /29

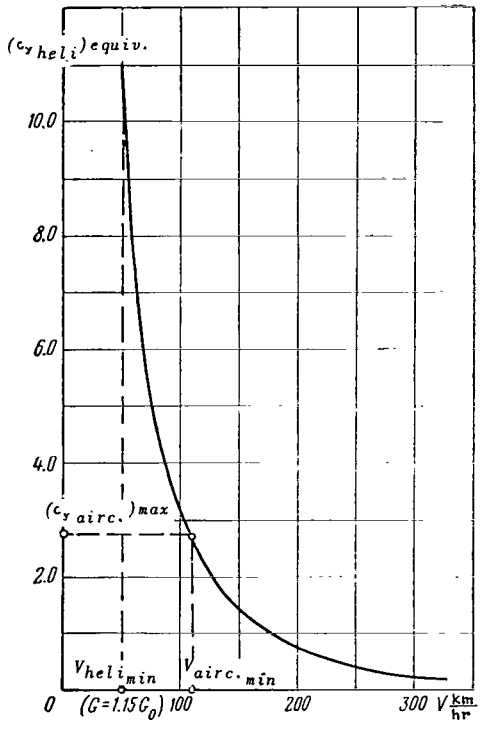

Fig.1.30 Dependence of $(c_{y_{heli}})_{eq}$ on Flying Speed.

However, a greater flying weight does not always mean a greater useful load.

At equal relative fuel weight (about 10%), the ordinary airplane of the "Caribou" type has a range of 1000 km, i.e., twice that of a helicopter taking off without a run.

The Breguet-941 STOL aircraft (at a fuel weight 12 - 13% of the flying weight) has twice the range of the helicopter or of the XC-142 VTOL aircraft.

If, in helicopters, the fuel weight is increased to 20 - 25% of the gross weight, then the range of the helicopter can be doubled and raised to 1000 km. This value is already close to the normal ranges of specially designed STOL aircraft.

The load ratio of helicopters taking off with a run and at increased fuel supply becomes higher than the load ratio of comparable aircraft and reaches 44 - 50%. This makes it possible to obtain equal productivity at almost the same takeoff weight of airplane and helicopter. For example, a transport helicopter of average lift capacity, just as a "Caribou"-type airplane, can transport a load of 3.2 tons over a range of 1000 km. It is true that the helicopter, in so doing, uses 2.5 times more fuel. However, it must be remembered that the airplane needs twice the area for taking

off and, what is quite important, the helicopter after having consumed half its fuel is able to land vertically, whereas the ordinary airplane cannot do so.

It must be emphasized that comparable airplanes and helicopters have practically the same power supply (0.23 - 0.25 hp/kg). One must also bear in mind that piston engines, operating on gasoline, have a lower fuel consumption at low altitudes than turboprops, so that the average turboprop helicopter operates under less advantageous conditions than the "Caribou" aircraft with piston engines.

Thus, the suggestion to use a takeoff run for the helicopter will permit doubling its range at the same useful load.

4. Takeoff Distance of Helicopter

We have already expressed the takeoff distance in terms of takeoff speed and acceleration. The takeoff speed, proportional to the minimum speed at which a helicopter can be supported in the air at an overload of 15% as opposed to the weight with which it can take off without a run, is not more than 60 - 70 km/hr. Let us now define the possible degree of linear acceleration, since the takeoff run is inversely proportional to acceleration. Let us find the possible initial acceleration. /30

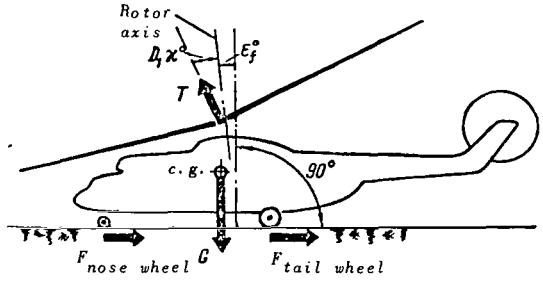

Fig.1.31 Forces Acting on Helicopter during Takeoff Run.

As agreed, let the helicopter develop a thrust amounting to only 0.85 G (takeoff weight) at the takeoff power. Then, allowing for some angle of inclination of the rotor axis to the vertical ε_f (here the difference in the compression of the struts and pneumatic tires of the nose and tail wheels is accounted for) and for the forward deviation of the resultant owing to deflection of the automatic pitch control mechanism through an angle $D_1\varkappa$, according to Fig.1.31, we find the initial acceleration:

$$j_0 = g\left[\frac{T}{G}\sin(D_1\varkappa + \varepsilon_f) - \left(1 - \frac{T}{G}\right)f\right]. \qquad (2.4)$$

Here, the second term on the right-hand side takes into account friction of the wheels against the ground, with a friction coefficient f. Adopting the usual notations of $\varepsilon_f = 6.5^\circ$, $D_1\varkappa = 10^\circ$, $\frac{T}{G} = 0.85$, and f = 0.12, we obtain $j_0 = 2.2$ m/sec^2.

Assuming a relative static propeller thrust of $\frac{P}{N} = 1.6$ kg/hp for the

airplane and using $\frac{N}{G}$ = 0.25 hp/kg, the initial acceleration will be

$$j_0 = g\left(\frac{P}{N}\frac{N}{G} - f\right) = 2.5 \text{ m/sec}^2$$

i.e., a value of the same order as for the helicopter.

Of course, the acceleration at the moment of takeoff is determined by the excess power, which is somewhat higher for the airplane. However, its propeller thrust decreases with an increase in speed whereas the rotor thrust increases; in fact, the angle of pitch of the helicopter, during the takeoff run, may even increase since, during takeoff, the tail wheels are able to lift off the ground at a thrust substantially less than the takeoff weight so that the takeoff run is completed on the nose wheel.

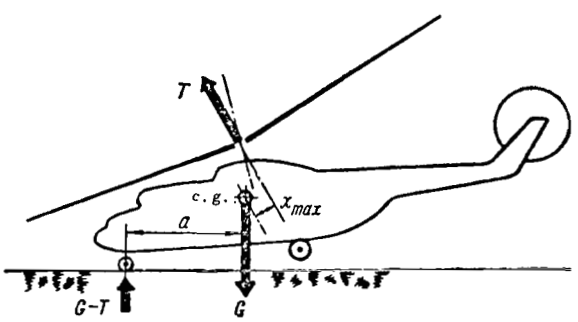

Fig.1.32 Forces Acting on a Helicopter during Takeoff on Nose Wheel.

It is obvious from Fig.1.32 that the thrust-to-weight ratio at which the tail wheels can lift off the ground (disregarding friction) will be

$$\left(\frac{T}{G}\right)_{\text{takeoff}} = 1 - \frac{x_{max}}{a}, \qquad (2.5)$$

where x_{max} is the distance from the center of gravity to the axis of the automatic pitch control mechanism at a maximal forward deflection of this mechanism [here it is assumed that the quantity $\left(\frac{x_{max}}{a}\right)^2$ can be neglected for unity].

Fig.1.33 Running Takeoff of Mi-6 Helicopter.

With the usual relations, this corresponds to a thrust-to-weight ratio of 0.8 - 0.85. Figure 1.33 shows a helicopter during the takeoff run, at a gross weight of $G_{max} = 1.15\ G$.

An exact calculation of the takeoff run can be carried out by the same /31 method proposed by the author 30 years ago for calculating the takeoff run of an autogiro (Ref.4).

Running takeoffs performed in practice have confirmed that, at a 15% overload of a helicopter as opposed to the maximal weight with which it can take off without a run, the takeoff run amounts to no more than 60 - 100 m in still air.

5. Criterion for Estimating the Economy of Various Transport Aircraft

In any comparison of two transport aircraft, attention is primarily centered on the lift capacity. Still, the speed of transport is also important. Actually, if a load can be transported more quickly, then more loads can be transported in unit time over a given distance at a smaller lift capacity.

This results in the well-known criterion of hourly productivity $G_{load} V_{av}$ t · km/hr (V_{av} is the average ground speed).

However, at what cost is the load transported?

If both aircraft have identical efficiency and range as well as takeoff /32 and landing properties satisfactory for fulfilling the mission, which should be given preference?

To answer this question we must know which of the aircraft is more economical. In military use, the advantages of any aircraft for solving transport problems, which sometimes arise at an appreciable distance from the supply bases, are determined primarily by cost data. Expenditures for construction of the machine itself, incurred in the past, are no longer of significance and have no effect on fulfilling the immediate task. Under such conditions, the economy of an aircraft is determined mainly by the amount of fuel consumed. Here, the transport of fuel constitutes a bottleneck that is decisive for the ability to solve the stated problems. The criterion of economy under such conditions is conveniently obtained by referring the hourly productivity to the weight of the fuel consumed during that time $G_{T\,hr}$:

$$L_{e.s} = \frac{G_l V}{G_{T\,hr}}. \tag{2.6}$$

Since the fuel consumption per kilometer is

$$q = \frac{G_{T\,hr}}{V}, \tag{2.7}$$

it follows that

$$L_{e.s} = \frac{G_l}{q}\ \text{km}. \tag{2.8}$$

The quantity $L_{e.s}$ has the dimension of length, so that we can call it the equivalent specific range of the aircraft. It represents the distance over which a given aircraft can fly in excess of the design range if the entire transported load is replaced by fuel. Still another meaning can be given to this quantity. It can be regarded as the distance over which an aircraft can carry one ton of cargo after having consumed one ton of fuel. It is clear that the quantity $L_{e.s}$ depends on the distance of transportation just as productivity depends on it. The farther the machine flies, the more fuel it needs and the smaller the cargo it can take at a given flying weight (maximal).

On the other hand, $L_{e.s}$ is the work expressed in ton-miles which a given aircraft can perform, having consumed one ton of fuel.

The inverse quantity of $L_{e.s}$, i.e., $\frac{1}{L_{e.s}}$, is fuel consumption in tons required for performing transportation work of 1 ton-mile or $\frac{1000}{L_{e.s}}$ kg/ton-mile.

We can also use other criteria that estimate economy, i.e., the cost of transporting one ton-mile in rubles. In these criteria, we can take into account the cost of the aircraft (to some extent, this is proportional to the empty weight of the aircraft), the service life of the components and power system, cost of operation and repair, etc.

In this problem, the military transport criterion $L_{e.s}$ or $\frac{1000}{L_{e.s}} = C_L$ is most important since it takes into account not only economy but also the real and ponderable requirement of supplying fuel for transportation equipment under military conditions. Therefore, we can disregard many other criteria but not this one.

We supplemented the values of $L_{e.s}$ and C_L for comparable aircraft by data on jet VTOL aircraft which, for hovering, use specially installed lifting jet engines or which take off by means of fans driven by the main engines. The fuel consumption of such aircraft, while hovering, constitutes such a large percentage of the takeoff weight that it must be taken into account when calculating the value of C_L; therefore, the corresponding formula takes the form /33

$$C_L = C_{L_{h.f}} + C_{L_{hov}}, \qquad (2.9)$$

where

$C_{L_{h.f}} = \frac{1000\, G_T}{G_{load} L}$ is the fuel consumption in horizontal flight;

$C_{L_{hov}} = 1000 \frac{t_{hov} C_{R_{hov}}}{\frac{G_{load}}{G} L}$ is the fuel consumption while hovering.

For an aircraft taking off by means of wing fans rotated by turbines mounted to their periphery, we have used data similar to those published for the experimental Ryan X-16 airplane constructed in the USA.

In the calculations, we disregarded the fact that the installation of the

lifting engines impairs the aerodynamic efficiency of a VTOL aircraft. It was assumed that, at ranges greater than 1000 km, VTOL aircraft of the indicated two types with a sustainer turbojet will fly at the design altitude at maximum aerodynamic efficiency, whereas at a reduction in flying range from 1000 to 50 km the operational ceiling decreases accordingly and any drop in aerodynamic efficiency leads to some increase in fuel consumption. The hovering time t_{hov} was taken as 6 min (3 min in takeoff and 3 min in landing).

Table 1.3 gives our calculated data for aircraft of different flying ranges and different forms of takeoff.

TABLE 1.3

Characteristics	Type of Takeoff: Vertical			With Short Run L_r <200 m			From Small Airfield L_r <400 m		From Concrete Airstrip L_r ≈800 m		Road Transportation	
Range L, km	<500			1000			1000		2000		—	—
Flying altitude H, m	500—2000			500—2000			3000		8000		—	—
Type of aircraft	Helicopter	VTOL Propeller Aircraft	Rotocraft	Helicopter	STOL Propeller Aircraft	Rotocraft	Light Transport Propeller Aircraft	STOL Propeller Aircraft (Overload Weight)	Turboprop Transport Aircraft	Turbojet Transport Aircraft	Truck on Highway	Cross-Country Truck
Takeoff run L_r, m	0	0	0	80	140	150	170	210	850	950	—	—
C_L, kg/t·km	0.8	0.9	1.3	0.9	0.6	1.4	0.4	0.5	0.3	0.5	0.13	0.4
V_{cr}, km/hr	250	460	280	240	400	280	250	400	600	800	60	30

To compare the economy of transport conveyances, the values of C_L are given for the Soviet truck ZIL-151 where it is assumed that the road between two points is longer by a factor of 1.5 than the air route. /34

Figure 1.34 shows the values of C_L as a function of flying range, for various VTOL aircraft. The value of the flying range L in calculating C_L was determined with consideration of a decrease in fuel consumption per kilometer as the aircraft became lighter due to depletion of the fuel. Assuming a linear dependence between consumption per kilometer and the weight of the aircraft, we must correct the value for the range, calculated from the above formulas where the per-kilometer consumption is accepted to be constant and corresponding to the takeoff weight, by the quantity

$$K_L = \frac{\log \frac{1}{1-\bar{G}_т}}{\bar{G}_т},$$

where $\bar{G}_T = \frac{G_T}{G}$ is the ratio of fuel weight to takeoff weight of the aircraft.

For VTOL aircraft, aircraft with a large fuel consumption for hovering, the reduction in flying weight due to the expenditure of fuel for hovering and in horizontal flight was taken into account. Figure 1.35 shows the curve of the correction coefficients K_L as a function of the values of $\bar{G}_T$.

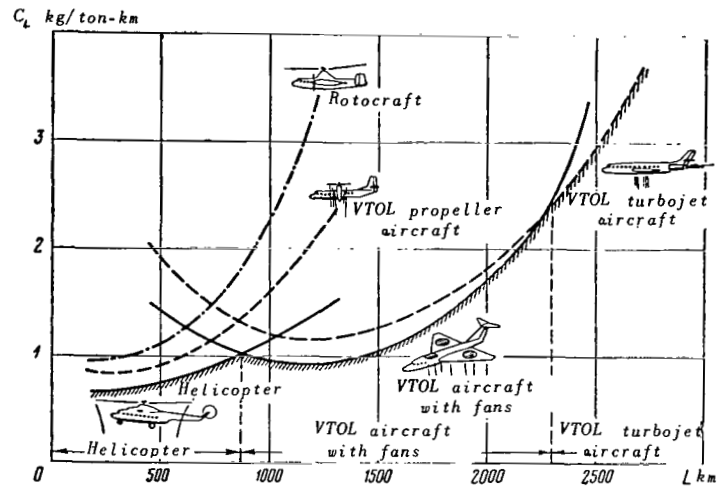

Fig.1.34 Dependence of C_L on Flying Range L.

For aircraft with takeoff run, the values of C_L at different flying ranges are given in Fig.1.36. The diagram also shows how the economy of transport means can be increased, at a given range, by using a takeoff run. The longer the takeoff, the larger the takeoff weight of the aircraft and hence the greater the weight of transported cargo.

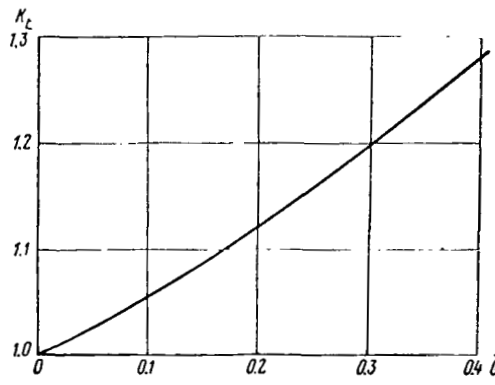

Fig.1.35 Dependence of Coefficient K_L on $\bar{G}_T$.

Such are the results of investigating fuel consumption for transporting one ton-mile with various types of transportation means.

As regards the cost of operating airplanes and helicopters, which naturally is determined not only by the cost of fuel but also by the service life and initial cost of the machine, we must bear in mind that the greater power/weight ratio of the VTOL aircraft compared to that of helicopters as well as the presence of transmissions in some types more or less balances this cost. As for safety in the case of engine failure /36

during takeoff or landing, all advantages are here on the side of helicopters since the propellers on an aircraft with a pivoted wing are not capable of autorotation, and engine failure (depletion of fuel) during landing of an aircraft of the type Breguet-941 may lead to flow separation and an uncontrollable descent because the wing is no longer washed by the propellers. Furthermore, there will always be the difficulty of providing controllability at low speeds in these machines.

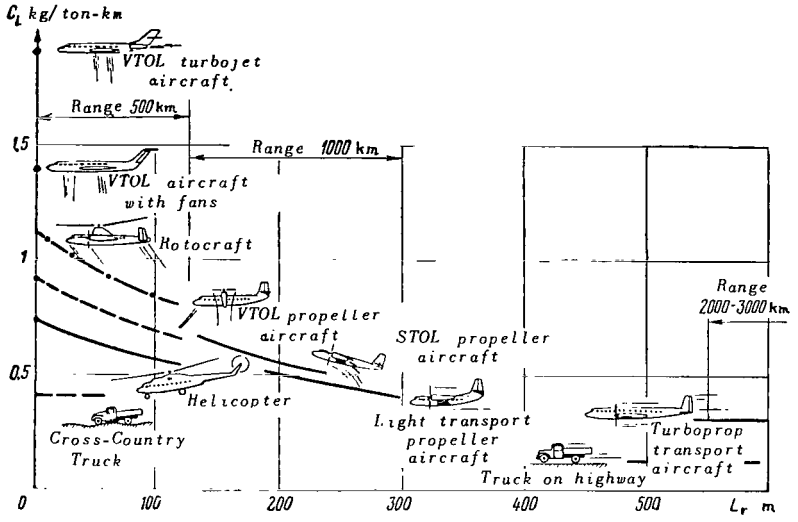

Fig.1.36 Dependence of C_L on Takeoff Run for Various Flying Ranges.

A further reduction in weight and fuel consumption of turboprop engines under development at present will lead to an increase in load factor of helicopters. The substantial increase in service life of rotor blades, reduction gears, and transmissions obtained in modern prototypes will equalize the amortization cost of airplanes and helicopters, after which the helicopter will become a full and equal member of the air transportation system in its most massive area.

6. Possibilities of Increase in Maximum Flying Speed

If the flying speed of VTOL and STOL aircraft is considered to be an important flying and tactical requirement, then the possibilities of rotocraft are far from exhausted with respect to further increase in speed.

If we equate the power required for horizontal flight and the net power of the engine, we can obtain the relation between maximum speed and power/weight ratio of the aircraft:

$$V_{max} = 270 \frac{N}{G} \frac{c_y}{c_x} \eta\xi, \qquad (2.10)$$

where

N = engine power;
G = gross weight of the aircraft.

It follows from eq.(2.10) that the maximum speed is directly proportional to the power/weight ratio N/G of the aircraft.

Figure 1.37 gives the curves of the required power/weight ratio as a function of flying speed for various aircraft. The curves for heavy rotocraft show that, to increase the flying speed above 300 - 320 km/hr, it is necessary to supplement the helicopter rotor with a second high-lift device - a wing; to reach speeds above 370 km/hr also propellers are needed, which means changing over to a rotocraft. Thus, by formulating the problem of achieving the highest speed possible at any price, it becomes possible to decide what VTOL aircraft configuration to use for different maximum flying speeds. However, it must be remembered that the transition from helicopter to rotocraft involves a loss in lift capacity, an increase in the cost of construction, etc. Even with a power/weight ratio of 0.45 hp/kg, which can presently be realized on rotocraft, the transition from helicopter to rotocraft will not produce a gain in speed by more than 30 - 40 km/hr.

/37

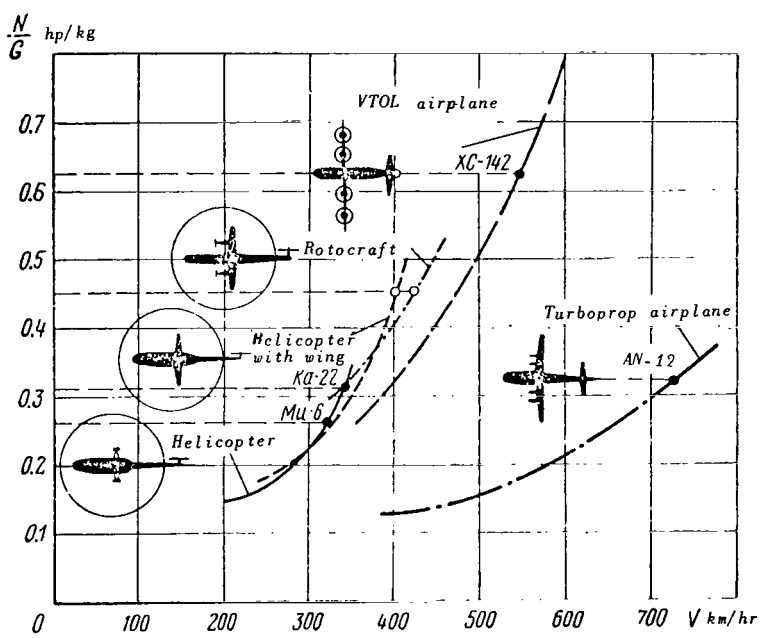

Fig.1.37 Power/Weight Ratio of Aircraft as a Function of Flying Speed.

Finally, the graph of the required power/weight ratio clearly shows the great difference in the power/weight ratio of VTOL aircraft and of rotocraft. At equal power/weight ratio, the rotocraft is somewhat inferior in speed to the propeller-driven VTOL airplane with a short range.

Section 3. Basic Principles of Design

1. Selection of Engine Horsepower and Rotor Span

In most cases, the helicopter designer is supplied with the desired lift capacity. Knowing the required speed, he estimates the necessary power/weight ratio. After assigning the current percentage of the useful load ratio, he determines the order of magnitude of the flying weight and hence the magnitude of the installed power. Having selected the number of engines in view of the end use of the helicopter (one engine for a light military machine, at least two engines for a passenger craft, etc.), he can select the most suitable engines among existing or scheduled types.

Usually, it will happen that the power of the possible combinations of engines does not match the desired power. This necessitates correcting the parameters of the helicopter in question, after selecting the optimum combination of existing engines. After this, the main problem facing the designer is to select the rotor span for the specific power plant.

How does one select disk loading?

It is known from statistics that disk loading rapidly increases with increasing flying weight and varies within 12 - 50 kg/m^2 as the weight increases from the lightest to the heaviest helicopter.

Disk loading, as a function of weight, varies even more than wing loading of an airplane. This is of importance since an increase in wing loading of an airplane can be compensated by an increase in length of takeoff run whereas, for helicopters, the takeoff run must always remain zero. /38

The weight of the rotor increases approximately in proportion to the cube of its span. However, at equal power the lift capacity of the helicopter as a whole increases in proportion to the 2/3 power with an increase in span. In addition, such flight data as ceiling, rate of climb, range, rate of descent in autorotation must be improved when the span is increased and hence disk loading is decreased.

It is impossible to calculate the parameters of an optimal design since there are too many contradictory considerations that the designer must weigh. The answer to this problem should also include a search into the past, an analysis of the development of helicopters with respect to size.

How is the next (larger) helicopter to be developed?

It is obvious that the prime requisite is to increase the installed power. However, to what extent? For example, if we retain the power/weight ratio (for considerations of economy) and then, if necessary, increase the rotor span so that the former disk loading remains, or else if we increase the power/weight ratio and then have the opportunity to increase disk loading provided that takeoff is vertical, will we actually obtain a comparatively smaller rotor span?

The best solution is obtained with the variant having the lowest construction

weight, i.e., providing a higher proportion of useful load.

Let us find the variation in load ratio of a helicopter when its size is increased for different power loading and disk loading.

We will examine the case in which a new larger helicopter is developed according to the same scheme as above.

Taking the static thrust (without consideration of the ground effect) to be equal to the weight, Joukowski's formula will furnish

$$T=G=(33.25\xi\eta ND)^{2/3}, \tag{3.1}$$

where

ξ = a coefficient smaller than unity characterizing the mechanical losses of power in the transmission and those due to cooling and equalization of the torque;

η = rotor efficiency representing the ratio of the useful power needed for supporting the aircraft in the air during hovering to the spent power.

We will write the expression for takeoff weight of a helicopter in the form

$$G=G_{use}+G_{nl}+k_{tr}N+\bar{G}_{l.s}G, \tag{3.2}$$

where

G_{use} = useful load of the helicopter;

G_{nl} = weight of the nonlifting elements of the helicopter;

G = takeoff weight of the helicopter;

k_{tr} = an empirical coefficient representing the ratio of engine weight and transmission to engine power;

$\bar{G}_{l.s}$ = relative weight of lifting system (rotor with hub and automatic pitch control mechanism) with respect to helicopter weight.

Change in load factor on increase in rotor span. We will attempt to determine the load factor $\frac{G_{use}}{G}$ of a heavier helicopter which differs from the original by the rotor span: /39

$$\frac{G_{use}}{G}=\frac{G-G_{nl}-k_{tr}N-\bar{G}_{l.s}G}{G}. \tag{3.3}$$

Assuming that, in this case, the power/weight ratio N/G remains constant, eq.(3.1), at a constant value of $\xi\eta$, will yield

$$G^{3/2}=\text{const}\,ND$$

or

$$\frac{G}{N}\sqrt{\frac{G}{D^2}}=\text{const.} \tag{3.4}$$

Hence the disk loading, i.e., the quantity

$$p=\frac{G}{\frac{\pi D^2}{4}}$$

also should remain constant.

On increasing the rotor span, if the size of the blades changes similarly while their number remains unchanged, the weight of the lifting system increases in proportion to the cube of the ratio of the rotor spans:

$$G_{l.s_2}=G_{l.s_1}\left(\frac{D_2}{D_1}\right)^3. \tag{3.5}$$

Consequently,

$$\overline{G}_{l.s_2}=\overline{G}_{l.s_1}\frac{G_1}{G_2}\left(\frac{D_2}{D_1}\right)^3. \tag{3.6}$$

Here the subscripts 1 and 2 pertain, respectively, to the original helicopter and to the helicopter under study ($D_2 > D_1$).

However, if the disk loading p is increased, flow separation at maximum speed can be avoided only by increasing the loading (mainly by increasing the number of blades since a relative increase in chord is less advantageous and causes a greater increase in weight because of the need for larger balancers to eliminate flutter).

In this case, when retaining the span and the tip speed of the blades, the weight of the lifting system will increase proportionally to p, i.e.,

$$G_{l.s_2}=G_{l.s_1}\frac{p_2}{p_1}\left(\frac{D_2}{D_1}\right)^3; \tag{3.7}$$

or

$$\overline{G}_{l.s_2}=\overline{G}_{l.s_1}\frac{D_2}{D_1}. \tag{3.8}$$

Substituting this expression into eq.(3.3), we obtain

$$\overline{G}_{use_2}=1-\overline{G}_{nl}-k_{tr}\left(\frac{N}{G}\right)_2-\overline{G}_{l.s_1}\frac{D_2}{D_1}. \tag{3.9}$$

The coefficient k_{tr} is the sum of the relative weights of engine and transmission:

$$k_{tr}=\frac{G_{eng}}{N}+\frac{G_{tr}}{N}. \tag{3.10}$$

The first addend remains unchanged (it characterizes the weight characteristic of a modern engine) and the second increases proportionally to the increase in rotor span. /40

Actually, if we assume that the weight of the transmission is proportional to the magnitude of its transmitted torque M_t, then we obtain

$$G_{tr_2}=G_{tr_1}\frac{M_{t_2}}{M_{t_1}}=G_{tr_1}\frac{N_2 n_1}{n_2 N_1}. \tag{3.11}$$

Keeping the tip speed constant (ωR = const), we have

$$\frac{n_1}{n_2}=\frac{D_2}{D_1}.$$

Hence,

$$\left(\frac{G_{tr}}{N}\right)_2=\left(\frac{G_{tr}}{N}\right)_1\frac{D_2}{D_1}. \tag{3.12}$$

At constant disk loading it follows from eq.(3.4) that

$$\frac{D_2}{D_1}=\sqrt{\frac{G_2}{G_1}}=\sqrt{m}, \tag{3.13}$$

where

$$m=G_2/G_1.$$

Then, considering also that

$$\frac{N_2}{G_2}=\frac{N_1}{G_1}$$

and

$$\left(\frac{G_{tr}}{N}\right)_2=\left(\frac{G_{tr}}{N}\right)_1\sqrt{m}, \tag{3.14}$$

we can transform eq.(3.9) into

$$\bar{G}_{use}=1-\bar{G}_{nl}-\frac{1}{q}\left(\frac{G_{eng}}{N}\right)-\left[\bar{G}_{l.s}+\frac{1}{q}\left(\frac{G_{tr}}{N}\right)_1\right]\sqrt{m}, \tag{3.15}$$

where

$$q=\left(\frac{G}{N}\right)_1=\left(\frac{G}{N}\right)_2.$$

Assuming for the original version: $\bar{G}_{nl}$ = 0.25; $\frac{G_{eng}}{N}$ = 0.2; $\frac{G_{tr}}{N}$ = 0.4; $\bar{G}_{l.s}$ = 0.18; $\frac{N}{G}$ = 0.28 and substituting these into eq.(3.15), we obtain (at $G_2 = G_1$)

$$\left(\frac{G_{use}}{G}\right)_1 = 0.402;$$

$$\bar{G}_{use} = 0.694 - 0.292\sqrt{m}. \tag{3.16}$$

Hence it is clear that the magnitude of the load ratio of a larger helicopter decreases monotonically with an increase in m (Fig.1.38).

The ratio of the useful load of helicopters can be represented as

$$\frac{G_{use_2}}{G_{use_1}} = \frac{G_2}{G_1}\frac{\left(\frac{G_{use}}{G}\right)_2}{\left(\frac{G_{use}}{G}\right)_1} = 2.49m\left\{0.75 - \frac{1}{q_1}\left(\frac{G_{eng}}{N}\right)_1 - \left[0.18 + \frac{1}{q_1}\left(\frac{G_{tr}}{N}\right)_1\right]\sqrt{m}\right\}. \tag{3.17}$$

It follows from eqs.(3.15) and (3.17) that it is impossible to construct /41 a larger helicopter while maintaining the same disk loading and the same power to weight ratio as those of the original helicopter, with a larger (or even the same as the previous) coefficient of the load ratio, although the absolute value of the useful load increases at first (Fig.1.40).

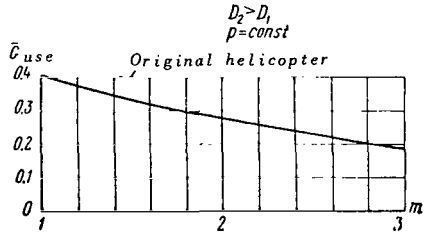

Fig.1.38 Dependence of Load Ratio on Scale m of Weight Increase when p = const.

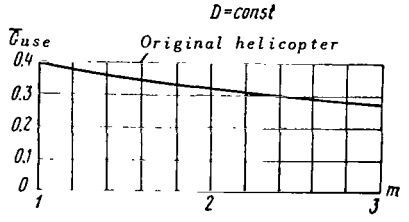

Fig.1.39 Dependence of Load Ratio on Scale m of Weight Increase when D = const.

Change in load ratio on increase in power/weight ratio without change in rotor span. Let us next examine the case where the rotor span remains unchanged while flying weight and engine power increase, i.e., the power/weight ratio of the helicopter and disk loading increase.

It follows from eq.(3.1) that the power/weight ratio of a helicopter should in this case increase according to the law

$$\left(\frac{N}{G}\right)_2 = \left(\frac{N}{G}\right)_1\sqrt{m}. \tag{3.18}$$

Equation (3.8) indicated that the relative weight of the lifting system remains constant. Keeping the ratio of engine weight to engine power constant, the relative weight of the engine increases in proportion to $\sqrt{m}$

$$\bar{G}_{eng}=\left(\frac{G_{eng}}{N}\right)_1 \frac{1}{q_1}\sqrt{m}. \tag{3.19}$$

The relative weight of the transmission also changes

$$\bar{G}_{tr}=\left(\frac{G_{tr}}{N}\right)_1 \frac{1}{q_1}\sqrt{m}. \tag{3.20}$$

Then the expression for the load ratio coefficient will take the form

$$\bar{G}_{use}=1-\bar{G}_{nl}-\bar{G}_{l.s}-\left[\frac{G_{tr}}{N}+\frac{G_{eng}}{N}\right]\frac{\sqrt{m}}{q_1}. \tag{3.21}$$

Substituting the numerical values, we have

$$\bar{G}_{use}=0.57-0.17\sqrt{m}.$$

The ratio of useful load to helicopter weight varies in the same manner as in the previous case (see Fig.1.39), i.e., decreases monotonically.

As we see (Fig.1.40), upon an increase in power at constant span, the useful load increases more rapidly than upon an increase in span at constant power/weight ratio.

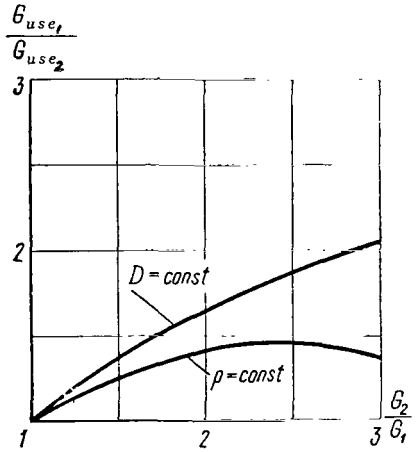

Fig.1.40 Ratio of Useful Load Weights as a Function of Flying Weight Ratio.

Thus, it is obvious that the disk loading depends on the weight characteristics of specific engines available to the designer for solving the formulated problem, namely to lift a prescribed useful load. It is obvious that the lighter the engine in comparison with a given prototype, the greater will be the optimum disk loading and the smaller will be the rotor span. /42

This is the reason for the small loads per square meter of the first airplanes and helicopters. These machines with their then low-power and high-weight engines with large loading were generally not airworthy.

Thus, the designer or researcher who wishes to project into the future should adopt some rules for decreasing the unit weight of engines, rotors, and nonlifting structural elements (by using new materials and increasing the effective design stresses)

aside from the possible discovery of new engine operating principles; only then will he be able to predict the potentialities of developing larger or more economic (load ratio, flying range) aircraft.

It would be natural to expect a pronounced increase in load ratio by returning to small helicopters and using the level of engine and rotor unit weights achieved in developing the heavy helicopters of the 1960s.

Actually, a comparison of recent helicopters with turboprops of the same weight category as the Mi-1 and Mi-4 helicopters showed that their load ratio almost doubled.

2. Analysis of Multirotor Configurations

Sooner or later, the designer is confronted with the problem of the expediency of further increasing the rotor span and the need to change to a twin- or multirotor configuration.

The lot production of still another blade size requires very large capital investment for building new steel mills, presses, and other expensive equipment required for finish-treating of spars and blade assembly. Therefore, the development of new blades is to some extent a Federal problem. At the same time, termination of the production of any one type of series-produced blade is impossible, since the existing inventory of helicopters is a steady consumer of blades because the blade life, as a rule, is considerably shorter than the service life of helicopters. Consequently, when initiating a new blade design new production facilities must be created to supplement those already available.

Therefore, after having developed the largest series-produced rotor, it is logical to attack the problem of the optimum multiple to be used. This renders the problem of configuration specific: it becomes necessary to double or triple also nonrotor units, i.e., rotors together with reduction gears and engines. /43

Actually, the number of combinations is not excessive: twin-rotor (side-by-side and fore-and-aft configurations) and three-rotor helicopters. The cumbersome four-rotor configuration need not be discussed here since the above configurations are able to provide the maximum required lift capacity of 40-50 tons. Another problem to be discussed is that of comparing single-rotor helicopters, designed for similar missions, with these configurations.

Fore-and-aft configuration. Since the induced velocities of the front and rear rotors are identical, the induced velocity of the system will differ only by the quantity of the average velocity of mutual induction

$$v_{av}=\frac{1}{2}\varkappa v_1, \tag{3.22}$$

where

v_1 = induced velocity in the rotor plane;
$\varkappa$ = coefficient of induction.

Then, the additional induced power of the system or of the rear rotor is

$$\Delta N_i = \frac{1}{2} \varkappa v_1 G. \tag{3.23}$$

If both rotors lie in the same horizontal plane and do not overlap, then $\varkappa = 2$; at $\frac{a}{R} = 0.2$ (Fig.1.41) we already have $\varkappa = 1.35$.

However, we should consider that the induced velocities are unevenly distributed over the disk so that the average velocities are larger, corresponding to another aspect ratio, i.e., to a smaller span or, what comes to the same, to a larger load p on the supporting surface. Therefore, we will take the expression for the average velocity of mutual induction, referred to the entire craft, as

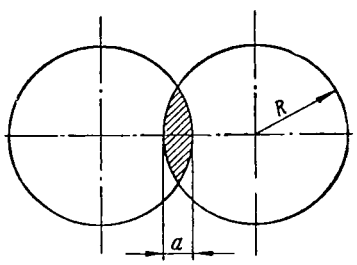

Fig.1.41 For Determining Rotor Overlap.

$$v_{av} = 0.75 v_1 = 0.75 \frac{4p}{V\Delta}. \tag{3.24}$$

Then the rate of climb of a helicopter of a fore-and-aft configuration can be expressed by the rate of climb of a single-rotor helicopter

$$V_y^t = V_y - \frac{3p}{V\Delta}, \tag{3.25}$$

where

V_y^t = rate of climb of a tandem (fore-and-aft configuration) helicopter;
V_y = rate of climb of a single-rotor helicopter;
Δ = relative air density.

Thus, whereas the Mi-4 helicopter with blades of mixed design has a vertical rate of climb, at a flying speed of 100 km/hr, of 3.6 m/sec, the vertical speed of the tandem-rotor helicopter (Fig.1.42) with two such power plants decreases by the quantity

$$\Delta V_y^t = V_y - V_y^t = \frac{3 \cdot 21}{28} = 2.25 \text{ m/sec},$$

i.e., the rate of climb of the tandem-rotor helicopter is 1.35 m/sec.

Consequently, the flying characteristics of the fore-and-aft machine substantially differ from those of the original single-rotor helicopter from which the power plants were taken.

The rate of climb is determined by the transverse span of the helicopter, /44 its engine power, and the takeoff weight of the helicopter prescribed by the designer. It can be stated that, if these parameters are given, the maximum possible rate of climb will be determined regardless of the configuration of the planned helicopter and the type of its power plant.

In addition to power expended for lifting weight, there are also power

expenditures for mechanical, profile, and induced drag. Thus, if the takeoff weight of the helicopter of a fore-and-aft configuration is twice the weight of a single-rotor helicopter, the magnitude of rate of climb can be maintained only by increasing the power of the tandem-rotor helicopter to more than the double power, by an amount of

$$\Delta N = G_t \frac{3p}{75V\Delta}.$$

If we only double the power of the tandem-rotor helicopter, its rate of climb will decrease, as indicated above. Such a doubling would be especially unsuitable for heavy helicopters with large disk loading; thus, at values of $p = 40$ kg/m^2 and $V = 40$ m/sec the loss of rate of climb ΔV_y^t at an altitude of $H = 3000$ m, in comparison with the original single-rotor helicopter, will be 4 m/sec, i.e., such a helicopter will not be able to fly if $V_y < 4.5 - 5.0$ m/sec.

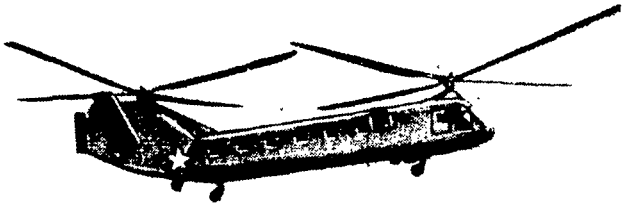

Fig.1.42 Yak-24 Helicopter.

Comparative data of two Soviet helicopters Mi-4 and Yak-24 of different configurations but having the same engines and supporting systems (these are doubled on the Yak-24 helicopter) show that the fore-and-aft helicopter has a vertical ground speed 2.6 m/sec lower than that of the single-rotor helicopter and that, at altitudes of 1000 - 2000 m, the loss in vertical speed reaches 3 - 3.5 m/sec. The service ceiling also drops by a factor of 2 for the fore-and-aft helicopter.

Figure 1.43 shows the change in torque distribution with respect to the rotor shafts, measured in flight on one of the fore-and-aft helicopters. At $\mu = 0.1 - 0.25$, the rear rotor consumes about double the power of the front rotor.

This nonuniformity in loading of the rear and front reduction gears and rotors substantially reduces the lifetime of the rear rotor parts or else necessitates development of a more powerful and heavy reduction gear. It is impossible to use the main reduction gear of the original single-rotor helicopter as the rear reduction gear of the tandem helicopter.

The large induced losses due to mutual interference of the rotors in fore-and-aft helicopters, which amount to 20 - 25% of the power at cruising speed, /45

greatly impair its efficiency in comparison with the single-rotor helicopter in which the power expenditure for driving the rear rotor in horizontal flight is negligible.

Side-by-side configuration. This configuration is another solution to the old problem of how to build a "bridge" connecting the rotors. How can one define the difference between such fore-and-aft and side-by-side "bridges"?

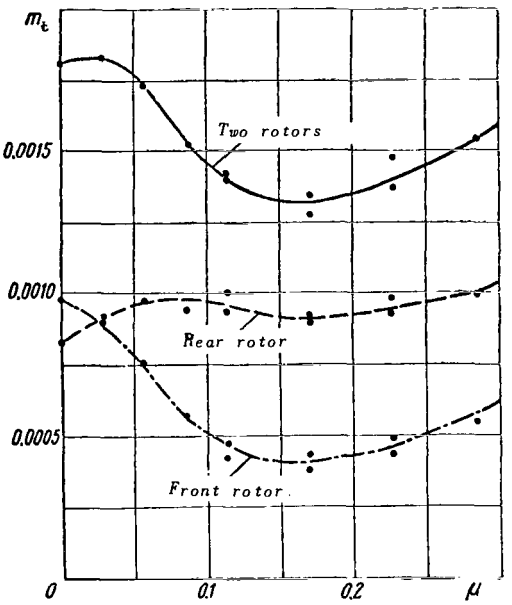

Fig.1.43 Change in Torque Distribution with Respect to Rotor Shafts as a Function of their Operation.

From the viewpoint of mutual interference during hovering, there are no fundamental differences in the operation of the rotors of either type of helicopter configuration. However, the losses from propeller wash over the wing in a side-by-side helicopter may be greater than from wash over the fuselage in a fore-and-aft helicopter. Therefore, the characteristics of vertical takeoff are poorer for the side-by-side configuration with a wing. Nevertheless, in forward flight the rate of climb of the side-by-side helicopter increases by an amount of

$$\Delta V_y = \frac{1}{2}\,\varkappa v_1 = 0.375 v_1 = \frac{1.5p}{V\Delta}$$

in comparison with the original single-rotor helicopter, due to a decrease of induced drag (the "span" of the side-by-side helicopter being twice that of the original single-rotor machine).

It can be demonstrated that, between the load ratio of a side-by-side helicopter and a single-rotor helicopter, the following relation exists:

$$\left(\frac{G_{use}}{G}\right)_{s.s} = (1-\xi_{rear})^{2.3}\left[\left(\frac{G_{use}}{G}\right)_{s.r} - \xi_T - \frac{1}{2}\,\xi_G\right],$$

where

$\xi_{rear} = \frac{N_{rear}}{N_{eng}}$ = a coefficient taking into account power expenditures at the rear rotor in a single-rotor helicopter taken equal to 0.09;

$\xi_T = \frac{\Delta T_w}{T_1}$ = a coefficient taking into account thrust losses due to wash over the wing, taken equal to 0.07;

$\xi_G = \frac{G_w - G_{rear}}{T_1}$ = a coefficient taking into account the variation in weight on changing from a single-rotor helicopter to a two-rotor helicopter of side-by-side configuration.

Let us assume that the wing weight is 12% of the weight of the single-rotor

helicopter and that of the rear transmission with rotor, 10%.

The above formula shows that, in a side-by-side helicopter constructed from two single-rotor helicopters, it is impossible to achieve the load ratio of the single-rotor helicopter.

If a side-by-side helicopter is designed from scratch, it might result /46
in a much better construction since the designer of a side-by-side helicopter will not use the same load per square meter as the designer of a single-rotor helicopter had been using. In fact, this factor will be made greater and the helicopter will become more compact. On the other hand, when designing a fore-and-aft helicopter from scratch it is natural to select a smaller load per area and a higher power/weight ratio than is usually done.

It must be borne in mind that, in designing a side-by-side helicopter, there must be means available for "controlling" the frequency of natural oscillations of the wing with power plants and rotors, both in the vertical and horizontal plane, since this configuration has a multitude of possible vibration modes whose frequencies may enter into resonance with the forced frequencies induced by the rotor. Furthermore, in the case of high-power and thus heavy engines mounted to the wing tips, the side-by-side helicopter almost certainly will have a vibration mode of a frequency close to or even smaller than the rotor rpm, at which the rotors will vibrate on horizontal displacement. This may set up oscillations of the "ground resonance" type not only on the ground but also in the air. Therefore, the designer who has decided to design a side-by-side helicopter is faced with the difficult task of making the wing as small as possible in area, light in weight, and sufficiently rigid in bending and torsion.

However, despite certain difficulties in designing side-by-side helicopters and shortcomings of fore-and-aft configurations, designers will have to resort to them as a means of increasing lift capacity. This becomes obvious when considering the difficulties in developing rotors and reduction gears of super-heavy single-rotor helicopters.

Selection of configuration. An analysis shows that, in changing over to side-by-side or fore-and-aft helicopters with doubling of the power plants, it is impossible to double the useful load lifted by the single-rotor helicopter. If this could be achieved at all, it would be at the price of an appreciable loss in such flying and tactical data as takeoff and landing properties, rate of climb, dynamic ceiling, etc. Thus, the transition from the single-rotor to the multirotor helicopter must be done over an increase in power/weight ratio.

However, the selection of the configuration can be largely influenced by factors such as end use of the helicopter and tactical, technical, or operational requirements. The designer often prefers to adhere to the configuration for which he has more data and experience, if other conditions permit selecting several approximately equivalent configurations. In some cases, the designer is forced to give preference to a previously used configuration even when another configuration might offer some advantages.

Let us give an example to illustrate the point. The payload of a helicopter

with standard range amounts to about 20% of flying weight. Depending on the helicopter design, this weight may vary by 5% to either side. This means that, at identical takeoff weight, a good helicopter will lift a payload weighing 25% of the machine itself, whereas a poorly designed helicopter will lift only 15% of its weight. Thus, the second helicopter will be quite inferior with respect to lift capacity. This should be taken into account, on the one hand, in solving the problem of selecting the helicopter configuration and, on the other hand, in estimating the rationality of some particular configuration on the basis of a comparative analysis of data of existing designs.

CHAPTER II

/47

ROTOR AERODYNAMICS

Section 1. Development of Rotor Theory and Methods of Experimental Determination of its Characteristics

The idea of using a rotor in place of a wing as a lifting system was born in 1923. The Spanish engineer Juan de la Cierva, after the airplane of his design had stalled and crashed, decided to develop an autorotating sustaining system whose wing-blade combination would not lose speed at a low or even zero forward speed of the apparatus.

An experiment carried out by him in 1924 in the laboratory of Quadro-Ventos in Madrid, which showed the unlikely high values of the aerodynamic efficiency of an autorotating rotor as a lifting system, induced a theoretical investigation of the aerodynamics of autorotating rotors, carried out in England by Glauert in 1926 and later developed in 1928 by Lock for the case of hinged blades.

Thus, experiment generates theory and the endeavor to extrapolate the results of theory to practice gives rise to new experiments which more thoroughly reveal the physical nature of various phenomena, which in turn leads to a new close examination and development of theory. Only in the unity of theory and practice is it possible to describe the development of rotor aerodynamics up to the present state of the art. Thus, in 1928 the Glauert-Lock theory was first published. As is known, in this theory the magnitudes of thrust T, longitudinal force H, and torque M_t are determined as a function of the kinematic parameter

$$\mu = \frac{V \cos \alpha}{\omega R},$$

of the angle of rotor blade setting φ, and of the flow coefficient

$$\lambda = \frac{V \sin \alpha - v}{\omega R},$$

which represents the ratio of the velocity of the air flowing through the disk to the tip speed ωR (Fig.2.1). Consequently, the coefficients of the moments and forces can be expressed as

$$\left.\begin{aligned} m_t &= f(\varphi, \mu, \lambda); \\ C_T &= f(\varphi, \mu, \lambda); \\ C_H &= f(\varphi, \mu, \lambda). \end{aligned}\right\} \qquad (1.1)$$

According to the momentum theorem (see Sect.3), we have /48

$$Y \approx T \approx 2\varrho\pi R^2 V' v. \qquad (1.2)$$

After determining from this the induced velocity v

$$v=\frac{T}{2\varrho\pi R^2V'}=\frac{C_T\varrho\pi R^4\omega^2}{4\varrho\pi R^3\omega\sqrt{\mu^2+\lambda^2}}=\frac{C_T\omega R}{4\sqrt{\mu^2+\lambda^2}} \tag{1.3}$$

and substituting this expression into the formula for λ,

$$\lambda=\mu\tan\alpha-\frac{C_T}{4\sqrt{\mu^2+\lambda^2}},$$

we obtain the expression for the angle of attack of the craft:

$$\tan\alpha=\frac{\lambda}{\mu}+\frac{C_T}{4\mu\sqrt{\mu^2+\lambda^2}}. \tag{1.4}$$

For calculating the aerodynamic characteristics of an autogiro, Iock proposed deriving the unknown value of the quantity λ from the conditions of autorotation, i.e., equating the expression for torque on the rotor shaft to zero:

$$M_t=f(\varphi,\lambda,\mu)=0. \tag{1.5}$$

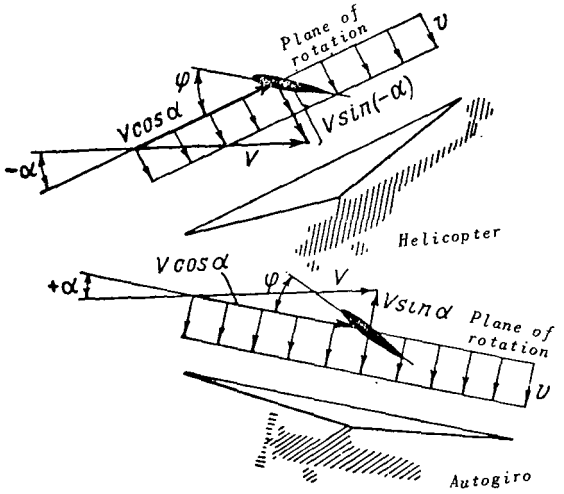

Fig.2.1 Velocity Components of Air Flowing through the Rotor Disk.

Since the angle of blade setting φ and the characteristic of the regime μ were prescribed quantities, the value of λ was determined from the quadratic equation (2.47) representing eq.(1.5) in a developed form. For a given value of the velocity of rotation ωR, flying speed V, angle of setting φ, and known λ, the only possible angle of attack of the autogiro α at which steady autorotation occurred was found from eq.(1.4). In this case, the equation (see Sect.2)

$$\frac{C_t}{\sigma}=t=f(\varphi,\mu,\lambda)=a_\infty\left[\frac{\lambda}{2}+\varphi\left(\frac{1}{3}+\frac{\mu^2}{2}\right)\right] \tag{1.6}$$

yielded the value of the thrust coefficient while the corresponding equation furnished the value of the coefficient of longitudinal force so that the polar /49 of a freely autorotating rotor could be determined as a function of the angle of attack. This polar, like the polar of a wing, could be used in the aerodynamic

calculation of the autogiro. Such a method was published in 1931 by I.P.Bratukhin (Ref.11).

In 1934, the author* (Ref.4), in his study of overspeed of the autogiro rotor during the takeoff run, determined the unknown values of thrust and torque from eqs.(1.4), (1.5), and (1.6) and prescribed values for the angle of attack α, angle of blade setting φ, and initial peripheral velocity and flying speed, i.e., the parameter μ, which made it possible to calculate the aerodynamic characteristics for cases of unsteady motion. The following method of determining the flow coefficient λ was proposed:

Substituting expression (1.6) into eq.(1.4) will yield a polynomial of the fourth power in both λ and μ; thus, it is difficult in practical work to determine λ at known μ or vice versa, since each time it would be necessary to solve a fourth-degree equation. A study of the dependence of λ on μ at given values of α and φ shows that, with the exception of a small segment of negative λ near $\mu = 0$, the curve $\lambda = f(\mu)$ represents a straight line with a high degree of accuracy. The equation of the family of these straight lines at different values of α and φ has the form

$$\lambda = \mu \tan\alpha - \sqrt{\frac{a_\infty \sigma \varphi \tan\alpha}{12}}. \qquad (1.7)$$

Equation (1.7) yields the dependence of λ on μ, α, φ, and σ; its use, together with the above formulas, permits calculating the thrust and torque coefficients. It is thus possible to calculate the aerodynamic characteristics of the autogiro rotor for any unsteady operating conditions when the torque created on the rotor by the air flow produces spinning or braking of the blades, depending on the angle of attack and the value of μ.

This still left the necessity of finding a method of applying this theory (developed by Glauert and Lock for an autogiro) to calculation of the aerodynamic characteristics of a helicopter, i.e., to their determination under forced rotation of the rotor by an engine. Such a method was proposed by the author in 1945, in collaboration with V.N.Yaroshenko (Ref.9).

To determine the torque necessary for flight under given conditions it is logical to use the above system of equations. Here, it was convenient to prescribe the value of the thrust coefficient t, since the rotor thrust is easily determined if it is approximately assumed that the thrust, under steady horizontal flying conditions, is equal to the helicopter weight.

Using prescribed values of the rpm and determining t from the expression

$$t = \frac{G}{\frac{\rho}{2} \sigma \pi R^4 \omega^2}, \qquad (1.8)$$

* Here and elsewhere in Section 1, the author is M.L.Mil'.

the quantity λ can be found from eq.(1.6), the torque from eq.(2.47) and the angle of attack of the helicopter α which corresponds to these conditions, from eq.(1.4).

Even before the present stage of helicopter development, practical autogiro engineering required the solution of certain stability problems; designers in various countries attacked the problem of determining the damping produced by the hinged rotor during vibrations of the craft. Analyses of flight accidents with autogiros showed the necessity for studying the flapping motion of blades /50 and for finding methods of retaining autorotation during aerobatic maneuvers of the craft. This led to the theory of a rotor for hinged blade attachment with curvilinear motion, which the author developed in 1939 and which represents a more general case than the Glauert-Lock theory established for steady rectilinear motion.

Finally, in 1940 A.N.Mikhaylov worked out a method of equivalent rotors, which simplifies the application of the Lock theory to a rotor equipped with an automatic pitch control mechanism (Ref.15).

The application of these methods to the aerodynamic calculation of Soviet autogiros between 1931 and 1940 and of the Mi-1 and Mi-4 helicopters in 1947-1952 showed highly satisfactory agreement between design characteristics and flight-test characteristics. Since these first autogiros and helicopters flew at relatively low speeds and thus at small values of μ, the inaccuracies of the theory due to the assumption of smallness of this parameter, made by Glauert and Lock, were nonessential. However, more complex problems were still to come: the development of more powerful and faster helicopters, which implied constant improvement of the theory.

The Glauert-Lock theory, as is known, makes a number of assumptions (including uniform distribution of induced velocities) so as to permit integrating the equations in a finite form. Thus, the c_y of the section was expressed as a linear function of the angle of attack $c_y = a_\infty \alpha$, while c_{xp} was taken as some average quantity independent of the angle of attack. The forces acting on the profile, i.e., on the section of the disk where - in forward flight - the air flows around the blade from the trailing edge (this region is small at small values of μ) were inaccurately determined. The radial component of the resultant velocity in the blade direction was also disregarded. The blade itself was assumed to be rectilinear, flat (not twisted), and of constant chord.

During the period of 1932-1943, many researchers - Whittle and Bailey in the USA, Hohenemzer and Zissing in Germany, and others - further refined this theory in that methods were found for integrating equations in a finite form while doing away with many previously accepted assumptions. The concept of the effective radius of a blade, smaller than the actual, was introduced for taking account of tip losses. The coefficients c_y and c_x represented more complex functions of the angle of attack, etc.

The most important improvement of the classical theory during the postwar years was the application of methods of numerical integration to the calculation of flapping motion and aerodynamic forces. This permitted the direct use of the experimental characteristics of profiles, taken for the necessary value of the

Reynolds numbers and Mach number, in determining c_y and c_x of the section as a function of the angle of attack and thus to take into account also the effect of compressibility.

Later, it became possible to introduce into the calculations not only the initial geometric shape of the blade but also its deformations due to bending in the plane of thrust and in plane of rotation and, what is especially important, due to torsion.

However, the use of such a cumbersome method for practical calculations became possible only after appearance of electronic computers. Thus, the modern method of rotor calculation, as presented in this book on the basis of studies made by A.S.Braverman and M.N.Tishchenko, was a step-by-step process.

However, even after all these refinements there still remained the rather rough assumption of a uniform distribution of induced velocities over the rotor disk, which not only led to an inaccuracy in determining induced power losses but also to errors in determining the true angles of attack of individual blade sections and hence to errors in the profile power, thrust, and longitudinal force. /51

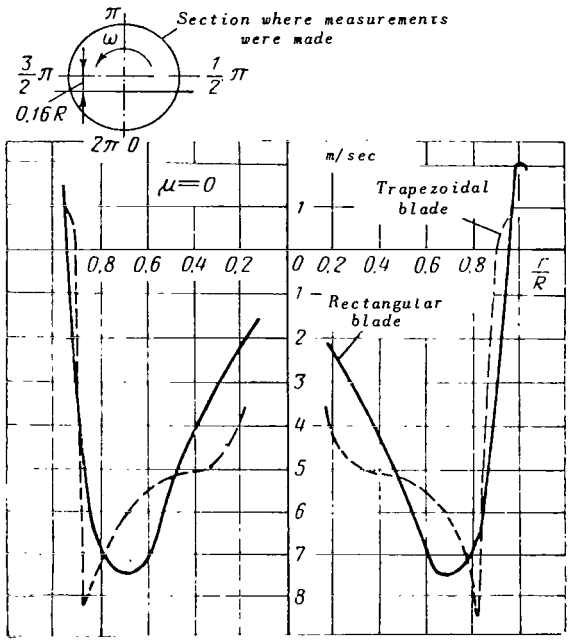

Fig.2.2 Induced Velocity Distribution in Hovering.

Thus, further refinement of the theory could be expected from the development of the vortex theory which is the only one capable of determining the distribution of induced velocities in relation to the forces acting on each given blade element.

However, development of such a theory required greater insight into the physical aspects of the phenomenon. Here again it was necessary to resort to experiment.

Experimental studies of flow around a rotor in a wind tunnel followed by removal of the induced velocity field, carried out in 1946 by the author together with M.K.Speranskiy, clearly showed that the vortex system known from a propeller operating under conditions of axial circulation flow and representing [for the case of circulation constant along the blade (Γ = const)] a central vortex with blade-tip vortices shed by the blades, is transformed - at small values of μ - into a system similar to the rectangular vortex system characteristic for a wing. In turn, the induced velocity distribution obtained from experiment (Figs.2.2, 2.3, and 2.4) fully confirmed the possibility of an

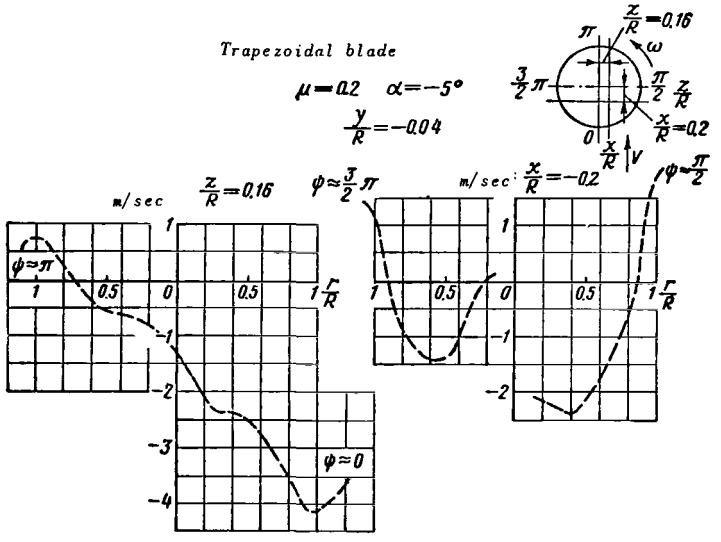

Fig.2.3 Induced Velocity Distribution in Forward Flight (μ = 0.2).

approximate representation of the induced velocity field, proposed by Kusner and Glauert, in the form of a funnel during the hovering phase (Fig.2.5) and in the form of a cylinder truncated by an inclined plane during forward flight (Fig.2.6). This configuration could be used for refining the Glauert-Lock theory without resorting to the vortex theory. These experimental facts gave rise to a sequence of theoretical works, which were based both on the approximate vortex pattern of rectangular vortices suitable for describing conditions at medium and high flying speeds and on various more general theories which examine a system of vortices trailing from each element of the blade.

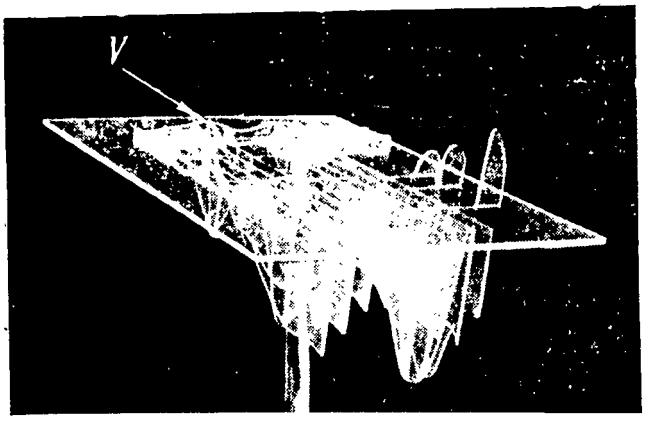

Fig.2.4. Three-Dimensional Model of Induced Velocity Field of a Rotor.

It is necessary to say that even before appearance of these experimental data, G.I.Maykopar examined the vortex theory of rotors, having proposed that the vortex cylinder slopes in direction of flight, which then served as incentive for a series of more or less accurate studies in this area.

Subsequently, L.S.Vil'dgrube was successful in developing the vortex theory in the USSR, followed later by V.E.Baskin.

In all these theories for determining the angle of attack of the blade section it was necessary to define not only the known kinematic parameters α, μ, ψ, and φ but also the vertical component of the induced velocity v as a result of the action at a given point of all vortices in the region surrounding the rotor. The induced velocities are found by the Biot-Savart formula as a function of the circulation in the blade section: /53

$$\Gamma = \frac{1}{2} c_y b U.$$

Hence it is clear that, since the induced velocity determining the angle of attack of the section is a function of circulation and since the latter, in turn, can be determined in terms of c_y which is a function of the angle of attack of the section in which the induced velocity enters, all these problems reduce to quite complex equations and can be solved only by approximation methods and, in particular, by methods of successive approximations. Generally, first the magnitude of c_y is determined under the assumption of constancy in the distribution of induced velocities over the disk, after which the calculation is repeated during which process the induced velocity is determined from the vortex theory. The integral value of the coefficient of thrust is then compared with the assigned value, and leads to calculation of successive approximations.

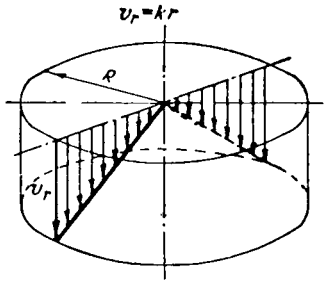

Fig.2.5 Induced Velocity Distribution according to the Law of the Triangle

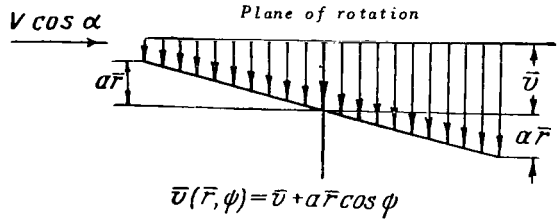

Fig.2.6 Linear Induced Velocity Distribution.

Without here examining the essence of various vortex theories which, specifically, differ by the assumption of finiteness or infiniteness of the number of blades, or the principles of methods for calculating the induced velocity (see Chapt.II, Sect.5), we will estimate their general significance and role in the refinement of calculations of the flying characteristics of the single-rotor helicopter.

Let us examine the maximum value of the air in determining the induced power, assuming a uniform and funnel-shaped induced velocity distribution. After this, we will compare the induced rotor power under the condition of constancy of thrust for the case of a uniform induced velocity distribution over the disk and corrections for the funnel.

The funnel-shaped induced velocity distribution is represented by the law

of the triangle (Fig.2.5):

$$v_r = kr,$$

where v_r is the induced velocity at a radius r of the blade.

According to the momentum theorem, the elementary thrust is /54

$$dT = \varrho 2\pi r 2 v_r^2.$$

Integrating from 0 to R, we obtain

$$T = \varrho \pi R^2 v_t^2,$$

where v_t is the induced velocity in the blade tip section.

For the case of uniform induced velocity distribution, the thrust is

$$T_1 = \varrho 2\pi R^2 v^2.$$

Equating T_1 and T, we obtain

$$\varrho \pi R^2 v_t^2 = 2\pi R^2 \varrho v^2,$$

whence

$$v_t = v\sqrt{2}.$$

Consequently,

$$v_r = v_t \frac{r}{R} = v \frac{r}{R} \sqrt{2}.$$

The induced power is determined from the following formulas:

$$dN_{ind} = dT v = 4\pi \varrho v_r^3 r dr;$$

$$N_{ind} = 4\pi \varrho \int_0^R v_r^3 r dr.$$

Substituting into the last formula the value of $v_r = kr$, we obtain the expression for power in the case of an induced velocity distribution according to the law of the triangle:

$$N_{ind_{tri}} = \frac{4}{5} R^2 \varrho 2^{3/2} v^3 = 2.26\pi R^2 \varrho v^3.$$

This power is greater by a factor of 1.13 than the power N_{ind} for the case of uniform velocity distribution, since

$$\frac{N_{ind_{tri}}}{N_{ind}} = \frac{2.26\pi R^2 \varrho v^3}{2\pi R^2 \varrho v^3} = 1.13.$$

Thus, the funnel-shaped induced velocity distribution increases the induced losses by about 13%. Consequently, the difference in the relative efficiency amounts to about 10%. This is a high value so that, for calculating the thrust and power of a rotor in a hovering regime, it is logical to use methods of the momentum or vortex theory which permit taking into account the additional power loss due to nonuniform induced velocity distribution over the disk.

In an approximate calculation, the induced losses calculated by the formula

$$N_{ind} = Tv,$$

can be increased by about 13%.

In hovering, the expended power is the sum of induced power and profile power, where the former amounts to 75% of the total required power. At cruising speed, the induced power is only 20 - 30% and at maximum speed, about 10%. Thus, at high flying speeds the maximum refinement in the required power, as a result of taking the nonuniform induced velocity distribution into consideration, /55 can be not more than 1 - 2% in power and not more than 1% in flying speed.

Of course, using (analogous to the effective aspect ratio of an airplane) an effective rotor radius somewhat smaller than the actual radius, it becomes possible to introduce an experimental correction to the aerodynamic calculation which had been based on the theory of constant induced velocity distribution. This correction may be particularly important in determining the rate of climb and ceiling for heavily loaded rotors.

Thus, it is obvious that, in calculating the flight data, there is no need for much more complex calculations of the aerodynamic rotor characteristics based on the vortex theory.

Refinement of the section angles of attack given by the vortex theory becomes necessary only in calculating the stresses set up in the blade, especially at low speeds where the aerodynamic forces inducing blade vibrations in second and higher harmonics actually are the result of the blade encountering the vortex field. According to the theories stipulating v = const, these stresses - for all practical purposes - are equal to zero.

It must be assumed that further refinement of the velocity field may be of importance in determining the boundary conditions at which flow separation begins. However, for this purpose it suffices to refine only the pattern of the induced velocity distribution in the form of longitudinal pitch, which leads to a variation in the flapping motion (b_1) and to some redistribution of the angles of attack.

At the same time, the concept of induced velocity distribution in the form of a funnel (Fig.2.5) and especially the assumption of its buildup from front to rear (Fig.2.6) result in substantial variations in the flapping motion (specifically in b_1) and in the lateral force S, which has been taken into account by various authors.

1. Classification of Rotor Theories

It is obvious from this account that only two of the theories of a real rotor differ fundamentally. Both are based on a study of forces acting on the blade element. Such an approach to the helicopter rotor was first used by N.Ye.Zhukovskiy (Ref.1) as long ago as in his investigations on the effect of wind on the thrust of a helicopter rotor.

In the first of these theories, the induced velocity distribution over the disk is prescribed, regardless of the forces acting on the blade elements. Its average value can be determined from the momentum theorem.

In the second theory, the induced velocities of each blade element are a function of forces acting on all blades, which in turn are a function of these induced velocities and are usually determined by means of the Biot-Savart formula.

Let us call the first the classical theory which encompasses the Glauert-Lock theory and its subsequent development, while the second will be designated as the vortex theory.

The classical theory is conceivable with integration in finite form, while the vortex theory proposes only numerical solution methods.

It is also of use to study the momentum theory of an ideal rotor, which can be used in developing energy methods for aerodynamic calculation and in interpreting the results of an experimental determination of the aerodynamic rotor characteristics.

Although the development of the classical theory in its numerical methods is nearing completion due to the use of computers, the vortex theory still /56
presents various problems. Thus, in most vortex theories, when calculating the circulation flow, the quantity c_y is taken as a linear function of the angle of attack since it can be refined. For simplification, the vortex system is considered to be two- or three-dimensional but linear. This simplification can be compensated later.

Thus, the vortex theory, having inherited all refinements introduced during the development of the numerical calculation methods of the classical theory, is presently becoming the most accurate theory. In its development, there is no need to use the assumption of steady flow around the blade sections and the section polar can be refined by using experimental data as to the influence of centrifugal forces on phenomena in the boundary layer.

Proceeding from this classification, let us give a further account of the rotor theory.

2. Development of Experimental Methods

Experimental methods for determining the aerodynamic rotor characteristics are being developed simultaneously with the described development trends of the

theory.

After the first experiments in Madrid in the 1930s, researchers in many countries began experimenting with rotors in wind tunnels. Experiments based on procedures by V.G.Petrunin at TsAGI were carried out (1931-1936) on models of autorotating rotors of 1.2 m diameter, in which the three components of force and torque were measured and the blade flapping recorded.

The experimental technique was greatly improved. In particular, it became possible to obtain the fuselage polar in the presence of an operating rotor. Measurement of flapping at the hub of an autorotating rotor, turning in the tunnel air stream about the translational velocity vector [which permitted estimating the rotor damping in roll (see Sect.2)] was the most noteworthy achievement by V.G.Petrunin in these experiments.

However, it soon became clear that small Reynolds numbers in the case of flow around the blade section led to such extensive distortions of the profile polar on the model, in comparison with a full-scale craft, that it was impossible to use these results directly.

In 1944, the author together with I.F.Morozov at TsAGI set up experiments on a rotor of D = 2.5 m, which no longer concerned only the autorotation regime but also included the helicopter regimes.

The testing facility for the rotor model of 2.5 m diameter is shown in Fig.2.7. Tests on this model were first made in the coordinates δ, $m_t = f(\varphi)$ for μ = const and t = const (see Fig.2.8), where $\delta \approx \frac{t_x}{t_y}$. The tests, conducted for three types of blades of different shape and twist, made it possible to judge the propulsive properties of the rotors. However, the main thought behind these experiments lay in the possibility of estimating the degree of perfection of the theory in comparison with calculations.

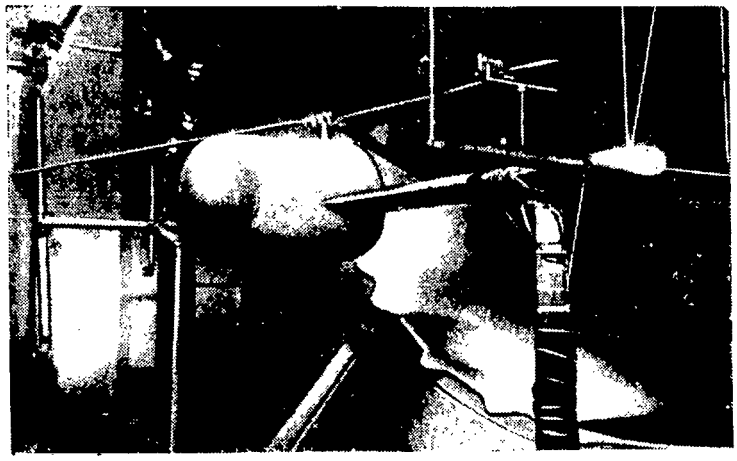

Fig.2.7 Testing Facility for Rotor Models.

Whereas our first helicopters were calculated with reasonable accuracy by the classical theory presented in Section 2, the Mi-6 helicopter with 11,000-hp turboprop engines had already passed into a region of flying speeds - and hence of values of μ (more than 0.4) and Mach numbers - where the Glauert-Lock theory yielded appreciable errors. In preparation of this, a full-scale helicopter test stand was constructed at the TsAGI on which the author, together with M.K. Speranskiy, determined the characteristics of 14.5-m rotors in a large wind tunnel. The next problem was that of converting the experimental data obtained for a specific rotor to another load factor and to other Mach numbers. These calculations are presented in Section 6. /57

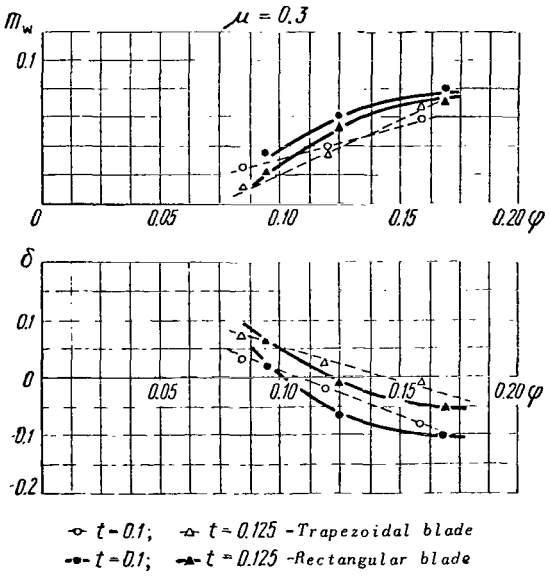

Fig.2.8 Aerodynamic Rotor Characteristics (Model Test).

Because of the need to refine the theoretical methods of calculating aerodynamic loads on a blade element, a series of experiments were carried out in recent years, whose results yield a more detailed explanation of the circulation flow pattern around the blade profile under actual rotor operating conditions. In this respect, interesting data can be obtained by measuring the pressure distribution over the blade chord in flight. By integrating the pertaining pressure distribution diagrams, it is possible to obtain the actual in-flight aerodynamic loads acting on the profile and varying relative to the rotor azimuth. In making such experiments on models, V.E.Baskin and A.S.D'yachenko found that, as the blade passes into the region of vortex trailing from the tip of the advancing blade, there is a marked jump in blade loading. /58

No doubt, the further development in helicopter engineering toward an increase of flying speeds will require new experiments and the development of test stands for experimental determination of the aerodynamic characteristics at even larger values of μ while retaining similarity of Mach and Reynolds numbers.

Section 2. Classical Theory of a Rotor with Hinged Blade Attachment; General Case; Curvilinear Motion

The rotor theory for rectilinear motion of a helicopter or autogiro was developed by Glauert and Lock and has been described at numerous occasions [see (Ref.36, 37, 2, 11, 23)]. The theory presented below is a further development of the Glauert-Lock theory, for the more general case where the helicopter is in curvilinear motion so that the rotor axis describes a rotary motion in space. Such motion takes place during steady curvilinear flight of the craft, for example, during turning and also during vibrations relative to the longitudinal or

transverse axis caused by piloting or external factors.

Rotor Theory in Curvilinear Motion

Here, all the assumptions made by Lock are accepted in the general theory, namely: The induced velocity in the absence of rotation of the rotor axis is considered as uniformly distributed over the rotor disk; the change in the law of its distribution over the disk pertains only to the superposed effect of rotation of the entire craft, i.e., the initial pattern remains the same as for Lock's pattern.

Likewise, we adopt the assumptions of linearity $c_y = f(\alpha)$ and the admissibility of replacing the coefficient c_x by some average quantity $c_{xp_{av}}$ which is identical for all blade sections.

We will take into account blade tip losses, i.e., consider that no lift is developed at some tip portion of the blade and that the drag forces, just as the inertia forces, act on the entire radius. The method of obtaining the expressions for forces and moments here is analogous to the Lock method, so that we will not repeat the derivation of the fundamental equations here and only discuss expressions that differ in the case of curvilinear motion.

A special role is played here by the Coriolis forces of inertia arising upon rotation of the rotor. These forces will be discussed in most detail.

The results to be presented here contain the basic relations of the Glauert-Lock theory for rectilinear motion and, furthermore, permit answering the following questions:

a) What is the flapping motion of the blades in curvilinear motion of the entire craft?
b) How does the position of the aerodynamic resultant change in the case of rotation of the entire craft in some direction (for example, to the left or to the right) and is there a tendency to accelerate or decelerate this rotation?
c) What peculiarities does the autorotation regime of a rotor exhibit in the presence of rotation? /59

Along with an investigation of these problems we will also discuss the effect of the configuration of the hub, profile, and blade centering on the behavior of the rotor from the viewpoint of stability and safety of the craft.

The obtained results are common for any rotor with hinged blade attachment, be it the rotor of an autogiro or of a helicopter.

In addition to answering the above questions which are of independent interest, the results of the analysis yield some necessary data for studying the controllability and dynamic stability of the mentioned craft.

1. Coordinate System and Physical Scheme of the Phenomenon

Coordinate system. The phenomenon is examined in a coordinate system fixed

with respect to the craft (Fig.2.9). This is a right-handed system (for right-hand rotation of the rotor) in which the z-axis is directed along the axis of rotation of the rotor and the x-axis backward with respect to the direction of the velocity of the center of gravity of the craft. The angular position of the blade ψ is reckoned from the x-axis.

Physical scheme of the phenomenon. We will study a rotor rotating in space together with the craft at a constant angular velocity and, in so doing, maintaining a constant angle of attack with the flight path.

Such rotation occurs, for example, in turning.

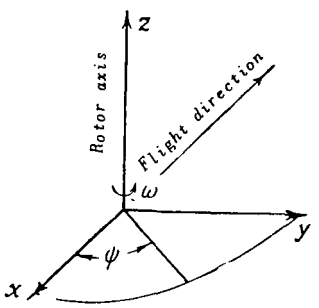

Fig.2.9 Coordinate System.

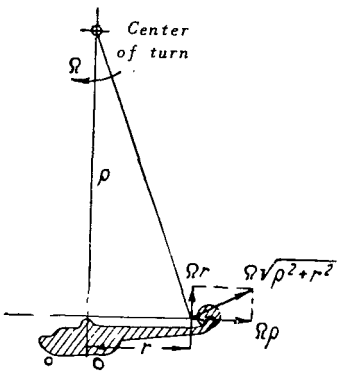

Fig.2.10 Velocity Diagram of Rotor in Turning.

We are interested here in the manner in which the radius of rotation of the craft is to be taken into consideration.

For this, let us examine a helicopter executing a turn of radius ρ at a large angle of bank γ_b, close to 90°.

The velocity diagram in the plane of symmetry of the craft, in this case close to the turning plane, is shown in Fig.2.10.

The relative flow velocity at a distance r from the center of the rotor can be divided into two components: velocity $\Omega\rho$ directed along the tangent to the path of the center of the rotor hub (we will call this the turning speed) and velocity Ωr directed perpendicular to the rotor plane.

The distance from the center of the rotor hub to the center of gravity of the helicopter will be neglected for the radius of curvature of the path.

If we now transfer the center of rotation of the craft to the center of the rotor hub, it should become possible, in addition to the indicated velocities, to also allow for the additional centrifugal forces acting on the blades. /60

As is known, in the case of a steady turn without sideslip, the resultant of the centrifugal force and the force of gravity lies in the plane of symmetry of the craft.

Thus, these forces, proportional to $\Omega^2\rho$, can be regarded as an increase in blade weight. Obviously, this increase is the overload n.

The expression for the coning angle a_0 contains a term taking the blade weight into account:

$$\Delta a_0 = -\frac{S_{h.h}}{I_{h.h}\omega^2}, \tag{2.1}$$

where $S_{h.h}$ is the static moment of the blade weight relative to the horizontal hinge.

For turning, we thus have

$$\Delta a_{0_t} = -\frac{S_{h.h}n}{I_{h.h}\omega_t^2}. \tag{2.2}$$

It is known that, in turning, the revolutions of the rotor increase. If $\omega_t = \omega\sqrt{n}$, which roughly takes place during autorotation, then, substituting ω_t into eq.(2.2), we obtain

$$\Delta a_0 = \Delta a_{0_t}, \tag{2.3}$$

i.e., during steady curvilinear motion of the rotor without sideslip, the decrease in coning angle due to the weight of the blades remains constant regardless of the overload.

In the usual case, Δa_0 is not more than 0.3°; this quantity can be either neglected or taken into account, regardless of how this is done in the theory for rectilinear motion. Therefore, we will here discuss the following scheme: The rotor moves at a constant angle of attack and executes a rotary motion relative to the axis going through its center.

2. Inertia Forces Acting on the Blade

At curvilinear motion of the helicopter, the rotor blade executes four rotary motions in space.

First, it rotates about the hub axis Oz with an angular velocity ω; secondly, it rotates together with the axis Oz in space with a velocity Ω having the components Ω_x and Ω_y; finally, it vibrates relative to the axes of the flapping and drag hinges making an angle $\beta = f(\psi)$ with the plane perpendicular to the hub axis and an angle $\xi = f(\psi)$ relative to its own mean position.

Below, we will neglect the blade motion for the drag hinge, in view of its relative smallness.

Let us examine the elementary inertia forces acting on the blade during

rotation of the rotor. The centrifugal force C

$$dC = m\omega^2 r dr \tag{2.4}$$

is perpendicular to the rotor axis and directed along the radius.

The centrifugal forces generated during rotation with angular velocities /61
Ω_x and Ω_y will be

$$\left.\begin{aligned} dC_{\Omega_x} &= m\Omega_x^2 r \sin\psi\, dr, \\ dC_{\Omega_y} &= m\Omega_y^2 r \cos\psi\, dr. \end{aligned}\right\} \tag{2.5}$$

These forces also lie in the plane of rotation and, accordingly, are perpendicular to the vectors Ω_x and Ω_y.

The inertia force of flapping, perpendicular to the blade, is

$$dJ = m\frac{d^2\beta}{dt^2} r\, dr. \tag{2.6}$$

The Coriolis inertia forces K produced by the rotations ω, Ω_x, and Ω_y, perpendicular to the plane of rotation, are

$$\left.\begin{aligned} dK_{\Omega_x} &= -2m\Omega_x \omega r \cos\psi\, dr; \\ dK_{\Omega_y} &= -2m\Omega_y \omega r \sin\psi\, dr. \end{aligned}\right\} \tag{2.7}$$

The Coriolis inertia forces generated during blade flapping, i.e., during rotation with an angular velocity Ω, are as follows:

- component in the plane of rotation

$$\left.\begin{aligned} dK'_{\beta\Omega_x} &= 2m\Omega_x \frac{d\beta}{dt} r\, dr; \\ dK'_{\beta\Omega_y} &= -2m\Omega_y \frac{d\beta}{dt} r\, dr; \end{aligned}\right\} \tag{2.8}$$

- component perpendicular to the plane of rotation

$$\left.\begin{aligned} dK''_{\beta\Omega_x} &= -2m\Omega_x \beta \frac{d\beta}{dt} r \sin\psi\, dr; \\ dK''_{\beta\Omega_y} &= -2m\Omega_y \beta \frac{d\beta}{dt} r \cos\psi\, dr. \end{aligned}\right\} \tag{2.9}$$

The Coriolis inertia forces due to flapping and rotation at angular velocity

$$dK_{\beta\omega} = -2m\omega\beta \frac{d\beta}{dt} r\, dr \tag{2.10}$$

lie in the plane of rotation and are perpendicular to the blade.

The diagram of the inertia forces generated during curvilinear motion is given in Fig.2.11. The forces dC, dJ, $dK''_{\beta\Omega_x}$, and $dK''_{\beta\Omega_y}$ are not shown.

In studying the blade flapping relative to the flapping hinge, we will take into account only forces with respect to eqs.(2.4), (2.6), and (2.7), since any forces $dK''_{\beta\Omega}$ [eq.(2.9)] of a higher order of smallness can be neglected for the inertia forces of flapping or for the forces dK_Ω and since also all centrifugal forces produced by rotations Ω_x and Ω_y [eq.(2.5)] can be neglected for the principal centrifugal force [eq.(2.4)]; the ratio $\left(\frac{\Omega}{\omega}\right)^2$, for all practical purposes, is not greater than 0.01.

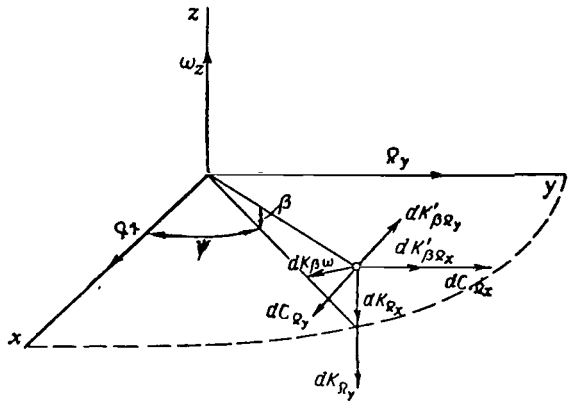

Fig.2.11 Diagram of inertia Forces.

These centrifugal forces [eq.(2.5)] are accounted for in studies of the equilibrium relative to the axis of rotation in the expression for torque. /62

In addition to inertia forces, aerodynamic forces act on the blade element.

With the aim of obtaining a clearer view over the effect of inertia forces and to check whether the general equations derived below correctly describe the phenomenon, we will first simplify the problem.

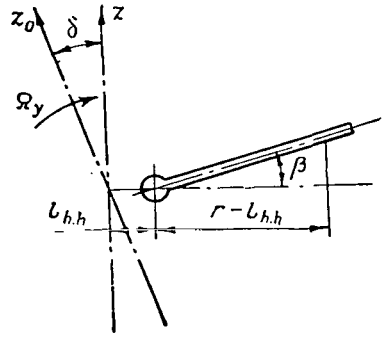

Fig.2.12 For Determining the Flapping Motion of the Rotor.

We will completely disregard all aerodynamic effects and study the motion of blades hinged to the hub and rotating by inertia in a vacuum while their axis of rotation is turning.

Motion of hinged rods rotating by inertia during hub rotation. Let us examine the general case of a hub whose horizontal (flapping) hinges are at some distance $l_{h.h}$ from the axis of rotation.

Let the rotor rotate about the z-axis at an angular velocity ω (Fig.2.12).

The axis of rotation z turns backward at a constant angular velocity Ω_y and, at some instant of time, is deflected through the angle δ from the original position z_0. Taking, as reference plane, the plane perpendicular to the z-axis and assuming smallness of the angle δ, eqs.(2.4), (2.6), and (2.7) can be used for deriving the expressions for the moments of the acting forces relative to the axis of the flapping hinge.

The moment of the inertia forces of flapping (with the positive moment tending to raise the blade upward) reads

$$M_J = -\int_{l_{h.h}}^{R} m\frac{d^2\beta}{dt^2}(r-l_{h.h})^2\,dr =$$

$$= -\frac{d^2\beta}{dt^2}\left(\int_{l_{h.h}}^{R} mr^2\,dr - 2\int_{l_{h.h}}^{R} ml_{h.h}\,r\,dr + \int_{l_{h.h}}^{R} ml_{h.h}^2\,dr\right).$$

Since, for modern helicopters, the ratio $\frac{l_{h.h}}{R}$ usually is not more than 0.02, we can assume that /63

$$\int_{l_{h.h}}^{R} mr^2\,dr \approx \int_{0}^{R} mr^2\,dr \approx I_{h.h}; \tag{2.11}$$

$$\int_{l_{h.h}}^{R} mr\,dr \approx \int_{0}^{R} mr\,dr \approx S_{h.h}, \tag{2.12}$$

and since the integral containing $l_{h.h}^2$ can be disregarded, we have

$$M_J = -\frac{d^2\beta}{dt^2}(I_{h.h} - 2S_{h.h}l_{h.h}).$$

Having designated

$$\varepsilon = \frac{S_{h.h}}{I_{h.h}}l_{h.h}, \tag{2.13}$$

we obtain

$$M_J = -I_{h.h}\frac{d^2\beta}{dt^2}(1-2\varepsilon). \tag{2.14}$$

The moment of centrifugal forces is

$$M_C = -\int_{0}^{R} \beta m\omega^2 r(r-l_{h.h})\,dr = -I_{h.h}\omega^2\beta(1-\varepsilon). \tag{2.15}$$

Here, we assume the angle β to be small and consider that the vector of angular velocity ω is directed along the axis of rotation z.

The moment of the Coriolis inertia forces is

$$M_{K\ell} = -2\int_{0}^{R} m\Omega_y\omega\sin\psi r(r-l_{h.h})\,dr = -2I_{h.h}\Omega_y\omega(1-\varepsilon)\sin\psi. \tag{2.16}$$

Equating the sum of all moments to zero, we obtain the equation of blade motion:

$$I_{h.h}\frac{d^2\beta}{dt^2}(1-2\varepsilon) + I_{h.h}\omega^2\beta(1-\varepsilon) = -2I_{h.h}\Omega_y\omega(1-\varepsilon)\sin\psi.$$

After dividing by $(1 - \varepsilon)^2$, neglecting ε^2, and setting $\omega = \frac{d\psi}{dt}$, we finally obtain

$$\frac{d^2\beta}{d\psi^2} + \beta(1+\varepsilon) = -2\frac{\Omega_y}{\omega}(1+\varepsilon)\sin\psi. \tag{2.17}$$

Let us find the particular solution of this equation. Setting $\beta = N \sin \psi$ and substituting into the equation, we obtain

$$\beta = -\frac{2\Omega_y}{\varepsilon\omega}(1+\varepsilon)\sin\psi.$$

The general solution of this equation will be

$$\beta = A\cos\sqrt{1+\varepsilon}\psi + B\sin\sqrt{1+\varepsilon}\psi - \frac{2\Omega_y}{\varepsilon\omega}(1+\varepsilon)\sin\psi. \tag{2.18}$$

Substituting the initial values of $\psi = \frac{\pi}{2}$; $\beta = 0$; $\frac{d\beta}{d\psi} = 0$, we then determine the values of A and B: /64

$$\left.\begin{aligned} A &= \frac{2\Omega_y}{\varepsilon\omega}(1+\varepsilon)\cos\sqrt{1+\varepsilon}\,\frac{\pi}{2}, \\ B &= \frac{2\Omega_y}{\varepsilon\omega}(1+\varepsilon)\sin\sqrt{1+\varepsilon}\,\frac{\pi}{2}. \end{aligned}\right\} \tag{2.19}$$

Substituting these values into eq.(2.18) and assuming $\psi_1 = \psi - \frac{\pi}{2}$ (here, ψ_1 is the angle reckoned from the position of the blade at the initial moment, when $t = 0$), we obtain

$$\beta = \frac{2\Omega_y}{\varepsilon\omega}(\cos\sqrt{1+\varepsilon}\psi_1 - \cos\psi_1)(1+\varepsilon). \tag{2.20}$$

From this, it is easy to obtain also the solution of β for the case of hinges intersecting the rotor axis ($l_{h.h} = \varepsilon = 0$).

We will evaluate the indeterminate form by the L'Hospital rule:

$$\beta_{\varepsilon=0} = \frac{2\Omega_y}{\omega}\lim_{\varepsilon\to 0}\frac{\frac{\partial}{\partial\varepsilon}(\cos\sqrt{1+\varepsilon}\psi_1 - \cos\psi_1)}{\frac{\partial}{\partial\varepsilon}(\varepsilon)} = -\frac{\Omega_y}{\omega}\psi_1\sin\psi_1.$$

Since the rotation is assumed to be uniform, then, having introduced $\psi_1 = \omega t$, we find

$$\delta = \Omega_y t = \frac{\Omega_y}{\omega}\psi_1, \tag{2.21}$$

and, substituting $\psi_1 = \psi - \frac{\pi}{2}$, we obtain finally

$$\beta = \frac{\Omega_y}{\omega} \psi_1 \cos\psi = \delta \cos\psi. \tag{2.22}$$

This result can be obtained also by direct solution of the differential equation (2.17) in which it is assumed that $\varepsilon = 0$.

It follows from eq.(2.22) that, in the case of a hub with intersecting hinges with the rotor axis deflected backward at an angle δ, the blade will be deflected in the opposite direction through the same angle.

This means that the plane of the blade tips in space remains constant while the rotor hub turns.

The result is correct and has physical meaning.

The solution for β is plotted in Fig.2.13 in the case of superposed ($\varepsilon = 0$) and spaced hinges (for $\varepsilon = 0.2$*) at $\frac{\Omega_y}{\omega} = 0.01$. The curves were constructed on the basis of eqs.(2.20) and (2.22).

/65

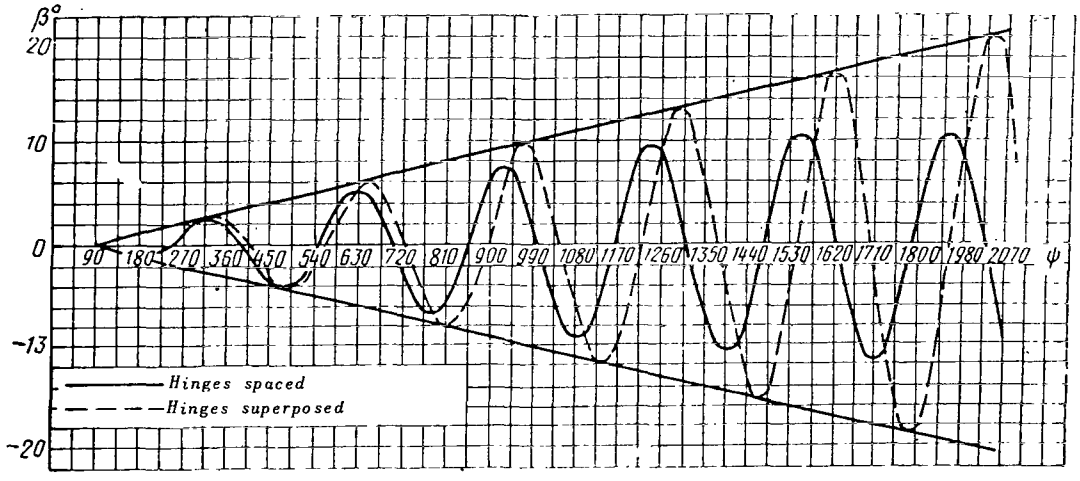

Fig.2.13 Flapping Angle β vs. Azimuthal Position of Blade.

As indicated by Fig.2.13, over a certain interval of time the motion of the blades almost coincides, i.e., their position in space is constant; after this, the blade on a hub with spaced hinges gradually starts following the axis of /66 rotation, i.e., the plane of rotation of the blade approaches the plane of rotation of the hub, with some phase shift.

---

* Such a large value of ε is used to make the graph clearer. In practice, ε does not exceed 0.02.

At this time, however, the angle of turn of the hub is already so great that a further analysis is useless since the blades are physically restrained in their arresting devices on the hub and since the above theory holds only for small δ.

Thus, the study of short-time oscillations shows that the rotor with small hinge spacing is practically equivalent to a rotor with intersecting hinges, i.e., it retains its position in space unchanged.

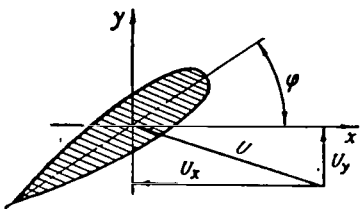

Fig.2.14 Velocity Diagram of Blade Element.

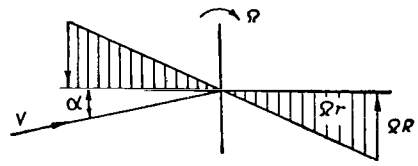

Fig.2.15 Change of Velocity Field during Rotor Rotation.

In the subsequent analysis we will disregard hinge spacing, and assume $\varepsilon = 0$. Furthermore, we have reason to believe that the aerodynamic forces (as will be shown below) entrain the plane of rotation of the blades beyond the motion of the hub so that equilibrium is established between the blades and the inertia forces that tend to keep the rotor position in space constant; thus, the plane of rotation follows the motion of the hub with some lag.

3. Aerodynamic Forces Acting on the Blade

Let us assume that the aerodynamic forces acting on a blade element lie in a plane perpendicular to the blade axis and depend only on the velocity component lying in this plane.

The coordinate axes lying in a plane perpendicular to the blade axis are situated such that the Ox axis is parallel to the plane of rotation and the Oy axis, perpendicular to it, lies in a plane containing the rotor axis.

Let us now decompose the velocity acting on the blade element into the components U_x and U_y (Fig.2.14). These are equal to

$$U_x = r\omega + \mu R\omega \sin\psi; \tag{2.23}$$

$$U_y = \lambda R\omega - r\frac{d\beta}{dt} - \mu R\omega\beta\cos\psi + \Omega_y r\cos\psi - \Omega_x r\sin\psi. \tag{2.24}$$

Here, eq.(2.23) is the same as in rectilinear motion. In eq.(2.24) only the last two terms are added, which take into account the effect of rotary motion of the axis. Consideration of these terms gives the change in velocity field of the rotor, which becomes analogous to that depicted in Fig.2.15.

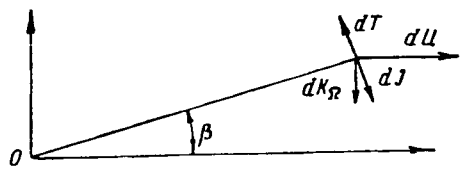

Fig.2.16 Forces Acting on a Blade Element.

Taking the new values of U_x and U_y into account, all elementary forces acting on the rotor blade can be obtained.

As derived by Lock, the elementary aerodynamic forces and moments are expressed in terms of velocity components of the element in the following manner: /67

$$dT = \frac{1}{2} b\varrho a_\infty (\varphi U_x^2 + U_x U_y)\, dr; \tag{2.25}$$

$$dM = \frac{1}{2} b\varrho (c_{x p_{av}} U_x^2 - a_\infty \varphi U_x U_y - a_\infty U_y^2)\, r\, dr; \tag{2.26}$$

$$dH = \frac{dM_t}{r} \sin\psi - \beta\, dT \cos\psi; \tag{2.27}$$

$$dS = -\frac{dM_t}{r} \cos\psi - \beta\, dT \sin\psi. \tag{2.28}$$

4. Equation of Moments Relative to Flapping Hinge

The equation of moments relative to the flapping hinge can be written as follows (see scheme in Fig.2.16):

$$-\int_0^R \frac{d^2\beta}{dt^2} mr^2\, dr - \int_0^R \beta m\omega^2 r^2\, dr - \int_0^R 2m\Omega_y \omega \sin\psi r^2\, dr - \\ - \int_0^R 2m\Omega_x \omega \cos\psi r^2\, dr + \int_0^{BR} dTr - \int_0^R mgr\, dr = 0. \tag{2.29}$$

After integration, we obtain

$$-I_{h.h} \frac{d^2\beta}{dt^2} - I_{h.h}\omega^2\beta + \int_0^{BR} dTr = 2I_{h.h}\Omega_y \omega \sin\psi + 2I_{h.h}\Omega_x \omega \cos\psi + S_{h.h}.$$

Let us change from differentiation with respect to t to differentiation with respect to ψ, assuming $\frac{d\psi}{dt} = \omega$:

$$\frac{d\beta}{dt} = \frac{d\beta}{d\psi}\omega; \quad \frac{d^2\beta}{dt^2} = \frac{d^2\beta}{d\psi^2}\cdot\omega^2,$$

and then rewrite the equation of moments, after dividing it by $I_{h.h}\omega^2$:

$$\frac{d^2\beta}{d\psi^2} + \beta = \frac{1}{I_{h.h}\omega^2}\int_0^{BR} dTr - 2\frac{\Omega_y}{\omega}\sin\psi - 2\frac{\Omega_x}{\omega}\cos\psi - \frac{S_{h.h}}{I_{h.h}\omega^2}. \tag{2.30}$$

Using eqs.(2.23) and (2.24), we write out the expressions for U_x^2 and $U_x U_y$ entering eq.(2.25) for dT:

$$U_x^2 = r^2\omega^2 + 2\omega^2 Rr\mu \sin\psi + \mu^2 R^2\omega^2 \sin^2\psi; \tag{2.31}$$

/68

$$\begin{aligned} U_x U_y = {} & \lambda\omega^2 Rr - \frac{d\beta}{dt}\omega r^2 - \beta\mu\omega^2 Rr\cos\psi - \Omega_x \omega r^2 \sin\psi + \\ & + \lambda\mu\omega^2 R^2 \sin\psi - \frac{d\beta}{dt}\mu\omega Rr\sin\psi - \beta\mu^2\omega^2 R^2 \sin\psi\cos\psi - \\ & - \Omega_x \omega\mu Rr\sin^2\psi + \Omega_y \omega r^2\cos\psi + \Omega_y \omega\mu Rr\sin\psi\cos\psi. \end{aligned} \tag{2.32}$$

The thrust moment is

$$\begin{aligned} \int_0^{BR} dTr = \frac{1}{2} b\rho a_\infty \int_0^{BR} (\varphi U_x^2 + U_x U_y)\, rdr = \frac{1}{2} b\rho a_\infty R^4\omega^2 \Big(& \frac{B^4}{4}\varphi + \frac{2}{3}B^3\varphi\mu\sin\psi + \\ & + \frac{B^2}{2}\varphi\mu^2\sin^2\psi + \frac{B^3}{3}\lambda - \frac{B^4}{4}\frac{d\beta}{d\psi} - \frac{B^3}{3}\beta\mu\cos\psi - \frac{B^4}{4}\frac{\Omega_x}{\omega}\sin\psi + \\ & + \frac{B^2}{2}\lambda\mu\sin\psi - \frac{B^2}{2}\beta\mu^2\sin\psi\cos\psi - \frac{B^3}{3}\frac{d\beta}{d\psi}\mu\sin\psi - \\ & - \frac{B^3}{3}\frac{\Omega_x}{\omega}\mu\sin^2\psi + \frac{B^4}{4}\frac{\Omega_y}{\omega}\cos\psi + \frac{B^3}{3}\frac{\Omega_y}{\omega}\mu\sin\psi\cos\psi \Big). \end{aligned} \tag{2.33}$$

Let us substitute expression (2.33) into eq.(2.30) and set $\gamma = \frac{b\rho a_\infty R^4}{2I_{h.h}}$; this finally yields

$$\begin{aligned} \frac{d^2\beta}{d\psi^2} + \frac{d\beta}{d\psi}\gamma\Big(\frac{B^4}{4} + \frac{B^3\mu\sin\psi}{3}\Big) + \beta\Big(1 + \frac{B^3}{3}\gamma\mu\cos\psi + B^2\gamma\mu^2\sin 2\psi\Big) = \\ = \gamma\Big(\frac{B^3}{3}\lambda - \frac{B^4}{4}\frac{\Omega_x}{\omega}\sin\psi + \frac{B^2}{2}\lambda\mu\sin\psi - \frac{B^3}{3}\frac{\Omega_x}{\omega}\mu\sin^2\psi + \\ + \frac{B^4}{4}\frac{\Omega_y}{\omega}\cos\psi + \frac{B^3}{3}\frac{\Omega_y}{\omega}\frac{1}{2}\mu\sin 2\psi + \frac{B^4}{4}\varphi + \frac{2}{3}B^3\varphi\mu\sin\psi + \\ + \frac{B^2}{2}\varphi\mu^2\sin^2\psi\Big) - 2\frac{\Omega_y}{\omega}\sin\psi - 2\frac{\Omega_x}{\omega}\cos\psi - \frac{S_{h.h}}{I_{h.h}\omega^2}. \end{aligned} \tag{2.34}$$

The particular solution of the differential equation (2.34) can be represented as the series

$$\beta = a_0 - a_1\cos\psi - b_1\sin\psi - a_2\cos 2\psi - b_2\sin 2\psi - \ldots$$

It is known from solutions obtained with retention of only five terms in the expression of β and from practical experiments that, in the usual case of ($\Omega = 0$), the second harmonics of the angle β are small in comparison with the first.

For greater clarity and simplicity of the derivations (while fundamentally retaining an accurate pattern) we will discard, in solving the problem, the second harmonics in the expression for β, i.e., we take β in the form

$$\beta = a_0 - a_1\cos\psi - b_1\sin\psi. \tag{2.35}$$

We then find the derivatives $\frac{d\beta}{d\psi}$ and $\frac{d^2\beta}{d\psi^2}$ and substitute them into eq.(2.34). Discarding terms containing functions of double angles, we derive

$$\begin{aligned} a_0+\frac{B^3}{6}\frac{\Omega_x}{\omega}\gamma\mu+a_1\gamma\frac{B^2}{4}\left(B^2-\frac{1}{2}\mu^2\right)\sin\psi- \\ -\left[b_1\gamma\frac{B^2}{4}\left(B^2+\frac{1}{2}\mu^2\right)-\frac{B^3}{3}a_0\gamma\mu\right]\cos\psi=\gamma\left[\frac{B^3}{3}\lambda+\frac{\varphi}{4}B^2(B^2+\mu^2)\right]- \\ -\frac{S_{h.h}}{I_{h.h}\omega^2}+\left(\frac{B^2}{2}\gamma\lambda\mu-\frac{B^4}{4}\frac{\Omega_x}{\omega}\gamma+\frac{2}{3}B^3\varphi\gamma\mu-2\frac{\Omega_y}{\omega}\right)\sin\psi+ \\ +\left(\frac{B^4}{4}\frac{\Omega_y}{\omega}\gamma-2\frac{\Omega_x}{\omega}\right)\cos\psi. \end{aligned} \tag{2.36}$$

Since eq.(2.36) is an identity, we equate the coefficients of sin ψ, cos ψ, and of the free term, whence we obtain the coefficients of flapping motion. /69

The free term is

$$a_0=\gamma\left[\frac{B^3}{3}\lambda+\frac{\varphi}{4}B^2(B^2+\mu^2)-\frac{B^3\Omega_x}{6\omega}\mu\right]-\frac{S_{h.h}}{I_{h.h}\omega^2}. \tag{2.37}$$

The coefficient of sin ψ is

$$a_1\gamma\frac{B^2}{4}\left(B^2-\frac{1}{2}\mu^2\right)=\frac{B^2}{2}\gamma\lambda\mu-\frac{B^4\Omega_x}{4\omega}\gamma+\frac{2}{3}B^3\varphi\gamma\mu-2\frac{\Omega_y}{\omega},$$

from which it follows that

$$a_1=2\mu\left(\lambda+\frac{4}{3}B\varphi\right)\frac{1}{B^2-\frac{1}{2}\mu^2}-\left(B^4\frac{\Omega_x}{\omega}+\frac{8\Omega_y}{\gamma\omega}\right)\frac{1}{B^2\left(B^2-\frac{1}{2}\mu^2\right)}. \tag{2.38}$$

The coefficient of cos ψ is

$$b_1\gamma\frac{B^2}{4}\left(B^2+\frac{1}{2}\mu^2\right)-\frac{B^3}{3}a_0\gamma\mu=\frac{B^4\Omega_y\gamma}{4\omega}-2\frac{\Omega_x}{\omega},$$

whence

$$b_1=\frac{4}{3}\mu a_0\frac{B}{B^2+\frac{1}{2}\mu^2}-\left(B^4\frac{\Omega_y}{\omega}-\frac{8\Omega_x}{\gamma\omega}\right)\frac{1}{B^2\left(B^2+\frac{1}{2}\mu^2\right)}. \tag{2.39}$$

For the conditions of rectilinear motion we obtain

$$a_0'=\gamma\left[\frac{B^3}{3}\lambda+\frac{\varphi}{4}B^2(B^2+\mu^2)\right]-\frac{S_{h.h}}{I_{h.h}\omega^2}, \tag{2.40}$$

$$a_1' = 2\mu\left(\lambda + \frac{4}{3} B\varphi\right) \frac{1}{B^2 - \frac{1}{2}\mu^2},$$

$$b_1' = \frac{4}{3} \mu a_0 \frac{B}{B^2 + \frac{1}{2}\mu^2}.$$

Then eqs.(2.37), (2.38), and (2.39) can be rewritten as

$$\left.\begin{aligned} a_0 &= a_0' - \gamma \frac{B^3 \Omega_x}{6\omega} \mu, \\ a_1 &= a_1' - \left(B^4 \frac{\Omega_x}{\omega} + \frac{8\Omega_y}{\gamma\omega}\right) \frac{1}{B^2\left(B^2 - \frac{1}{2}\mu^2\right)}, \\ b_1 &= b_1' - \left(B^4 \frac{\Omega_y}{\omega} - \frac{8\Omega_x}{\gamma\omega}\right) \frac{1}{B^2\left(B^2 + \frac{1}{2}\mu^2\right)}. \end{aligned}\right\} \qquad (2.41)$$

We have examined the particular solution of eq.(2.34). Investigations of the general solution of this equation characterizing the natural vibrations of the blade show that the blade is stable and, after having been deflected from its path normal for the given regime, will return to it under strong damping during one or two revolutions of the rotor.

This means that the new flapping motion of the blades, described by eqs.(2.41) and caused by the presence of angular velocity of rotation of the craft, is established rather promptly (within one revolution of the rotor). /70

The obtained expressions hold for rotors with large γ. Equation (2.41) shows that, under the effect of angular velocity, the cone of the blades rotates together with the shaft, lagging behind it by a constant angle Δa_1 and is also deflected in a perpendicular direction. Thus, the plane of this new slope is shifted in phase relative to the plane of rotation of the rotor axis.

This shift $\Delta\psi$ in the case of longitudinal rotation is characterized by the relation

$$\tan \Delta\psi = \frac{\Delta b_1}{\Delta a_1},$$

where Δb_1 and Δa_1 are determined by eqs.(2.41).

Equations (2.41) can be used for compiling a table (see Table 2.1) showing the direction of flapping of the cone under the effect of angular velocity.

Deflection of the cone in the case of complex motion of the rotor (for example, to the front and right) is easily obtained by means of eqs.(2.41). Thus, for the particular case $\gamma = 8$ and $\Omega_x = \Omega_y$ we obtain Table 2.2.

TABLE 2.1

Mode of Revolution of Rotor Axis	Mode of Deflection of Cone
Pitches	Forward and left
Banks to the left	Right and forward
Dives	Backward and right
Banks to the right	Left and backward

TABLE 2.2

Mode of Revolution of Rotor Axis	Mode of Deflection of Cone
Dives and banks to the right	Backward
Dives and banks to the left	To right
Pitches and banks to the right	To left
Pitches and banks to the left	Forward

The deflection of the cone during rotation is easily determined if we recall that it is deflected to the side opposite to the rotation (in the plane of rotation) and, furthermore, is deflected in a perpendicular direction opposite to the direction of the gyro reaction (a right-handed gyroscope, on sloping backward, is deflected to the right while the additional slope of the cone occurs to the left).

5. Physical Meaning of the Obtained Result

Equations (2.41) show that, in response to rotation of the rotor axis to some side, the axis of the cone in this direction will lag (the plane of the blade tips, relative to the shaft axis, is deflected to the opposite side) and, furthermore, will incline in a direction perpendicular to the rotation.

It is not difficult to demonstrate that the lateral inclination is caused by aerodynamic forces and the lag by inertia forces.

As a typical example, let us examine the case $\mu = 0$; $B = 1$.

Let us assume that the rotor revolves backward; $\Omega_y > 0$; $\Omega_x = 0$. Then, /71 according to eq.(2.24),

$$U_y=\lambda R\omega-r\frac{d\beta}{dt}-\mu R\beta\cos\psi+\Omega_y r\cos\psi=U_{y_{st}}+\Delta U_y,$$

where $U_{y_{st}}$ is the expression for U_y when $\Omega = 0$.

The angle of attack of the forward blade sections ($\psi = \pi$), assuming $\lambda =$ = const, decreases by

$$\Delta\alpha_{r_1}=\frac{\Delta U_y}{U_x}=-\frac{\Omega_y}{\omega},$$

while the angle of attack of the blade sections stationary with respect to the flow increases by the quantity

$$\Delta\alpha_{r_2}=\frac{\Omega_y}{\omega}.$$

Under the effect of the change in moments of aerodynamic forces occurring in this case, the flapping motion of the blades will change until a new equilibrium of the moments and a corresponding flapping motion are established. As follows from the condition of zero hinge moment, the angles of attack of the blade sections should return to their previous value corresponding to rectilinear motion (since no new forces appeared and the velocities U_x remained constant).

This is realized when the real axis of rotation of the cone swept by the blades is deflected leftward by the same angle $\Delta\alpha$ (the axis is inclined to the right to reduce the angle of attack of the advancing blade in the case of regular stationary flight).

Actually, the formula for b_1 [eq.(2.39)] will yield in this case:

$$b_1=b_1'-\frac{\Omega_y}{\omega},$$

i.e., the slant of the cone to the right, occurring in rectilinear flight, decreases by the indicated quantity.

Now let us examine the effect of inertia forces. The additional force acting during the rotation is the force due to Coriolis acceleration. Its moment, according to eq.(2.7), is

$$M_K=-\int_0^R 2m\Omega_y\omega r^2\sin\psi\,dr=-2I_{h.h}\Omega_y\omega\sin\psi,$$

i.e., during backward rotation of the rotor the advancing blade $\left(\psi=\frac{\pi}{2}\right)$ is acted on by the moment $M_K = 2I_{h.h}\Omega_y\omega$ which tends to depress the blade.

This new moment changes the blade flapping. Equilibrium is established when, as a consequence of this flapping, the angles of attack of the blade sections in a forward position increase so that the additional aerodynamic moment equalizes the moment of the Coriolis forces.

An increase in the blade angle of attack at the position $\psi=\frac{\pi}{2}$ is achieved when the real axis of rotation of the cone described by the blades is deflected forward (under rectilinear flight conditions, the axis is inclined backward so that the angles of attack of the advancing blades diminish).

Actually, eq.(2.38) for a_1 yields /72

$$a_1=a_1'-\frac{8\Omega_y}{\gamma\omega},$$

i.e., during backward rotation of the rotor, the cone follows the rotor axis with some lag, being deflected forward from it through the angle $\frac{8\Omega_y}{\gamma\omega}$.

6. Equation of Torque

The elementary moment due to aerodynamic forces can be written in the form of eq.(2.26):

$$dM_t = \frac{1}{2} b\varrho (c_{x p_{av}} U_x^2 - a_\infty \varphi U_x U_y - a_\infty U_y^2) r\, dr.$$

Here the braking moment is considered to be positive. In addition to these forces, additional inertia forces [eqs.(2.5), (2.8), and (2.10)] appear in the plane of rotation owing to rotation of the rotor axis in space.

The expressions $U_x U_y$ and U_y^2 in curvilinear motion can be represented by eqs.(2.23) and (2.24) in the following form:

$$\begin{aligned}
U_x U_y &= U_x U_{y_{st}} + U_x \Delta U_y;\\
U_x \Delta U_y &= -\Omega_x \omega\mu R r \sin^2\psi - \Omega_x \omega r^2 \sin\psi + \\
&\quad + \Omega_y \omega r^2 \cos\psi + \Omega_y \omega\mu R r \sin\psi\cos\psi;\\
U_y &= U_{y_{st}} + \Delta U_y;\\
\Delta U_y &= -\Omega_x r \sin\psi + \Omega_y r \cos\psi;\\
U_y^2 &= U_{y_{st}}^2 + \Delta U_y^2;
\end{aligned} \tag{2.42}$$

$$\begin{aligned}
\Delta U_y^2 = &-2\Omega_x \omega\lambda R r \sin\psi + 2\frac{d\beta}{d\psi}\Omega_x \omega r^2 \sin\psi + \\
&+ 2\beta\Omega_x \omega\mu R r \sin\psi\cos\psi + 2\Omega_y \omega\lambda R r \cos\psi - \\
&- 2\frac{d\beta}{d\psi}\Omega_y \omega r^2 \cos\psi - 2\beta\Omega_y \omega\mu R r \cos^2\psi - \\
&- 2\Omega_x \Omega_y r^2 \sin\psi\cos\psi + \Omega_x^2 r^2 \sin^2\psi + \Omega_y^2 r^2 \cos^2\psi.
\end{aligned} \tag{2.43}$$

Then, transforming the expression dM_t and adding the moments due to inertia forces according to eqs.(2.5), (2.8), and (2.10), we obtain

$$dM_t = dM_{t_{st}} + \Delta dM_t$$

where

$$\begin{aligned}
\Delta dM_t &= \Delta dM_{t_{st}} + \Delta dM_{t_{inert}};\\
\Delta dM_t &= -\frac{1}{2} b\varrho a_\infty (\varphi U_x \Delta U_y + \Delta U_y^2) r\, dr + \\
&+ m\left[-2\Omega_y \frac{d\beta}{dt}\sin\psi - 2\Omega_x \frac{d\beta}{dt}\cos\psi + \left(\Omega_y^2 - \Omega_x^2\right)\sin\psi\cos\psi - \right.\\
&\left. - 2\beta \frac{d\beta}{dt}\omega\right] r^2\, dr;
\end{aligned} \tag{2.44}$$

$$M_t = M_{t_{st}} + \int_0^{BR} \Delta dM_{t_{aero}} + \int_0^{R} \Delta dM_{t_{inert}}. \qquad (2.45)$$

Assuming $\beta = a_0 - a_1 \cos\psi - b_1 \sin\psi$ and substituting into eq.(2.44) the /73 expressions $U_x \Delta U_y$ and ΔU_y^2 from eqs.(2.42) and (2.43), we obtain, according to eq.(2.45),

$$\begin{aligned} M_t = M_{t_{st}} + \frac{1}{2} b\varrho a_\infty \int_0^{BR} [&\varphi\Omega_x\omega\mu Rr^2 \sin^2\psi + \varphi\Omega_x\omega r^3 \sin\psi - \\ &- \varphi\Omega_y\omega r^3 \cos\psi - \varphi\Omega_y\omega\mu Rr^2 \sin\psi\cos\psi + 2\Omega_x\omega\lambda Rr^2 \sin\psi - \\ &- 2a_1\Omega_x\omega r^3 \sin^2\psi + 2b_1\Omega_x\omega r^3 \sin\psi\cos\psi - 2(a_0 - a_1\cos\psi - \\ &- b_1\sin\psi)\Omega_x\omega\mu Rr^2 \sin\psi\cos\psi - 2\Omega_y\omega\lambda Rr^2\cos\psi + \\ &+ 2a_1\Omega_y\omega r^3 \sin\psi\cos\psi - 2b_1\Omega_y\omega r^3\cos^2\psi + \\ &+ 2(a_0 - a_1\cos\psi - b_1\sin\psi)\Omega_y\omega\mu Rr^2\cos^2\psi + 2\Omega_x\Omega_y r^3 \sin\psi\cos\psi - \\ &- \Omega_x^2 r^3 \sin^2\psi - \Omega_y^2 r^3\cos^2\psi]\,dr + \int_0^R m[-2a_1\Omega_y\omega\sin^2\psi + \\ &+ 2b_1\Omega_y\omega\sin\psi\cos\psi + (\Omega_y^2 - \Omega_x^2)\sin\psi\cos\psi - \\ &- 2(a_0 - a_1\cos\psi - b_1\sin\psi)(a_1\sin\psi - b_1\cos\psi)\omega^2]r^2\,dr. \end{aligned}$$

The moment due to z_b of the blades per revolution is

$$\begin{aligned} M_t = \frac{z_b}{2\pi}\int_0^{2\pi} M_1\,d\psi = M_{t_{st}} + \frac{1}{2} z_b b\varrho a_\infty R^4\omega^2 \times \\ \times\left[\frac{B^3}{6}\frac{\Omega_x}{\omega}\varphi\mu - \frac{B^4}{4}\frac{\Omega_x}{\omega}a_1 - \frac{B^4\Omega_y}{4\omega}b_1 + \right. \\ \left. + \frac{B^3\Omega_y}{3\omega}a_0\mu - \frac{B^4}{8}\left(\frac{\Omega_x}{\omega}\right)^2 - \frac{B^4}{8}\left(\frac{\Omega_y}{\omega}\right)^2\right] + \\ + z_b I_{h.h}\omega^2\left(\frac{\Omega_x}{\omega}b_1 - \frac{\Omega_y}{\omega}a_1\right). \end{aligned} \qquad (2.46)$$

Here $M_{t_{st}}$ is the moment due to aerodynamic forces, obtained in the theory for rectilinear motion

$$\begin{aligned} M_{t_{st}} = m_{t_{st}}\frac{1}{2}z_b b\varrho R^4\omega^2 = m_{t_{st}}\frac{1}{2}\sigma\varrho(\omega R)^2 FR; \\ m_{t_{st}} = a_\infty\left[\frac{c_{xp_{av}}}{4a_\infty}(1+\mu^2) - \frac{B^3}{3}\varphi\lambda - \frac{B^2}{2}\lambda^2 - \frac{a_1^2}{8}\left(B^4 + \frac{3}{2}B^2\mu^2\right) - \right. \\ \left. - \frac{B^2}{4}a_0^2\mu^2 + \frac{B^3}{3}a_0 b_1\mu - \frac{b_1^2}{8}\left(B^4 + \frac{B^2}{2}\mu^2\right) - \frac{B^2}{2}a_1\lambda\mu\right]. \end{aligned} \qquad (2.47)$$

We then write the expression for m_t by means of eqs.(2.46) and (2.47):

$$m_t = a_\infty \left[\frac{c_{xp_{av}}}{4a_\infty}(1+\mu^2) - \frac{B^3}{3}\varphi\lambda - \frac{B^2}{2}\lambda^2 - \right.$$
$$- \frac{a_1^2}{8}\left(B^4 + \frac{3}{2}B^2\mu^2\right) - \frac{B^2}{4}a_0^2\mu^2 + \frac{B^3}{3}a_0 b_1 \mu -$$
$$\left. - \frac{b_1^2}{8}\left(B^4 + \frac{B^2}{2}\mu^2\right) - \frac{B^2}{2}a_1\lambda\mu \right] +$$
$$+ \frac{B^3}{6}\frac{\Omega_x}{\omega}\varphi\mu - \frac{B^4}{4}\frac{\Omega_x}{\omega}a_1 - \frac{B^4\Omega_y}{4\omega}b_1 + \frac{B^3\Omega_y}{3\omega}a_0\mu -$$
$$- \frac{B^4}{8}\left(\frac{\Omega_x}{\omega}\right)^2 - \frac{B^4}{8}\left(\frac{\Omega_y}{\omega}\right)^2 + \frac{1}{\gamma}\left(\frac{\Omega_x}{\omega}b_1 - \frac{\Omega_y}{\omega}a_1\right). \qquad (2.48)$$

7. Rotor Thrust and Angle of Attack /74

The rotor thrust is

$$T = \frac{z_b}{2\pi}\int_0^{2\pi} d\psi \int_0^{BR} dT = \frac{z_b}{2\pi}\int_0^{2\pi} d\psi \int_0^{BR} \frac{1}{2} b\rho a_\infty (\varphi U_x^2 + U_x U_y)\, dr.$$

Substituting the values of U_x and U_y from eqs.(2.23) and (2.24) and integrating, we obtain

$$T = \frac{1}{2} z_b b\rho a_\infty R^3\omega^2 B\left[\frac{\lambda B}{2} + \frac{\varphi}{3}\left(B^2 + \frac{3}{2}\mu^2\right) - \frac{B\Omega_x}{4\omega}\mu\right]. \qquad (2.49)$$

Setting

$$T = \frac{1}{2} t_\sigma \rho \pi R^4 \omega^2 = t_\sigma \frac{1}{2}\rho(\omega R)^2 F, \qquad (2.49')$$

we find

$$t = a_\infty B\left[\frac{\lambda B}{2} + \frac{\varphi}{3}\left(B^2 + \frac{3}{2}\mu^2\right) - \frac{B\Omega_x}{4\omega}\mu\right]. \qquad (2.50)$$

As we see, the expression for the thrust coefficient has been somewhat changed; nevertheless, assuming $\frac{\Omega_x}{\omega} = 0$, we obtain the same expression as for the case of rectilinear motion. The formula for the angle of attack, after determining the induced velocity, is obtained from the expression

$$T = 2\pi R^2 \rho V' v, \qquad (2.51)$$

where V′ is the resultant velocity,

$$V' = \sqrt{(V\sin\alpha - v)^2 + V^2\cos^2\alpha}. \qquad (2.52)$$

Substituting T and V by their expressions and remembering that

$$\lambda=\frac{V\sin\alpha-v}{\omega R};\quad \mu=\frac{V\cos\alpha}{\omega R},$$

we obtain

$$\tan\alpha=\frac{\lambda}{\mu}+\frac{ct}{4\mu\sqrt{\lambda^2+\mu^2}}, \tag{2.53}$$

i.e., the usual expression for the angle of attack in which only t has a new value. Writing this in expanded form, we derive

$$\tan\alpha=\frac{\lambda}{\mu}+\frac{\sigma a_\infty B\left[\frac{\lambda B}{2}+\frac{\varphi}{3}\left(B^2+\frac{3}{2}\mu^2\right)-\frac{B\Omega_x}{4\omega}\mu\right]}{4\mu\sqrt{\lambda^2+\mu^2}}. \tag{2.54}$$

8. Lateral Force

According to eq.(2.28), the elementary lateral force is

$$dS=-\frac{dM_t}{r}\cos\psi-\beta\,dT\sin\psi.$$

We can represent dS as

$$dS=dS_{st}+\Delta\,dS,$$

where dS_{st} is the elementary lateral force for the case of rectilinear motion:

$$\Delta\,dS=-\frac{\Delta dM_t}{r}\cos\psi-\beta\Delta\,dT\sin\psi. \tag{2.55}$$

In eq.(2.55) we can replace $\Delta dM_t = \Delta dM_{t_{aero}}$ since the inertia forces /75
when summed with respect to z_b-blades will give zero. It is easy to demonstrate this by means of eq.(2.44):

$$\int_0^R\frac{\Delta\,dM_{t_{inert}}}{r}\cos\psi=\int_0^R\frac{\Delta\,dM_{t_{inert}}}{r}\sin\psi=0.$$

Then, using eqs.(2.44), (2.42), and (2.43), we obtain

$$\begin{aligned}\frac{\Delta dM_{t_{aero}}}{r}\cos\psi=\frac{1}{2}b\varrho a_\infty[&\varphi\Omega_x\omega\mu Rr\sin^2\psi\cos\psi+\\&+\varphi\Omega_x\omega r^2\sin\psi\cos\psi-\varphi\Omega_y\omega r^2\cos^2\psi-\varphi\Omega_y\omega\mu Rr\sin\psi\cos^2\psi+\\&+2\Omega_x\omega\lambda Rr\sin\psi\cos\psi-2a_1\Omega_x\omega r^2\sin^2\psi\cos\psi+\\&+2b_1\Omega_x\omega r^2\sin\psi\cos^2\psi-2(a_0-a_1\cos\psi-b_1\sin\psi)\Omega_x\omega\mu Rr\sin\psi\cos^2\psi-\\&-2\Omega_y\omega\lambda Rr\cos^2\psi+2a_1\Omega_y\omega r^2\sin\psi\cos^2\psi-\end{aligned} \tag{2.56}$$

$$-2b_1\Omega_y\omega r^2\cos^3\psi+2(a_0-a_1\cos\psi-b_1\sin\psi)\Omega_y\omega\mu Rr\cos^3\psi+$$
$$+2\Omega_x\Omega_y r^2\sin\psi\cos^2\psi-\Omega_x^2 r^2\sin^2\psi\cos\psi-\Omega_y^2 r^2\cos^3\psi]\,dr.$$

Setting

$$dT=dT_{st}+\Delta\,dT=dT_{st}+\frac{1}{2}b\varrho a_\infty U_x\Delta U_y\,dr, \tag{2.57}$$

we find, by means of eq.(2.42),

$$\beta\Delta\,dT\sin\psi=\frac{1}{2}b\varrho a_\infty(a_0-a_1\cos\psi-b_1\sin\psi)(-\Omega_x\omega\mu Rr\sin^3\psi-$$
$$-\Omega_x\omega r^2\sin^2\psi+\Omega_y\omega r^2\sin\psi\cos\psi+\Omega_y\omega\mu Rr\sin^2\psi\cos\psi). \tag{2.58}$$

The lateral force of the rotor can be represented in the form

$$S=S_{st}+\Delta S,$$

where

$$\Delta S=-\frac{z_b}{2\pi}\int_0^{2\pi}\int_0^{BR}\frac{\Delta\,dM_{t_{aero}}}{r}\cos\psi\,dr\,d\psi-$$
$$-\frac{z_b}{2\pi}\int_0^{2\pi}\int_0^{BR}\beta\Delta\,dT\sin\psi\,dr\,d\psi. \tag{2.59}$$

Substituting eqs.(2.56) and (2.58) into eq.(2.59) and integrating, we obtain

$$\Delta S=\frac{1}{2}z_b b\varrho R^3\omega^2 a_\infty\left[\frac{\Omega_x}{\omega}\frac{B^2}{2}\left(\frac{a_0B}{3}-\frac{5}{8}b_1\mu\right)+\right.$$
$$\left.+\frac{\Omega_y}{\omega}\frac{B^2}{2}\left(\frac{\varphi B}{3}+\lambda+\frac{7}{8}a_1\mu\right)\right]. \tag{2.60}$$

Substituting S_{st} by its value of /76

$$S_{st}=\frac{1}{2}z_b b\varrho R^3\omega^2 a_\infty\left\{b_1\left[\varphi\left(\frac{B^3}{3}+\frac{1}{2}B^2\mu^2\right)+\right.\right.$$
$$\left.+\frac{3}{4}\left(B^2\lambda+\frac{B^2}{3}a_1\mu\right)\right]-\frac{3}{2}a_0\mu\left(B\lambda+\frac{B^2}{2}\varphi\right)+ \tag{2.61}$$
$$\left.+a_0a_1\left(\frac{B^3}{6}-B\mu^2\right)\right\},$$

we finally obtain

$$S=\frac{1}{2}\sigma\varrho\pi R^4\omega^2 a_\infty\left\{b_1\left[\varphi\left(\frac{B^3}{3}+\frac{B^2}{2}\mu^2\right)+\frac{3}{4}\left(B^2\lambda+\frac{1}{3}B^2a_1\mu\right)\right]-\right.$$
$$\left.-\frac{3}{2}a_0\mu\left(B\lambda+\frac{B^2}{2}\varphi\right)+a_0a_1\left(\frac{B^3}{6}-B\mu^2\right)+\right.$$

$$+\frac{\Omega_x}{\omega}\frac{B^2}{2}\left(\frac{a_0 B}{3}-\frac{5}{8}b_1\mu\right)+\frac{\Omega_y}{\omega}\frac{B^2}{2}\left(\frac{\varphi B}{3}+\lambda+\frac{7}{8}a_1\mu\right)\Big\}. \qquad (2.62)$$

9. Longitudinal Force

According to eq.(2.27), the elementary longitudinal force is

$$dH=\frac{dM_t}{r}\sin\psi-\beta\,dT\cos\psi.$$

Setting

$$dH=dH_{st}+\Delta\,dH,$$

we find

$$\Delta\,dH=\frac{\Delta dM_{t_{aero}}}{r}\sin\psi-\beta\Delta\,dT\cos\psi. \qquad (2.63)$$

Analogous to eq.(2.56),

$$\begin{aligned}\frac{\Delta\,dM_{t_{aero}}}{r}\sin\psi=\frac{1}{2}\,b\varrho a_\infty\Big[&\varphi\Omega_x\omega\mu Rr\sin^3\psi+\varphi\Omega_x\omega r^2\sin^2\psi-\\&-\varphi\Omega_y\omega r^2\sin\psi\cos\psi-\varphi\Omega_y\omega\mu Rr\sin^2\psi\cos\psi+2\Omega_x\omega\lambda Rr\sin^2\psi-\\&-2a_1\Omega_x\omega r^2\sin^3\psi+2b_1\Omega_x\omega r^2\sin^2\psi\cos\psi-\\&-2(a_0-a_1\cos\psi-b_1\sin\psi)\,\Omega_x\omega\mu Rr\sin^2\psi\cos\psi-\\&-2\Omega_y\omega\lambda Rr\sin\psi\cos\psi+2a_1\Omega_y\omega r^2\sin^2\psi\cos\psi-2b_1\Omega_y\omega r^2\sin\psi\cos^2\psi+\\&+2(a_0-a_1\cos\psi-b_1\sin\psi)\,\Omega_y\omega\mu Rr\sin\psi\cos^2\psi+\\&+2\,\Omega_x\Omega_y r^2\sin^2\psi\cos\psi-\Omega_x^2 r^2\sin^3\psi-\Omega_y^2 r^2\sin\psi\cos^2\psi\Big]\,dr.\end{aligned} \qquad (2.64)$$

Analogous to eq.(2.58),

$$\begin{aligned}\beta\Delta\,dT\cos\psi=\frac{1}{2}\,b\varrho a_\infty(a_0-a_1\cos\psi-b_1\sin\psi)(&-\Omega_x\omega\mu Rr\sin^2\psi\cos\psi-\\&-\Omega_x\omega r^2\sin\psi\cos\psi+\Omega_y\omega r^2\cos^2\psi+\Omega_y\omega\mu Rr\sin\psi\cos^2\psi).\end{aligned} \qquad (2.65)$$

Let us use the same notations as in the calculation of the lateral force, namely

$$H=H_{st}+\Delta H;$$

$$\Delta H=\frac{z_b}{2\pi}\int_0^{2\pi}\int_0^{BR}\frac{\Delta\,dM_{t_{aero}}}{r}\sin\psi\,dr\,d\psi-\frac{z_b}{2\pi}\int_0^{2\pi}\int_0^{BR}\beta\Delta\,dT\cos\psi\,dr\,d\psi. \qquad (2.66)$$

Substituting here eqs.(2.64), (2.65) and integrating, we obtain /77

$$\Delta H=\frac{1}{2}z_b b\varrho R^3\omega^2 a_\infty\left[\frac{\Omega_x}{\omega}\frac{B^2}{2}\left(\frac{\varphi B}{3}+\lambda+\frac{1}{8}a_1\mu\right)-\frac{\Omega_y}{\omega}\frac{B^2}{2}\left(\frac{a_0 B}{3}+\frac{1}{8}b_1\mu\right)\right]. \qquad (2.67)$$

The expression of the longitudinal force for rectilinear motion has the form

$$H_{st}=\frac{1}{2}z_b b\varrho R^3\omega^2 a_\infty\left[\frac{c_{xp_{av}}}{2a_\infty}\mu-\frac{B^2}{2}\varphi\lambda\mu+\frac{B^3}{3}\varphi a_1-\right.$$
$$\left.-\frac{B^3}{6}a_0b_1+\frac{B^2}{4}a_0^2\mu+\frac{3}{4}B^2a_1\lambda+\frac{B^2}{4}a_1^2\mu\right]. \tag{2.68}$$

Summing eqs.(2.67) and (2.68), we finally obtain

$$H=\frac{1}{2}\sigma\varrho\pi R^4\omega^2 a_\infty\left[\frac{c_{xp_{av}}}{2a_\infty}\mu-\frac{B^2}{2}\varphi\lambda\mu+\frac{B^3}{3}\varphi a_1-\frac{B^3}{6}a_0b_1+\right.$$
$$+\frac{B^2}{4}a_0^2\mu+\frac{3}{4}B^2a_1\lambda+\frac{B^2}{4}a_1^2\mu+\frac{\Omega_x}{\omega}\frac{B^2}{2}\left(\frac{\varphi B}{3}+\lambda+\frac{1}{8}a_1\mu\right)-$$
$$\left.-\frac{\Omega_y}{\omega}\frac{B^2}{2}\left(\frac{a_0B}{3}+\frac{1}{8}b_1\mu\right)\right]. \tag{2.69}$$

10. Consideration of the Change in the Law of Induced Velocity Distribution during Curvilinear Motion

In curvilinear motion, a change both in magnitude and in character of the induced velocity distribution over the rotor disk should occur owing to the presence of new forces, namely Coriolis inertia forces; the moments produced by these forces are balanced (in the case of hinged blade attachment) by the redistribution of aerodynamic forces.

It is logical that, if the angles of attack of the blade sections at a given angular position in curvilinear motion do not change in comparison with those existing in rectilinear motion, then both the forces and the induced velocities caused by them also will remain constant.

Assuming that the rotor revolves backward ($\Omega_y > 0$), the angle of attack of blade section, at $\mu = 0$, $B = 1$, will be

$$\alpha_r=\varphi+\frac{U_y}{U_x}=\varphi+\frac{\lambda R\omega-r\omega a_1\sin\psi+r\omega b_1\cos\psi+\Omega_y r\cos\psi}{r\omega}.$$

Substituting here the expressions for a_1 and b_1 obtained from eqs.(2.38) and (2.39) and setting $\mu = 0$, $B = 1$, and $\Omega_x = 0$, i.e.,

$$a_1=-\frac{8\Omega_y}{\gamma\omega};\quad b_1=-\frac{\Omega_y}{\omega},$$

we obtain

$$\alpha_r=\varphi+\frac{\lambda R}{r}-\frac{8\Omega_y}{\gamma\omega}\sin\psi.$$

The angles of attack in the forward and rear positions ($\psi = 0$, $\psi = \pi$), as shown above, do not change when λ = const, i.e., the kinematic change in velocity

of the disk ($\Omega_y r \cos\psi$) does not produce a change in the angles of attack of the blades thanks to the corresponding change in flapping motion.

The above statements also hold for $\mu \neq 0$. The curves of the azimuthal change in angle of attack of the blade section, plotted in Fig.2.23, for rectilinear motion and for rotation of the axis in a longitudinal direction also show that, at azimuths $\psi = 0$ and $\psi = \pi$, the angles of attack, for all practical purposes, remain constant*. /78

The change in angles of attack, for the example under study, takes place from the right and left of this position, the maximum change occurring when $\psi = \frac{\pi}{2}$ and $\psi = \frac{3}{2}\pi$, which corresponds to the azimuth of the maximum value of the Coriolis inertia forces.

Thus, it can be assumed that the previous distribution law of forces and induced velocities over the disk is superposed by aerodynamic forces equalizing the moments due to the Coriolis inertia forces and the resultant velocities. These forces have a maximum in a plane perpendicular to the direction of rotation, so that the induced velocity field will be tilted in this direction.

The vertical components of the Coriolis forces are expressed, according to eq.(2.7), in the following manner:

$$\left.\begin{aligned} K_{\Omega_y} &= -\int_0^R 2m\Omega_y \omega r \sin\psi\, dr = -2S_{h.h}\,\Omega_y \omega \sin\psi; \\ K_{\Omega_x} &= -\int_0^R 2m\Omega_x \omega r \cos\psi\, dr = -2S_{h.h}\,\Omega_x \omega \cos\psi. \end{aligned}\right\} \tag{2.70}$$

These forces are linearly distributed over the radius and are periodic.

It can be assumed that the aerodynamic forces and their induced velocities, equalizing the Coriolis forces at each angular position, obey the same law of change both with respect to azimuth and radius of the blade. Then the induced velocity in the case of curvilinear motion can be expressed in the form

$$v = v_0 + v_1 \frac{r}{R}\sin\psi + v_2 \frac{r}{R}\cos\psi. \tag{2.71}$$

Here, the velocity directed downward is considered to be positive. Let us denote

$$\left.\begin{aligned} p_y &= \frac{v_1}{v_0} = C\frac{|K_{\Omega_y}|}{T}; \\ p_x &= \frac{v_2}{v_0} = C\frac{|K_{\Omega_x}|}{T}. \end{aligned}\right\} \tag{2.72}$$

* The difference in the angle of attack of the section, at $\psi = 270^\circ$, for rotation in a transverse direction (see Fig.2.22) is due to a change in λ.

Here, $|K_{\Omega_y}|$ and $|K_{\Omega_x}|$ are the absolute values of the Coriolis forces at angular positions where they reach a maximum. In calculating v_0, it was assumed that this velocity is constant over the radius. Assuming an additional induced velocity as a linear function of the radius, we should, from the condition of equality of momentum, introduce some factor C into the expressions for p_x and p_y. At $C = \frac{3}{2}$ /79

$$\left.\begin{aligned} p_y &= \frac{3S_{h.h}z_b}{\frac{1}{2}\sigma\varrho\pi R^4 t}\,\frac{\Omega_y}{\omega}; \\ p_x &= \frac{3S_{h.h}z_b}{\frac{1}{2}\sigma\varrho\pi R^4 t}\,\frac{\Omega_x}{\omega}. \end{aligned}\right\} \qquad (2.73)$$

Substituting v_1 and v_2 by their values from eqs.(2.72), we obtain

$$v = v_0 + p_y v_0 \frac{r}{R}\sin\psi + p_x v_0 \frac{r}{R}\cos\psi.$$

We then express the mean induced velocity in terms of the magnitude of thrust. According to the law of momentum

$$v_0 = \frac{T}{2\pi R^2 \varrho V'}. \qquad (2.74)$$

Here V' is the resultant velocity determined from eq.(2.52). Substituting the expressions for T and V' from eqs.(2.49) and (2.52), we obtain

$$v_0 = \frac{\sigma t \omega R}{4\sqrt{\lambda^2+\mu^2}}.$$

Let us denote

$$\lambda_1 = \frac{v_0}{\omega R} = \frac{\sigma t}{4\sqrt{\lambda^2+\mu^2}}. \qquad (2.75)$$

Then, the velocity component U_y of the blade element will have the form

$$\begin{aligned} U'_y = {} & \lambda R\omega - p_y\lambda_1 r\omega\sin\psi - p_x\lambda_1 r\omega\cos\psi - r\frac{d\beta}{dt} - \\ & - \mu R\omega\beta\cos\psi + \Omega_y r\cos\psi - \Omega_x r\sin\psi. \end{aligned} \qquad (2.76)$$

To the expression $U_x U_y$ obtained for v = const, we then add the terms

$$\begin{aligned} U_x\Delta' U_y = {} & -p_y\lambda_1 r^2\omega^2\sin\psi - p_y\lambda_1\omega^2 R r\mu\sin^2\psi - \\ & - p_x\lambda_1 r^2\omega^2\cos\psi - p_x\lambda_1\omega^2 R r\mu\sin\psi\cos\psi. \end{aligned} \qquad (2.77)$$

The expression for the rotor thrust will have the form

$$T=\frac{z_b}{2\pi}\int_0^{2\pi}\int_0^{BR}\frac{1}{2}b\varrho a_\infty(\varphi U_x^2+U_xU_y+U_x\Delta'U_y)\,dr\,d\psi,$$

which, in the expression for the coefficient t, will give the additional term

$$\Delta' t=-\frac{B^2}{4}p_y\lambda_1\mu.$$

In the expression for the thrust moment, we obtain the additional terms

$$\Delta'\int_0^{BR}dTr=\frac{1}{2}b\varrho a_\infty\int_0^{BR}U_x\Delta'U_y r\,dr=$$

$$=-\frac{1}{2}b\varrho a_\infty R^4\omega^2\left(\frac{B^3}{6}p_y\lambda_1\mu+\frac{B^4}{4}p_y\lambda_1\sin\psi+\frac{B^4}{4}p_x\lambda_1\cos\psi\right).$$

Substituting the expression for the thrust moment (with these additional /80 terms) into eq.(2.30), we obtain the following expressions of the flapping coefficients, with consideration of a variable law of induced velocity distribution:

$$a_0=\gamma\left[\frac{B^3}{3}\lambda+\frac{\varphi}{4}B^2(B^2+\mu^2)-\frac{B^3}{6}\mu\left(\frac{\Omega_x}{\omega}+p_y\lambda_1\right)\right]-\frac{S_{h.h}}{I_{h.h}\omega^2}; \tag{2.78}$$

$$a_1=2\mu\left(\lambda+\frac{4}{3}B\varphi\right)\frac{1}{B^2+\frac{1}{2}\mu^2}-\left(B^4\frac{\Omega_x}{\omega}+\frac{8\Omega_y}{\gamma\omega}+B^4p_y\lambda_1\right)\frac{1}{B^2\left(B^2-\frac{1}{2}\mu^2\right)}; \tag{2.79}$$

$$b_1=\frac{4}{3}\mu a_0\cdot\frac{B}{B^2+\frac{1}{2}\mu^2}-\left(B^4\frac{\Omega_y}{\omega}-\frac{8\Omega_x}{\gamma\omega}-B^4p_x\lambda_1\right)\frac{1}{B^2\left(B^2+\frac{1}{2}\mu^2\right)}. \tag{2.80}$$

Let us now derive the formula for torque in the case of a variable law of induced velocity distribution.

We find the expression for U_y^2. Let us denote

$$U_y'=U_y+\Delta'U_y;$$

$$\Delta'U_y=-p_y\lambda_1r\omega\sin\psi-p_x\lambda_1r\omega\cos\psi, \tag{2.81}$$

where U_y is taken with respect to eq.(2.24), i.e., without consideration of a variable induced velocity.

Then,

$$U_y'^2=U_y^2+2U_y\Delta'U_y+\Delta'U_y^2=$$

$$=U_y^2-2\lambda p_y\lambda_1\omega^2R\dot{r}\sin\psi-2\lambda p_x\lambda_1\omega^2Rr\cos\psi+$$

$$+2\frac{d\beta}{d\psi}p_y\lambda_1\omega^2r^2\sin\psi+2\frac{d\beta}{d\psi}p_x\lambda_1\omega^2r^2\cos\psi+$$
$$+2\beta p_y\lambda_1\mu\omega^2Rr\sin\psi\cos\psi+2\beta p_x\lambda_1\mu\omega^2Rr\cos^2\psi-2\Omega_y\omega p_y\lambda_1r^2\sin\psi\cos\psi+$$
$$+2\Omega_x\omega p_y\lambda_1r^2\sin^2\psi-2\Omega_y\omega p_x\lambda_1r^2\cos^2\psi+2\Omega_x\omega p_x\lambda_1\sin\psi\cos\psi+ \quad (2.82)$$
$$+p_y^2\lambda_1^2\omega^2r^2\sin^2\psi+2p_yp_x\lambda_1^2\omega^2r^2\sin\psi\cos\psi+p_x^2\lambda_1^2\omega^2r^2\cos^2\psi.$$

The expression for dM_t' reads

$$dM_t'=\frac{1}{2}b\varrho(c_{xp_{av}}U_x^2-a_\infty\varphi U_xU_y'-a_\infty U_y'^2)r\,dr.$$

We can represent this in the form

$$dM_t'=\frac{1}{2}b\varrho[c_{xp_{av}}U_x^2-a_\infty\varphi(U_xU_y+\Delta'U_xU_y)-$$
$$-a_\infty(U_y^2+2U_y\Delta'U_y+\Delta'U_y^2)]r\,dr$$

or

$$dM_t'=dM_t+\Delta'dM_t,$$

where

$$\Delta'dM_t=-\frac{1}{2}b\varrho a_\infty(\varphi\Delta'U_xU_y+2U_y\Delta'U_y+\Delta'U_y^2)r\,dr. \quad (2.83)$$

Substituting here the necessary expressions from eqs.(2.77) and (2.82) /81 and integrating, we obtain

$$\Delta'M_t=\frac{z_b}{2\pi}\int_0^{2\pi}\int_0^{BR}\Delta'dM_t\,d\psi=\frac{1}{2}z_bb\varrho R^4\omega^2a_\infty\left[\frac{B^3}{6}\varphi p_y\lambda_1\mu+\frac{B^4}{4}a_1p_y\lambda_1+\right.$$
$$+\frac{B^4}{8}(p_y^2+p_x^2)\lambda_1^2-\frac{B^4}{4}b_1p_x\lambda_1+\frac{B^3}{3}a_0p_x\lambda_1\mu- \quad (2.84)$$
$$\left.-\frac{B^4}{4}\left(\frac{\Omega_y}{\omega}p_x\lambda_1-\frac{\Omega_x}{\omega}p_y\lambda_1\right)\right]$$

or, setting $m_t' = m_t + \Delta'm_t$, we obtain for $\Delta'm_t$ the expression

$$\Delta'm_t=a_\infty\left[\frac{B^3}{3}\mu\left(\frac{\varphi}{2}p_y\lambda_1+a_0p_x\lambda_1\right)+\frac{B^4}{4}\left(a_1p_y\lambda_1-b_1p_x\lambda_1+\right.\right.$$
$$\left.\left.+\frac{1}{2}p_y^2\lambda_1^2+\frac{1}{2}p_x^2\lambda_1^2-\frac{\Omega_y}{\omega}p_x\lambda_1+\frac{\Omega_x}{\omega}p_y\lambda_1\right)\right]. \quad (2.85)$$

We now determine the expressions for $p_x\lambda_1$ and $p_y\lambda_1$ with the aid of eqs.(2.73) and (2.75), assuming λ to be small in comparison with μ (which holds for $\mu \geq 0.15$):

$$\left.\begin{aligned} p_x\lambda_1 &= \frac{3S_{h.h}}{2\pi\varrho R^4}\,\frac{z_b}{\mu}\,\frac{\Omega_x}{\omega};\\ p_y\lambda_1 &= \frac{3}{2}\,\frac{S_{h.h}}{\varrho\pi R^4}\,\frac{z_b}{\mu}\,\frac{\Omega_y}{\omega}. \end{aligned}\right\} \qquad (2.86)$$

Obviously, the additional terms in the expressions for the flapping coefficients and in the expression for the torque do not depend on λ.

Equations (2.86) show that the smaller the value of μ, the greater will be the influence of distortion in the induced velocity distribution. This becomes understandable if we recall that the smaller the translational velocity, the greater should be the induced velocity caused by an aerodynamic force of the same magnitude. The fact that the quantities $p_x\lambda_1$ and $p_y\lambda_1$ do not depend on λ greatly facilitates the calculation of the flapping coefficients and forces from the variable induced velocity. The calculation in this case is performed in the same manner as for a constant induced velocity, except that a_0, a_1, and b_1 are calculated from eqs.(2.78), (2.79), and (2.80) and the expression for m_t from eq.(2.48); to the obtained value, we add the term $\Delta' m_t$ calculated from eq.(2.85).

ANALYSIS OF OBTAINED RESULTS

11. Blade Flapping

To illustrate the point, we made various calculations of a rotor in curvilinear motion.

Design data:

rotor diameter, D = 14 m;
loading coefficient, σ = 0.065;
static moment of blade relative to axis of flapping hinge, $S_{h.h}$ = = 142 kg • m;
angle of blade setting, $\varphi = 3^\circ$, $a_\infty = 5.7$.

All calculations were performed for the regime of autorotation.

Figure 2.17 shows the variation in flapping coefficients, calculated for a constant value $\mu = 0.3$ and different values of the ratio $\frac{\Omega_x}{\omega}$ (rotation in transverse direction). /82 We see from Fig.2.17 that, on rotation to the left, $\left(\frac{\Omega_x}{\omega} > 0\right)$ b_1 increases while a_1 decreases, i.e., the cone described by the blades is deflected to the right and forward. In rotation to the right $\left(\frac{\Omega_x}{\omega} < 0\right)$, we have a decrease in b_1 and an increase in a_1, which indicates deflection of the cone to the left and backward. The coning angle a_0 slightly increases with rotation to the left and decreases with rotation to the right.

Consideration of the change in the induced velocity distribution leads to an even greater change in b_1 at an angular velocity Ω_x.

Curve b_1 calculated for a variable induced velocity is plotted in Fig.2.17 as a broken line. For practical purposes, we can disregard the changes in a_0 and a_1 due to variable induced velocity.

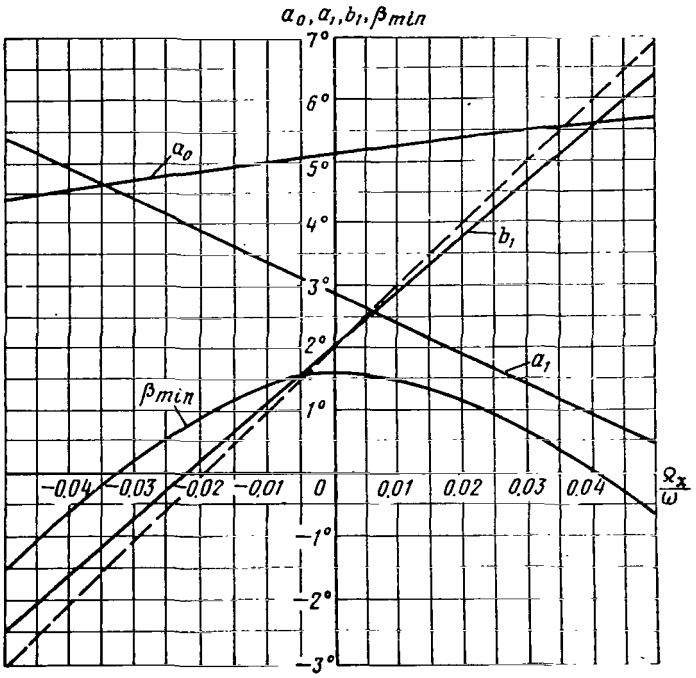

Fig.2.17 Flapping Coefficients in Transverse Rotation of Craft ($\mu = 0.3$).

Figure 2.17 also gives the curve for the values $\beta_{min} = a_0 - \sqrt{a_1^2 + b_1^2}$, which shows a marked decrease in β_{min} for rotation to either left or right. This means that the reserve of blade overhang decreases markedly toward the lower arresting device. The blades will pass lower, the greater the angular velocity of the roll and the smaller the value of γ.

Figure 2.18 gives the same curves for the case of rotation of the craft in longitudinal direction. In conformity with the foregoing, during rotation in a dive, a_1 increases and b_1 decreases, i.e., the plane of the blade tips is displaced backward and to the left, whereas during rotation in pitch it is shifted forward and to the right. Curve β_{min} shows that nose-down rotation causes the greatest decrease in β_{min}, i.e., the blades pass very far below the plane of rotation, /83 whereas pitching rotation in this sense is most favorable.

Figures 2.17 and 2.18 pertain to craft whose control is not accomplished by means of an automatic pitch control mechanism (for example, by ailerons and rudders, by deflecting the hub of autogiros with direct control). Both Figs.2.17 and 2.18 indicate that, for such craft in curvilinear motion (for example, during a sharp bank or going into a dive), the change in β_{min} may be much greater than its variation over the entire speed range of the craft in rectilinear flight. This should be taken into consideration in selecting the position of the lower arresting device of blade flapping. On a helicopter, the pilot, in deflecting the automatic pitch control, reduces the deflection of the blade cone in curvilinear flight; thus, the reserves of the angle toward the lower arresting device do not diminish so severely.

/83

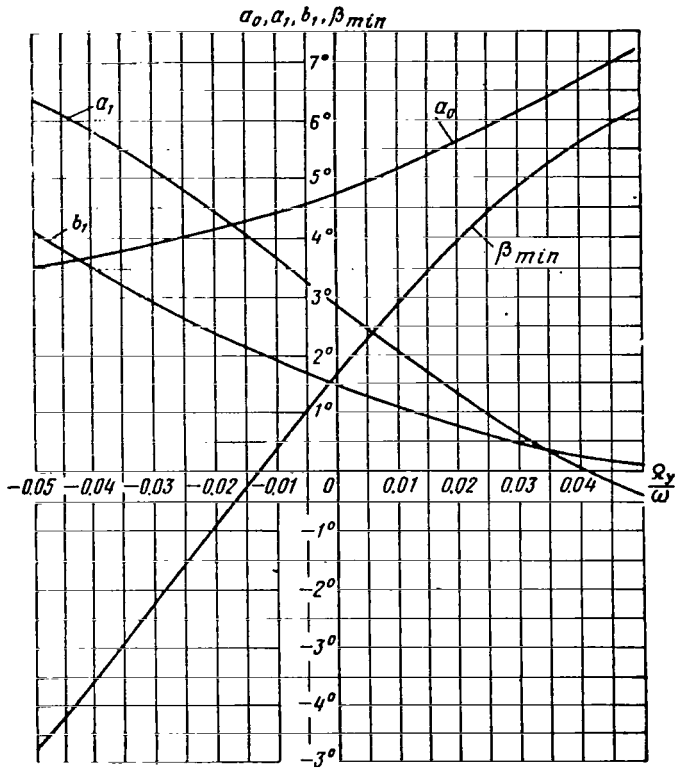

Fig.2.18 Flapping Coefficients in Longitudinal Rotation of the Craft (μ = 0.3).

/84

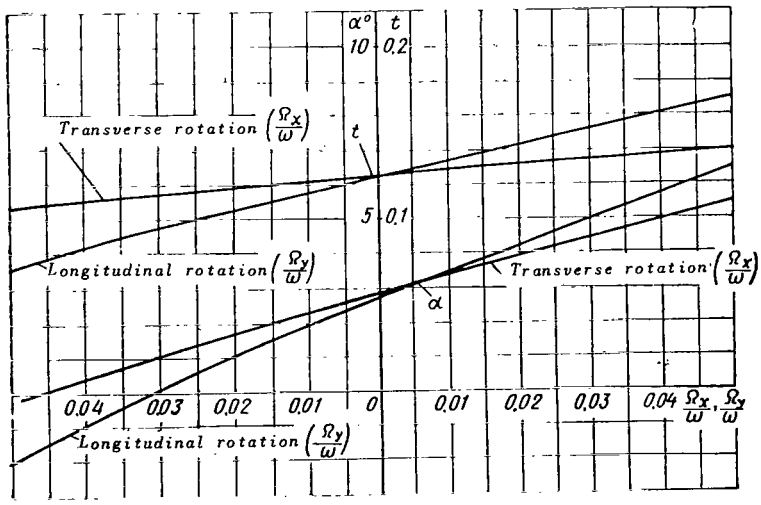

Fig.2.19 Change in Angle of Attack and Thrust Coefficient of a Rotor, as a Function of the Angular Velocity of Rotation of the Craft at Constant μ = 0.3.

12. Effect of Curvilinear Motion at Autorotation of the Rotor

In the aerodynamic calculation of a rotor in autorotating regime, eq.(2.48) is used for determining λ, which permits finding the value of λ, if $m_t = 0$ is assumed and φ, μ, Ω_x, and Ω_y are known. However, in practice this quadratic equation becomes very cumbersome after substitution of the values of a_0, a_1, and b_1. For determining the value of λ it is more convenient, after plotting the dependence of m_t on λ, to read from the graph the value of λ at which m_t vanishes. When constructing the plot of m_t, the coefficients a_0, a_1, and b_1 should be determined from eqs.(2.37), (2.38), and (2.39).

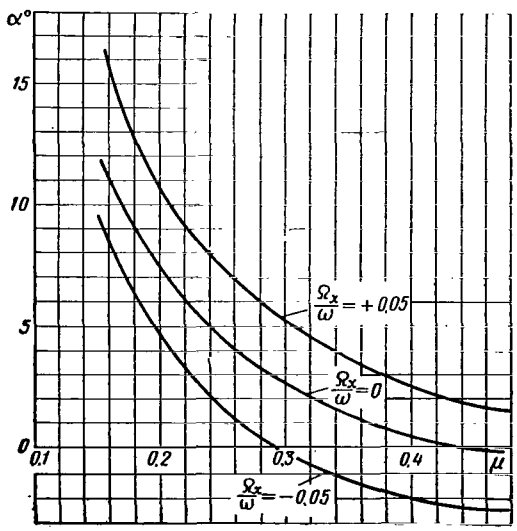

Fig.2.20 Angle of Attack of Rotor in Autorotation.

Figure 2.19 gives the values of the angle of attack of the rotor and the thrust coefficient t, obtained for a constant value $\mu = 0.3$ at different angular velocities of rotation of the craft. /84

Figure 2.19 indicates that, to maintain a constant value of μ at constant flying speed in the presence of angular velocity, the magnitude of the angle of attack must be changed and the more so, the larger the angular velocity. When the craft rotates to the left, a constant value of μ can be maintained only by increasing the angle of attack over that in rectilinear motion, whereas in rotation to the right the angle of attack must be reduced. This is explained physically by the fact that, in rotation to the left, the rotor disk is inclined forward (in addition to being inclined to the right), which reduces the angle between velocity and plane of rotation of the blade tips in space. In rotation to the right, the opposite occurs. It can be assumed that, to maintain a constant value of μ, the angle between the velocity of flow and the plane of rotation of the blade tips must remain constant at any angular velocity Ω.

Figure 2.20 gives the values of the angles of attack as a function of μ, obtained at different angular velocities of rotation of the entire craft. It can be seen that, if rotation of the axis begins and proceeds at a constant angle of attack (i.e., angle between velocity and a plane perpendicular to the rotor axis), then steady autorotation will occur only at a new value of μ, differing from the former. Thus, in rotation of the craft to the left at a constant angle of attack μ will increase and in rotation to the right, it will decrease. /85

If in addition to the angle of attack also the flying speed is kept constant, the rpm of the rotor will decrease on rotation to the left and will increase on rotation to the right.

To illustrate this phenomenon, Fig.2.21 gives the revolutions of a rotor at angles of attack of α = +4.5°, 2.8°, and 1.5° (μ_0 = 0.25, 0.30, 0.35 in rectilinear motion) as a function of the velocity of rotation in transverse direction.

The number of revolutions in rectilinear flight is taken as n_0 = 200 rpm. The rpm in the presence of rotation n_Ω is obtained from the following considerations:

$$n_0 = 9.55 \frac{V \cos \alpha}{\mu_0 R};$$

$$n_\Omega = 9.55 \frac{V \cos \alpha}{\mu_\Omega R};$$

$$n_\Omega = n_0 \frac{\mu_0}{\mu_\Omega}.$$

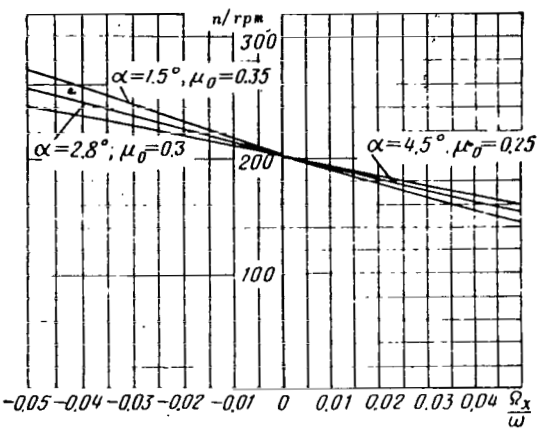

Fig.2.21 Rotor Revolutions in Autorotating Regime, as a Function of $\frac{\Omega_x}{\omega}$.

The value of μ_Ω is determined from Fig.2.20 at the intersection of the ordinate α = const with the curve $\alpha = f(\mu)$ for the corresponding angular velocity.

As a consequence of the above effect of an increase in angle of attack necessary for maintaining steady autorotation at a given μ, there exists the risk of the rotor losing autorotation at high flying speeds in the case of rotation of the craft to the left.

If the helicopter begins to rotate sharply to the left at large μ while its angle of attack remains constant, the rotor revolutions will decrease rapidly and μ will increase further. This is aggravated by the fact that the forward inclination of the resultant of the rotor, generated when the craft rotates to the left, will per se (against the will of the pilot) create a diving moment which tends to decrease the angle of attack even more. The latter circumstance, increasing the abruptness of drop in rpm as the craft rotates, involves an increase in angles of attack with respect to the blade sections, which causes flow separation and marked increase in drag.

Figures 2.22 and 2.23 give the variation in angles of attack, calculated for sections of r = 0.5 at μ = 0.3, for the case of stationary flight and for different directions of rotation of the craft. As seen here, the angles of attack with respect to the sections increase markedly on left-hand rotation and nose-down of the helicopter. This is due to the fact that, in the cases under consideration, an increase in angles of attack at angular settings of the blade of ψ = 270° and ψ = 180° (where the angles of attack of the sections are already large) is required to balance the moment of the Coriolis forces.

Taking the variable induced velocity into consideration will always increase the variation in angles of attack with respect to azimuth.

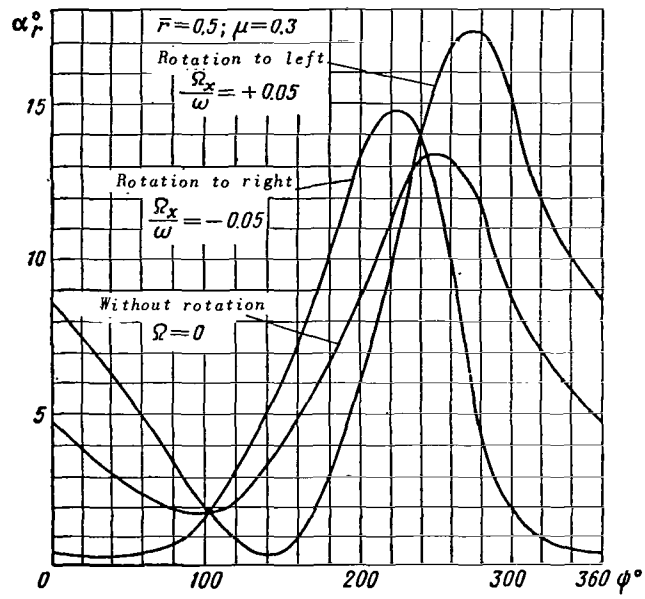

Fig.2.22 Angle of Attack of Blade Section vs. Azimuth.

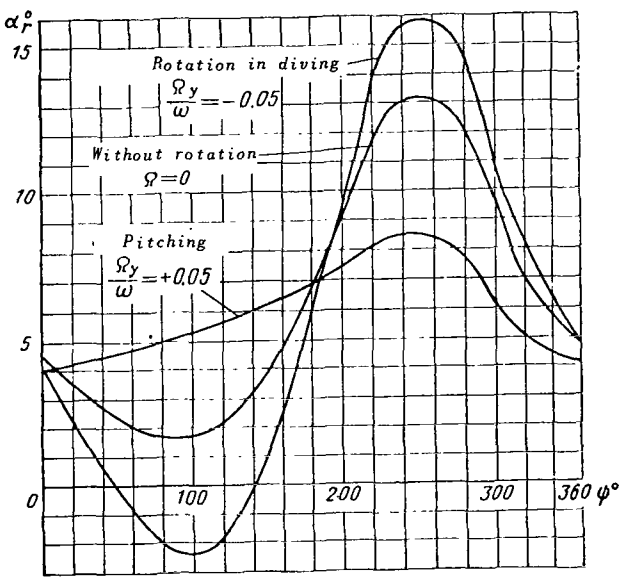

Fig.2.23 Angle of Attack of Blade Section vs. Azimuth.

Based on wind-tunnel tests /86 of blades with two profiles, of which profile No.1 has higher /87 values of $c_{y_{max}}$ and α_{cr} than profile No.2, we plotted the curves of the reserve of autorotation in Fig.2.24 (Ref.11):

$$\alpha-\alpha_0-\tan^{-1}\frac{c_x}{c_y}=f(\alpha-\alpha_0),$$

where α_0 is the angle of attack at which $c_y = 0$ for the profile. The diagram shows that, in the case $\varphi = 3^\circ$, the range of angles of attack at which an accelerating moment is produced on the blade element extends from $\alpha_r = 4^\circ$ to $\alpha_r = 15^\circ$ for the profile No.2, and is much greater for the profile No.1, reaching a value of 30°.

In profile No.2, during left-hand rotation of the craft with a ratio of $\frac{\Omega_x}{\omega} = 0.05$ at $\mu = 0.3$, a decelerating moment will be produced even on the section $\bar{r} = 0.5$, over an appreciable portion of the disk. To maintain autorotation at given μ, an even larger angle of attack of the rotor is required; if the angle of attack is kept unchanged, the rotor rpm will drop and the flapping motion will increase greatly.

This brings us to the conclusion that a constant (according to Fig.2.21) decrease in rotor rpm on left-hand rotation of the helicopter and an increase in rpm on right-hand rotation will take place only up to some small value of $\frac{\Omega_x}{\omega}$, whose magnitude is determined exclusively by the aerodynamic blade characteristics. At large values of

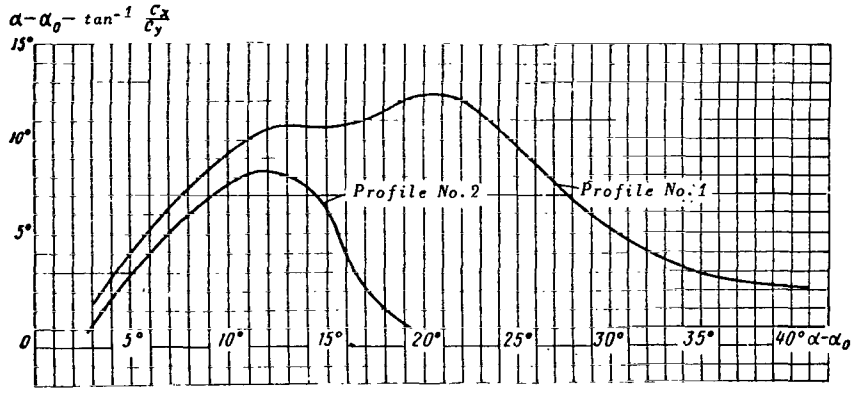

Fig.2.24 Curves of the Autorotation Reserve of Blades.

$\frac{\Omega_x}{\omega}$ the rotor rpm on rotation to the left will drop more abruptly - even as far as loss of autorotation - as a result of flow separation, whereas in rotation to the right the rpm will first cease to increase and then, at large values of $\frac{\Omega_x}{\omega}$, begin to decrease.

Thus, for a rotor with blade profiles of large autorotation reserves one can safely permit a much greater angular velocity than for a rotor with poor blade profiles.

13. Behavior of the Resultant of Aerodynamic Forces in Curvilinear Helicopter Motion

/88

According to general considerations, the resultant in the case of curvilinear helicopter motion is deflected in a manner similar to the deflection of the cone described by the blades in space. Thus, the resultant lags on the side opposite the rotation and, in addition, is deflected in a perpendicular direction by an amount proportional to the ratio $\frac{\Omega}{\omega}$.

The lag of the resultant causes, relative to the center of gravity of the craft, a moment counteracting the rotation. This constitutes a damping moment which is larger, the greater the angular velocity of rotation of the craft.

The inclination of the resultant in perpendicular direction in the case of lateral rotation causes a change in angle of attack, whereas in the case of longitudinal rotation the inclination of the craft is to the right or to the left.

Figure 2.25 gives the variation in the quantity $\frac{S}{T}$ characterizing the angle of inclination of the resultant in the lateral plane, as a function of the

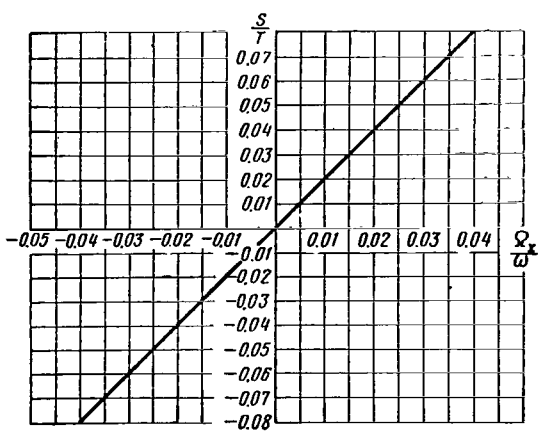

Fig.2.25 Lateral Inclination of the Resultant as a Function of the Velocity of Rotation in Transverse Direction.

angular velocity of banking $\frac{\Omega_x}{\omega}$ (at $\mu = 0.3$).

The formula for the lateral force in rectilinear motion does not yield the values of S close to full-scale values (owing to the poor convergence of the calculated flapping coefficients to the real coefficients); however, the variation in lateral force as a function of the angular velocity is correctly given by eq.(2.62).

The slope of the curve $\frac{S}{T} = f\left(\frac{\Omega_x}{\omega}\right)$ is close to that of the curve $b_1 = f\left(\frac{\Omega_x}{\omega}\right)$. This circumstance can be used for an approximate calculation of the damping forces and moments of the rotor with respect to the degree of variation in the flapping coefficients.

The magnitude of the component of the damping moment acting in the plane of angular velocity of the craft is readily determined from the formula /89

$$M = T\delta y,$$

where

y = distance between center of hub and center of gravity of the craft;
δ = angle of lag of the resultant in rotation.

According to eqs.(2.80) and (2.86), we can take, for $\mu \geq 0.2$

$$\delta = -\frac{\Omega_x}{\omega}\left(\frac{8}{\gamma} + \frac{3}{2}\frac{S_{h.h}k}{\varrho\pi R^4\mu}B^4\right)\frac{1}{B^2\left(B^2 + \frac{1}{2}\mu^2\right)}K_1.$$

Here, K_1 is a coefficient taking into account the change in the flow coefficient λ during rotation of the craft. The coefficient K_1 can be determined from experiment. If no experimental data are available, we can take $K_1 = 1$.

The intensity of interaction, expressed by the slope of the curve S/T as a function of Ω_x/ω, may decrease on further increase of this ratio above a certain value, owing to flow separation in the blade sections.

As a result of the above-described phenomenon of decrease in rpm and hence in thrust during autorotation while the craft rotates to the left (with a rotor of right rotation), the damping and thus also the controllability of the craft is less in the case of left-hand rotation than in the case of right-hand rota-

tion.

The use of an optimum supporting blade profile extends the permissible range of the angles of attack of the blade sections so much that, with proper arrangement of the helicopter, the critical magnitude of the angular velocity of rotation of the helicopter will not be reached in actual service.

EFFECT OF ROTOR PARAMETERS AND HUB DESIGN ON FLAPPING AND DAMPING OF THE ROTOR

Blade flapping and deflection of the resultant in curvilinear motion of a helicopter are affected by the characteristics of the rotor itself, which changes its aerodynamics under these conditions.

Below, we will examine the effect on flapping and damping of the rotor, the moment characteristics of the blade profile, its transverse centering, and hub design.

Let us take a hub with a flapping compensator, with kinematic dependence of the angle of blade setting on the flapping angle - such that the angle of blade setting decreases with increasing flapping angle.

14. Rotor with a Profile Having a Variable Center of Pressure

Until now, we discussed a rotor having blades with profiles of constant center of pressure and with a flexural axis coinciding with the center of pressure. Let us now examine a rotor having blades with a variable center of pressure.

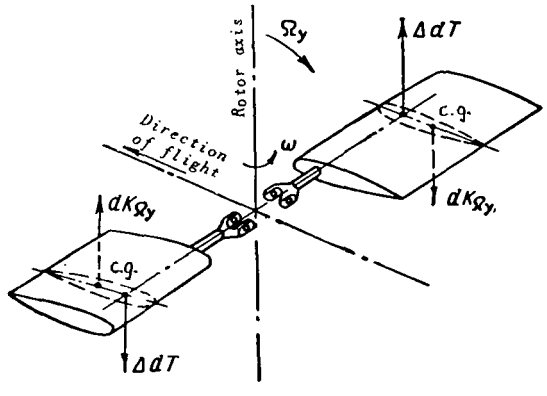

Fig.2.26 Diagram of the Effect of Coriolis Forces Producing Blade Twist in Curvilinear Motion.

Recalling the variations in the angle of attack distribution of the blade sections with respect to azimuth as they occur in curvilinear motion, it is easy to show that, if the coefficient of the moment relative to the flexural axis of the blade c_m depends on the angle of attack of the section, then the aerodynamic moment producing blade twist will vary in relation to its angular position. This, as a result of blade twisting, will cause a change in the flapping motion and in the position of the resultant. Let us suppose that the flexural axis is located aft of the aerodynamic center and that the profile, at $\alpha_r = 0$, has a diving moment /90

($c_{m0} < 0$), i.e., with increasing α_r the center of pressure of the blade section shifts forward and the diving moment c_m decreases.

As an example, let us examine the case of left-hand rotation of the craft.

The character of the angle of attack variation of the blade sections, for rotation to the left, is plotted in Fig.2.22. For the blade in forward position ($\psi = \pi$), the angles of attack decrease almost to zero whereas for the blade located aft of ($\psi = 0$) they increase appreciably. Therefore, the forward blade is twisted in diving, i.e., the angle of setting decreases, whereas the rearward blade is twisted very little (with the velocity U_x being identical in both positions).

To balance the angles of attack of such blades, providing zero hinge moment, the cone of the blades and hence the resultant should be deflected to the left. This additional inclination of the resultant to the left, occurring in left rotation, decreases the resistance of the rotor to rotation of the craft, i.e., damping, and may cause the helicopter to bank at large angular velocities. This effect produces pressure on the control stick directed toward the side of banking.

The above discussion shows that, if the flexural axis of the blade is located in front of the aerodynamic center, i.e., if $\frac{dc_m}{d\alpha} < 0$, the damping moment of the rotor resisting rotation of the craft, increases.

15. Effect of Blade Centering

If we assume that the center of gravity of the blade section is located at some distance b_f from the focus of the profile (positive b_f - backward), then during rotary motion of the rotor axis a couple, produced by the Coriolis and aerodynamic forces, arises on the blades. This is shown schematically in Fig.2.26.

The expression of the moment producing the blade twist (a positive moment will twist the blade toward an increase in angle) will have the form

$$M_b = -\int_0^R b_f (dK_{\Omega_y} + dK_{\Omega_x}).$$

Substituting dK_{Ω_x} and dK_{Ω_y} by their expression from eq.(2.7), we obtain /91

$$M_b = \int_0^R 2b_f m (\Omega_y \omega \sin\psi + \Omega_x \omega \cos\psi) r\, dr.$$

It is obvious here that the moment varies periodically.

The angle of twist of the blade, under assumption of constant mass, a value

of b_f, and torsional rigidity, is determined by the formula

$$\varphi_{twp} = \int_0^R \frac{M\,dr}{GI_p} = \frac{2}{3}\frac{b_f mR^3}{GI_p}\omega^2\left(\frac{\Omega_y}{\omega}\sin\psi + \frac{\Omega_x}{\omega}\cos\psi\right).$$

Assuming that a linearly twisted blade is equivalent to a blade with a constant angle of setting equal to the angle of setting of the first blade at the section r = 0.75 R, we find

$$\varphi_{twp_{0.75R}} = 0{,}61\,\frac{b_f mR^3}{GI_p}\omega^2\left(\frac{\Omega_y}{\omega}\sin\psi + \frac{\Omega_x}{\omega}\cos\psi\right).$$

Let us derive an additional periodic variation in angle of setting

$$\Delta\nu = \bar{\nu}_1\cos\psi + \bar{\bar{\nu}}_1\sin\psi,$$

where

$$\bar{\bar{\nu}}_1 = A\frac{\Omega_y}{\omega};\quad \bar{\nu}_1 = A\frac{\Omega_x}{\omega},\quad A = 0{,}61\,\frac{b_f mR^3\omega^2}{GI_p}.$$

The periodic variation in angle of setting leads to a variation in inclination of the cone during rotation.

The flapping coefficients take the form (for constant induced velocity)

$$\left.\begin{aligned} a_1 &= a_1' - \left(B^4\frac{\Omega_x}{\omega} + \frac{8\Omega_y}{\gamma\omega}\right)\frac{1}{B^2\left(B^2 - \frac{1}{2}\mu^2\right)} + \\ &\quad + A\frac{\Omega_y}{\omega}\frac{\left(1+\frac{3}{2}\mu^2\right)}{B^2 - \frac{1}{2}\mu^2}, \\ b_1 &= b_1' - \left(B^4\frac{\Omega_y}{\omega} - \frac{8\Omega_x}{\gamma\omega}\right)\frac{1}{B^2\left(B^2 + \frac{1}{2}\mu^2\right)} - \\ &\quad - A\frac{\Omega_x}{\omega}\frac{\left(1+\frac{3}{2}\mu^2\right)}{B^2 + \frac{1}{2}\mu^2}. \end{aligned}\right\} \qquad (2.87)$$

If the center of gravity is located aft of the aerodynamic center ($b_f > 0$, $A > 0$), an additional inclination of the cone and hence of the resultant to the side of rotation of the craft will occur. If the c.g. is ahead of the a.c., then the additional inclination increases the damping moment of the rotation.

The angles of twist $\bar{\nu}_1$ and $\bar{\bar{\nu}}_1$ are easily determined if the dynamic twist of the blade in rectilinear flight is calculated and the angle of twist ν_0 is /92

known (Ref.6). The relation between these angles is determined by the formulas

$$\left.\begin{aligned}\tilde{\nu}_1 &= \nu_0 \frac{2}{A} \frac{\Omega_y}{\omega},\\ \bar{\nu}_1 &= \nu_0 \frac{2}{A} \frac{\Omega_x}{\omega}.\end{aligned}\right\} \tag{2.88}$$

16. Rotor with Flapping Compensator

Let us now examine a rotor whose blades change in pitch φ, as a function of the flapping angle β. There are many methods of accomplishing such kinematics. Figure 2.27 shows one of the methods of changing pitch in relation to the flapping angle β (turned flapping hinge), where φ varies in accordance with the law:

$$\varphi = \theta_0 - \beta \tan\sigma_1.$$

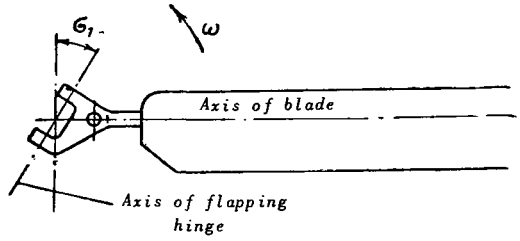

Fig.2.27 Diagram of Blade with Turned Hinge.

The flapping angle β, in this case, is the angle between the blade axis and the plane of rotation. Not wanting to complicate the results, we will take the case $\mu = 0$. The variation in flapping motion obtained for regimes with $\mu = 0$ can be extrapolated to the case $\mu > 0$.

Let the craft be inclined in space at a constant angular velocity having the components Ω_x and Ω_y.

The velocity components of the blade element will take the form

$$U_x = r\omega;$$

$$U_y = \lambda\omega R - r\frac{d\beta}{dt} + \Omega_y r\cos\psi - \Omega_x r\sin\psi.$$

Assuming $\varphi = \theta_0 - \beta \tan\sigma_1$, we construct, as above, the equation of moments relative to the horizontal (flapping) hinge for B = 1:

$$\begin{aligned}&\frac{d^2\beta}{d\psi^2} + \frac{d\beta}{d\psi}\frac{\gamma}{4} + \beta\left(1 - \frac{\gamma}{4}\tan\sigma_1\right) = \gamma\left(\frac{\lambda}{3} + \frac{\theta_0}{4}\right) +\\ &+ \frac{\gamma}{4}\frac{\Omega_y}{\omega}\cos\psi - \frac{\gamma}{4}\frac{\Omega_x}{\omega}\sin\psi - 2\frac{\Omega_y}{\omega}\sin\psi - 2\frac{\Omega_x}{\omega}\cos\psi.\end{aligned} \tag{2.89}$$

The particular solution of this equation has the usual form

$$\beta = a_0 - a_1\cos\psi - b_1\sin\psi,$$

while the coefficients of the series have the values /93

$$\left.\begin{aligned} a_0 &= \gamma\left(\frac{\lambda}{3}+\frac{\theta_0}{4}\right)\frac{1}{1+\frac{\gamma}{4}\tan\sigma_1}, \\ a_1 &= -\left[\frac{\Omega_y}{\omega}\left(\frac{8}{\gamma}+\tan\sigma_1\right)+\frac{\Omega_x}{\omega}\left(1-\frac{8}{\gamma}\tan\sigma_1\right)\right]\frac{1}{1+\tan^2\sigma_1}, \\ b_1 &= \left[\frac{\Omega_x}{\omega}\left(\frac{8}{\gamma}+\tan\sigma_1\right)-\frac{\Omega_y}{\omega}\left(1-\frac{8}{\gamma}\tan\sigma_1\right)\right]\frac{1}{1+\tan^2\sigma_1}. \end{aligned}\right\} \qquad (2.90)$$

Equations (2.90) show that, in the case of a turned hinge, the deflection of the cone described by the blades and hence the resultant will take place at a smaller phase shift than in the case of a conventional hub. The absence of phase shift means that, in transverse rotation, there should be no change in longitudinal inclination of the resultant, i.e., at $\frac{\Omega_y}{\omega} = 0$, we should have $a_1 = 0$ and, conversely, at $\frac{\Omega_x}{\omega} = 0$, $b_1 = 0$. This condition is satisfied if

TABLE 2.3

γ	8	6	4.6
σ_1, deg	45	37	30

$$\tan\sigma_1 = \frac{\gamma}{8}. \qquad (2.91)$$

The values of σ_1, shown in Table 2.3, are derived with respect to the value of γ.

TABLE 2.4

	$\gamma = 8$		$\gamma = 4.6$	
	$\sigma_1 = 0$	$\sigma_1 = 45°$	$\sigma_1 = 0$	$\sigma_1 = 30°$
a_1	$-\frac{\Omega_y}{\omega}$	$-\frac{\Omega_y}{\omega}$	$-1.74\frac{\Omega_y}{\omega}$	$-1.74\frac{\Omega_y}{\omega}$
b_1	$-\frac{\Omega_y}{\omega}$	0	$-\frac{\Omega_y}{\omega}$	0
$\tan^{-1}\frac{b_1}{a_1}$	45°	0	30°	0

It is of interest that the condition of absence of phase shift $\tan\sigma_1 = \gamma/8$ yields the same magnitude of damping (lag of the resultant) as for a rotor

without flapping compensator. For example, for longitudinal rotation we obtain the values indicated in Table 2.4.

It is obvious that the absence of phase shift in transverse rotation at constant angle of attack ensures maintenance of μ in the autorotation regime, i.e., prevents a decrease in rotor rpm or in controllability during rotation.

ROTOR FLAPPING IN CURVILINEAR MOTION OF THE ROTOR AXIS AT VARIABLE ANGULAR VELOCITY

Below, we will derive formulas for determining the flapping coefficients of blades in the presence of uniformly accelerated and harmonic oscillation of the rotor axis. For simplicity, we will take the case where $\mu = 0$. It is shown that, for both laws of variation in angular velocity of the rotor axis, the flapping coefficients and hence the longitudinal and lateral forces of the rotor will vary by the same amount - proportional to the angular velocity - as in the case of uniform rotation of the rotor axis. Furthermore, terms appear that depend on the angular acceleration of the rotor axis. /94

17. Uniformly Accelerated Rotation of the Rotor Axis

Let us first examine the case of rotation of the rotor axis in pitching at variable angular velocity*

$$\Omega_y = At. \tag{2.92}$$

Let us substitute $t = \frac{\psi}{\omega}$ and put $k = \frac{A}{\omega}$. We can then write

$$\Omega_y = k\psi. \tag{2.93}$$

We then derive the expression for forces and their moments relative to the flapping hinge.

The velocities in the blade section, assuming $v = \text{const}$, $\mu = 0$, $\Omega_y = k\psi$, $\Omega_x = 0$, and $B = 1$, can be obtained from eqs.(2.23) and (2.24):

$$\left.\begin{aligned} U_x &= r\omega, \\ U_y &= \lambda\omega R + k\psi r\cos\psi - r\frac{d\beta}{dt}. \end{aligned}\right\} \tag{2.94}$$

Then, the thrust moment takes the form

$$M_T = \frac{1}{2}\int_0^R b\varrho a_\infty(\varphi U_x^2 + U_x U_y) r\,dr = \tag{2.95}$$

---

* By turning the coordinate axes through an angle ψ_0, all results obtained below can be extrapolated to the case of rotation in any direction.

$$= \frac{1}{2} b\varrho a_\infty R^4 \omega^2 \left(\frac{\lambda}{3} + \frac{\varphi}{4} - \frac{1}{4} \frac{d\beta}{d\psi} + \frac{k\psi}{4\omega} \cos\psi \right).$$

The moment due to the Coriolis force is

$$M_K = -2I_{h.h} k\psi\omega \sin\psi. \tag{2.96}$$

The inertia force of rotational acceleration reads

$$dj_\varrho = m \frac{d\Omega_y}{dt} r \cos\psi \, dr,$$

where

$$\frac{d\Omega_y}{dt} = \frac{d(k\psi)}{dt} = k\omega.$$

The moment of this force is

$$M_{j_\varrho} = \int_0^R mk\omega \cos\psi r^2 \, dr = I_{h.h} \, k\omega \cos\psi. \tag{2.97}$$

The equations of moments relative to the flapping hinge, after canceling by $I_{h.h} \cdot \omega^2$, will take the form

$$\frac{d^2\beta}{d\psi^2} + \frac{\gamma}{4} \frac{d\beta}{d\psi} + \beta = \gamma \left(\frac{\lambda}{3} + \frac{\varphi}{4} \right) + \frac{k}{\omega} \cos\psi - 2 \frac{k}{\omega} \psi \sin\psi + \frac{\gamma}{4} \frac{k}{\omega} \times \times \psi \cos\psi - \frac{S_{h.h}}{I_{h.h} \omega^2}. \tag{2.98}$$

The particular solution to this equation has the form

$$\beta = a_0 - \bar{a}_1 \psi \cos\psi - \bar{b}_1 \psi \sin\psi - c_1 \cos\psi - d_1 \sin\psi. \tag{2.99}$$

Let us find the derivative of β with respect to ψ: /95

$$\frac{d\beta}{d\psi} = \bar{a}_1 \psi \sin\psi - \bar{a}_1 \cos\psi - \bar{b}_1 \psi \cos\psi - \bar{b}_1 \sin\psi + c_1 \sin\psi - d_1 \cos\psi;$$

$$\frac{d^2\beta}{d\psi^2} = \bar{a}_1 \psi \cos\psi + 2\bar{a}_1 \sin\psi + \bar{b}_1 \psi \sin\psi - 2\bar{b}_1 \cos\psi + c_1 \cos\psi + d_1 \sin\psi.$$

We next substitute these values into the left-hand side of eq.(2.98), yielding

$$\frac{\gamma}{4} \bar{a}_1 \psi \sin\psi - \frac{\gamma}{4} \bar{b}_1 \psi \cos\psi + \left(2\bar{a}_1 - \frac{\gamma}{4} \bar{b}_1 + \frac{\gamma}{4} c_1 \right) \sin\psi - - \left(2\bar{b}_1 + \frac{\gamma}{4} \bar{a}_1 + \frac{\gamma}{4} d_1 \right) \cos\psi + a_0 = \gamma \left(\frac{\lambda}{3} + \frac{\varphi}{4} \right) + + \frac{k}{\omega} \cos\psi - 2 \frac{k}{\omega} \psi \sin\psi + \frac{\gamma}{4} \frac{k}{\omega} \psi \cos\psi - \frac{S_{h.h}}{I_{h.h} \omega^2}. \tag{2.100}$$

Since eq.(2.100) is an identity, then, by equating the coefficients of like terms, we obtain the following system of equations for determining the coefficients of the series

$$\left.\begin{aligned} \frac{\gamma}{4}\bar{a}_1 &= -\frac{2k}{\omega}, \\ -\frac{\gamma}{4}\bar{b}_1 &= \frac{\gamma}{4}\frac{k}{\omega}, \\ 2\bar{a}_1 - \frac{\gamma}{4}\bar{b}_1 + \frac{\gamma}{4}c_1 &= 0, \\ 2\bar{b}_1 + \frac{\gamma}{4}\bar{a}_1 + \frac{\gamma}{4}d_1 &= -\frac{k}{\omega}; \end{aligned}\right\} \tag{2.101}$$

$$a_0 = \gamma\left(\frac{\lambda}{3} + \frac{\varphi}{4}\right) - \frac{S_{h.h}}{I_{h.h}\omega^2}. \tag{2.102}$$

From eqs.(2.101) we obtain

$$\bar{a}_1 = -\frac{8}{\gamma}\frac{k}{\omega}; \tag{2.103}$$

$$\bar{b}_1 = -\frac{k}{\omega}; \tag{2.104}$$

$$c_1 = -\frac{k}{\omega}\left(1 - \frac{64}{\gamma^2}\right); \tag{2.105}$$

$$d_1 = \frac{12}{\gamma}\frac{k}{\omega}. \tag{2.106}$$

Thus, the solution for β can be written in the following form:

$$\begin{aligned} \beta = \gamma\left(\frac{\lambda}{3} + \frac{\varphi}{4}\right) + \frac{8}{\gamma}\frac{k\psi}{\omega}\cos\psi + \\ + \frac{k\psi}{\omega}\sin\psi + \frac{k}{\omega}\left(1 - \frac{64}{\gamma^2}\right)\cos\psi - \frac{12}{\gamma}\frac{k}{\omega}\sin\psi. \end{aligned} \tag{2.107}$$

It is easy to see that the quantity $\frac{k\psi}{\omega}$ is none other than the ratio of the instantaneous angular velocity $\Omega = k\psi$ to the velocity ω. Thus, the coefficients of the first terms in eq.(2.107) are analogous to those previously obtained for Ω_y = const, namely

$$a_1 = -\frac{8\Omega_y}{\gamma\omega}, \quad b_1 = -\frac{\Omega_y}{\omega}.$$

The terms containing sin ψ in the expression for β are derived from the influence of inertia forces generated as a result of nonuniform rotation. In backward rotation, the inertia forces tend to lift the blade which is in the rear position; this causes a change in the flapping motion and a decrease in angles of attack so as to attain equilibrium. In so doing the axis of the cone tilts /96

to the left.

So far we have investigated the particular solution for eq.(2.98), characterizing forced oscillations of the blade. Let us now examine the general solution of eq.(2.98) without the right-hand member, i.e., the equation

$$\frac{d^2\beta}{d\psi^2}+\frac{\gamma}{4}\frac{d\beta}{d\psi}+\beta=0.$$

Setting $\gamma = 8$ in the particular case, we find the solution in the form

$$\beta=C_1e^{-\psi}+C_2\psi e^{-\psi}. \tag{2.108}$$

The general solution of eq.(2.98) then becomes

$$\begin{aligned}\beta=C_1e^{-\psi}+C_2\psi e^{-\psi}+\gamma\left(\frac{\lambda}{3}+\frac{\varphi}{4}\right)+\\ +\frac{8k\psi}{\gamma\omega}\cos\psi+\frac{k\psi}{\omega}\sin\psi-\frac{12k}{\gamma\omega}\sin\psi.\end{aligned} \tag{2.109}$$

The values of the coefficients C_1 and C_2 are found from the initial conditions $\psi = 0$; $\beta = 0$; $\beta' = 0$:

$$\left.\begin{aligned}C_1&=-\gamma\left(\frac{\lambda}{3}+\frac{\varphi}{4}\right);\\ C_2&=-\frac{4k}{\gamma\omega}+\gamma\left(\frac{\lambda}{3}+\frac{\varphi}{4}\right).\end{aligned}\right\} \tag{2.110}$$

As we see from eq.(2.108), the terms containing C_1 and C_2 decay extremely rapidly; thus, in one revolution ($\psi = 2\pi$) the degree of perturbation diminishes tenfold: $e^{-\psi} = e^{-2\pi} \approx 0.002$, $\psi e^{-\psi} \approx 0.012$.

This furnishes a justification to use only the particular solution of eq.(2.107), neglecting free oscillations of the blade, a procedure also confirmed by experiment.

A comparison with experiment showed that, under static operating conditions, the induced velocity distribution over the disk has a substantial influence on flapping; the refined formulas for the flapping coefficients are given elsewhere (Ref.8).

For a rotor with a flapping compensator, the flapping motion of the rotor is determined from the formulas:

$$a_0=\gamma\left(\frac{\lambda}{3}+\frac{\theta_0}{4}\right)\frac{1}{1+\frac{\gamma}{4}\tan\sigma_1}-\frac{S_{h.h}}{I_{h.h}\omega^2}\frac{1}{1+\frac{\gamma}{4}\tan\sigma_1}; \tag{2.111}$$

$$\bar{a}_1 = -\frac{k}{\omega}\left(\frac{8}{\gamma} + \tan\sigma_1\right)\frac{1}{1+\tan^2\sigma_1}; \tag{2.112}$$

$$\bar{b}_1 = -\frac{k}{\omega}\left(1 - \frac{8}{\gamma}\tan\sigma_1\right)\frac{1}{1+\tan^2\sigma_1}; \tag{2.113}$$

$$c_1 = -\left[\bar{a}_1\left(\tan\sigma_1 + \frac{8}{\gamma}\right) - \bar{b}_1\left(1 - \frac{8}{\gamma}\tan\sigma_1\right) + \frac{4}{\gamma}\frac{k}{\omega}\tan\sigma_1\right]\frac{1}{1+\tan^2\sigma_1}; \tag{2.114}$$

$$d_1 = -\left[\bar{a}_1\left(1 - \frac{8}{\gamma}\tan\sigma_1\right) + \bar{b}_1\left(\tan\sigma_1 + \frac{8}{\gamma}\right) + \frac{4k}{\gamma\omega}\right]\frac{1}{1+\tan^2\sigma_1}. \tag{2.115}$$

A comparison of eqs.(2.112) and (2.113) for $\bar{a}_1$ and $\bar{b}_1$ followed by comparing them with the previously obtained expressions (2.103) and (2.104) for a rotor without flapping compensator, will show that the lag of the cone and hence of the resultant in a direction opposite to the rotation will be practically the same, whereas the inclination in a perpendicular direction will decrease. /97

18. Harmonic Oscillation of the Rotor Axis

Let us now examine the case in which the rotor axis executes a harmonic oscillation in space at angular velocity

$$\Omega_y = A\sin\nu t = A\sin p\psi,$$

where $p = \frac{\nu}{\omega}$ with ν being the vibration frequency of the craft.

Since damping of the free oscillations of rotary-wing craft is small, the harmonic law describes oscillations of the craft close to the true oscillations. We again obtain the expressions for the moments of forces relative to the axis of the flapping hinge. The velocities in the blade section, assuming as usual $\mu = 0$, $B = 1$, are equal to

$$\left.\begin{aligned} U_x &= r\omega, \\ U_y &= \lambda\omega R + A\sin p\psi\, r\cos\psi - r\frac{d\beta}{dt}. \end{aligned}\right\} \tag{2.116}$$

The thrust moment is

$$M_T = \int_0^R \frac{1}{2} b\varrho a_\infty (\varphi U_x^2 + U_x U_y) r\, dr =$$

$$= \frac{1}{2} b\varrho a_\infty R^4\omega^2\left(\frac{\lambda}{3} + \frac{\varphi}{4} - \frac{1}{4}\frac{d\beta}{d\psi} + \frac{A\sin p\psi\cos\psi}{4\omega}\right). \tag{2.117}$$

The moment of the Coriolis force reads

$$M_K = -2\int_0^R mA\sin p\psi\omega r\sin\psi\, dr = -2I_{h.h}\,\omega A\sin p\psi\sin\psi. \tag{2.118}$$

The moment of the inertia force of rotational acceleration is

$$M_{j_{\mathfrak{a}}}=\int_0^R m\frac{d\Omega_y}{dt}r\cos\psi r\,dr=I_{h.h}\,Ap\omega\cos p\psi\cos\psi.$$

The equation of moments, after canceling by $I_{h.h}\cdot\omega^2$, is written in the form

$$\frac{d^2\beta}{d\psi^2}+\frac{\gamma}{4}\frac{d\beta}{d\psi}+\beta=-\frac{2A}{\omega}\sin p\psi\sin\psi+\frac{\gamma}{4}\frac{A}{\omega}\sin p\psi\cos\psi+$$
$$+\frac{A}{\omega}p\cos p\psi\cos\psi+\gamma\left(\frac{\lambda}{3}+\frac{\varphi}{4}\right). \qquad (2.119)$$

The solution to this equation (assuming that we can neglect the free motion of the blade, according to the foregoing) is found in the form of

$$\beta=a_0-a_1'\cos(p\psi-\psi)-b_1'\sin(p\psi-\psi)-a_1''\cos(p\psi+\psi)-b_1''\sin(p\psi+\psi).$$

Substituting this solution into the equation of motion of the blade, we find the values of the coefficients:

$$a_1'=\frac{A}{\omega}\,\frac{-\frac{\gamma^2}{32}(p-1)-(p^2-2p)+\frac{p}{2}(p^2-2p)}{\frac{\gamma^2}{16}(p-1)^2+(p^2-2p)^2};$$

$$b_1'=\frac{A}{\omega}\,\frac{\frac{\gamma}{8}(p^2-2p)+\frac{\gamma}{4}(p-1)-\frac{\gamma}{4}\frac{p}{2}(p-1)}{\frac{\gamma^2}{16}(p-1)^2+(p^2-2p)^2};$$

/98

$$a_1''=\frac{A}{\omega}\,\frac{\frac{\gamma^2}{32}(p+1)+(p^2+2p)+\frac{p}{2}(p^2+2p)}{\frac{\gamma^2}{16}(p+1)^2+(p^2+2p)^2};$$

$$b_1''=\frac{A}{\omega}\,\frac{\frac{\gamma}{8}(p^2+2p)-\frac{\gamma}{4}(p+1)-\frac{\gamma}{4}(p+1)\frac{p}{2}}{\frac{\gamma^2}{16}(p+1)^2+(p^2+2p)^2}.$$

Disregarding powers of p greater than the first (since p does not exceed 0.03 - 0.04) and expressing sin (pψ ± ψ) and cos (pψ ± ψ) in terms of the product of the form sin pψ cos ψ, cos pψ sin ψ, cos pψ · cos ψ, sin pψ · sin ψ, we obtain

$$\beta=a_0+\frac{8}{\gamma}\frac{A}{\omega}\sin p\psi\cos\psi-\left(\frac{64}{\gamma^2}+1\right)\frac{A}{\omega}p\cos p\psi\cdot\cos\psi+$$
$$+\frac{A}{\omega}\sin p\psi\sin\psi+\frac{4}{\gamma}\frac{A}{\omega}p\cos p\psi\sin\psi.$$

Recalling that

$$A \sin p\psi = \Omega_y,$$

$$pA \cos p\psi = \frac{d\Omega_y}{d\psi} = \frac{1}{\omega} \frac{d\Omega_y}{dt},$$

we find that the flapping motion, in the case of harmonic oscillations of the rotor axis in space, can be represented in the form

$$\beta = a_0 + \left[\frac{8}{\gamma} \frac{\Omega_y}{\omega} - \left(\frac{64}{\gamma^2} + 1 \right) \frac{d\Omega_y}{dt} \frac{1}{\omega^2} \right] \cos \psi + \left[\frac{\Omega_y}{\omega} + \frac{4}{\gamma} \frac{d\Omega_y}{dt} \frac{1}{\omega^2} \right] \sin \psi. \quad (2.120)$$

Thus, the longitudinal inclination of the cone of the rotor during rotation in a longitudinal plane will be

$$a_1 = -\frac{8}{\gamma} \frac{\Omega_y}{\omega} + \left(\frac{64}{\gamma^2} + 1 \right) \frac{d\Omega_y}{dt} \frac{1}{\omega^2}, \quad (2.121)$$

and the lateral inclination becomes

$$b_1 = -\frac{\Omega_y}{\omega} - \frac{4}{\gamma} \frac{d\Omega_y}{dt} \frac{1}{\omega^2}. \quad (2.122)$$

These expressions, relative to the magnitude of the terms proportional to the angular velocity of the rotor shaft, coincide with those previously obtained for uniform and uniformly accelerated rotation and thus can be used, in the general case of helicopter motion, for determining forces and moments of the rotor, damping the helicopter motion.

For a rotor with a flapping compensator, eqs.(2.121), (2.122) vary proportional to eqs.(2.102) - (2.106).

CHARACTERISTICS OF ROTOR AERODYNAMICS DETERMINED BY HINGED BLADE ATTACHMENT

/99

Hinged blade attachment has a substantial effect on the aerodynamics of the rotor; therefore, an understanding of the role and physical meaning of flapping motion will help the reader toward a better study of the characteristics of rotor aerodynamics. These questions are presented below. Furthermore, a simple graphic derivation of formulas for calculating the flapping coefficients is given.

19. Physical Meaning of Blade Flapping

The equation of blade flapping in steady rectilinear flight can be represented as

$$\frac{d^2\beta}{d\psi^2}+\beta=\frac{\gamma}{a_\infty}m_{h.h}-\frac{gS_{h.h}}{I_{h.h}\omega^2}, \tag{2.123}$$

where

$$\frac{\gamma}{a_\infty}=\frac{\varrho bR^4}{2I_{h.h}}; \quad m_{h.h}=\int_0^1\frac{dt}{d\bar{r}}\bar{r}d\bar{r}.$$

Here, $S_{h.h}$ is the mass static moment of the blade relative to the flapping hinge.

As shown above [see eq.(2.33)], the expression for $\frac{dt}{d\bar{r}}$ contains the flapping angle β and the angular velocity $\frac{d\beta}{d\psi}$; this demonstrates that the flapping motion relative to the flapping hinge is damped by aerodynamic forces.

Owing to appreciable aerodynamic damping [with linearization of the equation, i.e., on the assumption that $c_y = a_\infty a_r$, the average (per revolution) coefficient of $\frac{d\beta}{d\psi}$ in eq.(2.34) is equal to $\frac{\gamma}{4}B^2 \approx 1 - 1.7$], the natural oscillations of the blade rapidly die out and the flapping motion of the blade becomes a forced oscillation due to the thrust moment. Since the natural frequency of the blade is close to the rpm of the rotor [the average (per revolution) coefficient of β in eq.(2.34) is equal to 1], the blade reaches its maximum oscillation amplitude upon a variation in thrust moment with the frequency of the rotor revolutions, i.e., with respect to the first harmonic.

The correlation between the amplitudes of the second harmonic of flapping and the thrust moment is by approximately a factor of 10 less than for the first harmonic. Therefore, despite the fact that the amplitude of the second harmonic of the thrust moment is high, blade flapping occurs mainly with respect to the first harmonic.

Thus, the bulk of the flapping motion of the blade is described by the equation

$$\beta=a_0-a_1\cos\psi-b_1\sin\psi. \tag{2.124}$$

Let us substitute eq.(2.124) into the equation of flapping motion (2.123). The left-hand side of the equation is equal to a_0:

$$\frac{d^2\beta}{d\psi^2}+\beta=a_0. \tag{2.125}$$

The equation of flapping takes the form

$$\frac{\gamma}{a_\infty} m_{h.h} = a_0 + \frac{gS_{h.h}}{I_{h.h}\omega^2}. \qquad (2.126)$$

It follows from eq.(2.125) that, in each section of the blade, the sum of the inertia force of flapping and of the component of the centrifugal force normal to the blade axis is proportional to a_0 and is a constant, remaining unchanged upon rotation of the blade although the flapping angle of the blade changes. This means that the first harmonic of the moment of inertia forces relative to the horizontal hinge is equal to zero. Therefore, as shown by eq.(2.126), the thrust moment of the blade relative to the flapping hinge should be the same at all azimuths. Herein lies the basic characteristic of a rotor with flapping hinges and the physical meaning of blade flapping with respect to the first harmonic: The blade moves about the horizontal hinge so that, as a result of the redistribution of aerodynamic forces over the blade caused by the flapping, the thrust moment relative to the horizontal hinge does not change at all azimuths. /100

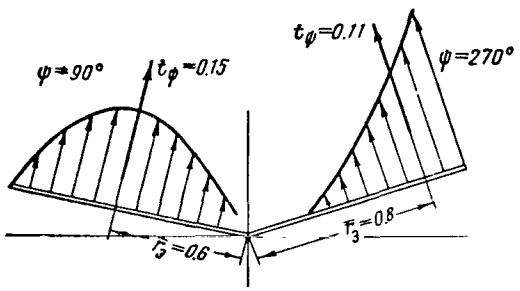

Fig.2.28 Distribution of Thrust over the Blade Radius at Identical Magnitude of Thrust Moment Relative to the Horizontal Hinge.

20. Redistribution of Aerodynamic Forces over the Rotor Disk due to Flapping

Equality of the magnitude of the thrust moment of the blade relative to the flapping hinge at every azimuth will not result in blade thrust, calculated only with consideration of the first harmonics of flapping which are the same at all azimuths, since the distribution of thrust over the radius changes from azimuth to azimuth (Fig.2.28). However, owing to flapping of the rotor with hinged blade retention, the first harmonic of the change of blade thrust decreases steeply.

The blade thrust depends on the flapping motion mainly with respect to the additional relative flow normal to the blade axis* produced during flapping of the blade elements, which changes the true angle of attack of the element. The changes which introduce first-harmonic flapping into the distribution of true angles of attack over the rotor disk are appreciable. For example, the additional vertical velocity of the air $\Delta\overline{U}_y = a_1\overline{r}$ of a blade element at azimuth $\psi = 90^\circ$ and of the same element at azimuth $\psi = 270^\circ$ is the same in magnitude but opposite in direction. However, owing to the difference in the horizontal components of the relative flow, the true angle of attack of the element decreases

* For simplicity, we will call the velocity of the air normal to the blade axis the "vertical" velocity.

little at $\psi = 90^\circ$ and increases much more at $\psi = 270^\circ$. This explains the local increase of the true angles of attack of the blade sections in the region $\psi = 270^\circ$ and the occurrence of flow separation at high flying speeds for a rotor with hinged blades (Fig.2.29).

Above, we determined the relative vertical velocity of the flow at azimuths $\psi = 90^\circ$ and $\psi = 270^\circ$. This was found equal to, respectively, $-a_1 r\omega$ and $a_1 r\omega$. The expressions have a simple explanation.

Figure 2.30 shows a rotor whose blades have different flapping angles at azimuths $\psi = 0^\circ$ and $\psi = 180^\circ$, i.e., the axis of the cone of the blades is deflected backward ($a_1 \neq 0$). Here, the blades have a maximum vertical velocity with respect to absolute magnitude on passing through azimuths $\psi = 90^\circ$ and /101

$\psi = 270^\circ$ since the blade, in the same time interval $\Delta t = \frac{\Delta\psi}{\omega}$, is vertically displaced by the largest magnitude ($p > n$). At azimuths $\psi = 0^\circ$ and $\psi = 180^\circ$, the vertical velocity of the blades is equal to zero.

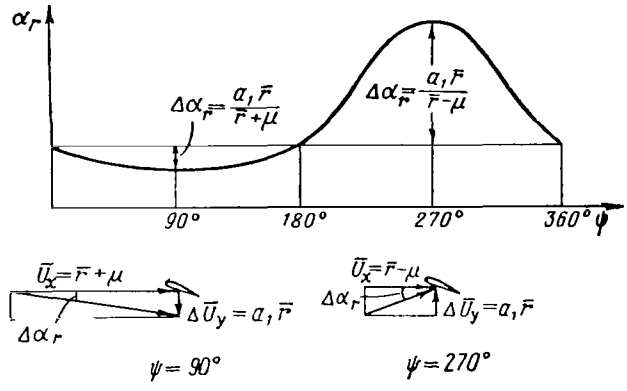

Fig.2.29 Variation in Angle of Attack of the Blade Section with Respect to Azimuth, due to Blade Flapping.

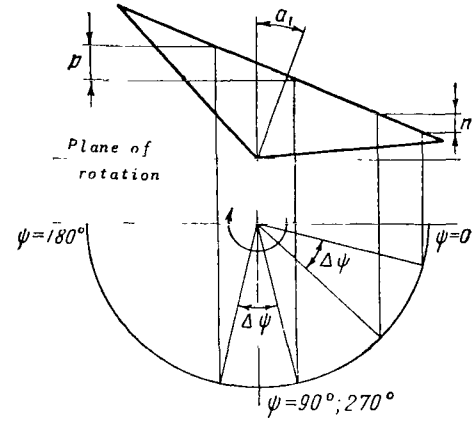

Fig.2.30 Displacement of Blade Section Relative to Plane of Rotation on Blade Turning.

Thus, a change in vertical velocity and, consequently, in true angle of attack and blade thrust at azimuths ψ and $\psi + \pi$ will take place on variations in the blade flapping angles at azimuths $\psi + \frac{\pi}{2}$ and $\psi + \frac{3}{2}$ and vice versa. Bearing this in mind, it is easy to understand how the rotor flapping will vary if, for some reason, a cyclic change of the true angles of attack takes place or an additional moment relative to the flapping hinges appears on the blades.

For example, if because of blade twisting or for some other reason the angles of attack of the sections increase to a maximum at azimuth ψ and decrease maximally at azimuth $\psi + \pi$, then an additional flapping motion of the blades is

established so that the blades occupy the lowest position at azimuth $\psi - \frac{\pi}{2}$ and, when flapping upward, reduce the true angles of attack to a value at which the condition of constancy of thrust moment relative to the horizontal hinge is observed at all azimuths. The highest position of the blades is at azimuth $\psi + \frac{\pi}{2}$ after which they drop, restoring the diminished angles of attack. Along with the variation in flapping with respect to the first harmonic, the forces H and S also vary (Fig.2.31):

$$\Delta H = T\Delta\beta\sin\psi;$$
$$-\Delta S = T\Delta\beta\cos\psi.$$

It was shown above that, despite the large first harmonic at velocity U, the first harmonic of the variation in blade thrust with respect to azimuth is relatively small, since it substantially decreases because of the flapping. The second harmonic of blade thrust is larger and the third smaller than the first harmonic. /103

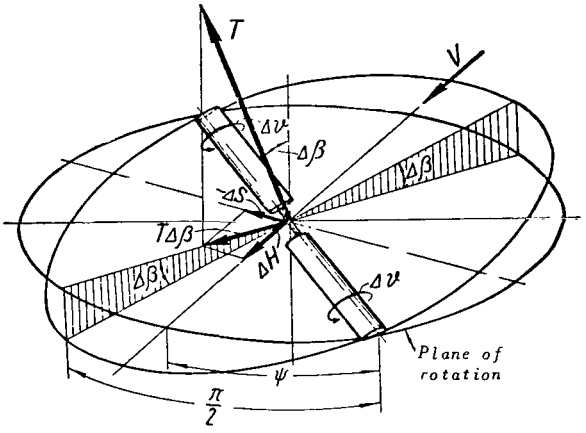

Fig.2.31 Variation in Flapping and Longitudinal and Lateral Forces due to Dynamic Twist of the Blade with Respect to the First Harmonic.

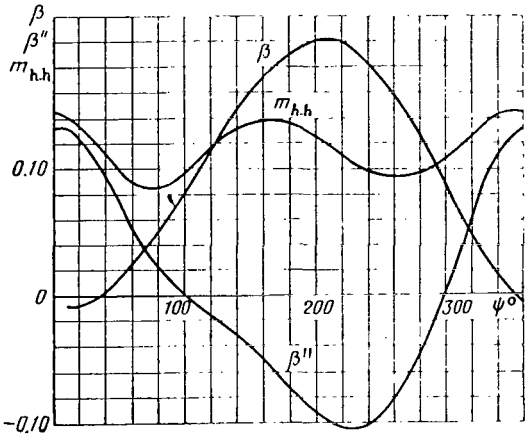

/102

Fig.2.32 Variation in Flapping Angle, Angular Acceleration of Flapping, and Thrust Moment of Blade Relative to Flapping Hinge as a Function of Azimuth.

The second harmonic of blade thrust causes second-harmonic flapping motion of the blade

$$\Delta\beta = -a_2\cos 2\psi - b_2\sin 2\psi, \tag{2.127}$$

which is equalized by the moment of inertia forces

$$I_{h.h}\omega^2\left(\frac{d^2\Delta\beta}{d\psi^2} + \Delta\beta\right) = I_{h.h}\omega^2(3a_2\cos 2\psi + 3b_2\sin 2\psi) \tag{2.128}$$

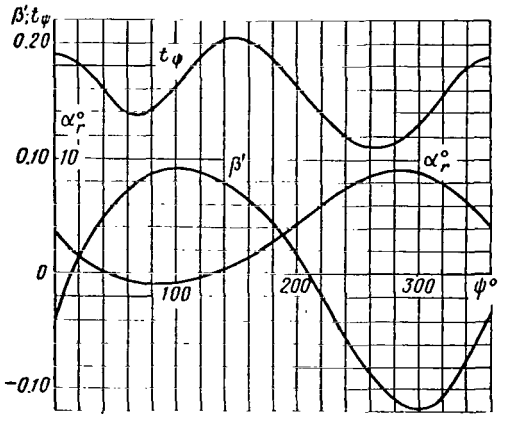

Fig.2.33 Variation in Angular Velocity of Flapping, Angle of Attack of Section at $\bar{r} = 0.975$, and Blade Thrust as a Function of Azimuth.

and creates some redistribution of aerodynamic forces of the blade with respect to azimuth, which is less extensive than for the first harmonic.

The higher harmonics of flapping are very small and have practically no effect on the blade aerodynamics.

The graphs in Figs.2.32 and 2.33 are an illustration of our statements on blade flapping and variation in aerodynamic forces with respect to azimuth. The diagrams were obtained by rough calculation, on the assumption of uniform induced velocity distribution over the rotor disk and without consideration of elastic oscillations of the blade which affect the magnitude of the upper harmonics of flapping and blade thrust.

The calculation was performed for the following initial data:

$$\bar{V}=0.30;\ t_y=0.16;\ \alpha=-9.4°;\ M_0=0.6;\ \frac{v}{a_\infty}=0.9;\ k=0,\ l_{h.h}=0.$$

The curves show the kinematic characteristics of flapping β, $\frac{d\beta}{d\psi}$, $\frac{d^2\beta}{d\psi^2}$, thrust, and thrust moment of blade t_ψ, $m_{h.h}$, and angle of attack of section α_r at $\bar{r} = 0.975$.

We see from this example and from Table 2.11 that, beginning with the second harmonic, the flapping coefficients markedly decrease and, beginning with the third harmonic, the decay coefficients of blade thrust diminish. Thus, the angle and angular velocity of flapping as well as the angle of attack of the blade section vary mainly with respect to the first harmonic, i.e., with the frequency of the rotor revolutions. The second harmonic becomes manifest in angular acceleration of the blade, whereas the blade thrust and its moment relative to the flapping hinge vary mainly with respect to the second harmonic.

21. Approximate Derivation of Formulas for Flapping Coefficients

On the basis of the properties of blade flapping, described in Subsection 19, we will derive approximate expressions for determining the flapping coefficients a_1 and b_1 obtained in Subsection 4. For simplicity, we will take B = 1 and /104 will disregard small terms of the order of μ^2 so as to obtain expressions with an accuracy to μ.

On the basis of the constancy of the thrust moment at all azimuths, we will equate the thrust moments for azimuths differing by 180°. This method permits

a better definition of the mechanism of equalization of thrust moments by means of flapping, under different conditions of blade flow at azimuths differing by 180°.

The angle of backward tilt of the axis of the rotor cone a_1 is determined from an examination of azimuths $\psi = 90^\circ$ and $\psi = 270^\circ$; the angle of sideward tilt of the axis of the cone toward the side of the advancing blade ($\psi = 90^\circ$) is determined from azimuths $\psi = 0^\circ$ and $\psi = 180^\circ$.

The superposition of the translational velocity of flight on the rotary motion of the rotor is responsible for the different operating conditions of the blades at azimuths 90° and 270°. At azimuth $\psi = 90^\circ$ the velocities are added and at azimuth $\psi = 270^\circ$, subtracted. Therefore, the coefficient a_1 is equal to zero during static operation of the rotor and increases with an increase in flying speed $V \left(\text{or } \mu = \frac{V \cos \alpha}{\omega R} \right)$.

At azimuth $\psi = 90^\circ$, the relative flow in the plane of rotation is equal to $U_x = \omega R(\bar{r} + \mu)$. Here, in the region of large velocities, the backward displacement of the axis of the rotor cone causes a lifting of the blade and a decrease in the vertical component of the relative flow $U_y = \omega R(\lambda - a_1 \bar{r})$, which reduces the true angles of attack of the sections.

At azimuth $\psi = 270^\circ$, the relative flow in the plane of rotation is small, while the vertical velocity and the true angles of attack of the sections increase: $U_x = \omega R(\bar{r} - \mu)$; $U_y = \omega R(\lambda + a_1 \bar{r})$.

Let us then construct the equations for the elementary thrust moment, take the integral from $\bar{r} = 0$ to $\bar{r} = 1$ at both azimuths and, equating the results, find the expression for a_1. We can also equate to zero the moment of the thrust difference at azimuth $\psi = 90^\circ$ and $\psi = 180^\circ$:

$$\frac{1}{a_\infty} \int_0^1 \left[\left(\frac{dt}{d\bar{r}} \right)_{\psi=90^\circ} - \left(\frac{dt}{d\bar{r}} \right)_{\psi=270^\circ} \right] \bar{r} d\bar{r} = 0, \tag{2.129}$$

where

$$\frac{1}{a_\infty} \left(\frac{dt}{d\bar{r}} \right)_{\psi=90^\circ} = \varphi (\bar{r} + \mu)^2 + (\bar{r} + \mu)(\lambda - a_1 \bar{r});$$

$$\frac{1}{a_\infty} \left(\frac{dt}{d\bar{r}} \right)_{\psi=270^\circ} = \varphi (\bar{r} - \mu)^2 + (\bar{r} - \mu)(\lambda + a_1 \bar{r}).$$

Hence,

$$a_1 = 2\mu \left(\frac{3}{4} \varphi + \lambda \right). \tag{2.130}$$

Owing to the velocity difference of the oncoming flow at azimuths $\psi = 90^\circ$ and $\psi = 270^\circ$, the quantity a_1 will vary even at the same change in angle of attack or vertical velocity for the blade at these azimuths. For example, upon an increase in angle of attack of the rotor, equal vertical velocities appear at the blade sections at azimuths $\psi = 90^\circ$ and $\psi = 270^\circ$. To have the blade thrust moment increments at these azimuths identical, the angles of attack of the

sections at azimuth $\psi = 90^\circ$ should be decreased further and, at azimuth $\psi = 270^\circ$, increased again. Obviously, this will occur upon an increase in a_1.

This is an important property of a rotor with hinged blades: Upon an increase in angle of attack of the helicopter owing to an increase in a_1, the longitudinal force H increases and a destabilizing moment appears relative to the center of gravity of the helicopter, causing an even greater increase in angle of attack; the helicopter is statically unstable with respect to the angle of attack. /105

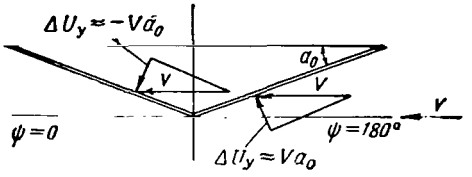

Fig.2.34 Variation in Velocity U_y as a Function of the Coning Angle a_0.

We should note that a_1 does not depend on the inertia characteristics of the blades, since a_1 equalizes the aerodynamic "asymmetry" in rotor operation.

The presence of the coning angle is responsible for the difference in vertical velocity U_y of the air relative to the blade, at azimuths $\psi = 0^\circ$ and $\psi = 180^\circ$ (Fig.2.34).

For a blade in the forward position ($\psi = 180^\circ$), the velocity of the air is directed from the bottom upward; to reduce the true angle of attack the blade, on passing the azimuths 90 - 270°, is lifted upward. During the second half of the revolution the blade drops, which increases the true angles of attack. Thus, the axis of the rotor cone is displaced laterally, toward the side of the advancing blade ($\psi = 90^\circ$).

Let us now derive the expression for the coefficient b_1. The velocity components of flow around the blade sections are equal to:

at azimuth $\psi = 0$,

$$U_x = \omega R\bar{r}; \quad U_y = \omega R(\lambda + b_1\bar{r} - \mu a_0);$$

at azimuth $\psi = 180^\circ$,

$$U_x = \omega R\bar{r}; \quad U_y = \omega R(\lambda - b_1\bar{r} + \mu a_0).$$

Equating the thrust moments of the blade at these azimuths, we obtain

$$b_1 = \frac{4}{3}\mu a_0. \tag{2.131}$$

The coefficient b_1 equalizes the aerodynamic "asymmetry" caused by the presence of a_0. Since a_0 depends on the mass characteristic of the blade γ, it follows that also b_1 depends on γ.

22. Effect of Nonuniformity of the Induced Velocity Field on the Flapping Motion

Next, we will define the variation in the flapping coefficients a_1 and b_1

for the case in which an additional vertical velocity appears on the sections and an additional periodic moment relative to the flapping hinge acts on the blade:

$$\Delta U_y = -U_1 \cos\psi - U_2 \sin\psi; \tag{2.132}$$

$$\Delta M = -M_1 \cos\psi - M_2 \sin\psi. \tag{2.133}$$

The blade thrust moment is the only moment able to balance the additional first-harmonic moment caused by a variation in the vertical velocity and in the moment ΔM.

The linear thrust of the blade receives an increment owing to a change in the flapping coefficients by a quantity Δa_1 and Δb_1. In this case, the equation of flapping has the form

$$\int_0^R dTr = I_{h.h}\omega^2 a_0 - M_1 \cos\psi - M_2 \sin\psi. \tag{2.134}$$

In conformity with eq.(2.134), we can examine the following equalities: /106

$$\left(\int_0^R dTr\right)_{\psi=90^\circ} + M_2 = \left(\int_0^R dTr\right)_{\psi=270^\circ} - M_2; \tag{2.135}$$

$$\left(\int_0^R dTr\right)_{\psi=0^\circ} + M_1 = \left(\int_0^R dTr\right)_{\psi=180^\circ} - M_1 \tag{2.136}$$

or, in dimensionless form,

$$\frac{1}{a_\infty}\left(\int_0^1 \frac{dt}{d\bar{r}}\bar{r}d\bar{r}\right)_{\psi=90^\circ} + \frac{1}{\gamma I_{h.h}\omega^2} M_2 = \frac{1}{a_\infty}\left(\int_0^1 \frac{dt}{d\bar{r}}\bar{r}d\bar{r}\right)_{\psi=270^\circ} - \frac{1}{\gamma I_{h.h}\omega^2} M_2; \tag{2.137}$$

$$\frac{1}{a_\infty}\left(\int_0^1 \frac{dt}{d\bar{r}}\bar{r}d\bar{r}\right)_{\psi=0^\circ} + \frac{1}{\gamma I_{h.h}\omega^2} M_1 = \frac{1}{a_\infty}\left(\int_0^1 \frac{dt}{d\bar{r}}\bar{r}d\bar{r}\right)_{\psi=180^\circ} - \frac{1}{\gamma I_{h.h}\omega^2} M_1. \tag{2.138}$$

The equality (2.137) can also be described differently:

$$\frac{1}{a_\infty}\int_0^1 \left[\left(\frac{dt}{d\bar{r}}\right)_{\psi=90^\circ} - \left(\frac{dt}{d\bar{r}}\right)_{\psi=270^\circ}\right]\bar{r}d\bar{r} = -2\,\frac{1}{\gamma I_{h.h}\omega^2} M_2 \tag{2.139}$$

or, expressing $\frac{dt}{d\bar{r}}$ in the form of

$$\frac{dt}{d\bar{r}} = \left(\frac{dt}{d\bar{r}}\right)_{a.v} - \left(\frac{\bar{\bar{dt}}}{d\bar{r}}\right)_1 \cos\psi - \left(\frac{\bar{\bar{\bar{dt}}}}{d\bar{r}}\right)_1 \sin\psi, \tag{2.140}$$

$$\frac{1}{a_\infty}\int_0^1 \left(\frac{\bar{\bar{dt}}}{d\bar{r}}\right)_1 \bar{r}\,d\bar{r} = \frac{1}{\gamma I_{h.h}\omega^2} M_2. \tag{2.141}$$

The physical meaning of eq.(2.141) is obvious: The flapping hinge moment, varying with respect to the first harmonic, is equalized by the moment of the first harmonic of thrust*.

Henceforth we will use the equality (2.139) and, accordingly, the equality (2.142):

$$\frac{1}{a_\infty}\int_0^1 \left[\left(\frac{dt}{d\bar{r}}\right)_{\psi=0^\circ} - \left(\frac{dt}{d\bar{r}}\right)_{\psi=180^\circ}\right]\bar{r}\,d\bar{r} = -2\frac{1}{\gamma I_{h.h}\omega^2} M_1, \tag{2.142}$$

and determine only the flapping coefficient increments. /107

Let us examine the azimuths $\psi = 90^\circ$ and $\psi = 270^\circ$ (Fig.2.35):

$$\frac{1}{a_\infty}\Delta\left(\frac{dt}{d\bar{r}}\right)_{\psi=90^\circ} = -(\Delta a_1 \bar{r} + \bar{U}_2)(\bar{r} + \mu);$$

$$\frac{1}{a_\infty}\Delta\left(\frac{dt}{d\bar{r}}\right)_{\psi=270^\circ} = (\Delta a_1 \bar{r} + \bar{U}_2)(\bar{r} - \mu);$$

$$\frac{1}{a_\infty}\left[\Delta\left(\frac{dt}{d\bar{r}}\right)_{\psi=90^\circ} - \Delta\left(\frac{dt}{d\bar{r}}\right)_{\psi=270^\circ}\right] = -2\Delta a_1 \bar{r}^2 - 2\bar{U}_2\bar{r}.$$

---

* We will give the expressions for $\left(\frac{\bar{\bar{dt}}}{d\bar{r}}\right)_1$ and $\left(\frac{\bar{dt}}{d\bar{r}}\right)_1$ (with an accuracy to μ^2):

$$\frac{1}{a_\infty}\left(\frac{\bar{\bar{dt}}}{d\bar{r}}\right)_1 = \bar{r}^2 a_1 - \mu\lambda - 2\bar{r}\mu\varphi;$$

$$\frac{1}{a_\infty}\left(\frac{\bar{dt}}{d\bar{r}}\right)_1 = \frac{1}{a_\infty}\left[\left(\frac{dt}{d\bar{r}}\right)_{a.v} - \left(\frac{dt}{d\bar{r}}\right)_{\psi=0}\right] = (\varphi\bar{r}^2 + \lambda\bar{r}) -$$
$$-[\varphi\bar{r}^2 + \bar{r}(\lambda + b_1\bar{r} - \mu a_0)] = \bar{r}\mu a_0 - \bar{r}^2 b_1.$$

However $\left(\frac{\bar{dt}}{d\bar{r}}\right)_1$ is not equal to $\left(\frac{dt}{d\bar{r}}\right)_{a.v} - \left(\frac{dt}{d\bar{r}}\right)_{\psi=90^\circ}$ since the term $-\mu a_1\bar{r}$ in the expression $\left(\frac{dt}{d\bar{r}}\right)_{\psi=90^\circ}$ is the coefficient of $\sin^2\psi$ and does not pertain to the first harmonic.

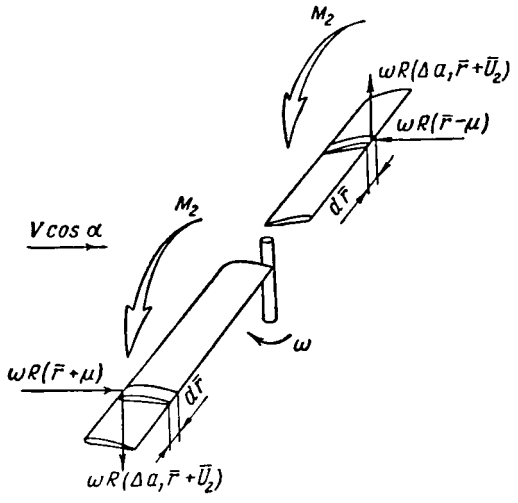

Fig.2.35 For Deriving the Expressions for Δa_1.

From the equality (2.139) we obtain

$$\Delta a_1 = -4\int_0^1 \bar{U}_2\bar{r}^2 d\bar{r} + \frac{4}{\gamma I_{h.h}\omega^2} M_2. \qquad (2.143)$$

Next, let us examine the azimuths $\psi = 0$ and $\psi = 180^\circ$ (Fig.2.36):

$$\frac{1}{a_\infty}\Delta\left(\frac{dt}{d\bar{r}}\right)_{\psi=0^\circ} = (\Delta b_1\bar{r} - \bar{U}_1)\bar{r};$$

$$\frac{1}{a_\infty}\Delta\left(\frac{dt}{d\bar{r}}\right)_{\psi=180^\circ} = -(\Delta b_1\bar{r} - \bar{U}_1)\bar{r};$$

$$\frac{1}{a_\infty}\left[\Delta\left(\frac{dt}{d\bar{r}}\right)_{\psi=0^\circ} - \Delta\left(\frac{dt}{d\bar{r}}\right)_{\psi=180^\circ}\right] = 2\Delta b_1\bar{r}^2 - 2\bar{U}_1\bar{r}.$$

From the equality (2.142) we obtain

$$\Delta b_1 = 4\int_0^1 \bar{U}_1\bar{r}^2 d\bar{r} - \frac{1}{\gamma I_{h.h}\omega^2} M_1. \qquad (2.144)$$

Using eqs.(2.143) and (2.144), we then derive the formulas for determining the flapping coefficient increments, with consideration of a nonuniform induced velocity distribution over the rotor disk. /108

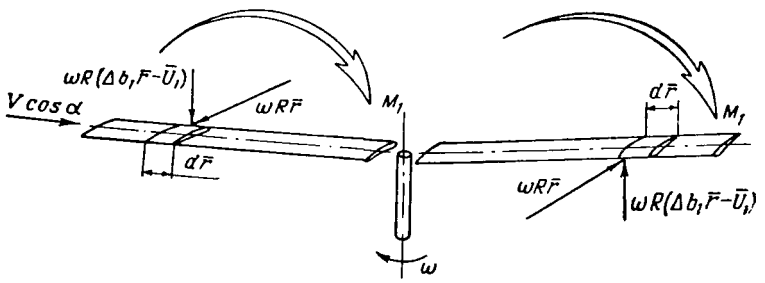

Fig.2.36 For Deriving the Expressions for Δb_1.

In first approximation, the induced velocity distribution can be described by the equation (see Fig.2.6)

$$\bar{v}(r, \psi) = \bar{v} + \bar{a}r\cos\psi. \qquad (2.145)$$

Since the positive direction of the additional vertical velocity ΔU_y is from the bottom up and that of the induced velocity from the top down, a com-

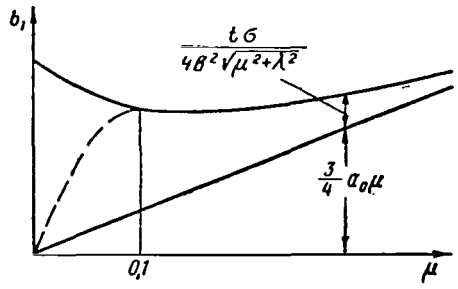

Fig.2.37 Variation in b_1 as a Function of μ.

parison of eqs.(2.145) and (2.132) will yield

$$\left.\begin{aligned}\bar{U}_1&=a\bar{r};\\ \bar{U}_2&=0.\end{aligned}\right\} \qquad (2.146)$$

Substituting eq.(2.146) into eqs.(2.143) and (2.144), we obtain the sought expressions:

$$\left.\begin{aligned}\Delta a_1&=0;\\ \Delta b_1&=4a\int_0^1\bar{r}^3d\bar{r}=a.\end{aligned}\right\} \qquad (2.147)$$

Thus, the backward deflection of the axis of the rotor cone will not change, whereas the lateral deflection will increase by an angle numerically equal to the increment of the relative induced velocity at the blade tip in both forward and rear positions. If we assume that $a = \bar{v}^*$, i.e., that the induced velocity at the leading end of the disk is equal to zero and at the trailing end equal to double the mean value, then

$$\Delta b_1=\bar{v}=\frac{t\sigma}{4B^2\sqrt{\mu^2+\lambda^2}}, \qquad (2.148)$$

while the total value of backward deflection of the cone axis will be

$$b_1=\frac{4}{3}\mu a_0+\frac{t\sigma}{4B^2\sqrt{\mu^2+\lambda^2}}. \qquad (2.149)$$

A longitudinal tilt of the induced velocity field also affects the magnitude of the longitudinal and lateral forces of the rotor. Let us derive the formulas for determining h and s:

$$h=a_\infty\left[-\frac{1}{2}\lambda\mu\varphi+\frac{1}{3}\varphi a_1+\frac{3}{4}\lambda a_1+\frac{1}{4}\mu\left(a_0^2+a_1^2\right)-\right.$$
$$\left.-\frac{a_0b_1}{6}+\frac{1}{2}\bar{v}\left(\frac{a_0}{3}+\frac{b_1\mu}{8}\right)\right]+\frac{1}{2}\mu c_{xp_{av}}; \qquad (2.150)$$

$$s=a_\infty\left\{b_1\left[\varphi\left(\frac{1}{3}+\frac{1}{2}\mu^2\right)+\frac{3}{4}\left(\lambda+\frac{1}{3}a_1\mu\right)\right]-\frac{3}{2}\mu a_0\left(\lambda+\frac{1}{2}\varphi\right)+\right. \qquad /109$$
$$\left.+a_0a_1\left(\frac{1}{6}-\mu^2\right)-\frac{1}{2}\bar{v}\left(\frac{\varphi}{3}+\lambda+\frac{7}{8}\mu a_1\right)\right\}. \qquad (2.151)$$

Equations (2.149) - (2.151) can be used at $\mu > 0.1 - 0.05$. Therefore, in Fig.2.37 which gives the curve of b_1 as a function of μ, the sector from $\mu = 0$ to $\mu = 0.1$ contains a broken curve laid approximately through the points $\mu = 0$,

* The quantity a, as related to the flight regime, can be determined from data given elsewhere (Ref.25).

at which $b_1 = 0$ and $\mu = 0.1$.

By means of eqs.(2.143) and (2.144) we can also obtain the approximate expressions for determining the flapping coefficient increments during curvilinear motion of a helicopter, which were derived in Subsection 4.

METHOD OF CALCULATING THE AERODYNAMIC CHARACTERISTICS OF A ROTOR FOR AZIMUTHAL VARIATION OF BLADE PITCH

23. Equivalent Rotor Theory

It will be shown below that a rotor whose blade pitch changes cyclically with respect to the first harmonic

$$\varphi = \varphi_0 - \bar{\varphi}_1 \cos\psi - \bar{\bar{\varphi}}_1 \sin\psi, \tag{2.152}$$

can be regarded in the aerodynamic design as a rotor with a constant pitch equal to φ_0, but with a different angle of attack. On this basis, the method of determining the aerodynamic characteristics of a rotor with a pitch variable in azimuth is called the equivalent rotor theory.

The equivalent rotor theory furnishes an explanation for the mode of variation in rotor characteristics with deflection of the automatic pitch control mechanism. The formulas for calculating $\bar{\varphi}_1$ and $\bar{\bar{\varphi}}_1$ in relation to the angle of deflection of the automatic pitch control and the kinematic characteristics of the rotor hub are given in Subsections 25 - 28. Data published earlier (Ref.15, 14) were used in presenting the material.

First, let us examine the problem formally:

Substituting eq.(2.152) into the equation of flapping and, for simplicity, retaining only the first harmonics, a series of transformations will yield

$$\begin{aligned}\frac{1}{\gamma}a_0 = {} & \frac{1}{4}\varphi_0(1+\mu^2) + \frac{1}{3}\lambda - \frac{1}{3}\bar{\bar{\varphi}}_1\mu + \left[\frac{1}{3}\mu a_0 - \frac{1}{4}b_1\left(1+\frac{1}{2}\mu^2\right) - \right. \\ & \left. - \frac{1}{4}\bar{\varphi}_1\left(1+\frac{1}{2}\mu^2\right)\right]\cos\psi + \left[\frac{2}{3}\mu\varphi_0 + \frac{1}{2}\lambda\mu + \frac{1}{4}a_1 \times \right. \\ & \left. \times\left(1-\frac{1}{2}\mu^2\right) - \frac{1}{4}\bar{\bar{\varphi}}_1 - \frac{3}{8}\bar{\bar{\varphi}}_1\mu^2\right]\sin\psi = 0.\end{aligned} \tag{2.153}$$

Below, in Subsections 23 and 24, only the pitch components φ_0, $\bar{\varphi}_1$, and $\bar{\bar{\varphi}}_1$ will be contained in the formulas so that, for simplicity, we will omit the subscript "0" of φ_0.

From eq.(2.153), the following formulas are obtained for the flapping coefficients: /110

$$a_0=\gamma\left[\frac{\lambda}{3}+\frac{1}{4}\varphi(1+\mu^2)-\frac{1}{3}\bar{\varphi}_1\mu\right]; \tag{2.154}$$

$$a_1=\frac{2\mu}{1-\frac{1}{2}\mu^2}\left(\lambda+\frac{4}{3}\varphi-\bar{\bar{\varphi}}_1\mu\right)-\bar{\bar{\varphi}}_1; \tag{2.155}$$

$$b_1=\frac{4}{3\left(1+\frac{1}{2}\mu^2\right)}a_0\mu+\bar{\varphi}_1. \tag{2.156}$$

It is obvious that, on making the substitution $\lambda_{eq} = \lambda - \bar{\bar{\varphi}}_1\mu$, eqs.(2.154) to (2.156) can be rewritten in the form

$$a_0=\gamma\left[\frac{\lambda_e}{3}+\frac{1}{4}\varphi(1+\mu^2)\right]; \tag{2.157}$$

$$a_1=\frac{2\mu}{1-\frac{1}{2}\mu^2}\left(\lambda_e+\frac{4}{3}\varphi\right)-\bar{\bar{\varphi}}_1; \tag{2.158}$$

$$b_1=\frac{4}{3\left(1+\frac{1}{2}\mu^2\right)}a_0\mu+\bar{\varphi}_1. \tag{2.159}$$

A comparison of these formulas with eqs.(2.40) for a rotor with constant pitch readily shows that a_0 and the first terms of the expressions for a_1 and b_1 coincide, provided that both rotors have equal μ and φ, and that the λ of the rotor with constant pitch is equal to λ_{eq}. Henceforth we will denote all quantities pertaining to a rotor with constant pitch by the subscript "eq" or "e" (for equivalent).

The coincidence of the formulas enables us to determine the flapping coefficients of a rotor with variable pitch from the formulas for the flapping coefficients of a rotor with constant pitch, adding $\bar{\varphi}_1$ and $\bar{\bar{\varphi}}_1$:

$$a_0=a_{0_e}; \tag{2.160}$$

$$a_1=a_{1_e}-\bar{\bar{\varphi}}_1; \tag{2.161}$$

$$b_1=b_{1_e}+\bar{\varphi}_1. \tag{2.162}$$

In so doing it is necessary to satisfy the conditions of equivalence of the rotor with variable pitch and the rotor with constant pitch:

$$\mu=\mu_e; \tag{2.163}$$

$$\lambda-\bar{\bar{\varphi}}_1\mu=\lambda_e; \tag{2.164}$$

$$\varphi=\varphi_e. \tag{2.165}$$

Now we are convinced that the following relations are satisfied:

$$\bar{U}_x=\bar{r}+\mu\sin\psi=\bar{U}_{x_e}; \tag{2.166}$$

$$(\varphi_e-\varphi)\bar{U}_x=\bar{U}_y-\bar{U}_{y_e} \tag{2.167}$$

or

$$-\Delta\varphi\bar{U}_x=(\bar{\varphi}_1\cos\psi+\bar{\bar{\varphi}}_1\sin\psi)\bar{U}_x=\Delta\bar{U}_y. \tag{2.168}$$

Actually, on the basis of eqs.(2.160) - (2.165), we represent both sides /111 of the equality (2.168) in expanded form:

$$-\Delta\varphi\bar{U}_x=(\bar{\varphi}_1\cos\psi+\bar{\bar{\varphi}}_1\sin\psi)(\bar{r}+\mu\sin\psi);$$

$$\Delta\bar{U}_y=\Delta\lambda-\bar{r}(\Delta a_1\sin\psi-\Delta b_1\cos\psi)-\mu\Delta a_0\cos\psi+\mu\Delta a_1\cos^2\psi+$$

$$+\mu\Delta b_1\sin\psi\cos\psi=\bar{\bar{\varphi}}_1\mu-\bar{r}(-\bar{\bar{\varphi}}_1\sin\psi-\bar{\varphi}_1\cos\psi)-$$

$$-\bar{\bar{\varphi}}_1\mu\cos^2\psi+\bar{\varphi}_1\mu\sin\psi\cos\psi=(\bar{\varphi}_1\cos\psi+\bar{\bar{\varphi}}_1\sin\psi)(\bar{r}+\mu\sin\psi).$$

It is obvious that the equality (2.168) is valid here.

It follows directly from eq.(2.168) that

$$\alpha_r=\varphi+\frac{U_y}{U_x}=\varphi_e+\Delta\varphi+\frac{U_{y_e}}{U_x}+\frac{\Delta U_y}{U_x}=\varphi_e+\frac{U_{y_e}}{U_x}=\alpha_{r_e}. \tag{2.169}$$

Thus, the angles of attack at all blade sections for the rotor with variable pitch and for the rotor with constant pitch equivalent to it are equal.

Likewise, we can show that

$$\frac{dt}{d\bar{r}}=\left(\frac{dt}{d\bar{r}}\right)_e; \tag{2.170}$$

$$t_\psi=t_{\psi_e}; \tag{2.171}$$

$$t=t_e. \tag{2.172}$$

Equations (2.168) - (2.170) show that a decrease or increase in linear thrust, produced by a change in pitch of the blade at a given azimuth, is due to a decrease or increase in $\bar{U}_y$ at the same azimuth when calculating on the basis of the equivalent rotor theory.

At equal thrust coefficients, the relative induced velocities are also equal

$$\bar{v}=\frac{t\sigma}{4B^2\sqrt{\mu^2+\lambda^2}}\approx\frac{t_e\sigma}{4B^2\sqrt{\mu_e^2+\lambda_e^2}}=\bar{v}_e, \tag{2.173}$$

from which it follows, based on eqs.(2.163) and (2.164), that

$$\lambda \approx \mu\alpha - \bar{v};$$

$$\lambda_e \approx \mu_e \alpha_e - \bar{v}_e;$$

$$\lambda - \lambda_e = \mu(\alpha - \alpha_e) = \bar{\bar{\varphi}}_1 \mu; \tag{2.174}$$

$$\alpha_e = \alpha - \bar{\bar{\varphi}}_1.$$

We represent the expression for $\frac{dq}{d\bar{r}}$ in the form [see eq.(3.56)]

$$\frac{dq}{d\bar{r}} \approx -\frac{dt}{d\bar{r}} \frac{\bar{U}_y}{\bar{U}_x} + c_{xp_{av}} \bar{U}_x^2. \tag{2.175}$$

Using eqs.(2.168) and (2.170), we find /112

$$\frac{dq}{d\bar{r}} = -\left(\frac{dt}{dr}\right)_e \frac{\bar{U}_{y_e}}{\bar{U}_x} + c_{xp_{av}} \bar{U}_x^2 - \left(\frac{dt}{d\bar{r}}\right)_e \frac{\Delta \bar{U}_y}{\bar{U}_x} = \left(\frac{dq}{d\bar{r}}\right)_e -$$

$$-\left(\frac{dt}{d\bar{r}}\right)_e (\bar{\varphi}_1 \cos\psi + \bar{\bar{\varphi}}_1 \sin\psi); \tag{2.176}$$

$$q_\psi = q_{\psi_e} - t_\psi (\bar{\varphi}_1 \cos\psi + \bar{\bar{\varphi}}_1 \sin\psi);$$

$$m_t = \frac{1}{2\pi} \int_0^{2\pi} d\psi \int_0^1 \frac{dq}{d\bar{r}} \bar{r} d\bar{r} = m_{t_e} - \frac{1}{2\pi} \int_0^{2\pi} (\bar{\varphi}_1 \cos\psi + \bar{\bar{\varphi}}_1 \sin\psi)\, d\psi \int_0^1 \left(\frac{dt}{d\bar{r}}\right) \bar{r} d\bar{r}. \tag{2.177}$$

Since, for a rotor with flapping hinges, the value of the integral $\int_0^1 \left(\frac{dt}{d\bar{r}}\right) \bar{r} d\bar{r}$ is constant at all azimuths, the integral with respect to ψ must be equal to zero. Consequently, the average per-revolution magnitude of the torque coefficients of the rotors is identical:

$$m_t = m_{t_e}. \tag{2.178}$$

However, at equal azimuths the values of $\frac{dq}{d\bar{r}}$, q_ψ, and m_{t_ψ} for both rotors are not the same and the rotors have a different variable component of flapping motion about the drag hinge.

Let us now derive formulas for determining the coefficients h and s of the rotor with variable pitch from the corresponding coefficients of the rotor with constant pitch: h_{eq} and s_{eq}. On the basis of eqs.(2.161), (2.162), (2.171), and (2.177) we then obtain

$$\Delta h_\psi = -t_{\psi_e} \Delta\beta \cos\psi + \Delta q_\psi \sin\psi = -t_{\psi_e} \times$$

$$\times [(\bar{\bar{\varphi}}_1 \cos\psi - \bar{\varphi}_1 \sin\psi)\cos\psi + (\bar{\varphi}_1 \cos\psi + \bar{\bar{\varphi}}_1 \sin\psi)\sin\psi] = -t_{\psi_e} \bar{\bar{\varphi}}_1; \tag{2.179}$$

$$\Delta s_\psi = -t_{\psi_e}\Delta\beta\sin\psi - \Delta q_\psi\cos\psi = t_{\psi_e}\bar{\varphi}_1. \tag{2.180}$$

Consequently,

$$\Delta h = \frac{1}{2\pi}\int_0^{2\pi}(-t_{\psi_e})\,\bar{\bar{\varphi}}_1 d\psi = -t_e\bar{\bar{\varphi}}_1;$$

$$h = h_e - t_e\bar{\bar{\varphi}}_1; \tag{2.181}$$

$$s = s_e + t_e\bar{\varphi}_1. \tag{2.182}$$

Finally, let us define the relation of the coefficients of forces in the velocity axes. It follows from eqs.(2.172), (2.174), and (2.181) that

$$t_y \approx t \approx t_{y_e}; \tag{2.183}$$

$$t_x \approx t\alpha + h = t_e\alpha_e + h_e + t_e\Delta\alpha + \Delta h = t_{x_e} + t_e\bar{\bar{\varphi}}_1 - t_e\bar{\bar{\varphi}}_1 = t_{x_e}. \tag{2.184}$$

Equations (2.183) and (2.184) show that a rotor with different $\bar{\varphi}_1$ and $\bar{\bar{\varphi}}_1$ at identical μ, λ_{eq}, φ has identical t_y and t_x. Consequently, at equal μ, t_y, t_x the rotor with a cyclic variation of pitch and the rotor with a constant pitch have equal φ, λ_{eq}, α_{eq}, but different α. This characteristic of a hinged rotor manifests itself in that, at equal t_y and t_x (at equal flying weight, speed, and altitude) but at different $\bar{\bar{\varphi}}_1$ (different centering or angles of stabilizer setting), the helicopter will have different angles of attack and angles of pitch. This is shown in Fig.2.38: The rotor with constant pitch and the rotor with variable pitch, at equal μ, t_y, t_x have equal α_{eq} but different α; consequently, the helicopter with a deflected automatic pitch control mechanism in the same flying regime will occupy a new position in space. /113

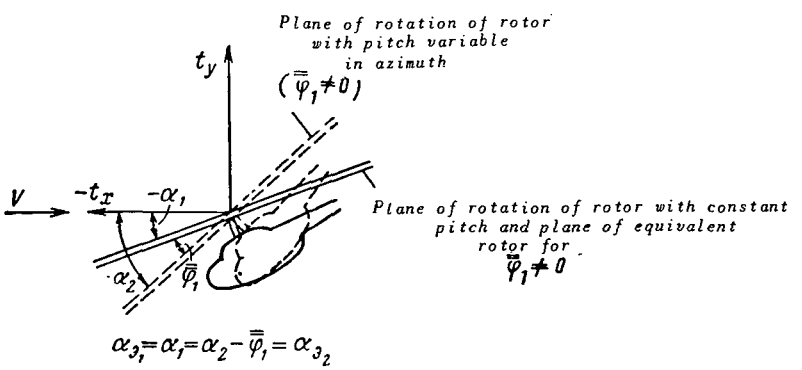

Fig.2.38 Angles of Pitch of Helicopter at Same Flying Regime but Different Deflections of Automatic Pitch Control.

An important consequence of eqs.(2.178), (2.183), and (2.184) is the possibility of mathematically determining the interdependence of the coefficients μ,

t_y, t_x, m_t irrespective of whether or not the rotor has a cyclic variation of pitch with respect to azimuth since, for any $\bar{\varphi}_1$ and $\bar{\bar{\varphi}}_1$, the coefficients t_y, t_x, m_t do not change. This property of the rotor greatly simplifies the aerodynamic design of a helicopter.

The above-derived formulas of the equivalent rotor theory will remain valid even if they are not derived from eq.(2.153) and even in the absence of assumptions of uniformity of the induced velocity field (without discarding higher harmonics of flapping) and of other assumptions. Consequently, also here transformations based on the equivalent rotor theory will hold. The higher harmonics of flapping and the loads acting on the blade in the thrust plane, for a rotor with pitch varying as a function of the first harmonic and for a rotor with constant pitch, are identical if the conditions of equivalence of the regimes (2.163) - (2.165) are satisfied.

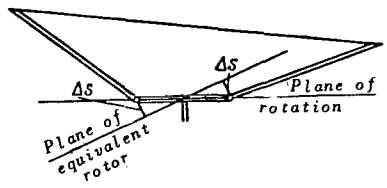

Fig.2.39 Displacement Δs of the Flapping Hinges Relative to the Plane of the Equivalent Rotor.

The equivalent rotor theory is not applicable in the case of widely spaced flapping hinges, since relative to the new reference plane, i.e., relative to the plane of the equivalent rotor, the blades execute an additional displacement Δs (Fig.2.39) together with the flapping hinges, which does not occur when calculating a rotor relative to the plane of rotation and is not taken into account in design formulas.

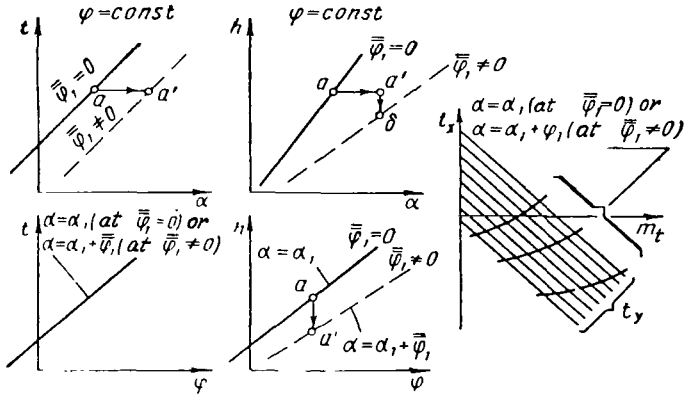

Fig.2.40 Reconstruction of the Aerodynamic Characteristics for a Rotor with Pitch Varying in Azimuth.

Finally, for a rotor with constant pitch all dimensionless characteristics are defined upon prescribing three quantities (μ, λ, φ or any other three quantities), whereas for the rotor with variable pitch five quantities (μ, λ, φ, $\bar{\varphi}_1$, $\bar{\bar{\varphi}}_1$ or any other five) must be known for determining the dimensionless /114

characteristics in the related axes.

Thus, it has been proved that the calculation of a rotor with variable pitch can be replaced by the simpler calculation of a rotor with variable pitch, i.e., stipulating equivalence of the flying regimes (2.163) - (2.165), with subsequent conversion by the above formulas.

The sequence of calculation is as follows:

From the quantities μ, λ, φ, $\bar{\varphi}_1$, $\bar{\bar{\varphi}}_1$ which are known for the rotor with variable pitch, we find μ_e, λ_e, φ_e.

We then determine a_{0_e}, a_{1_e}, b_{1_e}, t_e, m_{t_e}, h_e, s_e, t_{y_e}, t_{x_e}.

From the conversion formulas, we find a_0, a_1, ... t_x.

The equivalent rotor theory is often used in determining the aerodynamic characteristics of a rotor from graphs. If the graphs are constructed for a rotor with constant pitch, their change for a rotor with variable pitch will be as shown in Fig.2.40. In the graphs for the angle of attack at φ = const (upper plots) the curves of t are equidistantly shifted by $\Delta\alpha = \bar{\bar{\varphi}}_1$, and each point of the curves of h is shifted by $\Delta\alpha = \bar{\bar{\varphi}}_1$ to the right and by $\Delta h = -t\bar{\bar{\varphi}}_1$ downward. On the graphs for rotor pitch, at α = const (lower plots) the marking of the angles of attack is changed (for $\bar{\bar{\varphi}}_1 \neq 0$, each curve corresponds to an angle of attack greater by $\bar{\bar{\varphi}}_1$), and the curves of h, in addition, are shifted by $\Delta h = -t\bar{\bar{\varphi}}_1$. The graphs of m_t, t_y, t_x, a_0, and of higher harmonics of flapping a_n, b_n (n = 2, 3, ...) are modified like the graphs of t, whereas the graphs of s, a_1, b_1 are modified like the graphs of h. On the graphs of the aerodynamic characteristics in the velocity axes (the plot on the right in Fig.2.40) for a rotor with $\bar{\bar{\varphi}}_1 \neq 0$, the marking of the angles of attack is also changed.

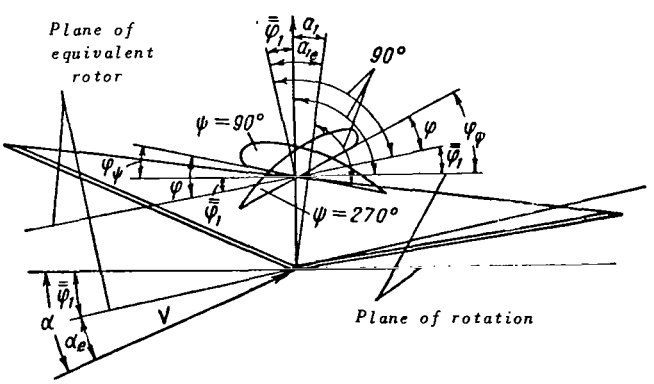

Fig.2.41 For Determining the Position of the Equivalent Rotor Plane.

Let us now derive formulas correlating the characteristics of the rotor with variable pitch and its equivalent rotor with constant pitch, on the basis of geometric relations.

Figure 2.41 gives a side view of the rotor and two blade sections at azi-

muths 90 and 270°. If we draw a plane turned about the blade axis through an angle $\Delta\varphi_{\psi=90^\circ} = -\bar{\bar{\varphi}}_1$ to the plane of rotation, then the blade pitch relative to the turned plane will be identical and equal to the mean value of pitch per revolution. This plane is the plane of the equivalent rotor. The angle of attack of the equivalent rotor $\alpha_e = \alpha - \bar{\bar{\varphi}}_1$. If $\bar{\bar{\varphi}}_1 \neq 0$, an analogous picture is obtained on viewing the rotor from the azimuth $\psi = 0$, i.e., the plane of the equivalent rotor is turned, relative to the plane of rotation, through an angle $\bar{\bar{\varphi}}_1$ in the side plane of the helicopter. /115

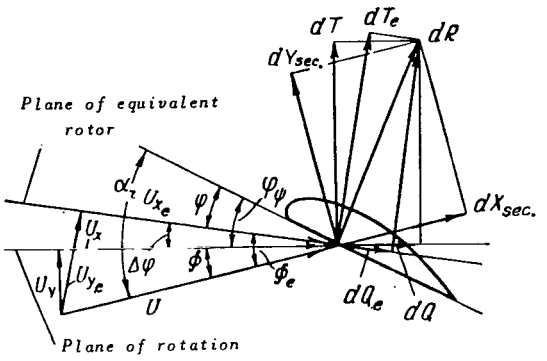

Fig.2.42 Velocity and Elementary Force Components of Blade Sections in Different Reference Planes.

Thus it is obvious that, for a rotor with pitch varying cyclically with respect to the first harmonic, we can select another plane of reference relative to which the rotor pitch does not change. Therefore, relative to the new reference plane we can determine forces, moments, and flapping of the rotor by formulas derived for the rotor with constant pitch. In so doing, it must be taken into account that the new reference plane has a different angle of attack and that the results of the calculation pertain to axes related with it and should be converted to axes related with the plane of rotation of the rotor. This constitutes the geometric meaning of the formulas derived above.

The position of the aerodynamic force of the rotor relative to the velocity vector of flight does not depend on the selection of the reference plane; therefore, its components on the velocity axes, i.e., lift and propulsive forces, are equal [see eqs.(2.183) and (2.184)].

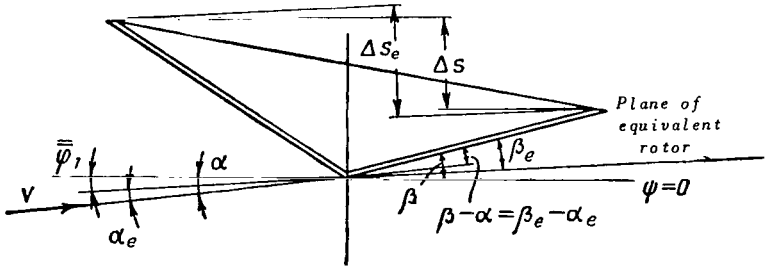

Fig.2.43 For Determining the Difference $\bar{U}_y - \bar{U}_{y_e}$ at Azimuths $\psi = 0^\circ$ and $\psi = 180^\circ$.

Let us now outline the changes occurring when calculating the elementary forces of the blade section on change-over to the new reference plane. Figure 2.42 shows the blade section at azimuth ψ. The section has a setting

angle φ_ψ relative to the plane of rotation and a setting angle φ relative to the plane of the equivalent rotor. The angle of attack of the blade section, i.e., the angle between the chord of the blade and the vector of the total relative velocity of flow around the section U, does not depend on selection of the reference plane [see eq.(2.169)]. The relations between the components of U at small values of $\Delta\varphi$ are equal [see eqs.(2.166) and (2.168)]: $\bar{U}_{x_e} \simeq \bar{U}_x$; $\bar{U}_{y_e} \simeq U_y + \bar{U}_x\Delta\varphi$ or $\Delta\bar{U}_y \simeq -\Delta\varphi\bar{U}_x$. /116

As indicated above, the last expression shows that any decrease or increase in load per unit length of the section due to a change in blade pitch at a given azimuth for an equivalent rotor with constant pitch is the result of a decrease or increase in U_y at the same azimuth.

Let us define the reason for the variation in U_y at the characteristic azimuths $\psi = 0$ and 90°. At azimuth $\psi = 0$, U_y and U_{y_e} are equal:

$$\bar{U}_y = \mu(\alpha - \beta) - \bar{v} - \bar{r}\frac{d\beta}{d\psi};$$

$$\bar{U}_{y_e} = \mu(\alpha_e - \beta_e) - \bar{v}_e - \bar{r}\left(\frac{d\beta}{d\psi}\right)_e.$$

We see from Fig.2.43 that, at $\psi = 0$, the value of β changes on changing to another reference plane by the same quantity as α so that $\alpha - \beta = \alpha_e - \beta_e$. This means $\bar{U}_y - \bar{U}_{y_e} = -\bar{r}\left[\frac{d\beta}{d\psi} - \left(\frac{d\beta}{d\psi}\right)_e\right]$.

If $\Delta\varphi = -\bar{\varphi}_1 \cos\psi$, then the plane of the equivalent rotor is inclined laterally relative to the plane of rotation by an angle $\bar{\varphi}_1$, on account of which $\frac{d\beta}{d\psi} - \left(\frac{d\beta}{d\psi}\right)_e = -\bar{\varphi}_1$ and $(\bar{U}_y - \bar{U}_{y_e})_{\psi=0} = \bar{\varphi}_1\bar{r} = -\Delta\varphi_{\psi=0}\bar{U}_{x_{\psi=0}}$.

Thus, when the pitch of the blade at azimuth $\psi = 0$ changes by $-\bar{\varphi}_1$, a change to the equivalent plane in the calculation will lead to a decrease in $\bar{U}_y$ owing to a decrease in the flapping rate relative to the plane of the equivalent rotor by a quantity equal to $\bar{\varphi}_1\bar{r}$.

If $\Delta\varphi = -\bar{\varphi}_1 \sin\psi$, then $\frac{d\beta}{d\psi} = \left(\frac{d\beta}{d\psi}\right)_e$ and $\Delta U_y = \Delta\varphi = 0$.

At azimuth $\psi = 90^\circ$, U_y is equal to

$$\bar{U}_y = \mu\alpha - \bar{v} - \bar{r}\frac{d\beta}{d\psi};$$

$$\bar{U}_{y_e} = \mu\alpha_e - \bar{v}_e - \bar{r}\left(\frac{d\beta}{d\psi}\right)_e;$$

$$\bar{U}_y - \bar{U}_{y_e} = \mu(\alpha - \alpha_e) - \bar{r}\left[\frac{d\beta}{d\psi} - \left(\frac{d\beta}{d\psi}\right)_e\right].$$

If $\Delta\varphi = -\bar{\varphi}_1 \cos\psi$, then at $\psi = 90^\circ$ $\frac{d\beta}{d\psi} = \left(\frac{d\beta}{d\psi}\right)_e$, $\alpha = \alpha_e$, and $\Delta U_y = \Delta\varphi = 0$.

If $\Delta\varphi = -\bar{\bar{\varphi}}_1 \sin\psi$, then $\alpha - \alpha_e = \bar{\bar{\varphi}}_1$, $\frac{d\beta}{d\psi} - \left(\frac{d\beta}{d\psi}\right)_e = -\bar{\bar{\varphi}}_1$* and /117

$$\Delta\bar{U}_y = \mu\bar{\bar{\varphi}}_1 + \bar{r}\bar{\bar{\varphi}}_1 = \bar{\bar{\varphi}}_1(\bar{r}+\mu) = -\Delta\varphi_{\psi=90^\circ}\bar{U}_{x\psi=90^\circ}.$$

Consequently, when the blade pitch decreases at azimuth $\varphi = 90^\circ$, the changeover to the plane of the equivalent rotor produces the same decrease in aerodynamic force as a result of the fact that $U_{y_e} < U_y$ owing to a decrease in angle of attack of the equivalent rotor and an increase in flapping rate relative to the equivalent rotor.

In conformity with Fig.2.42, the formulas for converting the load per unit length in the blade section will be

$$\frac{dt}{d\bar{r}} = \left(\frac{dt}{d\bar{r}}\right)_e;$$

$$\frac{dq}{d\bar{r}} = \left(\frac{dq}{d\bar{r}}\right)_e + \left(\frac{dt}{d\bar{r}}\right)_e \Delta\varphi.$$

Thus, all formulas of the equivalent rotor theory are in essence only formulas for converting from one system of axes to another.

24. Derivation of Formulas for a Rotor with Flapping Hinges as for a Rotor without Hinges. Conditions of Equivalence of Hinged and Rigid Rotors

In the Glauert-Lock theory, when deriving formulas for the coefficients of forces, torque, and flapping, the flapping angle of the direction of forces in space is reckoned from a plane relative to which the setting angle of the blade in rotation remains constant. Obviously the plane of the equivalent rotor meets these requirements.

In this Subsection, we will derive formulas for the coefficients of forces and torque of a rotor, except that we conceive the hinged rotor as rigid relative to the axis of the cone described by the blades. In so doing, we will take the plane of the blade tips as the reference plane rather than the plane of the equivalent rotor. Relative to this new plane, the blade setting angle changes in rotation but there is no flapping; this simplifies the expression for the velocity component of the flow past the blade U_y normal to the reference plane. Since U_y enters the expressions for elementary forces more complexly than the setting angle, the formulas for the coefficients of forces and torque in the tip plane are simplified.

This method gives individual formulas applicable to the calculation of a

* Figure 2.43 shows the displacements of the blade Δs relative to the plane of rotation and plane of equivalent rotor during a half-revolution of the blade; it is obvious that $\left(\frac{d\beta}{dt}\right)_e > \frac{d\beta}{dt}$.

rotor both with constant blade setting and with a setting angle variable relative to the plane of rotation.

Occasionally, approximate expressions for the longitudinal and lateral forces of the rotor enter the aerodynamic calculations and especially the stability calculations:

$$\left.\begin{aligned} h &= ta_1; \\ s &= tb_1. \end{aligned}\right\} \qquad (2.185)$$

Obviously, these expressions are valid if the forces directed parallel to the plane of the blade tips are equal to zero, i.e., if the resultant of all aerodynamic forces is perpendicular to the plane of the tips. /118

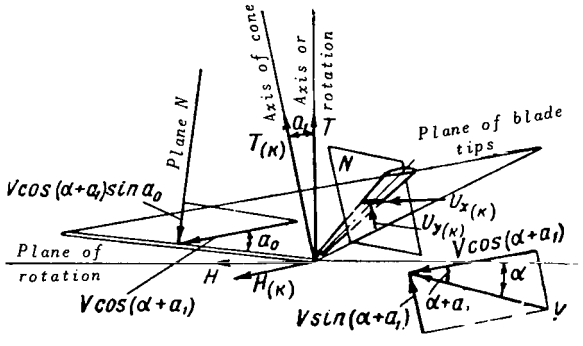

Fig.2.44 Velocity Components of Flow Past the Blade.

The obtained expressions for the coefficients of forces parallel to the plane of the blade tips are additions for refining eqs.(2.185).

Finally, we will derive various formulas while retaining the assumptions of the Glauert-Lock theory. Blade flapping can be taken into account only with an accuracy to the first harmonic. For a rotor with infinitely heavy blades (a_0 = b_1 = s = 0, the coefficients of higher harmonics of flapping are also equal to zero) such formulas were derived by Lock (Ref.37).

Let us now derive these formulas.

The velocity components of flow past the blade in a plane normal to its axis (Fig.2.44, plane N) are the component parallel to the plane of the blade tips

$$U_{x_{(\kappa)}} \approx \omega r + V\cos(\alpha+a_1)\sin\psi \approx \omega R(\bar{r}+\mu\sin\psi) = \omega R\bar{U}_{x_{(\kappa)}}, \qquad (2.186)$$

and the component normal to $U_{x_{(\kappa)}}$

$$\begin{aligned} U_{y_{(\kappa)}} &\approx V\sin(\alpha+a_1) - v - V\cos(\alpha+a_1)\cos\psi\sin a_0 \approx \\ &\approx \omega R(\lambda+\mu a_1 - a_0\mu\cos\psi) = \omega R(\lambda_{(\kappa)} - a_0\mu\cos\psi) = \omega R\bar{U}_{y_{(\kappa)}}, \end{aligned} \qquad (2.187)$$

where

$$\lambda_{(\kappa)} = \lambda + a_1\mu; \qquad (2.188)$$

$\lambda_{(\kappa)}$ characterizes the velocity of the airflow through the plane of the blade tips.

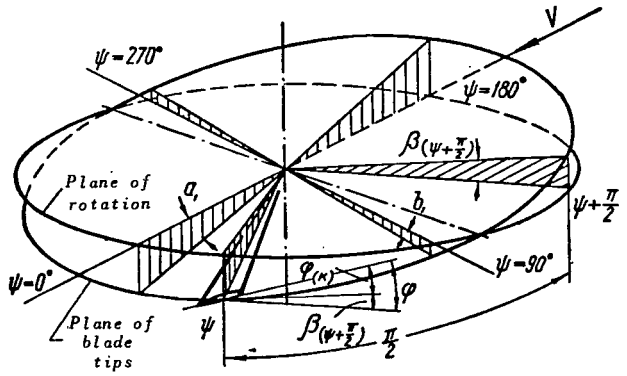

Fig.2.45 For Determining the Blade Setting Angle Relative to the Plane of the Blade Tips.

Let us first examine a rotor having a pitch constant with respect to azimuth. In the section normal to the blade axis at azimuth ψ, the angle between the plane of rotation and the plane of the blade tips is equal to $\beta_{\psi+\frac{\pi}{2}} = a_1 \sin\psi - b_1 \cos\psi$ (Fig.2.45). Therefore, the relation between the quantities pertaining to the plane of rotation and the plane of the tips, in conformity with Fig.2.46, is as follows:

$$\varphi_{(к)} = \varphi - \beta_{\psi+\frac{\pi}{2}} = \varphi - a_1 \sin\psi + b_1 \cos\psi; \quad (2.189)$$

$$U_{x_{(к)}} \approx U_x; \quad (2.190)$$

/119

$$U_{y_{(к)}} \approx U_y + U_x \beta_{\psi+\frac{\pi}{2}} = U_y + U_x (a_1 \sin\psi - b_1 \cos\psi); \quad (2.191)$$

$$T_{(к)} \approx T; \quad (2.192)$$

$$Q_{(к)} = Q - T\beta_{\psi+\frac{\pi}{2}} = Q - T(a_1 \sin\psi - b_1 \cos\psi). \quad (2.193)$$

The expression for the angle of attack of the blade section obviously should not depend on the selection of the reference plane. We will demonstrate this, after substituting eqs.(2.189) - (2.191) into the expression for the angle of attack of the section:

$$\alpha_r = \varphi + \tan^{-1}\frac{U_y}{U_x} \cong \varphi + \frac{U_y}{U_x} = \frac{\varphi U_x + U_y}{U_x} = \frac{\varphi U_x + U_{y_{(к)}} - U_x \beta_{\psi+\frac{\pi}{2}}}{U_x} =$$

$$= \frac{\left(\varphi - \beta_{\psi+\frac{\pi}{2}}\right) U_{x_{(к)}} + U_{y_{(к)}}}{U_{x_{(к)}}} = \frac{\varphi_{(к)} U_{x_{(к)}} + U_{y_{(к)}}}{U_{x_{(к)}}} = \alpha_{r_{(к)}}. \quad (2.194)$$

The expressions for the coefficients of aerodynamic forces of a blade element in the plane N have the usual form (see Fig.2.46):

$$\left(\frac{dt}{dr}\right)_{(к)} = (c_y \cos\Phi_{(к)} + c_{xp} \sin\Phi_{(к)}) \overline{U}_x^2 \approx a_\infty (\varphi_{(к)} \overline{U}_x^2 + \overline{U}_{y_{(к)}} \overline{U}_x);$$

$$\left(\frac{dq}{dr}\right)_{(к)} = (c_{xp} \cos\Phi_{(к)} - c_y \sin\Phi_{(к)}) \overline{U}_x^2 \approx c_{xp} \overline{U}_x^2 - a_\infty (\varphi_{(к)} \overline{U}_x \overline{U}_{y_{(к)}} + \overline{U}_{y_{(к)}}^2).$$

Omitting intermediate computations, we can give the final formulas:

$$\left(\frac{dt}{d\bar{r}}\right)_{(\kappa)} = a_\infty\left[\varphi_{(\kappa)}\left(\bar{r}^2+\frac{1}{2}\mu^2\right)+\lambda_{(\kappa)}\bar{r}+\mu\left(2\varphi_{(\kappa)}\bar{r}+\lambda_{(\kappa)}\right)\sin\psi-\right.$$
$$\left.-a_0\mu\bar{r}\cos\psi-\frac{1}{2}a_0\mu^2\sin 2\psi-\frac{1}{2}\mu^2\varphi_{(\kappa)}\cos 2\psi\right]; \qquad (2.195)$$

$$\left(\frac{dq}{d\bar{r}}\right)_{(\kappa)} = c_{xp_{\text{ср}}}\left(\bar{r}^2+\frac{1}{2}\mu^2\right)+a_\infty\left(\varphi_{(\kappa)}\lambda_{(\kappa)}\bar{r}-\lambda_{(\kappa)}^2-\frac{1}{2}a_0^2\mu^2\right)+$$
$$+\left(2\mu c_{xp_{a\nu}}\bar{r}-a_\infty\varphi_{(\kappa)}\lambda_{(\kappa)}\mu\right)\sin\psi+a_\infty\left(2\mu\lambda_{(\kappa)}a_0+\varphi_{(\kappa)}a_0\mu\bar{r}\right)\cos\psi+$$
$$+\frac{1}{2}a_\infty a_0\varphi_{(\kappa)}\mu^2\sin 2\psi-\frac{1}{2}\mu^2\left(c_{xp_{a\nu}}+a_\infty a_0^2\right)\cos 2\psi, \qquad (2.196)$$

where $c_{xp_{av}}$ is the average value of c_{xp} over the disk.

To determine $\frac{dq}{d\bar{r}}$ we must use eq.(2.193): /120

$$\frac{dq}{d\bar{r}}=\left(\frac{dq}{d\bar{r}}\right)_{(\kappa)}+\left(\frac{dt}{d\bar{r}}\right)_{(\kappa)}\left(a_1\sin\psi-b_1\cos\psi\right). \qquad (2.197)$$

Substituting $\varphi_{(k)}$ with respect to eq.(2.189) into the expression for $\left(\frac{dt}{dr}\right)_{(k)}$ and integrating, we obtain

$$t_{(\kappa)}=a_\infty\left[\frac{1}{2}\left(\lambda_{(\kappa)}-a_1\mu\right)+\frac{\varphi}{3}\left(1+\frac{3}{2}\mu^2\right)\right]=$$
$$=a_\infty\left[\frac{1}{2}\lambda+\frac{\varphi}{3}\left(1+\frac{3}{2}\mu^2\right)\right]=t. \qquad (2.198)$$

Since, in reality, the rotor blades have flapping hinges, the condition of flapping motion

$$\frac{1}{\gamma}a_0=\int_0^1\left(\frac{dt}{d\bar{r}}\right)\bar{r}d\bar{r}, \qquad (2.199)$$

is satisfied, which yields

$$a_0=\gamma\left[\frac{1}{3}\left(\lambda_{(\kappa)}-a_1\mu\right)+\frac{\varphi}{4}\left(1+\mu^2\right)\right]=\gamma\left[\frac{\lambda}{3}+\frac{\varphi}{4}\left(1+\mu^2\right)\right]; \qquad (2.200)$$

$$a_1=\frac{2\mu}{1+\frac{3}{2}\mu^2}\left(\lambda_{(\kappa)}+\frac{4}{3}\varphi\right)=\frac{2\mu}{1-\frac{1}{2}\mu^2}\left(\lambda+\frac{4}{3}\varphi\right); \qquad (2.201)$$

$$b_1=\frac{4a_0\mu}{3\left(1+\frac{1}{2}\mu^2\right)}. \qquad (2.202)$$

Let us derive the expressions for the coefficients of longitudinal and lateral forces parallel to the plane of the blade tips.

The elementary longitudinal and lateral forces are equal to

$$\left(\frac{dh}{d\bar{r}}\right)_{(\kappa)}=\left(\frac{dq}{d\bar{r}}\right)_{(\kappa)}\sin\psi-\left(\frac{dt}{d\bar{r}}\right)_{(\kappa)}a_0\cos\psi; \tag{2.203}$$

$$\left(\frac{ds}{d\bar{r}}\right)_{(\kappa)}=-\left(\frac{dq}{d\bar{r}}\right)_{(\kappa)}\cos\psi-\left(\frac{dt}{d\bar{r}}\right)_{(\kappa)}a_0\sin\psi. \tag{2.204}$$

Substituting eqs.(2.195) and (2.196) into these equations and integrating /121 the elementary forces over the blade radius and azimuths, we obtain the following expressions for the coefficients of average per-revolution forces:

$$h_{(\kappa)}=\frac{c_x p_{av}\mu}{2}-\frac{a_\infty}{2}\left[\lambda_{(\kappa)}\left(\varphi\mu-\frac{a_1}{2}\right)-\frac{a_0}{2}\left(a_0\mu-\frac{2b_1}{3}\right)\right]; \tag{2.205}$$

$$s_{(\kappa)}=-\frac{a_\infty}{2}\left\{a_0\left[\frac{3}{2}\varphi\mu-\frac{a_1}{3}(1+3\mu^2)\right]+3\lambda_{(\kappa)}\left(a_0\mu-\frac{b_1}{6}\right)\right\}. \tag{2.206}$$

With consideration of these expressions, the coefficients of longitudinal and lateral forces of the rotor are equal to

$$h=h_{(\kappa)}+ta_1; \tag{2.207}$$

$$s=s_{(\kappa)}+tb_1. \tag{2.208}$$

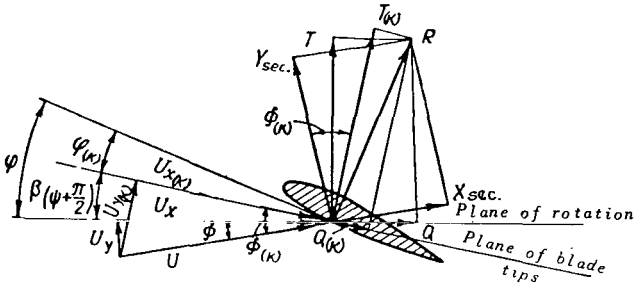

Fig.2.46 Velocity and Elementary Force Components of the Blade Section for Different Reference Planes.

Calculations show that use of the approximate formulas (2.185) leads to an error in determining h, equal to 10 - 30% (toward the side of a decrease, a larger figure always pertains to small thrust coefficients t). The derivatives of the coefficient h with respect to μ, α, φ can be determined from eq.(2.185). Determination of the coefficient s and its derivatives by means of eq.(2.186) gives a result differing greatly from calculations by means of eq.(2.208). Equation (2.208), just as eq.(2.61) of the Glauert-Lock theory, at uniform induced velocity distribution, only approximately determines s, but calculations by means of eq.(2.208) are closer to the experimental data than calculations by means of eq.(2.185).

Practical calculations show that the value of the coefficient s in autorotation is close to zero and amounts to only a small portion of the value of the product tb_1. At average values of m_t (horizontal flying regime) the value of s is smaller than that of tb_1 and we can roughly consider $s = \frac{1}{2}tb_1$. At maximum power conditions, the value of s is equal to or higher than tb_1.

The torque coefficient of the rotor is determined from the expression

$$m_{t_{(\kappa)}} = \frac{1}{2\pi}\int_0^{2\pi} d\psi \int_0^1 \left(\frac{dq}{d\bar{r}}\right)_{(\kappa)} \bar{r}\,d\bar{r}. \tag{2.209}$$

Since eq.(2.209) provides for integration with respect to ψ within limits from zero to 2π, all harmonics of the expression for $\left(\frac{dq}{d\bar{r}}\right)_{(\kappa)}$ vanish on integration. Therefore, it suffices to substitute into eq.(2.209) only the center portion of $\left(\frac{dq}{d\bar{r}}\right)_{0(\kappa)}$:

$$\left(\frac{dq}{d\bar{r}}\right)_{0(\kappa)} = \frac{1}{2} c_{xp_{av}} \mu^2 + c_{xp_{av}} \bar{r}^2 + a_\infty \left[\frac{1}{2} a_1 \lambda_{(\kappa)} \mu - \right.$$
$$\left. - \frac{1}{2} a_0^2 \mu^2 - \lambda_{(\kappa)}^2 - \left(\varphi \lambda_{(\kappa)} - \frac{1}{2} a_0 b_1 \mu\right)\bar{r}\right]. \tag{2.210}$$

Substituting eq.(2.210) into eq.(2.209) and integrating, we obtain

$$m_{t_{(\kappa)}} = -\frac{1}{2} a_\infty \left[\lambda_{(\kappa)}\left(\lambda_{(\kappa)} + \frac{2}{3}\varphi - \frac{a_1\mu}{2}\right) + \frac{a_0\mu}{2}\left(a_0\mu - \frac{2}{3} b_1\right)\right] +$$
$$+ \frac{1}{4} c_{xp_{av}} (1+\mu^2). \tag{2.211}$$

We will demonstrate that $m_t = m_{t_{(\kappa)}}$. In fact, using eq.(2.197), we find m_t: /122

$$m_t = \frac{1}{2\pi}\int_0^{2\pi} d\psi \int_0^1 \left[\left(\frac{dq}{d\bar{r}}\right)_{(\kappa)} + \left(\frac{dt}{d\bar{r}}\right)_{(\kappa)} (a_1 \sin\psi - b_1 \cos\psi)\right] \bar{r}\,d\bar{r} =$$
$$= m_{t_{(\kappa)}} + \frac{1}{2\pi}\int_0^{2\pi} (a_1 \sin\psi - b_1 \cos\psi)\, d\psi \int_0^1 \frac{dt}{d\bar{r}}\, \bar{r}\,d\bar{r}. \tag{2.212}$$

It is known from the equation of blade flapping relative to the flapping hinge that the expression for the thrust moment of the blade $\left(\int_0^1 \frac{dt}{d\bar{r}}\,\bar{r}d\bar{r}\right)$ does not contain first harmonics ψ; consequently, the integral with respect to ψ is equal to zero. Thus, the coefficient of the average per-revolution torque m_t is determined by eq.(2.211) (the instantaneous values of m_{t_ψ} are not mutually equal, i.e., $m_{t_{(\kappa)\psi}} \neq m_{t_\psi}$).

It is also easy to prove the equality of the expressions for m_t [eqs.(2.211) and (2.48)] by taking their difference:

$$m_t - m_{t_{(\kappa)}} = a_\infty \left[\frac{1}{8} a_1 \left(2\lambda\mu + \frac{1}{2}\mu^2 a_1 - a_1 + \frac{8}{3}\varphi\mu\right) + \frac{1}{24} b_1 \left(4\mu a_0 + 3b_1 - \frac{3}{2} b_1 \mu^2\right)\right].$$

The expressions in the brackets are equal to zero, since they represent formulas [eqs.(2.201) and (2.202)] for determining the flapping coefficients a_1 and b_1. Thus, it has been proved that $m_t = m_{t_{(k)}}$.

The lift and propulsive forces of the rotor do not depend on the mode of calculating the components of the resultant force of the rotor in the related axes, whether relative to the plane of rotation or relative to the plane of the blade tips. They are equal to (considering $\cos a_1 \approx 1$, $\sin a_1 \approx a_1$)

$$t_{y_{(\kappa)}} = t_{(\kappa)} \cos(\alpha + a_1) - h_{(\kappa)} \sin(\alpha + a_1) = t \cos\alpha - h \sin\alpha = t_y; \tag{2.213}$$

$$t_{x(\kappa)} = t_{(\kappa)} \sin(\alpha + a_1) + h_{(\kappa)} \cos(\alpha + a_1) = t \sin\alpha + h \cos\alpha = t_x. \tag{2.214}$$

The formulas derived in this Subsection are simpler than those of the Glauert-Lock theory. They are also of interest in that they permit tracing the manner in which, and the factors by which, the formulas for calculating a rigid rotor (simplest case) are transformed into formulas for a hinged rotor. The change in formulas takes place for the following reasons:

1. Change in angle of attack of the rotor owing to deflection of the angle of rotation of a rigid rotor through an angle a_1. In place of λ we introduce $\lambda_{(k)} = \lambda + a_1\mu$ into the formulas for a rigid rotor:

$$t_{(\kappa)} = a_\infty \left[\frac{\lambda_{(\kappa)}}{2} + \frac{\varphi}{3} \left(1 + \frac{3}{2} \mu^2 \right) \right];$$

$$h_{(\kappa)} = -\frac{a_\infty}{2} \mu \lambda_{(\kappa)} \varphi;$$

$$s_{(\kappa)} = 0;$$

$$m_{t_{(\kappa)}} = -\frac{a_\infty}{2} \lambda_{(\kappa)} \left(\lambda_{(\kappa)} + \frac{2}{3} \varphi \right).$$

2. Cyclic change of rotor pitch relative to the deflected plane of rotation of the rigid rotor: /123

$$\varphi_{(\kappa)} = \varphi - \bar{\varphi}_{1(\kappa)} \cos\psi - \bar{\bar{\varphi}}_{1(\kappa)} \sin\psi.$$

With consideration of the cyclic change of pitch, the formulas for a rigid rotor take the form

$$t_{(\kappa)} = a_\infty \left[\frac{\lambda_{(\kappa)}}{2} - \frac{\bar{\bar{\varphi}}_{1(\kappa)} \mu}{2} + \frac{\varphi}{3} \left(1 + \frac{3}{2} \mu^2 \right) \right];$$

$$h_{(\kappa)} = -\frac{a_\infty}{2} \lambda_{(\kappa)} \left(\varphi\mu - \frac{\bar{\varphi}_{1(\kappa)}}{2} \right) + \frac{c_x p_{av} \mu}{2};$$

$$s_{(\kappa)} = -\frac{a_\infty}{4} \lambda_{(\kappa)} \bar{\varphi}_{1(\kappa)};$$

$$m_{t_{(\kappa)}} = -\frac{a_\infty}{2}\lambda_{(\kappa)}\left(\lambda_{(\kappa)} + \frac{2}{3}\varphi - \frac{\bar{\bar{\varphi}}_{1(\kappa)}\mu}{2}\right) + \frac{c_{xp_{av}}}{4}(1+\mu^2),$$

where $\bar{\bar{\varphi}}_{1_{(k)}} = a_1$, $\bar{\varphi}_{1_{(k)}} = -b_1$ for the case in which the blade pitch does not change relative to the axis of rotation.

We note that, in calculating a rigid rotor with variable pitch, it is impossible to use a new reference plane relative to which the pitch is constant, i.e., the equivalent rotor theory. This is due to the fact that the blades, on rotating, do not lie in a new reference plane but actually leave it, i.e., perform flapping motion relative to it, and the rigid rotor theory does not hold for the new reference plane.

3. The coning angle of a rigid rotor in forward flight creates a cyclic change in the velocity component $\bar{U}_y$ of the section flow (see Fig.2.34): $\Delta U_y = -\mu a_0 \cos\psi$. Furthermore, owing to the presence of the coning angle the blade thrust is projected onto the plane of the tips, supplementing the forces $h_{(k)}$ and $s_{(k)}$. These factors further complicate the formulas, so that they acquire a form which, after the substitutions $\bar{\varphi}_{1_{(k)}} = -b_1$ and $\bar{\bar{\varphi}}_{1(k)} = a_1$, coincides with that of eqs.(2.198), (2.205), (2.206), and (2.211):

$$t_{(\kappa)} = a_\infty\left[\frac{\lambda_{(\kappa)}}{2} - \frac{\bar{\bar{\varphi}}_{1(\kappa)}\mu}{2} + \frac{\varphi}{3}\left(1 + \frac{3}{2}\mu^2\right)\right]; \tag{2.215}$$

$$h_{(\kappa)} = -\frac{a_\infty}{2}\left[\lambda_{(\kappa)}\left(\varphi\mu - \frac{\bar{\bar{\varphi}}_{1(\kappa)}}{2}\right) - \frac{a_0}{2}\left(a_0\mu + \frac{2}{3}\bar{\varphi}_{1(\kappa)}\right)\right] + \frac{c_{xp_{av}}\mu}{2}; \tag{2.216}$$

$$s_{(\kappa)} = -\frac{a_\infty}{2}\left\{a_0\left[\frac{3}{2}\varphi\mu - \frac{\bar{\bar{\varphi}}_{1(\kappa)}}{3}(1+3\mu^2)\right] + 3\lambda_{(\kappa)}\left(a_0\mu + \frac{\bar{\varphi}_{1(\kappa)}}{6}\right)\right\}; \tag{2.217}$$

$$m_{t_{(\kappa)}} = -\frac{a_\infty}{2}\left[\lambda_{(\kappa)}\left(\lambda_{(\kappa)} + \frac{2}{3}\varphi - \frac{\bar{\bar{\varphi}}_{1(\kappa)}\mu}{2}\right) + \frac{a_0\mu}{2}\times\right.$$

$$\left.\times\left(a_0\mu + \frac{2}{3}\bar{\varphi}_{1(\kappa)}\right)\right] + \frac{c_{xp_{av}}}{4}(1+\mu^2). \tag{2.218}$$

4. Change-over from the plane of the blade tips to the plane of rotation /124 according to the expressions

$$\left.\begin{aligned} t &= t_{(\kappa)};\\ h &= h_{(\kappa)} + ta_1;\\ s &= s_{(\kappa)} + tb_1;\\ m_t &= m_{t_{(\kappa)}}. \end{aligned}\right\} \tag{2.219}$$

When using eqs.(2.215) - (2.218) for calculating a rotor with flapping hinges according to the condition of flapping motion [eq.(2.199)], a_0, $\bar{\varphi}_{1(\kappa)}$, and $\bar{\bar{\varphi}}_{1(\kappa)}$ will be equal to

$$\left.\begin{aligned} a_0 &= \gamma\left[\frac{\lambda_{(\kappa)}}{3} - \frac{\bar{\bar{\varphi}}_{1(\kappa)}\mu}{3} + \frac{\varphi}{4}(1+\mu^2)\right], \\ \bar{\varphi}_{1(\kappa)} &= -\frac{4a_0\mu}{3\left(1+\frac{1}{2}\mu^2\right)}, \\ \bar{\bar{\varphi}}_{1(\kappa)} &= \frac{\frac{2\mu}{1+\frac{3}{2}\mu^2}\left(\lambda_{(\kappa)}+\frac{4}{3}\varphi\right)}{1-\frac{1}{2}\mu^2} = \frac{2\mu}{1-\frac{1}{2}\mu^2} \times \\ &\quad \times\left(\lambda_{(\kappa)} - \bar{\bar{\varphi}}_{1(\kappa)}\mu + \frac{4}{3}\varphi\right). \end{aligned}\right\} \qquad (2.220)$$

Let us next examine a rotor with pitch varying in azimuth.

Equations (2.215) - (2.218) without any changes are applicable also to calculating a rotor with variable pitch.

In this case, the conditions of equality of the setting angles relative to the plane of the blade tips are

$$\left.\begin{aligned} \bar{\varphi}_{1(\kappa)} &= -b_1 + \bar{\varphi}_1; \\ \bar{\bar{\varphi}}_{1(\kappa)} &= a_1 + \bar{\bar{\varphi}}_1, \end{aligned}\right\} \qquad (2.221)$$

where $\bar{\varphi}_{1(\kappa)}$, $\bar{\bar{\varphi}}_{1(\kappa)}$, and a_0, as before, are determined in conformity with the condition of zero moment at the flapping hinge in accordance with eqs.(2.220). In place of the term $\lambda_{(\kappa)} - \bar{\bar{\varphi}}_{1(\kappa)}\mu$ it is convenient to substitute $\lambda - \bar{\bar{\varphi}}_1\mu$ into eq.(2.220).

Thus, the calculation of a rotor with variable pitch is accomplished by means of formulas derived in this Subsection and differing only by the fact that a_1 and b_1 are not equal to $\bar{\bar{\varphi}}_{1(\kappa)}$ and $\bar{\varphi}_{1(\kappa)}$ and are found from eq.(2.221) after determining $\bar{\bar{\varphi}}_{1(\kappa)}$ and $\bar{\varphi}_{1(\kappa)}$.

The angles $\bar{\varphi}_{1(\kappa)}$ and $\bar{\bar{\varphi}}_{1(\kappa)}$ should be equal to the angles between the plane of the blade tips and the plane relative to which the rotor pitch is constant, i.e., the plane of the equivalent rotor. Consequently,

$$\left.\begin{aligned} \bar{\varphi}_{1(\kappa)} &= -b_{1_e}, \\ \bar{\bar{\varphi}}_{1(\kappa)} &= a_{1_e}, \\ \lambda_{(\kappa)} &= \lambda_e + a_{1_e}\mu. \end{aligned}\right\} \qquad (2.222)$$

Thus, without introducing the concept of an equivalent rotor we obtained /125

eqs.(2.220) and (2.221), after actually relating the quantities pertaining to the plane of the blade tips with their corresponding quantities of an equivalent rotor.

The formulas derived in this Subsection yield the conditions of equivalence of a rotor with and without flapping hinges: Rotors are "equivalent" if their angles of attack differ by a quantity equal to a_1, and a rotor without flapping hinges has a coning angle and components of cyclic pitch change determinable by eq.(2.220) or eq.(2.221).

Here, it is assumed that the flapping hinges are located on the axis of rotation of the rotor or close to it and we can disregard the effect of second and higher harmonics of flapping on the aerodynamic characteristics of the rotor.

The geometric meaning of the conditions of rotor equivalence is that, upon satisfying these conditions, the position of the blades of both rotors relative to the velocity vector of the oncoming flow and their setting angles at all azimuths are identical. It is obvious that, in this case, the thrust moment of the blade relative to the axis of rotation of a rotor without flapping hinges is equal to zero.

If, for a helicopter with a rotor without flapping hinges, the cyclic variation of rotor pitch for balancing the longitudinal and transverse moments is such that eqs.(2.220) are not satisfied, then the aerodynamic characteristics of the rotor differ from those of a rotor with flapping hinges. For example, by creating a transverse moment by a lateral shift of the center of gravity of the helicopter toward the side of the advancing blade ($\psi = 90^\circ$), we can reduce the angles of attack of the blade sections at azimuth $\psi = 270^\circ$ and thus eliminate flow separations for a rotor without flapping hinges.

25. General Expressions for Determining the Components of Blade Pitch Change φ_0, $\bar{\varphi}_1$, and $\bar{\bar{\varphi}}_1$

In Subsections 23 and 24, we presented a method of calculating the aerodynamic characteristics of a rotor with a blade pitch cyclically varying in the first harmonic

$$\varphi = \varphi_0 - \bar{\varphi}_1 \cos\psi - \bar{\bar{\varphi}}_1 \sin\psi. \qquad (2.223)$$

Let us now derive formulas for determining the components of blade pitch change φ_0, $\bar{\varphi}_1$, and $\bar{\bar{\varphi}}_1$.

The blade pitch established by the control units of the helicopter - control of the overall rotor pitch and inclination of the automatic pitch control mechanism - is represented in the form

$$\theta = \theta_0 - \theta_1 \sin\psi - \theta_2 \cos\psi. \qquad (2.224)$$

We assume that the design and working principle of the automatic pitch control are known to the reader [see, for example (Ref.12)].

In addition, the blade pitch of helicopters is usually changed during blade flapping, which is achieved by a special arrangement of blade turning levers and flapping hinges. The hubs of such rotors are called hubs with "flapping compensator". Let us examine several schemes of hubs with a flapping compensator: Cardanic and non-Cardanic hubs differing in control of blade rotation about the axial hinge, and also hubs with an offset and with a turned flapping hinge (Fig.2.47).

/126

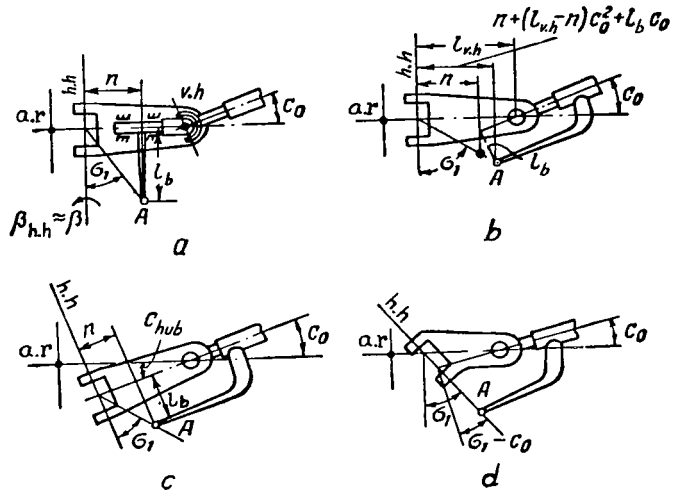

Fig.2.47 Schematic Sketches of Rotor Hubs. a - Cardanic; b - Non-Cardanic; c - With offset hinge; d - With turned hinge; v.h = Vertical hinge; a.r = Axis of rotation; h.h = Horizontal hinge.

In the first scheme (a), the blade turning lever does not participate in moving the blade relative to the drag hinge but participates in others. In the third scheme (c), the flapping hinge is located such that, in horizontal flying regimes, the blade axis is practically perpendicular to the axis of the flapping hinge and goes through the middle between its bearings. /127

In these schemes, the interdependence of setting angle and flapping angle of the blade is accomplished by displacement of the ball bearing of the blade lever A from the axis of the flapping hinge ($n \neq 0$). In the fourth scheme of the hub (d), the interdependence of pitch and flapping angle is achieved by rotation of the axis of the flapping hinge.

In all schemes, the blade is shown in a position inclined about the drag hinge through an angle $c_0 = \xi_{av}$. The flapping angle of the blade β is in a plane perpendicular to the plane of rotation and goes through the axis of the blade. Since the angle c_0 is small, the angle of turn about the flapping hinge in the first three schemes can be considered equal to the flapping angle of the

blade: $\beta_{h.h} = \frac{\beta}{\cos c_0} \approx \beta$ and, in the fourth scheme, as equal to

$$\beta_{h.h} = \frac{\beta}{\cos(c_1 - c_0)}. \qquad (2.225)$$

We derive the formulas in the following sequence: First we determine the mode of blade pitch change if the axial hinge had seized and the ball bearing of the blade-turning lever A was disconnected from the rod of the automatic pitch control mechanism. This change in blade pitch, taking place without turning of the blade in the axial hinge, is called "kinematic change of pitch". We will denote it by $\Delta\varphi_{kin}$.

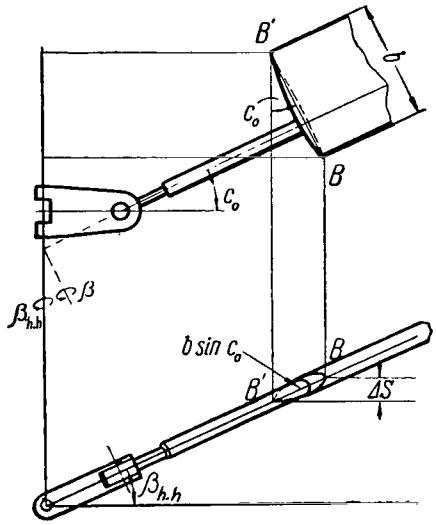

Fig.2.48 Kinematic Change of Blade Pitch.

We then determined the amount by which the blade is turned in the axial hinge, owing to the fact that the point A is connected by a rod with the automatic pitch control and cannot be displaced in flapping. This change of pitch is designated by $\Delta\varphi_{a.h}$. The overall change of pitch $\Delta\varphi_c$ is equal to the sum of $\Delta\varphi_{kin}$ and $\Delta\varphi_{a.h}$:

$$\Delta\varphi_c = \Delta\varphi_{kin} + \Delta\varphi_{a.h}. \qquad (2.226)$$

The kinematic change of blade pitch in flapping is due to the blade axis being perpendicular to the axis of the flapping hinge. Its derivation is clear from Fig.2.48. Point B, referring to the leading edge of the blade, during flapping of the blade is displaced relative to the plane of rotation by a greater amount than point B′ referring to the trailing edge. Consequently, the blade changes its angle relative to the plane of rotation:

$$\Delta\varphi_{kin} = \frac{\Delta s}{b} = \frac{b \sin c_0 \beta_{h.h}}{b} = \beta \tan c_0. \qquad (2.227)$$

The derivation of $\Delta\varphi_{kin}$ is illustrated also by the drawing shown in Fig.2.49.

It is obvious that, when the flapping hinge rotates together with the blade during flapping of the blade relative to the drag hinge (hubs of Sikorsky helicopters, Fig.2.50), there is no kinematic change of pitch. Such a change is virtually absent in the scheme shown in Fig.2.47c (hubs of Mil' helicopters) since, in horizontal flying regimes $c_{hub} \approx c_0$,

$$\Delta\varphi_{kin} = \beta \tan(c_0 - c_{hub}) \approx 0. \qquad (2.228)$$

In the scheme of a hub with a turned flapping hinge (scheme d in Fig.2.47; such a scheme for the drag hinge is sometimes used for tail rotors of single- /128
rotor helicopters),

$$\Delta\varphi_{kin} = -\beta\tan(\sigma_1 - c_0). \tag{2.229}$$

Now let us find $\Delta\varphi_{a.h}$. If point A in Fig.2.47 were not connected by a rod with the automatic pitch control mechanism, then during flapping of the blade it would be displaced relative to the axis of rotation by an amount $\Delta s = n\beta$ for a Cardanic (universal) hub and $\Delta s = [n + (l_{v.h} - n)c_0^2 + l_b c_0]\beta \approx [n + l_b c_0]\beta$ for

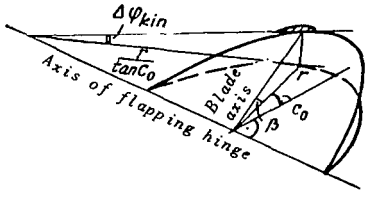

Fig.2.49 Kinematic Change of Blade Pitch.

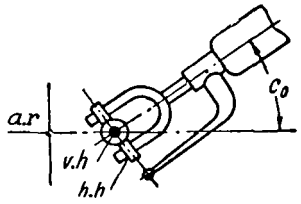

Fig.2.50 Schematic Sketch of Hub of Sikorsky Helicopter.

a non-Cardanic (nonuniversal) hub. Since point A cannot have such a displacement, the blade in flapping turns about the axial hinge by an amount of

$$\Delta\varphi_{a.h} = -\frac{\Delta s}{l_b} = \frac{n}{l_b}\beta = -\tan\sigma_1\beta \tag{2.230}$$

for the universal hub and

$$\Delta\varphi_{a.h} = -\left(\frac{n}{l_b} + c_0\right)\beta = -(\tan\sigma_1 + c_0)\beta \tag{2.231}$$

for the nonuniversal hub.

For a hub with an offset flapping hinge, we have

$$\Delta\varphi_{a.h} = -[\tan\sigma_1 + (c_0 - c_{hub})]\beta \approx -\tan\sigma_1\beta. \tag{2.232}$$

For a hub with a turned hinge, $\Delta\varphi_{a.h} = 0$.

Thus, the total change of blade pitch during flapping motion is equal to:

for a universal hub

$$\Delta\varphi_c = \Delta\varphi_{kin} + \Delta\varphi_{a.h} = (-\tan\sigma_1 + \tan c_0)\beta \approx -(\tan\sigma_1 - c_0)\beta; \tag{2.233}$$

for a nonuniversal hub and a hub with offset hinge

$$\Delta\varphi_c = -\tan\sigma_1 \cdot \beta; \tag{2.234}$$

for a hub with turned hinge*

* For simplicity in Subsection 16, we take $c_0 = 0$, $\Delta\varphi_c = -\beta\tan\sigma_1$.

$$\Delta\varphi_c = -\tan(\sigma_1 - c_0)\beta \approx -(\tan\sigma_1 - c_0)\beta. \qquad (2.235)$$

The dependence of pitch on the angle β, in the general form, is expressed by

$$\Delta\varphi_c = -k\beta, \qquad (2.236)$$

where k is a coefficient of the flapping compensator.

The value of k is determined from eqs.(2.233) to (2.235).

Our derived expressions for k do not take into account additional changes in the setting angle, such as those caused by inclination of the rod of the automatic pitch control mechanism, etc. Therefore, the quantity k should be corrected by measurements on a manufactured hub or its model. This is deter- /129
mined as the partial derivative $k = \frac{\partial\varphi}{\partial\beta}$ at an average blade pitch and blade angle of deflection relative to the drag hinge equal to c_0.

For further computations, the quantity k is conveniently represented as the tangent of some angle δ:

$$k = \tan\delta. \qquad (2.237)$$

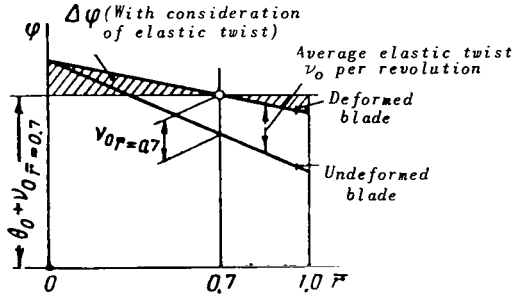

Fig.2.51 Rotor Pitch and Blade Twist, with Consideration of Average Elastic Twist per Revolution.

The blade pitch is equal to the sum of the angle θ established by the controls and the angle $\Delta\varphi_c$:

$$\varphi = \theta_0 - \theta_1\sin\psi - \theta_2\cos\psi - k\beta. \qquad (2.238)$$

Substituting into eq.(2.238) the expression for β with an accuracy to the first harmonic, we obtain

$$\varphi = (\theta_0 - ka_0) - (\theta_1 - kb_1)\sin\psi - (\theta_2 - ka_1)\cos\psi. \qquad (2.239)$$

Comparing this with eq.(2.223), we find

$$\varphi_0 = \theta_0 - ka_0,\quad \bar{\varphi}_1 = \theta_2 - ka_1,\quad \bar{\bar{\varphi}}_1 = \theta_1 - kb_1. \qquad (2.240)$$

We recall that, in the calculations by the Glauert-Lock theory, the blade pitch is counted from the zero-lift angle of the profile:

$$\varphi_0 = \varphi_{\text{pl.ref}} - \alpha_0 = \theta_0 - ka_0 - \alpha_0. \qquad (2.240')$$

For a rotor with a flapping compensator, the equivalent rotor theory does not take into account the change of blade pitch with respect to harmonics higher than the first, in view of the fact that this change is produced by higher harmonics of blade flapping. Higher harmonics of the change of pitch can be accounted for by specially derived formulas.

This also pertains to the average elastic twist over the blade with respect to higher harmonics and also to higher harmonics of the change of pitch due to elasticity of the automatic pitch control mechanism. The average elastic twist over the blade in the first harmonic $\bar{\nu}_{1_{av}}$ and $\bar{\bar{\nu}}_{1_{av}}$ must be introduced into the expressions for $\bar{\varphi}_1$ and $\bar{\bar{\varphi}}_1$. The average twist per revolution ν_0 must be subdivided into average twist over the blade $\nu_{0_{av}}$ and variable twist over the blade radius $\nu_0 - \nu_{0_{av}}$; the first is introduced into the expression for φ_0, and the second is added to the geometric twist of the blade $\Delta\varphi$ (Fig.2.51).

Averaging of the elastic twist of the blade (this can be determined in flight tests or by calculation; an estimate of the magnitude of twist can be made from the magnitude of the hinge moment of the blade) is carried out by means of the formulas /130

$$\left.\begin{aligned} \nu_{0_{av}} &= \frac{\int_0^1 \nu_0 \bar{r}^2 d\bar{r}}{\int_0^1 \bar{r}^2 d\bar{r}} = 3\int_0^1 \nu_0 \bar{r}^2 d\bar{r} \approx \nu_{0_{\bar{r}=0.7}}, \\ \bar{\nu}_{1_{av}} &= 3\int_0^1 \bar{\nu}_1 \bar{r}^2 d\bar{r} \approx \bar{\nu}_{1_{\bar{r}=0.7}}, \\ \bar{\bar{\nu}}_{1_{av}} &= 3\int_0^1 \bar{\bar{\nu}}_1 \bar{r}^2 d\bar{r} \approx \bar{\bar{\nu}}_{1_{\bar{r}=0.7}}. \end{aligned}\right\} \qquad (2.241)$$

With consideration of the elastic twist of the blade, eqs.(2.240) take the form

$$\varphi_0 = \theta_0 - ka_0 + \nu_{0_{av}}; \qquad (2.242)$$

$$\bar{\varphi}_1 = \theta_2 - ka_1 + \bar{\nu}_{1_{av}}; \qquad (2.243)$$

$$\bar{\bar{\varphi}}_1 = \theta_1 - kb_1 + \bar{\bar{\nu}}_{1_{av}}. \qquad (2.244)$$

With the use of eqs.(2.161) and (2.162), we find

$$\bar{\varphi}_1 = \theta_2 - ka_{1_e} + k\bar{\bar{\varphi}}_1 + \bar{\nu}_{1_{av}}; \quad \bar{\bar{\varphi}}_1 = \theta_1 - kb_{1_e} - k\bar{\varphi}_1 + \bar{\bar{\nu}}_{1_{av}}.$$

Solving this system relative to $\bar{\varphi}_1$ and $\bar{\bar{\varphi}}_1$ we obtain

$$\bar{\varphi}_1 = -k\frac{a_{1_e} + kb_{1_e}}{1+k^2} + \frac{\theta_2 + k\theta_1}{1+k^2} + \frac{\bar{\nu}_{1_{av}} + k\bar{\bar{\nu}}_{1_{av}}}{1+k^2}; \qquad (2.245)$$

$$\bar{\bar{\varphi}}_1 = -k\frac{b_{1_e}-ka_{1_e}}{1+k^2} - \frac{-\theta_1+k\theta_2}{1+k^2} - \frac{\bar{\bar{v}}_{1_{av}}+k\bar{v}_{1_{av}}}{1+k^2}. \tag{2.246}$$

26. Determination of Flapping Coefficients of Rotor with Flapping Compensator

After substituting eqs.(2.245) and (2.246) into eqs.(2.161) and (2.162), we obtain the following expressions for the flapping coefficients a_1 and b_1:

$$a_1 = \frac{a_{1_e}+kb_{1_e}}{1+k^2} + \frac{-\theta_1+k\theta_2}{1+k^2} + \frac{-\bar{\bar{v}}_{1_{av}}+k\bar{v}_{1_{av}}}{1+k^2}; \tag{2.247}$$

$$b_1 = \frac{b_{1_e}-ka_{1_e}}{1+k^2} + \frac{\theta_2+k\theta_1}{1+k^2} + \frac{\bar{v}_{1_{av}}+k\bar{\bar{v}}_{1_{av}}}{1+k^2}. \tag{2.248}$$

The first addends on the right-hand side of eqs.(2.247) and (2.248) determine the flapping motions of a rotor having a flapping compensator with an undeflected automatic pitch control mechanism $\theta_2 = \theta_1 = 0$ and without consideration of elastic twist. For simplification of the formulas we write them in the form

$$\bar{a}_1 = \frac{a_{1_e}+kb_{1_e}}{1+k^2}; \tag{2.249}$$

$$\bar{b}_1 = \frac{b_{1_e}-ka_{1_e}}{1+k^2}. \tag{2.250}$$

The presence in the kinematic scheme of the hub of a flapping compensator /131 greatly affects the flapping coefficients of the rotor. Upon an increase of k the inclination of the axis of the rotor cone to the side of the advancing blade ($\psi = 90^\circ$) $\bar{b}_1$ decreases. When $k = \frac{b_{1_e}}{a_{1_e}}$ we have $\bar{b}_1 = 0$, and with a further increase of k, $\bar{b}_1$ becomes negative, i.e., the axis of the cone is inclined to the side of the retreating blade ($\psi = 270^\circ$).

The backward inclination of the axis of the rotor cone $\bar{a}_1$ upon an increase in k varies differently. At a small value of the coefficient of the flapping compensator $\left(k < \frac{b_{1_e}}{a_{1_e}}\right)$, the axis of the rotor cone is still inclined toward the advancing blade and the setting angle of the blade increases at azimuth $\psi = 90^\circ$ ($\Delta\varphi_k = -k\beta$) and decreases at azimuth $\psi = 270^\circ$. Therefore, the coefficient $\bar{a}_1$ increases. At $k = \frac{b_{1_e}}{a_{1_e}}$, $\bar{b}_1 = 0$ and the setting angle at azimuth $\psi = 90^\circ$ and $\psi = 270^\circ$ will not change. Thus, $\bar{a}_1 = a_{1_e}$. On further increase in k, the angle $\bar{b}_1$ becomes negative and the setting angle at azimuth $\psi = 90^\circ$ decreases, whereas at azimuth $\psi = 270^\circ$ it increases. Therefore, the coefficient $\bar{a}_1$ decreases.

For a single-rotor helicopter, the tail rotor has no automatic pitch control so that the blade flapping is determined by the quantities a_0, $\bar{a}_1$, b_1 (the elastic twist of the tail rotors being small).

The maximum flapping angle of the blade in this case is equal to

$$\beta_{max} = a_0 + \Delta\beta = a_0 + \sqrt{a_1^2 + b_1^2} = a_0 + \frac{\sqrt{a_{1_e}^2 + b_{1_e}^2}}{\sqrt{1 + k^2}}. \qquad (2.251)$$

Equations (2.249) - (2.251) show that the flapping compensator decreases the magnitude of the variable portion of the flapping motion* $\Delta\beta$ and changes the azimuth at which the flapping angle has an extreme value $\tan \psi_{\beta_{min}} = \frac{\bar{b}_1}{\bar{a}_1}$. Both the first and second factor may be of significance for a single-rotor helicopter: the first decreases the variable loads on the blade of the tail rotor and the second changes the gap between the blades of the tail rotor and the tail boom.

For helicopters of side-by-side configuration, the gap between the blades and the fuselage is determined mainly by the quantity b_1. It is expedient to select a kinematic scheme of the automatic pitch control mechanism such that a deflection of this mechanism will not influence the quantity b_1 (usually only course control of a helicopter is accomplished by the automatic pitch control, i.e., change in a_1). Consequently, for helicopters of side-by-side configuration we must take into account, when selecting the magnitude of the flapping compensator and disregarding the elasticity of the automatic pitch control and of the blades $b_1 = \bar{b}_1$, that the quantity $\bar{b}_1$ should be higher or lower depending on the direction of rotation of the rotors.

For coaxial helicopters the gap between the blades of the upper and lower rotors depends on the quantity b_1 (because of the mutual interference of the rotors, the operating conditions of the upper and lower rotors are not the same so that also the difference of the coefficients a_1 of the rotors has an influence on the gap). As we see from Fig.2.52 this gap is

$$\Delta = H + R\beta_{up.} - R\beta_{low.} = H - R(b_{1_{up.}} + b_{1_{low.}}).$$

It is obvious that to increase the gap we must select a magnitude of the coefficient of the flapping compensator such that $b_{1_{up.}} = b_{1_{low.}} = 0$. /132

The value of b_1 of single-rotor and fore-and-aft helicopters and the value of a_1 of helicopters of any configuration are determined by balancing the helicopter. The pilot, deflecting the control stick and acting on $a_{1_{con}}$ and $b_{1_{con}}$,

---

* R.A.Mikheyev determined that $\Delta\beta$ decreases somewhat less than $\sqrt{1 + k^2}$-fold, since tail rotors with $k = 0$ and $k \neq 0$ should be considered at an identical angle of attack and since α_e of a rotor with $k \neq 0$ is less than α_e of a rotor with $k = 0$; due to this fact, the quantity a_{1_e} of the former, at equal thrust, is greater than that of the latter.

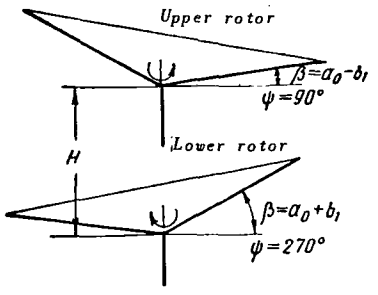

Fig.2.52 For Determining the Gap between Rotors of Coaxial Helicopters.

establishes a_1, b_1, h, and s in such a manner that the helicopter is in balance. However, at the required values of a_1 or b_1 the quantities $a_{1_{con}}$ and $b_{1_{con}}$ depend on $\bar{a}_1$ and $\bar{b}_1$; consequently, the flapping compensator influences the deflection of the helicopter controls in flight, i.e., its "balancing curves".

27. Determination of the Components of Blade Pitch Change $\bar{\varphi}_1$ and $\bar{\bar{\varphi}}_1$ after Deflection of the Automatic Pitch Control

The second addends on the right-hand side of eqs.(2.245) and (2.246) determine the increment of the components of cyclic pitch change and the flapping coefficients of a rotor with a flapping compensator, after manipulation of the automatic pitch control. They represent the change in position of the blade cone and the directions of forces and moments relative to the rotor shaft when the helicopter controls are manipulated. We denote these by $\bar{\bar{\varphi}}_{1_{con}}$ and $\bar{\varphi}_{1_{con}}$ or $a_{1_{con}}$ and $b_{1_{con}}$:

$$\bar{\bar{\varphi}}_{1_{con}} = -a_{1_{con}} = -\frac{-\theta_1 + k\theta_2}{1+k^2}; \tag{2.252}$$

$$\bar{\varphi}_{1_{con}} = b_{1_{con}} = \frac{\theta_2 + k\theta_1}{1+k^2}. \tag{2.253}$$

Let us now establish the relation between the angles of inclination of the automatic pitch control and the magnitude of the angles θ_1 and θ_2.

Figure 2.53 shows a diagram of the hub and automatic pitch control in top view along the rotor shaft. The arrangement of the flapping hinges is not shown, since this has no influence on our derivations (only the expression for k depends on it). The segments AA′ are projections of the inclined rods of the automatic pitch controls; point A is the coupling of the rod with the blade turning lever, while point A′ is the coupling of the rod with the automatic pitch control itself.

The rotor blades are shown in positions at which $\Delta\varphi_{con} = \theta_2(\psi = 180^\circ)$ and $\Delta\varphi_{con} = \theta_1(\psi = 270^\circ)$; here the hub and automatic pitch control are turned, relative to the longitudinal axis of the helicopter, through the angles $\psi_{hub} = 180^\circ + c_0$ and $\psi_{hub} = 270^\circ + c_0$.

The angles of turn of the automatic pitch control will de denoted by the letters $\varkappa$ and η, where $\varkappa$ is the turn mainly causing deflection of the blade cone in the longitudinal plane of the helicopter and η in the transverse plane.

Let the automatic pitch control be deflected through an angle $\varkappa$ relative to the axis 00′ located at an angle $\Delta\psi_{con}$ to the transverse plane of the helicopter.

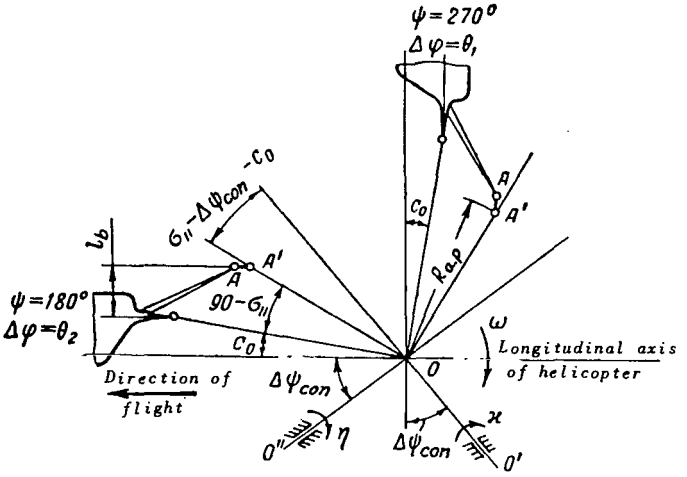

Fig.2.53 Kinematic Diagram of Hub and Automatic Pitch Control.

Considering that the vertical displacements of the points A and A′ are equal to ($S_A = S'_A$), we find

$$\left.\begin{aligned}\theta_2^{(x)} &= \frac{S_A}{l_b} = x\frac{R_{a.p}}{l_b}\sin(\sigma_{11} - \Delta\psi_{con} - c_0) = \bar{D}_2 x;\\ \theta_1^{(x)} &= -x\frac{R_{a.p}}{l_b}\cos(\sigma_{11} - \Delta\psi_{con} - c_0) = -\bar{D}_1 x.\end{aligned}\right\} \qquad (2.254)$$

Similar expressions are obtained on deflection of the automatic pitch control relative to the axis 00″ through an angle η

$$\left.\begin{aligned}\theta_2^{(\eta)} &= \eta\frac{R_{a.p}}{l_b}\cos(\sigma_{11} - \Delta\psi_{con} - c_0) = \bar{D}_1\eta,\\ \theta_1^{(\eta)} &= \eta\frac{R_{a.p}}{l_b}\sin(\sigma_{11} - \Delta\psi_{con} - c_0) = \bar{D}_2\eta.\end{aligned}\right\} \qquad (2.255)$$

Let us determine the increments of the flapping coefficients of the rotor when the automatic pitch control is deflected through the angles x and η, substituting the obtained relations into eqs.(2.252) and (2.253)

$$a_{1\,con}^{(x)} = x\frac{R_{a.p}}{l_b}\frac{\cos(\sigma_{11} - \Delta\psi_{con} - c_0) + k\sin(\sigma_{11} - \Delta\psi_{con} - c_0)}{1 + k^2} = \qquad (2.256)$$

$$= x\frac{R_{a.p}}{l_b}\cos\delta\cos(\sigma_{11} - \Delta\psi_{con} - c_0 - \delta);$$

$$a_{1\,con}^{(\eta)} = -\eta\frac{R_{a.p}}{l_b}\cos\delta\sin(\sigma_{11} - \psi_{con} - c_0 - \delta); \qquad (2.257)$$

$$b_{1\,con}^{(x)} = x\frac{R_{a.p}}{l_b}\cos\delta\sin(\sigma_{11} - \psi_{con} - c_0 - \delta); \qquad (2.258)$$

$$b_{1_{con}}^{(\eta)} = \eta \frac{R_{a.p}}{l_b} \cos\delta \cos(\sigma_{11} - \Delta\psi_{con} - c_0 - \delta). \tag{2.259}$$

Usually, the angles are so selected that $\cos(\sigma_{11} - \Delta\psi_{con} - c_0 - \delta) > \sin(\sigma_{11} - \Delta\psi_{con} - c_0 - \delta)$; consequently, the deflection of the automatic pitch control through an angle $\varkappa$ mainly causes a change in the coefficient a_1, /134 whereas a deflection through an angle η will change the coefficient b_1. The product $\frac{R_{ap}}{l_b} \cos\delta \cos(\sigma_{11} - \Delta\psi_{con} - c_0 - \delta)$, which is dependent on the kinematic scheme of the hub, constitutes a relation between the longitudinal inclination of the axis of the rotor cone and the angle $\varkappa$. This is denoted by D_1:

$$D_1 = \frac{R_{a.p}}{l_b} \cos\delta \cos(\sigma_{11} - \Delta\psi_{con} - c_0 - \delta). \tag{2.260}$$

The product $\frac{R_{ap}}{l_b} \cos\delta \sin(\sigma_{11} - \Delta\psi_{con} - c_0 - \delta)$ characterizes the inclination of the axis of the rotor cone in a lateral direction. This is denoted by D_2:

$$D_2 = \frac{R_{a.p}}{l_b} \cos\delta \sin(\sigma_{11} - \Delta\psi_{con} - c_0 - \delta). \tag{2.261}$$

The value of the coefficients D_1 and D_2 can be refined by testing the full-scale hub or its model. For this, the blades are set in an azimuthal position (shown in Fig.2.53) and relative to the flapping hinge at an angle $\beta = \beta_{av} = a_0$. After deflecting the automatic pitch control through an angle $\varkappa$, the increments of the setting angles, i.e., the angles θ_2 and θ_1, are measured.

The values of $\bar{D}_1$, $\bar{D}_2$, D_1, and D_2 are found from the expressions

$$\bar{D}_1 = -\frac{\theta_1}{\varkappa};$$

$$\bar{D}_2 = \frac{\theta_2}{\varkappa};$$

$$D_1 = \frac{\bar{D}_1 + k\bar{D}_2}{1+k^2} = \frac{1}{\varkappa} \frac{-\theta_1 + k\theta_2}{1+k^2};$$

$$D_2 = \frac{\bar{D}_2 - k\bar{D}_1}{1+k^2} = \frac{1}{\varkappa} \frac{\theta_2 + k\theta_1}{1+k^2}.$$

The quantity k is also found from tests (see Subsect.25).

Thus,

$$\bar{\varphi}_{1_{con}} = -a_{1_{con}} = -D_1\varkappa + D_2\eta; \tag{2.262}$$

$$\bar{\varphi}_{1_{con}} = b_{1_{con}} = D_1\eta + D_2\varkappa. \tag{2.263}$$

Helicopter designers often accomplish the kinematics of the automatic pitch control in which $D_2 = 0$. This is done so that, with a longitudinal deflection of the control stick causing inclination of the automatic pitch control by an angle κ, only the coefficient a_1 is changed, i.e., so that the resultant force is deflected strictly in the longitudinal plane of the helicopter. This creates a moment relative to the center of gravity of the helicopter, also acting in the longitudinal plane of the craft. However, the motion of helicopters is so interconnected in all directions that there is no sense to rigorously insist on the condition of coincidence of the directions of action of the moment and deflection of the control stick.

For helicopters of side-by-side and coaxial configurations, for which special demands are made on the quantity b_1, the coefficient D_2 should be equal to zero so that b_1 does not change when the automatic pitch control is deflected longitudinally forward or backward.

We see from eq.(2.261) that $D_2 = 0$, when /135

$$\Delta\psi_{con} = \sigma_{11} - c_0 - \delta. \tag{2.264}$$

If, in the kinematic scheme of the hub and automatic pitch control, a value of $\sigma_{11} - c_0 - \delta \neq 0$ is obtained, then the plane of inclination of the cone axis will not coincide with the plane of inclination of the automatic pitch control but will lead the plane of inclination of the automatic pitch control by an angle of

$$\zeta = \sigma_{11} - c_0 - \delta. \tag{2.265}$$

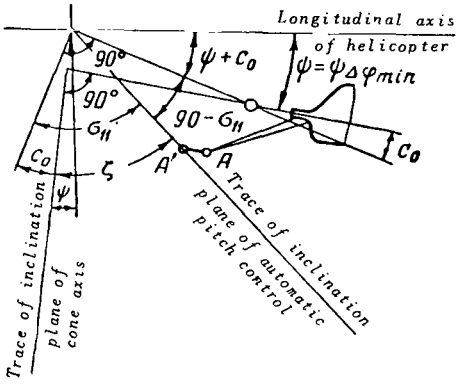

Fig.2.54 Position of Blade at Instant of Maximum Pitch Change (Hub without Flapping Compensator).

Let us explain the derivation of the lead angle, assuming - for simplicity - that the coefficient of the flapping compensator is equal to zero ($\delta = 0$). In this case, the cyclic change of the setting angle is produced exclusively by inclination of the automatic pitch control.

Figure 2.54 shows a blade in a position at which its setting angle has a maximum value since the point A' of the rod, connecting the blade turning lever with the automatic pitch control, lies in the plane of inclination of the automatic pitch control. The plane of inclination of the cone axis is perpendicular to the blade position. We see from Fig.2.54 that $\zeta = \sigma_{11} - c_0$. The angle ζ is nonzero since the mechanism changing the pitch is designed such that, for a maximum change of blade pitch at some azimuth ψ, the automatic pitch control will be deflected at an azimuth differing by an angle $90^\circ - \sigma_{11} + c_0$. If $\sigma_{11} \neq c_0$, then the plane of inclination of the automatic pitch control will not coincide with that of the cone axis.

At $\delta \neq 0$, the cyclic change of the setting angle is not only directly due

to deflection of the automatic pitch control but also to the fact that the change of flapping, caused by deflection of the mechanism, in turn changes the angle of blade setting. Here, the azimuth of the maximum total change of setting angle lags by angle $\delta = \tan^{-1}k$ behind the azimuth of the maximum change of setting angle due directly to inclination of the automatic pitch control. Therefore, at $\delta \neq 0$ the lead angle is determined by eq.(2.265).

For the plane of inclination of the cone axis to coincide with the longitudinal or with the transverse plane of the helicopter (so-called "independent" control), the axes of inclination of the automatic pitch control 00′ and 00″ should be turned to the longitudinal and transverse planes of the helicopter through an angle $\Delta\psi_{con} = \zeta$.

It follows from eq.(2.260) that, with "independent" control, the coefficient will be

$$D_1 = \frac{R_{a.p}}{l_b}\cos\delta. \tag{2.266}$$

If for a hub $c_0 = 0$ the rod of the automatic pitch control is vertical, then /136

$$\frac{R_{a.p}}{l_b} = \frac{1}{\cos\sigma_{11}} \tag{2.267}$$

and

$$D_1 = \frac{\cos\delta}{\cos\sigma_{11}}. \tag{2.268}$$

28. Sequence of Aerodynamic Calculation of a Rotor with Variable Pitch

Thus, the expressions for the components of cyclic pitch change are written in the form

$$\bar{\varphi}_1 = \bar{D}_1\eta + \bar{D}_2\chi - ka_1 + \bar{\nu}_{1_{av}} = D_1\eta + D_2\chi - k\bar{a}_1 + \frac{\bar{\nu}_{1_{av}} + k\bar{\bar{\nu}}_{1_{av}}}{1+k^2}; \tag{2.269}$$

$$\bar{\bar{\varphi}}_1 = -\bar{D}_1\chi + \bar{D}_2\eta - kb_1 + \bar{\bar{\nu}}_{1_{av}} = -D_1\chi + D_2\eta - k\bar{b}_1 - \frac{\bar{\bar{\nu}}_{1_{av}} + k\bar{\nu}_{1_{av}}}{1+k^2}. \tag{2.270}$$

For brevity, the last addends of eqs.(2.269) and (2.270) are omitted in what follows.

Let us now derive the expressions for determining the coefficients h and s:

$$h = h_e - t\bar{\bar{\varphi}}_1 = h_e + tk\bar{b}_1 + t(D_1\chi - D_2\eta) = h_e + tk\bar{b}_1 + ta_{1_{con}}; \tag{2.271}$$

$$s = s_e + t\bar{\varphi}_1 = s_e - tk\bar{a}_1 + t(D_1\eta + D_2\chi) = s_e - tk\bar{a}_1 + tb_{1_{con}}. \tag{2.272}$$

The flapping coefficients of the rotor are

$$a_1 = \bar{a}_1 + D_1\varkappa - D_2\eta; \tag{2.273}$$

$$b_1 = \bar{b}_1 + D_1\eta + D_2\varkappa. \tag{2.274}$$

For helicopter flight with sideslip, eqs.(2.269) - (2.274) should be corrected. For example (Fig.2.55),

$$a_1 = \bar{a}_1 + (D_1\varkappa - D_2\eta)\cos\beta_{s.s} - (D_1\eta + D_2\varkappa)\sin\beta_{s.s}; \tag{2.275}$$

$$b_1 = \bar{b}_1 + (D_1\eta + D_2\varkappa)\cos\beta_{s.s} + (D_1\varkappa - D_2\eta)\sin\beta_{s.s}, \tag{2.276}$$

since the inclination of the cone axis and of the aerodynamic force produced by deflection of the automatic pitch control is determined along axes related with the helicopter regardless of the direction of the velocity vector. The angles a_1, $\bar{a}_1$, b_1, $\bar{b}_1$, just as the forces H and S, are the angles and forces along axes fixed with respect to the direction of the velocity vector.

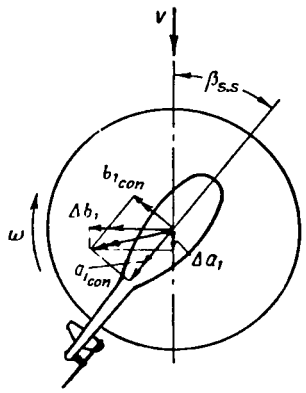

Fig.2.55 Decomposition of $a_{1_{con}}$ and $b_{1_{con}}$ into Velocity Axes during Helicopter Flight with Sideslip.

If we represent h_e and s_e in terms of components lying in the plane of the blade tips [eqs.(2.207) and (2.208)], we obtain

$$h = h_{(\varkappa)} + ta_1 = h_{(\varkappa)} + t\bar{a}_1 + t(D_1\varkappa - D_2\eta); \tag{2.277}$$

$$s = s_{(\varkappa)} + tb_1 = s_{(\varkappa)} + t\bar{b}_1 + t(D_1\eta + D_2\varkappa). \tag{2.278}$$

Equations (2.269) and (2.270) show that, for /137 a rotor with a flapping compensator, $\bar{\varphi}_1$ and $\bar{\bar{\varphi}}_1$ depend not only on the angles of deflection of the automatic pitch control but also on the flapping coefficients of the equivalent rotor. This substantially complicates the calculation of a rotor with a flapping compensator since, in determining the initial data for calculating the equivalent rotor λ_e, φ, μ, it is necessary to know the coefficients a_{1_e}, b_{1_e}, a_0. However, when any five quantities characterizing the operation of a rotor with variable pitch are prescribed, it is always possible to select a calculation sequence (sometimes pre-assigning several values of λ_e or φ and constructing auxiliary graphs) which will contain all coefficients of forces, moments, and flapping of the rotor.

Let us give a typical example. At given t (rotor thrust approximately equal to helicopter weight), μ, θ_0, $\varkappa$, and η, the aerodynamic calculation sequence for the rotor can be as follows: Assigning various values of λ_e, the expression obtained from eqs.(2.157)* and (2.242)

* We recall that φ_0 entered the formulas in Subsections 3 - 24. For simplicity, the subscript "0" of φ was omitted.

$$\varphi_e = \varphi_0 = \frac{\theta_0 + \nu_{0_{av}} - \frac{k\gamma}{3}\lambda_e}{1 + \frac{k\gamma}{4}(1+\mu^2)},$$

will yield φ_0, after which eq.(2.50) will give $t_e = t$.

After determining, either by trial and error or graphically, the values of λ_e and φ_0 at which t is equal to the prescribed value, eq.(2.40) will furnish a_0, a_{1_e} and b_{1_e}. Then, eqs.(2.249), (2.250), (2.269), and (2.270) will be used for determining $\bar{a}_1$, $\bar{b}_1$, $\bar{\varphi}_1$, and $\bar{\bar{\varphi}}_1$. We now have all data necessary for calculating the characteristics of the equivalent rotor and their conversion in the axis of a rotor with variable pitch. To determine h, s, and m_t we can also use formulas derived in Subsection 24, obtaining - in the above-described sequence - $\bar{\varphi}_{1(k)}$, $\bar{\bar{\varphi}}_{1(k)}$, and $\lambda_{(k)}$ from eqs.(2.222).

The aerodynamic calculation and the calculation of helicopter balancing are performed in the same sequence.

As shown in Subsection 23, the aerodynamic characteristics of a rotor in a velocity coordinate system - $t_x = f(t_y, m_t)$ at constant values of μ and M_0 - do not depend on $\bar{\varphi}_1$ and $\bar{\bar{\varphi}}_1$; therefore, the computation can be performed from the characteristics of a rotor with constant pitch: $t_{x_e} = f(t_{y_e}, m_{t_e})$ for the same values of μ ($\mu = \bar{V}$) and M_0. From the aerodynamic calculation, we obtain the coefficients t_{x_e} and t_{y_e}; at any value of $\bar{\varphi}_1$ and $\bar{\bar{\varphi}}_1$ in a given flying regime, the characteristics of the equivalent rotor* will not change and will correspond to the found values of μ, t_{x_e}, and t_{y_e}. Thus, as a result of the aerodynamic calculation, we will obtain all characteristics of the equivalent rotor. /138
After this, we calculate $\theta_0 = \varphi_0 + ka_0$, $\bar{a}_1$, $\bar{b}_1$ and, from eqs.(2.271), (2.272) or (2.277), (2.278), the components h and s which do not depend on $a_{1_{con}}$ and $b_{1_{con}}$. From the condition of helicopter balancing, i.e., from the condition of equating to zero the longitudinal and transverse moments, we find $a_{1_{con}}$ and $b_{1_{con}}$ and follow this by calculating $\varkappa$, η, a_1, b_1, h, and s.

Section 3. Momentum Theory of Rotor

In the momentum theory of a rotor, the aerodynamic forces and the power required by the rotor are found by applying general theorems of mechanics to the flow around the rotor.

This theory is used in approximate calculations in which both the induced

---

* The characteristics of the equivalent rotor for any $\bar{\bar{\varphi}}_1$ are the same when assuming that the parasite drag of the fuselage (and also the angle of attack of the wing of a winged helicopter) does not depend on $\bar{\bar{\varphi}}_1$ and is determined as some average value $(\bar{\bar{\varphi}}_1)_{av}[\alpha = \alpha_e - (\bar{\bar{\varphi}}_{1av})]$. Usually, this assumption is valid. If it is not, it will be necessary to perform second-approximation calculations from the value of $\bar{\bar{\varphi}}_1$ obtained from the balancing calculation.

and profile power of the rotor are determined on the basis of simplifying assumptions or from precalculated graphs. In this case, there is no need to determine the angles of attack and elementary aerodynamic forces in each blade section, a fact responsible for the simplicity of the formulas.

In the momentum theory, the components of the aerodynamic forces of the rotor along the velocity of flight (drag) and normal to it (lift) are determined, which makes this theory convenient for use in helicopter calculations.

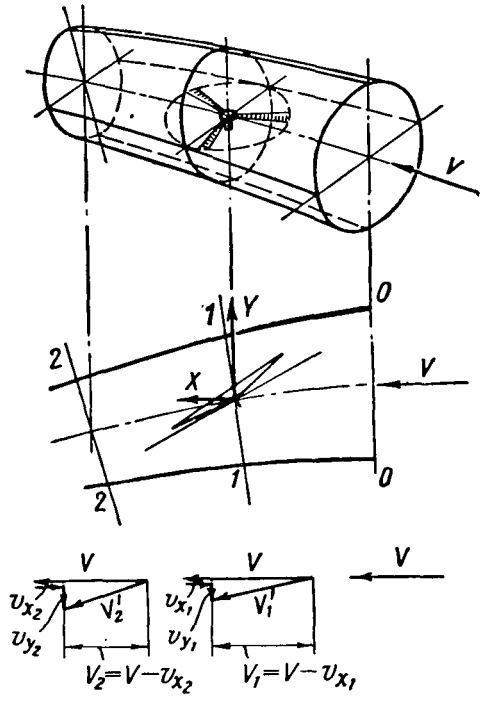

Fig.2.56 Model of Airflow around Rotor.

1. Theory of an Ideal Helicopter Rotor

When creating lift and drag (or propulsive force), the rotor thrusts an air mass downward and forward (or backward).

Glauert postulated that the rotor acts on an air mass passing through the area of a circle placed normal to the flow incident on the rotor. The diameter of the circle was to be equal to the diameter of the rotor (Fig.2.56). This postulate is based on the fact that the same flow boundaries are selected both for the propeller and for the wing, with uniform induced velocity distribution. For the propeller, this is entirely obvious since the flow boundary is determined by the area swept by the blades; for the wing, the possibility of selecting such a flow boundary is given by the vortex theory. Recently developed vortex theories of a rotor rather accurately /139 confirm the correctness of Glauert's hypothesis concerning the air mass participating in the generation of the aerodynamic forces of a rotor.

In the ideal rotor theory (Ref.21), it is postulated that the air flows at the same velocity over the entire area of the circle: The air stream does not mix with the surrounding air, so that it is proposed that the air is an inviscid fluid. Furthermore, it is assumed that profile losses of power and vorticity of the stream are absent.

A model of the airflow and its velocity components in three sections - far upstream of the rotor (section 0-0), along the rotor axis (section 1-1), and far downstream of the rotor (section 2-2) - are shown in Fig.2.56. The induced velocity corresponding to the rotor lift Y is denoted by the vector v_y, while the induced velocity corresponding to the rotor drag X, is represented by the vector v_x ($\vec{v}_y \| \vec{Y}$, $\vec{v}_x \| \vec{X}$) and the velocity of the undisturbed flow, by V. All

vectors are shown for positive direction, with the subscripts corresponding to the section number.

From the theorem of moment of momentum follow the relations

$$\left.\begin{aligned} Y &= m(v_{y_2} - v_{y_0}) = mv_{y_2}; \\ X &= m(V - V_2) = mv_{x_2}, \end{aligned}\right\} \tag{3.1}$$

where m is the air mass flowing per second through the section 0-0, 1-1, or 2-2.

The variation in kinetic energy of the per-second air mass is

$$E = E_2 - E_0 = \frac{1}{2} m(V_2^2 + v_{y_2}^2 - V^2). \tag{3.2}$$

Equating eq.(3.2) to the expression of energy imparted to the air by the rotor in unit time

$$E = Yv_{y_1} + X(v_{x_1} - V) = m(v_{y_2}v_{y_1} + v_{x_2}v_{x_1} - v_{x_2}V), \tag{3.3}$$

we obtain

$$V_2^2 + v_{y_2}^2 - V^2 = 2(v_{y_2}v_{y_1} - v_{x_2}V + v_{x_2}v_{x_1}).$$

After transformation, this expression is reduced to the form

$$v_{y_2}(v_{y_2} - 2v_{y_1}) = v_{x_2}(2v_{x_1} - v_{x_2}),$$

which indicates that, in the examined flow, the following conditions are satisfied:

$$v_{y_1} = \frac{1}{2} v_{y_2} \tag{3.4}$$

and

$$v_{x_1} = \frac{1}{2} v_{x_2}. \tag{3.5}$$

These relations show that the induced velocities in the rotor plane are one half those far downstream of the rotor.

The power supplied to an ideal rotor is expended only for creating kinetic energy of the flow and thus is equal to it. Making use of eq.(3.3), we have

$$75N = Yv_{y_1} - X(V - v_{x_1}). \tag{3.6}$$

The weight rate of flow of air m per second is equal to the product of the mass density and the volume rate of flow of air per second:

$$m = \varrho FV', \tag{3.7}$$

where V' is the resultant of the velocities V, v_{y_1} and v_{x_1}:

$$V'=\sqrt{V_1^2+v_{y_1}^2}=\sqrt{(V-v_{x_1})^2+v_{y_1}^2}. \tag{3.8}$$

To account for the so-called tip losses of the rotor, the following method is used: In calculating the forces and induced velocities, the air mass flowing through an effective area $F_{eff} = B^2F$ smaller than the area swept by the blades is introduced. Usually, for forward flight regimes we take $B^2 = 0.94 - 0.96$ [the effective radius of the rotor $R_{eff} = BR = (0.97 - 0.98)R$]. The power is calculated on the basis of the mass of air flowing through the actual area. Therefore, by means of eqs.(3.1) and (3.4) to (3.8), with consideration of tip losses, we obtain /140

$$Y=2B^2\varrho F v_{y_1}\sqrt{(V-v_{x_1})^2+v_{y_1}^2}; \tag{3.9}$$

$$X=2B^2\varrho F v_{x_1}\sqrt{(V-v_{x_1})^2+v_{y_1}^2}; \tag{3.10}$$

$$75N=\frac{1}{B^2}[Yv_{y_1}-X(V-v_{x_1})]. \tag{3.11}$$

Let us now change over to dimensionless quantities - coefficients of forces, moments (power), and velocity:

$$C_Y=4B^2\bar{v}_y\bar{V}'=4B^2\bar{v}_y\sqrt{(\bar{V}-\bar{v}_x)^2+\bar{v}_y^2}; \tag{3.12}$$

$$C_X=4B^2\bar{v}_x\bar{V}'=4B^2\bar{v}_x\sqrt{(\bar{V}-\bar{v}_x)^2+\bar{v}_y^2}; \tag{3.13}$$

$$\bar{m}_t=\frac{1}{B^2}[C_Y\bar{v}_y-C_X(\bar{V}-\bar{v}_x)]. \tag{3.14}$$

In these expressions we omitted the subscripts since, from now on, we will be concerned only with the velocities in section 1-1 and, for simplicity, will not give them a subscript.

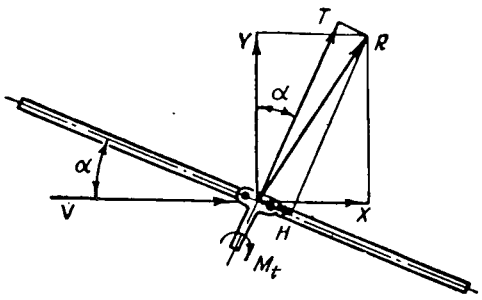

Fig.2.57 Decomposition of the Resultant Aerodynamic Force of a Rotor into Velocity and Body-Fixed Axes.

Equations (3.12) to (3.14) describe the general case where any aerodynamic system creates lift and drag (or propulsion) and consumes or yields power. Therefore, these expressions also are valid for a propeller and for a wing. For a propeller, $C_Y = v_y = 0$ must be substituted into eqs.(3.12) to (3.14) and for a wing which does not inject engine power into the flow, $m_t = 0$. (For a wing, one usually takes $\bar{v}_x \ll \bar{V}$, $\bar{v}_y < \bar{V}$.)

In the rotor theory, it is conventional to use quantities in rotor-fixed coordinates C_T, C_H, μ, λ, etc.

Introduction of the angle of attack of the rotor yields the following relations between the coefficients of forces and velocities, in different coordinate systems (Figs.2.57 and 2.58):

$$C_T = C_Y \cos\alpha + C_X \sin\alpha; \tag{3.15}$$

$$\bar{v}_t = \bar{v}_y \cos\alpha + \bar{v}_x \sin\alpha; \tag{3.16}$$

$$C_H = C_X \cos\alpha - C_Y \sin\alpha; \tag{3.17}$$

/141

$$\bar{v}_h = \bar{v}_x \cos\alpha - \bar{v}_y \sin\alpha; \tag{3.18}$$

$$\bar{V}'^2 = (\bar{V}\cos\alpha - \bar{v}_h)^2 + (\bar{V}\sin\alpha - \bar{v}_t)^2 = \mu^2 + \lambda^2; \tag{3.19}$$

$$\mu = \bar{V}\cos\alpha - \bar{v}_h; \tag{3.20}$$

$$\lambda = \bar{V}\sin\alpha - \bar{v}_t. \tag{3.21}$$

Substituting eq.(3.12) and (3.13) into eqs.(3.15) and (3.17) we obtain formulas for the coefficients C_T and C_H:

$$C_T = 4B^2 \bar{v}_t \sqrt{\mu^2 + \lambda^2}; \tag{3.22}$$

$$C_H = 4B^2 \bar{v}_h \sqrt{\mu^2 + \lambda^2}; \tag{3.23}$$

$$\bar{m}_t = \frac{1}{B^2}(C_T \bar{v}_t + C_H \bar{v}_h - C_X \bar{V}) = \frac{1}{B^2}\left\{C_T \bar{v}_t \left[1 + \left(\frac{C_H}{C_T}\right)^2\right] - C_X \bar{V}\right\}; \tag{3.24}$$

$$\bar{m}_t = -\frac{1}{B^2}(C_T \lambda + C_H \mu). \tag{3.25}$$

Let us now study the velocity polygon of a rotor and derive a number of additional relations facilitating the calculation of rotor characteristics.

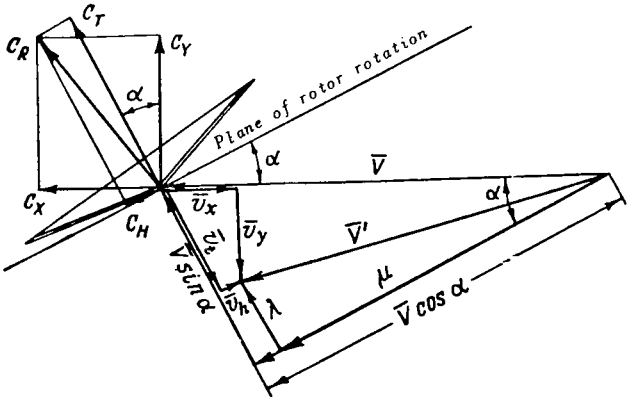

Fig.2.58 Velocity Polygon of Rotor.

The velocity and force polygons are shown in Figs.2.58 and 2.59. The latter diagram, as a supplement to Fig.2.58, shows the vector of the resultant induced velocity

$$\vec{u} = \vec{v}_y + \vec{v}_x = \vec{v}_t + \vec{v}_h$$

as well as the angles ζ and δ, as follows:

ζ - angle between the velocity of the undisturbed stream (flying speed) and resultant velocity in the rotor region, $\zeta > 0$ at $C_Y > 0$;

δ - angle between the normal to the velocity of the undisturbed stream and resultant aerodynamic force of rotor.

Since $\vec{C}_R \parallel \vec{u}$, the angle between the vectors $\vec{v}_y$ and $\vec{u}$ will also be equal to δ.

The angles ζ and δ and the flying speed $\bar{V}$ completely determine the velocity polygon. To determine the velocity polygon in terms of vectors in a fixed coordinate system, one more quantity must be known, such as - for example - the angle of attack of the rotor α. /142

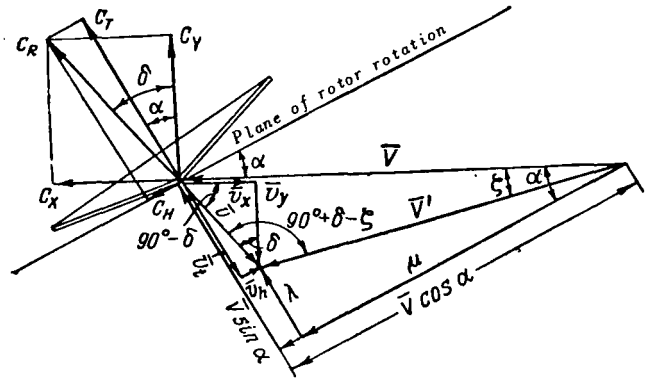

Fig.2.59 Velocity Polygon of Rotor.

Let us write out the main relations between forces and velocities in the velocity polygon:

$$\frac{C_X}{C_Y}=\frac{\bar{v}_x}{\bar{v}_y}=\tan\delta; \tag{3.26}$$

$$\frac{\bar{v}_y}{\bar{V}-\bar{v}_x}=\tan\zeta; \tag{3.27}$$

$$\frac{\bar{u}}{\sin\zeta}=\frac{\bar{V}'}{\cos\delta}=\frac{\bar{V}}{\cos(\zeta-\delta)}; \tag{3.28}$$

$$\left.\begin{aligned} C_Y&=C_R\cos\delta,\\ C_X&=C_R\sin\delta;\end{aligned}\right\} \tag{3.29}$$

$$\left.\begin{aligned} \bar{v}_y&=\bar{u}\cos\delta,\\ \bar{v}_x&=\bar{u}\sin\delta.\end{aligned}\right\} \tag{3.30}$$

Using these relations, eqs.(3.12) - (3.14) can be written in another form

$$C_Y=4B^2\bar{v}_y\bar{V}'=4B^2\bar{V}^2\frac{\sin\zeta\cos^2\delta}{\cos^2(\zeta-\delta)}; \tag{3.31}$$

$$C_X=C_Y\tan\delta; \tag{3.32}$$

$$\bar{m}_t=\frac{1}{B^2}\left[C_Y\bar{v}_y-C_X(\bar{V}-\bar{v}_x)\right]=\frac{C_Y}{B^2}(\bar{V}-\bar{v}_x)\times$$

$$\times\left(\frac{\bar{v}_y}{\bar{V}-\bar{v}_x}-\frac{C_X}{C_Y}\right)=\frac{C_Y}{B^2}\bar{V}\tan(\zeta-\delta)=\frac{C_Y}{B^2\bar{V}^2}\bar{V}^3\tan(\zeta-\delta). \tag{3.33}$$

Equations (3.31) to (3.33) are of interest in that the two independent variables ζ and δ correlate the coefficients C_Y, C_X, and $\bar{m}_t$ at any value of $\bar{V}$, which is a consequence of the similarity of the velocity polygons in regimes in which the ratios $\frac{C_Y}{\bar{V}^2}$ and $\frac{C_X}{\bar{V}^2}$ are equal.

Having assigned a series of values to the angles ζ and δ, we can find /144 the ratios $\frac{C_Y}{B^2\bar{V}^2}$, $\frac{C_X}{B^2\bar{V}^2}$, $\frac{m_t}{\bar{V}^3}$ and construct a graph for their correlation.

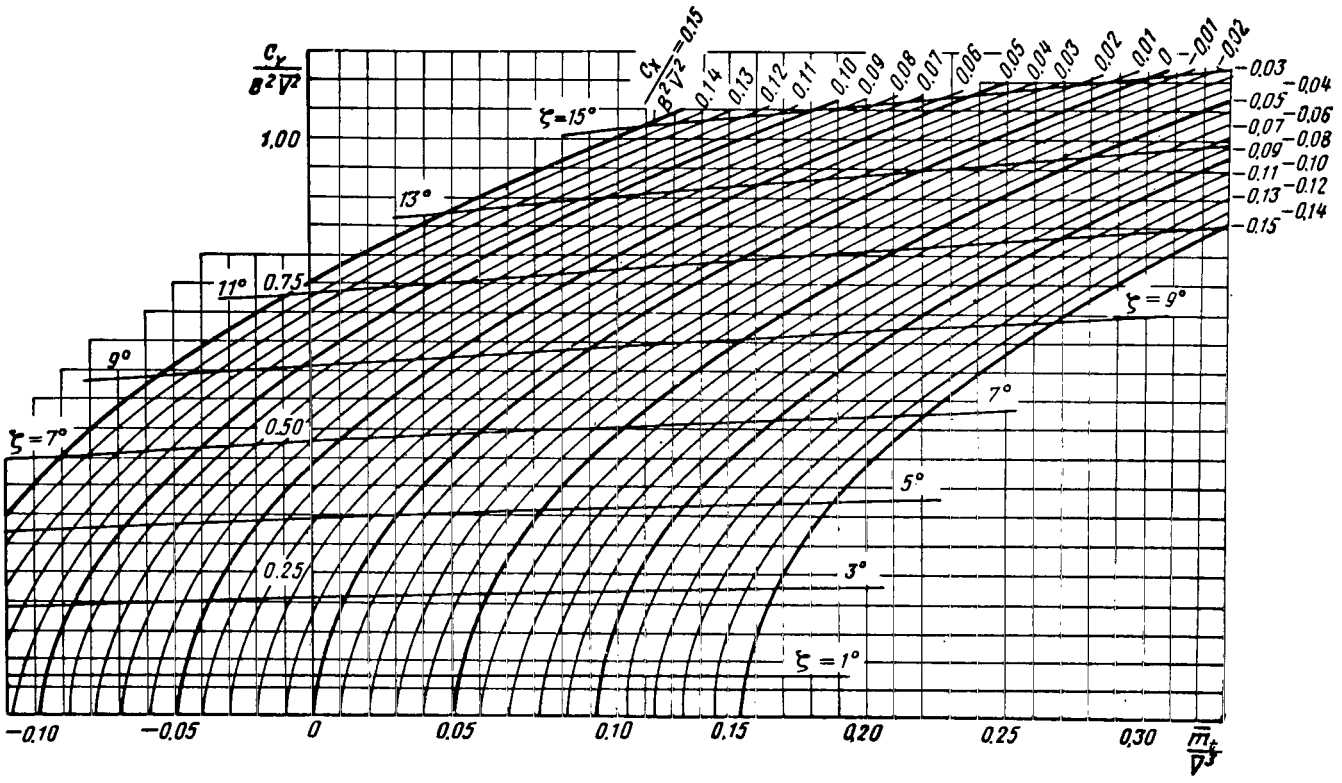

Fig.2.60 Interrelation of Coefficients of Lift, Propulsive Force, and Torque of an Ideal Rotor $\left(\frac{C_y}{B^2\overline{V}^2} < 1.0\right)$

At $C_Y = 0$ ($\zeta = 0$), eqs.(3.31) to (3.33) are not applicable; therefore, in constructing the graph, we used eqs.(3.13) and (3.14) transformed into

$$\frac{C_X}{B^2\bar{V}^2} = 4\frac{\bar{v}_x}{\bar{V}}\left(1-\frac{\bar{v}_x}{\bar{V}}\right); \tag{3.34}$$

$$\frac{\bar{m}_t}{\bar{V}^3} = -\frac{C_X}{B^2\bar{V}^2}\left(1-\frac{\bar{v}_x}{\bar{V}}\right). \tag{3.35}$$

Such graphs (Figs.2.60 and 2.61) are convenient for solving problems of aerodynamic design.

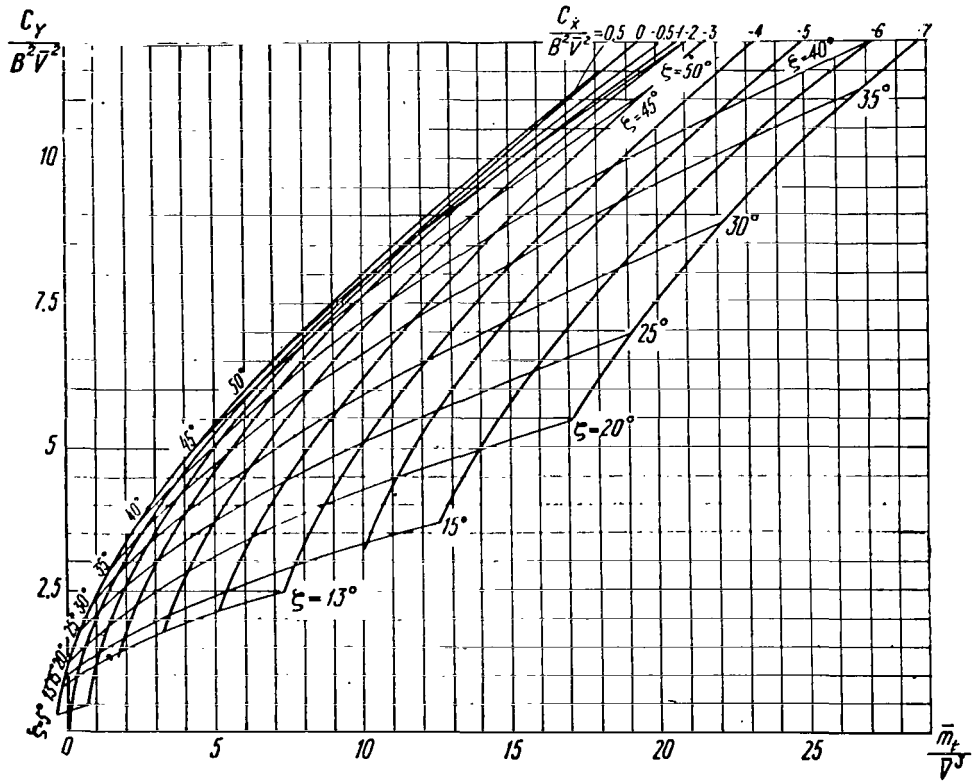

Fig.2.61 Interrelation of Coefficients of Lift, Propulsive Force, and Torque of an Ideal Rotor $\left(\frac{C_Y}{B^2\bar{V}^2} = 1.0 - 12.0\right)$.

To determine the quantities entering the velocity polygon of a rotor, we must know - in addition to $\bar{V}$ - angles ζ and δ. The angle ζ is determined rather accurately by means of graphs (see Figs.2.60 and 2.61), while the angle δ is determined from C_Y and C_X: $\delta = \tan^{-1}\frac{C_X}{C_Y}$.

At small ζ and δ (large $\overline{V}$, small C_Y) eqs.(3.31) to (3.33) are simplified. /145 Actually, we have

$$\left.\begin{aligned} C_Y &= 4B^2\overline{V}^2\zeta; \\ C_X &= C_Y\delta; \\ \overline{m}_t &= \frac{1}{B^2}C_Y\overline{V}(\zeta-\delta). \end{aligned}\right\} \tag{3.36}$$

Substituting the first two equalities into the third, we obtain

$$\overline{m}_t \simeq \frac{1}{B^2}(C_Y\overline{V}\zeta - C_Y\overline{V}\delta) \simeq \frac{C_Y^2}{4B^4\overline{V}} - \frac{1}{B^2}C_X\overline{V}. \tag{3.37}$$

At small angles of attack

$$\overline{m}_t \simeq \frac{1}{B^2}(C_T\overline{V}\zeta - C_X\overline{V}) \simeq \frac{1}{B^2}(C_T\overline{v} - C_X\overline{V}) \simeq \frac{C_T^2}{4B^4\overline{V}} - \frac{1}{B^2}C_X\overline{V}. \tag{3.38}$$

The expression for $\overline{m}_t$ is generally used in this form in aerodynamic calculations of a helicopter in flying regimes at $\overline{V} \geq 0.15$.

To calculate flying regimes with large ζ (at small $\overline{V}$), which are not covered by the graphs shown in Figs.2.60 and 2.61, we must use eqs.(3.12) to (3.14). Substituting into eq.(3.13)

$$\overline{v}_y = \overline{v}_x\frac{C_Y}{C_X} \tag{3.39}$$

and transforming, we obtain

$$\left(\frac{C_X}{4B^2}\right)^2 = \frac{\overline{v}_x^2}{2}\left[(\overline{V}-\overline{v}_x)^2 + \sqrt{(\overline{V}-\overline{v}_x)^4 + \frac{C_Y^2}{4B^2}}\right]. \tag{3.40}$$

This expression permits constructing graphs for the aerodynamic characteristics of a rotor $C_X = f(\overline{m}_t)$, for any selected values of $\overline{V}$ and C_Y: Assigning $\overline{v}_x$, we find C_X, then $\overline{v}_y$, and finally $\overline{m}_t$ from eq.(3.14) (the sign of C_X coincides with the sign of $\overline{v}_x$).

To calculate the characteristics of an ideal rotor, we can also use the following expressions:

$$\begin{aligned} C_R = 4B^2\overline{u}\,\overline{V}' &= 4B^2\overline{u}\sqrt{(\overline{V}-\overline{u}\sin\delta)^2 + (\overline{u}\cos\delta)^2} = \\ &= 4B^2\overline{u}\sqrt{\overline{V}^2 - \overline{u}(2\overline{V}\sin\delta - \overline{u})}. \end{aligned} \tag{3.41}$$

Let us then transform eq.(3.41) into

$$1=\frac{\bar{u}^2}{\frac{C_R}{4B^2}}\left[\frac{\bar{V}^2}{\frac{C_R}{4B^2}}-\sqrt{\frac{\bar{u}}{\frac{C_R}{4B^2}}}\left(2\sin\delta\sqrt{\frac{\bar{V}}{\frac{C_R}{4B^2}}}-\sqrt{\frac{\bar{u}}{\frac{C_R}{4B^2}}}\right)\right], \qquad (3.42)$$

from where it is obvious that we can construct the graph of the dependence of $\tilde{u}=\frac{\bar{u}}{\sqrt{\frac{C_R}{4B^2}}}$ on $\tilde{V}=\frac{\bar{V}}{\sqrt{\frac{C_R}{4B^2}}}$ and δ. Such a graph, borrowed from another publication (Ref.2), is shown in Fig.2.62. In this diagram, the broken line is the approximate curve which can be used as basis for calculating the vortex-ring state at $\delta = +60^\circ$ and $\delta = +90^\circ$; for this curve, the ideal rotor theory does not hold.

A determination of the induced velocity of the rotor is of independent interest.

If the angles ζ and δ are known, the ratio of the induced velocity to the flying speed can be determined by expressions derived from eqs.(3.26) and (3.27): /146

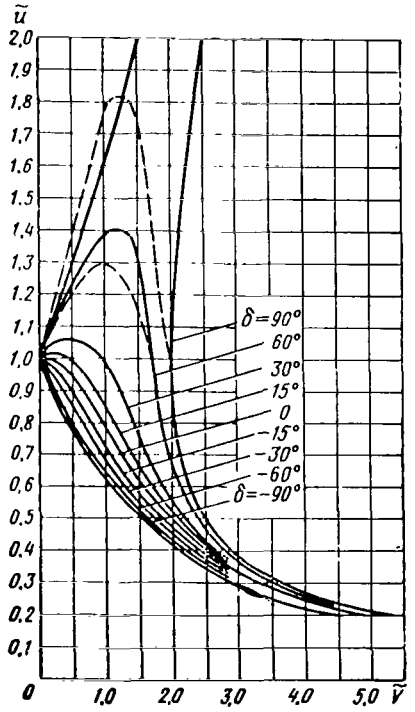

Fig.2.62 Induced Velocity $\tilde{u}$ as a Function of $\tilde{V}$ and δ.

$$\frac{v_y}{V}=\frac{\bar{v}_y}{\bar{V}}=\frac{\sin\zeta\cos\delta}{\cos(\zeta-\delta)}=\frac{1}{\frac{1}{\tan\zeta}+\tan\delta}; \qquad (3.43)$$

$$v_x=v_y\tan\delta. \qquad (3.44)$$

If the angle of attack of the rotor is known, the velocities v_t and v_h can be obtained from eqs.(3.16) and (3.18).

In the operating condition $C_X = \bar{v}_x = 0$, the velocity $\bar{v}_y$ is determined from the expression:

$$\bar{v}_y=\bar{V}\sqrt{\sqrt{\frac{1}{4}+\left(\frac{C_Y}{4B^2\bar{V}^2}\right)^2}-\frac{1}{2}}. \qquad (3.45)$$

At small angles ζ and δ, the relation $\bar{v}_x \ll \bar{V}$ is satisfied, so that

$$\bar{v}_y=\frac{C_Y}{4B^2\sqrt{\bar{V}^2+\bar{v}_y^2}} \qquad (3.46)$$

or

$$\bar{v}_t=\frac{C_T}{4B^2\sqrt{\bar{V}^2+\bar{v}_t^2}}; \qquad (3.46')$$

$$\bar{v}_x=\frac{C_X}{4B^2\sqrt{\bar{V}^2+\bar{v}_y^2}} \qquad (3.47)$$

At $\bar{V} \geq 0.15$ and at small angles of attack (more accurately, if $\tilde{V} \geq 2.0$ and at small δ where - in conformity with Fig.2.62 - $\tilde{u} \approx \frac{1}{\tilde{V}}$) the simplified expressions widely used in the calculations will rather accurately yield the induced velocities

$$\bar{v} = \bar{v}_y = \frac{C_Y}{4B^2\bar{V}} = \bar{v}_t = \frac{C_T}{4B^2\mu} = \tag{3.48}$$

$$= \frac{t\sigma}{4B^2\bar{V}};$$

$$\bar{v}_x = \bar{v}_h = 0. \tag{3.49}$$

In these cases, the induced velocity is denoted by the letter v without subscript, for simplicity.

2. Derivation of the Expression for the Torque Coefficient of a Real Rotor

Equations (3.14) and (3.37) were derived above for determining the torque coefficient of an ideal rotor, when considering the rotor as an active disk influencing its own circumflow. These expressions are interesting in that $\bar{m}_t$ is represented as an explicit function of the coefficients of lift and propulsive force C_Y and C_X. In the same form, the expression for $\bar{m}_t$ can be derived also /147 for a real rotor. This derivation was originated by L.S.Vil'dgrube. The obtained equation is valid for nonuniform induced velocity distribution over the rotor disk and takes into account the forces of the profile drag of the blades.

As is known from the classical theory (Sects.2 and 4), the components of the dimensionless velocity of flow past the blade sections (at $t_{h.h} = 0$, $\cos\beta \approx 1$) are equal to

$$\bar{U}_x = \frac{U_x}{\omega R} = \bar{r} + \bar{V}\cos\alpha\sin\psi; \tag{3.50}$$

$$\bar{U}_y = \frac{U_y}{\omega R} = \bar{V}\sin\alpha - \bar{v} - \bar{V}\cos\alpha\sin\beta\cos\psi - \bar{r}\frac{d\beta}{d\psi}. \tag{3.51}$$

The components of the aerodynamic forces located in a plane perpendicular to the blade axis are expressed by the equations

$$dt = (c_y\cos\Phi + c_{xp}\sin\Phi)\bar{U}^2\bar{\bar{b}}d\bar{r}; \tag{3.52}$$

$$dq = (c_{xp}\cos\Phi - c_y\sin\Phi)\bar{U}^2\bar{\bar{b}}d\bar{r}. \tag{3.53}$$

Substituting, into eqs.(3.52) and (3.53), the expressions

$$\sin\Phi = \frac{U_y}{U} \text{ and } \cos\Phi = \frac{U_x}{U},$$

we obtain

$$dt = (c_y\bar{U}_x + c_{xp}\bar{U}_y)\bar{U}\bar{\bar{b}}d\bar{r}; \tag{3.54}$$

$$dq=(c_{xp}\bar{U}_x-c_y\bar{U}_y)\bar{U}\bar{\bar{b}}d\bar{r}. \tag{3.55}$$

Solving eq.(3.54) relative to $c_y\bar{U}\bar{\bar{b}}d\bar{r}$

$$c_y\bar{U}\bar{\bar{b}}d\bar{r}=\frac{dt}{\bar{U}_x}-\frac{c_{xp}\bar{U}_y\bar{U}\bar{\bar{b}}d\bar{r}}{\bar{U}_x}$$

and substituting this into eq.(3.55), we obtain

$$dq=c_{xp}\left(\bar{U}_x+\frac{\bar{U}_y^2}{\bar{U}_x}\right)\bar{U}\bar{\bar{b}}d\bar{r}-\frac{\bar{U}_y}{\bar{U}_x}dt=c_{xp}\frac{\bar{U}^3}{\bar{U}_x}\bar{\bar{b}}d\bar{r}-dt\frac{\bar{U}_y}{\bar{U}_x}. \tag{3.56}$$

The elementary torque of the rotor is

$$dm_t=dq\bar{r}. \tag{3.57}$$

From this, after substituting dq from eq.(3.56) and $\bar{r}$ from eq.(3.50) we obtain

$$dm_t=c_{xp}\bar{U}^3\bar{\bar{b}}d\bar{r}-dt\bar{U}_y-dq\bar{V}\cos\alpha\sin\psi. \tag{3.58}$$

For further transformations of eq.(3.58) we use eq.(3.51) and the expressions for the elementary longitudinal and propulsive forces:

$$dh=dq\sin\psi-dt\sin\beta\cos\psi; \tag{3.59}$$

$$dt_x=dh\cos\alpha+dt\sin\alpha. \tag{3.60}$$

As a result we obtain /148

$$\begin{aligned}dm_t&=c_{xp}\bar{U}^3\bar{\bar{b}}d\bar{r}+dt\bar{v}+dt\bar{r}\frac{d\beta}{d\psi}-dt\bar{V}\sin\alpha+dt\sin\beta\cos\psi\bar{V}\cos\alpha-\\&-dq\sin\psi\bar{V}\cos\alpha=c_{xp}\bar{U}^3\bar{\bar{b}}d\bar{r}+dt\bar{v}+dt\bar{r}\frac{d\beta}{d\psi}-dt\bar{V}\sin\alpha-\\&-dh\bar{V}\cos\alpha=c_{xp}\bar{U}^3\bar{\bar{b}}d\bar{r}+dt\bar{v}+dt\bar{r}\frac{d\beta}{d\psi}-dt_x\bar{V}.\end{aligned} \tag{3.61}$$

We then integrate the elementary torques with respect to the rotor area:

$$m_t=\int_0^{2\pi}d\psi\int_0^1 dm_t=\int_0^{2\pi}\int_0^1 c_{xp}\bar{\bar{b}}\bar{U}^3d\bar{r}d\psi+\int_0^{2\pi}d\psi\int_0^1 dt\bar{v}+\int_0^{2\pi}\int_0^1 dt\bar{r}\frac{d\beta}{d\psi}d\psi-\bar{V}\int_0^{2\pi}d\psi\int_0^1 dt_x. \tag{3.62}$$

The equation of blade flapping has the form

$$\int_0^R dTr=I_{h.h}\omega^2\left(\frac{d^2\beta}{d\psi^2}+\beta\right)-S_{h.h}g,$$

so that $\int_0^1 dt\bar{r}$ is proportional to the sum $\frac{d^2\beta}{d\psi^2} + \beta - \text{const}$. Therefore,

$$\int_0^{2\pi}\int_0^1 dt\bar{r}\,\frac{d\beta}{d\psi}\,d\psi \doteq \int_0^{2\pi}\frac{d\beta}{d\psi}\left(\frac{d^2\beta}{d\psi^2}+\beta-\text{const}\right)d\psi=\int_0^{2\pi}\frac{d\beta}{d\psi}\,d\left(\frac{d\beta}{d\psi}\right)+$$
$$+\int_0^{2\pi}\beta d\beta-\text{const}\int_0^{2\pi}d\beta=\frac{1}{2}\left(\frac{d\beta}{d\psi}\right)^2\Big|_0^{2\pi}+\frac{1}{2}\,\beta^2\Big|_0^{2\pi}-\text{const}\,\beta\Big|_0^{2\pi}=0, \tag{3.63}$$

since β and $\frac{d\beta}{d\psi}$ at $\psi = 0$ and $\psi = 2\pi$ have an identical value [V.E.Baskin gives such a derivation of eq.(3.63)].

Thus, the expression for m_t can be represented as

$$m_t=\int_0^{2\pi}\int_0^1 c_{xp}\bar{U}^3\bar{b}d\bar{r}d\psi+\int_0^{2\pi}d\psi\int_0^1 dt\bar{v}-t_x\bar{V}. \tag{3.64}$$

For simplicity, we derived the expression for m_t on the basis of eqs.(3.50) and (3.51) for $\bar{U}_x$ and $\bar{U}_y$. More accurate expressions, taking account of the component of induced velocity v_h,

$$\bar{U}_x=\bar{r}+(\bar{V}\cos\alpha-\bar{v}_h)\sin\psi; \tag{3.65}$$

$$\bar{U}_y=\bar{V}\sin\alpha-\bar{v}_t-(\bar{V}\cos\alpha-\bar{v}_h)\sin\beta\cos\psi-\bar{r}\,\frac{d\beta}{d\psi}, \tag{3.66}$$

will yield, after analogous computations, the following expression for m_t:

$$m_t=\int_0^{2\pi}\int_0^1 c_{xp}\bar{\bar{b}}\bar{U}^3d\bar{r}\,d\psi+\int_0^{2\pi}d\psi\int_0^1(dt_y\bar{v}_y-dt_x\bar{v}_x)-t_x\bar{V}. \tag{3.67}$$

The first integral in eq.(3.67) contains the forces of profile drag and the second the forces of induced drag. We designate them, respectively, as /149

$$m_{pr}=\int_0^{2\pi}\int_0^1 c_{xp}\bar{\bar{b}}\bar{U}^3d\bar{r}\,d\psi;$$

$$m_{ind}=\int_0^{2\pi}d\psi\int_0^1 dt_y\bar{v}_y-dt_x\bar{v}_x.$$

For an ideal rotor for which $c_{xp} = 0$ and for which the induced velocities are uniformly distributed, we obtain from eq.(3.67) with an approximate consideration of tip losses,

$$m_t=\frac{1}{B^2}\left[t_y\bar{v}_y-t_x(\bar{V}-\bar{v}_x)\right]$$

or, multiplying both sides of the equality by the loading factor,

$$\overline{m}_t = \frac{1}{B^2}[C_Y \overline{v}_y - C_X(\overline{V} - \overline{v}_x)]. \qquad (3.68)$$

Equation (3.68) coincides with eq.(3.14) obtained in the ideal rotor theory.

We note that in the expression for m_t used for calculations in the classical theory, the term taking account of the profile drag of the blades does not coincide with that obtained above and, in conformity with eq.(3.55) and (3.57), is equal to

$$m'_{pr} = \int_0^{2\pi}\int_0^1 c_{xp}\overline{U}\,\overline{U}_x\overline{r}\,\overline{\overline{b}}\,d\overline{r}\,d\psi.$$

The discrepancy of these expressions is due to the fact that the profile drag forces enter not only into the expression for $\frac{dq}{d\overline{r}}$ but also into the expression for $\frac{dt}{d\overline{r}}$ and thus into t_x and t_y as well; if c_{xp} is taken into account at some fixed values of the angle of attack α and the pitch φ of the rotor (i.e., true angle of attack of the section as is done in calculations by the classical theory), then both m_t (by an amount m'_{pr}) and t_x and t_y also will change. When calculating m_t by eq.(3.67), the term m_{pr} determines the increment in m_t, provided identical values of t_x and t_y are maintained, which obviously occurs at different α and φ for rotors with different c_{xp}.

Since it is of greater interest to compare rotors with different profile drag of the blades at identical t_x and t_y, the profile losses of the rotor are estimated with respect to the quantity m_{pr} calculated at angles of attack and pitches of the rotors corresponding to the same value of the coefficients t_x and t_y.

For the reasons presented above it is obvious that, for changing from an ideal rotor with certain t_y and t_x to a real rotor with the same t_y and t_x, the profile losses must be determined from the expression for m_{pr}.

It also follows from eq.(3.67) that the influence of a nonuniform induced velocity distribution over the rotor disk at given t_y and t_x is directly determined by the quantity m_{ind}. Furthermore, the form of the induced velocity distribution influences the angles of attack of the blade sections and thus also the quantity m_{pr}.

The flapping angle of the blades does not directly enter into the coefficient m_t owing to the fact that the integral (3.63) is equal to zero. However, flapping does influence the distribution of c_{xp}, dt, and v over the rotor disk and hence the quantity m_{pr} and m_{ind}. /150

3. Rotor Profile Losses

As shown above, at given values of the coefficients t_y and t_x the rotor profile losses are determined by the expression

$$m_{pr} = \int_0^{2\pi} \int_0^1 c_{xp} \bar{U}^3 \bar{\bar{b}}\, d\bar{r}\, d\psi. \tag{3.69}$$

With consideration of the radial velocity component of flow past the blade (see Fig.2.91), the profile losses are determined by the expression

$$m_{pr} = \int_0^{2\pi} \int_0^1 c_{xp} (U^2 + \bar{V}^2 \cos^2\alpha \cos^2\psi)^{3/2} \bar{\bar{b}}\, d\bar{r}\, d\psi. \tag{3.70}$$

Equation (3.70) should be used at small values of M_0 and t_y, i.e., in cases when the coefficient c_{xp} is determined mainly by friction forces. At large M_0 and t_y, when regions of flow separation and an increase in wave drag appear on the rotor, the profile drag of the sections is determined by the velocity component of the stream U normal to the blade axis, and eq.(3.69) must be used for calculating m_{pr}.

To calculate m_{pr} it is necessary to know the distribution of the profile drag coefficient c_{xp} and velocity of flow $\bar{U}$ about the blade sections over the rotor disk. Consequently, a calculation of m_{pr} is a laborious task and, in practice, can be performed only on high-speed computers.

Figures 2.63 - 2.70 give graphs of m_{pr} as a function of the coefficients t_y, t_x, $\bar{V}$, $M_0 = \frac{\omega R}{a}$ for a rotor with rectangular blades and a loading factor of $\sigma = 0.091$. The rotor blades (variant II in Table 2.10) have a linear geometric twist $\Delta\varphi = 7^\circ$. The blade profile is as follows: at the shank, up to $\bar{r} = 0.85$ - NACA 230 with a relative thickness $\bar{c} = 12\%$, at the end of the velocity profile with a relative thickness $\bar{c} = 9\%$. The coefficient c_{xp} obtained on exposing the model to an airstream increased by $\Delta c_{xp} = 0.002$ and pertains to a rotor having a high profile drag owing to poor manufacture. The aerodynamic characteristics of the profiles are given in Section 4, 3.

The calculation was carried out by means of eq.(3.69). Here, it was assumed that the induced velocity is constant over the rotor disk and was determined by eq.(3.46).

The method of calculation and the remaining assumptions are described in Section 4.2 and 4.4.

We see from the graphs that at numbers $M_0 = 0.6 - 0.7$ the quantity m_{pr} greatly depends on t_y and t_x.

At $M_0 \leq 0.5$, the quantity m_{pr} depends little on t_x and increases somewhat upon an increase of t_y.

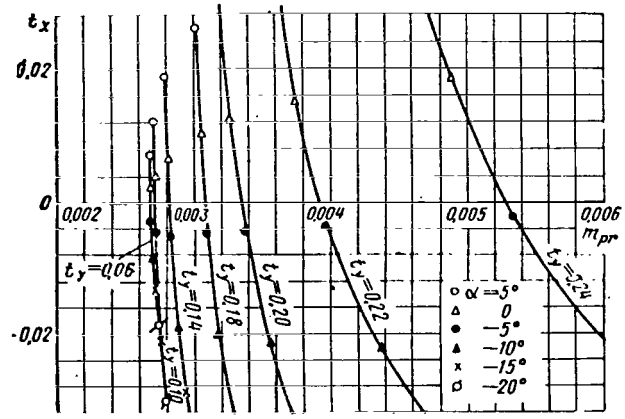

Fig.2.63 Coefficient of Profile Power of Rotor ($\bar{V}$ = 0.15; M_o = 0.6; σ = 0.091).

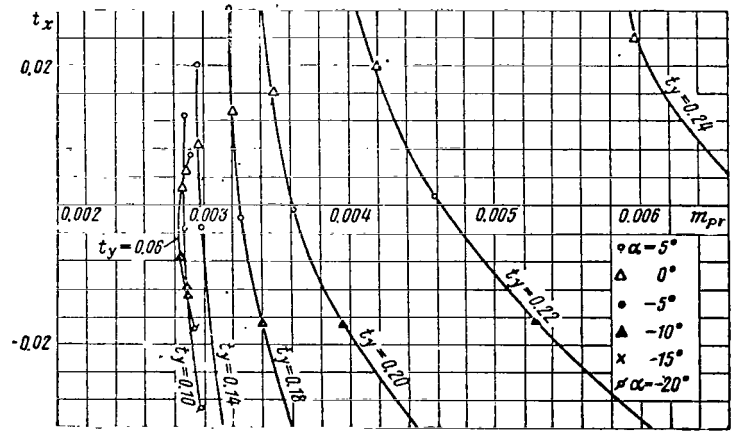

Fig.2.64 Coefficient of Profile Power of Rotor ($\bar{V}$ = 0.2; M_o = 0.6; σ = 0.091).

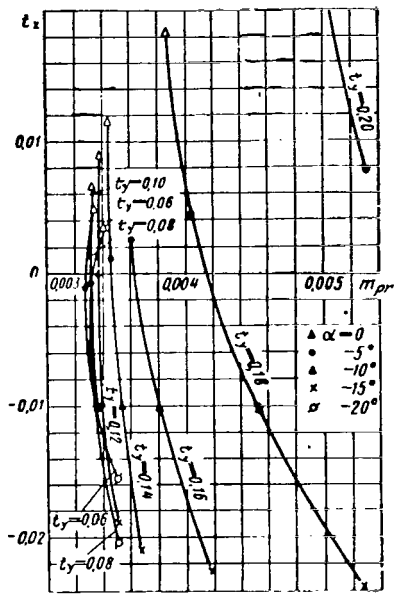

Fig.2.65 Coefficient of Profile Power of Rotor ($\bar{V}$ = 0.3; M_o = 0.6; σ = 0.091).

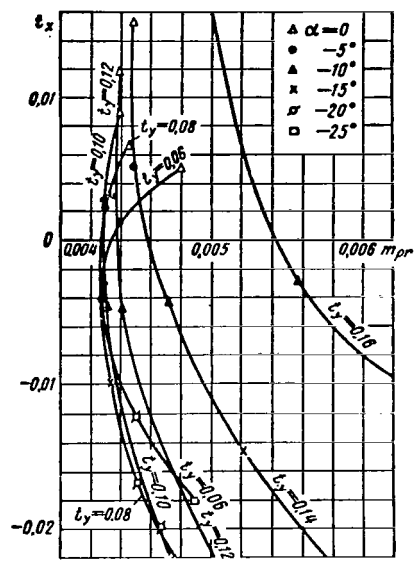

Fig.2.66 Coefficient of Profile Power of Rotor ($\bar{V}$ = 0.4; M_o = 0.6; σ = 0.091).

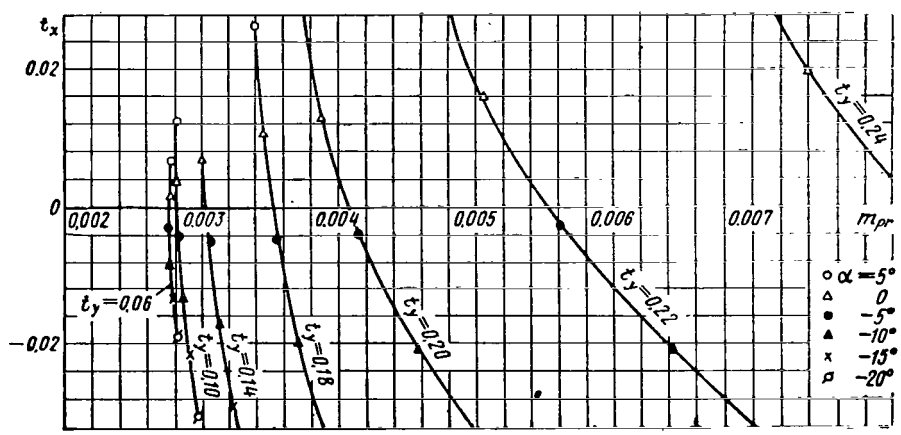

Fig.2.67 Coefficient of Profile Power of Rotor ($\bar{V}$ = 0.15; M_o = 0.7; σ = 0.091).

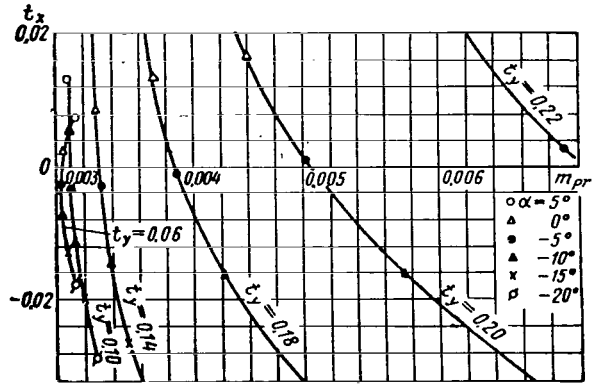

Fig.2.68 Coefficient of Profile Power of Rotor ($\bar{V}$ = 0.2; M_o = 0.7; σ = 0.091).

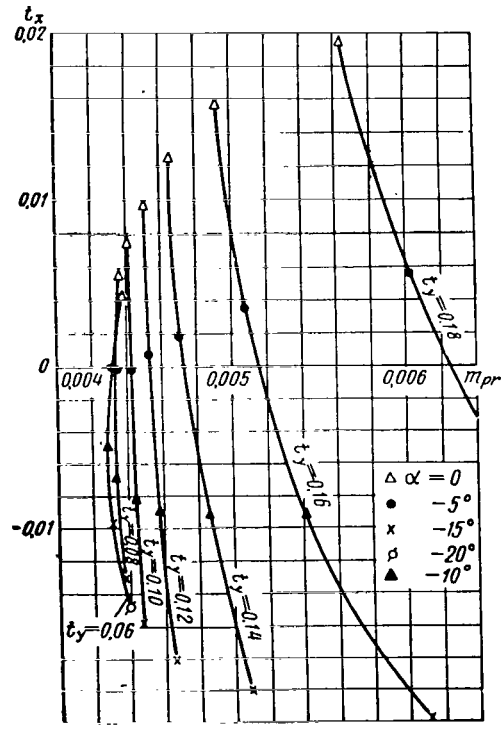

Fig.2.69 Coefficient of Profile Power of Rotor ($\bar{V}$ = 0.3; M_o = 0.7; σ = 0.091).

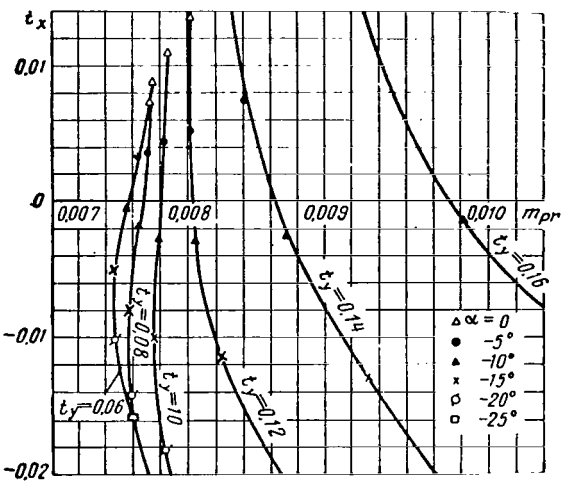

Fig.2.70 Coefficient of Profile Power of Rotor ($\bar{V}$ = 0.4; M_0 = = 0.7; σ = 0.091).

The materials for determining /154 m_{pr} for blades with other geometric characteristics are presented below in Subsections 4 - 6.

4. Certain Considerations in Selecting Blade Shape and Profile

The power expended to overcome profile losses of the rotor constitutes a large portion of the total required power of the helicopter. As shown in Fig.3.52, about 50% of the required power is expended for overcoming the profile drag of blades in horizontal flight.

Since the induced losses constitute a smaller portion of the losses than the profile losses, we can consider that the conclusions as to the effect of the geometric characteristics of the blade on profile losses pertain also to the total power of the rotor, especially at high flying speeds when the induced velocities are small and the induced losses do not exceed 12 - 15% of the total power.

Figures 2.71 - 2.74 contain comparative graphs of the profile drag coefficient m_{pr} for rotors with five blade variants:

Variant I - trapezoidal twisted blade with high-speed profile at tip;
Variant II - rectangular twisted blade with high-speed profile at tip (rotor described above);
Variant III - rectangular twisted blade with NACA 23012 profile;
Variant IV - rectangular twisted blade with symmetric NACA 0012 profile;
Variant V - trapezoidal flat blade with high-speed profile at tip.

A detailed description of all blade variants is given in Table 2.10.

A comparison of the blades is carried out for average and large lift coefficients, at two values of $\bar{V}$: 0.2 and 0.4.

A comparison shows that at low Mach number $M_0 \leq 0.5$ the trapezoidal /155 twisted blade, at all values of the propulsive force, has approximately 8% less profile power losses than the rectangular twisted blade. Since, in horizontal flight, about one half of the required power is expended to overcome the profile drag of the blades, a decrease in m_{pr} by 8% will lead to a decrease in the required power coefficient $m_{t_{h.f}}$ by 4%.

Therefore, for light helicopters for which M_0 is small and $\bar{V}_{max} \approx 0.3$, the optimum planform of the blade is trapezoidal.

The plane blade in an autorotation regime does not differ from a twisted

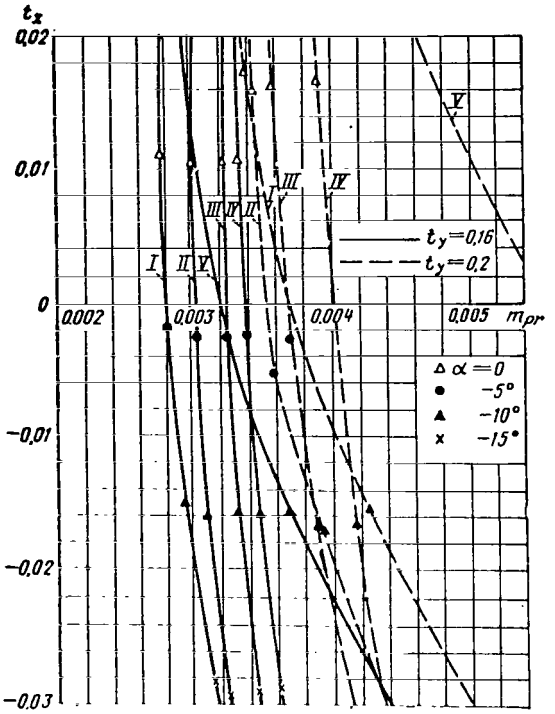

Fig.2.71 Coefficient of Profile Power of Rotors with Blades of Different Shape ($\bar{V}$ = 0.2; M_0 = = 0.6; σ = 0.091).

blade, but becomes appreciably worse than the twisted blade in helicopter regimes, especially at large $\bar{V}$. It can be used for a helicopter only at small and average values of t_y and $M_0 < 0.6$.

When varying the blade profile at small peripheral velocities, m_{pr} will vary within 5 - 12%. The symmetric profile is somewhat better than the asymmetric; at $\bar{V}$ = 0.2, the blade with a thin high-speed profile on the tip has smaller losses.

We should mention that the influence of the quality of manufacture of the profile on m_{pr} can prove to be greater than the effect of the type of profile: Δm_{pr} for different profiles is about 0.0002 (the maximum difference at large t_y is not more than 0.0004), whereas owing to difference in the type of construction and quality of manufacture of the blade the profile drag coefficient of blade sections may differ by an appreciable amount going /157 as high as 0.003 - 0.004 (see Sect.4, 3), which gives a difference in profile losses - in conformity with eq.(3.71) - of

$$\Delta m_{pr} = \frac{0.003}{4}(1 + 3 \cdot 0.3^2) \simeq 0.001.$$

At high Mach number M_0 (M_0 = 0.7; ωR = 230 - 238 m/sec), the use of a high-speed profile at the blade tip markedly reduces profile losses.

The decrease in m_{pr} amounts to 0.0015 at $\bar{V}$ = 0.2 and 0.004 at $\bar{V}$ = 0.4. This reduces m_{pr} by 40 - 45% and the total required power, by 20 and 25% respectively.

In flying regimes ($t_x < 0$) of helicopters, m_{pr} is greatly affected by the geometric twist of the blade. A straight blade is not used in helicopter regimes, and in autorotation regimes its profile drag does not differ from that of a twisted blade.

The trapezoidal blade is better than the rectangular one in autorotation regimes and at low propulsive force. In helicopter regimes where the angles of attack of the tip sections of the trapezoidal blade are larger, the difference in m_{pr} decreases while at large t_x the rectangular blade becomes better.

At moderate Mach number M_0 (M_0 = 0.6; ωR = 197 - 204 m/sec) the peculiari-

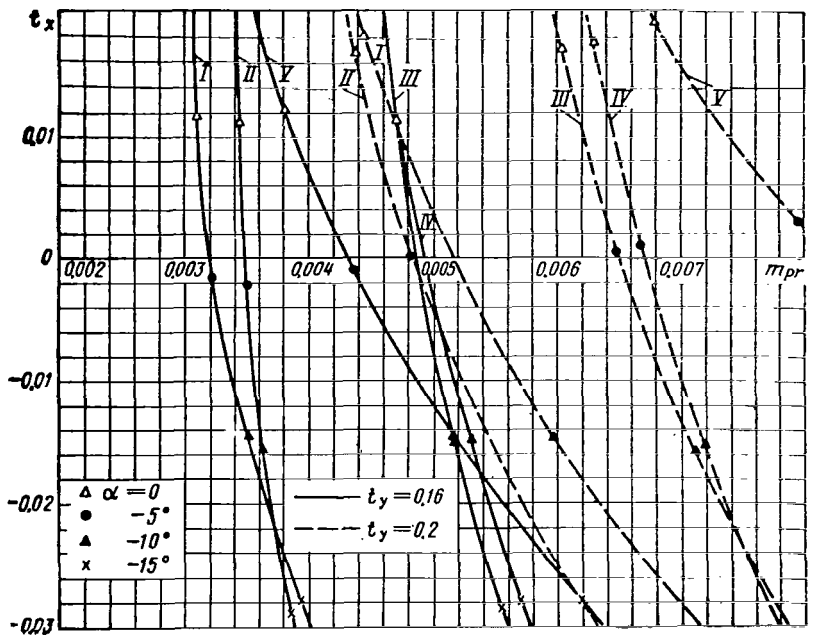

Fig.2.72 Coefficient of Profile Power of Rotors with Blades of Different Shape ($\bar{V}$ = 0.2; M_o = 0.7; σ = 0.091).

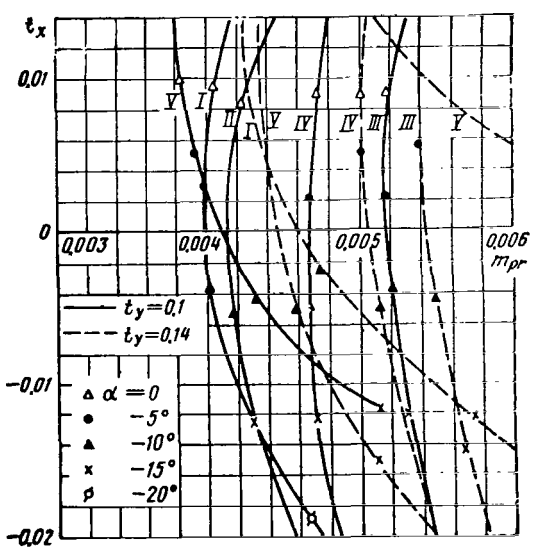

Fig.2.73 Coefficient of Profile Power of Rotors with Blades of Different Shape ($\bar{V}$ = 0.4; M_o = 0.6; σ = 0.091).

ties of the curves of m_{pr}, which were noted at $M_0 = 0.7$ (to a larger extent, at $\bar{V} = 0.4$), begin to appear: The twisted blade with a high-speed profile at the tip becomes better, and the straight blade in helicopter regimes becomes appreciably worse than the twisted blade.

A comparison of rectangular and trapezoidal blades for $M_0 = 0.6 - 0.7$ shows that at $\bar{V} = 0.4$ and also at $\bar{V} = 0.2$ for large t_y the former has the advantage, whereas for medium and small t_y at $\bar{V} = 0.2$ the trapezoidal blade becomes of advantage. In general, the rectangular blade is preferable for heavy and medium helicopters, whereas it is preferable to use trapezoidal blades for rotocraft for which the coefficients t_y and t_x of the rotor are small at large $\bar{V}$, owing to the installation of a wing and a tractor propeller.

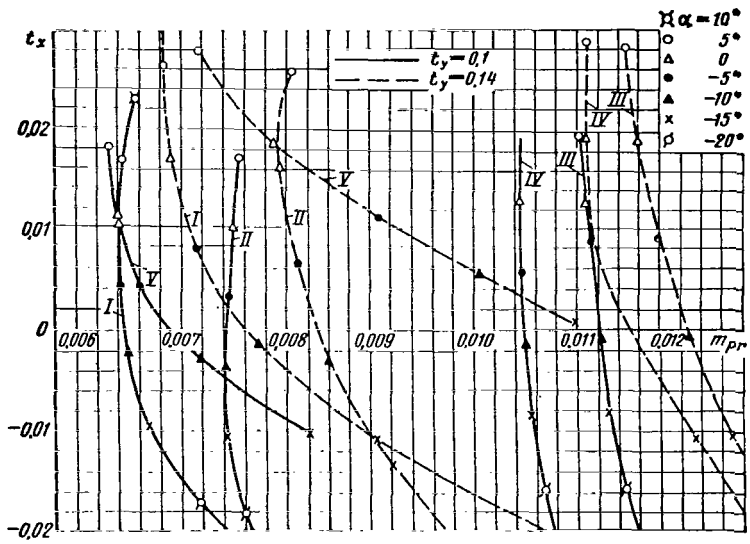

Fig.2.74 Coefficient of Profile Power of Rotors with Blades of Different Shape ($\bar{V} = 0.4$; $M_0 = 0.7$; $\sigma = 0.091$).

At $\bar{V} = 0.4$, the profile losses are quite large even with a high-speed profile at the blade tip: m_{pr} is twice that at $M_0 = 0.4 - 0.5$. To estimate the possibility of decreasing the quantity m_{pr}, Figs.2.75 and 2.76 give graphs of m_{pr} for blades of the variants I and II and also for a rectangular blade with an increased geometric twist (variant VI), for an expansible blade ($\eta = 0.5$; variant VII), and for a rectangular blade with an increase to $\bar{r} = 0.75$ of the part with a high-speed profile (variant VIII). We see from Figs.2.75 and 2.76 that, in horizontal flight and especially in autorotation regime, the trapezoidal blade remains preferable. At large values of t_y, the optimum blade is the blade with increased twist, which reduces m_{pr} at $\bar{V} = 0.2$ by 20% ($m_{t_{h.f}}$ by 10%) and at $\bar{V} = 0.4$ by 10% ($m_{t_{h.f}}$ by 5%). Consequently, the use of a blade with greater twist raises the dynamic as well as the static ceiling of the helicopter, increases the static thrust (see Fig.2.171), negligibly increases the maximum

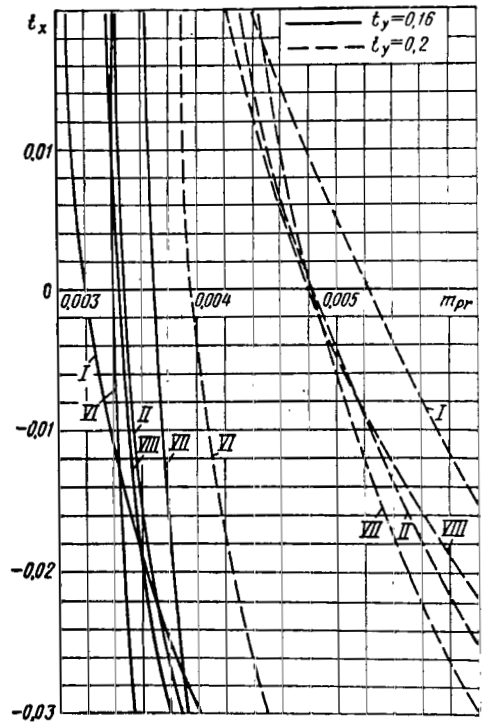

Fig.2.75 Coefficient of Profile Power of Rotors with Different Blade Shapes ($\overline{V}$ = 0.2; M_o = 0.7; σ = 0.091).

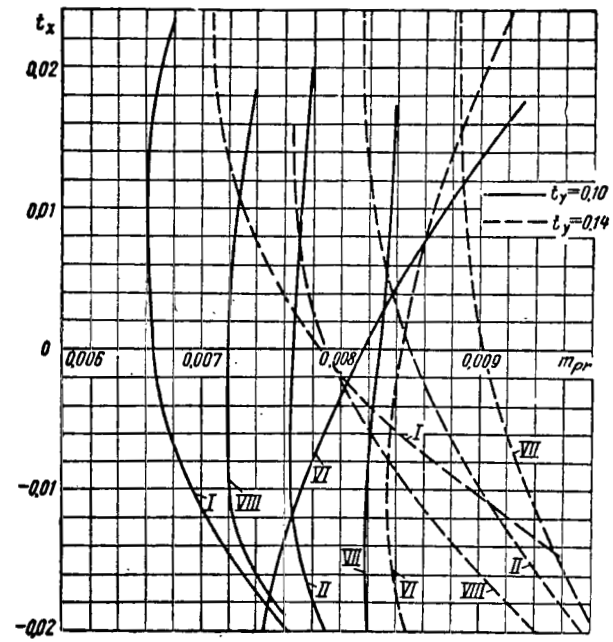

Fig.2.76 Coefficient of Profile Power of Rotors with Different Blade Shapes ($\overline{V}$ = 0.4; M_o = 0.7; σ = 0.091).

speed, and appreciably increases the rate of descent in autorotation. An enlargement of the blade portion with the high-speed profile slightly reduces the value of m_{pr}.

The obstacle in using blades with greater geometric twist lies in the increase of dynamic stresses in the blade spar, whereas for blades with an enlarged high-speed profile, the increase of hinge moments is the obstacle.

The expansible blade is preferable over the rectangular design only at very large values of the propulsive force coefficient t_x.

A comparison of the graphs of m_{pr} for $M_0 = 0.6$ and $M_0 = 0.7$ shows that, in a rotor with our high-speed profile at the tip, it is impossible to avoid a pronounced increase in profile losses at $M_0 = 0.7$, for all blade variants.

The method of utilizing graphs of m_{pr} for rotors with these types of blades but with a different loading factor is described in Section 6.

5. Approximate Determination of Rotor Profile Losses

The quantity m_{pr} is most reliably determined from graphs plotted for each specific rotor. If there are no such calculations, the data of Figs.2.63 - 2.74 can be used for an approximate estimate of m_{pr}.

At small M_0, the approximate equation (3.72), derived on the assumption of constancy of the coefficient c_{xp} in all blade sections, can be used for determining m_{pr}.

TABLE 2.5

η	1	2	3	4
P	1.0	0.94	0.91	0.88

Let us derive eq.(3.72). For a rectangular blade, we have $\bar{b}$ = const = 1.0. Having taken

$$\bar{U}^3=(\bar{U}_x^2+\bar{U}_y^2)^{3/2}\approx(\bar{r}+\bar{V}\sin\psi)^3,$$

we obtain

$$m_{pr}=\int_0^{2\pi}d\psi\int_0^1 c_{xp}\bar{U}^3\bar{\bar{b}}\,d\bar{r}=c_{xp_{av}}\int_0^{2\pi}d\psi\int_0^1\bar{U}^3\,d\bar{r}= \\ =\frac{1}{4}c_{xp_{av}}(1+3\bar{V}^2), \tag{3.71}$$

where $c_{xp_{av}}$ is the average value of the coefficient c_{xp} over the rotor disk.

For trapezoidal blades, m_{pr} is smaller than for rectangular blades. This is taken into account by the coefficient P which is pre-assigned in relation to the blade taper η (Fig.2.77) in Table 2.5.

To account for the influence of the radial velocity component of flow past the blade, m_{pr} is calculated by eq.(3.70). An approximate estimate (Ref.25, 36) shows that, to account for this component, the coefficient of $\bar{V}^2$ in eq.(3.71) /160 should be changed from 3 to 5.

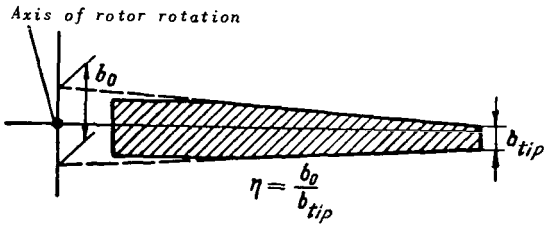

Fig.2.77 For Determining Blade Taper.

Thus, the final formula for determining m_{pr} reads

$$m_{pr} = \frac{1}{4} c_{xp_{av}} (1 + 5\bar{V}^2) P. \qquad (3.72)$$

The average profile drag coefficient $c_{xp_{av}}$ over the disk is determined as a function of the average lift coefficient c_{y_0} over the disk; the latter is found from eq.(3.74) whose derivation is given below:

$$Y = \frac{1}{2} \varrho c_{y_0} b \frac{k}{2\pi} \int_0^{2\pi} d\psi \int_0^R U^2 dr =$$

$$= \frac{1}{2} \varrho c_{y_0} bR(\omega R)^2 \frac{k}{2\pi} \int_0^{2\pi} d\psi \int_0^1 \bar{U}^2 d\bar{r}.$$

Substituting

$$\bar{U}^2 \approx (\bar{r} + \bar{V} \sin\psi)^2$$

and integrating, we obtain

$$Y = \frac{1}{2} \varrho c_{y_0} \frac{kb}{\pi R} \pi R^2 (\omega R)^2 \frac{1}{3} \left(1 + \frac{3}{2} \bar{V}^2\right) =$$
$$= \frac{1}{2} \varrho c_{y_0} \sigma F (\omega R)^2 \frac{1}{3} \left(1 + \frac{3}{2} \bar{V}^2\right). \qquad (3.73)$$

Expressing Y in terms of the dimensionless coefficient C_Y or t_y, we find

$$c_{y_0} = \frac{C_Y}{\sigma} \frac{3}{1 + \frac{3}{2} \bar{V}^2} = \frac{3 t_y}{1 + \frac{3}{2} \bar{V}^2}. \qquad (3.74)$$

Having determined c_{y_0}, the profile polar in the section $\bar{r} = 0.7$ will yield $c_{xp_{av}}$.

L.S.Vil'dgrube proposed to take into account the planform of the blade by the coefficient P and to determine $c_{xp_{av}}$ as a function of c_{y_0}.

6. Effect of Air Compressibility on Rotor Profile Losses

At average and large M_0 (for profiles generally used at $M_0 > 0.55 - 0.6$, i.e., at $\omega R > 185 - 200$ m/sec) it is necessary to supplement m_{pr}, calculated from eq.(3.72), by the term Δm_{co} which takes into account the increment in

profile power produced by the increase in profile drag coefficients of sections over which the flow has high Mach numbers. Thus, /161

$$m_{pr} = \frac{1}{4} c_{x p_{av}} (1 + 5\bar{V}^2) P + \Delta m_{co}. \qquad (3.75)$$

The coefficient of the increment in profile power Δm_{co} should be determined with consideration of the actual distribution of the angles of attack of the blade sections over the rotor disk, since an increment in profile drag due to an increase in M_0 generally occurs in all blade sections. Figures 2.78 and 2.79 show M.N.Tishchenko's graphs of the variation in the profile power coefficient of a blade as a function of its azimuthal position in the plane of rotation. We see from Fig.2.78 that, at low flying speed ($\bar{V} = 0.2$) but at large thrust coefficient, the profile power of the blades increases at all azimuths as the M_0 increases. At high flying speeds (see Fig.2.79), the increment in profile power occurs mainly at azimuths of 30 - 150°.

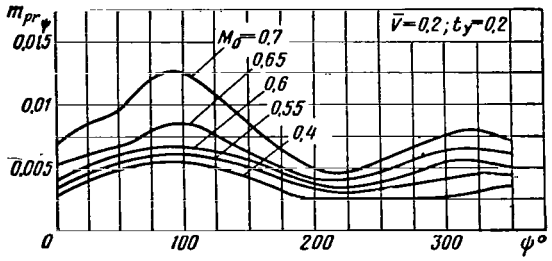

Fig.2.78 Variation in Profile Power Coefficient of Blade with Respect to Azimuth.

The graphs of Δm_{co} for the variant II of the rotor are given in Figs.2.80 to 2.84. The quantity Δm_{co} is defined as the difference between the profile power coefficient m_{pr} at the examined M_0 and at $M_0 = 0.4$ at identical values of the coefficients $\bar{V}$, t_y, t_x:

$$\Delta m_{co}(M_0) = m_{pr}(M_0) - m_{av}(M_0 = 0.4). \qquad (3.76)$$

It follows from Figs.2.80 - 2.84 that Δm_{co} is a function not only of $\bar{V}$ and the Mach number M_0 but also of the coefficients t_y and t_x. The coefficients t_y and t_x have an especially strong effect at small $\bar{V}$ at which, in conformity with Fig.2.78, the increment in m_{pr} occurs at all azimuths. Upon an increase in $\bar{V}$ the increment in m_{pr} occurs mainly in the region $\psi = 90°$ (see Fig.2.79) where the angles of attack of the sections are close to zero regardless of the value of t_y. Consequently, at $\bar{V} = 0.4$ and $\bar{V} = 0.5$ the influence of t_y and t_x on the quantity Δm_{co} is insignificant.

We see from Figs.2.80 - 2.84 that, at large M_0, $\bar{V}$, and t_y, Δm_{co} is large. The quantity Δm_{co} greatly increases when $M_0 > 0.55 - 0.6$. At near-separation values of t_y when $\bar{V} = 0.15$ and $\bar{V} = 0.2$, Δm_{co} has a high value already at $M_0 > 0.5$.

So as to keep the increase in required power of a helicopter, due to the compressibility effect, from exceeding 15 - 18%, the rotor of the variant II should be used when $M_0 = 0.7$ at $\bar{V} \leq 0.3$, and when $M_0 = 0.65$ at $\bar{V} \leq 0.4$. For example, when $M_0 = 0.7$, $\bar{V} = 0.3$, $t_y = 0.15$, and $t_{x_{h.f}} = -0.0075$, the increment

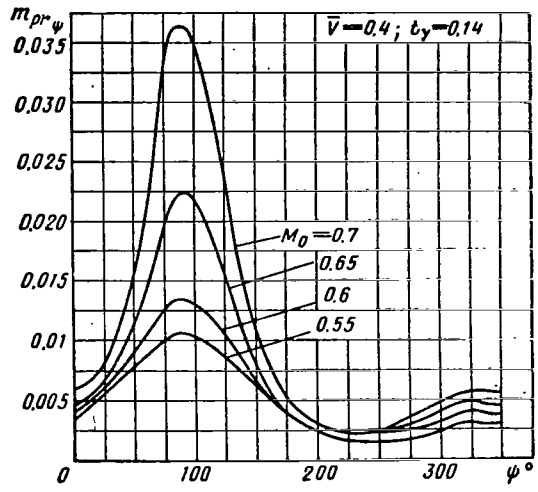

Fig.2.79 Azimuthal Variation in Profile Power Coefficient of Blade.

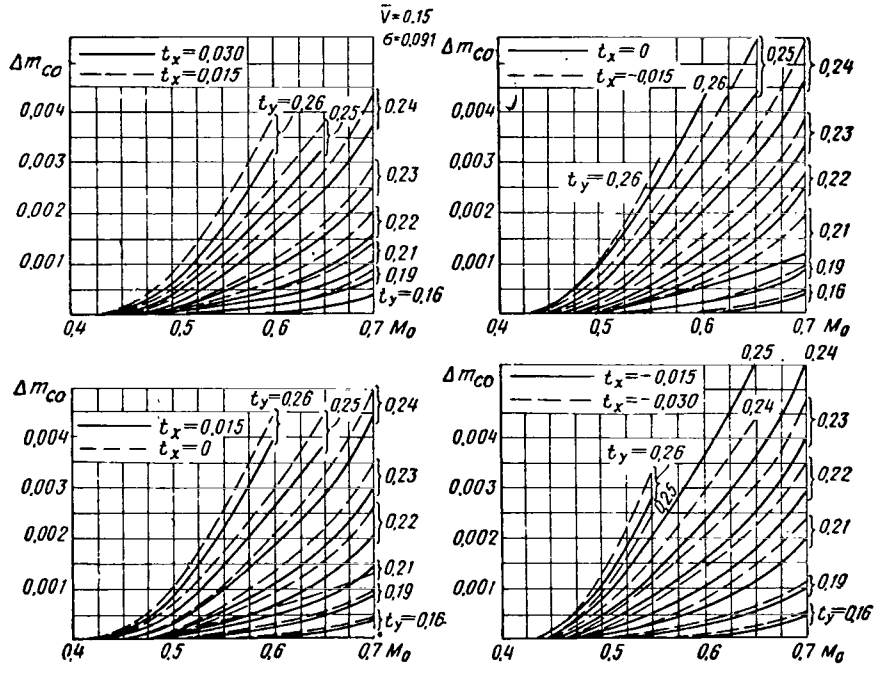

Fig.2.80 Increment in Profile Power Coefficient of Rotor, due to Air Compressibility.

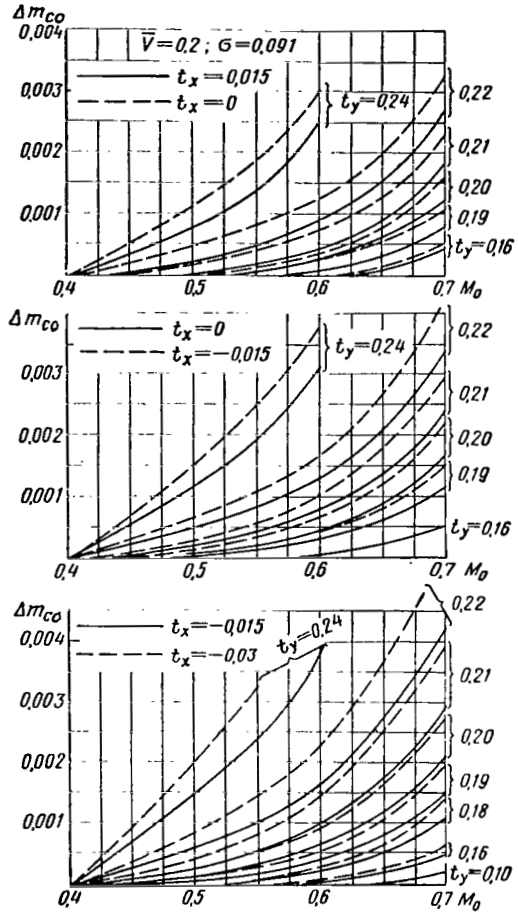

Fig.2.81 Increment in Profile Power Coefficient of Rotor, due to Air Compressibility.

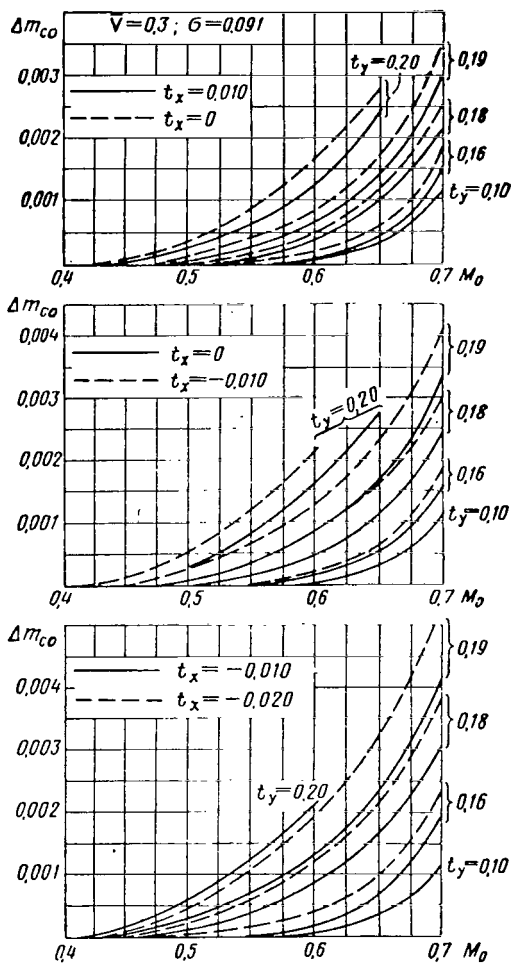

Fig.2.82 Increment in Profile Power Coefficient of Rotor, due to Air Compressibility.

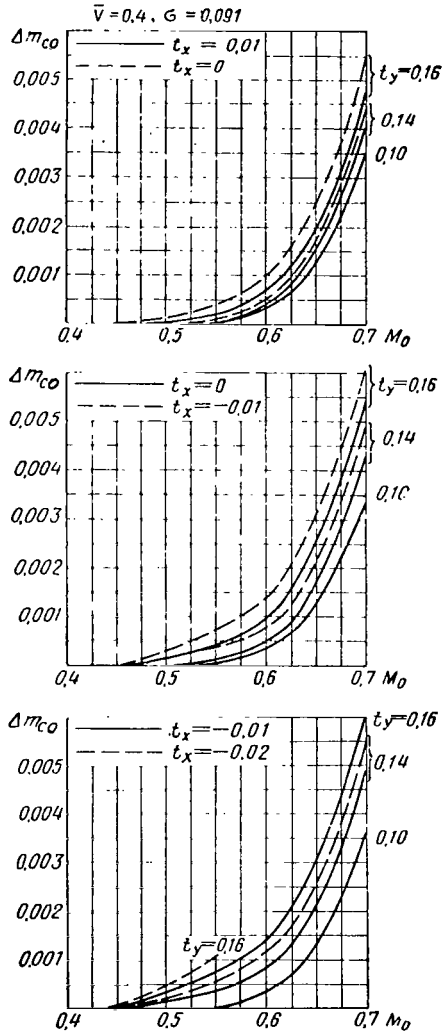

Fig.2.83 Increment in Profile Power Coefficient of Rotor, due to Air Compressibility.

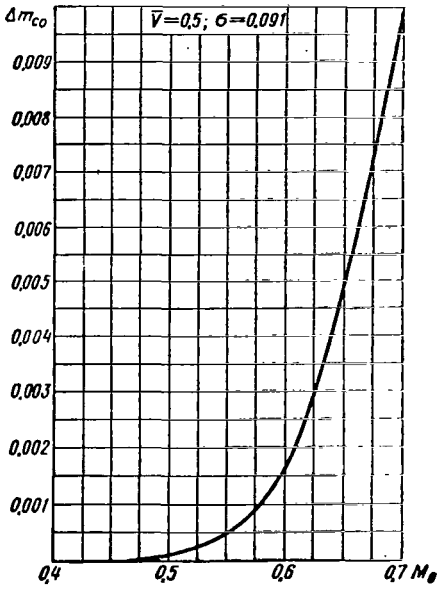

Fig.2.84 Increment in Profile Power Coefficient of Rotor, due to Air Compressibility.

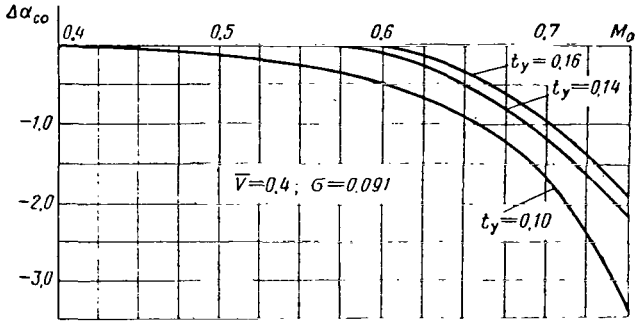

Fig.2.85 Increment in Angle of Attack of Rotor, due to Air Compressibility at Constant Coefficient of Propulsive Force.

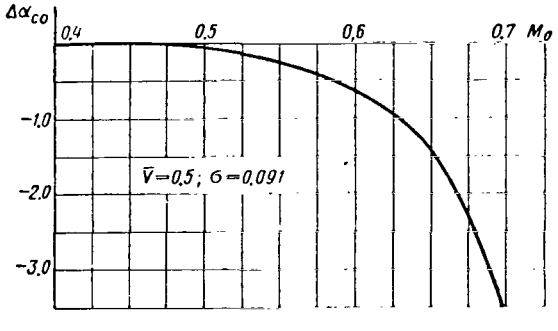

Fig.2.86 Increment in Angle of Attack of Rotor, due to Air Compressibility at Constant Coefficient of Propulsive Force.

in profile power will be $\Delta m_{co} = 0.0016$ which amounts to 18% of $m_{t_{h.f}}$. When $M_o = 0.65$, $\bar{V} = 0.4$, $t_y = 0.13$, and $t_{x_{h.f}} = -0.0133$, the increment in profile power will be $\Delta m_{co} = 0.002$ which amounts to 16% of $m_{t_{h.f}}$.

Since, at large $\bar{V}$, the increment in $m_{pr\psi}$ occurs mainly at azimuths close to 90°, the increase in Δm_{co} at large $\bar{V}$ is intimately connected with the relation between the Mach number of the blade-tip section at $\psi = 90°$, equal to $M_{fl} + M_o = M_o(1 + \bar{V})$, and the critical Mach number of the section profile. The critical Mach number M_{cr} is determined at $\alpha = 0$ since, in the tip sections at $\psi = 90°$, we have $\alpha_r \approx 0$. /167

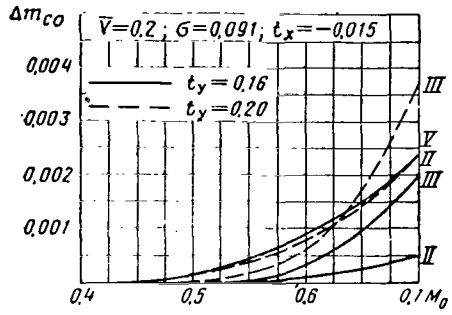

Fig.2.87 Increment in Profile Power Coefficient, due to Air Compressibility for Rotors with Blades of Different Shape.

These data show that a 15 - 18% increase in required power, due to the compressibility effect, occurs at $M_{fl} + M_o = 0.91$, i.e., $M_{fl} + M_o$ is larger by 0.1 than M_{cr} of the high-speed profile when $\alpha = 0$ (see Fig.2.99). At $M_{fl} + M_o = M_{cr} + 0.15$, the increase in required power is about 30%. At $M_{fl} + M_o = M_{cr}$, the compressibility effect is virtually absent. These relations between M_o, M_{fl}, and M_{cr} of the blade profile can be used when selecting M_o for a helicopter with high flying speeds.

Since, on an increase in M_o, the angle of attack of the rotor should be more negative so as to retain identical values of the coefficients t_y and t_x, the graphs for the increment in rotor angle of attack are given in Figs.2.85 and 2.86:

$$\Delta\alpha_{co}(M_0) = \alpha(M_0) - \alpha(M_0 = 0.4). \qquad (3.77)$$

No graphs were constructed for $\bar{V} \approx 0.15 - 0.3$ since, at all t_y and t_x, the quantity $\Delta\alpha_{co}$ does not exceed 1°.

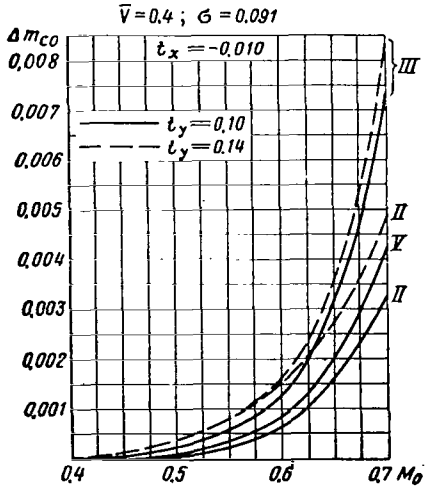

Fig.2.88 Increment in Profile Power Coefficient, due to Air Compressibility for Rotors with Blades of Different Shape.

Figures 2.87 and 2.88 show comparative graphs of Δm_{co} for rotors with blades of the variants II, III, and V. Calculations showed that the quantity Δm_{co} is greatly affected by the type of profile (this is seen from a comparison of the variants II and III) and by the geometric twist of the blade (variant V, straight blade). The planform of the blade plays a role only at large t_y in which case, for trapezoidal blades where flow separation begins earlier, Δm_{co} is greater than for rectangular blades. The planform of the blade plays a minor role at large M_o in view of the fact

that, as will be shown in Section 4.7, a variation in planform will cause a change in the angles of attack of the sections mainly at azimuths ψ = 250 - 340° where profile losses are small in the pre-separation regime.

A comparison of blades with a high-speed profile at the tip (variant II) and without it (variant III) used in the calculation, will show that a high-speed profile must be established at the blade tip when $M_0 > 0.6 - 0.625$.

The graphs of Δm_{c_0} and $\Delta\alpha_{c_0}$ should be calculated for each specific rotor. However, if no such calculations are available, the data in Figs.2.80 - 2.88 can be used for an approximate estimate of Δm_{c_0}.

The graphs in Figs.2.80 - 2.88 are laid out also for taking into account /168
the influence of the Mach number M_0 on the aerodynamic characteristics of a rotor, for cases in which the rotor characteristics experimentally determined at low M_0 are to be used also at high M_0. Furthermore, the graphs are useful for aerodynamic calculations to avoid interpolation of the Mach number M_0 if the calculated M_0 values do not coincide with those for which the graphs of the aerodynamic characteristics were plotted.

To use the graphs shown in Figs.2.80 - 2.83 for rotors with similar blades but with a different loading factor, it is necessary to recalculate the coefficient t_x for σ = 0.091 (Sect.6).

7. Induced Losses of a Real Rotor

Assuming a constant induced velocity over the entire rotor disk, the torque coefficient can be obtained from the graphs in Figs.2.60 and 2.61. The interdependence of the ratios $C_Y/B^2\bar{V}^2$, $C_X/B^2\bar{V}^2$, and $\bar{m}_t/\bar{V}^3$, which was derived in the theory of an ideal rotor, is valid when these ratios are determined with respect to the total forces Y and X taken with consideration of the profile drag, since the forces of the profile drag also create induced velocities so that the velocity polygons and all relations given in Subsection 1 remain in force. We must add the profile losses to the $\bar{m}_t$ obtained in this manner.

Consequently,

$$\bar{m}_t = \frac{\bar{m}_{t_{id}}}{\bar{V}^3}\bar{V}^3 + \bar{m}_{pr}, \tag{3.78}$$

where

$$\frac{\bar{m}_{t_{id}}}{\bar{V}^3}\bar{V}^3 = \frac{1}{B^2}\left(C_Y\bar{v}_y + C_X\bar{v}_x - C_X\bar{V}\right) = \frac{1}{B^2}\left(C_R\bar{u} - C_X\bar{V}\right).$$

The addend in the expression for $\bar{m}_t$, containing the product of the aerodynamic force and the induced velocity $C_R\bar{u}$, will be called the induced losses of the rotor.

In calculating the induced losses, we introduce a correction for taking into account the nonuniform induced velocity distribution over the rotor disk.

As follows from eq.(3.67), the induced losses of a real rotor are determined by means of the formula

$$m_{ind}=\int_0^{2\pi} d\psi \int_0^1 dt_R \bar{u}=\int_0^{2\pi} d\psi \int_0^1 (dt_y \bar{v}_y - dt_x \bar{v}). \tag{3.79}$$

However, to calculate ordinary helicopter regimes, at $t_y > t_x$, an approximate expression is used

$$m_{ind}=\int_0^{2\pi} d\psi \int_0^1 dt \bar{v}. \tag{3.80}$$

First, just as in the ideal rotor theory, we determine m_{ind} under the assumption of constant induced velocity over the entire rotor disk. With this assumption and with an approximate consideration of tip losses, the expression for m_{ind} takes the simple form

$$m_{ind}=\frac{1}{B^2}\int_0^{2\pi} d\psi \int_0^B dt\bar{v}=\frac{1}{B^2}\, t\bar{v}. \tag{3.81}$$

For flying regimes at $\bar{V} \geq 0.15$, substitution of eq.(3.48) for $\bar{v}$ will yield

$$m_{ind}=\frac{t^2\sigma}{4B^4\bar{V}}. \tag{3.82}$$

We will demonstrate that eq.(3.82) holds not only for the assumption of constant induced velocity over the rotor disk but also for an induced velocity distribution obeying the law

$$\bar{v}(\bar{r},\psi)=\bar{v}+a\bar{r}\cos\psi, \tag{3.83}$$

where a is a constant.

According to eq.(3.83), the induced velocity has a minimum value in the forward portion of the rotor disk ($\psi = \pi$, $\bar{r} = 1$) and increases linearly in the direction of the velocity flow. In a direction perpendicular to the velocity flow, the induced velocity remains constant. Thus, the form of the induced velocity diagram is a cylinder cut off by a plane turned toward the plane of rotation of the rotor about an axis perpendicular to the direction of motion (see Fig.2.6); the angle of turn is characterized by the quantity a; $\bar{v}$, the average induced velocity of the disk, is determined from eqs.(3.46) or (3.48).

The induced velocity diagram described by eq.(3.83) is close in character to the time-average induced velocity diagram found from experiment (see Fig.2.3).

Let us substitute eq.(3.83) into eq.(3.80) and find

$$m_{ind}=\int_0^{2\pi} d\psi \int_0^1 dt(\bar{v}+a\bar{r}\cos\psi)=\bar{v}\int_0^{2\pi} d\psi \int_0^1 dt + a\int_0^{2\pi}\cos\psi\, d\psi \int_0^1 dt\bar{r}.$$

The integral in the first addend is equal to the rotor thrust coefficient. The integral for radius in the second addend is proportional to the sum (see Subsect.2) $\frac{d^2\beta}{d\psi^2} + \beta$ – const for a rotor with flapping hinges. With an accuracy to the first harmonics of flapping, the sum $\frac{d^2\beta}{d\psi^2} + \beta = a_0$; consequently, $\int_0^1 d\bar{t}\bar{r}$ is a quantity independent of the azimuthal position of the blade. Therefore, $\int_0^{2\pi} \cos\psi \, d\psi \int_0^1 d\bar{t}\bar{r} = 0$.

Thus, for the induced velocity distribution in accordance with eq.(3.83) the induced losses are also determined by eq.(3.81). Calculations based on the vortex theory for a rotor with an infinite number of blades show that, owing to differences in the induced velocity diagram from eq.(3.83), the induced losses of a rotor with twisted blades are about 5% greater. Taking $B^4 = 0.92$, the induced losses of the rotor in flying regimes at $\bar{V} \geq 0.15$ are determined by the expression

$$m_{ind} = \frac{1.05}{0.92 \cdot 4} \frac{t^2\sigma}{\bar{V}} = 0.285 \frac{t^2\sigma}{\bar{V}}. \tag{3.84}$$

In flying regimes with small $\bar{V}$, the quantity $\bar{m}_{ind}$ is found from eq.(3.85) /170 where $\tilde{u}$ is determined as a function of C_R, $\bar{V}$, and δ from the graph in Fig.2.62:

$$\bar{m}_{ind} = \frac{1.05}{B^2} C_R \bar{u} = \frac{1.05}{2B^3} C_R^{3/2} \tilde{u} = 0.56 C_R^{3/2} \tilde{u}, \tag{3.85}$$

where, just as in eq.(3.84), 1.05 is a coefficient taking into account the increase in induced losses.

The dependence of $\tilde{u}$ on $\tilde{V}$ can be refined by flight tests. After determining the required rotor power from flight tests for a number of horizontal flying speeds and after calculating the parasite drag of the helicopter, we find $C_{Y_{h.f}}$, $C_{X_{h.f}}$ (see Chapt.III, Sect.1.2) as well as C_R, $\bar{m}_{t_{h.f}}$, and then $\tilde{V}$ and $\tilde{u}$ from the expressions

$$\tilde{V} = \bar{V} \frac{1}{\sqrt{\frac{C_R}{4B^2}}} = 1.96 \frac{\bar{V}}{\sqrt{C_R}}; \tag{3.86}$$

$$\tilde{u} = \frac{\bar{m}_{t_{h.f}} - \bar{m}_{pr} + \frac{1}{B^2} C_{X_{h.f}} \bar{V}}{0.56 C_R^{3/2}}. \tag{3.87}$$

The graph of $\tilde{u} = f(\tilde{V})$ obtained from flight tests of the Mi-4 helicopter is shown in Fig.2.89.

The tests were performed at different heights between rotor and surface of the airfield h. In flights close to the ground, the quantity $\tilde{u}$ was affected by

the "air cushion". The values of $\tilde{u}$ in the influence domain of the "air cushion" are plotted on the graph for different values of $\bar{h} = \frac{h}{R}$.

The graph of $\tilde{u}$ in Fig.2.89 was obtained for low horizontal flying speeds, when $\delta = \delta_{h.f} \approx 0$. However, the diagram can be used approximately for values of δ within limits from $+5^\circ$ to -20°. Calculations made from the graph of $\tilde{u}$, shown in Fig.2.62, revealed that instead of determining the product $\tilde{u}C_R^{3/2}$ we can calculate the product $\tilde{u}C_Y^{3/2}$ ($C_Y = C_R \cos\delta$), determining $\tilde{u}$ for $\delta = 0$ and $\bar{V} = 1.96 \frac{\bar{V}}{\sqrt{C_y}}$:

$$\tilde{u}\left(\delta, \frac{\bar{V}}{\sqrt{C_R}}\right) C_R^{3/2} \approx \tilde{u}\left(\delta = 0, \frac{\bar{V}}{\sqrt{C_Y}}\right) C_Y^{3/2}. \qquad (3.88)$$

Thus, in calculating the rotor characteristics at low flying speeds, $\bar{m}_{ind}$ is determined from the expression

$$\bar{m}_{ind} = 0.56\tilde{u}C_Y^{3/2}. \qquad (3.89)$$

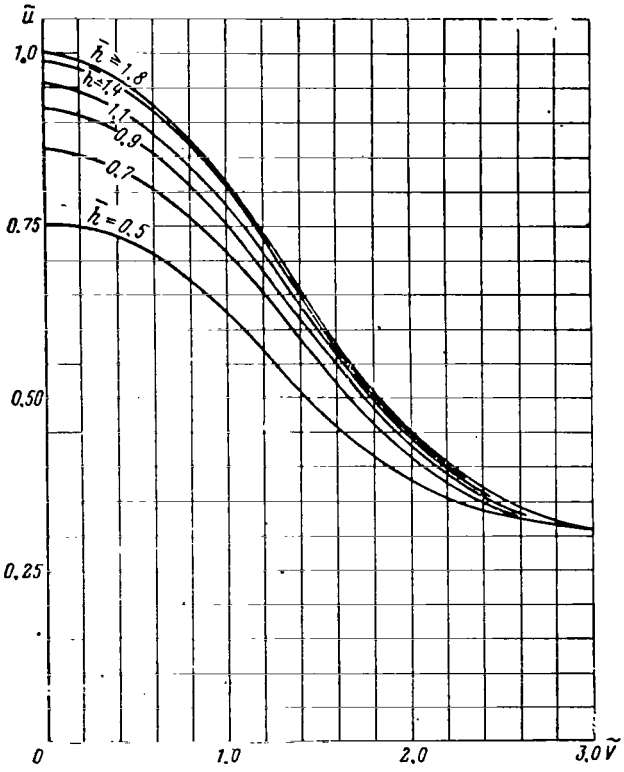

Fig.2.89 Induced Velocity $\tilde{u}$ as a Function of $\bar{V}$ and $\bar{h}$ (Based on Flight Tests of the Mi-4 Helicopter).

Equation (3.89) can be used both for calculating the rotor power required for horizontal flight at low flying speeds and for determining the propulsive force of the rotor when calculating the takeoff distance of a helicopter or the towing force of a towing helicopter. These calculations are substantially simplified because of the fact that, for determining the velocity coefficient $\bar{V}$, it suffices to know C_Y and not C_R.

The graph of the average induced velocity $\tilde{u}$ for a rotor system (with consideration of mutual interference) of the Yak-24 fore-and-aft helicopter is shown in Fig.2.90. Figure 2.90 also contains the curve $\tilde{u}$ for the Mi-4 helicopter outside the earth's influence. This graph can be used approximately for determining $\tilde{u}$ of all helicopters of single-rotor configuration /171 and of fore-and-aft helicopters with an excess of rotors y_k (see Fig.3.8) close to $\bar{y}_k = 0.057$, just as for the Yak-24.

Turning to these curves, we can find $\tilde{u}$ for fore-and-aft helicopters with other $\bar{y}$ and also for helicopters of side-by-side configuration, after determining $\tilde{u}$ at high flying speeds ($\bar{V} \geq 0.15$) from eq.(3.87), based on data of an aerodynamic calculation. Such a curve is plotted in Fig.2.90 for a helicopter of side-by-side configuration with a coefficient of mutual induction $\varkappa_{ss} = -0.4$.

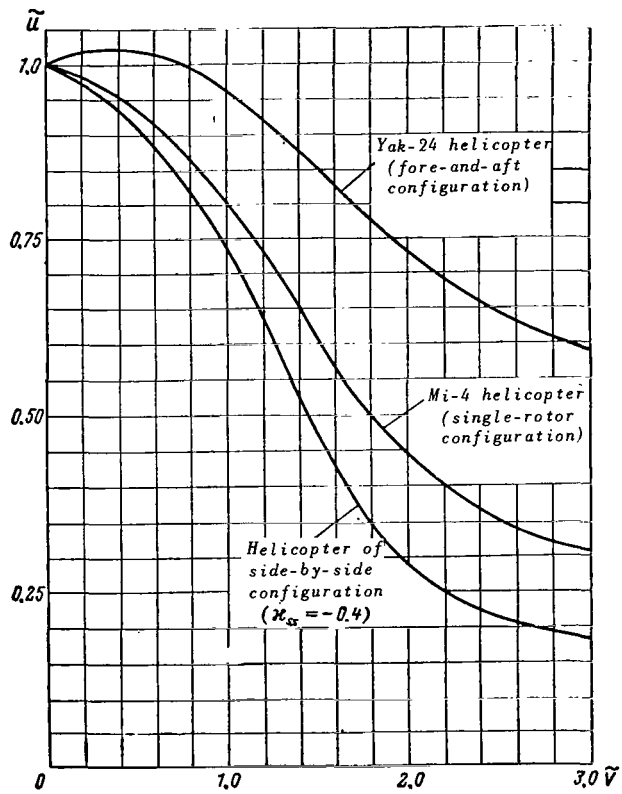

Fig.2.90 Induced Velocity $\tilde{u}$ vs. $\tilde{V}$ for Helicopters of Various Configurations.

It is interesting to note that at low $\tilde{V}$ for a fore-and-aft helicopter the induced velocity coefficient, owing to the mutual interference of the rotors, is greater than in a hovering regime. Consequently, its required power at low flying speeds is greater than in the hovering regime.

Thus, a fore-and-aft helicopter has poor flying characteristics at low flying speeds (in acceleration, in takeoff runs when taking off like an airplane, and in towing); they are substantially worse than those of single-rotor and side-by-side helicopters.

Since $\tilde{u}$ depends on the ratio $\frac{V}{\sqrt{C_Y}}$, which is directly proportional to the ratio $\frac{V}{\sqrt{p}}$ (p being the load per square meter of the rotor area, $p = \frac{T}{F}$), the flying speed has a different effect on the required power for helicopters with different p. Therefore, for helicopters with a larger p, the wind in this case lowers the required power less or increases the maximum rotor thrust in hovering. /172

* * *

Thus, for calculating the torque coefficient of a lift-producing rotor and a propulsive force with coefficients t_y, t_x exposed to an air stream with dimensionless velocity $\bar{V} \geq 0.15$, we can use the following expression:

$$m_t = m_{pr} + \frac{1.05}{4B^4}\frac{t_y^2 \sigma}{\bar{V}} - \frac{1}{B^2} t_x \bar{V} = \\ = m_{pr} + 0.285\frac{t_y^2 \sigma}{\bar{V}} - 1.04 t_x \bar{V}. \qquad (3.90)$$

Owing to the necessity of taking tip losses into account, the coefficients B^2 are often omitted in the term $\frac{1}{B^2} t_x \bar{V}$ so that eq.(3.90) takes the following form:

$$m_t = m_{pr} + 0.285 \frac{t_y^2 \sigma}{\bar{V}} - t_x \bar{V}. \tag{3.91}$$

The coefficient m_{pr} is determined as indicated in Subsections 3 - 6 of this Section.

8. Determination of Angle of Attack and Pitch of Rotor /173

The momentum theory gives no data on the angle of attack of the rotor. Determination of the angle of attack of the rotor α and its characteristics in a rotor-fixed coordinate system (forces T, H), however, is necessary for calculating the rotor pitch, for refining the magnitude of parasite drag of the non-lift-producing parts of the helicopter, and mainly for determining the equilibrium conditions of the helicopter moment relative to the center of gravity (balancing) and its stability.

It is obvious that, when forces with coefficients C_Y and C_X are generated during some operating regime of the rotor, the determined mean dimensionless induced velocities $\bar{v}_y$ and $\bar{v}_x$ over the disk must correspond to these operating conditions. However, the angle of attack of the rotor may differ here and depends on the type of rotor (hinged or rigid), on the blade shape, etc. To determine the angle of attack of the rotor use must be made of the classical theory, wherein the found magnitude of the angle of attack depends on the assumptions contained in this theory.

Let us determine the angle of attack and pitch of the rotor.

To each point of the curves of m_{pr} (see Figs.2.63 - 2.74) there corresponds a certain rotor angle of attack. The angles of attack are laid off on these curves so that, in determining m_{pr} from Figs.2.63 - 2.74, the angle of attack of the rotor can be located. The rotor setting is found from graphs of $t_y = f(a, \theta_0, \bar{V})$ (see Figs.2.115 and 2.116) or from eq.(2.50) of the Glauert-Lock theory (Sect.3), wherein μ and λ are determined from eqs.(3.20), (3.21).

If the profile power coefficient is determined from eq.(3.72) rather than from the graphs in Figs.2.63 - 2.74, then α_e which is the angle of attack of an equivalent rotor (see Sect.2), is calculated from the approximate equation (3.95). This formula is derived on the basis of the following relations:

$$t_x = t \sin \alpha_e + h_e \cos \alpha_e \approx t\alpha_e + h_e. \tag{3.92}$$

Assuming $h_e \approx ta_{1_e}$, we find from eq.(3.92)

$$\alpha_e \approx \frac{t_x}{t} - a_{1_e}. \tag{3.93}$$

The flapping coefficient a_{1_e} can be expressed by the approximate relation [eq.(3.94)] derived from formulas of the Glauert-Lock theory:

$$a_{1_e} = 2\bar{V}\left[t\left(\frac{4}{a_\infty} - \frac{\sigma}{4B^2\bar{V}}\right) - \bar{V}\alpha_e\right]. \tag{3.94}$$

After transformation of eqs.(3.93) and (3.94), we obtain the formula for determining α_e :

$$\alpha_e = \frac{1}{1-2\bar{V}^2}\left[\frac{t_x}{t} - 2\bar{V}t\left(\frac{4}{a_\infty} - \frac{\sigma}{4B^2\bar{V}}\right)\right]. \tag{3.95}$$

At large Mach numbers M_0 for $V \geq 0.4$, the increment in angle of attack is found from the graphs in Figs.2.85 and 2.86.

After α_e is determined, μ, λ, φ, and other data are found.

Having determined α, eqs.(3.15) and (3.17) will permit finding the coefficients of thrust and longitudinal force of the rotor.

Section 4. Classical Rotor Theory. Method of Numerical Integration

/174

When calculating the aerodynamic characteristics of a rotor in regimes with large $\bar{V}$, M_0, and t_y, many of the assumptions of the Glauert-Lock theory lead to substantial errors. For commonly used rotors, we can consider that $\bar{V} \geq 0.3$-0.35; $M_0 \geq 0.55 - 0.6$; and t_y close to $t_{y_{cr}}$, based on the condition of flow separation.

In calculating such regimes it is primarily necessary to discard the approximation of the profile characteristics stipulated in the Glauert-Lock theory: $c_y = a_\infty \alpha_r$ and $c_{xp} = c_{xp_{av}}$, where a_∞ and $c_{xp_{av}}$ are constants at all points of the disk regardless of the angle of attack α_r and the Mach number of the blade section.

In practice it is impossible to give a sufficiently accurate analytical expression for the dependence of c_y and c_{xp} on α and M. Therefore, in the refined calculation methods the angle of attack and the Mach number are found at each point of the swept disk after which c_y and c_{xp} are determined from the graphs of the profile characteristics.

For calculating the distribution of the angles of attack, the flapping angle of the blade β must be known; however, this can be determined only if the thrust moment relative to the flapping hinge is known. The latter can be found when the distribution of the angles of attack is known. Therefore, the calculation can be constructed either on the basis of determining, by the method of successive approximations, the flapping coefficients with respect to the first 2 - 3 harmonics, or on the basis of determining β and $\frac{d\beta}{d\psi}$ by numerical integra-

tion of the equation of flapping; the second method of calculation, which has become widespread, will be described below.

Practical application of such a laborious computational process is possible only with the use of high-speed digital computers. Under this condition, the previously used assumptions for overcoming mathematical difficulties can be discarded. Unavoidable assumptions are only those due to our lack of knowledge of individual problems at the present state of art of rotor aerodynamics. Such assumptions include:

Determination of c_y and c_{xp} of sections, neglecting the angles of sideslip $\left(\text{equal to } \frac{\bar{U}_z}{\bar{U}}\right)$ and variations in the boundary layer produced by centrifugal forces arising on blade rotation; c_y and c_{xp} of the sections are determined from the aerodynamic characteristics of the profile obtained in a plane-parallel flow.

Neglect of the effect of unsteady circulation of flow about the blade sections, which involves a complex motion, on the aerodynamic characteristics of the profile.

Neglect of the fuselage and hub effects on rotor aerodynamics, and others.

The method of calculation permits taking into account (within the assumptions given above) individual features of the blade profiles and to select a profile on the basis of quantitative data rather than of qualitative considerations, as was done previously.

The aerodynamic characteristics can be calculated together with calculation of blade deformation and with consideration of the induced velocity distribution caused by a vortex system of arbitrary form; the computational effort depends on the accuracy requirements and on the capability of the computer such as memory capacity and speed of computation.

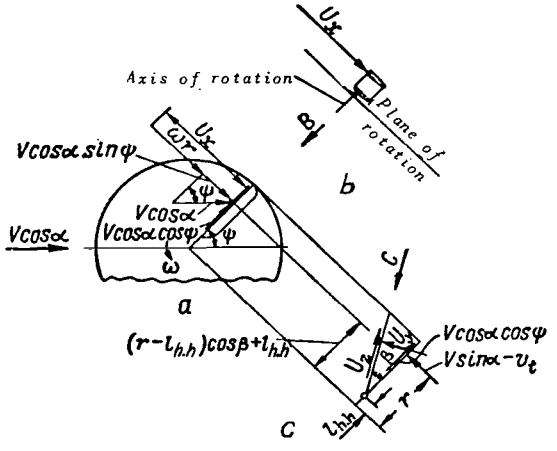

Fig.2.91 For Determining the Component of Relative Velocity of Flow around the Blade Section.

1. Formulas for Calculating Forces and Moments of a Rotor /175

First, let us derive formulas for determining the components of the relative velocity of flow about the blade sections. These differ from the formulas derived in Section 2 in that they take into account the spacing of the flapping hinges and do not consider the angles β and Φ to be small.

The component U_x (Fig.2.91a, b) is directed perpendicular to the blade axis and is located in a plane parallel to the plane of rotation (or located in the

plane of rotation when the flapping angle of the blade relative to the flapping hinge is zero). As shown in Fig.2.91, U_x is composed of the projection of the flying speed, equal to V cos α sin ψ, and the peripheral speed of the section $\omega[r - l_{h.h}) \cos \beta + l_{h.h}]$:

$$U_x = \omega[(r - l_{h.h}) \cos \beta + l_{h.h}] + V \cos \alpha \sin \psi. \tag{4.1}$$

Changing to relative qualities, we obtain

$$\bar{U}_x = \frac{U_x}{\omega R} = (\bar{r} - \bar{l}_{h.h}) \cos \beta + \bar{l}_{h.h} + \bar{V} \cos \alpha \sin \psi =$$

$$= (\bar{r} - \bar{l}_{h.h}) \cos \beta + \bar{l}_{h.h} + \mu \sin \psi, \tag{4.2}$$

where

$$\mu = \frac{V \cos \alpha}{\omega R} = \bar{V} \cos \alpha. \tag{4.3}$$

Strictly speaking, with consideration of flow stagnation in the region of the rotor equal to the induced velocity v_h, the flow velocity in the plane of rotation is equal to V cos α - v_h. Therefore, the dimensionless coefficient μ must be determined from eq.(3.20). This introduces no complications if the calculation is made at a given μ, and the dimensionless flying speed $\bar{V}$ is determined from eq.(3.20) when $\bar{v}_h$ is already known. If the calculation is made at a given $\bar{V}$, then for simplification we will determine μ by the approximate equation (4.3). /176

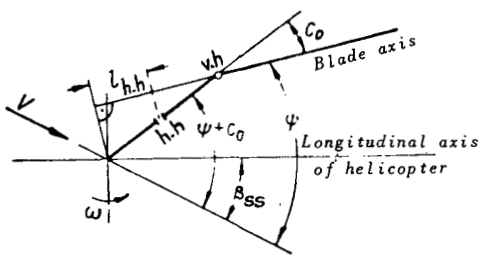

Fig.2.92 For Determining the Position of Blade, Hub, and Longitudinal Axis of the Helicopter Relative to the Flight Direction.

In this Chapter, we will not discuss blade flapping relative to the drag hinge. The variable part of the angle of deflection of the blade about the drag hinge is negligible and it can be considered that all blades turn about the drag hinge through an identical angle $\xi_{av} = c_0$. Therefore, at some azimuthal position of the blade ψ, the rotor hub is turned through an angle $\psi + c_0$ toward the projection of the flying speed and through an angle $\psi + c_0 - \beta_{ss}$ to the longitudinal axis of the helicopter, if the craft is flying with sideslip (Fig.2.92).

The component U_z (see Fig.2.91a, c) directed along the blade axis, is equal to

$$U_z \approx V \cos \alpha \cos \psi \cos \beta. \tag{4.4}$$

This component determines the angle of sideslip in flow through the blades.

The component U_y is directed perpendicular to the blade axis and is located in the blade flapping plane (being parallel to the shaft axis when the flapping angle of the blade is equal to zero).

As shown in Fig.2.91c, the component U_y is composed of the following speeds:
projection of the speeds perpendicular to the plane of rotation of the rotor, $V \sin \alpha - v_t$;
projection of the component of flying speed, $V \cos \alpha \cos \psi$;

peripheral speed of flapping, $(r - l_{h.h}) \frac{d\beta}{dt}$.

The sum of these speeds is equal to

$$U_y = (V \sin \alpha - v) \cos \beta - V \cos \alpha \cos \psi \sin \beta - (r - l_{h.h}) \frac{d\beta}{dt}, \tag{4.5}$$

where v is the induced velocity component perpendicular to the plane of rotation (v_t in Sect.3).

On replacing the differentiation with respect to time by a differentiation with respect to the angle of blade rotation ($\psi = \omega t$) and changing over to relative quantities, we obtain

$$\begin{aligned} \overline{U}_y = \frac{U_y}{\omega R} = (\overline{V} \sin \alpha - \overline{v}) \cos \beta - \overline{V} \cos \alpha \cos \psi \sin \beta - \\ - (\overline{r} - \overline{l}_{h.h}) \frac{d\beta}{d\psi} = \lambda(r, \psi) \cos \beta - \mu \cos \psi \sin \beta - (\overline{r} - \overline{l}_{h.h}) \frac{d\beta}{d\psi}. \end{aligned} \tag{4.6}$$

Here the flow coefficient $\lambda(r, \psi)$ at nonuniform induced velocity distribution /177 is equal to

$$\begin{aligned} \lambda(r, \psi) = \overline{V} \sin \alpha - \overline{v}(r, \psi) = \overline{V} \sin \alpha - [\overline{v} - \Delta \overline{v}(r, \psi)] = \\ = \lambda + \Delta \overline{v}(r, \psi), \end{aligned} \tag{4.7}$$

whence

$$\lambda = \overline{V} \sin \alpha - \overline{v}, \tag{4.7'}$$

where
$\overline{v}$ and $\Delta \overline{v}$ (r, ψ) = mean and variable portions of the dimensionless induced velocity;
λ = average flow coefficient over the disk.

The geometric sum of the components U_x and U_y is equal to the relative flow velocity through the blade section in a plane normal to the blade axis:

$$\overline{U} = \sqrt{\overline{U}_x^2 + \overline{U}_y^2}. \tag{4.8}$$

The angle β and the angular velocity $\frac{d\beta}{d\psi}$ of the flapping motion of the

blade, which are determined from the flapping equation, enter the expressions for U_x, U_y, U_z.

Without the simplifying assumptions made in Section 2, the flapping equation has the form

$$I_{h.h}\omega^2\frac{d^2\beta}{d\psi^2}+(I_{h.h}\cos\beta-l_{h.h}S_{h.h})\omega^2\sin\beta=$$

$$=\int_{l_{h.h}}^{R}\frac{dT}{dr}(r-l_{h.h})\,dr-gS_{h.h} \qquad (4.9)$$

or, in dimensionless form,

$$\frac{d^2\beta}{d\psi^2}+\left(\cos\beta-\frac{l_{h.h}S_{h.h}}{I_{h.h}}\right)\sin\beta=\frac{\gamma}{a_\infty}m_{h.h}-\frac{gS_{h.h}}{I_{h.h}\omega^2}, \qquad (4.10)$$

where

$$\left.\begin{aligned}\frac{\gamma}{a_\infty}&=\frac{\varrho b_{0.7}R^4}{2I_{h.h}};\\ m_{h.h}&=\int_{\bar{l}_{h.h}}^{1}\frac{dt}{d\bar{r}}(\bar{r}-\bar{l}_{h.h})\,d\bar{r}.\end{aligned}\right\} \qquad (4.11)$$

To calculate the flying regimes common for a helicopter, we can assume a small value of the angle β. Then the flapping equation is simplified to

$$\frac{d^2\beta}{d\psi^2}+\left(1-\frac{l_{h.h}S_{h.h}}{I_{h.h}}\right)\beta=\frac{\gamma}{a_\infty}m_{h.h}-\frac{gS_{h.h}}{I_{h.h}\omega^2}. \qquad (4.12)$$

To determine the angle of attack of the blade section α_r, we examine the drawing (Fig.2.93) in a plane perpendicular to the blade axis (view along the arrow C in Fig.2.91).

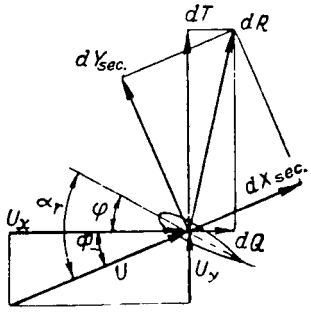

Fig.2.93 Speeds and Aerodynamic Forces of Blade Element.

Figure 2.93 shows that air with a relative velocity U, directed at an angle Φ to the plane of rotation, will flow over the blade section turned through an angle φ to the plane of rotation (φ being the blade pitch in the studied section). The angle of attack of the blade section is equal to /178

$$\alpha_r=\varphi+\Phi; \qquad (4.13)$$

$$\Phi=\tan^{-1}\frac{U_y}{U_x}; \qquad (4.14)$$

$$\alpha_r=\varphi+\tan^{-1}\frac{U_y}{U_x}=\varphi+\tan^{-1}\frac{\bar{U}_y}{\bar{U}_x}. \qquad (4.15)$$

The blade pitch in the examined section depends on the following: overall

pitch of the rotor θ_0 equal to the blade pitch in the section $\bar{r} = 0.7$ at $\beta = 0$ and without cyclic change of pitch; angle of twist $\Delta\varphi$ of the section relative to the section $\bar{r} = 0.7$; flapping angle of the blade in the presence of a flapping compensator; cyclic change of blade pitch. The sum of these terms is equal to

$$\varphi = \theta_0 + \Delta\varphi - k\beta - \theta_1 \sin\psi - \theta_2 \cos\psi - \sum_{n=0}^{\infty} (\bar{\nu}_n \cos n\psi + \bar{\bar{\nu}}_n \sin n\psi), \tag{4.16}$$

where

θ_1 and θ_2 = components of cyclic change of blade pitch, with deflection of the automatic pitch control;

$\bar{\nu}_n$ and $\bar{\bar{\nu}}_n$ = components of elastic twist of the blade.

The aerodynamic forces per unit length in the section $\bar{r}$ are determined by the coefficients c_y and c_x for the profile of the section under study, taken in relation to α_r. Since, in determining α_r, the induced velocity in the section was taken into account, the coefficients c_y and c_x are taken for a profile with infinite elongation.

The Mach and Reynolds numbers in the section are

$$M = \frac{U}{a} = \frac{\omega R}{a} \bar{U} = M_0 \bar{U}; \tag{4.17}$$

$$\mathrm{Re} = \frac{Ub}{\nu} = \frac{\omega R b_{0.7}}{\nu} \bar{\bar{b}}\bar{U} = \frac{a b_{0.7}}{\nu} \bar{\bar{b}} M. \tag{4.18}$$

Since the Re for helicopters is rather high, the coefficients c_y and c_{xp} of the sections will be considered (for simplification) to depend only on the Mach number in the section. Therefore, the aerodynamic characteristics of the profile for each M are taken at Re corresponding to a given Mach and mean chord and flight altitude:

$$\mathrm{Re} = \left(\frac{a}{\nu}\right)_{\alpha\nu} b_{0.7} M. \tag{4.19}$$

The lift and drag per unit length of the section will then be

$$\frac{dY_{sec.}}{dr} = \frac{1}{2} \varrho U^2 b c_y; \tag{4.20}$$

$$\frac{dX_{sec.}}{dr} = \frac{1}{2} \varrho U^2 b c_{xp}, \tag{4.21}$$

while their components directed along the axes relative to the rotor, i.e., /179
the thrust dT and the resistance to rotation dQ, will read

$$\frac{dT}{dr} = \frac{dY_{sec.}}{dr} \cos\Phi + \frac{dX_{sec.}}{dr} \sin\Phi; \tag{4.22}$$

$$\frac{dQ}{dr} = \frac{dX_{sec.}}{dr} \cos\Phi - \frac{dY_{sec.}}{dr} \sin\Phi. \tag{4.23}$$

Substituting, into eqs.(4.22) and (4.23), the expressions for cos Φ and sin Φ from eqs.(4.24) and (4.25)

$$\cos\Phi=\frac{U_x}{U}; \tag{4.24}$$

$$\sin\Phi=\frac{U_y}{U} \tag{4.25}$$

and the expressions for $\frac{dY_{sec.}}{dr}$ and $\frac{dX_{sec.}}{dr}$ from eqs.(4.20) and (4.21), we finally obtain

$$\frac{dT}{dr}=\frac{1}{2}\varrho bU(c_yU_x+c_{xp}U_y); \tag{4.26}$$

$$\frac{dQ}{dr}=\frac{1}{2}\varrho bU(c_{xp}U_x-c_yU_y) \tag{4.27}$$

or, in relative quantities,

$$\frac{dt}{d\bar{r}}=(c_y\bar{U}_x+c_x\bar{U}_y)\bar{U}\bar{\bar{b}}; \tag{4.28}$$

$$\frac{dq}{d\bar{r}}=(c_{xp}\bar{U}_x-c_y\bar{U}_y)\bar{U}\,\bar{\bar{b}}. \tag{4.29}$$

The antitorque moment of the blade per unit length, or the section torque, is determined from the formula (in relative quantities)

$$\frac{dm_t}{d\bar{r}}=\frac{dq}{d\bar{r}}[(\bar{r}-\bar{l}_{h.h})\cos\beta+\bar{l}_{h.h}]. \tag{4.30}$$

After integrating the loads per unit length over the blade radius, we obtain expressions for determining the forces and torque of the blade. Since these quantities depend on the blade position in the plane of rotation (its azimuthal position ψ), they are given the subscript ψ:

$$t_\psi=\int_{\bar{l}_{h.h}}^{1}\frac{dt}{d\bar{r}}d\bar{r}; \tag{4.31}$$

$$q_\psi=\int_{\bar{l}_{h.h}}^{1}\frac{dq}{d\bar{r}}d\bar{r}; \tag{4.32}$$

$$m_{t_\psi}=\int_{\bar{l}_{h.h}}^{1}\frac{dq}{d\bar{r}}[(\bar{r}-\bar{l}_{h.h})\cos\beta+\bar{l}_{h.h}]\,d\bar{r}. \tag{4.33}$$

The blade thrust is directed at an angle β to the axis of the rotor. Its projections onto the rotor axis and onto the plane of rotation are equal to $t_\psi\cos\beta$ and $t_\psi\sin\beta$.

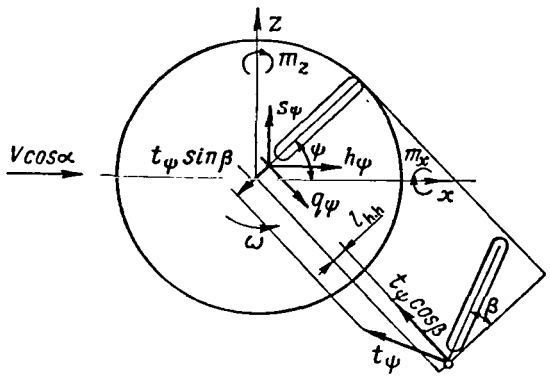

Fig.2.94 For Determining Coefficients of Longitudinal and Transverse Blade Forces.

On mapping the blade forces in the plane of rotation onto the longitudinal and transverse axes of the rotor, we find the longitudinal and transverse forces of the blade (Fig.2.94): /180

$$h_\psi = -t_\psi \sin\beta\cos\psi + q_\psi \sin\psi; \qquad (4.34)$$

$$s_\psi = -t_\psi \sin\beta\sin\psi - q_\psi \cos\psi. \qquad (4.35)$$

The component $t_\psi \cos\beta$ creates the longitudinal and lateral moments of aerodynamic forces $m_{z_{A\psi}}$ and $m_{x_{A\psi}}$:

$$m_{z_{A\psi}} = -t_\psi \cos\beta \bar{l}_{h.h} \cos\psi; \qquad (4.36)$$

$$m_{x_{A\psi}} = -t_\psi \cos\beta \bar{l}_{h.h} \sin\psi. \qquad (4.37)$$

In order to determine the blade forces and moments in a dimensionless form, the dimensionless coefficients must be multiplied by $\frac{1}{z_b}\frac{1}{2}\rho\sigma(\omega R)^2 F$ and $\frac{1}{z_b}\frac{1}{2}\rho\sigma(\omega R)^2 FR$.

The instantaneous value of rotor forces and moments can be found by summing the forces and moments of all blades at a selected instant of time (one blade being at an angle ψ, the second at an angle $\psi + \frac{2\pi}{z_b}$, the third at an angle $\psi + 2\frac{2\pi}{z_b}$, and so on).

The average per-revolution forces and moments created by the blade are equal to the integral with respect to ψ from eqs.(4.31) - (4.37) divided by 2π. On multiplying the result by the number of blades, we find the average forces and moments of the rotor per revolution.

In a dimensionless form, the average per-revolution forces and moments of aerodynamic forces are determined by the expressions

$$t = \frac{1}{2\pi}\int_0^{2\pi} t_\psi \cos\beta\, d\psi; \qquad (4.38)$$

$$h = \frac{1}{2\pi}\int_0^{2\pi} h_\psi\, d\psi; \qquad (4.39)$$

$$m_t = \frac{1}{2\pi}\int_0^{2\pi} m_{t_\psi}\, d\psi; \qquad (4.40)$$

/181

$$s=\frac{1}{2\pi}\int_0^{2\pi} s_\psi\, d\psi; \tag{4.41}$$

$$m_{z_A}=\frac{1}{2\pi}\int_0^{2\pi} m_{z_{A\psi}}\, d\psi=-\frac{1}{2\pi}\bar{l}_{h.h}\int_0^{2\pi} t_\psi \cos\beta\cos\psi\, d\psi; \tag{4.42}$$

$$m_{x_A}=\frac{1}{2\pi}\int_0^{2\pi} m_{x_{A\psi}}\, d\psi=-\frac{1}{2\pi}\bar{l}_{h.h}\int_0^{2\pi} t_\psi \cos\beta\sin\psi\, d\psi. \tag{4.43}$$

A force equal to the sum of the inertia forces of blade flapping is transmitted through the flapping hinge to the rotor hub (Fig.2.95). Its projection, directed parallel to the rotor shaft axis,

$$J_{y_\psi}=-\int_{l_{h.h}}^{R} m\frac{d^2\beta}{dt^2}(r-l_{h.h})\cos\beta\, dr=-S_{h.h}\,\omega^2\frac{d^2\beta}{d\psi^2}\cos\beta, \tag{4.44}$$

creates longitudinal and lateral moments of the rotor

$$M_{z_J}=\frac{z_b}{2\pi}\int_0^{2\pi}-J_{y_\psi}l_{h.h}\cos\psi\, d\psi=\frac{z}{2\pi}S_{h.h}\,\omega^2 l_{h.h}\int_0^{2\pi}\frac{d^2\beta}{d\psi^2}\cos\beta\cos\psi\, d\psi, \tag{4.45}$$

$$M_{x_J}=\frac{z_b}{2\pi}\int_0^{2\pi}-J_{y_\psi}l_{h.h}\sin\psi\, d\psi=\frac{z_b}{2\pi}S_{h.h}\,\omega^2 l_{h.h}\int_0^{2\pi}\frac{d^2\beta}{d\psi^2}\cos\beta\cos\psi\, d\psi, \tag{4.46}$$

which should be summed with the moments of aerodynamic forces [see eqs.(4.42) and (4.43)].

We note that the integral expressions (4.42), (4.43), (4.45), and (4.46) contain sin ψ or cos ψ, due to which the moments are created by the first harmonics of thrust and inertia forces. Therefore, the moments of the inertia force are greater in magnitude than the moments of the aerodynamic force, since the first harmonic of t_ψ is small because of blade flapping.

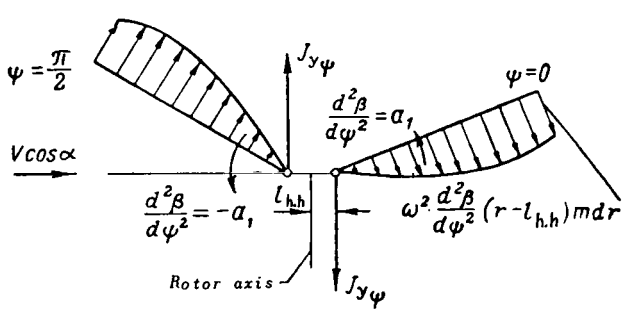

Fig.2.95 Generation of Rotor Moment Created by Inertia Forces of Flapping Motion.

The lift and drag coefficients of the rotor are determined by changing from the body-fixed system of axes to a velocity system: /182

$$t_y = t\cos\alpha - h\sin\alpha; \tag{4.47}$$

$$t_x = t\sin\alpha + h\cos\alpha. \tag{4.48}$$

2. Method of Calculation

The initial data for calculation are the dimensionless rotor characteristics: geometric blade characteristics (variation in twist $\Delta\varphi$, relative chord $\bar{b}$, and profile over the blade length), load factor of the rotor σ, aerodynamic profile characteristics, stagger of the flapping hinges $t_{h.h}$, mass and weight characteristics of the blade $\left(\frac{\gamma}{a_\infty} = \frac{\rho b_{0.7} R^4}{2I_{h.h}}$ and $\frac{gS_{h.h}}{\omega^2 I_{h.h}}\right)$, coefficient of the flapping compensator k.

The operating regime of the rotor is given the following dimensionless data: angle of attack of rotor α, coefficients of velocity and lift $\bar{V}$, t_y, Mach number M_0, deflection of controls $\varkappa$, η (or angles θ_1 and θ_2).

The sequence of the calculation is as follows: In first approximation, the magnitude and distribution of the induced velocity v and the rotor pitch θ_0 are assigned. The induced velocity can be taken from eq.(3.46) or from experimental data. The rotor pitch is determined either by the Glauert-Lock theory with conversion by means of eq.(2.242) or is assigned arbitrarily (for example, $\theta_0 = t_y$).

Let us select the azimuth with which to begin the calculation ψ_0 and the initial values of β_0 and β_0' (for brevity, we denote: $\beta' = \frac{d\beta}{d\psi}$, $\beta'' = \frac{d^2\beta}{d\psi^2}$). Usually, we take $\psi_0 = 0$ or $\psi_0 = 270^\circ$; β_0 and β_0' can be determined by the Glauert-Lock theory or we can assume $\beta_0 = \beta_0' = 0$ (which, for all practical purposes, does not lengthen the calculation since the natural oscillations of the blade decay rapidly).

At the initial azimuth we calculate μ, λ, $\bar{U}_x$, $\bar{U}_y$, $\bar{U}$, φ, α_r, and M at all radii, and then determine c_y and c_{xp} from the graphs of the aerodynamic characteristics of the profiles. Next, $\frac{dt}{d\bar{r}}$ and $m_{h.h}$ are determined, and from the flapping equation (4.10) we find β_0''. From β_0'', β_0', and β_0 we find, by numerical integration, β and β' at the next azimuth and continue the calculation in this sequence at other azimuths.

In the method of calculation compiled and programmed by M.N.Tishchenko, integration of the flapping equation of the blade with respect to azimuth is performed by the Euler method with conversion. From the values of β_i, β_i', β_i'' at azimuth ψ_i we find the preliminary values of $\beta'_{i+1_{pr}}$ and $\beta_{i+1_{pr}}$ at azimuth ψ_{i+1} from the expressions

$$\beta'_{i+1_{pr}} = \beta'_i + \beta''_i \Delta\psi;$$

$$\beta_{i+1_{pr}} = \beta_i + \frac{\beta'_i + \beta'_{i+1}}{2} \Delta\psi,$$

where $\Delta\psi = \psi_{i+1} - \psi_i$.

Then, from eq.(4.10) we calculate the preliminary value of the thrust moment coefficient relative to the flapping hinge $(m_{h.h})_{i+1_{pr}} = f(\beta_{i+1_{pr}}, \beta'_{i+1_{pr}})$. /183

Furthermore, assuming first that in the section between azimuths ψ_i and ψ_{i+1} there is a uniformly accelerated motion with an average acceleration $\frac{1}{2}(\beta''_i + \beta'_{i+1_{pr}})$ and secondly that $\beta''_{i+1_{pr}}$ can be found from eq.(4.10) with respect to $(m_{h.h})_{i+1_{pr}}$ and β_{i+1}, the system of equations

$$\beta'_{i+1} = \beta'_i + \frac{\beta''_{i+1_{pr}} + \beta''_i}{2} \Delta\psi;$$

$$\beta_{i+1} = \beta_i + \frac{\beta'_{i+1} + \beta'_i}{2} \Delta\psi;$$

$$\beta''_{i+1_{pr}} = \frac{\gamma_b}{a_\infty} (m_{h.h})_{i+1_{pr}} - \frac{gS_{h.h}}{I_{h.h}\omega^2} - \left(\cos\beta_{i+1} - \frac{l_{h.h}\delta_{h.h}}{I_{h.h}}\right)\sin\beta_{i+1}$$

will yield, by the iterative method, the final values of β'_{i+1} and β_{i+1}. Then, knowing β'_{i+1} and β_{i+1}, we calculate the final values of $m_{h.h_{i+1}}$ and β_{i+1}.

The calculations showed that, with this method, integration can be performed with an interval $\Delta\psi = 12^\circ$.

Integration of the loads per unit length over the radius, as well as forces and moments of the blade with respect to azimuth, is accomplished by the trapezoidal method. For example,

$$t_\psi = \sum_{i=2}^{k-1} \left(\frac{dt}{d\bar{r}}\right)_i \frac{\bar{r}_{i+1} - \bar{r}_{i-1}}{2} + \left(\frac{dt}{d\bar{r}}\right)_1 \frac{\bar{r}_2 - \bar{r}_1}{2} + \left(\frac{dt}{d\bar{r}}\right)_k \frac{\bar{r}_k - \bar{r}_{k-1}}{2};$$

$$t = \frac{1}{n} \sum_{i=1}^{n} (t_\psi \cos\beta)_i.$$

Here, k is the number of blade sections ($\bar{r}_k = 1$, $\bar{r}_1$ is the root section), and n is the number of calculated azimuths.

Using the described method, we then calculate one or two revolutions of the rotor and compare the values of β' and β'' with those which had been at this azimuth in the preceding revolution. The obtained value of t_y is compared with that assigned. If these values do not agree within the stipulated accuracy, then the difference $t_{y_{obt}} - t_{y_{assd}}$ is used for refining the value of θ_0 and

calculating another revolution of the rotor.

The calculation is considered completed as soon as t_y is equal to the assigned value, to the required accuracy, and as soon as β and β' in the last and preceding revolutions coincide.

As a result of the calculation, we determine the average forces and moments per revolution, the distribution of the section angles of attack, the thrust coefficient, and the blade flapping angle, which are represented as Fourier series with an accuracy to five terms:

$$t_\psi = t + \sum_{n=1}^{5} (\bar{t}_n \cos n\psi + \bar{\bar{t}}_n \sin n\psi); \tag{4.49}$$

$$\beta = a_0 - \sum_{n=1}^{5} (a_n \cos n\psi + b_n \sin n\psi). \tag{4.50}$$

Only the average induced velocity over the disk, determinable by eq.(3.46'), was taken into account in the calculations whose results are presented below /184 in Subsections 4 - 7. The blade was considered to be absolutely rigid in bending and torsion.

The integration interval was 12°, the number of calculated radii 12, and the accuracy within which t_y, β', and β had to coincide was $|\Delta t_y|_{max} = 0.002$; $|\Delta\beta'|_{max} = 0.002$; $|\Delta\beta|_{max} = 0.002$.

At the blade tip, $\frac{dt}{d\bar{r}}$ and $\frac{dq}{d\bar{r}}$ were calculated for $c_y = 0$ and c_{xp} corresponding to $c_y = 0$. At sections $\bar{r} \leq 0.975$, the calculation was made without any corrections for taking tip losses into account.

The calculation time of one flying regime on a computer performing 20,000 operations per second, is 40 - 75 sec.

3. Aerodynamic Characteristics of Profiles for Rotor Blades

Below we give the aerodynamic characteristics of NACA 230 and NACA 00 profiles and also of a high-speed profile suitable for use at the tip of helicopter blades. The first two profiles are taken at a relative thickness of 12% and the last profile, of 9%.

The aerodynamic characteristics of the profiles were obtained from test data on a rectangular airfoil model in a wind tunnel, with conversion to infinite aspect ratio and to full-scale Reynolds numbers taken for each Mach by means of eq.(4.19):

$$\mathrm{Re} = \left(\frac{a}{\nu}\right)_{av} b_{0.7} M = 20 \cdot 10^6 M.$$

The aerodynamic characteristics of the profiles in the angle of attack range from -2° to 15° and Mach numbers from 0.3 to 0.9 are given in Tables 2.6 - 2.8.

TABLE 2.6

PROFILE NACA 23012

	M \ α°	−2	1.0	3.5	7	9	11	12.5	14.5	15
c_y	0.3	−0.085	0.205	0.46	0.81	1.035	1.21	1.365	1.525	1.525
	0.4	−0.10	0.20	0.445	0.80	1.01	1.20	1.33	1.42	1.42
	0.5	−0.085	0.225	0.485	0.85	1.0	1.185	1.24	1.25	1.245
	0.6	−0.085	0.225	0.485	0.843	0.94	1.0	1.03	1.048	1.05
	0.7	−0.085	0.245	0.505	0.715	0.785	0.837	0.87	0.91	0.915
	0.8	−0.065	0.285	0.43	0.556	0.625	0.675	0.715	0.76	0.77
	0.85	−0.065	0.185	0.30	0.435	0.490	—	—	—	—
	0.9	−0.075	0.09	0.22	—	—	—	—	—	—
c_{xp}	0.3	0.008	0.008	0.010	0.015	0.018	0.022	0.029	0.045	0.05
	0.4	0.008	0.008	0.010	0.015	0.023	0.0355	0.043	0.07	0.074
	0.5	0.008	0.008	0.010	0.019	0.031	0.0575	0.0835	0.121	0.130
	0.6	0.008	0.009	0.0135	0.0365	0.0765	0.128	0.167	0.218	0.230
	0.7	0.009	0.013	0.0275	0.09	0.138	0.181	0.213	0.254	0.262
	0.8	0.0125	0.03	0.067	0.130	0.177	0.121	0.253	0.294	0.304
	0.85	0.028	0.049	0.080	0.145	0.185	—	—	—	—
	0.9	0.069	0.08	0.1075	—	—	—	—	—	—

TABLE 2.7 /185

PROFILE NACA 0012

	M \ α°	−2	1	3.5	7	9	11	12.5	14.5	15
c_y	0.3	−0.185	0.085	0.32	0.645	0.835	1.02	1.155	1.34	1.39
	0.4	−0.18	0.095	0.335	0.665	0.85	1.035	1.175	1.25	1.25
	0.5	−0.215	0.10	0.355	0.71	0.915	1.08	1.1	1.1	1.1
	0.6	−0.215	0.11	0.375	0.75	0.91	0.94	0.95	0.96	0.965
	0.7	−0.235	0.11	0.395	0.735	0.81	0.84	0.860	0.863	0.865
	0.8	−0.245	0.135	0.40	0.57	0.65	0.72	0.765	0.765	0.75
	0.85	−0.19	0.095	0.29	0.50	0.61	0.71	—	—	—
	0.9	−0.08	0.02	0.14	0.40	0.56	0.70	—	—	—
c_{xp}	0.3	0.0095	0.007	0.009	0.0125	0.0165	0.021	0.0240	0.029	0.034
	0.4	0.0095	0.007	0.009	0.0125	0.0165	0.021	0.0245	0.061	0.080
	0.5	0.0095	0.007	0.009	0.013	0.0185	0.031	0.051	0.106	0.126
	0.6	0.010	0.007	0.0105	0.021	0.039	0.074	0.1095	0.171	0.186
	0.7	0.010	0.0085	0.0185	0.061	0.0955	0.135	0.1675	0.211	0.221
	0.8	0.0245	0.016	0.046	0.095	0.131	0.1675	0.195	0.2285	0.236
	0.85	0.0415	0.036	0.061	0.1065	0.141	0.180	—	—	—
	0.9	0.069	0.069	0.0795	0.118	0.149	0.187	—	—	—

TABLE 2.8

HIGH-SPEED PROFILE

	M \ α°	—2	1.0	3.5	7	9	11	12.5	14.5	15
c_y	0.3	—0.065	0.235	0.485	0.835	1.035	1.18	1.165	1.115	1.1
	0.4	—0.065	0.23	0.485	0.835	1.035	1.10	1.09	1.06	1.05
	0.5	—0.065	0.245	0.50	0.86	1.015	1.015	1.0	0.99	0.99
	0.6	—0.065	0.26	0.53	0.90	0.98	0.96	0.965	0.96	0.96
	0.7	—0.07	0.30	0.60	0.96	0.96	0.935	0.935	0.95	0.95
	0.8	—0.07	0.36	0.63	0.81	0.87	0.87	0.89	0.935	0.945
	0.85	—0.12	0.325	0.55	0.77	0.86	0.86	—	—	—
	0.9	—0.165	0.175	0.46	0.815	—	—	—	—	—
c_{xp}	0.3	0.008	0.007	0.009	0.011	0.012	0.0245	0.065	0.12	0.133
	0.4	0.008	0.007	0.009	0.011	0.012	0.055	0.0975	0.142	0.15
	0.5	0.008	0.007	0.0095	0.0125	0.046	0.093	0.13	0.1765	0.1885
	0.6	0.008	0.007	0.010	0.025	0.060	0.110	0.1475	0.195	0.205
	0.7	0.008	0.0075	0.015	0.061	0.10	0.143	0.175	0.195	0.221
	0.8	0.0125	0.012	0.037	0.092	0.128	0.165	0.194	0.2125	0.2415
	0.85	0.021	0.026	0.053	0.11	0.15	0.19	—	—	—
	0.9	0.044	0.04	0.069	0.131	—	—	—	—	—

In the calculations whose results are given below, when $M < 0.3$ we took /186 the profile characteristics for $M = 0.3$, whereas when $M > 0.9$ the coefficients c_y and c_{xp} were determined by linear extrapolation with respect to $M = 0.85$ and $M = 0.9$. If the angle of attack of the blade sections varied within 72° to 180° and -7° to -180°, the characteristics of all profiles were determined regardless of M from Table 2.9. At angles of attack from 15° to 72° and from -2° to -7°, a linear interpolation was made between the corresponding values of c_y and c_{xp}.

TABLE 2.9

α°	72	105	170	—170	—105	—85	—70	—7
c_y	0.35	—0.33	—0.62	0.77	0.27	—0.2	—0.32	—0.62
c_{xp}	1.1	1.1	0.04	0.15	1.08	1.08	0.87	0.04

Figures 2.96 and 2.97 contain graphs of the coefficients c_y and c_{xp} as a function of α at all three Mach values.

For selecting a profile at a small portion of the blade (for example, at

the tip portion), graphs of the aerodynamic characteristics of the profiles as a function of angle of attack are more characteristic than the profile polars, since the angle of attack of the examined blade section depends little on c_y of this section and is determined mainly by the flight regime (t_y, $\overline{V}$, α) and the blade shape. Consequently, when the profile is changed, the angle of attack of the section is not changed (bearing in mind that α_0 of the profiles differ by less than 1 to 1.5°). To select the profile for a blade as a whole, the profile polars or the graphs of the aerodynamic characteristics of profiles constructed as a function of $\alpha - \alpha_0$ are more characteristic.

In Figs.2.98 and 2.99 we have constructed the graphs of α_{cr} and α^* as a function of the Mach number (α_{cr} is the critical angle of attack at which c_y of the section begins to decrease or a previous increase stops; $c_y = c_{y_{max}}$; α^* is the angle of attack at which a marked increase in c_{xp} begins, owing to flow separation or owing to wave drag). Since the Mach number of the blade section is approximately equal to

$$M \approx M_0 \overline{U}_x = M_0(\bar{r} + \overline{V}\sin\psi) = \bar{r}M_0 + M_{fl}\sin\psi,$$

the graphs in Figs.2.98 and 2.99 give the value of α at which an increase in profile drag begins and separation phenomena appear as a function of a combination of M_{fl}, M_0, $\overline{r}$, and ψ for the blade section. These graphs will be used in Subsection 8.

The graphs in Figs.2.96 and 2.97 indicate that, for M = 0.3, the NACA 23012 profile has $c_{y_{max}} = 1.53$, whereas the thinner high-speed profile has $c_{y_{max}} = 1.18$ at $\alpha_{cr} = 11°$. For the latter, a steep increase in c_{xp} begins as soon as $\alpha > 10.5°$. The NACA 0012 profile has $c_{y_{max}} = 1.4$.

At M = 0.6 - 0.7 and at average angles of attack, the profile characteristics are close together, whereas at M = 0.9 the high-speed profile is more advantageous, having the lowest value of c_{xp} at small angles of attack and a normal slope of dependence of c_y on α.

The results of calculating rotor profile losses for different profiles are described in Section 3.4: At low M_0, the rotor with symmetric NACA 0012 profile and, in certain cases, rotors with the thin high-speed profile on the blade tip have profile losses several percentages lower than rotors with other profiles; at high M_0, the rotor with the high-speed profile at the blade tip definitely has the upper hand.

The maximum permissible value of the lift coefficient, in terms of flow separation (see Subsect.7) of a rotor with a NACA 23012 profile is by a factor of 0.01 - 0.02 larger than for a rotor with a high-speed profile at the blade tip. /188

The aerodynamic characteristics of profiles should include corrections to account for the quality of manufacture and design features of the blades. The profile drag as well as the quantity $c_{y_{max}}$ are influenced by the flexibility and roughness of the surface (fabric skin or plywood cover, spacing of ribs), by the presence of projecting parts especially near the nose of the profile

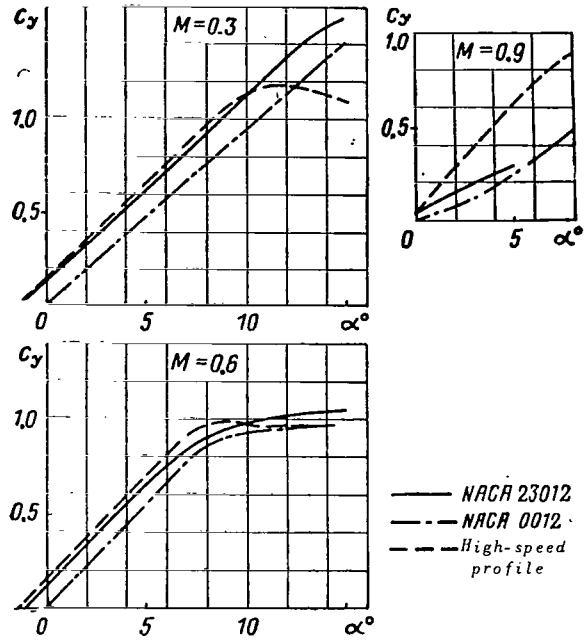

Fig.2.96 Lift Coefficient of Different Profiles.

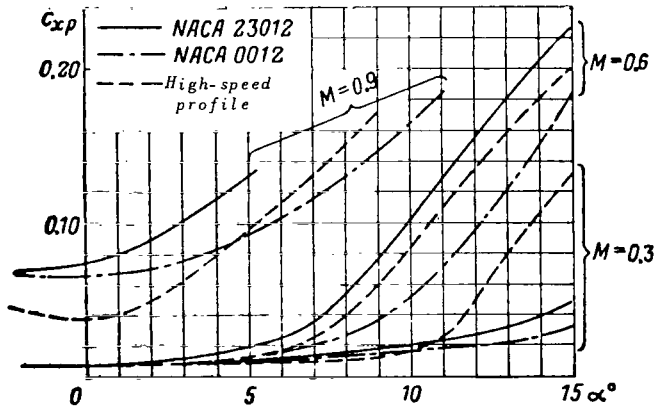

Fig.2.97 Profile Drag Coefficient of Different Profiles.

(de-icing system, rivets), leakage in the joints of the blade segments, and local deviations from the theoretical section profile.

On the basis of calculations, it is recommended to increase the c_{xp} values of the profile, obtained from model wind-tunnel tests, by Δc_{xp} equal to:

for blades with a nose in the form of a continuous spar of metal, plastic, or wood and with rigid shanks: 0.0 - 0.001;
for blades of segments with metal skin and ribs: 0.0015 - 0.0025;
for blades with veneer or fabric covering: 0.0025 - 0.005.

One or another value of Δc_{xp} is selected from the indicated interval, depending on the quality of blade manufacture.

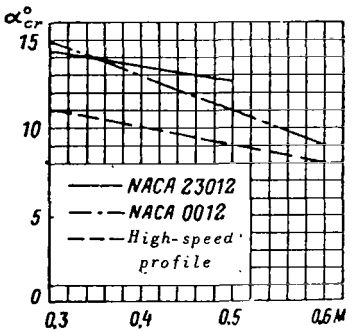

Fig.2.98 Critical Angle of Attack of Profiles as a Function of M.

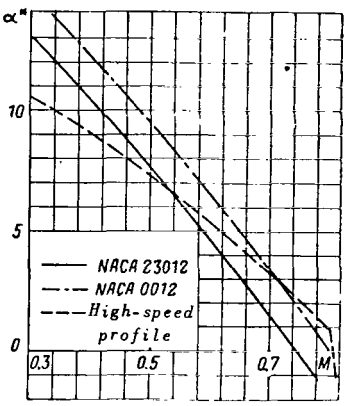

Fig.2.99 Angle of Attack α^* at which the Profile Drag Begins to Increase, as a Function of M.

4. Distribution of Aerodynamic Forces over the Rotor Disk

Only the average induced velocity over the disk was taken into account in the calculations whose results are described in Subsections 4 - 7; the error thus introduced into the total average characteristics of the rotor revolution at large and average values of $\overline{V}$ is small. The blade was considered to be absolutely rigid in bending and twisting. Calculations show that flexural deformations have practically no effect on the average aerodynamic per-revolution characteristics of the rotor whereas partial deformations, if the blade is insufficiently rigid, do have a noticeable effect. Preassigned torsional deformations can be taken into account by substitution into eq.(4.16).

The calculations were performed for eight variants of geometric blade characteristics, given in Table 2.10, with the following initial data: σ = /190

= 0.091; k = 0 and 0.4; $\frac{\gamma}{a_\infty}$ = 0.9 and 1.2; $i_{h.h} = \theta_1 = \theta_2 = 0$.

In this Subsection, we will examine the distribution of aerodynamic forces

TABLE 2.10

No. of Blade Variant	Blade Shape	Chord b		Taper Ratio η	Geometric Twist from $\bar{r}=0$ to $\bar{r}=1$, deg	Blade Profile		
		Root ($\bar{r}=0$)	Tip ($\bar{r}=1.0$)			From Root to $\bar{r}=0.75$	From $\bar{r}=0.75$ to $\bar{r}=0.85$	From $\bar{r}=0.85$ to $\bar{r}=1$
I	Trapezoidal twisted with high-speed profile	1.82	0.625	2.9	7	23012	Transitional	High-speed
II	Rectangular twisted with high-speed profile	1.0	1.0	1.0	7	23012	Transitional	High-speed
III	Rectangular twisted	1.0	1.0	1.0	7		NACA 23012	
IV	Rectangular twisted with symmetric profile	1.0	1.0	1.0	7		NACA 0012	
V	Trapezoidal flat with high-speed profile	1.82	0.625	2.9	0	23012	Transitional	High-speed
VI	Rectangular with high-speed profile and increased twist	1.0	1.0	1.0	15	23012	Transitional	High-speed
VII	Expanding with high-speed profile	0.59	1.176	0.5	7	23012	Transitional	High-speed
VIII	Rectangular with larger portion of high-speed profile	1.0	1.0	1.0	7	From root to $\bar{r}=0.65$, 23012	From $\bar{r}=0.65$ to $\bar{r}=0.75$, Transitional	From $\bar{r}=0.75$ to $\bar{r}=1$ High-speed

over the rotor disk. The assumption of constancy of induced velocity and the absence of blade deformations leads to errors in calculating the forces distributed over the rotor disk; consequently, the data in this Subsection are only approximate.

Let us examine rotors with blades of variants I and II in two helicopter flying regimes: one close to horizontal flight and one close to autorotation of the rotor; both regimes are taken at equal lift coefficients $t_y = 0.16$, dimensionless velocity $\overline{V} = 0.3$, and $M_0 = 0.6$. The results of rotor calculations in these regimes are given in Table 2.11.

TABLE 2.11

$t_y = 0.16$; $\overline{V} = 0.3$; $M_0 = 0.6$

Characteristics	Horizontal Flight				Autorotation		
	Rectangular Blade		Trapezoidal Blade		Rectangular Blade		Trapezoidal Blade
	$k=0$	$k=0.4$	$k=0$	$k=0$	$k=0$	$k=0.4$	$k=0$
$\alpha°$	−9.4	−9.4	−9.4	−10.3	1.4	1.4	1.4
λ	−0.0610	−0.06103	−0.0610	−0.065	−0.0048	−0.0048	−0.0048
$\theta_0°$	7.820	9.957	8.0320	8.45	3.576	5.62	3.550
t_x	−0.0095	−0.0101	−0.00795	−0.01	0.0168	0.0172	0.0180
m_t	0.00849	0.008698	0.00796	0.0086	0.000475	0.000365	−0.00015
h	0.0168	0.0162	0.01815	0.0186	0.0129	0.01327	0.0140
a_0	0.0997	0.09667	0.0949	0.0958	0.0926	0.09247	0.0877
a_1	0.0973	0.09535	0.108	0.1096	0.06938	0.07166	0.0772
b_1	0.0398	0.003355	0.0408	0.0405	0.0367	0.00857	0.0368
a_2	0.0069	0.006043	0.0078	0.0076	0.00559	0.00515	0.0062
b_2	−0.0025	−0.003146	−0.0024	−0.00276	−0.00203	−0.00269	−0.0012
a_3	0.0004	−0.000548	0.0005	0.000628	0.0003	0.000457	0.0003
b_3	0.00015	−0.0002637	0.00027	0.000177	0.00014	0.000175	0.0003
$\bar{t}_1$	−0.0059	0.003116	−0.0062	−0.00623	−0.0053	−0.0054	−0.0058
$\bar{\bar{t}}_1$	0.0219	0.0249	0.0233	0.0227	0.0289	0.0285	0.0312
$\bar{t}_2$	0.0309	0.03466	0.0377	0.0364	0.0249	0.0267	0.0300
$\bar{\bar{t}}_2$	−0.0143	−0.00963	−0.0149	−0.0167	−0.0120	−0.0153	−0.0138
$\bar{t}_3$	0.0062	0.0062	0.0078	0.00859	0.00427	0.00623	0.0051
$\bar{\bar{t}}_3$	0.0033	0.0089	0.0055	0.00407	0.00348	0.00317	0.0049

Table 2.11 shows that, in horizontal flight, the flapping motion of the blade is greater than in autorotation and that it is greater for the trapezoidal than for the rectangular blade. A comparison of the characteristics of rotors with rectangular and trapezoidal blades shows that, at equal α, t_y, and V, the rotor with trapezoidal blades has larger θ_0, h, a_1, b_1 and a smaller absolute propulsive coefficient t_x; at equal t_x, t_y, V (see the column with $\alpha = -10.3^\circ$) the rotor with trapezoidal blades has a more negative angle of attack, and the difference in the quantities θ_0, h, a_1, b_1 increases even more. This is responsible for the change in balancing characteristics of a helicopter when the trapezoidal blades are replaced by rectangular types (for example, there is a decrease in deflection of the automatic pitch control forward, owing to a decrease in the longitudinal force H and in the coefficient c_1). /191

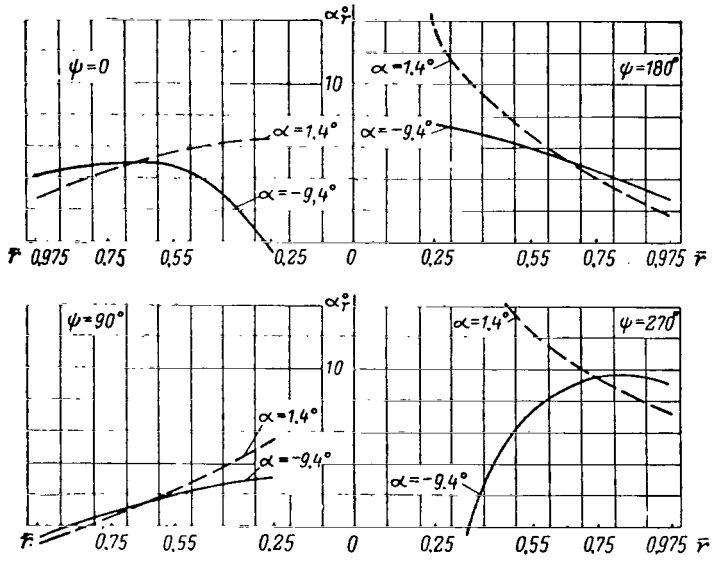

Fig.2.100 Angles of Attack of Sections as a Function of Blade Radius.

Figure 2.100 shows graphs of the variation in angles of attack of a rotor with rectangular blades with respect to blade radius at four azimuths: 0, 90, 180, and 270°. The solid lines refer to horizontal flight and the dashed lines to autorotation.

In horizontal flight, the angles of attack are negative at the blade root, at $\psi = 0$ and 270°. At azimuth $\psi = 0$ when the flapping angle is small, the vertical velocity component equal to about $V(\alpha + \beta) - v = V(\alpha + a_0 - a_1) - v$ (Fig.2.101) is large and directed downward, due to which the angle of attack at the blade root is small or negative at this azimuth. At azimuth $\psi = 270^\circ$ the roots are close to the zone of the backwash and are washed backward and upward. Therefore, they have large negative angles of attack.

In the middle and tip sections of the blade, the angles of attack are

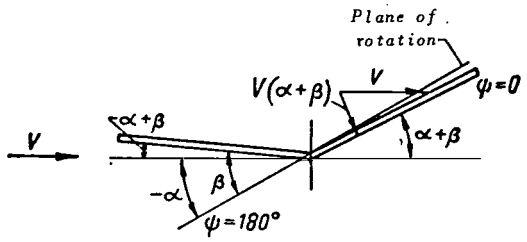

Fig.2.101 Component of Air Velocities Normal to Blade Axis at Azimuths $\psi = 0$ and $\psi = 180^\circ$.

greatly influenced by the peripheral velocity of flapping. This increases the angles of attack at azimuths of 270° and 0°, where the blade is shifted downward and decreases them at azimuths of 90° and 180°. The geometric twist of /192 the blade reduces the increase in angles of attack toward the blade tip at azimuths of 270° and 0° and decreases them even more at azimuths of 90° and 180°. The angles of attack are negative at the blade tip at azimuth of 90°.

In autorotation, the angle of attack of the rotor is positive so that the angles of attack of the blade root sections have a large positive value. At the blade tips, the angles of attack of the sections are less than in horizontal flight, since in autorotation the rotor has a small pitch and less flapping motion.

The distribution of the section angles of attack over the entire rotor disk with twisted rectangular blades is illustrated by the graph in Fig.2.102 (horizontal flight). The hatched circle in this diagram is the zone of backwash, along whose boundaries the section angle of attack is close to ±90°. Regions with negative section angles of attack are also shown by hatching.

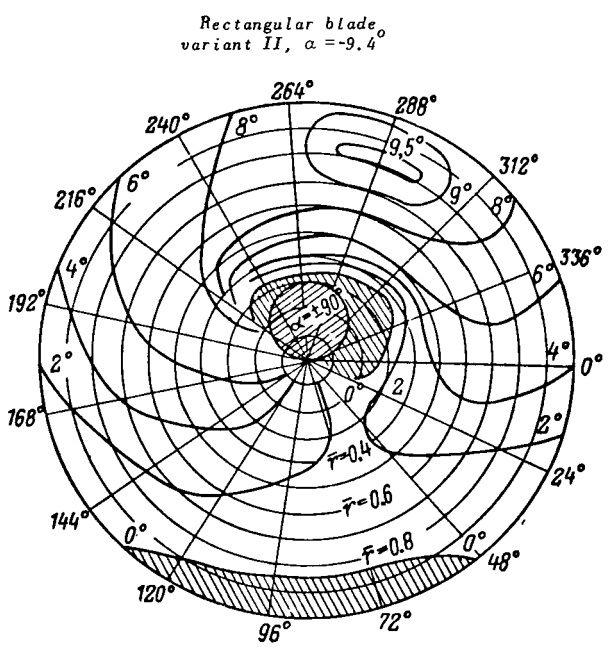

Fig.2.102 Distribution of Angles of Attack over Rotor Disk (Horizontal Flight).

Figure 2.102 shows that, in the zone bounded by azimuths of 270 - 300° and relative radii 0.7 - 1.0, the angles of attack reach a maximal value (for untwisted blades, the angles of attack are maximum at $\bar{r} = 1.0$). This region, in which flow separation takes place on increase in t_y and $\bar{V}$, has a noticeable effect on rotor operation as a whole. In /193 autorotation the separation region is located in the root portion of the blade at azimuths of 200 - 300°.

Calculations show that the maximum angles of attack of a trapezoidal blade are substantially larger than those of a rectangular blade. For a rotor with a flapping compensator, the maximum angles of attack at $\psi = 270^\circ$ decrease somewhat.

The linear thrust is extremely unevenly distributed over the radius and azimuth (see Fig.2.28), which is responsible for the occurrence of the large variable bending moments of the blade. It follows from Table 2.11 that, for the rotor with trapezoidal blades and for the rotor with a flapping compensator, the variable portion of thrust increases. The rotor with a flapping compensator has a larger fourth harmonic. These peculiarities of rotors must be taken into account when estimating vertical vibrations of helicopters. The magnitude of the variable thrust component depends on the rotor characteristic μ (or $\bar{V}$): the larger μ, the larger the variable component. At $\cos\psi - \bar{t}_1$, the coefficient of the first harmonic of thrust is very small; consequently, at small spacing of the flapping hinges the aerodynamic moment of the rotor relative to the transverse axis m_{z_A} [eq.(4.43)] need not be taken into consideration.

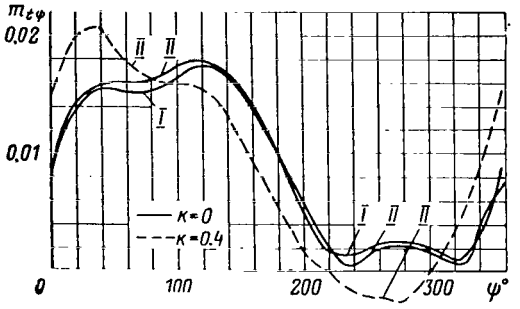

Fig.2.103 Torque Coefficient of Blade vs. Azimuth (Horizontal Flight).

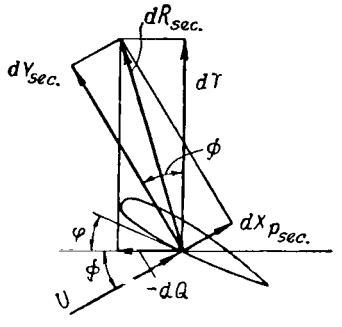

Fig.2.104 Acceleration Moment in Blade Section $dQ = dX_{p_{sec.}} \times \times \cos\Phi - dY_{sec.} \sin\Phi < 0$.

The torque coefficient of the blade m_{t_ψ} varies greatly with the azimuth (Fig.2.103). At azimuths where the section angles of attack increase (quadrants III and IV), m_{t_ψ} markedly decreases. In an autorotation regime, m_{t_ψ} is negative in the quadrants III and IV. This is due to the fact that, at these azimuths, the blade sections have large positive inflow angles Φ, as a result of which the projection of the lift of the blade section is directed forward and produces an accelerating moment (Fig.2.104). Thus, it is obvious that, in forward flight in autorotation regime, decelerating moments are produced in the quadrants I and II and accelerating moments in quadrants III and IV (during vertical descent of a helicopter in an autorotation regime, the decelerating moments are produced by the tip sections of the blade and the accelerating moments by the root sections).

It should be noted that a very large variable torque component, in a rotor with the usual stagger of drag hinges ($\bar{t}_{v.h} < 0.05$), produces a small (within 1°) flapping motion relative to the drag hinges, since the eigenfrequency of blade oscillation is by a factor of about 4 lower than the rotor rpm, i.e., the frequency of change of m_{t_ψ}.

In Section 2, we noted that, at equal t_y, t_x, and $\bar{V}$, the quantity m_t does /194 not depend on the amplitude of cyclic change of blade pitch, whereas a change

of m_{t_ψ} with respect to azimuth does. Actually, as shown in Fig.2.103, for a rotor with a flapping compensator m_{t_ψ} differs with respect to magnitude and phase.

5. Aerodynamic Characteristics of Rotor

The aerodynamic characteristics of a rotor are presented in graphs in the form of the dependence $t_x = f(m_t)$ with parameters t_y, α at M_{f1} = const (or $\bar{V}$ = = const), M_0 = const. These graphs are convenient for determining the coefficients t_x, m_t, and the angle of attack α from values of M_{f1}, $\bar{V}$, M_0, t_y known from an aerodynamic calculation.

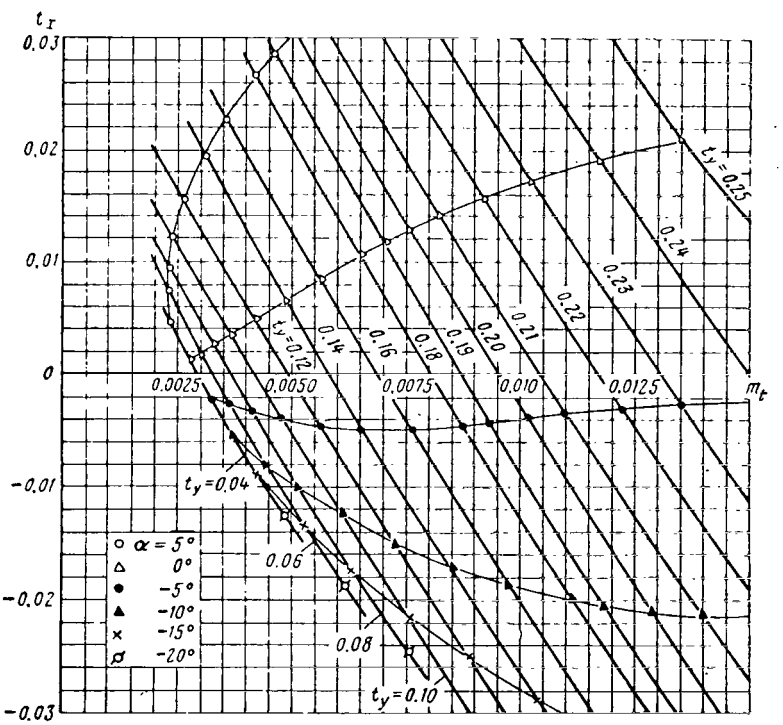

Fig.2.105 Aerodynamic Characteristics of Rotor (M_{f1} = 0.0975; $\bar{V}$ = 0.15; M_0 = 0.65; σ = 0.091).

Such graphs for a rotor with rectangular twisted blades with a high-speed profile at the tip (variant II of blades) are shown for M_0 = 0.65 in Figs.2.105 - 2.109.

We see from the graphs that the dependence of the propulsive coefficient t_x on the torque coefficient m_t is practically rectilinear, with the exception of near-separation values of t_y at negative t_x, where the rate of increment of m_t increases owing to an increase in profile losses. In these cases, curves with

different t_y become nonequidistant. The interval between the curves increases with increasing t_y, which can also be attributed to an increase in profile losses with increasing t_y.

Curves corresponding to very small values of the lift coefficient /195
($t_y < 0.1 - 0.08$) closely approach or intersect the curves corresponding to large values of t_y. This means that a decrease in rotor thrust coefficient (for example, when using a wing on a helicopter) to $t_y = 0.08$ and less it not recommended since, in this case, the propulsive force of the rotor does not increase. The upward deflection of the curves with small t_y upon a decrease in m_t shows that, at small t_y, the rotor is not in an autorotation regime.

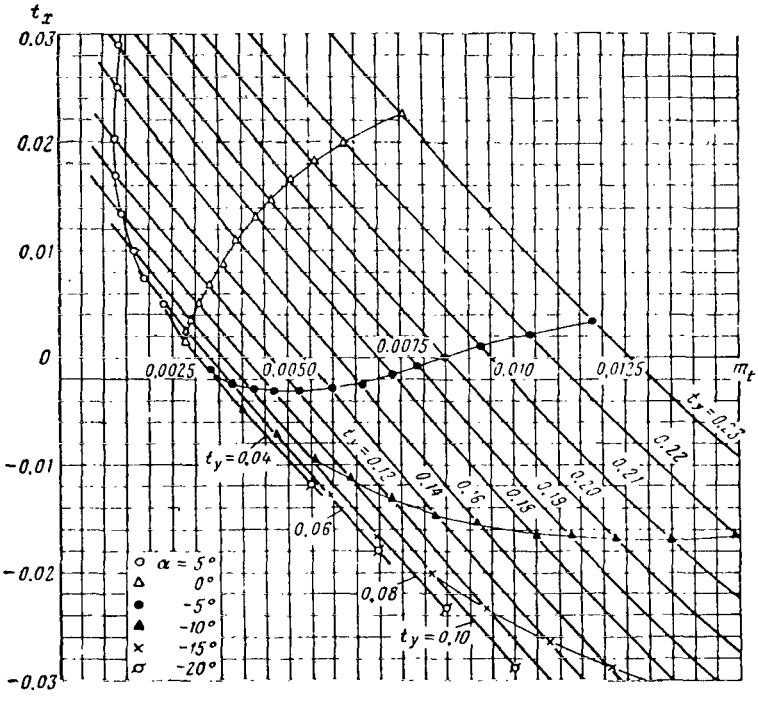

Fig.2.106 Aerodynamic Characteristics of Rotor ($M_{f1} = 0.13$; $\bar{V} = 0.2$; $M_o = 0.65$; $\sigma = 0.091$).

The advantages of the described graphs comprise: simple shape of the curves, facility of interpolation upon variations in the coefficient t_y, and the possibility of using them for different solidity ratios (see Sect.6). With the use of these graphs for calculating balancing and stability, we can determine the coefficients t and h by means of the conversion formulas (3.15) and (3.17).

To determine rotor pitch in the calculation, we use the dependence $\theta_o = f(m_t)$ with the parameter t_y at $\bar{V} = \text{const}$, $M_o = \text{const}$, or $t_y = f(\alpha)$ with the parameter θ_o at $\bar{V} = \text{const}$, $M_o = \text{const}$. The graphs of the relation $t_y = f(\alpha)$ are

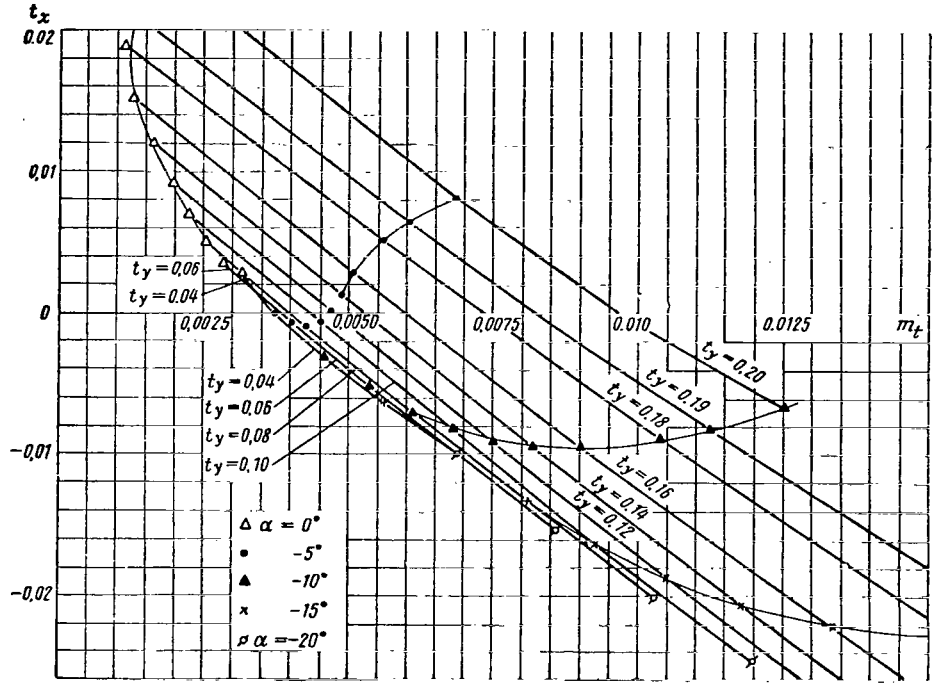

Fig.2.107 Aerodynamic Characteristics of Rotor (M_{t1} = 0.195; $\bar{V}$ = 0.3; M_0 = 0.65; σ = 0.091).

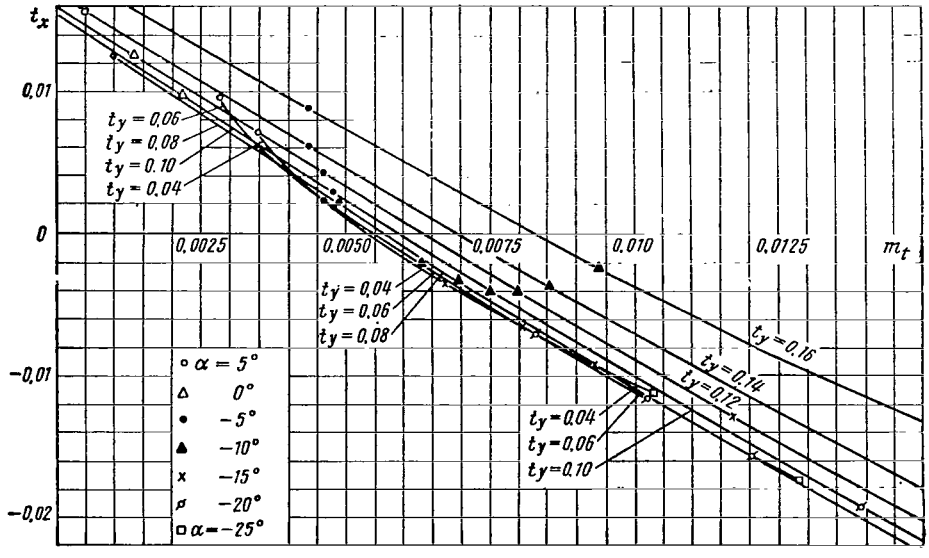

Fig.2.108 Aerodynamic Characteristics of Rotor (M_{t1} = 0.26; $\bar{V}$ = 0.4; M_0 = 0.65; σ = 0.091).

shown in Figs.2.115 and 2.116.

The aerodynamic characteristics of rotors with blades of different shapes are not presented here since, with the accepted assumption that regardless of blade shape the induced velocity is distributed uniformly over the rotor disk, the difference in the coefficient m_t at given t_y, t_x, $\bar{V}$, M_0 is determined entirely by the difference in m_{pr}. Therefore, our conclusions concerning the effect of blade shape obtained in examining graphs of m_{pr} in Section 3.3 remain unchanged. /197

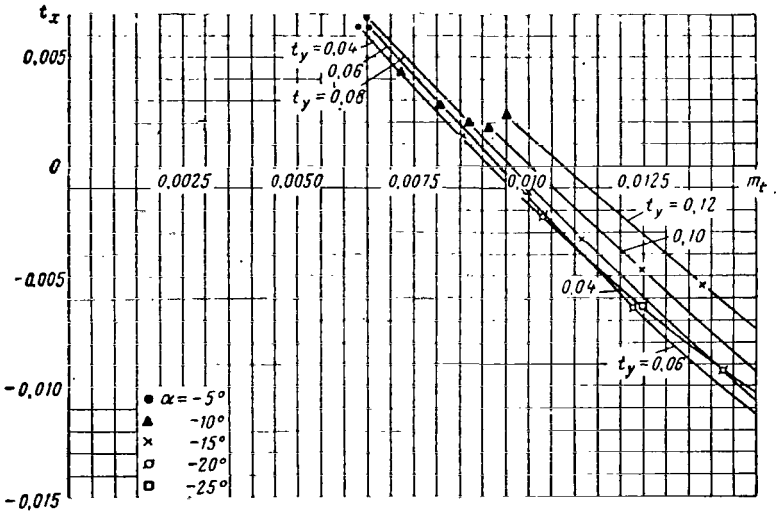

Fig.2.109 Aerodynamic Characteristics of Rotor (M_{f1} = 0.325; $\bar{V}$ = 0.5; M_0 = 0.65; σ = 0.091).

6. Aerodynamic Characteristics of Rotor in Autorotation Regime

The graphs of the characteristics of a rotor of the variant II in an autorotation regime - polars $t_y = f(t_{x_c})$, rotor performance K_c, pitch θ_{0_c}, and angle of attack α_c - are shown in Figs.2.110 - 2.113.

The graphs indicate that the rotor performance is lower than that of a wing (for more details on rotor performance see Sect.7 of Chapt.II). At small $\bar{V}$, autorotation of the rotor takes place at large positive angles of attack. Upon an increase in rotor rpm (of M_0) the rotor performance drops, the pitch decreases, and the angle of attack increases.

It is known that autorotation of a rotor is possible in the absence of forward speed and at any low flying speed. Therefore, the minimal permissible speed of an autogiro or helicopter on engine failure is not determined by flow separation at the wing, controllability loss or spinning, as would be the case in regular aircraft, but by the permissible vertical rate of descent. In vertical descent, the rotor develops approximately the same drag as a plate ($c_x \approx$ $\approx$ 1.28) with an area equal to the rotor disk area, with the vertical speed of

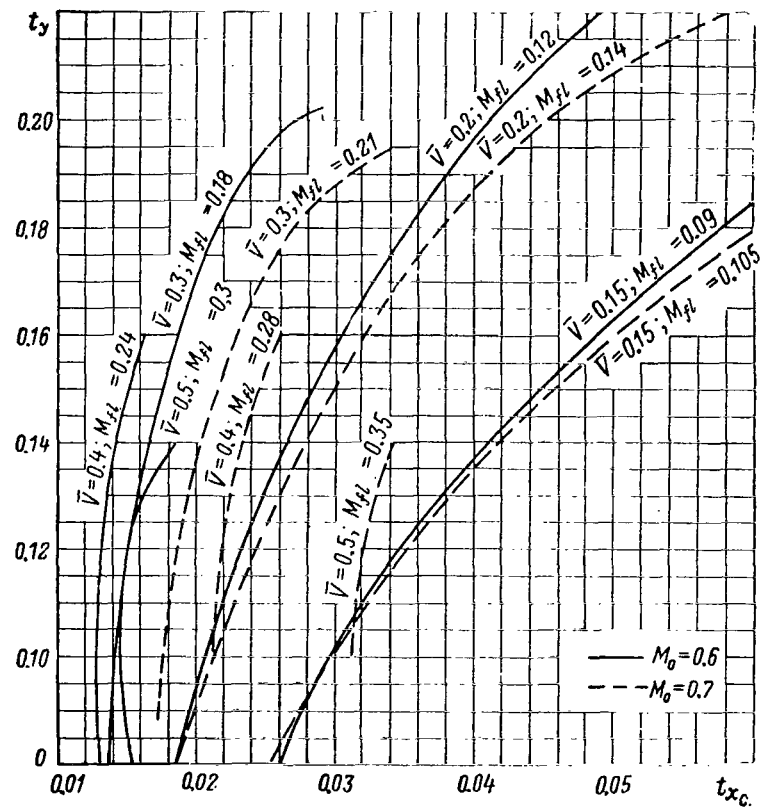

Fig.2.110 Polar of Rotor in Autorotation Regime (σ = 0.091).

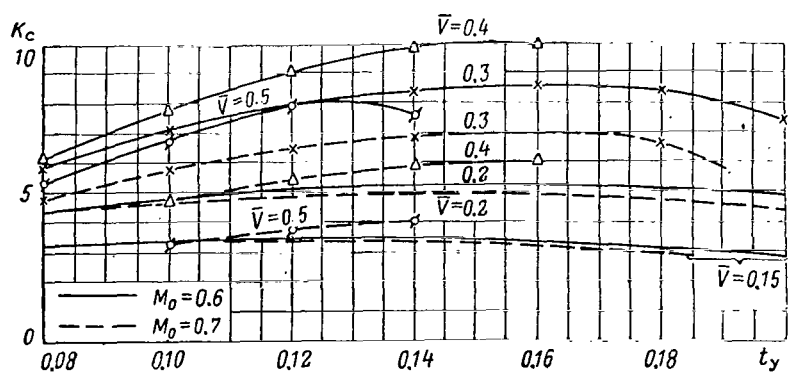

Fig.2.111 Rotor Performance in Autorotation Regime (σ = 0.091).

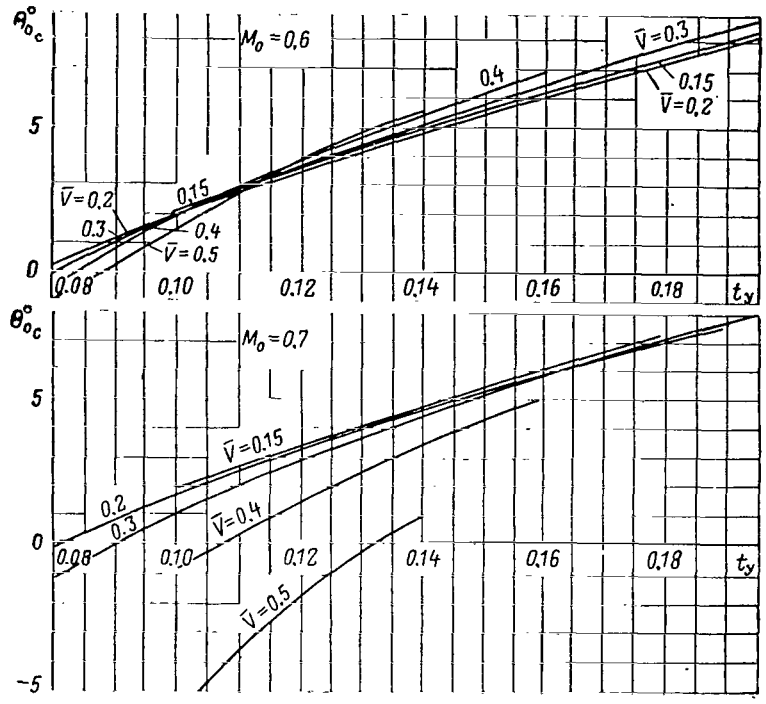

Fig.2.112 Rotor Pitch in Autorotation Regime.

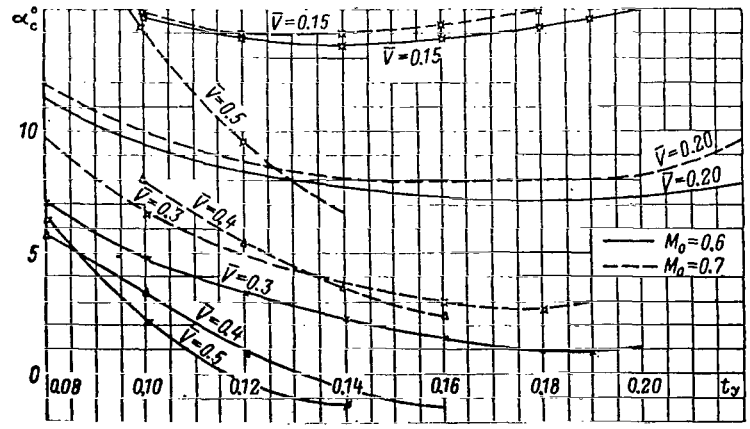

Fig.2.113 Angle of Attack of Rotor in Autorotation Regime (σ = 0.091).

descent of an autogiro being

$$V_y \approx \sqrt{\frac{G}{1/2 \cdot 1.28\, \varrho_0 \Delta F}} = 3.5 \sqrt{\frac{p}{\Delta}}.$$

In autogiros, the value of p was small and their rate of vertical descent was low.

Figure 2.104 shows that the acceleration (negative) moment in an autorotation regime is created by the projection of lift; consequently, autorotation is not possible at small rotor lift. Figure 2.114 gives a graph of the minimum lift coefficient in autorotation $(t_{y_c})_{min}$, which is either the autorotation limit or the value of t_y at which autorotation is generated at very large angles of attack and negative pitch. /200

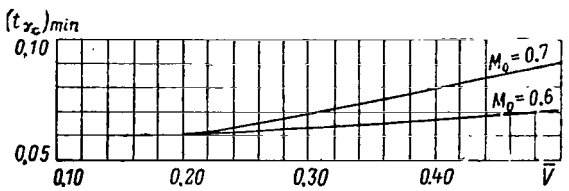

Fig.2.114 Minimum Lift Coefficient in Autorotation Regime.

In a helicopter with a large wing, the rotor lift markedly decreases during autorotation, and, since the rotor cannot have a very small coefficient t_y, autorotation occurs at a lower rpm than in helicopter regimes.

To estimate the influence of the geometric blade characteristics on the autorotation regime of a helicopter, we present the following data.

At optimum gliding speed ($\bar{V} = 0.2$) when $M_0 = 0.7$ for a helicopter with a rotor not having a high-speed profile at the blade tip, the vertical rate of descent increases by 1.7 m/sec and the flight-path angle $\theta_{f.p}$ by 2°; the pitch should be 0.5° smaller. The angle of attack increases by 1.8° while the pitching moment is retained ($\Delta\vartheta - \Delta\alpha + \Delta\theta_{f.p} \simeq 0$).

At $M_0 = 0.6$, the deterioration in autorotation characteristics is less by a factor of 2 - 3.

Change-over to trapezoidal blades reduces the vertical rate of descent by 0.65 m/sec and the flight-path angle by 0.8°.

7. Limit of Permissible Helicopter Flight Regimes (Flow Separation Limit)

As shown in Subsection 4, a rotor with flapping hinges has areas with large angles of attack of the blade sections. In helicopter flight regimes (horizontal flight, gain in altitude) these are located at the blade tip at azimuths of 270 - 300° and in the autorotation regime, at the blade root at azimuths of 200 - 300°.

An increase in lift coefficient t_y causes formation of a zone of supercritical angles of attack on the rotor.

Furthermore, the rotor disk contains zones of high and supercritical angles of attack, at sites where the blade passes close to vortices shed by the preceding blades. Here the blade enters a region of high upward-directed local induced velocities causing an increase in the angles of attack of individual sections.

As soon as the zones of supercritical angles of attack become large, the /201 rotor characteristics change noticeably: The dependence of t_y on the pitch and upward angle of attack becomes nonlinear, and the coefficients of flapping, longitudinal and lateral forces, and profile drag of the rotor all increase.

The limit of permissible regimes with respect to flow separation conditions is determined by the magnitude of the rotor lift coefficient t_y characterizing the average level of the section angles of attack, by the velocity coefficient $\overline{V}$ characterizing the degree of nonuniformity of distribution of the section angles of attack over the rotor disk, by the rotor angle of attack determining the character of the distribution of the section angles of attack, and also by the blade shape and the separation characteristics of its profile.

From the expressions for the coefficient t_y and $\overline{V}$

$$t_y = \frac{Y}{\frac{1}{2}\varrho\sigma(\omega R)^2 F} \approx \frac{G}{\frac{1}{2}\varrho\sigma(\omega R)^2 F};$$

$$\overline{V} = \frac{V}{\omega R},$$

it is obvious that, on a decrease in rotor rpm and an increase in flying speed and altitude, the coefficients t_y and $\overline{V}$ will increase so that the helicopter may enter a flow-separation regime. The phenomenon associated with flow separation at the rotor blades can be stopped rapidly by decreasing the pitch, increasing the rotor rpm, and reducing the flying speed.

Deep penetration into the flow-separation zone sometimes ends in catastrophe for the helicopter. One of the most important problems of selecting the helicopter parameters in designing and determining its flight characteristics is to ensure absence of flow separation in all permitted flying regimes. Owing to the possibility of entering the flow-separation zone, the maximum flying speeds and altitude are limited on helicopters and any decrease in rotor rpm below an established limit is impermissible. In order to avoid flow separation at high flying speeds, a wing is installed on helicopters to reduce rotor lift.

Flight tests show that flow separation manifests itself by an increase in blade stresses and in blade hinge moments, increase in helicopter vibrations, imbalance of the helicopter, and deterioration of controllability. Consequently, the manifestations of flow separation differ widely and are complex for determining the limit of separation by calculation. Flight tests and wind-tunnel tests of rotors yield insufficient data for establishing the overall limit of

flow separation. Therefore, the limiting values of the lift coefficients $t_{y_{cr}}$ obtained by calculation are given below.

Calculated graphs of permissible values of thrust coefficients are given in the literature (Ref.20, 24). In the first of these papers, the limiting flight regime is that regime at which the average lift coefficient of the blade at azimuth $\psi = 270^\circ$ becomes equal to the maximum lift coefficient of the profile $c_{y_{max}}$. In the second paper, the criterion of flow separation in helicopter flight regimes is taken as the equality of the angle of attack at the blade tip at azimuth $\psi = 270^\circ$ to some critical value α_{cr}: $\alpha_{cr} = 12^\circ$ in a regime corresponding to the start of separation phenomena, and $\alpha_{cr} = 16^\circ$ at the limiting flight regime with a large separation zone.

A shortcoming of both methods is that one does not know how to select $c_{y_{max}}$ or α_{cr} for a blade with a set of profiles. Furthermore, the degree of nonuniformity of distribution of the angles of attack over the rotor disk depends /202 on $\bar{V}$; at $t_y = t_{y_{cr}}$ and at large $\bar{V}$, the zone of increased angles of attack occupies a smaller portion of the disk than at small $\bar{V}$. Therefore, the appearance of supercritical angles of attack at large $\bar{V}$ has a less pronounced influence on the change in rotor characteristics than at small $\bar{V}$; this is not taken into account in the method presented in the second paper (Ref.24).

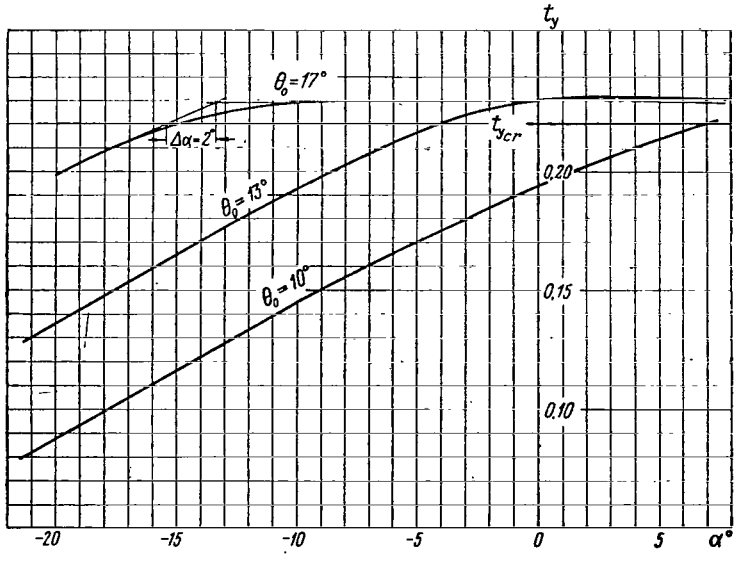

Fig.2.115 Change of Coefficient t_y as a Function of Angle of Attack and Pitch of Rotor ($\bar{V} = 0.2$; $M_0 = 0.7$).

In the separation limits constructed below, it is assumed that the permissible magnitude of the coefficient t_y is the value at which the character of the dependence of t_y on the angle of attack and pitch of the rotor begins to change. Such limits are constructed for rotors with different geometric characteristics

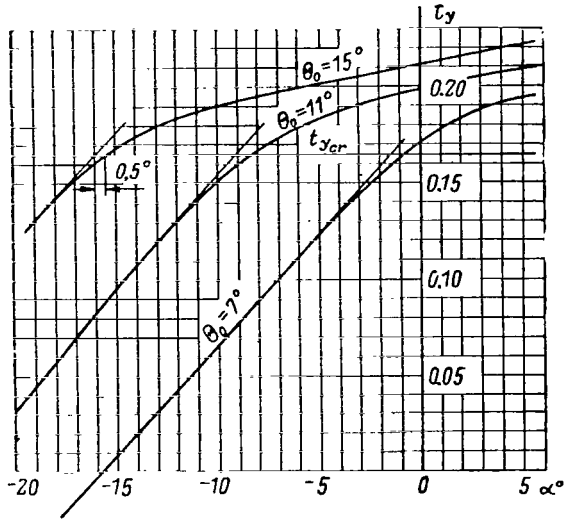

Fig.2.116 Change in Coefficient t_y as a Function of Rotor Angle of Attack and Pitch ($\overline{V}$ = 0.4; M_o = 0.7).

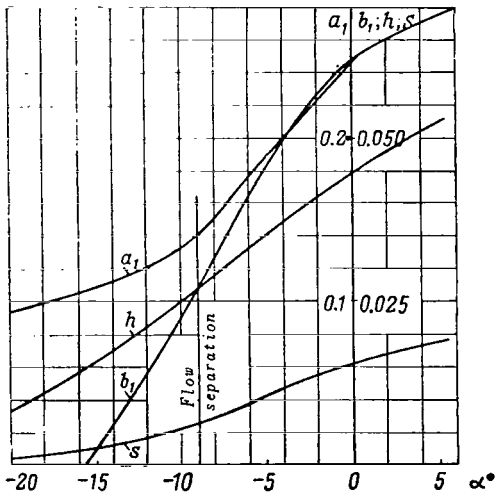

Fig.2.117 Dependence of Coefficients of Longitudinal and Lateral Forces h and s and of Flapping a_1 and b_1 on Rotor Angle of Attack ($\overline{V}$ = 0.4; M_o = 0.7; θ_o = 11°).

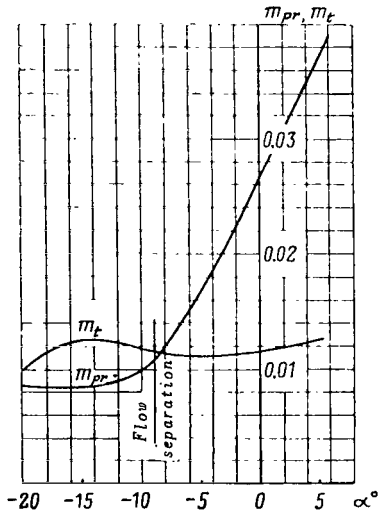

Fig.2.118 Dependence of Coefficients of Torque m_t and Profile Power m_{pr} on Rotor Angle of Attack ($\overline{V}$ = 0.4; M_o = 0.7; θ_o = 11°).

on the basis of calculations by the method presented in Subsection 2.

Figures 2.115 and 2.116 give graphs for the dependence of the coefficient t_y on the angle of attack and pitch of a rotor with blades of the variant II, at a flapping compensator coefficient of $k = 0.4$. Figure 2.115 indicates that, at $\bar{V} = 0.2$ when t_y reaches a certain value, the increase in t_y practically stops. The coefficient t_y has a limiting value which it cannot exceed at any α and θ_0°. Thus, because of the small $\bar{V}$, the flow separation extends over a large zone and there is a marked change in characteristics. Since the incipient deflection of the curve from the linear segment is not well-defined, we will use, at $\bar{V} = 0.2$ and for $t_{y_{cr}}$, a value of t_y less than the maximum by an amount corresponding to $\Delta\alpha = 2^\circ$ ($\Delta t_y \approx 0.01$).

At $\bar{V} = 0$, the maximum possible value of t_y is taken for t_{cr} (Sect.8). At large $\bar{V}$ (see Fig.2.116), the increase in t_y with respect to α markedly slows down at some value of t_y. The value of t_y at which the curve deviates from the linear law by $\Delta\alpha = 0.5^\circ$ is taken for $t_{y_{cr}}$.

Figures 2.115 and 2.116 indicate that the quantity $t_{y_{cr}}$ at given $\bar{V}$ and M_0 depends little on the rotor angle of attack.

Figures 2.117 and 2.118 give graphs for the dependence of the coefficients of longitudinal and lateral forces h and s, flapping a_1 and b_1, torque m_t, and profile power m_{pr} on the rotor angle of attack. These coefficients also change when $t_y = t_{y_{cr}}$: The forces of the rotor and the flapping motion of the blades increase backward and to the side of the advancing blade ($\psi = 90^\circ$), and the profile power coefficient increases markedly. The variable portion of rotor thrust, i.e., the second and higher harmonics, also increases substantially. /204

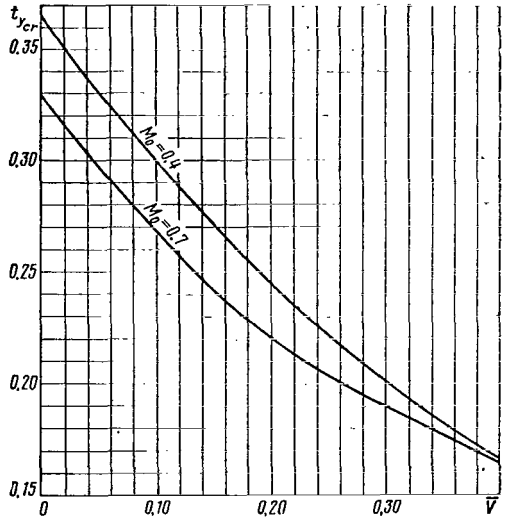

Fig.2.119 Dependence of $t_{y_{cr}}$ on $\bar{V}$ and M_0 (Rectangular Twisted Rotor with High-Speed Profile at the Blade Tip).

Thus, at $\bar{V} > 0$, the value of $t_{y_{cr}}$ is smaller than the maximum possible values of t_y; however, it can be assumed that, as soon as $t_y = t_{y_{cr}}$, the above-mentioned phenomena associated with flow separation will become manifest.

The curve for the dependence of $t_{y_{cr}}$ on $\bar{V}$ and M_0 is plotted in Fig.2.119. It is obvious that the quantity $t_{y_{cr}}$ decreases greatly upon an increase in $\bar{V}$. At small and medium $\bar{V}$, $t_{y_{cr}}$ decreases with increasing M_0, whereas at large $\bar{V}$ the effect of M_0 is insignificant.

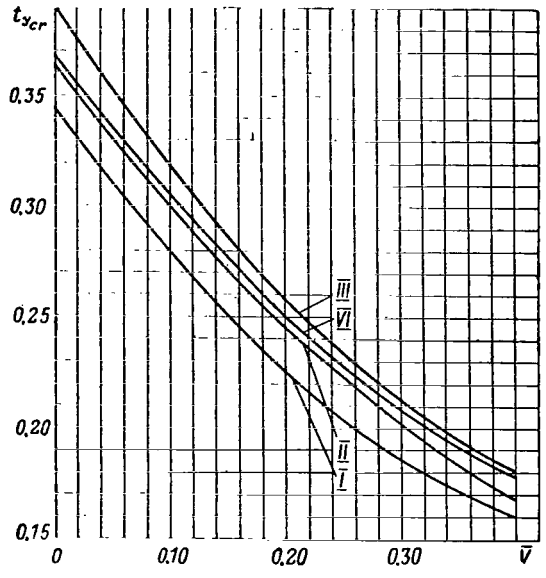

Fig.2.120 Dependence of $t_{y_{cr}}$ on $\bar{V}$ of Rotors with Blades of Different Shapes ($M_0 = 0.4$).

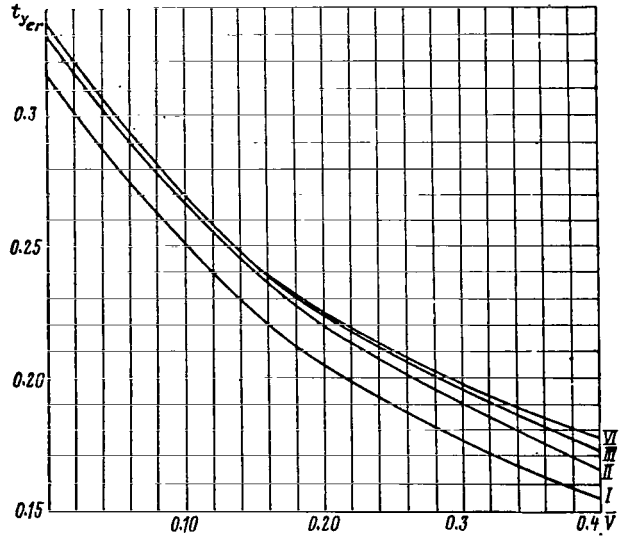

Fig.2.121 Dependence of $t_{y_{cr}}$ on $\bar{V}$ of Rotors with Blades of Different Shapes ($M_0 = 0.7$).

Figures 2.120 and 2.121 give graphs of $t_{y_{cr}}$ for blades with different geometric characteristics. The rotor with rectangular blades of NACA 230 profile (variant III) has the largest value of $t_{y_{cr}}$. The same rotor with a high-speed profile at the tip (variant II) has values of $t_{y_{cr}}$ smaller by 0.01 - 0.02. An increase in geometric twist of the blade increases $t_{y_{cr}}$ by approximately 0.01 (variant IV). The rotor with trapezoidal blades (variant I) has the smallest value of $t_{y_{cr}}$.

The graphs of $t_{y_{cr}}$ are approximate and obtained by calculation, but they do permit the helicopter designer to determine the limit of safe flying speeds before conducting special helicopter flight tests. Flight tests show that we can obtain a slightly larger value of t_y than the calculated values of $t_{y_{cr}}$. This is explained by the fact that our accepted $t_{y_{cr}}$ are smaller than the maximum possible values of t_y, and also by the fact that factors that increase $c_{y_{max}}$ were not taken into account in the calculations, namely effect of centrifugal /206 forces on the boundary layer and unsteady flow through the rotor blades.

8. Distribution of Profile Losses Over Rotor Disk. Dependence of Profile Losses on Aerodynamic Characteristics of Blade Profiles

In Section 3.3 we examined graphs of the coefficients of rotor profile losses. Let us define the extent of influence of aerodynamic characteristics of the blade profile, peripheral speed, and blade shape on the distribution of profile losses over the rotor disk and their total magnitude.

The required power of the rotor, referred to all-up weight, is proportional to $\bar{m}_t M_0^3$ [see eq.(5.16) in Chapt.III]:

$$\frac{N}{G} = \bar{m}_t M_0^3 \frac{a}{75\xi C_Y M_0^2} = \text{const}_1 \bar{m}_t M_0^3, \tag{4.51}$$

where

$$\bar{m}_t M_0^3 = \text{const}_2 + \bar{m}_{pr} M_0^3. \tag{4.52}$$

Thus, the required power of a helicopter at given M_{fl}, H, $p = \frac{G}{F}$, $\bar{c}_x = \frac{\Sigma c_x S}{F}$ is determined by the quantity $\bar{m}_{pr} M_0^3$ calculated at values of $C_Y M_0^2$ and $C_X M_0^2$ corresponding to the given quantities. For example, a helicopter has a load per square meter of the rotor disk area of $p = 35$ kg/m^2 and a parasite drag coefficient of $\bar{c}_x = 0.0075$; the calculated (operating) flight regime is $V = 275$ km/hr at a height of $H = 1000$ m. Under these conditions, the dimensionless coefficients of a helicopter are equal to

$$C_Y M_0^2 = \frac{p}{\frac{1}{2}\varrho a^2} = 0.00545;$$

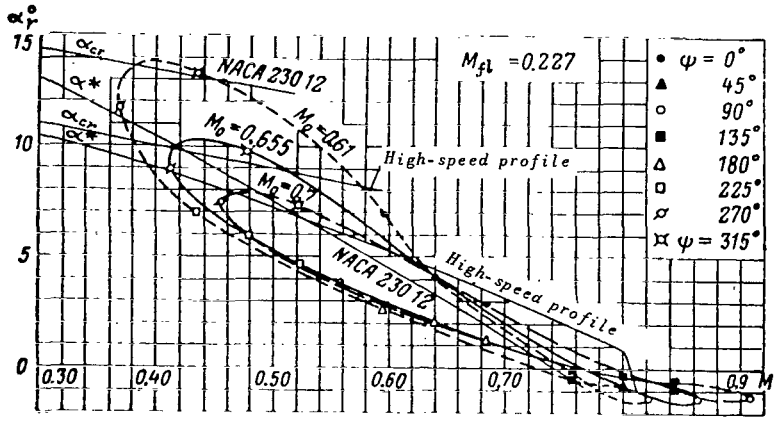

Fig.2.122 Angle of Attack at Blade Tip Section as a Function of M, for Three Values of Peripheral Rotor Speed (M_0).

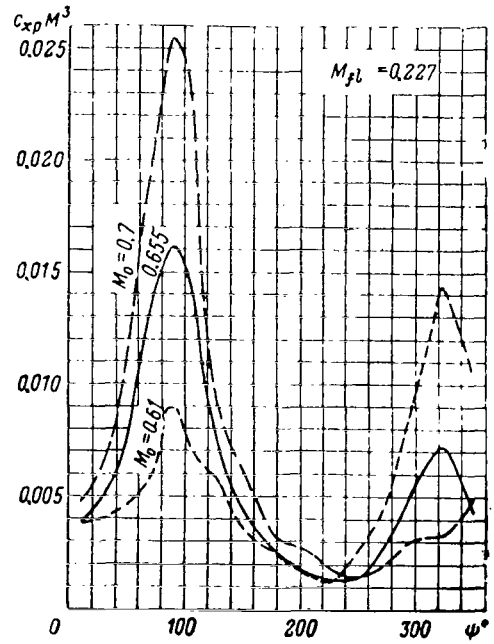

Fig.2.123 Profile Losses in Blade Tip Section as a Function of Azimuth Position of Blade, for Three Values of Rotor Peripheral Speed (M_0).

$$M_{fl} = \frac{V}{a} = 0.227;$$

$$C_X M_0^2 = \bar{c}_x M_{fl}^2 = 0.00039.$$

Let us give the results of calculations pertaining to the tip section of the blades $\bar{r} = 0.975$. Fig.2.122 is a graph for the angle of attack change of the tip section of a rectangular blade (variant II, $\sigma = 0.091$) with respect to azimuth, plotted as a function of M of the section for three values of the peripheral speed (M_0). We see from the graphs that the section has large angles of attack at small M and small negative angles at large M. By means of these graphs, it is easy to determine the location of flow separation zones at increased profile drag. For this, it is necessary to plot the curves of α_{cr} and α^* for the profile of the investigated section (see Figs.2.98 and 2.99) on the graphs in Fig.2.122. It is obvious that, for a high-speed profile and for $M_0 = 0.7$ ($\omega R = 235$ m/sec, $\bar{V} = 0.325$, $t_y = 0.1228$) the maximum angles of attack are low (1.5° lower than the critical values) but at azimuths $\psi = 35 - 140°$ deep penetration into the region of high c_{xp} takes place. At $M_0 = 0.655$ ($\omega R = 220$ m/sec, $\bar{V} = 0.347$, $t_y = 0.14$) the maximum angles of attack are close to critical and there are two zones of high profile drag: at azimuths $\psi = 55 - 120°$ and at azimuths $\psi = 270 - 0°$ when $\alpha = 10 - 5°$ and $M = 0.41 - 0.62$. When $M_0 = 0.61$ ($\omega R = 205$ m/sec, $\bar{V} = 0.373$, $t_y = 0.161$) the tip section at azimuths $\psi = 250 - 350°$ penetrates into the flow-separation zone and into the zone of high profile drag. There are no increases of profile losses at large M at azimuth $\psi = 90°$. /208

The permissibility of deeper penetration of the tip section into the flow-separation zone from the point of view of rotor behavior as a whole is characterized by the graph in Fig.2.119. In conformity with this graph, a flight regime with $M_0 = 0.61$ is permissible.

As shown above, the required power of a helicopter and the profile losses of the rotor are determined by the quantity $m_{pr} M_0^3$ which, for the examined section, is equal to

$$\frac{dm_{pr}}{dr} M_0^3 = \frac{1}{2\pi} \int_0^{2\pi} c_{xp} \bar{U}^3 \bar{b} M_0^3 d\psi = \frac{1}{2\pi} \bar{b} \int_0^{2\pi} c_{xp} M^3 d\psi. \qquad (4.53)$$

Figure 2.123 gives graphs for the product $c_{xp} M^3$ plotted against azimuth. The integral of eq.(4.53) is equal to (Table 2.12):

TABLE 2.12

M_0	0.7	0.655	0.61
$\frac{dm_{pr}}{d\bar{r}} M_0^3$	0.0073	0.0058	0.0056

Consequently, the greatest profile losses in the section under study occur at $M_0 = 0.7$ and the smallest losses, at $M_0 = 0.61$. At $M_0 = 0.655$, the profile losses are somewhat greater than at $M_0 = 0.61$, but local separation phenomena are absent.

Now let us assume that we were to change the profile in this section. Its angles of attack would then change slightly, while the zone of flow separation and high profile losses might change substantially. The curves of α_{cr} and α^* are also plotted in Fig.2.122 for the NACA 23012 profile. Obviously, at all M_0 the section would have no separation zones but would have a large zone of high profile losses at azimuths $\psi = 280 - 0 - 170^\circ$. Especially high will be the losses at $\psi = 90^\circ$, where M is greater than M_{cr} by 0.1 - 0.2. Since $\alpha_r < \alpha_{cr}$ at all ψ, the rpm of a rotor with this profile could be reduced.

Thus, the graph in Fig.2.122 gives the optimum dependence of α_{cr} and α^* on M of the profile, for the section under study at one of the design flight regimes.

For example, the rotor profile losses would decrease if the profile had $M_{cr} = 0.9$ at $\alpha \approx 0$ while retaining $\alpha^* = 7.5 - 5.5^\circ$ at M = 0.5 - 0.6. Then the best rotor rpm would correspond to $M_0 = 0.7$. The thin symmetric high-speed profile has a high value of M_{cr} at $\alpha \approx 0$, but a low value of α^* at M = 0.5 - 0.6.

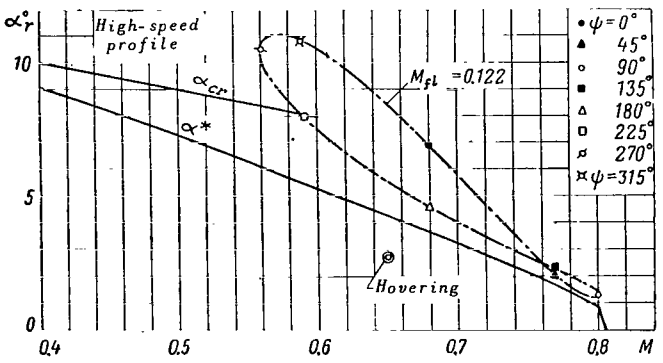

Fig.2.124 Angle of Attack of Blade Tip Section as a Function of Mach Number.

The profile with $M_{cr} = 0.8$ at $\alpha \approx 0$ and $\alpha^* = 4 - 7^\circ$ at M = 0.4 - 0.6 would be suitable for the examined flight regime for the case of $M_0 = 0.61$. A highly concave profile with a small relative thickness does have such characteristics; however, its use would considerably increase blade torsion and controls stress of the helicopter.

In selecting the profile, it must be considered that the dependence $\alpha_r = f(M)$ will be different in different flight regimes. Figure 2.124 gives a graph for a regime corresponding to flight close to the dynamic ceiling: $M_{fl} = 0.122$; $C_y M_0^2 = 0.0103$, $C_x M_0^2 = -0.00012$, $M_0 = 0.7$. We see from Fig.2.124 that, in this regime, the profile losses are very high. In conformity with Fig.2.119, this regime lies at the boundary of flow separation. In hovering flight near /209 the ground, at a lower peripheral speed, the examined section will have $\alpha_r = 2.7^\circ$, M = 0.65.

By suitable selection of blade shape, a certain influence can be exerted on the change in angles of attack at the blade tip with respect to azimuth and a better combination can be obtained of the dependence $\alpha_r = f(M)$ with the profile

characteristics. As typical example, Fig.2.125 gives a graph of $\alpha_r = f(M)$ for the tip section of blades of the variants I (trapezoidal), II (rectangular), VI (rectangular with increased twist) and VII (expanding) at $t_y = 0.12$, $t_x = -0.013$, $\bar{V} = 0.4$, $M_0 = 0.7$.

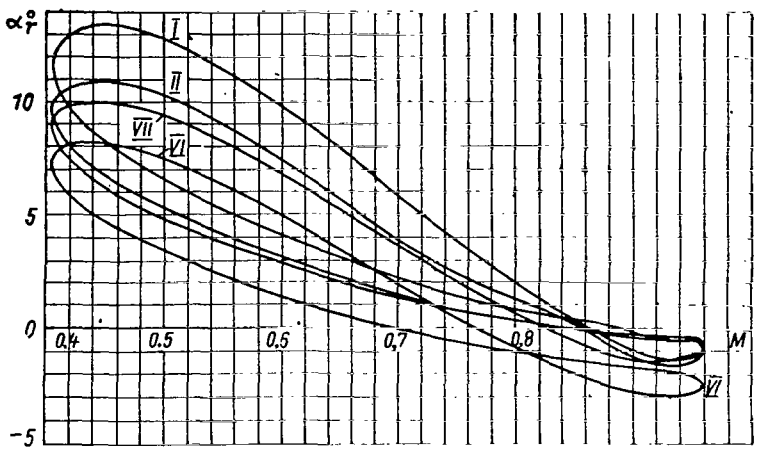

Fig.2.125 Angle of Attack of Blade Tip Section as a Function of Mach Number, for Rotors with Blades of Different Shapes.

Figure 2.125 shows that the trapezoidal blade, for which a reduction of chord at the tip ($\bar{b}_{tip} < 1$) leads to a decrease in profile losses, has the largest angles of attack at M = 0.4 - 0.7. The expanding blade, at these values of M, has angles of attack by 1° lower than those of the rectangular blade. The blade with increased twist has angles of attack by 1.7° lower at all azimuths than those of other blade variants.

The integral in eq.(4.53) should be calculated to obtain a quantitative estimate of the effect of a change of blade shape and profile. /210

It is clear from the foregoing that the azimuthal distribution of profile losses in each blade section depends on flight regime, peripheral speed, and blade profile. Main emphasis should be placed on selecting a suitable profile in the blade tip sections, where the largest profile losses occur. For illustration, Fig.2.126 shows the distribution of profile losses over the radius of a blade of variant II for $M_{f1} = 0.227$, $M_0 = 0.655$ at four azimuths, as well as the distribution of the average circumferential profile losses over the blade radius. Figure 2.126 indicates that about 35% of profile losses are accounted for by the tip portion of the blade from $\bar{r} = 1.0$ to $\bar{r} = 0.9$.

Section 5. Vortex Theory of Rotor

1. Problems in Vortex Theory

The main problem in the vortex theory of a rotor lies in the determination

of aerodynamic loads on the blade, with consideration of the nonuniform induced velocity field.

The solution of this problem permits:

1. Refining the aerodynamic characteristics of the rotor. These refinements are less important for the single-rotor helicopter and more important for multirotor helicopters, where the mutual induced effect is very strong and has a substantial influence on their flight characteristics.

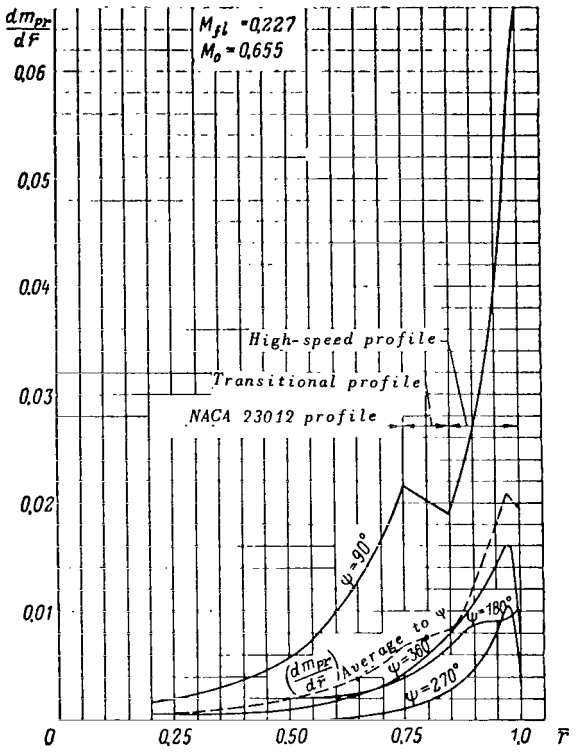

Fig.2.126 Distribution of Profile Losses over Blade Radius.

2. Determining both the constant and variable aerodynamic loads of the blade and from these loads calculating the oscillations of the blade and its deformations. Without consideration of the nonuniform induced velocity field, any determination of the variable aerodynamic loads on the blade in a number of flight regimes is quite inaccurate. Therefore, the rotor vortex theory must introduce the component of blade oscillations and the determination of variable stresses into the calculation, i.e., into the stress analysis of the blade. /211

Only by means of the vortex theory is it possible to explain such phenomena as the marked increase in variable loads on the blade and vibrations of the helicopter in low-speed regimes as well as the appearance of local flow separation zones at medium and high speeds.

In low-speed regimes, the induced velocity field is particularly nonuniform. This leads to the occurrence of appreciable variable aerodynamic forces acting on the blade. The blades begin to vibrate at increasing amplitude. Extensive variable stresses are set up in the blades. The variable forces transferred from the blades to the hub lead to increased vibrations of the entire helicopter. The explanation of this phenomenon is possible only by making use of the vortex theory.

At high and medium flying speeds, a phenomenon is observed which we can call induced flow separation. This phenomenon is a consequence of large induced velocities arising in the region of vortices shed from the blade tips. When the next blades pass below these vortices, appreciable surges in aerodynamic loads and, in certain regimes, even flow separation are created. This phenomenon was partially described elsewhere (Ref.17) and has been confirmed in flight tests.

A no less important problem of the vortex theory is the determination of the induced velocity field caused by the rotor in the stream flowing past the helicopter and its individual components in flight.

The character of flow past the wings of a helicopter, its fuselage, and stabilizer is largely determined by the velocity field induced by the rotor. The occurrence of induced velocities leads to additional downwash and to a change in the true angles of attack of the lifting elements and hence in the forces acting on all outer surfaces of the helicopter components. Therefore, to study the flow around these parts, it is necessary to determine the induced velocities at various points in the space surrounding the helicopter.

Thus, the vortex theory permits determining the induced downwash in the region of the helicopter wing and its stabilizer and hence the aerodynamic forces acting on them. Therefore, the theory also introduces the following components into the calculations of aerodynamic characteristics: balancing of the helicopter, characteristics of its stability, and controllability features in which these forces play a substantial role.

There are other phenomena for whose calculation the vortex theory is used. A sufficiently detailed description of all these phenomena is possible only in special works. Therefore, in this Section we will give only a brief account of the most important elements of the vortex theory, without detailed substantiations.

2. Theoretical Schemes for the Vortex Theory of a Rotor with a Finite Number of Blades

In the vortex theory, the rotor is replaced by a system of bound and free vortices. This system can be represented by a vortex sheet covered with horseshoe vortices (see Fig.2.128). The segments of these eddies located at the blade are known as bound vortices. Depending on the purpose of the calculation, we can use schemes in which the blade is replaced either by a bound lifting vortex (lifting-line scheme), or by a bound vorticity layer (scheme of a lifting-vortex surface). In the latter case (Fig.2.127), the blade is replaced by a system of bound vortices distributed over the blade chord with some strength γ_b so that

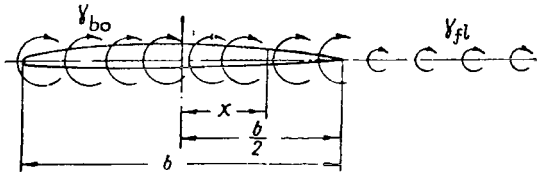

Fig.2.127 Flow around Blade Profile in Scheme of Lifting-Vortex Surface.

/212

$$\Gamma = \int_{-b/2}^{b/2} \gamma_{bo}\, dx, \qquad (5.1)$$

where

Γ = velocity circulation over a contour encompassing the blade section (Fig.2.128);

γ_{bo} = circulation per unit length of the bound vortices distributed over the profile chord.

The scheme of a lifting-vortex surface more accurately reflects the physical pattern of flow around the blade but is more complex in calculations. Therefore, to simplify calculations, the lifting-vortex surface is often replaced by a lifting-vortex line. In determining the induced velocities at a sufficient distance from the blade, this simplification does not produce excessive errors in the results and therefore is often used in calculations. The induced velocities close to the blade must be determined by the scheme of a lifting-vortex surface.

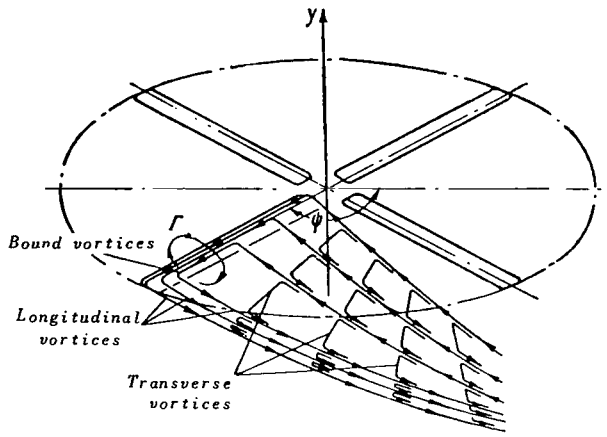

Fig.2.128 Diagram of Formation of a Vortex Sheet in Circulation of Flow about the Blade.

During operation of the rotor, the conditions of flow around the blade at different radii are dissimilar. Thus, the magnitude of circulation of the bound vortices varies over the blade radius. A change in circulation is accompanied by the formation of so-called longitudinal vortices (see Fig.2.128). The longitudinal vortices are a continuation of the bound vortices located on the blade and form the tails of horseshoe vortices extending to infinity. /213

The strength of the longitudinal vortices should be equal to the change in circulation of the bound vortices over the blade radius:

$$\gamma_{lo} = \frac{\partial \Gamma}{\partial \varrho}, \tag{5.2}$$

where

γ_{lo} = strength of longitudinal vortices per unit length;
Γ = total circulation of the bound vortices.

If the circulation of the bound vortex changes in time, also transverse vortices will trail from the blade. The circulation of transverse vortices is equal to the change in circulation of the bound vortices with respect to time

$$\gamma_{tr} = -\frac{\partial \Gamma}{\partial t}, \tag{5.3}$$

where γ_{tr} is the circulation of transverse vortices shed by the blade in unit time.

The strength of the transverse vortices per unit length can be determined as

$$\gamma_{tr} = -\frac{1}{U}\frac{\partial \Gamma}{\partial t}, \tag{5.4}$$

where U is the velocity component of relative flow, normal to the blade axis.

Transverse vortices, just as bound vortices, form part of the horseshoe vortices and merge along the edges with the longitudinal vortices. As a consequence, the circulation of the longitudinal vortices is variable over their length and changes by the magnitude of circulation of the transverse vortices merging there.

Under conditions of axial flow past the rotor, the circulation in the blade section Γ remains constant in time. Therefore, a vortex sheet consisting only of longitudinal vortices will be shed by the blade. Their strength proves to be constant over the length of the free vortex.

3. Form of Free Vortices

Under flying conditions, the free vortices shed by the blade are carried away from the rotor at a rate equal to the relative velocity of the flow passing through the rotor. These velocities, generally speaking, are different at different points of this flow. Therefore, the free vortices trailing from the blades are carried away from the rotor at different rates. As a result, a rather complex vortex system will exist downstream of the rotor, which, moreover, is continuously being deformed due to the mutual interference of the vortices. At some distance from the rotor, the vortex sheet begins to be dislodged and finally loses its original form.

It is extremely difficult to take into account deformations of the system of trailing vortices. Therefore, in theoretical methods of calculation few attempts have been made to take these deformations into consideration. Usually, most authors assume that the free vortex sheet is carried away from the rotor /214 at a constant rate equal to the mean velocity of flow through the rotor.

The components of this velocity with respect to the coordinate axes, referred to the peripheral speed of the blade tip ωR, are usually taken as equal to μ and $\lambda_{0\,av}$ ($\lambda_{0\,av}$ being the average velocity of the flow of the stream along the axis of the rotor, referred to ωR).

The average flow velocity $\lambda_{0\,av}$ is determined by the well-known formula:

$$\lambda_{0av}=\mu\tan\alpha-\frac{C_T}{4\sqrt{\mu^2+\lambda_{0av}^2}}.$$

With such an assumption, the trailing vortices are arranged over a downwash spiral surface. The longitudinal free vortices are located along downwash spiral lines, whereas the transverse vortices are arranged over the radial generatrix of this spiral surface. Therefore, as applied to a helicopter rotor it is preferable to divide the trailing vortices into spiral and radial rather than into longitudinal and transverse, as is done in the airfoil theory.

All free vortices trailing from the blades are located within an inclined cylindrical surface resting upended on the circumference of the rotor. The

vortex system enclosed within this surface is usually called a vortex column or a vortex cylinder.

Let us derive the equation of the line along which are located the free vortices shed from the blade at an arbitrary radius ρ. This line coincides with the wake of the blade in the flow passing through the rotor. Neglecting deviation of the blade from the plane of rotation, the coordinates of this line (see, for example, the coordinates of point A in Fig.2.130) can be written as follows:

$$\left.\begin{aligned} x &= -\varrho\cos\vartheta - \mu R(\psi_0 - v);\\ z &= -\varrho\sin\vartheta;\\ y &= -\lambda_{oav} R(\psi_0 - \vartheta), \end{aligned}\right\} \qquad (5.5)$$

where

$-\infty < \vartheta < \psi_0$;

$0 < \rho < R$;

ψ_0 = azimuth of the blade at the instant of time in question;

ϑ = azimuth of the blade at the instant of time of shedding the vortex.

All computations given below will be based only on such a form of the free vortices. We will disregard refinements introduced by consideration of their deformation.

4. Determination of the Induced Velocities by the Biot-Savart Formula

If the form of the free vortices is known, the Biot-Savart formula can be used for determining the induced velocities. This formula permits determining the elementary velocity $\vec{dv}$ induced at the point M by a vortex element of length dS (Fig.2.129). In vectorial form, the formula can be written as

$$\vec{dv} = \frac{\Gamma}{4\pi}\,\frac{\vec{dS}\times\vec{l}}{l^3}, \qquad (5.6)$$

where

$\vec{dv}$ = vector of the elementary induced velocity caused at the point M by a vortex element of length dS;

Γ = circulation of the vortex;

$\vec{dS}$ = vector of the vortex element;

$\vec{l}$ = vector proceeding from the point M where the induced velocity is calculated to the locus of the vortex element dS; /215

$l = |\vec{l}|$ = distance from the point M to the vortex element dS.

The direction of the vector $\vec{dv}$ is perpendicular to the plane formed by the vectors $\vec{dS}$ and $\vec{l}$.

To determine the induced velocity from the total vortex, eq.(5.6) must be integrated with respect to its length:

$$\vec{v}=\int_S \frac{\Gamma}{4\pi}\frac{\vec{dS}\times\vec{l}}{l^3}. \qquad (5.7)$$

Having taken such integrals over the length of all vortices, located both on the blade and shed by the rotor, we can obtain the total induced velocity at any point of space around the helicopter.

5. Use of the Biot-Savart Formula in Developing the Vortex Theory of a Rotor

Equation (5.7) can be used as basis of the rotor vortex theory. For this, it is necessary to determine the induced downwash in the rotor plane and take this into consideration when determining the true angles of attack of the blade sections. After this, the loads on the blades can be determined by formulas of the type

$$T=\frac{1}{2}c_y\varrho bU^2, \qquad (5.8)$$

where the value of c_y is taken with respect to profile wash, for angles of attack calculated with consideration of induced downwash.

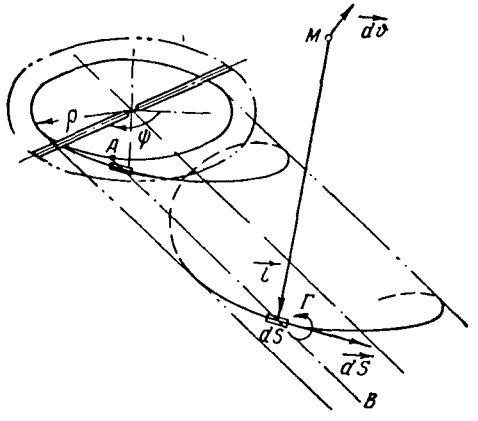

Fig.2.129 Diagram for Calculating Induced Velocities by the Biot-Savart Formula.

To determine the induced downwash on the rotor blade it suffices to calculate only the axial (parallel to the rotor axis) component of the induced velocity v_y. Then the downwash angle can be approximately determined by the formula

$$\Delta\alpha_v\cong\frac{v_y}{U_x}, \qquad (5.9)$$

where $\Delta\alpha_v$ is the change in angle of attack of the blade element due to downwash.

According to the rules of vector analysis, the projection of the product /216 of the vectors $\vec{dS}\times\vec{l}$ onto the y-axis can be calculated in the following manner:

$$(\vec{dS}\times\vec{l})_y=dS_zl_x-dS_xl_z, \qquad (5.10)$$

where dS_x and dS_z are projections of the vector $\vec{dS}$, while l_x and l_z are projections of the vector $\vec{l}$ onto the x- and z-axes; the direction of the x- and z-axes is shown in Fig.2.130.

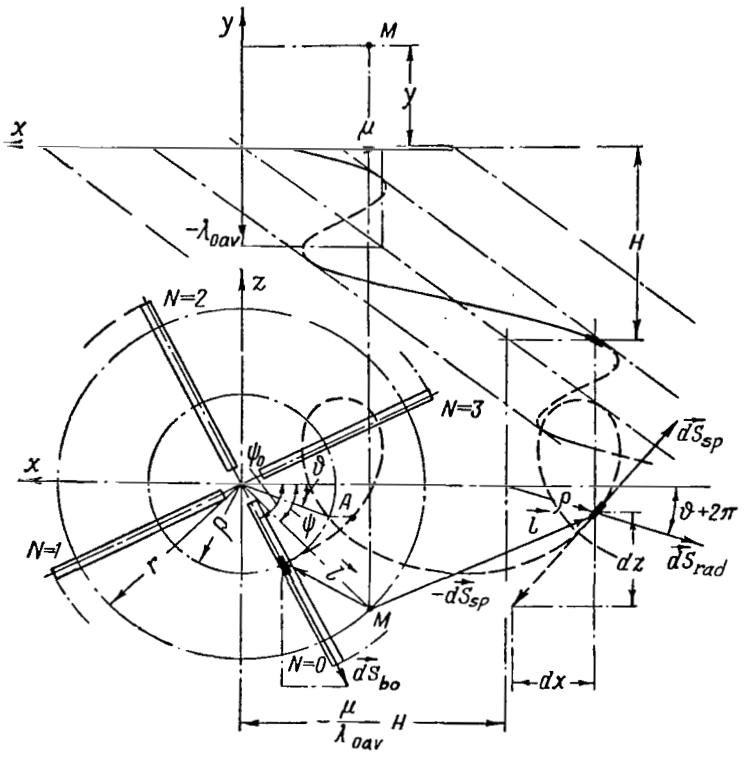

Fig.2.130 Diagram for Calculating Axial Components of Induced Velocities.

Correspondingly, the axial component of induced velocity can be obtained by a formula analogous to eq.(5.7):

$$v_y = \int_S \frac{\Gamma}{4\pi l^3} [dS_z l_x - dS_x l_z]. \tag{5.11}$$

Usually, the induced velocities are represented as the sum of three components:

$$v = v_{bo} + v_{sp} + v_{rad}, \tag{5.12}$$

where

v_{bo} = induced velocity from bound vortices;
v_{sp} = induced velocity from spiral vortices;
v_{rad} = induced velocity from radial vortices.

Let us construct the general formulas for calculating the axial components of induced velocities, without limiting ourselves to the case y = 0 (y being the coordinate of the point at which the induced velocity is calculated).

6. Axial Component of Induced Velocity from Bound Vortices /217

Bound vortices have a circulation equal to Γ_N and are located along the rotor blades. The subscript N denotes here the numeral of the rotor blade. We will consider that N = 0, 1, 2, ..., z_b - 1, where z_b is the number of blades in the rotor (see Fig.2.130).

The values of dS_x and dS_z entering eq.(5.11) for the bound vortices are equal to

$$\left.\begin{aligned}(dS_x)_{bo} &= -d\varrho\cos\psi_N,\\ (dS_z)_{bo} &= -d\varrho\sin\psi_N,\end{aligned}\right\} \tag{5.13}$$

where ψ_N is the azimuth of the blade with the numeral N.

Substituting eqs.(5.13) into eq.(5.11) and taking the integral of eq.(5.11) over the length of all rotor blades, we obtain

$$v_{bo} = \sum_{N=0}^{N=z_b-1}\int_0^R \Gamma_N K_N\, d\varrho, \tag{5.14}$$

where

$$K_N=\frac{1}{4\pi}\left[-\frac{l_x}{l^3}\sin\psi_N+\frac{l_z}{l^3}\cos\psi_N\right].$$

The values of l_x, l_z and l entering into K_N are determined by the formulas

$$\left.\begin{aligned}l_x&=r\cos\psi-\varrho\cos\psi_N,\\ l_z&=r\sin\psi-\varrho\sin\psi_N,\\ l&=\sqrt{l_x^2+l_z^2+y^2},\end{aligned}\right\} \tag{5.15}$$

where r is the radius of the circumference passing through the point at which the induced velocity is calculated, while

$$\psi_N=\psi_0+\frac{2\pi}{z_b}N. \tag{5.16}$$

Here, ψ_0 is the azimuth of the blade with the numeral N = 0.

Substituting the values of l_x and l_z into the formula for K_N, we obtain

$$K_N=\frac{1}{4\pi}\,\frac{r\sin(\psi-\psi_N)}{l^3}.$$

7. Axial Component of Induced Velocity from Spiral (Longitudinal) Vortices

In determining induced velocities from spiral vortices, we must sum the

velocities induced by vortices trailing from different radii of the blade. As in the determination of velocities from bound vortices, we must define here the total velocities induced by vortices shed from all rotor blades.

To use eq.(5.11) for this purpose, it is convenient to divide the vortex sheet into strips joining the vortices shed from a portion of the blade of length $d\rho$. Then the circulation of the vortices enclosed in this strip, in accordance with eq.(5.2), is equal to $\frac{\partial \Gamma_N}{\partial \rho} d\rho$.

To determine the values of dS_x and dS_z, we differentiate eqs.(5.5). Then (see Fig.2.130),

$$\left.\begin{aligned}(dS_x)_{sp} &= -dx = -(\varrho \sin\vartheta + \mu R)\, d\vartheta;\\ (dS_z)_{sp} &= -dz = \varrho \cos\vartheta\, d\vartheta.\end{aligned}\right\} \tag{5.17}$$

Using eq.(5.11), we obtain /218

$$v_{sp} = \sum_{N=0}^{z_b-1} \int_0^R \int_{\vartheta=-\infty}^{\psi_N} \frac{\partial \Gamma_N}{\partial \varrho} L_N\, d\varrho\, d\vartheta, \tag{5.18}$$

where

$$L_N = \frac{1}{4\pi}\left[\frac{l_x}{l^3}\varrho\cos\vartheta + \frac{l_z}{l^3}(\varrho\sin\vartheta + \mu R)\right].$$

The values of l_x, l_z, and l entering into L_N are determined by the formulas (see Fig.2.130):

$$\left.\begin{aligned}l_x &= \frac{\mu}{\lambda_{oav}} H_N + r\cos\psi - \varrho\cos\vartheta,\\ l_z &= r\sin\psi - \varrho\sin\vartheta,\\ l &= \sqrt{l_x^2 + l_y^2 + l_z^2},\end{aligned}\right\} \tag{5.19}$$

where

$$l_y = -(H_N + y).$$

The value of H_N, representing the distance along a normal to the plane of rotation, from the rotor to the point of the vortex sheet (see Fig.2.130), can be expressed in terms of the azimuth of the vortex sheet ϑ by means of the formula

$$H_N = \left(\psi_0 - \vartheta + \frac{2\pi}{z_b} N\right)\lambda_{oav} R, \tag{5.20}$$

where $N = 0, 1, 2, \ldots, z_b - 1$.

8. Axial Component of Induced Velocity from Radial (Transverse) Vortices

The circulation of radial vortices shed from the blade in unit time is equal to $-\frac{\partial \Gamma_N}{\partial t} \cdot dt$. In the vortex wake, these vortices are located over the radial generatrix. Therefore,

$$\left.\begin{aligned}(dS_x)_{rad} &= -d\varrho \cos\vartheta,\\ (dS_z)_{rad} &= -d\varrho \sin\vartheta.\end{aligned}\right\} \tag{5.21}$$

Using the same approach as above, we obtain

$$v_{rad} = -\sum_{N=0}^{z-1} \int_0^R \int_{t=-\infty}^{0} \frac{\partial \Gamma_N}{\partial t} M_N \, d\varrho \, dt, \tag{5.22}$$

where

$$M_N = \frac{1}{4\pi}\left[-\frac{l_x}{l^3}\sin\vartheta + \frac{l_z}{l^3}\cos\vartheta\right].$$

The values of l_x, l_z, and l entering into M_N are determined by eqs.(5.19).

Integration with respect to t in eq.(5.22) can be replaced by integration with respect to ϑ, bearing in mind that $\vartheta = \psi_N + \omega t$. Then,

$$v_{rad} = -\sum_{N=0}^{z_b-1} \int_0^R \int_{\vartheta=-\infty}^{\psi_N} \frac{\partial \Gamma_N}{\partial \vartheta} M_N \, d\varrho \, d\vartheta. \tag{5.23}$$

The functions K_N, L_N, and M_N entering into eqs.(5.14), (5.18), and (5.23) will henceforth be called the induction coefficients of the vortex element dS and a point with the coordinates r, ψ, and y. /219

9. Integrodifferential Equation of the Vortex Rotor Theory

To determine the aerodynamic load on the blade profile, the induced downwash must be determined from all trailing vortices and bound vortices of all blades, with the exception of the blade in question, since this vortex participates in the formation of lift expressed by Joukowski's formula:

$$T = \varrho U \Gamma. \tag{5.24}$$

In other words, the downwash from the bound vortices on a blade with the numeral N = 0 must be determined by calculating the induced velocity v_{b0} by a formula differing from eq.(5.14) in that the term with N = 0 is absent:

$$v_{bo} = \sum_{N=1}^{N=z_b-1} \int_0^R \Gamma_N K_N d\varrho. \tag{5.25}$$

We then equate the lifts determined by eqs.(5.8) and (5.24). This yields

$$\Gamma = \frac{1}{2} c_y b U. \tag{5.26}$$

If we limit ourselves to flight regimes in which it can be assumed that $c_y = c_y^{\alpha}\alpha$ and $U = U_x$ and if we represent the angle of attack α as

$$\alpha = \Phi_0 + \Delta\alpha_v, \tag{5.27}$$

(where Φ_0 is the inflow angle to the blade profile which would be present in the absence of induced downwash $\Delta\alpha_v$), and $\Delta\alpha_v$ is expressed in conformity with eq.(5.9), then eq.(5.26) can be written in the form

$$\Gamma = \frac{1}{2} c_y^{\alpha} b U_x \Phi_0 + \frac{1}{2} c_y^{\alpha} b v_y. \tag{5.28}$$

Substituting here the value of v_y determined by eqs.(5.12), (5.14), (5.18), and (5.23) and taking into account the refinement (5.25), we arrive at the integrodifferential equation analogous to the basic integrodifferential equation of finite wing theory (Ref.28):

$$\Gamma_0 = \frac{1}{2} c_y^{\alpha} b U_x \Phi_0 + \frac{1}{2} c_y^{\alpha} b \left[\sum_{N=1}^{z_b-1} \int_0^R \Gamma_N K_N \, d\varrho + \right.$$
$$\left. + \sum_{N=0}^{z_b-1} \int_0^R \int_{\vartheta=-\infty}^{\psi_N} \frac{\partial \Gamma_N}{\partial \varrho} L_N \, d\varrho \, d\vartheta - \sum_{N=0}^{z_b-1} \int_0^R \int_{\vartheta=-\infty}^{\psi_N} \frac{\partial \Gamma_N}{\partial \vartheta} M_N \, d\varrho \, d\vartheta \right]. \tag{5.29}$$

It is necessary to note that the functions U_x, Φ_0, Γ_N, $\frac{\partial \Gamma_N}{\partial \rho}$, $\frac{\partial \Gamma_N}{\partial \vartheta}$, K_N, L_N, and M_N entering here represent functions of the radius and azimuth of the blade. The function Φ_0 also depends on the flapping motion of the blade which, in turn, is a function of aerodynamic loads and hence of the values of Γ_N. Therefore, the integrodifferential equation (5.29) must be solved together with the equation of the flapping motion of the blade. /220

It is not possible to suggest any general method of solving this equation. In each individual case, the method of solution most suitable to the particular case is used in relation to the method of determining the induced velocities. As an example, we mention the method presented in Section 8 of Chapter I in Vol.II.

For a solution, the method of successive approximations is occasionally

used, which involves assuming at first that the induced velocity v_y is constant over the rotor disk and Γ_0 is calculated in the first approximation. In that case, the terms in brackets in eq.(5.29) are calculated and the new value of Γ_0 is found; the procedure is continued in this manner until the solution converges.

However, it must be borne in mind that convergence of this method is ensured only in individual particular cases and therefore must be separately checked each time.

Many authors, considering one or another method of successive approximations and believing it possible to restrict the process to the first approximation, only give a method of calculating induced velocities based on the values of circulation Γ, assuming them to be prescribed [see, for example, Baskin and Shi-Tsun (Ref.16, 22)]. Therefore, it often happens that only the operation of determining the induced velocities with respect to prescribed values of Γ is introduced into the vortex theory concept.

10. Constancy of Circulation of Trailing Vortices Along Straight Lines Parallel to the Axis of the Inclined Vortex Cylinder and Possible Simplifications

It was already noted in Subsection 2 that the circulation of spiral vortices is variable over their length because they merge with the radial vortices. Therefore, when calculating the integral in eq.(5.18) we must find the dependence $\frac{\partial\Gamma_N}{\partial\rho} = f(\vartheta)$. In like manner, when calculating the integral in eq.(5.23) it must be borne in mind that $\frac{\partial\Gamma_N}{\partial\vartheta}$ varies over the length of the vortex sheet along with the variable ϑ. This circumstance complicates calculation of the integrals in eqs.(5.18) and (5.23). Therefore, in calculating these it is convenient to make use of the fact that $\frac{\partial\Gamma_N}{\partial\rho}$ and $\frac{\partial\Gamma_N}{\partial\vartheta}$ are constant along straight lines parallel to the generatrix of the vortex cylinder.

Actually, in the case of steady flow past a rotor, vortices of identical strength will be shed from a certain radius of each blade at azimuth ψ. These vortices will be carried away from the rotor along a straight line parallel to the axis of the vortex column. Therefore, at any distance from the rotor, at a point of the vortex sheet with azimuth $\vartheta = \psi$ and radius $\rho = r$, the strength of the spiral and radial vortices is identical.

For further computation, it is important to note that any straight line passing within the vortex column and parallel to its axis intersects the vortex sheet at the points

$$H_n = \left(\psi_N - \vartheta + \frac{2\pi}{z_b} \cdot n\right)\lambda_{oav} R, \tag{5.30}$$

where

$n = 0, 1, 2, \ldots, \infty$;
ϑ = azimuth of the rotor reckoned only in the range from 0 to 2π;
ψ_N = azimuth of the blade for which the difference $(\psi_N - \vartheta)$ has the smallest positive value.

It follows from the structure of eqs.(5.18) and (5.23) that, to determine /221 the induced velocity at some point of space, it is first necessary to integrate, over the entire vortex sheet, a function representing the product of the strength of an element of this vortex sheet and the induction coefficients L_N and M_N, and then to sum the results obtained from the vortex sheet of each rotor blade separately.

However, in this case we need not integrate along the vortices comprising the vortex sheet. At first, we can sum the products of the strength of an element of the vortex sheet and the induction coefficients L_N and M_N along straight lines parallel to the axis of the vortex column. Here, by virtue of the strength of the vortices along the straight lines being constant, this operation reduces to summation of only the induction coefficients. Therefore, the elementary components of the induced velocity from these vortices can be represented as

$$\left.\begin{aligned} dv_{sp} &= \frac{\partial \Gamma_\vartheta}{\partial \varrho}\left(\sum_{n=0}^{\infty} L_N\right) d\varrho\, d\vartheta, \\ dv_{rad} &= -\frac{\partial \Gamma_\vartheta}{\partial \vartheta}\left(\sum_{n=0}^{\infty} M_N\right) d\varrho\, d\vartheta, \end{aligned}\right\} \tag{5.31}$$

where Γ_ϑ is the circulation of the bound vortex at the instant when the blade is at azimuth $\psi = \vartheta$.

After integrating these expressions over the entire rotor disk, we obtain formulas for determining the axial components of the induced velocities in the form

$$\left.\begin{aligned} v_{sp} &= \int_0^R \int_0^{2\pi} \frac{\partial \Gamma_\vartheta}{\partial \varrho}\left(\sum_{n=0}^{\infty} L_N\right) d\varrho\, d\vartheta, \\ v_{rad} &= -\int_0^R \int_0^{2\pi} \frac{\partial \Gamma_\vartheta}{\partial \vartheta}\left(\sum_{n=0}^{\infty} M_N\right) d\varrho\, d\vartheta. \end{aligned}\right\} \tag{5.32}$$

On the basis of these formulas, we can construct a computational method applicable in practice. This method was first used by M.N.Tishchenko.

It should be pointed out that, in the practical application of this method, the volume of computational operations is very large.

Thus, if for calculating the integrals in eq.(5.32) the circumference of

the rotor is divided with respect to azimuth into z_ψ sections and the blade into z_r sections with respect to radius, then for calculating the field of the axial induced velocity components in the rotor plane alone, the integrands in eqs.(5.32) must be calculated $(z_\psi z_r)^2$ times.

If we assume $z_\psi = 72$ ($\Delta\psi = 5^\circ$) and $z_r = 30$, then the quantity $(z_\psi z_r)^2$ will be equal to about 4.5×10^6. Therefore, this method can be effectively used only on computers with a speed substantially greater than 20,000 operations per second.

11. Characteristics of Using the Lifting-Line Scheme and Scheme of a Vortex Lifting Surface

It was pointed out above that the scheme of a vortex lifting line yields satisfactory results if the induced velocities are calculated at a sufficient distance from the blade. However, for determining the aerodynamic loads by eq.(5.8) it is necessary to calculate the induced velocities on the blade, /222
i.e., where the bound vortex is located according to the calculation scheme.

If the lifting-line scheme is used, then the induced velocities in the calculations begin to increase on approach to the lifting vortex and vanish at the vortex itself. This takes place in two cases:

1. If flow past the blade is unsteady and if radial (transverse) vortices are formed in the vortex wake.
2. If the spiral (longitudinal) vortices shed from the blade make an angle differing from $\pi/2$ with the blade axis, which always takes place in the case of oblique flow through the rotor since the blades have slip flow.

Consequently, the induced velocities in the lifting vortex will not vanish only in the case of axial flow past the rotor.

These difficulties can be overcome by neglecting the effect of radial vortices and rotor slip. Such an approach is widespread in practice and can be used whenever permissible with respect to the nature of the problem to be solved. However, this renders the solution rather approximate, which does not always suit the researcher.

The method of calculating with the scheme of a vortex lifting surface is free from this shortcoming. Therefore, when calculating the induced velocities in the blade region we can use methods based on replacement of the blade by a vortex surface, as is done in the theory of unsteady flow past an airfoil (Ref.30). However, this renders the problem of determining the induced velocities even more complex. Therefore, this approach is not yet in widespread practical use for rotor calculation, although work in this direction is in progress (Ref.19).

For practical purposes, we can use the method in which the free vortices shed by the blade are divided into vortices directly adjacent to the blade and vortices remote from the blade. After this, the induced velocities due to

vortices remote from the blade can be determined by the vortex lifting line scheme while, for calculating the velocities due to vortices adjacent to the blade, a method based on the vortex lifting surface scheme can be developed.

12. Division of Vortices into Types Close to and Remote from the Blade; Use of "Steady-Flow Hypothesis"

To facilitate an analysis of the influence of various elements of the vortex sheet on the magnitude of the aerodynamic load on the blade, it is convenient to divide free vortices into two classes (Ref.17). The first class includes vortices immediately adjoining the trailing edge of the blade in question and those shed from the blade during one revolution at some small azimuth angle $\Delta\psi$ ($\Delta\psi = 20 - 30^\circ$). Such vortices are called adjacent (to a given blade) and the induced velocities caused by these vortices are called intrinsic. The second class includes all other free vortices. These vortices are called remote, and the velocities induced by them are called extrinsic induced velocities.

Such a division is based on the fact that the vortices shed from the blade have a noticeable influence on the aerodynamic load of the blade only while they are sufficiently close to it. Upon removing the vortices by a distance of $20 - 30^\circ$ with respect to the rotor azimuth, their influence decreases but resumes its former extent when the blade executes one complete revolution and again approaches these vortices. Thus, the blade along its path encounters not only its own vortices but also the vortices shed from all other blades of the rotor. All these vortices usually fall into the general group of remote vortices. /223

In some cases, it is convenient in calculations to determine separately the velocity field induced by the remote vortices and to investigate the flow past a blade moving in this nonuniform field. With this approach, the flow past the blade will be similar to a flow past the wing of an airplane flying under conditions of turbulent air. In the same manner as for an airplane wing, when calculating the variable aerodynamic loads on a given blade, it is possible to consider the effect of trailing vortices directly adjacent to the blade by the so-called "steady-flow hypothesis". In this hypothesis, it is assumed that, in unsteady flow past a profile, the loads acting on the profile behave as though the flow pattern produced at a given instant of time remained unchanged for an arbitrarily long time. In the "steady-flow hypothesis", the effect of trailing vortices adjacent to the blade is disregarded.

Thus, the flow pattern of the blade can be represented in the following form: When the rotor rotates, the blade encounters the nonuniform field of extrinsic induced velocities caused by the effect of the total vortex system of the rotor with the exception of the vortices immediately adjoining the blade. Under the effect of this velocity field, the angles of attack of the blade sections vary constantly, and variable aerodynamic loads caused by the nonuniformity of this field begin to act on the blade. The magnitude of the variable aerodynamic loads is affected also by the free vortices adjacent to the blade and shed from it upon any change in the circulation flow. The effect of adjacent vortices is of the same nature as that in unsteady flow past a finite airplane wing.

13. Instantaneous and Mean Induced Velocities and Generation of Variable Aerodynamic Loads on the Blade

Calculation of induced velocities by the theoretical scheme with a finite number of blades makes it possible to determine the true (instantaneous) induced velocity at any point of space near the helicopter. The true induced velocities prove to be variable, fluctuating in time with the frequency of the vortices passing by a given point. One can distinguish time-invariant (mean) and time-variant components of induced velocities.

If we examine a point in space fixed with respect to the helicopter close to its rotor, then the time-variant induced velocities at this point will be caused both by bound and free vortices. However, in comparing their values, it becomes obvious that the variable induced velocities due to bound vortices and to free vortices adjacent to the blade are largest in value. These induced velocities fluctuate with the frequency of the rotor blades passing by the point in question. Generation of these velocities is related primarily with the formation of aerodynamic forces on the blade and is observed when the load on the blade remains constant in time, for example, in hovering flight. The velocity field induced by these vortices in this case rotates together with the blade.

Something similar happens in the case of oblique flow past the rotor in forward flight. Here, we can distinguish a certain component of the velocity field which, rotating together with the blade, does not excite variable aerodynamic loads on it. To calculate these loads, it is necessary to define the mode of variation of the induced velocities at a point rotating together with the /224 blade rather than at a fixed point of the rotor disk area.

With this approach, the main generator of variable aerodynamic forces on the blade is the nonuniformity of the extrinsic induced velocity field caused by vortices remote from the blade. Therefore, in the first approximation we can neglect the velocity field caused by vortices directly adjacent to the blade and investigate only the field of extrinsic induced velocities.

14. Characteristics of the Extrinsic Induced Velocity Field

An investigation of the extrinsic induced velocity field caused only by vortices remote from the blade permits the statement that their variable portion, at a point in space fixed with respect to the helicopter, will be smaller the greater the density of these vortices.

An increase in vortex density takes place, in particular, on any reduction in forward flying speed of the helicopter. The density also increases with an increase in rotor angle of attack, when the mean velocity of flow through the rotor decreases and the vortex sheet is not carried away rapidly enough from the plane swept by the blades. Such a situation specifically occurs in braking regimes of the helicopter before passing to the hovering state. As an example, Fig.2.131 gives a plan view of the vortex system shed only from the blade tips in a flying regime with $\mu = 0.05$. The pattern shown is incomplete, since only the three spiral vortices shed from the blade tips are given while the vortices shed from all other blade radii are omitted. The radial vortices are also left

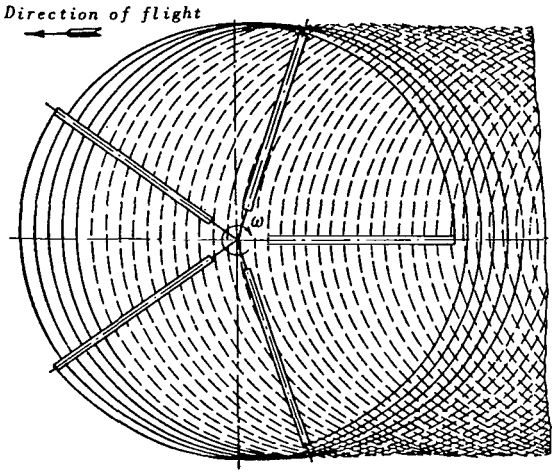

Fig.2.131 View of a Vortex System Shed by the Blade Tip in the μ = = 0.05 Regime.

out. However, even this pattern gives an idea of the extremely close spacing of vortices in low-speed regimes.

The variable portion of the extrinsic induced velocities decreases also with an increase in the number of rotor blades. At the limit for a rotor with an infinite number of blades, the variable components of the induced velocity become equal to zero.

To calculate the extrinsic induced velocity field, it is possible to use a scheme of a rotor with an infinite number of infinitely narrow blades. This scheme yields more accurate results, /225 the greater the density of the free vortex system of the rotor in the flight regime in question.

Upon changing from a given rotor to a design with an infinite number of blades, the local effect due to vortices immediately adjacent to the blade is reduced so greatly that, in first approximation, it can be assumed that this scheme does not allow for the effect of adjacent vortices, so that the field determined from this scheme will be closer to the extrinsic induced velocity field, the greater the density of the free vortices. Thus, a direct application of this scheme to the determination of variable aerodynamic loads on a given blade is equivalent to the use of the "steady-flow hypothesis".

The scheme with an infinite number of blades can also be used whenever it suffices to determine only the time-average part of the induced velocity. Use of this scheme leads to substantial simplifications of the problem and eliminates many difficulties arising with the scheme of a finite number of blades. Specifically, one of the advantages of this scheme is the fact that the induced velocities nowhere vanish.

In determining the downwash at the wing and stabilizer of a helicopter, when we are usually interested only in the constant portion of the loads, the scheme with an infinite number of blades can be used in all flying regimes and yields completely satisfactory results. The same probably holds for determination of the mutual interference of rotors, if the designer is interested only in their integral characteristics.

15. Vortex Theory of a Rotor with an Infinite Number of Blades

The vortex theory of a rotor with an infinite number of blades has been quite thoroughly developed. The solution of this problem was discussed specifically in the works of G.I.Maykopar, A.I.Slutskiy, L.S.Vil'dgrube, A.N.Proskuryakov, V.E.Baskin, Wang Shi-Tsun, and other authors. Each of them brought this

theory to ever greater perfection.

While working out the vortex theory of a rotor with an infinite number of blades, many methods were suggested which employed certain additional assumptions:

1. The vortex sheet trailing from a rotor is plane. This assumption formed the basis of the works by L.S.Vil'dgrube and L.O.Mel'ts, and substantially simplifies the calculations. Therefore, such an approach, which L.S.Vil'dgrube brought to a form convenient for practical use, became widespread.

2. It was proposed in a number of papers that the induced velocities can be determined rather accurately, with consideration of only the constant portion of the circulation of bound vortices or with the addition of one or two first harmonics of this circulation.

Recently, V.E.Baskin (Ref.16) and Wang Shi-Tsun (Ref.22) published papers in which they discarded these additional assumptions and brought the method of such calculation to a state completely convenient for practical use. Therefore, an account of only these two methods will be given below.

Vortex Theory of Wang Shi-Tsun

The vortex theory of a rotor proposed by Wang Shi-Tsun has been rather thoroughly presented in the author's work (Ref.22). Therefore, only the basic results will be repeated here.

16. Rotor Scheme

In all vortex theories examining a rotor with an infinite number of blades, it is proposed that the surface swept by the rotor is covered by continuously /226
distributed radial bound vortices with circulation variable over its radius and azimuth. The surface swept by the rotor is considered to be plane. The coning angle of the blades is disregarded.

Circulation of the bound vortices located along the radius in the rotor sector with an angle $\Delta\vartheta$ is taken as equal to

$$\Delta\Gamma_{bo} = \frac{z_b\Gamma}{2\pi}\Delta\vartheta,$$

where

Γ = circulation in the blade section at the examined radius and azimuth of the rotor;

z_b = number of blades in the rotor.

It is further assumed that there exists a spiral (longitudinal) free vortex with a circulation of

$$d(\Delta\Gamma_{sp}) = \frac{z_b}{2\pi}\frac{\partial\Gamma}{\partial\varrho}d\varrho\Delta\vartheta \qquad (5.33)$$

due to the rotor element under study.

As a consequence of the circulation of the bound vortex, varying with any change in the azimuth position of the blade, radial (transverse) vortices with a circulation of

$$d(\Delta\Gamma_{rad}) = -\frac{z_b}{2\pi}\cdot\frac{\partial\Gamma}{\partial\vartheta}\,d\vartheta\Delta\vartheta, \tag{5.34}$$

are also shed by the element in question.

The form of the surface over which the free vortices are arranged is represented as a downwash spiral surface, just as in the vortex theory of a rotor with a finite number of blades. However, now the vortex cylinder is filled with continuous free vortices rather than with discrete layers of widely spaced vortices, as had been the case in the theory with a finite number of blades.

17. Determination of Induced Velocities

To find the induced velocities due to trailing and bound vortices we used the Biot-Savart formula [eq.(5.6)]. As noted above, to determine the total induced velocities, it is necessary to sum all elementary induced velocities obtained from individual elements of all vortices comprising the vortex system. For this, integration in the form of eq.(5.7) must be carried out. Wang Shi-Tsun demonstrated that there is no need here to integrate along the downwash spiral lines along which lie the trailing vortices shed by the blade. It is simpler to integrate along the straight lines parallel to the axis of the inclined vortex cylinder (AB in Fig.2.129), since the vortices have identical strength along these straight lines. Such a method was used earlier by I.O. Mel'ts for the case of a plane vortex system.

Thus, in calculating induced velocities for the scheme of a rotor with an infinite number of blades, it is possible to carry out integration along straight lines parallel to the axis of the vortex cylinder rather than summation of individual discrete quantities, as is the case in the scheme with a finite number of blades (see Subsect.10).

Using this fact, Wang Shi-Tsun was able to calculate the above integrals and to obtain sufficiently simple formulas for determining all induced velocity components.

18. Calculation Formulas for Induced Velocity Determination

The induced velocities (Ref.22) are represented as the sum of three types:

$$\bar{v} = \bar{v}_{bo} + \bar{v}_{sp} + \bar{v}_{rad}, \tag{5.35}$$

where /227

$\bar{v}$ = total induced velocity;

$\bar{v}_{bo}$ = induced velocity due to bound vortices;

$\bar{v}_{sp}$ = induced velocity due to spiral (longitudinal) free vortices;
$\bar{v}_{rad}$ = induced velocity due to radial (transverse) free vortices.

All induced velocity components, entering eq.(5.35), pertain to the peripheral speed of the blade tip ωR.

Of greatest interest for practical application are the axial components (parallel to the rotor axis) of the induced velocity. In setting up the problem of calculating the rotor blade loads, axial induced velocity components need be determined only in its plane.

We will give the calculation formulas for determining the axial components in the rotor plane only. The formulas for other components, determinable outside this plane, can be found elsewhere (Ref.22).

The axial induced velocity components due to bound vortices are determined by the formula

$$\bar{v}_{bo} = -\frac{z_b}{8\pi^2}\int_0^1\int_0^{2\pi}\bar{\Gamma}\,\frac{\bar{r}\sin(\vartheta-\psi)}{\bar{l}^3}\,d\vartheta\,d\bar{\varrho}, \tag{5.36}$$

where $\bar{\Gamma}$ is the circulation in the blade section referred to ωR^2:

$$\bar{\Gamma}=\frac{\Gamma}{\omega R^2}. \tag{5.37}$$

The axial induced velocity components due to spiral and radial vortices are determined by the formulas

$$\left.\begin{aligned}
\bar{v}_{sp} &= \frac{z_b}{8\pi^2}\frac{1}{\sqrt{\mu^2+\lambda_{0av}^2}}\times\\
&\times\int_0^1\int_0^{2\pi}\frac{\partial\bar{\Gamma}}{\partial\bar{\varrho}}\left[\left(\mu+\bar{\varrho}\sin\vartheta\right)I_1-\bar{\varrho}\cos\vartheta I_2\right]d\vartheta\,d\bar{\varrho},\\
\bar{v}_{rad} &= \frac{z_b}{8\pi^2}\frac{1}{\sqrt{\mu^2+\lambda_{0av}^2}}\times\\
&\times\int_0^1\int_0^{2\pi}\frac{\partial\bar{\Gamma}}{\partial\vartheta}\left[\cos\vartheta I_1+\sin\vartheta I_2\right]d\vartheta\,d\bar{\varrho}.
\end{aligned}\right\} \tag{5.38}$$

Here,

$$\left.\begin{aligned}
I_1 &= \frac{(\bar{\varrho}\sin\vartheta-\bar{r}\sin\psi)\sqrt{\mu^2+\lambda_{0av}^2}}{\bar{l}^2\sqrt{\mu^2+\lambda_{0av}^2}+\mu\bar{l}\,(\bar{\varrho}\cos\vartheta-\bar{r}\cos\psi)},\\
I_2 &= \frac{(-\bar{\varrho}\cos\vartheta+\bar{r}\cos\psi)\sqrt{\mu^2+\lambda_{0av}^2}-\bar{l}\mu}{\bar{l}^2\sqrt{\mu^2+\lambda_{0av}^2}+\mu\bar{l}\left(\bar{\varrho}\cos\vartheta-\bar{r}\cos\psi\right)},
\end{aligned}\right\} \tag{5.39}$$

where

$$\bar{l}=\sqrt{\bar{\varrho}^2+\bar{r}^2-2\bar{\varrho}\bar{r}\cos(\vartheta-\psi)}. \tag{5.40}$$

For the variables entering eqs.(5.36) and (5.38) we will use the following notations:

$\bar{\rho}$ = relative radius of the blade section shedding the vortex;
$\bar{r}$ = relative radius of the rotor at which the induced velocity is determined; /228
ϑ = azimuth of the rotor shedding the vortex;
ψ = azimuth at which the induced velocity is determined.

Equations (5.35), (5.36), (5.38), and (5.39) permit determining the induced velocities if the circulation $\Gamma(\vartheta, \rho)$ is known at all azimuths ϑ and radii of the blade.

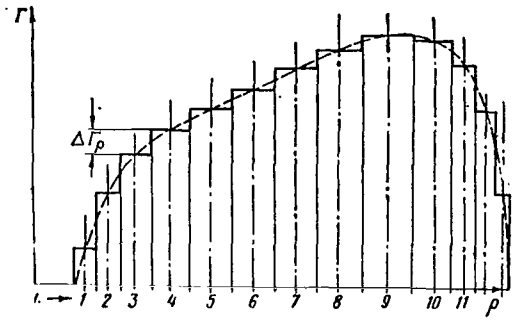

Fig.2.132 Distribution of Circulation over Blade Length, Used in the Calculation.

It should be noted that, in the vortex theory of a rotor with an infinite number of blades, one usually determines the total induced velocities, including the components due to bound vortices participating in the production of blade lift.

19. Application and Evaluation of the Possibilities of the Wang Shi-Tsun Vortex Theory

In the practical application of the Wang Shi-Tsun vortex theory, just as in a number of other schemes, the distribution of circulation Γ over the blade length is usually represented as a stepped line, as shown in Fig.2.132. The quantity $\frac{\partial \Gamma}{\partial \rho} d\rho$ is taken as approximately equal to

$$\frac{\partial \Gamma}{\partial \rho} d\rho = \Gamma_l - \Gamma_{l-1} = \Delta \Gamma_\rho, \tag{5.41}$$

where $\Delta\Gamma_\rho$ is the difference of circulation at two adjacent portions of the blade.

Such an approach is equivalent to replacing the vortex sheet by a number of discrete vortices. As a consequence, the induced velocity approaches infinity at points where these discrete vortices are shed by the blade. To avoid this, the induced velocities should be calculated with respect to the midsection at constant circulation.

In determining the circulation derivative with respect to blade azimuth, the circumference of the rotor is also divided into a finite number of sections and the derivative $\frac{\partial \Gamma}{\partial \vartheta} d\vartheta$ is taken as approximately equal to

$$\frac{\partial \Gamma}{\partial \vartheta} d\vartheta = \Gamma_l - \Gamma_{l-1} = \Delta \Gamma_l. \tag{5.42}$$

Thus, for a numerical determination of the integrals entering eqs.(5.36) and (5.38), we should first determine the values of Γ_ρ, $\Delta\Gamma_\rho$, and $\Delta\Gamma_t$, whose number N will be equal to

$$N = \frac{2\pi}{\Delta\psi} \cdot z_r, \tag{5.43}$$

where

z_r = number of sections over the radius into which the blade is divided;
$\Delta\psi$ = pitch with respect to blade azimuth over whose length the circulation is considered constant.

If we take $z = 30$ and $\Delta\psi = 5^\circ$, a determination of the induced velocities will require 2160 values of Γ_ρ, $\Delta\Gamma_\rho$, $\Delta\Gamma_t$ (a total of 6480 values). To determine the induced velocities at all 2160 points of the rotor, the operations needed /229 for determining the integrands in eqs.(5.36), and (5.38) would have to be repeated $(2160)^2$ times. It is obvious that the time required for this would handicap the practical applicability of this method, even when using high-speed computers. Therefore, the practical application of the Wang Shi-Tsun theory in such a form is possible only for a rather limited number of sections, taken over the radius and azimuth of the blade. On high-speed computers with a rate of 20,000 operations per second, the calculation can be performed under approximately the following conditions: $z_r = 10 - 12$; $\Delta\psi = 10 - 12^\circ$.

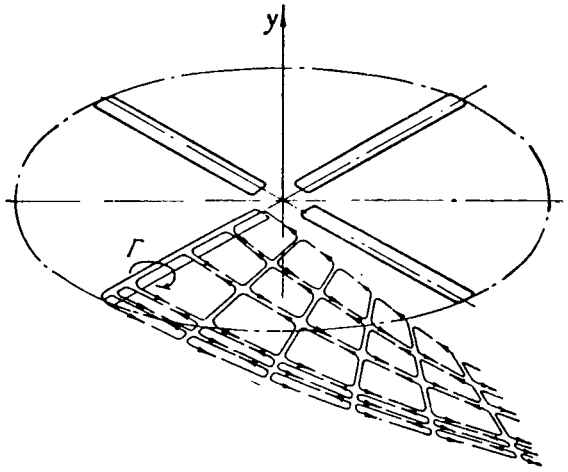

Fig.2.133 Diagram of Formation of Vortex Rings.

This shortcoming is eliminated if the circulation Γ and induced velocities are expanded in Fourier series in harmonics and if the process is limited to considering only a certain number of lower harmonics necessary for performing the calculation with satisfactory accuracy. For practical purposes, it usually suffices to restrict the process to the first 6 - 8 harmonics. This method was used in the theory of V.E.Baskin (Ref.16).

Vortex Theory of V.E.Baskin

The theory of V.E.Baskin was circulated in a limited edition in 1955 and later presented by the author in an unpublished report (Ref.16); as a consequence, the theory of V.E.Baskin is not very familiar to specialists interested in this problem. For this reason, the theory will be presented here in considerable detail but with certain simplifications which the author did not make.

20. Scheme of Rotor Flow

The vortex system, shown in Fig.2.128 and consisting of bound and free spiral and radial vortices, can be represented in a somewhat different form. We can consider that, during operation of the rotor, the blade continuously sheds infinitely small closed elementary vortex rings, with a circulation constant over the contour of the ring equal to the circulation of the bound vortex Γ in the blade section at the instant at which the vortex ring separates from it (Fig.2.133).

Since the circulation of the bound vortex varies over the radius and azimuth of the blade, the vortex rings trailing from it will have a different circulation at different points of the vortex sheet. Consequently, the free vortex sheet can be considered as consisting of continuously distributed, infinitely small vortex rings with different circulation Γ. /230

It is known from hydrodynamics [see (Ref.31, p.266)] that the induced velocities due to the vortex ring contour with a circulation Γ will be the same as those due to the layer of dipoles covering the surface stretched over this contour, with an intensity per unit area of

$$D=-\Gamma \tag{5.44}$$

and oriented along a normal to this surface. Here, the signs are selected on the basis that the circulation flow producing blade lift and the dipoles whose vector gives a positive projection onto the y-axis, are considered positive (Fig.2.134).

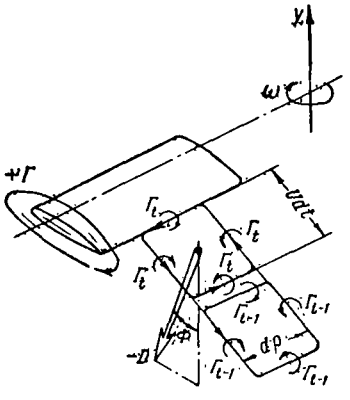

Fig.2.134 For Determining Induced Velocities from a Dipole Column.

Consequently, the free vortex sheet trailing from the blades can be replaced by a surface covered by a dipole layer.

On changing to a rotor with an infinite number of blades, this equality is somewhat modified. Aft of a rotor with an infinite number of blades, the vortex sheet fills the entire volume bounded by the downwash cylindrical surface tangent to the rotor circumference. This vortex system, as already mentioned, is called a vortex column. This column can be represented as filled with dipoles rather than with vortices. To determine the intensity of dipole distribution in the column, a layer of height dH, filled with vortices during the time dt, is cut from the column. During this time, vortex rings with a contour bounding the area

$$dF=Udtd\varrho \tag{5.45}$$

trail from all radii.

This contour can be replaced by dipoles with an intensity $D = -\Gamma$. On changing to an infinite number of blades, these dipoles are distributed over the

entire rotor circumference of radius r with an intensity of

$$D = -\frac{z_b \Gamma}{2\pi r} U dt. \tag{5.46}$$

If the circulation Γ is expressed in terms of the aerodynamic load per unit length from eq.(5.24), then

$$D = -\frac{z_b T\, dt}{2\pi \varrho r}. \tag{5.47}$$

We can determine the quantity dt entering this expression as

$$dt = \frac{dH}{V_y}, \tag{5.48}$$

where V_y is the average velocity of flow through the rotor:

$$V_y = \omega R \lambda_{0av}.$$

Let us then introduce the concept of relative aerodynamic load, so that /231

$$T = \frac{1}{2} c_y^{\alpha} \varrho b_{0,7} \omega^2 R^2 P. \tag{5.49}$$

Then,

$$D = -\frac{1}{4} \sigma c_y^{\alpha} \omega^2 R^2 \frac{P}{r} \frac{dH}{V_y}. \tag{5.50}$$

Thus, the problem reduces to determining the induced velocity field caused by the downwash column of dipoles whose intensity in a layer of thickness dH is determined by eq.(5.50).

21. Determination of Induced Velocities from the Dipole Column

Figure 2.134 shows that the plane of each of the elementary vortex rings trailing from the blade is inclined at some angle Φ to the plane of rotation of the rotor:

$$\Phi \approx \frac{U_y}{U_x}. \tag{5.51}$$

Correspondingly, at this same angle to the plane of rotation are inclined also the axes of the dipoles which, in V.E.Baskin's scheme, replace the elementary vortex rings.

Henceforth we will disregard this angle and will assume that the axes of all dipoles are directed perpendicular to the rotor plane. Baskin (Ref.16) did not use this simplification in deriving the basic relationships, but it is shown that - in calculating the axial induced velocity component - this is permissible.

To determine the induced velocities, let us examine a flow caused by dipoles filling an element of the vortex cylinder of a height equal to dH (see Fig.2.136).

Summing the induced velocities caused by all elements of the vortex column, we can obtain the total induced velocity.

22. Fluid Flow Induced by a Disk Covered with Dipoles

Fluid flow induced by a disk covered with dipoles can be determined as the solution of the Laplace equation with certain boundary conditions, which will be discussed below.

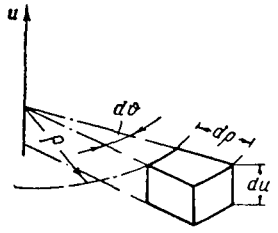

Fig.2.135 For Determining the Velocity Potential by the Laplace Equation.

The Laplace equation in cylindrical coordinates (Fig.2.135) can be written in the form

$$\frac{\partial^2\varphi}{\partial u^2}+\frac{\partial^2\varphi}{\partial\varrho^2}+\frac{1}{\varrho}\frac{\partial\varphi}{\partial\varrho}+\frac{1}{\varrho^2}\frac{\partial^2\varphi}{\partial\vartheta^2}=0, \qquad (5.52)$$

where φ is the velocity potential.

The velocity potential can be expanded in a Fourier series. Then,

$$\varphi=\sum_{m=0}^{\infty}(\bar{\varphi}_m\cos m\vartheta+\bar{\bar{\varphi}}_m\sin m\vartheta). \qquad (5.53)$$

Substituting eq.(5.53) into eq.(5.52), we obtain the equation for determining the coefficients of the sines and cosines entering eq.(5.53):

$$\frac{\partial^2\varphi_m}{\partial u^2}+\frac{\partial^2\varphi_m}{\partial\varrho^2}+\frac{1}{\varrho}\frac{\partial\varphi_m}{\partial\varrho}-\frac{m^2}{\varrho^2}\varphi_m=0. \qquad (5.54)$$

Solution of eq.(5.54) will be sought in the form /232

$$\varphi_m=e^{\mp ku}\chi(\varrho). \qquad (5.55)$$

Substituting eq.(5.55) into eq.(5.54), we obtain

$$\chi''(\varrho)+\frac{1}{\varrho}\chi'(\varrho)+\left(k^2-\frac{m^2}{\varrho^2}\right)\chi(\varrho)=0. \qquad (5.56)$$

This equation can be reduced to a canonical form, if we set

$$k\varrho=\bar{\varrho}.$$

Then,

$$\frac{\partial^2\chi}{\partial\bar{\varrho}^2}+\frac{1}{\bar{\varrho}}\frac{\partial\chi}{\partial\bar{\varrho}}+\left(1-\frac{m^2}{\bar{\varrho}^2}\right)\chi(\bar{\varrho})=0. \tag{5.57}$$

The general solution of this equation can be written in the form

$$\chi(\bar{\varrho})=AJ_m(\bar{\varrho})+BI_m(\bar{\varrho}). \tag{5.58}$$

The function $I_m(\bar{\rho})$ tends to infinity as $\bar{\rho}\to 0$. Therefore, if we restrict ourselves to a finite value of the potential, then

$$\varphi_m=Ae^{\pm ku}\cdot J_m(k\varrho). \tag{5.59}$$

If we use the condition that, as $u\to\infty$ also $\varphi_m\to 0$, then the solution of eq.(5.54) can be written as

$$\varphi_m=Ae^{-ku}J_m(k\varrho), \tag{5.60}$$

where $k\geq 0$.

The function φ_m will be the solution to eq.(5.54) at any value of $k=k_i$. Consequently, the solution of eq.(5.54) will also be the sum

$$\varphi_m=\sum_i A_i e^{-k_i u}J_m(k_i\varrho) \tag{5.61}$$

and the integral

$$\varphi_m=\int_0^\infty A(k)\,e^{-ku}J_m(k\varrho)\,dk, \tag{5.62}$$

where A(k) is an arbitrary function determined from the boundary conditions.

23. Boundary Conditions

It is known from hydrodynamics [see (Ref.31, p.82)] that the velocity potential on both sides of a surface covered by dipoles is associated with the density of these dipoles by the relation

$$D=\varphi_2-\varphi_1, \tag{5.63}$$

where

D = density of dipoles per unit surface, with the positive direction of the dipole axis coinciding with the u-axis;

φ_1 and φ_2 = velocity potentials on both sides of a surface covered by dipoles (Fig.2.136).

The fluid flow on both sides of the disk covered by dipoles is subject to equal conditions. Therefore, we can set

$$\varphi_2=-\varphi_1=\varphi. \tag{5.64}$$

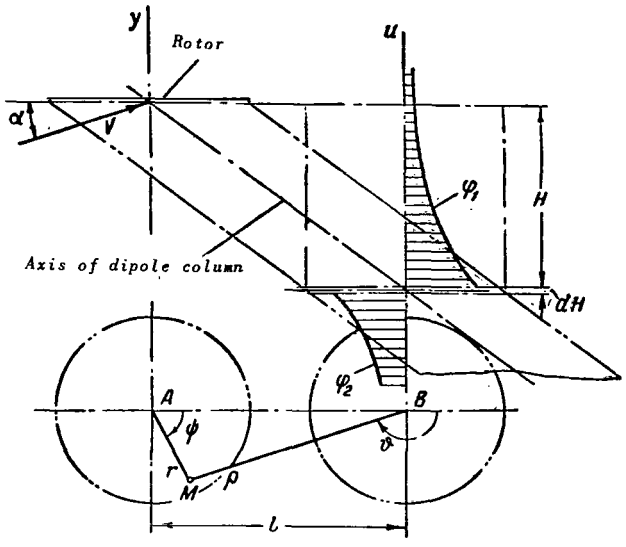

Fig.2.136 Diagram of Rotor Flow Used in the Calculation for Determination of Induced Velocities.

Then the value of the potential at the boundary of the disk on the side where $u > 0$, can be defined as

$$\varphi = -\frac{1}{2} D. \tag{5.65}$$

The boundary conditions for /233 flow induced by a disk covered by dipoles of a density D are determined from eq.(5.65) if $\rho \leq R$. If $\rho > R$, the potential in the disk plane is everywhere equal to zero ($\varphi = 0$).

The intensity of the dipoles covering the disk can be represented in form of a series:

$$D(\varrho, \vartheta) = \sum_{m=0}^{\infty} [\bar{D}_m(\varrho) \cos m\vartheta + \bar{\bar{D}}_m(\varrho) \sin m\vartheta]. \tag{5.66}$$

Then, using the boundary condition (5.65) for determining the arbitrary function A(k) in eq.(5.62), we can write the solution of the continuity equation (5.52) in the form

$$\varphi = -\frac{1}{2} \sum_{m=0}^{\infty} \int_0^{\infty} e^{-ku} J_m(k\varrho) k \times \times \left\{ \int_0^R [\bar{D}_m(\varrho) \cos m\vartheta + \bar{\bar{D}}_m(\varrho) \sin m\vartheta] J_m(k\varrho) \varrho \, d\varrho \right\} dk. \tag{5.67}$$

The derivation of this expression is given elsewhere (Ref.31).

24. Transformation of Eq.(5.67) to the Rotor Axes; Use of the Theorem of Addition of Cylindrical Functions

Equation (5.67) is written in cylindrical coordinates with the u-axis going through the center of the disk of thickness dH, cut out from the dipole column (see Fig.2.136). To transform this expression into coordinates related with the rotor, we can use the theorem of addition of cylindrical functions (Ref.34). /234 It follows from this theorem that

$$\cos m\vartheta J_m(k\varrho) = (-1)^m \sum_{n=-\infty}^{\infty} J_n(kr) J_{n+m}(kl) \cos n\psi, \tag{5.68}$$

$$\sin m\vartheta J_m(k\varrho) = -(-1)^m \sum_{n=-\infty}^{\infty} J_n(kr) J_{n+m}(kl) \sin n\psi. \Bigg\}$$

The velocity potential from the dipole layer is expanded in a Fourier series:

$$\varphi = \sum_{n=-\infty}^{\infty} (\bar{\varphi}_n \cos n\psi + \bar{\bar{\varphi}}_n \sin n\psi). \tag{5.69}$$

Then, using eqs.(5.68) and (5.69) and equating the coefficients of cos nψ and sin nψ with identical n in eq.(5.67), we obtain

$$\left.\begin{aligned} \bar{\varphi}_n &= -\frac{1}{2} \sum_{m=0}^{\infty} (-1)^m \int_0^{\infty} e^{-ku} J_n(kr) J_{n+m}(kl)\, k\, dk \times \\ &\quad \times \int_0^R \bar{D}_m(\varrho) J_m(k\varrho) \varrho\, d\varrho, \\ \bar{\bar{\varphi}}_n &= \frac{1}{2} \sum_{m=0}^{\infty} (-1)^m \int_0^{\infty} e^{-ku} J_n(kr) J_{n+m}(kl)\, k\, dk \times \\ &\quad \times \int_0^R \bar{\bar{D}}_m(\varrho) J_m(k\varrho) \varrho\, d\varrho. \end{aligned}\right\} \tag{5.70}$$

25. Determination of the Total Velocity Potential from the Entire Dipole Column

To determine the components of the total velocity potential represented as

$$\Phi = \sum_{n=-\infty}^{\infty} (\bar{\Phi}_n \cos n\psi + \bar{\bar{\Phi}}_n \sin n\psi), \tag{5.71}$$

eqs.(5.70) must be integrated over the entire dipole column (see Fig.2.136).

For this, we must first write out the values of $\bar{D}_m(\rho)$ and $\bar{\bar{D}}_m(\rho)$.

We note that within the vortex column the intensity of the dipoles, just as the strength of the vortices, is constant along straight lines parallel to the column axis. Therefore, the dipole intensity $D(\rho, \vartheta)$ in any layer cut out from the vortex column will be equal to the intensity of the dipoles trailing from the rotor at a point where $r = \rho$ and $\psi = \vartheta$.

If the relative aerodynamic load P [see eq.(5.50)] is represented in the /235 form

$$P = \sum_{m=0}^{\infty} (\bar{P}_m \cos m\psi + \bar{\bar{P}}_m \sin m\psi), \tag{5.72}$$

then we can write

$$\left.\begin{aligned}\bar{D}_m(\bar{\varrho}) &= -\frac{1}{4} c_y^{\alpha} \sigma \omega^2 R^2 \frac{1}{V_y} \frac{\bar{P}_m}{\bar{\varrho}} dH,\\ \bar{\bar{D}}_m(\bar{\varrho}) &= -\frac{1}{4} c_y^{\alpha} \sigma \omega^2 R^2 \frac{1}{V_y} \frac{\bar{\bar{P}}_m}{\bar{\varrho}} dH.\end{aligned}\right\} \tag{5.73}$$

Setting

$$\left.\begin{aligned}u &= H + y,\\ l &= \frac{V_x}{V_y} H\end{aligned}\right\} \tag{5.74}$$

and substituting eqs.(5.73) into (5.70), we can integrate the obtained expressions with respect to H. It is easy to demonstrate that, for performing this operation, we must determine the value of the integral

$$J(H) = \int_0^{\infty} e^{-kH} J_{n+m}\left(k \frac{V_x}{V_y} H\right) dH. \tag{5.75}$$

Referring to the handbook by Ruzhik [Ref.34, p.721, eq.(6.611.1)], we obtain

$$J(H) = \frac{1}{k} \frac{V_y}{\omega R} A_0 \tau^p, \tag{5.76}$$

where

$$A_0 = \frac{1}{\sqrt{\mu^2 + \lambda_{0av}^2}}, \tag{5.77}$$

$$\tau = \frac{\sqrt{\mu^2 + \lambda_{0av}^2} - |\lambda_{0av}|}{\mu}. \tag{5.78}$$

Here p = m + n, and eq.(5.76) is valid only if p > 0. Therefore, at m + + n < 0, eq.(5.76) takes the form

$$J(H) = \frac{1}{k} \frac{V_y}{\omega R} A_0 (-1)^p \tau^p, \tag{5.79}$$

where p = -(m + n).

Let us introduce the new variable

$$z = kR. \tag{5.80}$$

Then, using eqs.(5.76) and (5.80), we can write out the expressions for /236 the components of the velocity potential from the entire dipole column:

$$\left.\begin{aligned}
\overline{\Phi}_n &= \frac{1}{8} c_y^{\alpha} \sigma \omega R^2 \sum_{m=0}^{\infty} (-1)^m A_0 \tau^{n+m} \times \\
&\times \int_0^{\infty} e^{-z\bar{y}} J_n(z\bar{r})\, dz \int_0^1 \overline{P}_m(\bar{\varrho}) J_m(z\bar{\varrho})\, d\bar{\varrho}, \\
\overline{\overline{\Phi}}_n &= -\frac{1}{8} c_y^{\alpha} \sigma \omega R^2 \sum_{m=0}^{\infty} (-1)^m A_0 \tau^{n+m} \times \\
&\times \int_0^{\infty} e^{-z\bar{y}} J_n(z\bar{r})\, dz \int_0^1 \overline{\overline{P}}_m(\bar{\varrho}) J_m(z\bar{\varrho})\, d\bar{\varrho}.
\end{aligned}\right\} \qquad (5.81)$$

Here, all linear dimensions pertain to the radius of the rotor R, including $y\left(\bar{y} = \frac{y}{R}\right)$.

26. Determination of Induced Velocities

As already mentioned, we will determine only the axial induced velocity components. For this, we must take the derivative of the velocity potential with respect to y. We see from eq.(5.81) that only the term $e^{-z\bar{y}}$ depends on y. Therefore, the operation of differentiation leads to expressions differing from eq.(5.81) only in sign and in component z.

Before writing out the final formulas for determining the induced velocities, we will present them as a Fourier series:

$$\lambda = \sum_{n=0}^{\infty} (\bar{\lambda}_n \cos n\psi + \overline{\bar{\lambda}}_n \sin n\psi). \qquad (5.82)$$

Here, all induced velocity components are referred to the tip speed of the blade ωR. In determining the induced velocity components written in form of eq.(5.82), the following operations must be performed:

$$\left.\begin{aligned}
\bar{\lambda}_n &= \frac{1}{\omega R}\left(\frac{\partial \bar{\Phi}_n}{\partial y} - \frac{\partial \bar{\Phi}_{-n}}{\partial y}\right), \\
\overline{\bar{\lambda}}_n &= \frac{1}{\omega R}\left(\frac{\partial \overline{\bar{\Phi}}_n}{\partial y} - \frac{\partial \overline{\bar{\Phi}}_{-n}}{\partial y}\right).
\end{aligned}\right\} \qquad (5.83)$$

An exception is the determination of $\bar{\lambda}_0$, which is calculated as

$$\bar{\lambda}_0 = \frac{1}{\omega R} \frac{\partial \bar{\Phi}_0}{\partial y}. \qquad (5.84)$$

As a result of the actions provided for in eqs.(5.83) and (5.84), we obtain

$$\bar{\lambda}_0 = -\frac{1}{8} c_y^a \sigma A_0 \sum_{m=0}^{\infty} (-1)^m \tau^m \times$$

$$\times \int_0^{\infty} e^{-z\bar{y}} J_n(z\bar{r})\, z\, dz \int_0^1 \bar{P}_m(\bar{\varrho})\, J_m(z\bar{\varrho})\, d\bar{\varrho}; \tag{5.85}$$

$$\left.\begin{aligned} \bar{\lambda}_n &= -\frac{1}{8} c_y^a \sigma A_0 \sum_{m=0}^{\infty} [\tau^{n-m} + (-1)^m \tau^{n+m}] \times \\ &\times \int_0^{\infty} e^{-z\bar{y}} J_n(z\bar{r})\, z\, dz \int_0^1 \bar{P}_m(\bar{\varrho})\, J_m(z\bar{\varrho})\, d\bar{\varrho}; \\ \bar{\bar{\lambda}}_n &= -\frac{1}{8} c_y^a \sigma A_0 \sum_{m=0}^{\infty} [\tau^{n-m} - (-1)^m \tau^{n+m}] \times \\ &\times \int_0^{\infty} e^{-z\bar{y}} J_n(z\bar{r})\, z\, dz \int_0^1 \bar{\bar{P}}_m(\bar{\varrho})\, J_m(z\bar{\varrho})\, d\bar{\varrho}. \end{aligned}\right\} \tag{5.86}$$

It is assumed in these expressions that $n > m$. Therefore, in conformity with eq.(5.79), when $n < m$, in place of τ^{n-m} we must calculate $(-1)^{m-n}\tau^{m-n}$.

When performing operations with eqs.(5.83) we must bear in mind that

$$J_{-n}(z\bar{r}) = (-1)^n J_n(z\bar{r}).$$

Different methods can be suggested for calculating the integrals entering eqs.(5.85) and (5.86). One such method will be given in Section 8 of Chapter I of Vol.II, where a method of calculating elastic vibrations of a blade with consideration of a variable induced velocity field will be discussed.

It should be pointed out that, in certain particular cases, the integrals entering eqs.(5.85) and (5.86) can be calculated analytically (see Sect.8.6 of Chapt.I in Vol.II).

The vortex theory of V.E.Baskin permits obtaining results rather rapidly, if the person doing the calculations has at his disposal a computer with a rate of at least 20,000 operations per second. At this rate, the calculation can be performed in about 20 min. Therefore, if the problem is to determine the mean induced velocities with an accuracy to high harmonics and if the assumption that the vortex sheet is plane cannot be used, the best method for a determination of induced velocities is the Baskin vortex theory.

Section 6. Experimental Determination of Aerodynamic Characteristics of a Rotor

The most reliable methods of determining the aerodynamic characteristics of a rotor are flight tests of the helicopter with the rotor under study or with another similar rotor which can be regarded as a model of the investigated rotor, as well as wind-tunnel tests on full-scale rotors or large-scale models.

In this Section, we will present certain results of flight tests and wind-tunnel tests and give a brief description of the testing procedure. The tests /238 were carried out at research institutes by M.K.Speranskiy, A.I.Akimov, and others.

1. Flight Tests for Determining the Aerodynamic Characteristics of a Helicopter

The aerodynamic characteristics of a helicopter in a system of wind axes (Figs.2.105 - 2.109), i.e., in the form in which they are used in aerodynamic design, can be obtained from flight tests.

Selecting the flying speed, rotor rpm, flying weight, and flight altitude, flight tests will furnish constant values of M_{fl}, M_0, and the thrust coefficient of the helicopter t_{y_h} (below, p and T denote the pressure and temperature of the air):

$$M_{fl} = \frac{V}{a} = \frac{V}{20.1\sqrt{T}} = \text{const}_1 \frac{V}{\sqrt{T}};$$

$$M_0 = \frac{\omega R}{a} = \text{const}_2 \frac{n}{\sqrt{T}};$$

$$t_{y_h} \approx \frac{G}{\frac{1}{2}\varrho(\omega R)^2 \sigma F} = \frac{G}{\frac{1}{2}\varrho a^2 M_0 \sigma F} = \text{const}_3 \frac{G}{M_0^2 p},$$

since $$\frac{1}{2}\varrho a^2 = \frac{1}{2}\left(0.379\frac{p}{T}\right)(20.1\sqrt{T})^2 = \text{const}_4 p.$$

Fulfilling, under these conditions, various flight regimes with different engine powers - gliding at a different rate of descent, forward flight, and climbing with a different rate of ascent, we can obtain a sufficient number of points of the aerodynamic characteristics of the helicopter in the form of the dependence $t_{x_h} = f(m_t)$ for constant values of $\bar{V}$, t_{y_h}, and M_0. In an autorotation regime of the rotor, we obtain a point with $m_t \approx 0$ (Fig.2.137). The point $t_{x_h} = 0$ corresponds to a forward flight regime since, at this point, the propulsive force of the rotor is balanced by the parasite drag of the helicopter. Gliding of the helicopter corresponds to intermediate regimes. The regimes $t_{x_h} < 0$, i.e., a gain in altitude at a point where the engine power is maximal ($m_t = m_{t_{dis}}$), are obtained from the regime of maximum rate of ascent for a given flying speed.

As a result of tests, we will determine the aerodynamic characteristics of a helicopter which differ from the rotor characteristics in that the aerodynamics of the no-lift-producing parts of the helicopter is taken into account.

Thus, flight tests for determining the aerodynamic characteristics of a helicopter involve "flying by the seat of the pants" in which gliding, gain in altitude, and forward flight are performed at constant values of $V/\sqrt{T}$, $n/\sqrt{T}$, $\frac{G}{p}$.

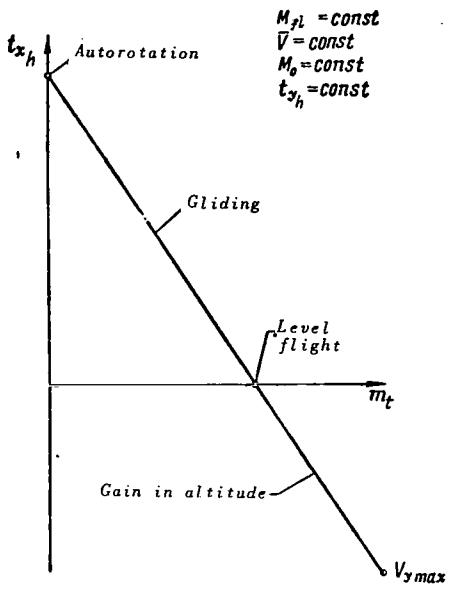

Fig.2.137 Coefficients of Forces and Torque of Rotor in Various Flight Regimes.

In addition to these quantities, the following are measured: vertical velocity V_y; inclination of the plane of rotation of the rotor to the horizon (pitch angle of the helicopter) ϑ; components of cyclic change of pitch $\bar{\varphi}_1$, $\bar{\bar{\varphi}}_1$ (or angles of deflection of the automatic pitch control $\varkappa$, η and the flapping coefficients); setting angle of the blade θ_0; and torque of the rotor M_t. The torque is measured by strain gages mounted to the rod of the reduction-gear frame.

The aerodynamic characteristics of a helicopter are determined from the expressions derived in Section 1 of Chapter III: /239

$$t_{y_h} = \frac{G\cos\theta_{fl.p}}{\frac{1}{2}\varrho(\omega R)^2\sigma F} \approx \frac{G}{\frac{1}{2}\varrho(\omega R)^2\sigma F}; \qquad (6.1)$$

$$t_{x_h} = -\frac{G\sin\theta_{fl.p}}{\frac{1}{2}\varrho(\omega R)^2\sigma F}; \qquad (6.2)$$

$$m_t = \frac{M_t}{\frac{1}{2}\varrho(\omega R)^2 R\sigma F}. \qquad (6.3)$$

The flight-path angle to the horizontal is

$$\theta_{fl.p} = \sin^{-1}\frac{V_y}{V}. \qquad (6.4)$$

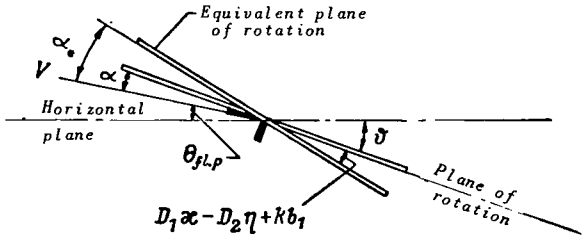

Fig.2.138 For Determining the Angle of Attack α and Equivalent Angle of Attack α_e in Flight.

The rotor angle of attack and the equivalent angle of attack are found from the following formulas (Fig.2.138):

$$\alpha = \vartheta - \theta_{fl.p}; \qquad (6.5)$$

$$\alpha_e = \alpha - \bar{\varphi}_1 = \alpha + D_1\varkappa - D_2\eta + k\bar{b}_1, \qquad (6.6)$$

where

$D_1\varkappa - D_2\eta$ = deflection of the equivalent plane of rotation of the rotor from the design plane of rotation at inclined automatic pitch control;

kb_1 = additional deflection of the equivalent plane of rotation of the rotor

in the presence of a flapping compensator.

At a methodologically correct conduction of tests, the root-mean-square error in determining t_{y_h} is 0.5% while, in determining m_t, it is 3.5%.

The results of flight tests with the helicopter Mi-1 are plotted in Fig.2.139. The helicopter had a three-blade rotor with trapezoidal twisted blades, D = 14.3 m, σ = 0.0504, blades with plywood planking except for the blade root ($\bar{r} < 0.59$) where the shank portion of the profile was covered with fabric. /240

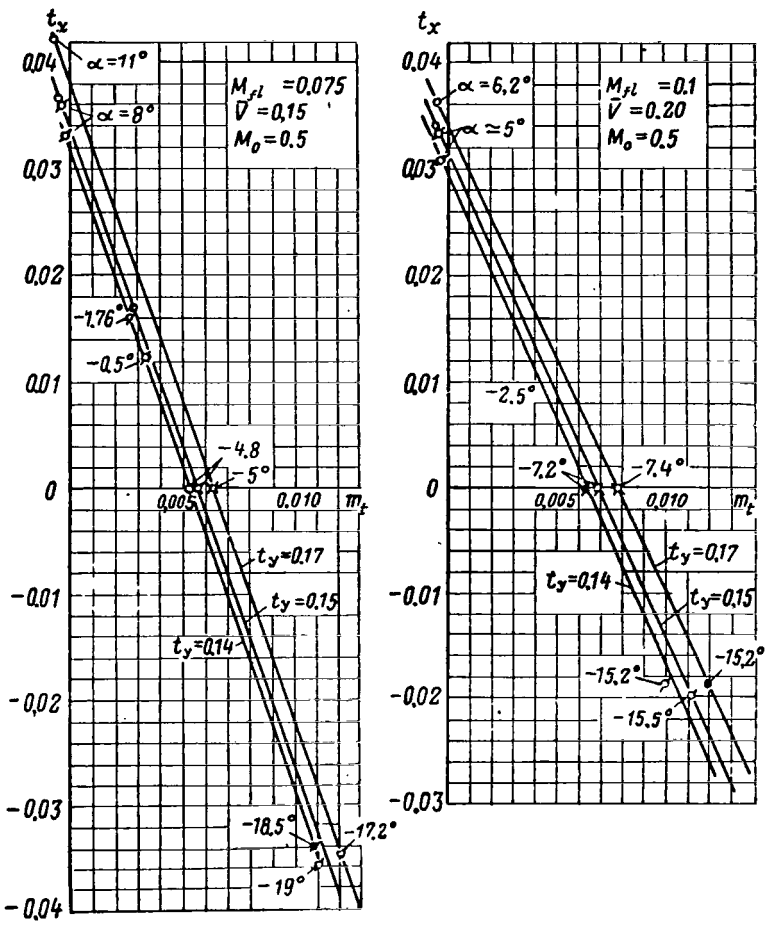

Fig.2.139 Coefficient of Propulsive Forces as a Function of Coefficient of Torque (Flight Tests of Mi-1 Helicopter).

The aerodynamic characteristics of the rotor are obtained by subtracting the coefficients of forces created by the nonlifting elements from the coefficients of forces of the helicopter. By analogy with eq.(1.3) from Chapter III, the coefficients of forces of the rotor are equal to

$$t_y = t_{y_h} - t_{y_f} = t_{y_h} - \bar{c}_{y_f}\frac{\bar{V}^2}{a}; \tag{6.7}$$

$$t_x = t_{x_h} - t_{x_{fus}} = t_{x_h} - \bar{c}_x\frac{\bar{V}^2}{a}, \tag{6.8}$$

where $\bar{c}_{y_f} = \frac{c_{y_f} S_f}{F}$ and $\bar{c}_x = \frac{\Sigma c_x S}{F}$.

The coefficients $\bar{c}_{y_f}$ and $\bar{c}_x$ of the Mi-1 helicopter were determined by testing a full-scale fuselage in a wind tunnel. The lift coefficient of the fuselage $\bar{c}_{y_f}$ is very small and we can disregard it in eq.(6.7).

It is necessary to bear in mind that the aerodynamic characteristics of /241
a rotor obtained from flight tests take into account the mutual interference of the lifting and nonlifting elements of the helicopter, a fact that increases the value of these data.

2. Wind-Tunnel Tests for Determining the Aerodynamic Characteristics of a Rotor

To determine the aerodynamic characteristics of full-scale helicopter rotors in a wind tunnel, the TsAGI has special facilities for testing two-, three-, and four-blade rotors with a diameter up to 15.5 m.

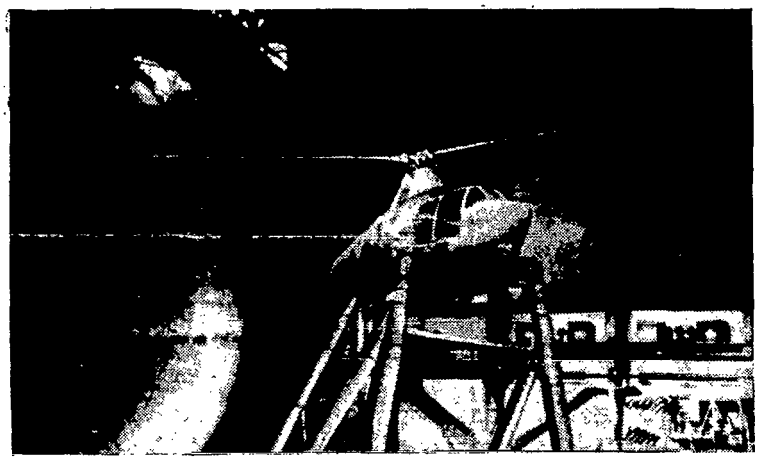

Fig.2.140 Facility for Testing Full-Scale Rotors in a Wind Tunnel.

The first facility for testing full-scale rotors with an engine power of 575 hp was created under the supervision of M.L.Mil' on the basis of the Mi-1 helicopter. Figure 2.140 gives a view of the unit mounted to the upper structure of the tunnel balance. The unit has a special damping suspension support, maintaining the permissible level of vibrations set up on the balance during start-

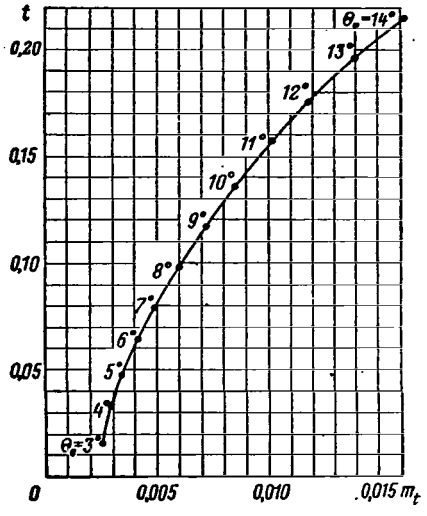

Fig.2.141 Aerodynamic Characteristics of Rotor (V = 0; M_0 = 0.5; σ = 0.0525; Experiment)

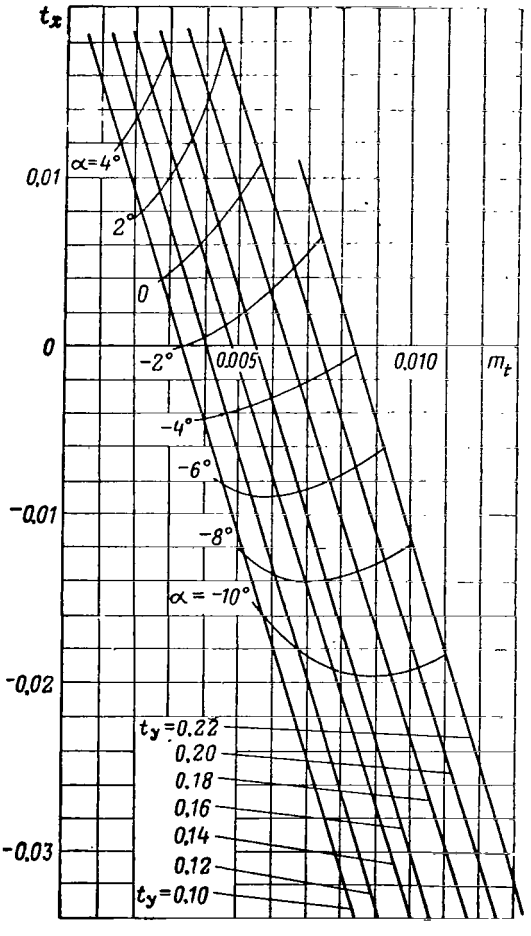

Fig.2.142 Aerodynamic Characteristics of Rotor (M_{t1} = 0.075; $\bar{V}$ = 0.15; M_0 = = 0.5; σ = 0.0525; Experiment).

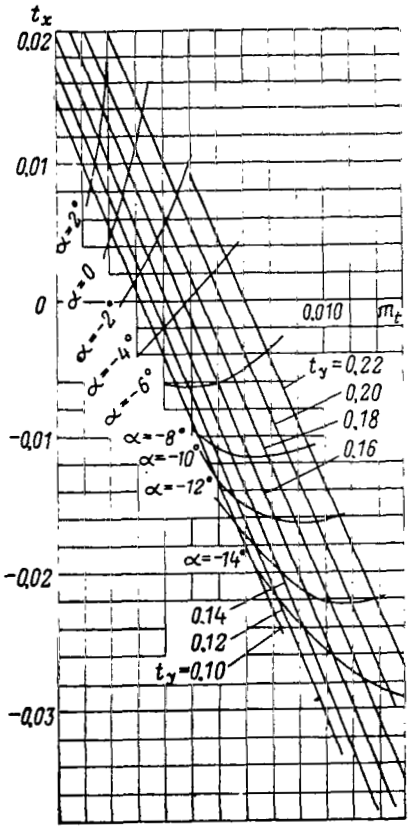

Fig.143 Aerodynamic Characteristics of Rotor (M_{f1} = 0.1; $\bar{V}$ = 0.2; M_0 = 0.5; σ = 0.0525; Experiment).

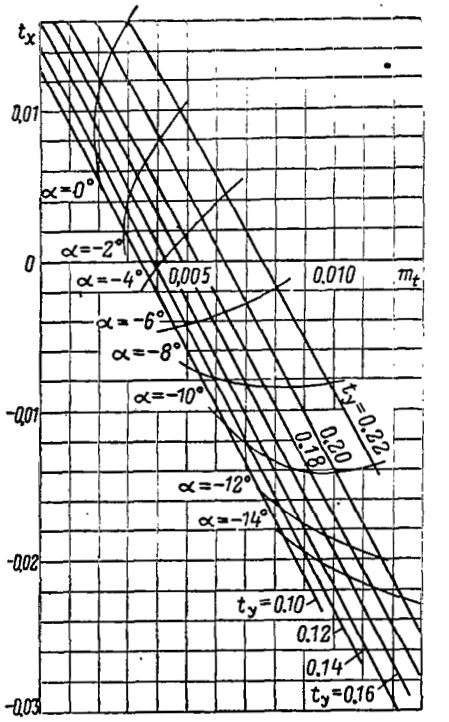

Fig.2.144 Aerodynamic Characteristics of Rotor (M_{f1} = 0.125; $\bar{V}$ = 0.25; M_0 = 0.5; σ = 0.0525; Experiment).

up, overspeeding, and normal operation of the rotor.

The aerodynamic forces and moments of the rotor in the axes of the wind tunnel are determined as the difference between the readings of the balance with the special unit operating, as well as with the unit minus rotor and hub (or with a nonrotating hub). The obtained moments and forces include the mutual interference of the rotor with the fuselage of the unit and the effect of the rotor hub. In some cases, corrections are introduced which take into account the effect of the rotor on the forces created by the fuselage of the unit. In such cases, and also when measuring with a strain-gage balance placed near the hub, the characteristics of the rotor include only the effect of the fuselage on the rotor and the effect of the rotor hub.

Figures 2.141 - 2.145 show the test-derived aerodynamic characteristics of the rotor of the Mi-1 helicopter, with metal blades of rectangular planform. The geometric characteristics of the blade are plotted in Fig.2.146: blade profile NACA 230, number of blades $z_b = 3$, diameter D = 14.5 m, solidity ratio /244 $\sigma = 0.0525$, mass characteristics of blade $\gamma = 4.5$, flapping compensator k = 0.56.

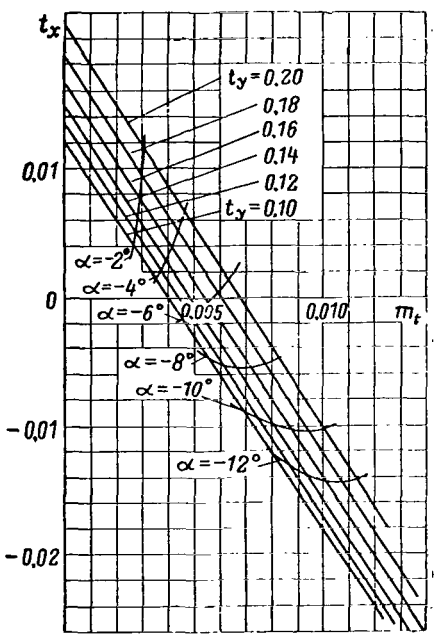

Fig.2.145 Aerodynamic Characteristics of Rotor ($M_{f1} = 0.15$; $\bar{V} = 0.3$; $M_0 = 0.5$; $\sigma = 0.0525$; Experiment).

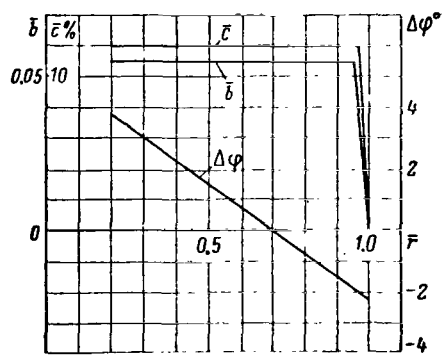

Fig.2.146 Geometric Characteristics of Blade.

The experiment was laid out so that the aerodynamic characteristics included the effect of the rotor hub and the mutual interference between fuselage and unit; this means that, in the aerodynamic design of a helicopter, allowance must be made for the parasite drag of the helicopter without rotor hub.

In this book, we use experimental data pertaining only to the aerodynamic design of the helicopter. Therefore, the graphs of the aerodynamic characteristics are given for components of forces in a system of wind axes t_y and t_x. The coefficients of forces t and h can be obtained by the conversion formulas [eqs.(3.15) and (3.17)].

The rotor angles of attack, plotted in Figs.2.142 - 2.145, correspond to zero deflection of the automatic pitch control mechanism. To reduce the volume of this book, the graphs of $t_y = f(\alpha, \theta_0, \bar{V})$ or $t_y = f(m_t, \theta_0, \bar{V})$, used for determining rotor pitch, are not given.

METHODS OF CONVERTING THE AERODYNAMIC CHARACTERISTICS OF A ROTOR

The conversion formulas presented below make it possible to use experimental data pertaining to some specific rotor for determining the aerodynamic characteristics of other rotors similar to the tested rotor with respect to dimensionless geometric characteristics. For example, the experimental graphs of the aerodynamic characteristics shown in Figs.2.142 - 2.145 can be used, with the help of the conversion formulas, for determining the characteristics of rotors with other solidity ratios if the rotors have rectangular blades, a twist of $5 - 9^\circ$, and a profile close to the NACA 230 profile. The characteristics can be extrapolated to other rotors, but with a lower degree of accuracy.

The use of the conversion formulas permits an appreciable reduction in the number of graphs of aerodynamic characteristics of rotors required for helicopter designs.

3. Conversion of Aerodynamic Characteristics to a Different Rotor Solidity Ratio

/245

Let us compare two rotors whose blades have identical distributions of twist angles and relative chord $\bar{\bar{b}} = \frac{b}{b_{0.7}}$ over the radius; the rotors are assumed to have either a different number of blades or a different chord $b_{0.7}$, i.e., a different solidity ratio. The magnitude of the mass characteristic of the blade γ has only a minor influence on the rotor characteristics so that the difference in γ can be disregarded; however, for rigorousness we will assume that γ of both rotors is identical.

At uniform induced velocity distribution over the disk of these rotors, the flapping motion of the blades and all dimensionless coefficients in the body axis system - t, h, m_t, and others - are identical if the rotors have equal values of the flight regime characteristic μ, collective pitch φ, and relative flow normal to the plane of rotation of the rotor λ:

$$\lambda = \frac{V \sin \alpha - v}{\omega R} = \mu \tan \alpha - \bar{v} \approx \mu \alpha - \bar{v}. \qquad (6.9)$$

It is easy to prove this from the formulas of the Glauert-Lock theory (Sect.2) which indicate that the expressions for all dimensionless coefficients contain four quantities: μ, λ, φ, and γ. These quantities fully determine the rotor kinematics; if they are equal, the velocity polygons in each rotor section will be alike, and the true angles of attack, c_y and c_{xp} will be equal.

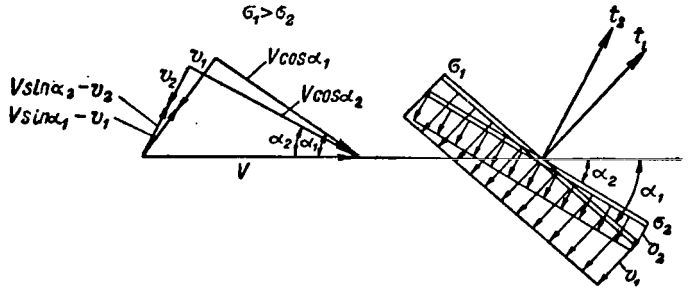

Fig.2.147 Air Velocity Components Normal (V sin α - v) and Parallel (V cos α) to the Rotor Plane at Different Values of σ and α.
V cos $\alpha_1 \approx$ V cos α_2; V sin $\alpha_1 - v_1 \approx$ V sin $\alpha_2 - v_2$.

At known μ, λ, and t, the angle of attack of the rotor is determined by the expression

$$\tan\alpha = \frac{\lambda}{\mu} + \frac{\bar{v}}{\mu} = \frac{\lambda}{\mu} + \frac{\sigma t}{4B^2\mu\sqrt{\mu^2+\lambda^2}}. \qquad (6.10)$$

Consequently, at equal dimensionless coefficients but different solidity ratios, the rotor angles of attack differ; the rotor with the larger solidity, i.e., with a larger dimensionless induced velocity, at equal t and at the same value of λ, will have a larger more positive angle of attack. Figure 2.147 illustrates the equality of the air velocity components normal (V sin α - v = $= \lambda\omega R$) and parallel (V cos $\alpha = \mu\omega R$) to the rotor plane at different mean induced velocities v and different rotor angles of attack α.

Using the subscripts "1" and "2" to denote the quantities pertaining to rotors with solidity ratios of σ_1 and σ_2, we can write the expression for the difference of the angles of attack of both rotors /246

$$\tan\alpha_1 - \tan\alpha_2 = \frac{(\sigma_1 - \sigma_2)t}{4B^2\mu\sqrt{\mu^2+\lambda^2}}$$

or, approximately for $\mu \geq 0.15$ at $\lambda^2 \ll \mu^2$,

$$\Delta\alpha = \alpha_1 - \alpha_2 = (\sigma_1 - \sigma_2)\frac{t}{4B^2\mu^2}. \qquad (6.11)$$

The difference in the angles of attack is expressed as the product of the

difference in the solidities and the ratio $\frac{t}{4B^2\mu^2}$. Consequently, at equal t and μ the difference in the angles of attack is proportional to the difference in σ.

Thus, at equal μ and φ all characteristics of the investigated rotors in body axes are identical if the rotors have angles of attack differing by a quantity $\Delta\alpha$, which is determined from eq.(6.11). To change over to characteristics in a system of wind axes, we use the formulas for converting from one system to another. Taking into account that the difference in the angles of attack of the rotors $\Delta\alpha$ is small, we obtain

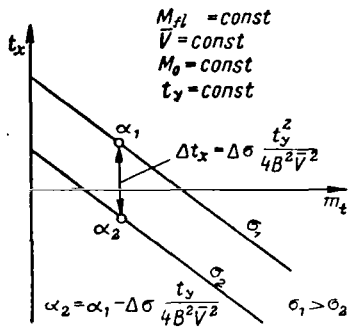

Fig.2.148 Reconstruction of the Dependence $t_x = f(m_t)$ on Change of the Rotor Solidity Ratio.

$$\bar{V}_1 \approx \bar{V}_2;$$
$$t_{y_1} \approx t_{y_2};$$
$$t_{x_1} \approx t_{x_2} + t_{y_2}\Delta\alpha.$$

Let us write out the final formulas for converting the aerodynamic characteristics of rotors with different solidity ratios:

$$\left.\begin{aligned} &\bar{V}_1 = \bar{V}_2;\\ &t_{y_1} = t_{y_2};\\ &t_{x_1} = t_{x_2} + (\sigma_1 - \sigma_2)\frac{t_y^2}{4B^2\bar{V}^2};\\ &m_{t_1} = m_{t_2};\\ &\alpha_1 = \alpha_2 + (\sigma_1 - \sigma_2)\frac{t_y}{4B^2\bar{V}^2}. \end{aligned}\right\} \qquad (6.12)$$

Equations (6.12) indicate that, on converting the characteristics, the value of the coefficients $\bar{V}$, t_y, and m_t is retained whereas t_x and α change by a quantity which is constant for given t_y and $\bar{V}$. This means that the reconstruction of the aerodynamic characteristics of a rotor, represented as the dependence $t_x = f(m_t)$ at $\bar{V}$ = const and t_y = const, reduces to a displacement of each curve along the ordinate by a quantity $\Delta t_x = \Delta\sigma \frac{t_y^2}{4B^2\bar{V}^2}$ (Fig.2.148).

Reconstruction of the characteristics need not be carried out in practice, since we can execute the aerodynamic design of a helicopter on the basis of the aerodynamic characteristics of a similar rotor with a different solidity ratio, with due regard for Δt_x. For example, in designing a helicopter with a solidity ratio σ_2 based on the aerodynamic characteristics of a rotor with a solidity ratio σ_1, the required torque coefficient $(m_{t_{h.f}})_2$ and the required power $N_{h.f_2}$ are determined in the following sequence:

a) We first determine

$$t_{y_2}=\frac{G}{1/2\,\varrho\,(\omega R)^2 F\sigma_2};$$

$$\overline{V}_2=\frac{V}{\omega R};$$

$$(t_{x_{h.f}})_2=-\bar{c}_x\frac{\overline{V}_2^2}{s_2}$$

b) For using the characteristics of a rotor with σ_1, we find

$$t_{x_1}=(t_{x_{h.f}})_2+(\sigma_1-\sigma_2)\frac{t_{y_2}^2}{4B^2\overline{V}_2^2};$$

$$\overline{V}_1=\overline{V}_2;$$

$$t_{y_1}=t_{y_2}.$$

c) From the characteristics of the rotor with σ_1, we determine m_{t_1}, α_1, φ_1.

d) We find $(m_{t_{h.f}})_2$, $\alpha_{h.f_2}$, $\varphi_{h.f_2}$ and the required power of the helicopter:

$$(m_{h.f})_2=m_{t_1};$$

$$\alpha_{h.f\,2}=\alpha_1-(\sigma_1-\sigma_2)\frac{t_{y_2}}{4B^2\overline{V}2};$$

$$\varphi_{h.f\,2}=\varphi_1;$$

$$N_{h.f\,2}=\frac{1}{150}\varrho\,(m_{t_{h.f}})_2(\omega R)^3 F\sigma_2.$$

The formulas derived above were obtained for rotors with uniform induced velocity distribution over the disk. For rotors with an infinite number of blades and nonuniform induced velocity distribution, no arguments or conversion formulas would change if at each point of the disk the induced velocities of the rotors with different solidity ratios differed by an identical quantity equal to $V\Delta\alpha$. In reality, the change in solidity ratio influences also the variable component of the induced velocity, i.e., the induced velocity diagrams do not differ by the same quantity. However, since we are converting the average per-revolution characteristics t_y, t_x, and m_t, which are mainly determined by the average portion of the induced velocity, the conversion formulas (6.12) can be used with sufficient reliability.

The proposed method of converting aerodynamic characteristics of rotors is similar to an analogous method for airplane propellers. It is also based on determining regimes in which the kinematic characteristics of the propellers with different solidity ratios are identical. The difference is that, for propellers with different σ, different flying speeds (different $\lambda_{t.p}$) are chosen, whereas for rotors for which the kinematics is determined not only by the normal velocity but also by the velocity component in the plane of rotation, the flying speed is retained but different angles of attack are chosen.

4. Conversion of Aerodynamic Characteristics on Variation in Minimum Profile Drag Coefficient of the Blade Sections c_{xp_0}

If the blades differ in magnitude of the minimum profile drag coefficient [different quality of manufacture of the profile (see Sect.4.3), different profiles differing mainly in c_{xp_0}], the following formulas can be used for converting the aerodynamic characteristics of the rotors. /248

The increments in the coefficients of torque and longitudinal force, according to the Glauert-Lock theory, will be equal to

$$\Delta m_t' = \frac{\Delta c_{xp}}{4}(1+\mu^2); \tag{6.13}$$

$$\Delta h = \frac{\Delta c_{xp}}{2}\mu, \tag{6.14}$$

where $\Delta c_{xp} = (c_{xp_0})_2 - (c_{xp_0})_1$.

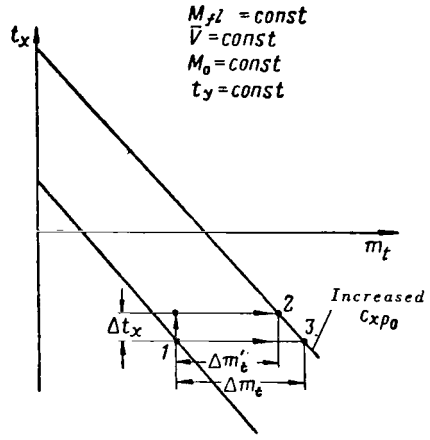

Fig.2.149 Reconstruction of the Dependence $t_x = f(m_t)$ on Variations in the Minimum Profile Drag Coefficient of the Blade Sections.

The remaining coefficients in the body axis system remain unchanged. The coefficient t_x increases by an amount equal to about Δh. Thus, the conversion formulas will be

$$\left.\begin{aligned} \bar{V}_2 &= \bar{V}_1; \\ t_{y_2} &= t_{y_1}; \\ t_{x_2} &= t_{x_1} + \frac{1}{2}\Delta c_{xp}\bar{V}; \\ m_{t_2} &= m_{t_1} + \frac{1}{4}\Delta c_{xp}(1+\bar{V}^2); \\ \alpha_2 &= \alpha_1; \\ \varphi_2 &= \varphi_1. \end{aligned}\right\} \tag{6.15}$$

The variation in the rotor characteristics upon conversion is illustrated in Fig.2.149.

Conversion can also be performed, provided there is constancy of the quantity t_x:

$$\left.\begin{aligned} \bar{V}_2 &= \bar{V}_1; \\ t_{y_2} &= t_{y_1}; \\ t_{x_2} &= t_{x_1}. \end{aligned}\right\}$$

Under this condition, the increment in torque will be equal to [see eq.(3.71)]

$$\Delta m_t = \Delta m_{pr} = \frac{1}{4}\Delta c_{xp}(1+3\bar{V}^2)$$

and, accordingly,

$$m_{t_2}=m_{t_1}+\frac{1}{4}\Delta c_{xp}(1+3\overline{V}^2). \tag{6.16}$$

By analogy with eq.(3.72), in place of eq.(6.16) we obtain

$$m_{t_2}=m_{t_1}+\frac{1}{4}\Delta c_{xp}(1+5\overline{V}^2)P. \tag{6.17}$$

Using eqs.(6.16) or (6.17), we change from point 1 in Fig.2.149 to point 3.

The nonrigorousness of the conversion formula lies in the fact that, while it does take into account the effect of an increment in c_{xp}, it disregards the fact that, at points 1 and 3, the angles of attack of the rotors are not mutually equal ($\alpha_1 = \alpha_2$; $\alpha_3 < \alpha_2$). Consequently, in these regimes there is a different distribution of the true angles of attack of the sections and therefore different induced and profile powers at identical profile polars. However, the conversion methods are approximate so that the indicated inaccuracy is of no practical value. /249

If the polars of the profiles differ not only in the quantity c_{xp_0} but also in their slope, the proposed method will not be valid. Therefore, it is unsuitable for converting aerodynamic characteristics to other Re and M_0 numbers. In these cases, the quantity Δm_t should be determined with consideration of the real values of α_r and c_{xp} at each point of the rotor disk.

5. Conversion of Aerodynamic Characteristics on Variation in the Peripheral Speed of the Rotor (M_0 Numbers)

Figures 2.80 - 2.88 in Section 3 give graphs for the increment in torque coefficient at Mach numbers greater than 0.4. The graphs show that at moderate values of the thrust coefficients the compressibility of air has a noticeable effect on the quantity m_t at M_0 greater than 0.55 - 0.6. Therefore, upon a change in M_0 beyond these limits (and at near-separation values of t_y at lower M_0) corrections must be introduced into the aerodynamic characteristics of the rotor. These corrections are determined from the graphs in Figs.2.80 - 2.88 as the difference of the values of Δm_{co} at the Mach numbers in question.

For example, if the experiment was carried out at M_0 equal to M_{0_1}, and the experimental data are used at M_0 equal to M_{0_2}, then the value of $m_{t_{exp}} = m_t(\overline{V}, t_y, t_x, M_{0_1})$ found from the experimental graphs, must be supplemented by

$$\delta m_{co}=\Delta m_{co}(M_{0_2})-\Delta m_{co}(M_{0_1}), \tag{6.18}$$

where Δm_{co} are determined at corresponding M_0 numbers and at the same values of $\overline{V}$, t_y, t_x.

Thus,

$$m_t(\overline{V}, t_y, t_x, M_{0_2}) = m_{t_{exp}}\ (\overline{V}, t_y, t_x, M_{0_1}) + \delta m_{co}. \tag{6.19}$$

At $\overline{V} > 0.3$ when M_0 changes, we must introduce a correction to the angle of attack of the rotor and, accordingly, to the blade pitch. These corrections are introduced analogously:

$$\alpha(\overline{V}, t_y, t_x, M_{0_2}) = \alpha_{exp}\ (\overline{V}, t_y, t_x, M_{0_1}) + \delta\alpha_{co}; \tag{6.20}$$

$$\delta\alpha_{co} = \Delta\alpha_{co}\ (\overline{V}, t_y, t_x, M_{0_2}) - \Delta\alpha\ \ (\overline{V}, t_y, t_x, M_{0_1}). \tag{6.21}$$

The blade pitch is determined in relation to $\overline{V}$, t_y, and α from the graphs of $t_y = f(\alpha, \theta_0, \overline{V})$ on the assumption that this dependence does not change with respect to M_0.

6. Conversion of Angle of Attack and Rotor Pitch on Variation in Inclination of the Automatic Pitch Control, Flapping Compensator, and Mass Characteristic of the Blade

As shown in Section 2, a change in the slope of the automatic pitch control and the flapping compensator will not cause a change in the coefficients t_y, t_x, and m_t provided that the equivalent rotor angle of attack $\alpha_e = \alpha - \varphi_1$ remains as before. Consequently, conversion of the rotor characteristics reduces to finding the new rotor angle of attack by means of the expression

$$\alpha_2 = \alpha_e + (\overline{\overline{\varphi}}_1)_2 = \alpha_1 - (\overline{\overline{\varphi}}_1)_1 + (\overline{\overline{\varphi}}_1)_2, \tag{6.22}$$

where $\overline{\overline{\varphi}}_1$ is determined by the formula /250

$$\overline{\overline{\varphi}}_1 = -D_1\chi + D_2\eta - k\frac{b_{1_e} - ka_{1_e}}{1 + k^2}.$$

The coefficients a_{1_e} and b_{1_e} are found from known values of a_1 and b_1 by means of eqs.(2.273), (2.274), (2.249), and (2.250). The rotor pitch is converted by the formula

$$\theta_{0_2} = \varphi_e + k_2 a_0 = \theta_{0_1} - a_0(k_1 - k_2). \tag{6.23}$$

On variation in the quantity $\frac{\gamma}{a_\infty}$, it can be considered that the coefficients a_0 and b_{1_e} entering eqs.(6.22) and (6.23) vary in direct proportion to the ratio of the new and old values of $\frac{\gamma}{a_\infty}$, i.e.,

$$(b_{1_e})_2 = (b_{1_e})_1 \left(\frac{\gamma}{a_\infty}\right)_2 \left(\frac{a_\infty}{\gamma}\right)_1;$$

$$a_{0_2} = a_{0_1} \left(\frac{\gamma}{a_\infty}\right)_2 \left(\frac{a_\infty}{\gamma}\right)_1.$$

In comparing experimental data with each other or with calculated data, one must also account for the effect of the rotor hub, as is done in the examples given below.

7. Examples of Using the Conversion Formulas

Comparison of calculated aerodynamic characteristics with experimental. The calculated aerodynamic characteristics of a rotor with rectangular blades $\sigma = 0.0525$ were obtained by the method presented in Section 4. The only difference between calculation and experiment, which should be taken into account when making a comparison, is the effect of the rotor hub on the experimental characteristics. Taking $\bar{c}_{x_{hub}} = 0.0015$, a reduction of the calculation to the experimental conditions requires the addition of the following increment to the calculated propulsive force of the rotor:

$$\Delta X_{hub} = \bar{c}_{x_{hub}} F \frac{\rho V^2}{2}$$

or, in dimensionless form,

$$\Delta t_{x_{hub}} = \bar{c}_{x_{hub}} \frac{\bar{V}^2}{\sigma}. \tag{6.24}$$

Thus, the experimental curves can be compared with the quantity

$$t'_x = t_{x_{calc}} + \Delta t_{x_{hub}} =$$
$$= t_{x_{calc}} + \frac{0.0015}{0.0525} \bar{V}^2 = t_{x_{calc}} + 0.0286 \bar{V}^2.$$

In Fig.2.150, experimental curves and converted calculated curves (t'_x) are plotted for $\bar{V} = 0.3$. The diagram indicates that, in powered flight regimes ($t_x = -0.01 - -0.02$), the difference in m_t is negligible whereas, in autorotation regime, the values of t_{x_c} differ by 5 - 15%. The convergence of the experimental and calculated curves is better at lower $\bar{V}$.

Comparison of experimental aerodynamic characteristics. Using the experimental aerodynamic characteristics of a rotor with trapezoidal blades of NACA 230 profile, plywood planking, $\sigma = 0.0865$, and $M_0 = 0.4$, the conversion formulas will yield the characteristics of a rotor with rectangular metal blades with NACA 230 profile, $\sigma = 0.0525$, and $M_0 = 0.5$, which can then be compared with the experimentally obtained characteristics shown in Figs.2.141 - 2.145. /251

The difference in the solidity ratio is taken into account by eq.(6.12):

$$t'_{x\,(\sigma=0.0525)} = t_{x\,(\sigma=0.0865)} + (0.0525 - 0.0865) \frac{t_y^2}{4B^2\bar{V}^2} =$$
$$= t_{x\,(\sigma=0.0865)} - 0.009 \frac{t_y^2}{\bar{V}^2}.$$

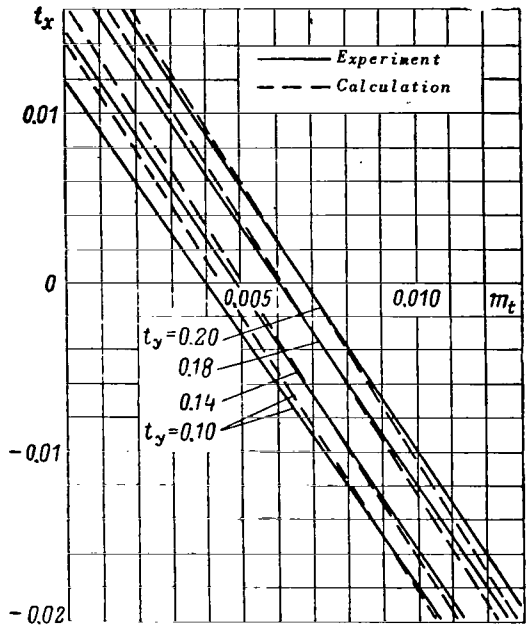

Fig.2.150 Comparison of Experimental and Calculated Aerodynamic Characteristics of Rotor (M_{f1} = 0.15; $\bar{V}$ = 0.3; M_0 = 0.5; σ = 0.0525).

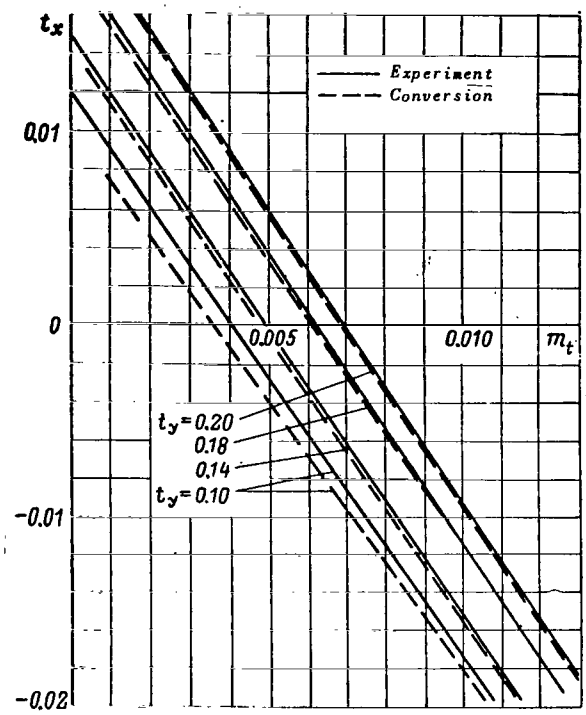

Fig.2.151 Comparison of Experimental and Converted Aerodynamic Characteristics of Rotor (M_{f1} = 0.15; $\bar{V}$ = 0.3; M_0 = 0.5; σ = 0.0525).

The difference in the profile power of the rotors, with consideration of the difference in blade planform, is found from the following expressions:

$$m_{pr\,(\sigma=0.0525)} = \frac{c_{xp_{av}}}{4}(1+5\bar{V}^2)P_1;$$

$$m_{pr\,(\sigma=0.0865)} = \frac{c_{xp_{av}}}{4}(1+5\bar{V}^2)P + \frac{\Delta c_{xp}}{4}(1+5\bar{V}^2)P; \qquad (6.25)$$

$$\Delta m_{pr} = -\frac{\Delta c_{xp}}{4}(1+5\bar{V}^2)P - \frac{c_{xp_{av}}}{4}(1+5\bar{V}^2)(P-P_1).$$

Admitting for the trapezoidal blade P = 0.92, $c_{xp_{av}}$ = 0.009 and in conformity with the recommendations in Section 4.3, Δc_{xp} = 0.0025, we find

$$\Delta m_{pr} = -\left[\frac{0.0025}{4}0.92 + \frac{0.009}{4}(0.92-1)\right](1+5\bar{V}^2) = -0.0004(1+5\bar{V}^2).$$

So as to make the conversion of the characteristics only with respect to one of the coefficients, namely with respect to t_x at m_t = const, we convert /252

Δm_{pr} to $\Delta t_{x_{pr}}$:

$$\Delta t_{x_{pr}} \approx \frac{\Delta m_{pr}}{\bar{V}}. \qquad (6.26)$$

The difference in the M_0 numbers is taken into account by eqs.(6.19), while Δm_{co} is determined from the graphs in Figs.2.80 - 2.88.

At a difference in solidity ratios, the hub drag results in a different increment of the coefficient t_x:

$$(\Delta t_{x_{hub}})_1 = \frac{\bar{c}_{x_{hub}}}{\sigma_1} \bar{V}^2;$$

$$(\Delta t_{x_{hub}})_2 = \frac{\bar{c}_{x_{hub}}}{\sigma_2} \bar{V}^2.$$

To convert the characteristics, we must subtract $(\Delta t_{x_{hub}})_1$ from the coefficient of the propulsive force of the experiment under conversion (σ_1) and add $(\Delta t_{x_{hub}})_2$:

$$t_{x(\sigma_2)} = t_{x(\sigma_1)} - \left(\frac{\bar{c}_{x_{hub}}}{\sigma}\right)_{(\sigma_1)} \bar{V}^2 + \left(\frac{\bar{c}_{x_{hub}}}{\sigma}\right)_{(\sigma_2)} \bar{V}^2. \qquad (6.27)$$

Since, in analyzing the experiment with trapezoidal blades, the drag of the nonrotating hub was excluded, we can take $\bar{c}_{x_{hub}} = 0.00075$ to account for hub rotation. Therefore, the conversion for the effect of the hub is performed by means of the expression /253

$$t_{x\,(\sigma=0.0525)} = t_{x\,(\sigma=0.0865)} - \left(\frac{0.00075}{0.0865} - \frac{0.0015}{0.0525}\right)\bar{V}^2 =$$

$$= t_{x\,(\sigma=0.0865)} + 0.02\bar{V}^2.$$

Thus, the final expression for converting the coefficient t_x has the form

$$t'_{x\,(\sigma=0.0525)} = t_{x\,(\sigma=0.0865)} - 0.009\,\frac{t_y^2}{\bar{V}^2} -$$

$$-0.0004\,\frac{1+5\bar{V}^2}{\bar{V}} + 0.02\bar{V}^2 + \frac{\delta m_{co}}{\bar{V}}.$$

For comparison purposes, Fig.2.151 gives the experimentally obtained and converted (t'_x) characteristics. For the most part, the agreement of the curves is satisfactory.

Section 7. Performance and Propulsive Efficiency Coefficient of a Rotor

The helicopter rotor produces lift and simultaneously acts as the prime

mover of the helicopter. Therefore, it is natural to characterize its lifting and propulsive properties in the same manner as a wing is characterized by the performance K_w and a tractor propeller by the efficiency $\eta_{t.p}$. These concepts permit definition of the degree of suitability of a rotor as a means for producing lift and propulsive force, as well as a rapid performance, in general form, of approximate calculations of the required power of a single-rotor helicopter, a helicopter with a wing and tractor propellers, or a multirotor helicopter, and proper selection of the regime of maximum performance (maximum range). Knowing the performance and efficiency, one can estimate directly the expediency of installing a wing and tractor propellers on a helicopter, determine what part of the total drag of a helicopter is made up by parasite drag and how much the required power can be reduced when the parasite drag is reduced, and find the rational distribution of power between tractor propellers and rotor.

A determination of rotor performance in an autorotation regime is carried out in the same manner as for a wing. The concept of rotor performance has been widely used in aerodynamic designs of autogiros. The rotor performance, together with a coefficient which we will call the propulsive efficiency coefficient, can be used also for calculating a helicopter, as we will demonstrate below.

Unlike in an airplane, where the wing and propeller are different units and K_w and $\eta_{t.p}$ can be examined independently of each other, in a helicopter the rotor performance K and the efficiency η are interrelated and the efficiency of a rotor in any regime is determined by the value of the product $K\eta$.

Let us first discuss the concepts of performance and efficiency, described in individual works on helicopter aerodynamics (K.Khokhenemzer and other authors).

1. Performance and Efficiency of Rotor Proposed by K.Khokhenemzer

/254

Rotor performance can be determined on the assumption that the actual propulsive force of the rotor (-X) is the difference between the ratio $\frac{75N}{V}$ and some arbitrary drag of the rotor $X_{arb}\left(-X = \frac{75N}{V} - X_{arb}\right)$, from which we determine the arbitrary drag of the rotor:

$$X_{arb} = \frac{75N}{V} + X.$$

Correspondingly, the rotor performance is

$$K = \frac{Y}{X_{arb}} = \frac{Y}{\frac{75N}{V} + X}. \qquad (7.1)$$

The ratio $\frac{75N}{V}$ would be equal to the propulsive force if the entire power were converted without losses into propulsive force. Since the actual propulsive

force is equal to $\frac{75N}{V} - X_{arb}$, it is obvious that all losses belong to X_{arb}.

Thus, the rotor is represented as a certain mechanism creating forces Y and X_{arb}; the power supplied to it creates, without losses, a propulsive force equal to $\frac{75N}{V}$ so that the total (actual) propulsive force is equal to $\frac{75N}{V} - X_{arb}$.

The arbitrary drag of the rotor is comparable with the drag of a wing plus the power losses of the tractor propeller, i.e.,

$$X_{arb_w} = X_w + \frac{75N_{t.p}}{V}(1 - \eta_{t.p}),$$

while the total propulsive force of the system "wing + tractor propeller" is equal to $\frac{75N_{t.p}}{V} - X_{arb_w}$.

As a second version it is proposed to consider that the lift of a rotor is produced without loss (without drag) and that all losses are accounted for by the generation of a propulsive force. The rotor is represented as some mechanism producing lift Y, while the power supplied to it is converted into propulsive force

$$-X = \frac{75N\eta}{V}.$$

Hence,

$$\eta = \frac{-XV}{75N} = \frac{-t_x\bar{V}}{m_t}. \qquad (7.2)$$

It is obvious that the efficiency η cannot be compared with $\eta_{t.p}$ but with /255 the difference $\eta_{t.p} - \frac{X_w}{\frac{75N_{t.p}}{V}}$, since the thrust of the propeller minus the wing drag is equal to

$$\frac{75N_{t.p}\eta_{t.p}}{V} - X_w = \frac{75N_{t.p}}{V}\left(\eta_{t.p} - \frac{X_w}{\frac{75N_{t.p}}{V}}\right).$$

The description of both versions of representing the characteristics of a rotor shows that they are both artificial and comparable only with combined characteristics of the wing and tractor propeller. This is the adverse side of the proposed concepts. Their favorable side is that the characteristics are described only by one quantity: either by performance or by efficiency.

The concepts of rotor performance (or efficiency) examined above are convenient for calculation, since they relate flying speed V and helicopter weight G (or propulsive force) with the required power. Actually, having set in eq.(7.1) G = Y and $Q_{par} = -X$, we obtain

$$N_{h.f} = \frac{V}{75}\left(\frac{G}{K} + Q_{par}\right). \qquad (7.3)$$

However, the sense of applying these concepts is predicated upon the convenience of use in calculation and in determining optimal parameters. Our concepts presented below also simplify the calculations and, furthermore, while retaining the sense and value of analogous concepts for airplanes, facilitate an investigation of composite rotary-wing aircraft.

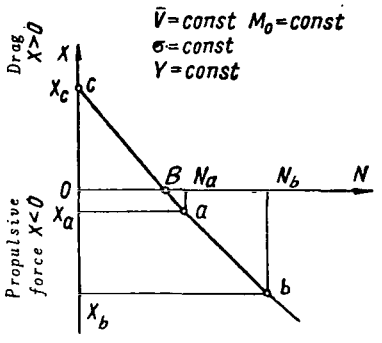

Fig.2.152 For Determining the Concepts of Performance and Efficiency of a Rotor.

2. Determination of Performance and Propulsive Efficiency of a Rotor

Let the rotor operate in the regime "a" (Fig.2.152) with a propulsive force X_a, requiring a power N_a. To increase the propulsive force to X_b while retaining the lift Y, the rotor must be tilted forward and the power must be raised to N_b. The efficiency of the rotor as a propulsion unit on changing from the regime "a" to the regime "b" is defined as the ratio of the power increment of the rotor as a prime mover $-\Delta XV$ to the increment of power supplied to the rotor:

$$\eta = \frac{-\Delta XV}{75\Delta N} = \frac{-\Delta t_x \bar{V}}{\Delta m_t} = \frac{(t_{x_a} - t_{x_b})\bar{V}}{m_{t_b} - m_{t_a}}. \qquad (7.4)$$

If, to increase the propulsive force of the rotor we were to install a tractor propeller and supply it with a power equal in magnitude to the difference $N_b - N_a = \Delta N$, then it would create a thrust of

$$P_{t.p} = \frac{75\Delta N \eta_{t.p}}{V}. \qquad (7.5)$$

A comparison of this expression with eq.(7.4) shows that the increment in propulsive force of the rotor $-\Delta X$ is characterized by its propulsive efficiency η just as the thrust of a tractor propeller is characterized by its efficiency $\eta_{t.p}$. /256

In a craft with a rotor installed to produce lift, the power can be supplied either to the rotor (helicopter: $N_{t.p} = 0$, $N_{rot} = N_b$, see Fig.2.152), or to the tractor propeller (autogiro: $N_{rot} = 0$, $N_{t.p} = N_b$), or distributed between the first ($N_{rot} = N_a$) and second ($N_{t.p} = N_b - N_a$). A comparison of η with $\eta_{t.p}$ shows which of these versions is better, i.e., whether it is expedient to install a tractor propeller for increasing the propulsive force of the craft or whether it is more advantageous to transmit the entire power to the rotor: if $\eta > \eta_{t.p}$, then $|X_b| > |X_a| + P_{t.p}$. More precisely, we must compare η with $\eta_{t.p} \frac{\xi_{t.p}}{\xi}$

(the ratio $\frac{\xi_{t.p}}{\xi}$ takes into account the difference in losses of power transmitted to the rotor and to the tractor propeller).

Thus, in order to obtain for a rotor, which is a lift-producing component as well as a propulsion unit, a coefficient analogous to the efficiency of a tractor propeller, it is necessary to investigate the increment in propulsive force (or drag) of the rotor when power is supplied to it. Therefore, we defined the propulsive efficiency of a rotor as the ratio of the increments of useful and expended work, although such a ratio is not actually the efficiency but only performs its role for craft with a rotor.

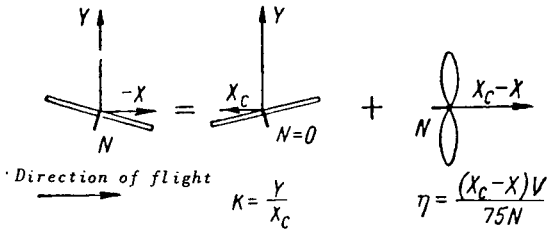

Fig.2.153 Model Representing a Rotor as Two Elements - Lifting and Propelling.

To determine the propulsive efficiency with respect to eq.(7.4) we must select some regime as the initial (we select here the point "a"). The drag of the rotor in this regime X_a determines its performance.

It is expedient to take, as initial regime, an autorotation regime (point "c" in Fig.2.152). In this regime, no power is supplied to the rotor which, in producing lift, also creates drag like a wing.

Thus, the work done by a rotor can be interpreted as follows: The lift is generated by the rotor in an autorotation regime without the expenditure of engine power, just as for a wing; in regimes with a supply of power the rotor creates a propulsive force which partially compensates (at $N < N_h$) or overcompensates (at $N > N_h$) the rotor drag in an autorotation regime. The propulsive efficiency characterizes the power losses of a rotor when changing to an engine (propulsion unit) regime. The rotor is replaced by the model shown in Fig.2.153, for which, in conformity with the foregoing, the expressions for η and K have the form

$$\eta=\frac{(t_{x_c}-t_x)\overline{V}}{m_t}; \tag{7.6}$$

$$K=\frac{t_y}{t_{x_c}}. \tag{7.7}$$

In eqs.(7.6), (7.7) and below the subscript "c" means that the indicated quantity refers to an autorotation regime.

In level flight, the propulsive force of the rotor is equal to the sum of the rotor drag t_{x_c} and the parasite drag of the helicopter $t_{x_c} - t_{x_{h.f}} = t_{x_c} + \overline{c}_x \frac{V^2}{\sigma}$. Consequently, the propulsive efficiency and performance of a helicopter in horizontal flight are equal to /257

$$\eta = \frac{(t_{x_c} - t_{x_{h.f}})\bar{V}}{m_{t_{h.f}}}; \tag{7.8}$$

$$K_h = \frac{t_y}{t_{x_c} - t_{x_{h.f}}} = \frac{t_y}{t_{x_c} + \bar{c}_x \frac{\bar{V}^2}{\sigma}} \tag{7.9}$$

or

$$K_h = \frac{t_y \bar{V}}{m_{t_{h.f}} \eta} = \frac{GV}{75 N_{h.f} \eta}. \tag{7.10}$$

We note that the quantity ($t_{x_c} - t_{x_{h.f}}$) represents the coefficient of the arbitrary propulsive force of the rotor in horizontal flight and is equal to the coefficient of the drag counteracted by the tractor propeller of an autogiro or helicopter for which, in horizontal flight, the rotor operates in an autorotation regime.

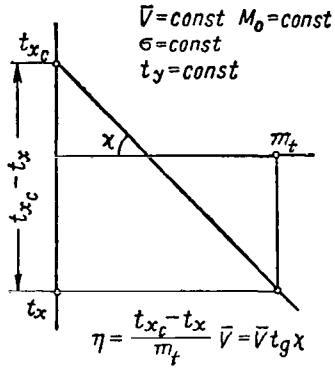

Fig.2.154 Determination of Rotor Efficiency at Linear Dependence of t_x on m_t.

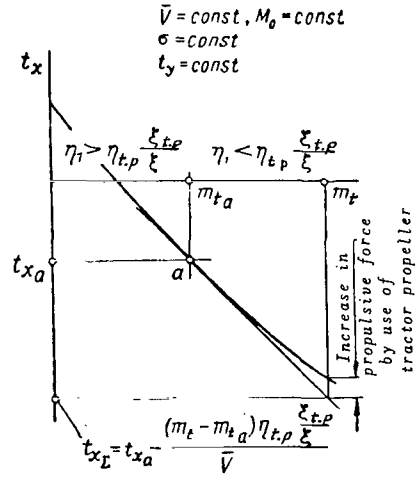

Fig.2.155 For Estimating the Expediency of Installing a Tractor Propeller on a Helicopter.

In eqs.(7.7), (7.9), and (7.10), the quantities K and K_h are the same as those used in autogiro calculations.

Use of the concepts of performance and propulsive efficiency for calculation is highly convenient in the case of linear dependence of t_x on m_t. Here, the quantity η does not depend on m_t or t_x, since the ratio $\frac{\eta}{V}$ is equal to the angle of slope of the straight lines $t_x = f(m_t)$ (Fig.2.154).

In place of the aggregate of the graphs (see Figs.2.105 - 2.109) constructed for several $\bar{V}$, the aerodynamic characteristics can be represented as two graphs: K and η as a function of t_y and $\bar{V}$ (see Fig.2.158), by means of which t_x is

determined from eqs.(7.7) and (7.6) at known values of t_y, $\bar{V}$, m_t, or else m_t is determined at known t_y, $\bar{V}$, t_x.

In the case of a nonlinear dependence of t_x on m_t, when η depends on m_t, the use of K and η in calculations offers no substantial advantages. Here, it is of interest to determine the propulsive efficiency with respect to the angle of inclination of the tangent to the curve $t_x = f(m_t)$ at the point in question /258

$$\eta_1 = \frac{\partial t_x}{\partial m_t}. \tag{7.11}$$

A comparison of η_1 with $\eta_{t.p} \frac{\xi_{t.p}}{\xi}$ permits determining whether the propulsive force of a craft can be increased by installing a tractor propeller. Let $\eta_1 = \eta_{t.p} \frac{\xi_{t.p}}{\xi}$ at the point "a" (Fig.2.155). It is obvious that, if $m_t < m_{t_a}$, we have $\eta_1 > \eta_{t.p} \frac{\xi_{t.p}}{\xi}$ and use of a tractor propeller is not advantageous. If the rotor operates in a regime with m_t greater than m_{t_a}, the installation of a tractor propeller may increase the propulsive force, the maximum gain being obtained when a power corresponding to m_{t_a} is transmitted to the rotor and to the tractor propeller ($m_t - m_{t_a}$).

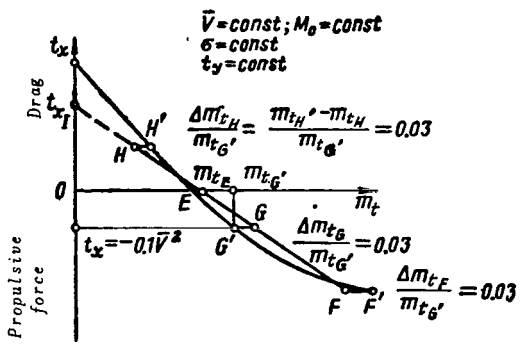

Fig.2.156 For Determining the Performance and Efficiency, at Nonlinear Dependence of t_x on m_t.

In the case of a nonlinear dependence of t_x on m_t, it is preferable, for approximate calculations with the concept of performance and efficiency, to replace the nonlinear dependence of t_x on m_t by a linear dependence. Such an approximation is made in the segment of the straight lines from $\alpha = -20^\circ$ and sometimes from $\alpha = -15^\circ$ at $\bar{V} = 0.15$ (point F in Fig.2.156) to the minimum value of m_t (point H in Fig.2.156) at which the greatest deviation of m_t from exact values does not exceed 3% of m_{t_G} at $t_x = -0.1\,\bar{V}^2$ (approximately a horizontal flight regime of helicopters).

The value of η and K, determined from the approximating segment HF, is calculated by the formulas

$$\eta = \frac{(t_{x_H} - t_{x_F})\bar{V}}{m_{t_F} - m_{t_H}}; \tag{7.12}$$

$$K = \frac{t_y}{t_{x_I}} = \frac{t_y \bar{V}}{\eta m_{t_E}}. \tag{7.13}$$

The efficiency determined by the angle of inclination of the linearized dependence $t_x = f(m_t)$ must be regarded as the propulsive efficiency, on the average, for the curve.

3. Performance and Efficiency of a Rotor, Obtained from Experimental Data

The graphs for the aerodynamic characteristics of a rotor in the form of the dependence $t_x = f(m_t)$ obtained from experiments in a full-scale wind tunnel are given in Section 6 in Figs.2.142 - 2.145. They pertain to a three-blade metal rotor with rectangular twisted blades, $\sigma = 0.0525$, and include the drag of the rotor hub. From these graphs and using eqs.(7.6), (7.7), we determine the dependence of K and η on t_y shown in Figs.2.157 and 2.158.

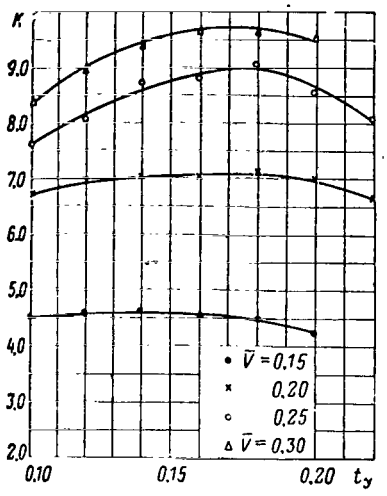

Fig.2.157 Rotor Performance according to Experimental Data ($M_0 = 0.5$; $\sigma = 0.0525$).

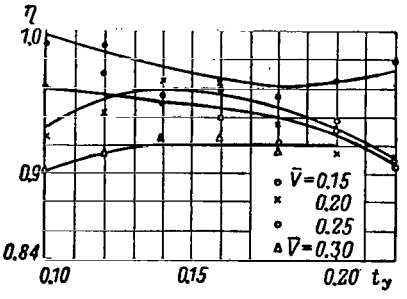

Fig.2.158 Rotor Efficiency according to Experimental Data ($M_0 = 0.5$; $\sigma = 0.0525$).

To define the character of the slope of the curves of K, let us examine the approximate expressions for K. According to the energy method of calculation (Sect.3), we have /259

$$m_{t_c} = 0 = t_y \bar{v}_c - t_{x_c} \bar{V} + m_{pr_c}; \tag{7.14}$$

$$\frac{1}{K} = \frac{t_{x_c}}{t_y} = \frac{\bar{v}_c}{\bar{V}} + \frac{m_{pr_c}}{t_y \bar{V}} = \frac{1}{K_{ind}} + \frac{1}{K_{pr}}; \tag{7.15}$$

$$\left.\begin{aligned} \frac{1}{K_{ind}} &= \frac{\bar{v}_c}{\bar{V}} = \frac{t_y}{4\bar{V}^2}; \\ \frac{1}{K_{pr}} &= \frac{m_{pr_c}}{t_y \bar{V}} = \frac{c_{xp_{av}}(1 + 3\bar{V}^2)}{4 t_y \bar{V}}. \end{aligned}\right\} \tag{7.16}$$

The increase in performance with an increase in V can be attributed to a decrease in induced and profile drags with an increase in V. At average values of t_y, the performance depends little on t_y since the induced part of the reciprocal performance increases with increasing t_y whereas the profile part decreases (up to incipient flow separation). At small t_y, the performance decreases owing to an increase in $\frac{1}{K_{pr}}$.

The maximum magnitude of rotor performance depends on $\bar{V}$, M_0, σ, quality of blade manufacture, and geometric blade characteristics. Optimum performance was not obtained in the experiments, owing to the low value of $\bar{V}_{max}$. The largest of the obtained values is $K_{max} = 9.7$ at $\bar{V} = 0.3$, $t_y = 0.17$.

Rotor performance is lower in magnitude than wing performance. This is explained by the fact that a rotor has greater profile losses than an airplane wing since, at equal flying speed, the flow across the blades has a much greater velocity U. In the case of undeflected mechanisms, the profile drag of a wing is by a factor of 2 - 2.7 less than that of a rotor. Upon deflection of the mechanisms, the profile drag of a wing increases appreciably and approaches the profile drag of a rotor.

A rotor and wing are closely adjacent in value of induced drag (at $t_w = D$ and at uniform induced velocity distribution, the induced drag is the same).

A decrease in performance at small $\bar{V}$ is inevitable both for a rotor and for a wing, owing to an increase in induced drag. However, the wing cannot have as low a performance as a rotor, since the wing cannot have as high a c_y as a rotor at $\bar{V} < 0.15$ [see eq.(4.37), Chapt.III]. /260

The propulsive efficiency of a rotor varies within the limits of 0.99 to 0.9. The curves of η intersect one another, and in some cases there is an appreciable scattering of the test points. The fact is that it is difficult to determine accurately the quantity η, since the scattering of the test points on graphs of $t_x = f(m_t)$ creates some indeterminacy in the angle of slope of the straight lines, which has a noticeable (within 3 - 5%) effect on the quantity η.

The inaccuracy in determining η, and also K, shows that when representing the characteristics of a rotor in the form of lifting and propelling elements it is impossible to estimate them separately with high accuracy. However, this does not mean that calculations performed with the use of K and η have a low accuracy, since when determining m_t by the formula

$$m_t = \frac{\left(\frac{t_y}{K} - t_x\right)\bar{V}}{\eta} \qquad (7.17)$$

the errors in determining η and K are compensated.

Figure 2.158 shows that, even if the low accuracy of determining the rotor efficiency is taken into consideration, this efficiency is greater than that of a tractor propeller. Since η is defined as the ratio of the increments of useful to expended work, it need not be less than 1.0. We will explain this. Let

us substitute into eq.(7.6) the expression for rotor power taken from the energy method of calculation

$$75N = 75N_{pr} + 75N_{ind} - XV. \tag{7.18}$$

Then eq.(7.6) takes the form

$$\eta = \frac{(X_c - X)V}{(X_c - X)V + 75(N_{ind} - N_{ind_c}) + 75(N_{pr} - N_{pr_c})}. \tag{7.19}$$

It is clear from eq.(7.19) that, if the induced and profile powers of the rotor which depend mainly on lift were not to change on a variation in the propulsive force, then the propulsive efficiency would be equal to 1.0. Actually, the differences of N_{ind} and N_{pr} are small, since we are examining the change of propulsive force at constant lift and flying speed, i.e., at approximately identical average values of induced velocity and true angles of attack of the blade sections. We can show that, for an identical propulsive force, these differences are respectively smaller than the induced and profile powers of a tractor propeller, as a result of which $\eta > \eta_{t.p}$.

Thus, in examining the lifting and propulsive properties of a rotor, we determined that the bulk of power losses (N_{ind} and N_{pr} in an autorotation regime) is accounted for by energy losses related with the production of lift, which determines the low performance of a rotor.

The propulsive efficiency of a rotor differs from 1.0, owing to the small difference in induced and profile losses in regimes with power supply to the rotor and in autorotation regimes; it is greater than the efficiency of a tractor propeller.

It should be borne in mind that the values of K and η, whose dependence on t_y is shown in Figs.2.157 and 2.158, are valid for regimes within limits in which the experiments are carried out. This means that m_t, calculated by eq.(7.17), can be correctly determined, if it is not greater than the maximum values of m_t up to which the experimental curves were plotted ($m_{t_{max}}$ = = 0.01 - 0.013). /261

4. Performance and Efficiency of a Rotor, Obtained from Calculated Graphs

The performance and efficiency of a rotor with rectangular twisted blades (variant II in Table 2.10), σ = 0.091, were determined from graphs of the aerodynamic characteristics obtained by calculation. In the case of nonlinear dependence $t_x = f(m_t)$, the quantities K and η were found from eqs.(7.12) and (7.13). The graphs of K and η are shown in Figs.2.159 and 2.160.

Rotor performance begins to decrease at $M_0 > 0.6$, especially at large $\bar{V}$; at $M_0 = 0.7$ and $\bar{V} = 0.3$, K diminishes by 1.5, and at $\bar{V} = 0.4$ by 3.5. At $M_0 = 0.7$, the performance at $\bar{V} = 0.3$ is greater than at $\bar{V} = 0.4$, and the maximum performance is equal to about 7.5.

The efficiency of a rotor, for $M_0 = 0.6 - 0.7$ at average and small values of t_y, has a higher value (more than 0.95). At near-separation values of t_y, the efficiency begins to drop markedly, but does not decrease when $t_y = t_{y_{cr}}$ less than 0.75 - 0.85.

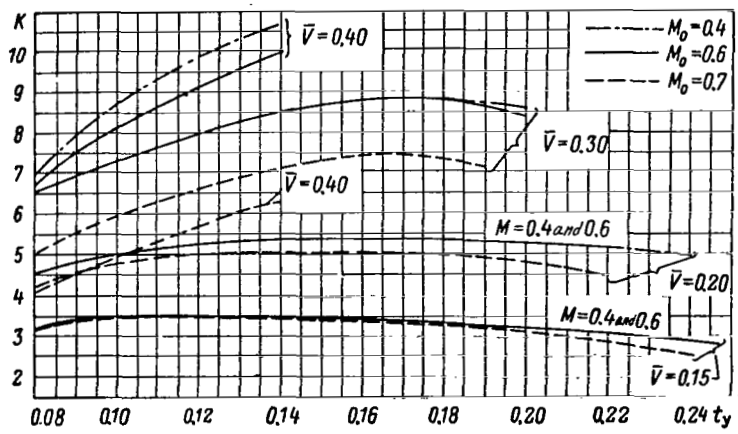

Fig.2.159 Rotor Performance (Calculation, $\sigma = 0.091$).

The values of K and η obtained as a result of linearization of the curves of $t_x = f(m_t)$ hold true within certain limits. The upper limit of applicability of the graphs of K and η are the values of the ratio $\frac{m_{t_{max}}}{t_y \bar{V}} = \left(\frac{75N}{YV}\right)_{max}$, given in Table 2.13.

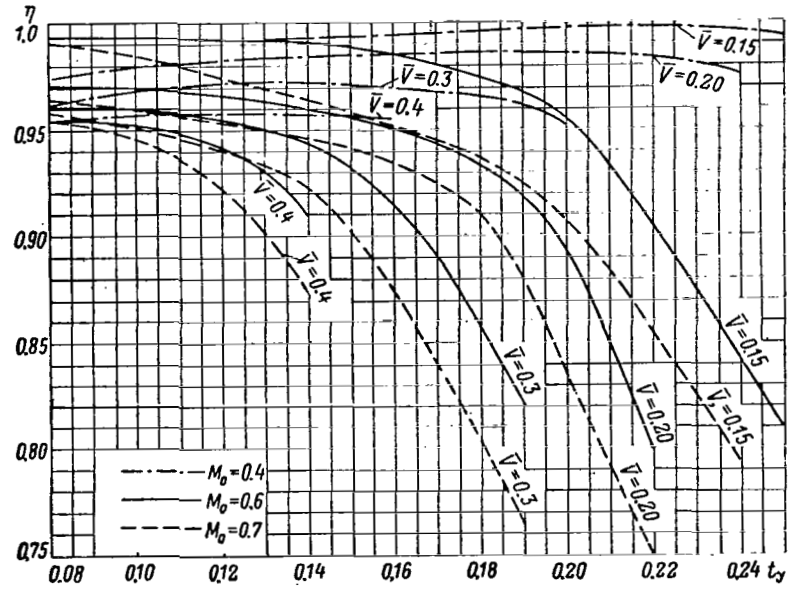

Fig.2.160 Rotor Efficiency (Calculation, $\sigma = 0.091$).

If the ratio $\frac{75N}{YV}$ obtained from calculation is less that that given in Table 2.13, the calculation will not differ by more than 3% from the calculation made from graphs of aerodynamic characteristics. Furthermore we note that the values of $\frac{75N}{YV}$ given in Table 2.13 correspond to flight regimes with $\alpha = -20^\circ$ /262 (sometimes -15° at $\bar{V} = 0.15$).

The lower limit of applicability of the graphs in Figs.2.159 and 2.160 is the autorotation regime or a powered glide. More accurately, the calculations for an autorotation regime are performed from the graphs of K_c shown in Fig.2.111, since the values of K found from the linearized curves may differ somewhat from K_c.

TABLE 2.13

$\bar{V}$	0.15	0.2	0.3	0.4
$\left(\frac{75N}{YV}\right)_{max}$	0.6	0.48	0.37	0.3

A comparison of the performance and efficiency of rotors having blades with different geometric characteristics shows that, at $M_0 = 0.4 - 0.5$, the blade profile influences the value of K to within several percents whereas η depends little on the blade profile. This means that rotors with different profiles require a power differing by ΔN, where ΔN is independent of the type of operating regime of the rotor, namely at either large or small propulsive force (in gliding or climbing).

For trapezoidal blades (variant I of the blades in Table 2.10), K is greater by 0.5 (at $\bar{V} = 0.2$) - 1.5 (at $\bar{V} = 0.4$), and η is lower by 0.01 (at $\bar{V} = 0.2$) - - 0.03 (at $\bar{V} = 0.4$) than for rectangular blades. This means that the greatest decrease in required power for a rotor with trapezoidal blades occurs at small propulsive forces. At large propulsive forces, the rotor with rectangular /263 blades having a larger η may prove to be better.

Comparative graphs of K and η at $M_0 = 0.7$ are shown in Figs.2.161 - 2.164. The diagrams show that, for a rotor without a high-speed profile at the blade tip (variants III, IV), K is smaller by 0.7 (at $\bar{V} = 0.2$) - 1.7 (at $\bar{V} = 0.4$) than for a rotor with a high-speed profile. For trapezoidal blades, K is higher by 0.5 - 1.0 and η lower by 0.02 - 0.08, respectively, than for a rotor with rectangular blades.

For a rotor with blades of increased geometric twist (variant VI) and with blades expanding toward the tip (variant VII) at $\bar{V} = 0.4$, the performance is 0.5 - 0.7 lower and the efficiency 0.05 - 0.15 higher. The very high value of η

for a rotor with increased twist is a consequence of the substantial decrease in profile losses upon an increase in propulsive force of the rotor (see Figs.2.75 and 2.76).

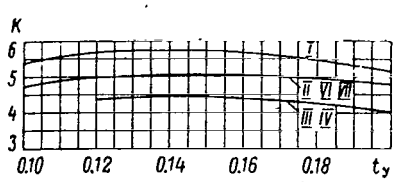

Fig.2.161 Performance of Rotors with Blades of Different Shape ($\bar{V}$ = 0.2; M_0 = 0.7).

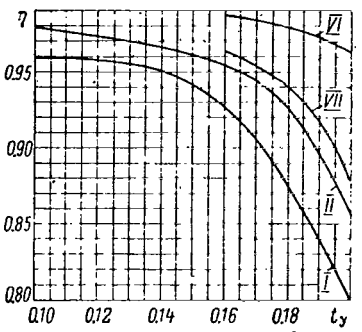

Fig.2.162 Efficiency of Rotors with Blades of Different Shape ($\bar{V}$ = 0.2; M_0 = 0.7).

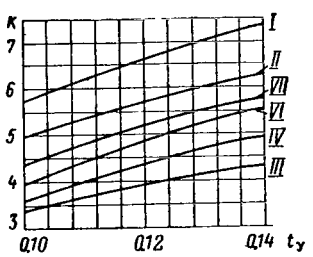

Fig.2.163 Performance of Rotors with Blades of Different Shape ($\bar{V}$ = 0.4; M_0 = 0.7).

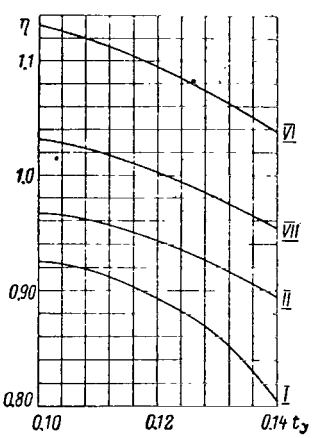

Fig.2.164 Efficiency of Rotors with Blades of Different Shape ($\bar{V}$ = 0.4; M_0 = 0.7).

5. Conversion of Performance and Efficiency on Variations in Rotor Parameters

In conformity with the formulas derived in Section 6, the performance of a rotor on variations in the solidity ratio and profile power coefficient is converted by the expression

$$\frac{1}{K}=\frac{1}{K_1}+\frac{(\sigma-\sigma_1)t_y}{4B^2\bar{V}^2}+\frac{\Delta m_{pr}\eta}{t_y\bar{V}}. \qquad (7.20)$$

A change in profile power coefficient should take into account a change /264
in c_{xp_0} of the profile (or Δc_{xp}, owing to the difference in the quality of blade manufacture) and a change in m_{pr} from the wave drag:

$$\Delta m_{pr} = \frac{\Delta c_{xp}}{4}(1+5\bar{V}^2)P + \delta m_{co}. \qquad (7.21)$$

The propulsive efficiency is independent of the difference in σ and Δc_{xp}. The quantity δm_{co} depends on t_x so that also η depends on t_x. However, for the sake of simplicity we need not convert η, and we substitute δm_{co} into eq.(7.21) at an average value of t_x.

6. General Comments on Rotor Efficiency and Performance

Figures 2.165 - 2.167 show the generalized graphs of K and η, which can be used for estimate calculations. Figure 2.165 gives the graph of K for σ = = 0.091, which is valid for average and large t_y. At small ($t_y \approx 0.1$), K is smaller by 0.2 (at $\bar{V} = 0.15$) - 1.5 (at $\bar{V} = 0.4$). Figure 2.166 contains the graph of η used for all t_y at $M_0 \leq 0.55$. For $M_0 > 0.55$, the efficiency must be corrected by a quantity $\Delta\eta$, which is plotted in Fig.2.167 as a function of t_y, M_0, $\bar{V}$.

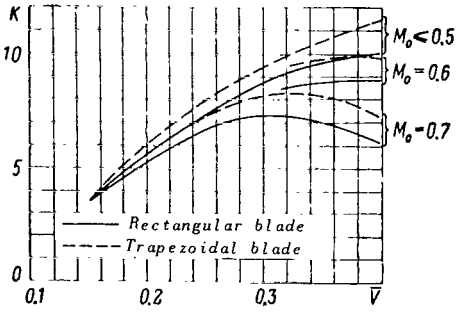

Fig.2.165 Generalized Graph of Rotor Performance (σ = 0.091).

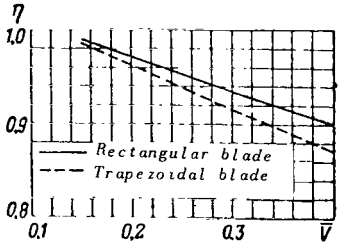

Fig.2.166 Generalized Graph of Rotor Efficiency ($M_0 \leq 0.5$).

Thus, as shown in Figs.2.165 - 2.167, the rotor performance is lower than the wing performance, and the propulsive efficiency of the rotor is higher than that of a tractor propeller. This is explained by the fact that the bulk of the power losses pertain to losses related with the production of lift, whereas the propulsive efficiency differs from unity owing to the small difference in induced and profile losses in regimes with power supply to the rotor and in autorotation regimes.

Thus, it is obvious that the installation of a wing with a performance higher than that of a rotor will increase the performance of the lifting system of a helicopter. The installation of a tractor propeller of an efficiency lower than the propulsive efficiency of a rotor will lead to some increase in required

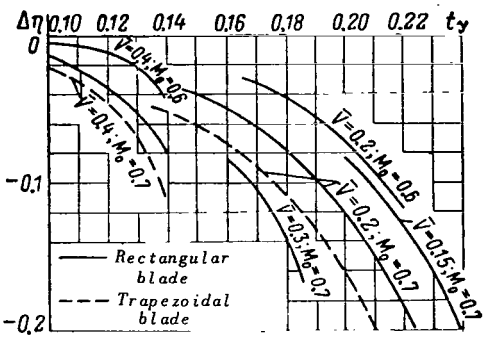

Fig.2.167 Correction for Rotor Efficiency as a Function of t_y, M_0, $\bar{V}$.

power. Therefore, a tractor propeller on a helicopter can be useful when the relief of the rotor load by the wing or the reserve of available power render the ratio $\frac{75N}{YV}$ greater than that shown in Table 2.13, since then the negative angle of attack of the rotor becomes greater than 20° (which is undesirable for design considerations, since the range of pitch angles of the helicopter and its parasite drag will increase). Furthermore, at larger $\frac{75N}{YV}$, the values of η may become smaller than $\eta_{t.p}$. A tractor propeller or another propeller may be required for realization of a large power excess $\left(\text{approximately } \frac{N}{G} > 0.35\right)$ when $\bar{V}_{max} > 0.45 - 0.5$ for a helicopter. /265

Quantitatively, the change in required power of a helicopter, on installation of a wing or tractor propeller, is small. Such an estimate will be made in Section 4, Chapter III.

Section 8. Calculation of Rotor Characteristics in Hovering and Vertical Ascent (Momentum Theory of Propellers)

The theory of a rotor in hovering and vertical ascent has been thoroughly presented in the literature on helicopter and propeller aerodynamics. In this Section, we will give some data pertaining to a calculation of rotors with peripheral speeds as they are in use at present.

The calculations were performed with regard to momentum theory of a rotor. This theory was selected because of the fact that introduction of linearized aerodynamic characteristics of the profile into the calculation can be replaced by introduction of the actual dependence of c_y and c_{xp} on α and M, obtained from wind-tunnel tests of the profile.

1. Brief Review of the Momentum Theory of Propellers

Figure 2.168 shows the velocity polygon in a blade section at a relative radius $\bar{r}$ in the regime of vertical climb. The resultant velocity of flow in the blade section U represents the sum of the vectors: flying speed V_y, peripheral velocity ωr, and induced velocity u. Since the vector of the resultant aerodynamic force of the section $\vec{dR}$ is directed opposite to the momentum vector, the induced velocity vector $\vec{u}$ is parallel to $\vec{dR}$.

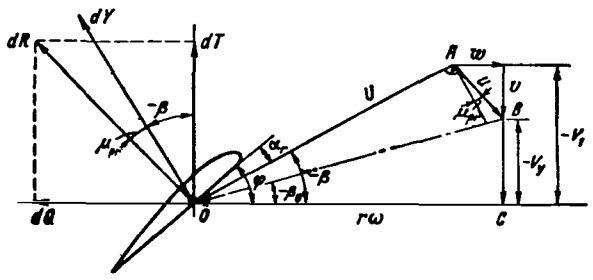

Fig.2.168 Velocity of Polygon in a Blade Section in Vertical Climb-Regime.

The mass flow through a circular section at a radius r of width dr is equal to /266

$$dm=\varrho 2\pi r\,dr\,|V_1|, \tag{8.1}$$

where V_1 is the vertical velocity component U.

Applying the momentum theorem to the ring and using the theorem of doubling the induced velocity far aft of the rotor, we obtain the equation

$$2dmu=z_b dR, \tag{8.2}$$

where $z_b dR$ is the resultant of the elementary aerodynamic forces created by all blades at radius r.

Substituting eq.(8.1) into eq.(8.2) and expressing dR in terms of the force coefficient $c_{R_{sec.}}$, we obtain the equation

$$4\pi\varrho\,|V_1|\,ur\,dr=z_b c_{R_{sec.}}\varrho\frac{U^2}{2}b\,dr. \tag{8.3}$$

Equation (8.3) can be represented in the form

$$|V_1|\,u=\frac{\sigma}{8\bar{r}}\bar{\bar{b}}c_{R_{sec.}}U^2. \tag{8.4}$$

This equation determines the relation between the velocity of the air and the coefficient of aerodynamic force in the blade section (the so-called "coupling equation").

Equation (8.4) holds for a stream flow through the rotor disk but is inapplicable in the region of the "vortex ring".

Expressing the velocities entering eq.(8.4) in terms of trigonometric functions of the angles of the velocity polygon, we can write eq.(8.4) in the trigonometric form:

$$\frac{\sin\beta\cdot\sin(\beta_0-\beta)}{\cos(\beta_0-\beta+\mu_{pr})}=\frac{\sigma\bar{\bar{b}}}{8\bar{r}}c_{R_{sec.}} \tag{8.5}$$

where β is the inflow angle.

The quantities μ_{pr} and β_0 are equal to

$$\mu_{pr}=\tan^{-1}\frac{c_{xp}}{c_y}; \tag{8.6}$$

$$\beta_0 = tan^{-1}\frac{\bar{V}_y}{\bar{r}}. \tag{8.7}$$

On the left-hand and right-hand sides of the equations, β_0 is a known quantity at a given $\bar{r}$; β, α_r, and μ_{pr} are unknown. However, if we assign α_r, then the characteristics of the profile will yield μ_{pr} and $c_{R_{sec.}}$, while eq.(8.8) will furnish β:

$$\beta = \alpha_r - \varphi = \alpha_r - (\theta_0 - ka_0 + \Delta\varphi). \tag{8.8}$$

The problem consists in determining α_r at which eq.(8.5) is satisfied. This value of α_r is found by successive approximations. Simultaneously with determining α_r, we find β, μ_{pr}, and $c_{R_{sec.}}$.

The loads per unit length in the thrust plane and in the plane of rotation as well as the torque per unit length are determined from the following formulas: /267

$$\frac{dt}{d\bar{r}} = \bar{b}c_{R_{sec.}}\bar{U}^2\cos(\mu_{pr} - \beta)\operatorname{sign} c_y; \tag{8.9}$$

$$\frac{dq}{d\bar{r}} = \bar{b}c_{R_{sec.}}\bar{U}^2\sin(\mu_{pr} - \beta)\operatorname{sign} c_y; \tag{8.10}$$

$$\frac{dm_t}{d\bar{r}} = \bar{r}\frac{dq}{d\bar{r}}. \tag{8.11}$$

The coefficients of thrust and power of the rotor are determined by numerical integration of eqs.(8.9) and (8.11).

For an approximate consideration of the tip losses, the loads per unit length in the thrust plane are not integrated up to the blade tip ($\bar{r} = 1$) but up to $\bar{r} = B$ whereby, according to another paper (Ref.2), we have

$$B = 1 - 4\frac{t\sigma}{z_b} = 1 - \frac{4}{\pi}\bar{b}_{0.7}t. \tag{8.12}$$

Equation (8.12) can be used when $z_b \geq 3$; at $z_b = 2$, the tip losses should be taken into account by more accurate methods.

The coning angle and profile power coefficient are found from the expressions

$$a_0 = \frac{\gamma}{a_\infty}\int_{r_0}^{B}\frac{dt}{d\bar{r}}\bar{r}\,d\bar{r}; \tag{8.13}$$

$$m_{pr} = \int_{r_0}^{1}\bar{b}c_{xp}\bar{U}^3\,d\bar{r}. \tag{8.14}$$

2. Results of Calculating the Characteristics of a Rotor

The aerodynamic characteristics of a rotor with rectangular twisted blades

having a high-speed profile at the tip (variant II in Table 2.10) for solidity ratios of the rotor σ = 0.0525; 0.069; 0.091; 0.11 (the number of blades is, respectively, z_b = 3; 4; 5; 6), k = 0.4, $\frac{\gamma}{a_\infty}$ = 1.28*, and for two values of M_0 are shown in Figs.2.169 and 2.170. Such graphs are used in check calculations of helicopters in order to determine the rotor thrust in a hovering regime, when power, flight altitude, and the rotor parameters F, σ, ωR are known. The sequence of the calculation is as follows: Having calculated m_t and M_0

$$m_t = \frac{75N}{1/2\,\varrho\,(\omega R)^3\,\sigma F} = \frac{75N_{eng}\,\xi}{1/2\,\varrho\,(\omega R)^3\,\sigma F}; \tag{8.15}$$

$$M_0 = \frac{\omega R}{a}, \tag{8.16}$$

the graphs can be used for finding the thrust coefficient t and for determining the rotor thrust

$$T = \frac{1}{2}\varrho\,(\omega R)^2\,\sigma F t. \tag{8.17}$$

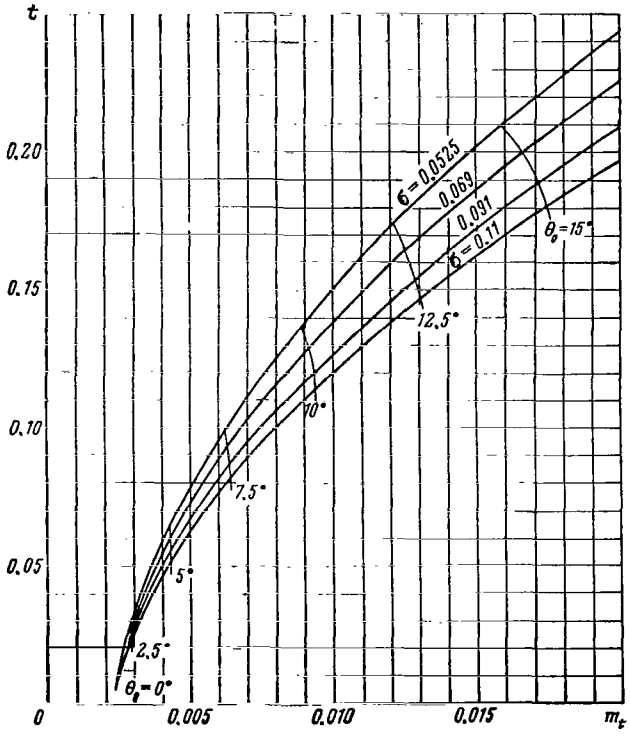

Fig.2.169 Aerodynamic Characteristics of a Rotor in Hovering Regime (M_0 = = 0.6).

The effect of the geometric /268 blade characteristics is illustrated by the graph in Fig.2.171, which indicates that the trapezoidal blade (variant I) and the rectangular blade with an increased twist (variant VI) at t = = 0.12 - 0.15 require 3 - 4% less power than a rectangular blade with moderate twist (variant II). Thus, an increase in geometric blade twist improves the rotor characteristics in hovering and in forward flight (with the exception of the regime of autorotation).

Figure 2.172 shows the radial distribution of the axial $\bar{v}$ and tangential $\bar{w}$ components of induced velocity. The slope of $\bar{v}$ and $\bar{w}$ with respect to $\bar{r}$ has a different character for blades of the examined shapes. For a rectangular blade with a geometric twist of 7° (variant II), $\bar{v}$ increases from the root to the tip of the blade; for a trapezoidal twisted blade and

* For other values of k and γ, the rotor pitch should be converted by eq.(6.23).

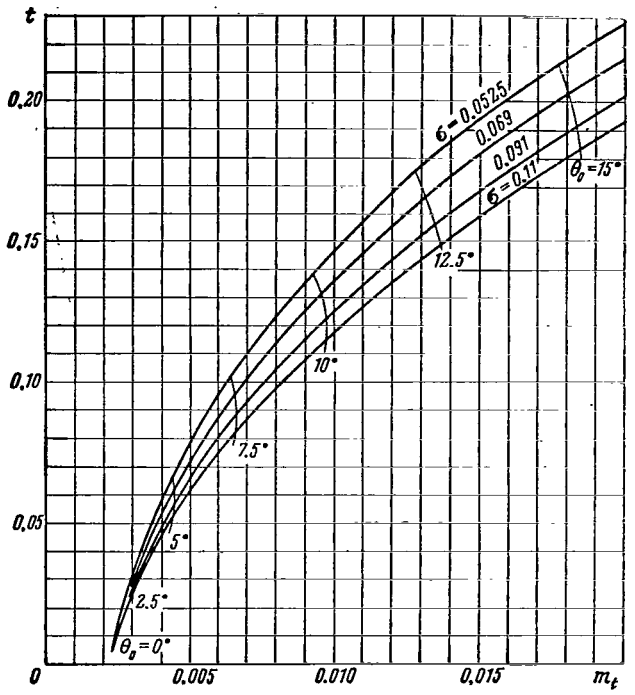

Fig.2.170 Aerodynamic Characteristics of Rotor in Hovering Regime (M_0 = 0.7).

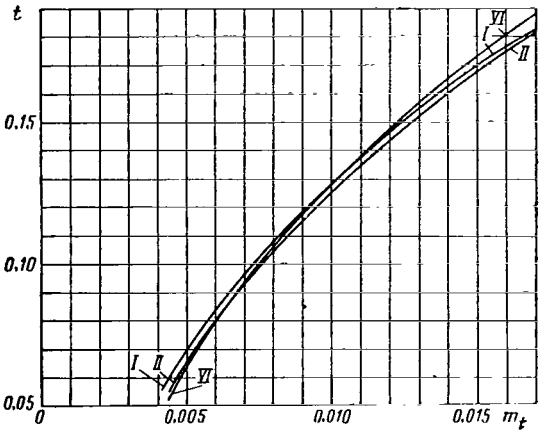

Fig.2.171 Aerodynamic Characteristics of Rotor with Blades of Different Shape in Hovering Regime (σ = 0.091; M_0 = 0.7).

for a rectangular blade with increased twist, the distribution of $\bar{v}$ in the tip portion of the blade is close to uniform, so that these blades have smaller induced losses. As indicated in Fig.2.172, the slipstream velocity $\bar{w}$ of the helicopter rotor is by one order of magnitude less than the axial induced velocity v.

For rectangular blades, the angles of attack of the sections α_r (Fig.2.173) decrease toward the blade tip, and the maximum angles of attack of the sections are at $\bar{r} = 0.3 - 0.5$. The trapezoidal twisted blade has a more uniform distribution of α_r over the outside half of the blade; this angle of attack distribution, compared to the rectangular blade, leads to earlier attainment of critical angles of attack and to a marked increase in c_{xp} at the effective blade portion.

/270

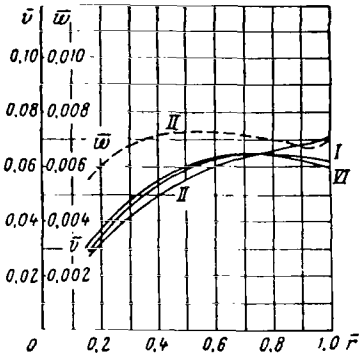

Fig.2.172 Radial Distribution of Axial $\bar{v}$ and Tangential $\bar{w}$ Components of Induced Velocity (t = 0.15).

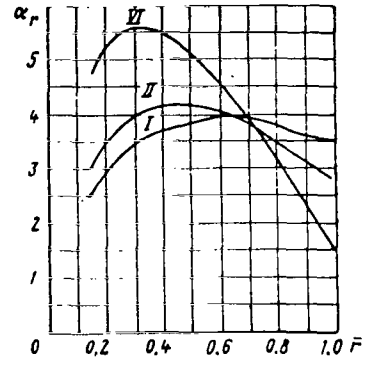

Fig.2.173 Radial Angle of Attack Distribution of Sections (t = 0.15).

Figure 2.174 shows the dependence of profile power on the thrust coefficient t and M_0 for a blade of the variant II. As we see from the graph, the effect of air compressibility becomes appreciable at $t > 0.15$. The graph in Fig.2.175 shows the effect of the geometric blade characteristics on the profile power. At $M_0 = 0.7$, the blade profile (variant III; blade without a high-speed profile at the tip) has the main effect while the blade shape has a smaller effect. An increase in geometric blade twist (variant VI) reduces the profile losses of the blade at large t.

To determine the effect of air compressibility, Fig.2.176 shows the graph of $\Delta m_{co}(M_0) = m_t(M_0) - m_t(M_0 = 0.4)$ for a blade of the variant II; for other blade shapes, this is shown in Fig.2.177. The compressibility graphs permit converting the rotor characteristics to other M_0 numbers and are also used in an approximate calculation of the rotor characteristics when m_{pr} is determined by eq.(8.28). We see from Fig.2.177 that, for the examined profiles, the blade without the high-speed profile, at $M_0 > 0.6$, shows a substantially greater increment in m_{pr} than the blade with the high-speed profile at the tip.

The values of the thrust coefficients t_{or} maximally permissible in view of the flow separation at the rotor blade (see Sect.4.7) were determined in hovering from the plot of thrust coefficient versus rotor pitch θ_0. This dependence

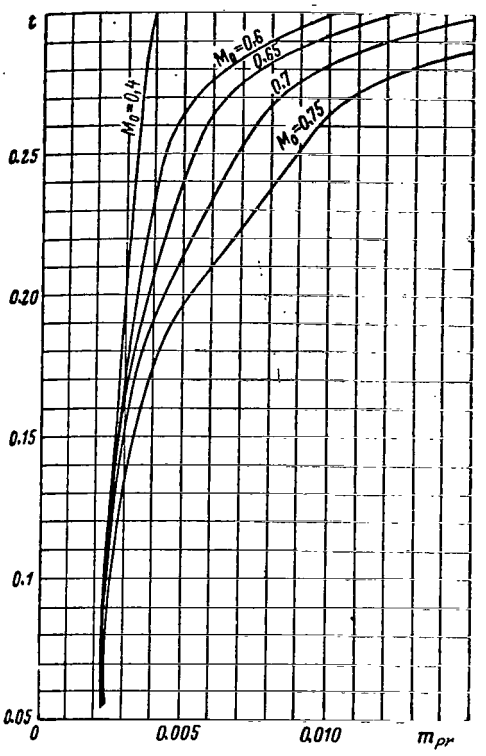

Fig.2.174 Profile Power Coefficient as a Function of Thrust Coefficient t and M_0.

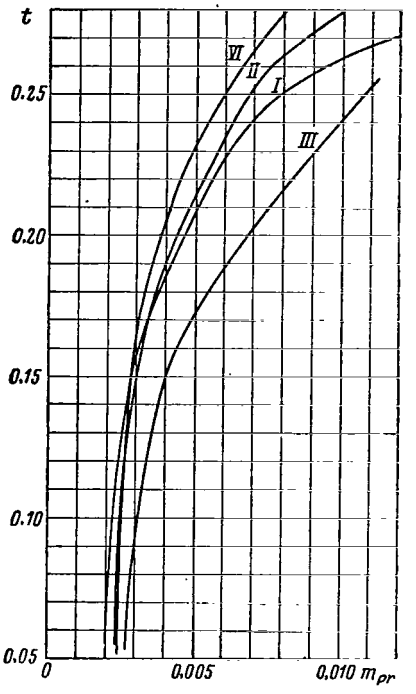

Fig.2.175 Profile Power Coefficient as a Function of Thrust Coefficient t for Rotors with Blades of Different Shape (M_0 = 0.7).

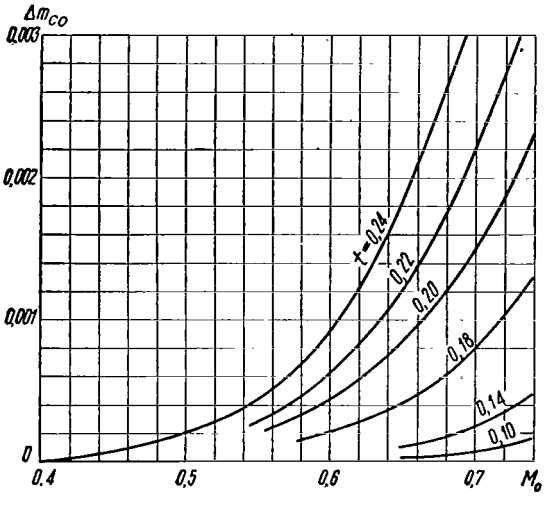

Fig.2.176 Increment in Profile Power Coefficient of the Rotor owing to Air Compressibility.

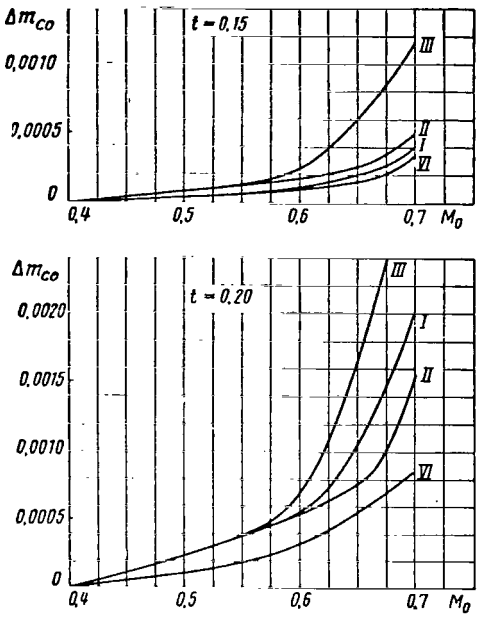

Fig.2.177 Increment in Profile Power Coefficient owing to Air Compressibility, for Rotors with Blades of Different Shape.

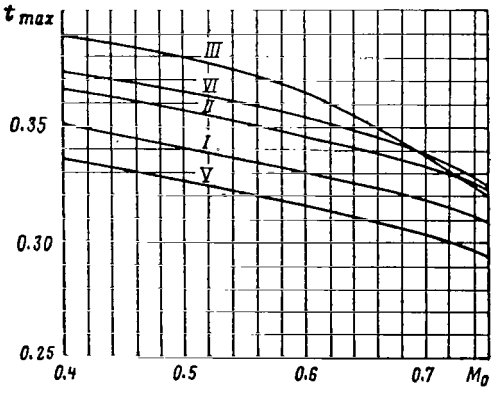

Fig.2.178 t_{max} as a Function of M_0, for Rotors with Blades of Different Shape.

is linear up to some value of t, after which the linearity is disturbed; the increase in t with increasing θ_0 decreases, after which t reaches a maximum t_{max}, which is taken as t_{cr} when constructing the limit of separation (Figs.2.119 to 2.121).

Figure 2.178 gives the graph of t_{max} as a function of M_0. The diagram shows that, in hovering, t_{max} decreases appreciably with increasing M_0. For a trapezoidal blade, t_{max} is smaller than for a rectangular type. An increase in geometric blade twist will increase t_{max}. The blade without a high-speed profile at the tip has a larger t_{max}; however, as soon as M_0 increases the difference in t_{max} will lessen.

According to the momentum theory and with an approximate consideration of tip losses, the solidity ratio does not affect the angle of attack distribution over the radius or the magnitude of the coefficients m_{pr}, Δm_{co}, t_{max}; consequently, the graphs in Figs.2.173 - 2.178, constructed for $\sigma = 0.091$, are valid for all σ.

3. Approximate Method of Determining the Dependence of m_t on t

/273

For vertical flight regimes of a helicopter, we can obtain an expression for m_t analogous to eq.(3.67) derived in Section 3 for flight with a horizontal velocity of

$$m_t = \int_0^1 (dt\bar{v} + dq\bar{w}) + \int_0^1 c_{xp}\bar{\bar{b}}\bar{U}^3\, d\bar{r} - t\bar{V}_y. \tag{8.18}$$

In this expression, $V_y < 0$ at a gain in altitude.

Introducing the designations for the terms representing the coefficients of induced and profile losses of the rotor,

$$m_{ind} = \int_0^1 dt\bar{v} + dq\bar{w}; \tag{8.19}$$

$$m_{pr} = \int_0^1 c_{xp}\bar{\bar{b}}\bar{U}^3\, d\bar{r}, \tag{8.20}$$

we can represent the expression for m_t in the form of

$$m_t = m_{ind} + m_{pr} - t\bar{V}_y. \tag{8.21}$$

Let us derive the approximate expressions for the components of m_t in hovering.

To determine m_{ind}, let us first assume that the induced velocity v is distributed uniformly over the blade radius and that w = 0.

Multiplying the left and right sides of eq.(8.4) by cos $(\mu_{pr} - \beta)$ and using

eq.(8.9), we obtain

$$8\bar{v}^2\bar{r}\,d\bar{r}=dC_T. \tag{8.22}$$

The average induced velocity over the disk $\bar{v}_{av}$ is found after integrating eq.(8.22) with respect to the blade radius from $\bar{r}$ = 0 to $\bar{r}$ = B:

$$\bar{v}_{av}=\frac{\sqrt{C_T}}{2B}. \tag{8.23}$$

According to eqs.(8.22) and (8.23), at constant induced velocity the elementary thrust coefficient is distributed linearly over the blade radius and is equal to

$$dC_T=\frac{2C_T}{B^2}\bar{r}\,d\bar{r}. \tag{8.24}$$

Consequently,

$$m_{ind}\simeq\int_0^1 dt\bar{v}=\frac{\bar{v}_{av}}{\sigma}\int_0^1 dC_T=\frac{C_T\bar{v}_{av}}{B^2\sigma}=\frac{t^{3/2}\sqrt{\sigma}}{2B^3}. \tag{8.25}$$

To take account of the nonuniformity of axial induced velocity distribution $\bar{v}$ and of the term $d\bar{q}\bar{w}$ (power losses due to twisting of the flow passing through the rotor), we will introduce into eq.(8.25) the coefficient Φ:

$$m_{ind}=\frac{\Phi}{2B^3}\sqrt{\sigma}t^{3/2}. \tag{8.26}$$

The coefficient Φ depends on the planform of the blade and on its geometric twist, on the solidity ratio, and also on the thrust coefficient. Calculations have shown that we can take the following average values of Φ: for a rectangular blade with a twist of 5 - 9°, a value of Φ = 1.05; for a blade with a twist /274
of 12 - 15°, Φ = 1.03. For a trapezoidal blade with taper η = 3 and twist of 5 - 9°, Φ = 1.03. The tip-loss coefficient B for rotors with σ = 0.0525 - 0.11 can be taken as equal to 0.98.

Thus, for a rectangular blade with a geometric twist of 5 - 9°, m_{ind} is determined by the formula

$$m_{ind}=0{,}56\sqrt{\sigma}t^{3/2}. \tag{8.27}$$

The profile loss coefficient of a rotor m_{pr} is most reliably determined by the graphs of $m_{pr}=f(t, M_0)$ (see Figs.2.174 and 2.175) which were calculated for a rotor with similar geometric characteristics. If there are no such graphs, then m_{pr} is found from

$$m_{pr}=\frac{c_{xp_{av}}}{4}P+\Delta m_{co}. \tag{8.28}$$

The first term determines the profile losses at small M_0, while the second term takes account of the increment in the profile loss coefficient owing to wave drag. An estimate of Δm_{co} can be made on the basis of the graphs in Figs.2.176 and 2.177.

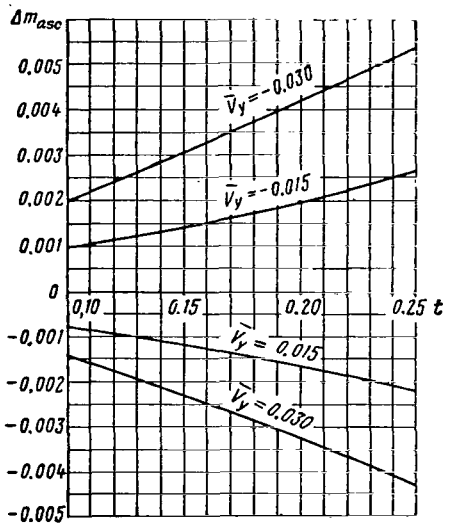

Fig.2.179 Graph of the Increment in Torque Coefficient of the Rotor in Ascent.

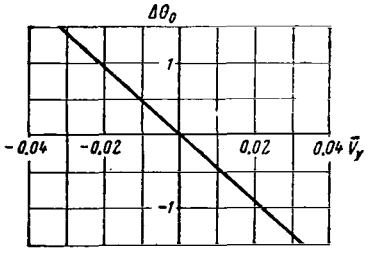

Fig.2.180 Graph of Increment in Rotor Pitch in Ascent.

The average profile drag coefficient of the blade $c_{xp_{av}}$ is determined by the profile polar at the section $\bar{r} = 0.7$, for an average lift coefficient c_{y_0}:

$$c_{y_0} \approx 3t. \qquad (8.29)$$

The coefficient P which depends on the blade shape, its solidity, and on the coefficient t can be taken as approximately equal to unity for a rectangular blade and for a trapezoidal blade with taper $\eta = 3$, $p = 0.91$ (see Table 2.5).

During a vertical ascent or descent, the magnitude of the induced velocity of the rotor and thus also m_{ind} will vary. Therefore, to determine m_t at $\bar{V}_y \neq 0$, it is not possible to add the term $t\bar{V}_y$ to m_t in hovering flight without considering the variation in m_{ind}. The graph of the increase in torque coefficient of a rotor during ascent Δm_{asc} as a function of $\bar{V}_y$ and t has been constructed for use in approximate calculations. This graph, shown in Fig.2.179, is obtained from results of calculations made by the momentum theory. The graph of the pitch increment $\Delta\theta_0$ during climb is given in Fig.2.180.

The approximate expressions for determining Δm_{asc} and $\Delta\theta_0$ can be obtained from the following considerations. During an ascent at low $\bar{V}_y$ the average induced velocity, according to the momentum theory (Ref.2), is equal to (recalling that, with our adopted rule of signs, $\bar{V}_y < 0$ in ascent) /275

$$\bar{v}_{asc} = \frac{\bar{V}_y}{2} + \frac{1}{2}\sqrt{\bar{V}_y^2 + \frac{C_T}{B^2}} \approx \frac{V_y}{2} + \frac{1}{2}\sqrt{\frac{C_T}{B^2}} = \frac{\bar{V}_y}{2} + \bar{v}_{hov}.$$

Consequently, in a climb m_t and θ_0 change by an amount of

$$\Delta m_{asc} = m_{ind_{asc}} - m_{ind_{hov}} - t\bar{V}_y = t(\bar{v}_{asc} - \bar{v}_{hov}) - t\bar{V}_y = -t\frac{\bar{V}_y}{2};$$

$$\Delta\theta_0 = \frac{\Delta V_1}{(\omega r)_{av}} = \frac{(\bar{v}_{asc} - \bar{V}_y) - \bar{v}_{hov}}{\bar{r}_{av}} = -\frac{\bar{V}_y}{2 \cdot 0.7} = -0.715\bar{V}_y$$

or

$$\Delta\theta_0^0 = -41\bar{V}_y.$$

The Δm_{asc} calculated by the approximation formula is somewhat smaller than in Fig.2.179.

Thus, the final expression for an approximate determination of the rotor torque coefficient as a function of the thrust coefficient and relative vertical speed has the form

$$m_t = \frac{\Phi}{2B^3}\sqrt{\sigma}\,t^{3/2} + \frac{c_{x p_{av}}}{4}P + \Delta m_{co} + \Delta m_{asc}. \qquad (8.30)$$

4. Conversion of Aerodynamic Characteristics on Variation in the Rotor Solidity Ratio

To determine the aerodynamic characteristics of a rotor in hovering flight, the method of conversion of characteristics can be used. This method should be employed if reliable characteristics of another rotor, close in relative geometric characteristics, are available.

The method of conversion of characteristics in flight regimes with forward speed, presented in Section 6, is based on a determination of the angle of attack of the rotor at which the velocity polygons, angles of attack of the sections, and elementary force are retained for a rotor with another σ in all blade sections, i.e., when there is similarity of regimes. In hovering, there are no similar regimes for rotors with different σ; therefore, the method of conversion of characteristics is based on the assumption that, at an identical thrust coefficient t, the induced power coefficient in conformity with eq.(8.25) is proportional to $\frac{\sqrt{\sigma}}{B^3}$ and the profile power coefficient is identical.

Thus, if the torque coefficient of the rotor of a solidity ratio σ_1 - m_{t_1} is known, then for a blade of a solidity ratio σ_2 the coefficient m_{t_2} for the same value of the thrust coefficient is determined by the formula

$$\begin{aligned} m_{t_2} &= m_{ind_1}\left(\frac{B_1}{B_2}\right)^3\sqrt{\frac{\sigma_2}{\sigma_1}} + m_{pr_1} = \\ &= (m_{t_1} - m_{pr_1})\left(\frac{B_1}{B_2}\right)^3\sqrt{\frac{\sigma_2}{\sigma_1}} + m_{pr_1}. \end{aligned} \qquad (8.31)$$

The values of m_{pr} and B are found from eqs.(8.28) and (8.12).

At an identical value of t for rotors with different σ, the angle of /276

attack of the blade sections should be practically the same; consequently, the rotor pitch varies by a quantity $\Delta\theta_0$ proportional to the difference of the average induced velocities.

We obtain the formula for determining $\Delta\theta_0$:

$$t_2 - t_1 = 0 \simeq \int_0^B \Delta a_1 \bar{U}^2 \, d\bar{r} = \int_0^B \left(\Delta\theta_0 - \frac{\Delta\bar{v}}{\bar{r}}\right)\bar{r}^2 \, d\bar{r};$$
$$\Delta\theta_0 \simeq \frac{3}{2B}\Delta\bar{v}_{av} \approx \frac{3}{4B^2}\sqrt{\bar{t}}\left(\sqrt{\sigma_2} - \sqrt{\sigma_1}\right). \tag{8.32}$$

Thus, the pitch of a rotor with a solidity ratio σ_2 is equal to

$$\theta_{0_2} = \theta_{0_1} + \frac{3}{4B^2}\sqrt{\bar{t}}\left(\sqrt{\sigma_2} - \sqrt{\sigma_1}\right). \tag{8.33}$$

5. Determination of Optimal Aerodynamic Parameters of a Rotor with Consideration of the Dependence of Characteristics on M_0

To select the optimal parameters of a rotor, it is convenient to use eq.(8.34) which correlates the rotor thrust, its diameter, and required power

$$T = (33.25\sqrt{\Delta}\eta_0 DN)^{2/3}. \tag{8.34}$$

Equation (8.34) includes the relative efficiency of the rotor η_0, characterizing the relation between the power of an ideal rotor and the actual power consumed by the rotor*:

$$\eta_0 = \frac{N_{id.}}{N} = \frac{C_T^{3/2}}{2\bar{m}_t} = \frac{t^{3/2}\sqrt{\sigma}}{2m_t}. \tag{8.35}$$

It is obvious that, at given N, D, and Δ (i.e., flight altitude), the greatest thrust of the rotor is achieved at a maximum value of η_0; therefore, the designer will strive to approach a maximum η_0. Usually, the graphs of η_0 are constructed as a function of t and σ for a value of M_0 corresponding to the average proposed values of the peripheral speed of the rotor (Fig.2.181). From this graph we select a reference point (i.e., values of t, σ) with a sufficiently large η_0. We can arbitrarily select the reference point regardless of the rotor diameter, since an inexact agreement of the value of M_0 obtained at the chosen t, σ, D with that for which the graph of η_0 was constructed, is considered permissible.

---

* The power of an ideal rotor is equal to the minimum possible power losses of a rotor which are directly related with the generation of force, while the actual power is equal to the sum of all power losses.

For a more accurate calculation (with consideration of the effect of M_0 on η_0), the use of graphs $\eta_0 = f(t, \sigma)$ constructed for different M_0 is inconvenient, since we cannot arbitrarily select a reference point on these graphs. Actually, eq.(8.15) can be represented in the form

$$\frac{75}{{}^1/_2 \varrho a^3} \frac{N}{F} = m_t \sigma M_0^3. \tag{8.36}$$

Consequently, at given N, D, H the product $m_t\sigma M_0^3$ should have a definite value, and on each curve of η_0 corresponding to definite values of σ, M_0, only one point (one m_t and, respectively, one t) satisfies eq.(8.36). Two broken curves are plotted in Fig.2.181 for two values of the product $m_t\sigma M_0^3$: the smaller value of $m_t\sigma M_0^3$ pertains to the larger rotor diameter. These curves show that, at /277
given rotor diameter and M_0, only the maximum η_0 on the broken curve can be selected and that it is impossible to realize larger values of η_0. Upon an increase in rotor diameter (lower broken curve) the maximum possible values of η_0 are still smaller and it is not apparent from the graph whether the rotor thrust determined by the product $\eta_0 D$ increases. Therefore, the graphs of η_0, constructed as a function of t, σ, and M_0 (or reconstructed as a function of $m_t\sigma M_0^3$, σ, M_0), are not suitable for selecting the optimal parameters of a rotor, especially if the rotor diameter varies.

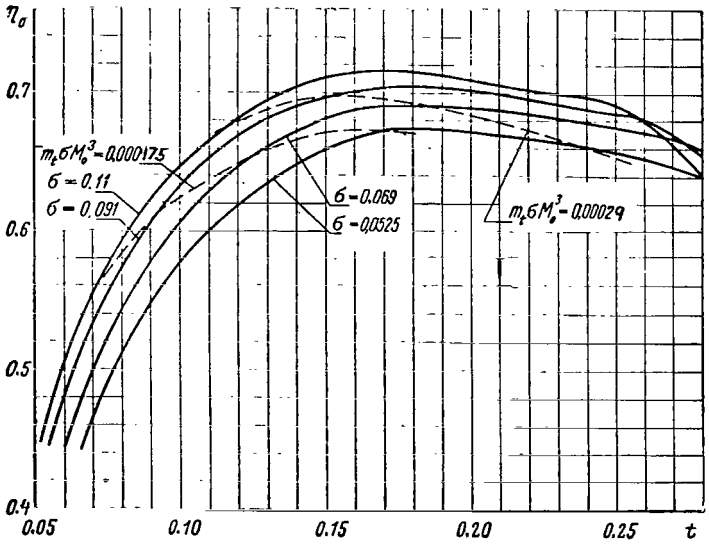

Fig.2.181 Relative Efficiency of Rotor as a Function of t and σ (M_0 = 0.65).

We will find a more convenient form of the graphs for selecting the optimal parameters of a rotor with consideration of the dependence of the characteristics on M_0. For this, we make use of eqs.(8.36) and (8.37); the latter is obtained from eqs.(8.15) and (8.17):

$$\frac{T}{N}\,\frac{a}{75}=\frac{t}{m_t M_0}. \qquad (8.37)$$

We can show that the ratio $\frac{t}{m_t M_0}$ on the right-hand side of eq.(8.37) is proportional to $(\eta_0 D)^{2/3}$. Actually, from eq.(8.36) we determine the rotor diameter D:

$$D=\sqrt{\frac{75N}{{}^1/_2\varrho a^3\,\frac{\pi}{4}\,m_t\sigma M_0^3}}=\frac{\text{const}\sqrt{N}}{(m_t\sigma)^{1/2}M_0^{3/2}},$$

and the product $\eta_0 D$:

$$\eta_0 D=\frac{(t\sigma)^{3/2}}{2m_t\sigma}\,\frac{\text{const}\sqrt{N}}{(m_t\sigma)^{1/2}M_0^{3/2}}=\text{const}\sqrt{N}\left(\frac{t}{m_t M_0}\right)^{3/2}.$$

It is obvious from this expression, just as from eq.(8.37), that at given N and H the maximum thrust of the rotor T_{max} is achieved at rotor parameters at which $\frac{t}{m_t M_0}$ has a maximum. Therefore, to find the optimal rotor parameters we must construct graphs of the dependence of the ratio $\frac{t}{m_t M_0}$ /278

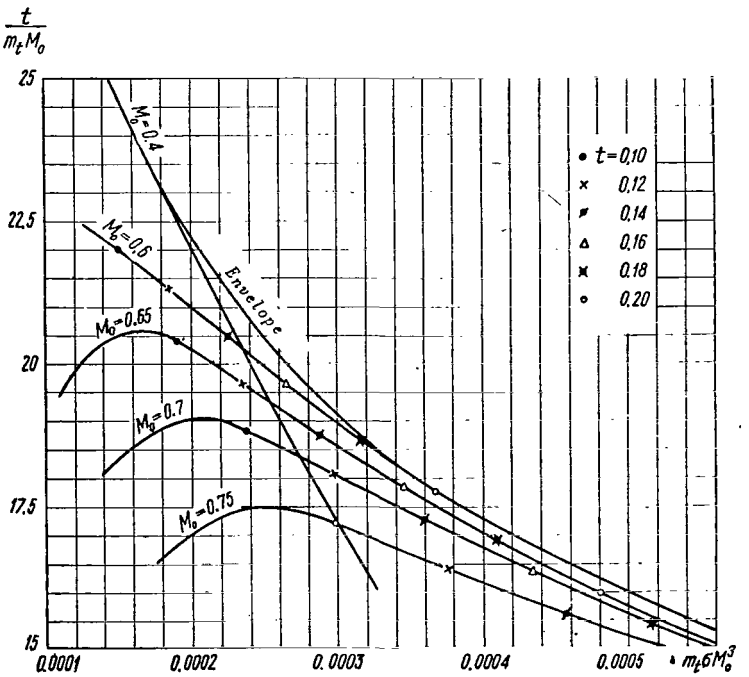

Fig.2.182 Ratio $\frac{t}{m_t M_0}$ as a Function of $m_t\sigma M_0^3$ at σ = 0.091.

on $m_t\sigma M_0^3$. These dependencies are shown at σ = const in Fig.2.182 and at M_0 = = const in Fig.2.183. The maximum values of $\frac{t}{m_t M_0}$ lie on the envelopes of these curves.

We see from Figs.2.182 and 2.183 that, at given D (i.e., $m_t\sigma M_0$ = const) and σ, there exists an optimal value of M_0' and at given D and ωR there exists σ_{opt}. If only D is given, then it follows from these graphs for a number of values of σ and M_0 that the rotor thrust increases with increasing σ and decreasing ωR (in the range of larger σ than that shown in Fig.2.183, it may happen that, if only D is given, also σ_{opt} and M_{0opt} exist). An increase in rotor diameter corresponds to a decrease in $m_t\sigma M_0^3$ and this, as we see from the graphs, will lead to an increase in rotor thrust, especially on a decrease in σ and M_0.

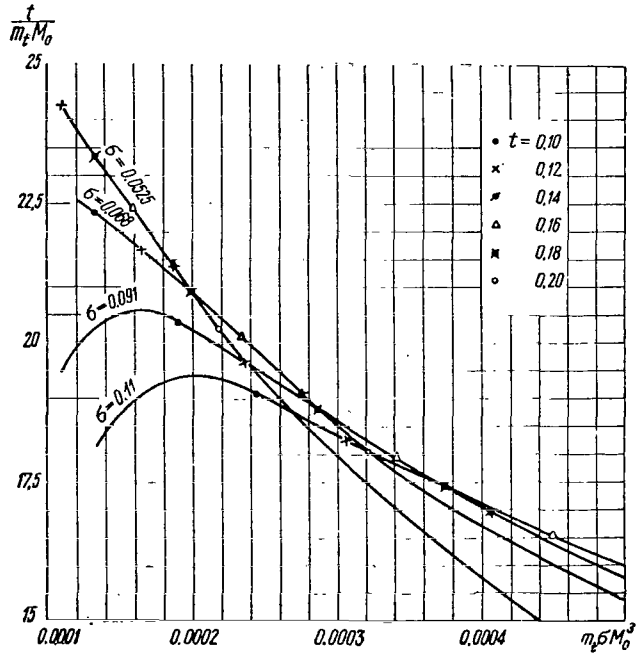

Fig.2.183 Ratio $\frac{t}{m_t M_0}$ as a Function of $m_t\sigma M_0^3$ at $M_0 = 0.65$.

All curves are closely spaced near the optimum of σ and M_0, so that any deviation from optimum values slightly changes the rotor thrust. For example, Fig.2.182 shows that, at $m_t\sigma M_0^3 = 0.0003$ and $\sigma = 0.091$, we have $\left(\frac{t}{m_t M_0}\right)_{max}$ = = 19.1 for $M_{0opt} \approx 0.55$ and $t_{opt} \approx 0.21$, whereas with a 10% increase in rotor rpm, i.e., for $M_0 = 0.6$ and $t \approx 0.176$ we have $\frac{t}{m_t M_0} = 18.8$; consequently, the /279

rotor thrust decreases by 1.6%. We find from Fig.2.183 that, at the same value of $m_t\sigma M_0^3$ and $M_0 = 0.65$, we have $\left(\frac{t}{m_t M_0}\right)_{opt} = 18.65$ for $\sigma_{opt} = 0.08$, $t_{opt} = 0.165$, whereas at $\sigma = 0.091$ and $t = 0.145$, we have $\frac{t}{m_t M_0} = 18.5$, i.e., the thrust diminishes by 0.8%.

To take account of the variation in the tail rotor losses upon a change in the parameters of the main rotor, the graphs of single-rotor helicopters should be constructed in the form of the dependence

$$\frac{t}{m_t(1+C\sqrt{m_t\sigma})M_0} \text{ from } m_t\sigma M_0^3(1+C\sqrt{m_t\sigma}),$$

where the coefficient reads

$$C=\frac{k_{bl}^{3/2}}{2\eta_{0_{tail}}}\frac{\left(\frac{D}{D_{tail}}\right)^{5/2}}{\left(1+\frac{D}{D_{tail}}\right)^{3/2}}.$$

The coefficient k_{bl}, which takes into account blanketing of the tail rotor by the tail boom, is taken to be equal to 1.03 - 1.06.

CHAPTER III

/280

AERODYNAMIC DESIGN OF A HELICOPTER

Section 1. Basic Equations for Aerodynamic Design of a Helicopter

1. Aerodynamic Design Principle of a Helicopter

The principle of aerodynamic design of a helicopter is calculating stable rectilinear flight regimes in a vertical plane in order to determine engine power, fuel consumption, angles of attack, setting angles, and other characteristics of a rotor during flight at different speeds and all possible altitudes. These data permit determining vertical speeds, range, and duration under different flying conditions, and also represent necessary material for studying the equilibrium conditions of moments (balancing and stability of the helicopter) and for stress analyses.

Of primary interest is the determination of the performance data of a helicopter, i.e., the limiting flight regimes: maximum and minimum horizontal flying speeds at all altitudes, ceiling, maximum rate of climb and range, minimum power of horizontal flight, and vertical rate of descent on engine failure.

2. Equation of Motion of a Helicopter

The flight characteristics of a helicopter are determined by solving equations of stable rectilinear motion of the craft in a vertical plane.

The equation expressing the sum of forces, equated to zero and directed along the flight path as well as along a normal to it, as shown in Fig.3.1, has the form

$$G \sin \theta_{fl\rho} + Q_{par} = -X; \tag{1.1}$$

$$G \cos \theta_{fl\rho} = Y, \tag{1.2}$$

where

X and Y = components of the resultant aerodynamic forces of the rotor directed along the flight path and along a normal to it; at $X < 0$, the rotor creates a propulsive force while at $X > 0$ it produces drag;

Q_{par} = parasite drag of the nonlifting parts of the helicopter;

$\theta_{fl.p}$ = angle of flight path of the helicopter to the horizontal.

It follows from Fig.3.1 and eqs.(1.1) and (1.2) that, in horizontal flight regimes ($\theta_{fl.p} = 0$), the lift of the rotor balances its drag. In flight /281
regimes along an inclined path, the propulsive force of the rotor compensates the drag plus the resistance to motion formed by the weight component directed

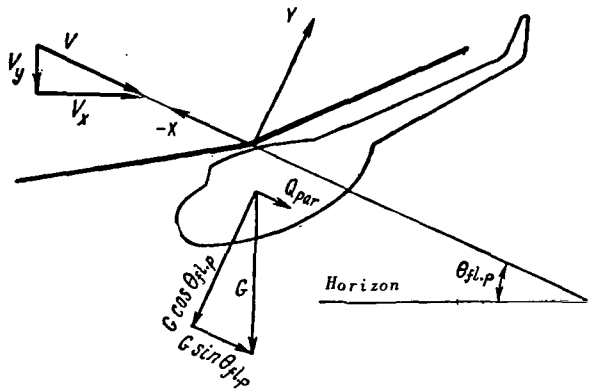

Fig.3.1 Forces Acting on a Helicopter in Steady Rectilinear Flight.

along the path, $G \sin \theta_{fl.p}$.

To determine the engine power in different flight regimes and to find regimes in which the maximum power of the engines should be utilized, the equations of motion must be supplemented by an equation expressing the condition of equality of the power absorbed by the rotor N_{rot} and the engine power transmitted to the rotor shaft

$$N_{rot} = N\xi. \tag{1.3}$$

To reduce eqs.(1.1) - (1.3) to a dimensionless form, let us refer the forces to the product $\frac{1}{2}\rho(\omega R)^2 \sigma F$, and the power to $\frac{1}{2}\rho(\omega R)^3 \sigma F$:

$$\frac{G}{\frac{1}{2}\rho(\omega R)^2 \sigma F} \sin\theta_{fl\rho} + \bar{c}_x \frac{\bar{V}^2}{\sigma} = -t_x; \tag{1.4}$$

$$\frac{G}{\frac{1}{2}\rho(\omega R)^2 \sigma F} \cos\theta_{fl\rho} = t_y; \tag{1.5}$$

$$\frac{75N\xi}{\frac{1}{2}\rho(\omega R)^3 \sigma F} = m_t. \tag{1.6}$$

Equation (1.4) can be then represented as

$$t_y \tan\theta_{fl\rho} + \bar{c}_x \frac{\bar{V}^2}{\sigma} = -t_x; \tag{1.7}$$

or

$$t_{y_{h.f}} \sin\theta_{fl\rho} + \bar{c}_x \frac{\bar{V}^2}{\sigma} = -t_x. \tag{1.8}$$

In eq.(1.8) and in what follows, the subscript "h.f." denotes quantities referring to horizontal flight.

The given quantities in the aerodynamic calculation are as follows: /282

flying weight of the helicopter G;
geometric rotor characteristics (twist, planform), solidity ratio σ and radius R;
peripheral rotor speed ωR;
air density ρ and velocity of sound "a" at design flight altitude;
drag coefficient of nonlifting parts of the helicopter $\bar{c}_x = \frac{\Sigma c_x S}{F}$;
engine characteristics: power N = N(H) and hourly fuel consumption G_{hr} =

$= G(N, H)$;
engine power utilization factor ξ.

In level flight ($\theta_{fl.p} = 0$), the number of given quantities is sufficient for determining the rotor lift coefficient by eq.(1.5). The problem of calculating level-flight regimes of a helicopter consists in determining, by means of eq.(1.7) and for different velocities $\overline{V}$, the required coefficient of propulsive force $t_{x_{h.f}}$, finding the values of $m_{t_{h.f}}$ from the aerodynamic rotor characteristics at known M_0, $t_{y_{h.f}}$ and $t_{x_{h.f}}$, and determining $N_{h.f}$ from eq.(1.6).

In maximum nonlevel flight regimes, m_t is known ($N = N_{max}$ in climbing and $N = 0$ in autorotation); the problem amounts to determining the values of t_x and t_y satisfying eqs.(1.5) and (1.7) from the rotor aerodynamic characteristics at different flying speeds at known M_0 and m_t; the flight-path angle $\theta_{fl.p}$ is obtained simultaneously.

3. Various Methods of Determining Aerodynamic Rotor Characteristics and Methods of Aerodynamic Design

As indicated in Subsection 2, the aerodynamic rotor characteristics, namely the interrelation of the four dimensionless rotor coefficients $\overline{V}$, t_y, t_{max}, m_t for a range of M_0 corresponding to the rpm and flight altitudes of the helicopter, should be known in the aerodynamic design.

In certain methods of aerodynamic design, the rotor characteristics are determined by an approximate theory in order to obtain simple formulas permitting a direct calculation of the helicopter performance data. Because of the approximate nature of these calculation methods, they are rarely used at present.

To increase the accuracy of aerodynamic calculations, it is expedient to separate the problems of determining the aerodynamic rotor characteristics from those of determining the helicopter performance data. With this approach, the aerodynamic rotor characteristics can be found beforehand and plotted on special graphs. This eliminates the need for introducing simplifications into the calculation of aerodynamic rotor characteristics. In the Mil'-Yaroshenko method, presented in Section 2, the following form of graphs is adopted: The angle of inclination of the resultant aerodynamic force of the rotor to the normal of the flight path δ, the torque coefficient m_t, and the angle of attack α are plotted as a function of the pitch φ for a series of values of the thrust coefficient t and the characteristic of the flight regime μ (see Fig.2.15).

A further development of the Mil'-Yaroshenko method resulted in a more convenient form of the graphs: dependence of the coefficient of propulsive rotor force t_x on m_t for various values of the lift coefficient t_y at $\overline{V} = \text{const}$ and $M_0 = \text{const}$. The graphs also give curves of constant values for the rotor angles of attack by means of which the latter can be defined (the angle of attack must be known for refining the parasite drag of the helicopter and for calculating a wing-type helicopter or other composites). /283

The graphs for the aerodynamic rotor characteristics can be plotted from

experiment or constructed from any rotor theory; the methods of determining the aerodynamic characteristics are presented in Sections 2, 4, 5, and 6 of Chapt.II.

The method of aerodynamic design in which graphs of the aerodynamic rotor characteristics are used, is presented in a very general form in Section 3.

It was shown in Section 7 of Chapter II that the aerodynamic rotor characteristics can be determined by using the concepts of performance and propulsive efficiency factor of the rotor. The method of aerodynamic design based on the use of these concepts is described in Section 4.

In many methods of aerodynamic design, the expression

$$m_t = \frac{1}{B^2} t_y \bar{v}_y - \frac{1}{B^2} t_x (\bar{V} - \bar{v}_x) + m_{pr} \approx \frac{t_y^2 \sigma}{4B^4 \bar{V}} - t_x \bar{V} + m_{pr},$$

derived in Section 3 of Chapter II, is used.

These represent rather simple but approximate calculation methods. One such method is described in Section 5.

4. Calculation of Composite and Multirotor Craft

For the aerodynamic design of composite and multirotor craft by the methods described in Sections 2 and 3, we will construct graphs of the total coefficients of the lifting and advancing systems of a composite craft: t_{x_Σ} (or δ_Σ) as a function of m_{t_Σ} for t_{y_Σ} = const. The total coefficients are found experimentally or can be obtained by calculation with respect to known aerodynamic characteristics of isolated elements of the lifting system of the craft. The design formulas for determining the total coefficients are given below, for certain special cases.

These formulas are also used in aerodynamic calculations based on the methods described in Sections 4 and 5, in which the lift distribution between individual elements of the lifting system of the craft must be known. One of the possible methods of determining the lift distribution between rotors and wing is given in Section 4. In this case, the formulas derived below are used for determining the total coefficients of the lifting system of the craft.

Single-rotor helicopter with wing. The summary coefficients t_{y_Σ}, t_{x_Σ}, and m_{t_Σ} are determined by the following expressions (Fig.3.2):

$$\left.\begin{aligned} t_{y_\Sigma} &= (t_y \cos \Delta\alpha_{rot} - t_x \sin \Delta\alpha_{rot}) + \frac{S_w}{F} \frac{\bar{V}^2}{\sigma} \times \\ &\times (c_{y_w} \cos \Delta\alpha_w - c_{x_w} \sin \Delta\alpha_w), \\ t_{x_\Sigma} &= (t_x \cos \Delta\alpha_{rot} + t_y \sin \Delta\alpha_{rot}) + \frac{S_w}{F} \frac{\bar{V}^2}{\sigma} \times \end{aligned}\right\} \quad (1.9)$$

$$\times (c_{x_w} \cos \Delta\alpha_w + c_{y_w} \sin \Delta\alpha_w),$$
$$m_{t_\Sigma} = m_t$$

or, approximately, by

/284

$$\left.\begin{aligned} t_{y_\Sigma} &= t_y + \frac{\bar{V}^2}{a} \frac{S_w}{F} c_{y_w}, \\ t_{x_\Sigma} &= (t_x + t_y \Delta\alpha_{rot}) + \frac{S_w}{F} \frac{\bar{V}^2}{a} (c_{x_w} + c_{y_w} \Delta\alpha_w). \end{aligned}\right\} \quad (1.9')$$

Figure 3.2 indicates that the angle between the plane of rotation of the rotor and the path velocity (or velocity of undisturbed flow), which we will call the angle of attack of the helicopter α_h, is equal to

$$\alpha_h = \alpha + \Delta\alpha_{rot}.$$

The angle of attack of the wing is correlated with the angle of attack of the rotor by

$$\alpha_w = \alpha_h - \Delta\alpha_w + \varepsilon_w = \alpha + \Delta\alpha_{rot} - \Delta\alpha_w + \varepsilon_w. \quad (1.10)$$

In these expressions we denote:

t_y, t_x, m_t, α, c_{y_w}, c_{x_w}, α_w = characteristics of isolated rotor and wing;
$\Delta\alpha_{rot}$ = mean downwash angle in the rotor region, induced by the wing;
$\Delta\alpha_w$ = mean downwash angle in the wing region, induced by the rotor;
S_w and ε_w = area and wing setting angle.

The slipstreams of rotor and wing are denoted by the vectors V′ and V″ in Fig.3.2. Considering that the flight velocity is many times greater than the additional vertical velocities of interference Δv, the velocities V′ and V″ are equal to

$$\left.\begin{aligned} V' &= \sqrt{V^2 + \Delta v_{rot}^2} \approx V; \\ V'' &= \sqrt{V^2 + \Delta v_w^2} \approx V. \end{aligned}\right\} \quad (1.11)$$

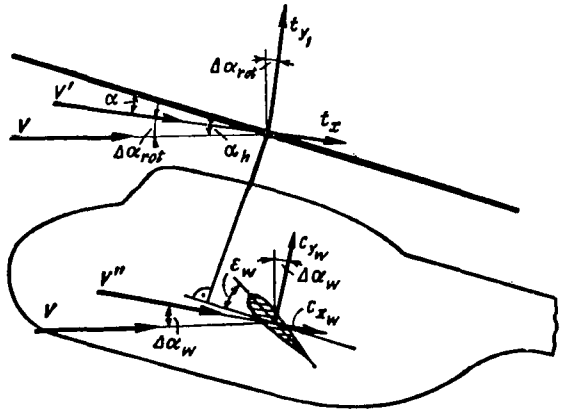

Fig.3.2 Velocities, Angles of Attack, and Forces of a Single-Rotor Helicopter with Wing.

The sequence of determining the total coefficients at known S_w and ε_w is as follows:

For selected $\bar{V}$, M_0, and t_{y_Σ}, assign c_{y_w} and find t_y from the first equation in the system (1.9′).

From the wing characteristic

$c_{y_w} = f(\alpha_w)$, find α_w.

Determine the downwash angles $\Delta\alpha_{r\,o\,t}$ and $\Delta\alpha_w$ (see below, Subsect.5).

From eq.(1.10), determine the angle of attack of the rotor and from the characteristics of the isolated rotor, find t_x and m_t. /285

Note that eq.(1.10) includes the angle of attack of the plane of rotation which, at $\bar{\bar{\varphi}}_1 \neq 0$, differs from the equivalent angle of attack (see Chapt.II, Sect.2).

Calculate t_{x_Σ}.

After carrying out such calculations for several values of c_{y_w}, find the dependence of t_{x_Σ} on m_t for given values of $\bar{V}$, M_0, and t_{y_Σ}. Perform these calculations for a series of values of t_{y_Σ}, $\bar{V}$, M_0, and then construct graphs of the aerodynamic characteristics of the lifting system of the craft.

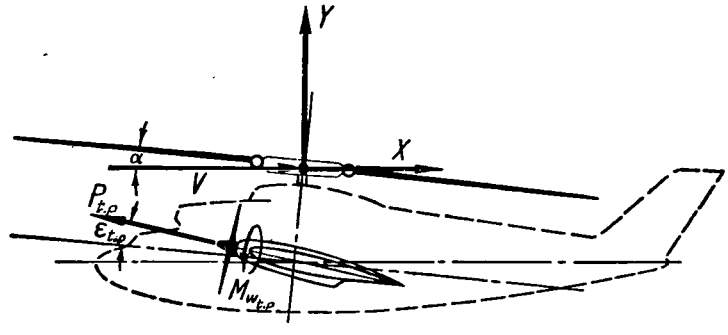

Fig.3.3 Forces Created by Rotor and Tractor Propeller.

It is obvious that, if the lift of the fuselage (nonlifting components) of the helicopter or a variation in its drag relative to the angles of attack must be taken into consideration, then the characteristics of the lifting system together with the fuselage of the helicopter can be determined in the same sequence.

Helicopter with tractor propellers. The additions to the total coefficients of the lifting system are expressed by the following formulas, which are evident from Fig.3.3 (interference of the tractor propellers with other elements of the system is disregarded):

$$\left.\begin{aligned} \Delta t_y &= \frac{P_{t.p}}{\frac{1}{2}\varrho\sigma(\omega R)^2\pi R^2}\sin(\alpha+\varepsilon_{t.p}) \approx 0, \\ \Delta t_x &= -\frac{P_{t.p}}{\frac{1}{2}\varrho\sigma(\omega R)^2\pi R^2}\cos(\alpha+\varepsilon_{t.p}) \approx -\frac{P_{t.p}}{\frac{1}{2}\varrho\sigma(\omega R)^2\pi R^2}, \end{aligned}\right\} \qquad (1.12)$$

$$\Delta m_t = \frac{75 N_{t.p} \frac{\xi}{\xi_{t.p}}}{\frac{1}{2} \varrho \sigma (\omega R)^3 \pi R^2}.$$

In these expressions $P_{t.p}$ and $N_{t.p}$ are the thrust and power of the tractor propeller, correlated by the ratio $75\ N_{t.p} = \frac{P_{t.p} V}{N_{t.p}}$.

When using a cruise jet engine with a thrust of $P_{t.p}$ on a helicopter, Δt_y and Δt_x will be determined by eqs.(1.12), and we will have $\Delta m_t = 0$.

Two-rotor helicopter of side-by-side configuration with a wing. For this /286 helicopter t_{y_Σ}, t_{x_Σ}, and m_{t_Σ} are determined by the following expressions:

$$\left.\begin{aligned} t_{y_\Sigma} &= 2(t_y \cos \Delta\alpha_{rot} - t_x \sin \Delta\alpha_{rot}) + \frac{S_w}{F} \frac{\bar{V}^2}{\sigma} \times \\ &\times (c_{y_w} \cos \Delta\alpha_w - c_{x_w} \sin \Delta\alpha_w), \\ t_{x_\Sigma} &= 2(t_x \cos \Delta\alpha_{rot} + t_y \sin \Delta\alpha_{rot}) + \frac{S_w}{F} \frac{\bar{V}^2}{\sigma} \times \\ &\times (c_{x_w} \cos \Delta\alpha_w + c_{y_w} \sin \Delta\alpha_w), \\ m_{t_\Sigma} &= 2m_t, \\ \alpha_w &= \alpha + \Delta\alpha_{rot} - \Delta\alpha_w + \varepsilon_w. \end{aligned}\right\} \qquad (1.13)$$

Unlike eqs.(1.9), here $\Delta\alpha_{rot}$ and $\Delta\alpha_w$ are the total angles of downwash induced both by mutual interference of the rotors and interference between rotors and wing.

The sequence of calculating the total coefficients is the same as for a single-rotor helicopter.

Equations (1.12) are added to eqs.(1.13) if tractor propellers are present.

Two-rotor helicopter of fore-and-aft configuration. Disregarding downwash in the region of the front rotor caused by the tail rotor, we can obtain the following relations (Fig.3.4):

$$\left.\begin{aligned} t_{y_\Sigma} &= t_{y_1} + (t_{y_2} \cos \Delta\alpha_{rot_2} - t_{x_2} \sin \Delta\alpha_{rot_2}) \approx t_{y_1} + t_{y_2}, \\ t_{x_\Sigma} &= t_{x_1} + (t_{x_2} \cos \Delta\alpha_{rot_2} + t_{y_2} \sin \Delta\alpha_{rot_2}) \approx t_{x_1} + \\ &+ (t_{x_2} + t_{y_2} \Delta\alpha_{rot_2}), \\ m_{t_\Sigma} &= m_{t_1} + m_{t_2}, \\ \alpha_2 &= \alpha_1 - \Delta\alpha_{rot_2} + \Delta\varepsilon_{rot_2}, \\ \bar{V}_1 &\approx \bar{V}_2. \end{aligned}\right\} \qquad (1.14)$$

In these expressions, we denote:

$\Delta\alpha_{rot_2}$ = mean downwash angle in the region of the tail rotor, induced by the front rotor;

$\Delta\varepsilon_{rot_e}$ = effective angle of advance of the tail rotor relative to the front rotor (with consideration of the difference in deflection of the automatic rotor pitch control):

$$\Delta\varepsilon_{rot_e} = \Delta\varepsilon_{rot} - (D_1\varkappa)_1 + (D_1\varkappa)_2. \qquad (1.15)$$

The subscript "1" denotes characteristics of the front rotor and the subscript "2", of the tail rotor. /287

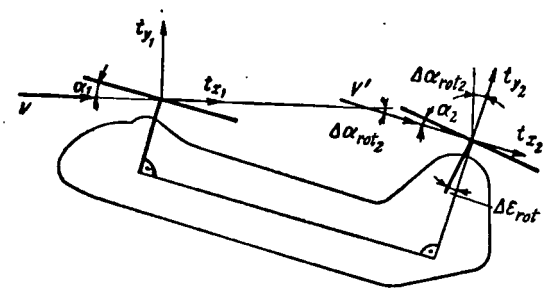

Fig.3.4 Velocities, Angles of Attack, and Forces for a Helicopter of Side-by-Side Configuration.

The performance data of a helicopter of fore-and-aft configuration can be uniquely determined if and only if the conditions of joint operation of front and tail rotors are known. Usually, such a condition is the relation between the thrust of the rotors determined by longitudinal balancing of the helicopter. Knowing this relation for selected $\overline{V}$, M_0, and t_{y_Σ}, it is possible to find t_{y_1} and t_{y_2} from the first equation of the system (1.14). After assigning α_1 and calculating $\Delta\alpha_{rot_2}$, we can determine α_2. From the characteristics of the isolated rotor, knowing $\overline{V}$, M_0, t_y, and α we then find t_x and m_t for both rotors. Furthermore, t_{x_Σ} and m_{t_Σ} are calculated and graphs of the aerodynamic characteristics of the lifting system are plotted.

5. Induction Coefficients of Two-Rotor Helicopters and Helicopters with a Wing

Determination of the lift and drag of the system of lifting elements is a complex problem for whose solution the induced velocity and loads per unit length in each section of the lifting elements should be found, with consideration of the effect of all vortices entering the system. When using high-speed computers, solution of this problem is possible in certain cases.

However, usually in aerodynamic designing, the computation is limited to determining the average downwash angles $\Delta\alpha$ of each of the elements of the lifting system. As shown in Subsection 4, the downwash angles permit finding the projection of forces of all elements of the lifting system onto the direction of motion and normal to it.

Equations (1.9) - (1.13) show that, for $\Delta\alpha > 0$ (i.e., for the vertical induced velocity component caused by other elements of the lifting system, Δv is directed from the top downward), the drag of the craft increases by an amount

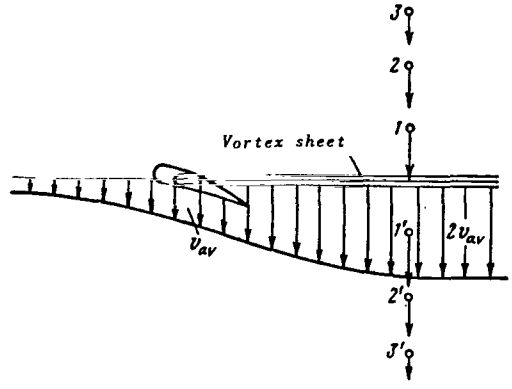

Fig.3.5 Induced Velocity Distribution of Wing (Points 1, 2, 3, 1′, 2′, 3′ are above and below the Vortex Sheet).

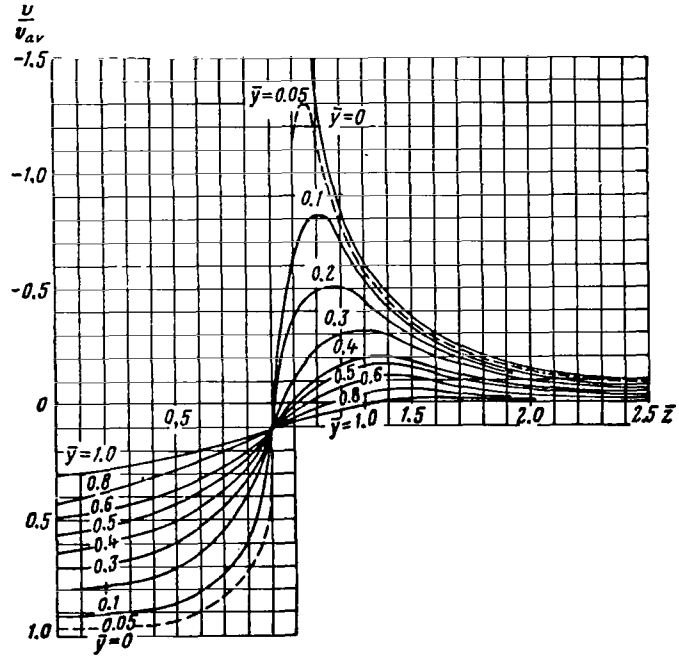

Fig.3.6 Induced Velocity Distribution along Wing Span $\bar{z}$ at Different Distances from Vortex Sheet $\bar{y}$.

$Y\Delta\alpha$ while, at $\Delta\alpha < 0$, the drag of the craft decreases.

The downwash angle of the i-th element of the lifting system induced by the n-th element is determined by the expression

$$\Delta\alpha_i = \frac{\Delta v_i}{V}, \tag{1.16}$$

where Δv_i is the vertical induced velocity component created by the n-th element at the focus of the i-th element, averaged over the area of the i-th element; Δv_i is proportional to the mean induced velocity in the plane of rotation of the n-th element:

$$\Delta\bar{v}_i = \varkappa_i \bar{v}_{a v_n} = \varkappa_i \frac{C_{Y_n}}{4B^2\bar{V}}. \tag{1.17}$$

The proportionality factor $\varkappa_i$ is called the induction coefficient. This depends on the mutual arrangement and dimensions of the i-th and n-th elements of the lifting system.

Let us recall how the induced velocity of the wing (or rotor) is distributed in space. At points downstream of the wing, the induced velocity increases and rather rapidly reaches double its initial value (Fig.3.5). An increase in induced rotor velocity will then take place within the rotor disk (Fig.2.3).

At points upstream of the wing, the induced velocity is virtually equal to zero, while it decreases at points above or below the vortex sheet (points 1, 1′, 2, 2′, 3, 3′ in Fig.3.5). In cross section, the induced velocity of the wing with an elliptic circulation distribution has the form shown in Fig.3.6: /289

Within the span of the wing or rotor $\left(\bar{z} = \frac{z}{l_w/2} < 1.0\right)$, the induced velocity is directed downward while at the periphery ($\bar{z} \geq 1.0$), it is directed upward.

Let us determine the magnitude of the induction coefficients.

The coefficients of mutual induction depend on the flight velocity ($\bar{V}$) and on the angle of attack of the rotors; our values of $\varkappa$ are averaged with respect to $\bar{V}$, approximate, and applicable to all flight regimes at $\bar{V} \geq 0.15$.

The rotors of a helicopter of side-by-side configuration, as is obvious from Fig.3.6, are located in the region where the induced velocities caused by the adjacent rotor are directed from the bottom up. In this configuration, the interference reduces the induced drag of the system. Here, the value of the mutual induction coefficients $\varkappa_{s.s}$ was taken from B.N.Yur'yev's book (Ref.2) to which corrections were applied for the fact that the induced velocities at azimuth $\psi = 90^\circ$ are greater than at azimuth $\psi = 270^\circ$. Therefore, the mutual induction coefficients depend on the direction of rotation of the rotors: When the azimuth $\psi = 90^\circ$ is between the rotors, these coefficients are approximately 25% higher than the mean values obtained elsewhere (Ref.2), while they are about 25% lower in another direction of rotation.

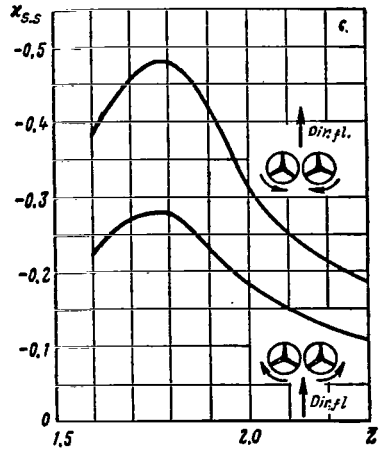

Fig.3.7 Coefficient of Mutual Induction of Rotors for Helicopters of Side-by-Side Configuration.

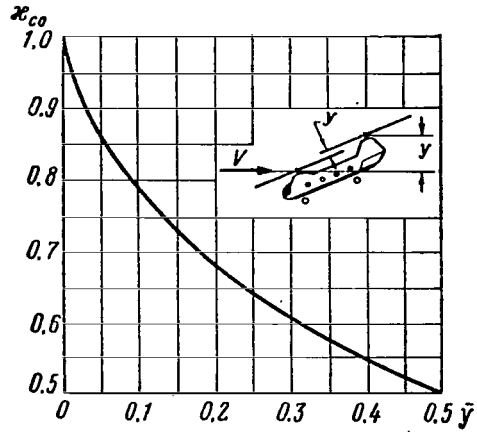

Fig.3.8 Coefficient of Mutual Induction of Rotors for Helicopters of Coaxial and Fore-and-Aft Configuration.

The graph of $\varkappa_{s.s}$ as a function of the distance between the rotor axes $\bar{z} = \frac{z}{R}$ is shown in Fig.3.7. It is obvious that the optimum distance between rotors, at which the least induced drag in forward flight occurs, is equal to $\bar{z} \approx 1.8$.

If, in helicopters of coaxial configuration, there is no vertical separation of the rotors, then the coefficient of mutual induction $\varkappa_{co}$ obviously will be equal to unity ($\Delta v = v_{av}$). When there is vertical separation, the induced velocity in the plane of the second rotor Δv will decrease ($\Delta v < v_{av}$) so that $\varkappa_{co} < 1$. The graph of $\varkappa_{co}$ as a function of the vertical separation of the rotors $y = \frac{\bar{y}}{R}$, taken from another paper (Ref.2), is shown in Fig.3.8.

According to the general theory of induction, the mean induced velocity of the system of lifting elements does not depend on their stagger in the direction of path velocity; consequently, for a helicopter of fore-and-aft configuration the mean magnitude of the additional induced velocity Δv is the same as for a coaxial helicopter (at equal $\bar{y}$). Since the tail rotor does not influence the front rotor, we have $\varkappa_{rot} = 0$; consequently, for the tail rotor located behind the front rotor, $\Delta v = 2\Delta v_{av}$ so that $\varkappa_{rot_2} = 2\varkappa_{co}$*. Thus, the mutual induction coefficients in helicopters of fore-and-aft configuration are also determined in accordance with Fig.3.8. /290

In terms of the general induction theory, a decrease in induced drag for

* In Chapter I, in eq.(3.22), we had $\varkappa = 2\varkappa_{co}$.

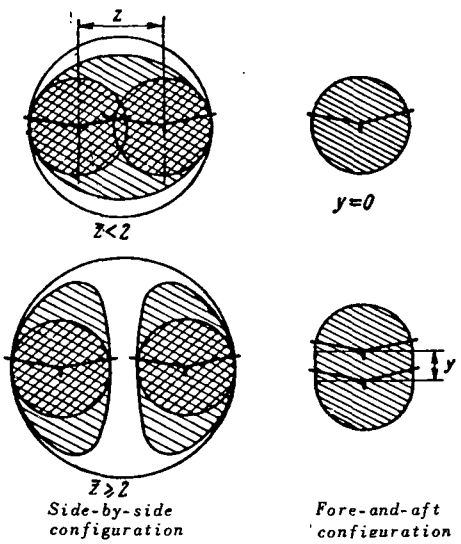

Fig.3.9 Effective Cross Section of Air Stream for Helicopters of Side-by-Side and Fore-and-Aft Configurations.

helicopters of side-by-side configuration ($\varkappa_{s.s} > 0$) and an increase in induced drag for helicopters of fore-and-aft and coaxial configurations ($\varkappa_{co} > 0$) is explained in the following manner: It is known that the induced drag of the system of lifting elements is directly proportional to the square of lift and inversely proportional to the mass of air participating in producing lift, or to the effective cross section of the air stream (see Fig.2.56). In the ideal case (uniform induced velocity distribution over the entire span), the effective cross section of the air stream is equal to a circumference whose diameter is equal to the span of the lifting system.

The effective stream cross section F_e for helicopters of side-by-side and fore-and-aft configurations is given in Fig.3.9. The sketch shows that, for the side-by-side helicopter, F_e is greater than the area of the two rotors ($\varkappa_{s.s} < 0$); at $\bar{z}_{s.s} > 2$, a gap effect appears and F_e decreases. In the fore-and-aft configuration without vertical separation of the rotors ($y = 0$), the effective stream cross section is the same as for a single rotor ($\varkappa_{co} = 1$); in the presence of vertical separation, F_e increases ($\varkappa_{co} < 1$).

Now let us examine the interference between rotor and wing for single-rotor and fore-and-aft helicopters (Figs.3.10 and 3.11). It is obvious that, if the wing of a single-rotor helicopter is very close to the rotor ($\bar{y} = 0$) and the spans of both rotor and wing are equal $\left(\bar{l}_w = \frac{l_w}{R} = 2.0\right)$, then $\varkappa_w \approx \varkappa_{rot} \approx 1.0$.

Upon an increase in $\bar{l}_w$, due to the fact that the induced velocity is directed upward outside the rotor, the induced velocity of the rotor averaged over the wing span will decrease ($\varkappa_w < 1.0$), while the induced velocity of the wing averaged over the rotor area will change little. Correspondingly, upon a decrease in $\bar{l}_w$, $\varkappa_w$ will change little whereas $\varkappa_{rot}$ will decrease. At $\bar{l}_w < 1.0$, when the wing is underneath the ineffective blade sections, $\varkappa_w$ will decrease. The graphs in Figs.3.10 and 3.11 are valid for a helicopter of fore-and-aft configuration, but must be taken with consideration of the mutual longitudinal displacement of both rotors and wings; for elements located aft, $\varkappa$ is doubled, /291 whereas for elements located forward, $\varkappa$ decreases to zero.

For a helicopter of side-by-side configuration, let us examine one of the rotors in calculating $\varkappa$. At $\bar{z} = 2.0$, half of the wing is underneath the rotor and half is outside the rotor (Figs.3.12 and 3.13); therefore, $\varkappa_w$ and $\varkappa_{rot}$ are smaller than 0.5 (they would be equal to 0.5, if the induced velocity were equal to zero outside the rotor disk or wing span and were uniformly distributed within their confines). Upon a decrease in $\bar{z}$, all larger components of the wing

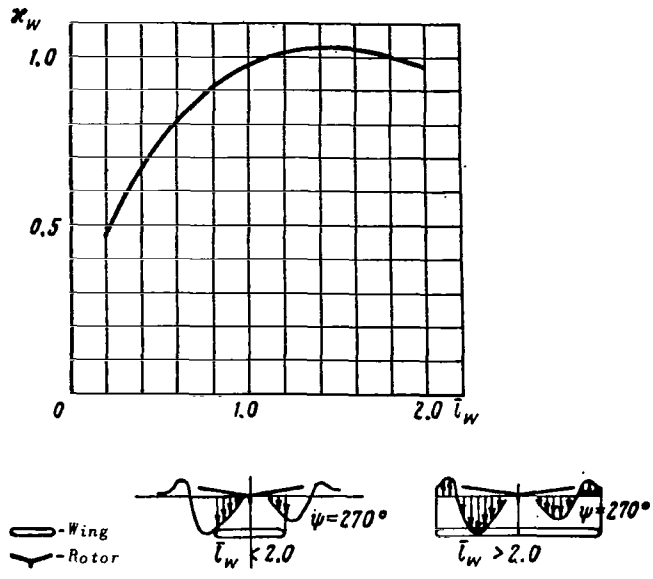

Fig.3.10 Induction Coefficient of Rotor for a Wing on Helicopters of Single-Rotor and Fore-and-Aft Configurations.

and rotor will be within the field of induced downward velocities, so that both $\varkappa_w$ and $\varkappa_{rot}$ will increase.

The numerical values of $\varkappa_w$ and $\varkappa_{rot}$ plotted in the graphs (Figs.3.10–3.13) are given for $\bar{y} = 0$. A decrease in $\varkappa$ at $y \neq 0$ can be determined from the graph of $\varkappa_{co} = f(\bar{y})$ in Fig.3.8, i.e.,

$$\varkappa_l(\bar{y}_1) = \varkappa_l(y=0)\varkappa_{co}(\bar{y}_1). \tag{1.18}$$

Thus, in accordance with eqs.(1.16) and (1.17), the downwash angles are determined by the formulas

$$\Delta\alpha_l = \varkappa_l \frac{C_{y_n}}{4B^2\bar{V}^2} = 0.26\varkappa_l \frac{C_{y_n}}{\bar{V}^2} = 0.26\varkappa_l \frac{t_{y_n}{}^a}{\bar{V}^2}. \tag{1.19}$$

The downwash angle of the rotor induced by the wing can also be found from the expression

$$\Delta\alpha_{rot} = \varkappa_{rot} \frac{c_{y_w}}{\pi\lambda_w} = \varkappa_{rot} \frac{t_{y_w}{}^a}{\bar{l}_w^2 \bar{V}^2}. \tag{1.20}$$

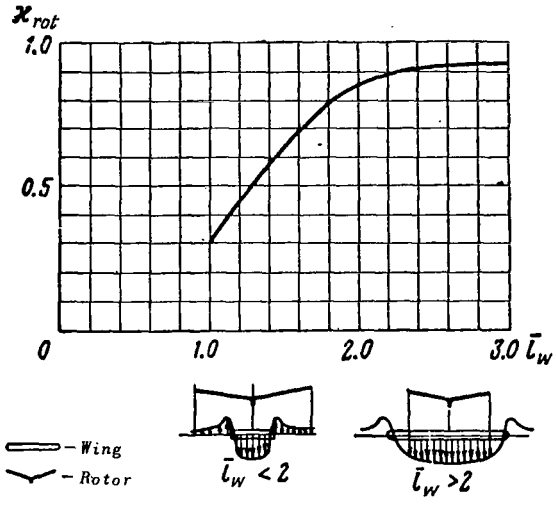

Fig.3.11 Induction Coefficient of Wing for a Rotor on Helicopters of Single-Rotor and Fore-and-Aft Configurations

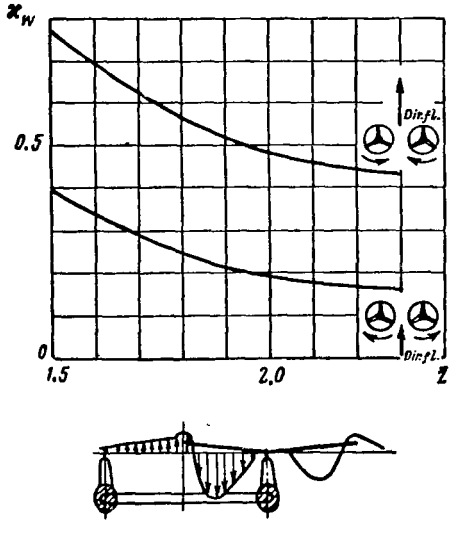

Fig.3.12 Induction Coefficient of Rotor for a Wing on Tandem Helicopter.

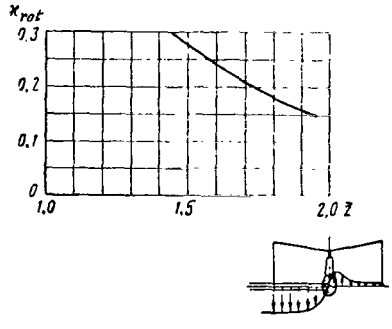

Fig.3.13 Induction Coefficient of Wing for Rotor on Tandem Helicopter.

Section 2. Aerodynamic Helicopter Design by the Mil'-Yaroshenko Method

Let us examine steady regimes of rectilinear motion of a helicopter with low flight-path angles to the horizontal.

Assuming the thrust of the rotor to be approximately equal to the weight and considering the revolutions of the rotor to be given, flight should always take place at a constant thrust coefficient t. In this case, the magnitude of the projection of the resultant onto the direction of motion can be varied only after having changed the angle of attack; at the same time, also the rotor pitch must be changed and hence the power transmitted to the rotor, so as to maintain balance of forces with respect to the vertical.

The method proposed below for designing a helicopter assumes, for each possible value of rotor pitch, that the aerodynamic rotor characteristics (thrust, longitudinal force, and torsion) are known.

1. Equations of Motion and Design Principle

Figure 3.14 shows the forces acting on a helicopter in steady rectilinear motion.

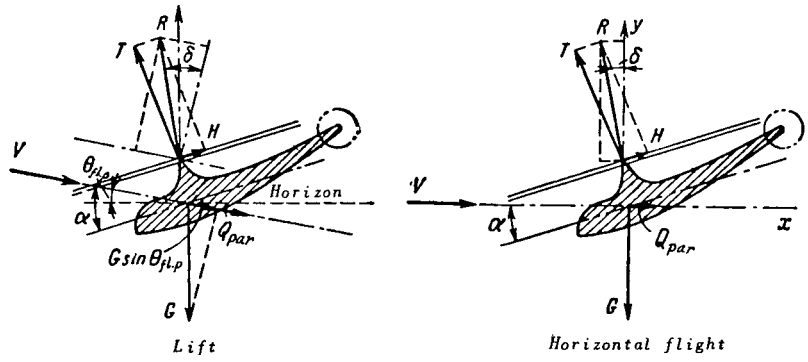

Fig.3.14 Forces Acting on a Helicopter in Steady Rectilinear Motion.

The equations of motion of a helicopter can be written in the form

$$\left.\begin{aligned} R\sin\delta + G\sin\theta_{fl.p} + Q_{par} = 0; \\ R\cos\delta - G\cos\theta_{fl.p} = 0. \end{aligned}\right\} \qquad (2.1)$$

The angle between the direction of the resultant and the normal to the path reads

$$\delta = \alpha + \tan^{-1}\frac{H}{T} = \alpha + \tan^{-1}\frac{h}{t}. \qquad (2.2)$$

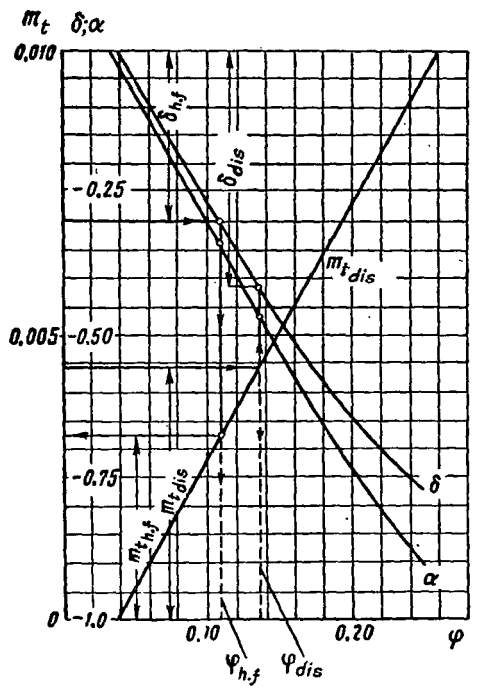

Fig.3.15 Aerodynamic Characteristics of Rotor (μ = 0.15; t = 0.13; σ = 0.065).

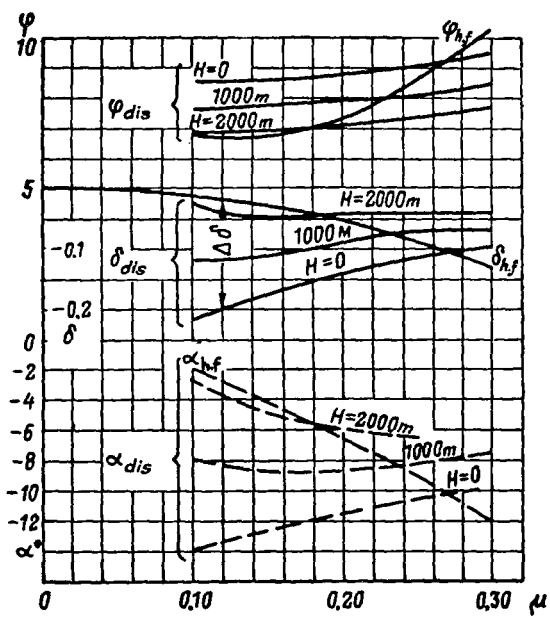

Fig.3.16 Required and Disposable Characteristics of Helicopter.

Below, we will assume that the angles δ and $\theta_{fl.p}$ are small. Furthermore, owing to the smallness of $\frac{H}{T}$ in flight regimes, we can assume the resultant force of the rotor as equal to the thrust (R = T). Then eqs.(2.1) can be rewritten in the form

$$\left.\begin{aligned} T\delta + G\theta_{fl.p} + Q_{par} = 0, \\ T = G. \end{aligned}\right\} \tag{2.3}$$

The angle of inclination of the forward resultant $\delta_{h.f}$ required for horizontal flight is found from eqs.(2.3), setting $\theta_{fl.p} = 0$: /295

$$\delta_{h.f} = -\frac{Q_{par}}{G}. \tag{2.4}$$

The flight-path angle for any given regime will be determined then from eqs.(2.3):

$$\theta_{fl.p} = -(\delta - \delta_{h.f}) = -\Delta\delta. \tag{2.5}$$

Thus, the problem consists in determining the possible angles of inclination of the resultant δ for each given regime.

Figure 3.15 shows the angle δ, the angle of attack α, and the torque coefficient of the rotor m_t relative to the condition of constancy of the thrust coefficient t, as a function of the blade pitch φ for a specific flight regime μ. The larger the setting angle φ, the more negative must be the angle of attack α of the entire helicopter, so as to maintain balance of forces with respect to the vertical, and the larger must be the angle of inclination of the forward resultant. The graphs in Fig.3.15 show that large setting angles often require a larger torque, i.e., a greater expenditure of power. Hence it is clear that, after determining the magnitude of the torque, it is possible - for example, from the total engine power as shown in Fig.3.15 - to obtain the maximum (disposable) pitch φ_{dis} for a given regime and hence the corresponding magnitudes of the angles of inclination of the resultant δ_{dis} and angle of attack α_{dis}. Conversely, on assigning the value of δ - for example, from the condition of horizontal flight - by means of eq.(2.4), it is possible to obtain the required blade setting angle φ, the torque coefficient m_t, and the angle of attack of the rotor α.

Figure 3.16 gives the resultant values of δ_{dis} and $\delta_{h.f}$ as a function of μ. The graphs in Fig.3.16 are also the main graphs for the calculation, by means of which all necessary flight data can be determined. The intercept of the curves determines

$$V_{max} = \mu_{max}\omega R. \tag{2.6}$$

The vertical velocities as a function of μ or V can be found from the formula

$$V_y = -V\theta_{fl.p}, \tag{2.7}$$

where the quantity $\theta_{fl.p} = -\Delta\delta$ is taken from the graph in Fig.3.16.

2. Determination of Aerodynamic Rotor Characteristics

The quantities m_t, δ, and α as a function of the pitch φ and at a given value of the thrust coefficient t - for example, similar to those shown in Fig.3.15 - which are necessary for calculation, can be determined experimentally or theoretically.

Within certain limits, the Glauert-Lock theory gives results close to reality (Sect.2, Chapt.II). These limits are bounded by a certain regime μ and by the magnitude of the thrust coefficient t, characterizing the value of the average working lift coefficient of the blade section c_y and thus determining the admissibility of assumptions made in the theory for the linear dependence of c_y on the angle of attack and for the possibility of adopting an average value of the coefficient of profile drag $c_{xp_{av}}$ = const which does not depend on the angle of attack of the section. /296

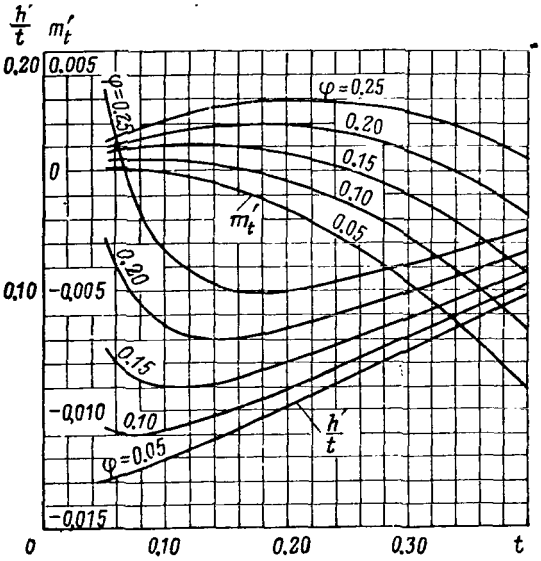

Fig. 3.17 Auxiliary Graphs for Calculation of Rotor Characteristics (μ = 0.1).

In the aerodynamic design of a helicopter it is convenient to define the flow coefficient λ on the basis of eq.(2.50) for the thrust coefficient (see Chapt.II). For this, we make use of the second equation of the above system (2.3) which expresses the condition that, for any rectilinear motion, the rotor thrust is approximately equal to the weight of the craft. Thus, the thrust coefficient in helicopter flight at a given rpm in all rectilinear regimes is constant, and its value is determined from the condition T = G. Then λ, at given values of μ and φ, will be determined from the equation

$$\lambda = \frac{2t}{a_\infty B^2} - \varphi\left(\frac{2}{3}B + \frac{\mu^2}{B}\right). \qquad (2.8)$$

If now we substitute the value of λ into the expression for h (2.68), m_t (2.47), and α (2.53) in Chapter II and plot their dependence on φ (see Fig.3.15), then each point of these curves will correspond to one of the possible regimes of rectilinear flight.

To simplify the calculations, let us plot graphs of the quantities

$$\left.\frac{h'}{t} = \frac{h - \frac{\mu}{2} c_{xp_{av}}}{t}\right\} \qquad (2.9)$$

and

$$m_t' = \frac{m_t}{a_\infty} - \frac{c_{xp_{av}}}{4a_\infty}(1+\mu^2)$$

as a function of t, where φ is a parameter.

Figures 3.17 - 3.20 show these graphs, plotted on the assumption that the coefficient of tip losses is B = 1 and that the mass characteristic of the blade is γ = 5. On a change in flight altitude, γ will vary in direct proportion to the variation in air density. As a consequence of a variation in γ, also $\frac{h'}{t}$ and m_t' will vary, but the changes in these quantities are small for values μ ≤ 0.3. /297

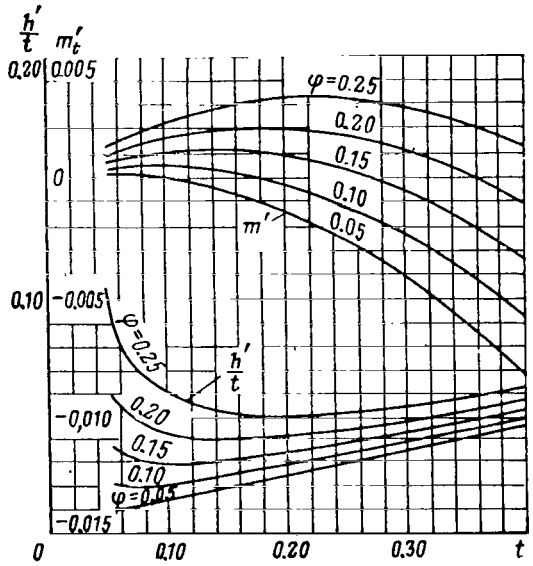

Fig.3.18 Auxiliary Graphs for Calculation of Rotor Characteristics (μ = 0.15).

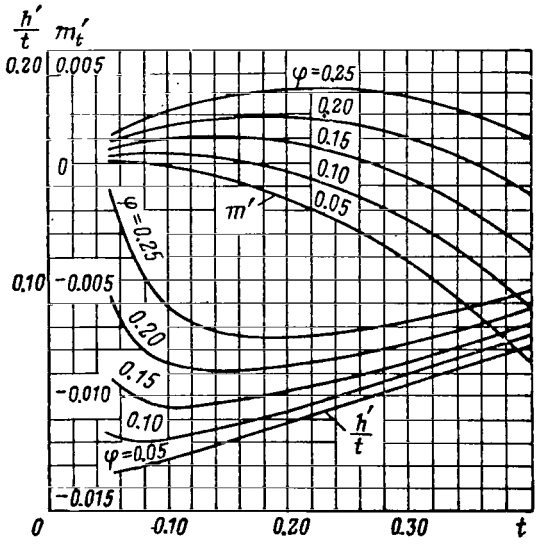

Fig.3.19 Auxiliary Graphs for Calculation of Rotor Characteristics (μ = 0.2).

The quantities m_t' and $\frac{h'}{t}$ represent components of the coefficients of torque and longitudinal force due only to lift and induced drag of the blades; the components of these coefficients due to the profile drag of the sections do not enter into eqs.(2.9). For values of μ within limits from 0.1 to 0.3 and for the usual profile surface finish, a value of $c_{xp_{av}} = 0.012$ gives satisfactory results. /298

3. Calculation of Flight Data

A selection of basic parameters usually precedes the aerodynamic design. Let us assume the rotor diameter as given.

Obtainment of optimum flight data in vertical regimes requires minimum loads on the disk area; therefore, the rotor diameter is selected as large as possible with respect to design and weight considerations. Also the magnitude of the solidity ratio σ is mostly predicated on design considerations.

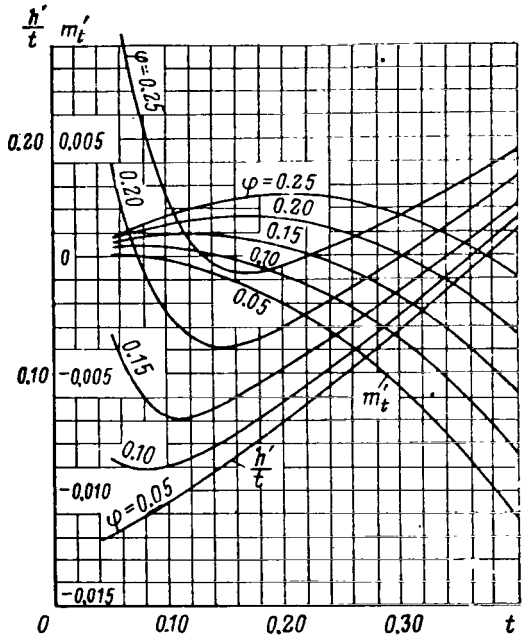

Fig.3.20 Auxiliary Graphs for Calculation of Rotor Characteristics (μ = 0.3).

The magnitude of blade loading which determines the working c_y of the section thus depends largely on the rotor rpm. For a rational selection of the rpm it is therefore suggested to assign 3 or 4 values of the angular rotor velocity and to perform a complete calculation for these.

As regards available power transmitted to the rotor, in the case of two- or multirotor configurations it is necessary to account for the efficiency of transmission and for losses due to cooling; in the case of a single-rotor configuration, the power expended for driving the tail rotor must also be taken into account. In first approximation, this power can be found for hovering flight and is taken as unchanged in forward flight, which will yield smaller values for the performance data in /299 forward flight than can be expected in reality.

The sequence of calculation is as follows: After assigning several values of ω, a series of values of t is derived; for given values of μ and φ, the rotor angle of attack α and the coefficients h and m_t are determined, and eq.(2.2) is used for defining the corresponding values of δ.

The found values of δ and m_t are plotted as a function of φ in the form of graphs similar to those in Fig.3.15, each of which is constructed for a definite value of μ. Then, plotting on the y-axis the values of the available torque coefficient

$$m_{t_{dis}} = \frac{75N_{rot}}{\sigma \frac{\varrho}{2} \pi R^2 (\omega R)^3}, \qquad (2.10)$$

the corresponding values of disposable δ_{dis}, α_{dis}, and φ_{dis} are obtained. The

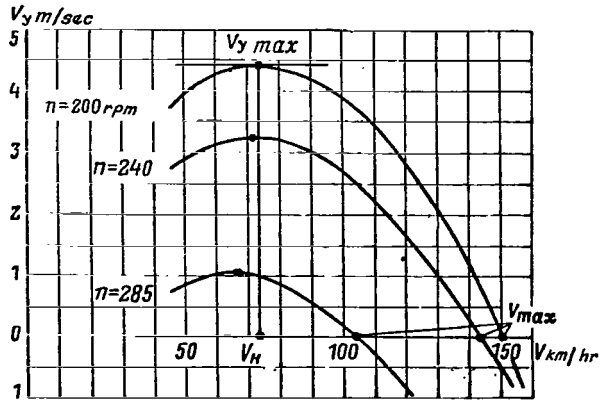

Fig.3.21 Rate of Climb of Helicopter as a Function of Flight Velocity.

next step is to determine the values of $\delta_{h.f}$, $\alpha_{h.f}$, $\varphi_{h.f}$, and $m_{t_{h.f}}$ required for horizontal flight and to construct a graph of these values plotted against μ (see Fig.3.16) in the same manner as presented above.

The power required for horizontal flight $N_{h.f}$ is found in terms of the torque coefficient $m_{t_{h.f}}$ by means of eq.(2.10).

Having determined, by eq.(2.7), the values of V_y as a function of V, we then construct the graphs shown in Fig.3.21. From these graphs, we find the values of $V_{y_{max}}$ and V_{max} and the optimum rate of climb V_c for each flight altitude and rotor rpm. Data corresponding to other altitudes can be determined in the same manner as that given above; the graphs, shown in Fig.3.15, should be constructed for values of t_H corresponding to a certain height on the basis of the relation

$$t_H = t_0 \frac{\varrho_0}{\varrho_H} = \frac{t_0}{\Delta}.$$

To obtain flight data for a helicopter with respect to height above ground, it is also possible to use the following method which does not require constructing the graphs shown in Fig.3.16. A change to another altitude is characterized by a change in ρ. The graphs /300 will remain unchanged if the value of the thrust coefficient is retained. Since

$$t = \frac{G}{\sigma \frac{\varrho}{2} \pi R^2 (\omega R)^2},$$

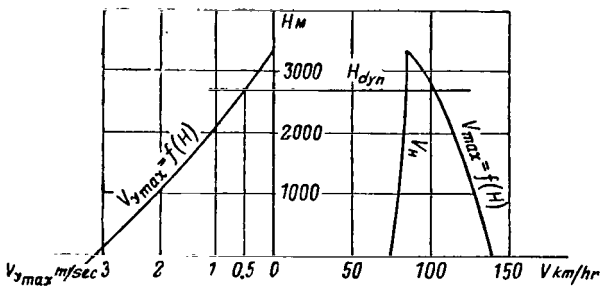

Fig.3.22 Graph of Helicopter Flight Data (n = 240 rpm).

then, for constancy of t, we must retain the equality $\rho_0 \omega_0^2 = \rho_H \omega_H^2$. Hence, we determine the value of ω_H at which t and thus also all other coefficients remain constant. The curve of $\delta_{h.f} = f(\mu)$ in Fig.3.16 remains the same, since the drag Q_{par} depends on $\rho\omega^2$, and this product does not change with height. The available torque coefficient must be calculated for power at an altitude, with consideration of the new value of angular velocity. If the power at altitude $N_H = AN_0$, then

$$(m_{t_{dis}})_H = (m_{t_{dis}})_0 A \sqrt{\Delta}.$$

Having $(m_{t_{dis}})_H$, the described process of obtaining δ_{dis}, φ_{dis}, and α_{dis} is repeated; the resultant values are plotted on graphs as shown in Fig.3.16. After determining $\Delta\delta$, graphs of $V_y = f(V)$ are plotted, finding $V_{y_{max}}$ and V_{max} as a function of rotor rpm for various heights taking for each height $n_H = n_0 \frac{1}{\sqrt{\Delta}}$.

These calculations must be carried out for at least three values of rotor rpm. Then, recording from the graphs the values $V_{y_{max}}$ and V_{max} with respect to /301 altitudes for given revolutions, a graph as shown in Fig.3.22 is plotted, from which we can determine the ceiling (dynamic) and also the variation in V_{max} with altitudes, at given revolutions.

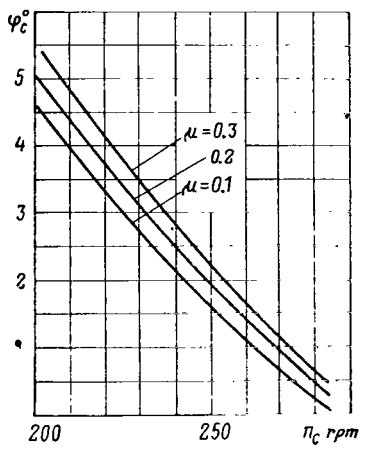

Fig.3.23 Rotor Pitch in Autorotation Regime.

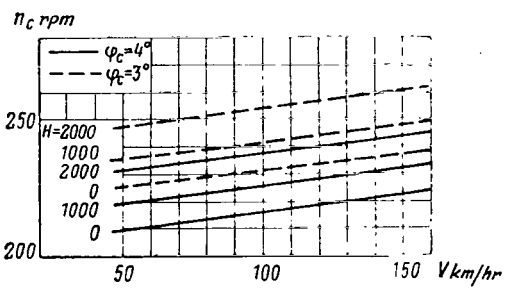

Fig.3.24 Rotor Rpm in Autorotation Regime.

The calculations for any weight can be made just as for any altitude, i.e., using the graphs shown in Fig.3.15 and changing only the value of n in conformity with the variation in weight.

From the condition $m_t = 0$, the pitch φ for an autorotation regime is determined. After constructing graphs (Fig.3.23) of the dependence of φ_c on the number of revolutions of the rotor m_c for each value of μ, we can find the rotor rpm in an autorotation regime as a function of flying speed and for any constant value of φ_c. The dependences $n_c = f(V)$ for different flight altitudes are plotted in Fig.3.24.

4. Limits of Applicability of the Method

The presented method permits analyzing the influence of numerous parameters

that determine the flight regime of a helicopter. Moreover, the degree of accuracy of the calculation of performance data, based on this method, is fully determined by the extent to which the theory underlying the calculation of rotor aerodynamics yields results close to reality.

In regimes μ within the limits from 0.1 to 0.3 and with thrust coefficients smaller than the maximum permissible, the section angles of attack are within the range for which the assumptions made in the theory are valid ($c_y = a_\infty \alpha_r$; $c_{x p_{av}} = \text{const}$).

At large values of μ and, in particular, at large blade setting angles, the section angles of attack in a large portion of the disk area exceed the critical value, and flow separation takes place. An ultimate analysis indicates that the theory in these regimes gives values of the longitudinal force, and especially of the torque, that are lower than reality, and also produces errors in the angle of attack. Thus, the results of the calculation by the proposed method should give higher values of maximum speed if this is determined in the region $\mu > 0.3$. The assumption of a uniform induced velocity distribution does not hold at small μ ($\mu < 0.15$). In reality, the induced losses are larger in these regimes owing to nonuniform induced velocity distribution so that the calculation will give larger values of the rate of climb of the craft.

These errors are small (of the order of 10%) for helicopters with low disk area loading, but markedly increase with increasing G/F, i.e., with increasing relative percentage of induced losses.

An increase in the accuracy of calculation of the flight data can be achieved by refining the theory or by using data obtained from wind-tunnel tests.

Section 3. General Method of Aerodynamic Design for Rotary Wing Aircraft

In this method of calculation, just as in the Mil'-Yaroshenko method, the first step is to plot - on special graphs - the aerodynamic rotor characteristics. Then, the propulsive force coefficient t_x is plotted against the torque coefficient m_t, for constant values of the coefficients t_y, M_{fl} (or $\overline{V}$), M_o (see Figs.2.142 - 2.145). To calculate a helicopter with a combined lifting system, the same graphs are plotted for the total coefficients; the design formulas for determining the total coefficients were derived in Section 1.4. Thus, this /302 method of calculation encompasses all types of rotary wing aircraft.

In determining the performance, i.e., in solving the equations of motion, no simplifying assumptions are made and the accuracy of the calculation is determined by the accuracy of the graphs of aerodynamic characteristics of the lifting system and by the correctness of estimating the parasite drag of the helicopter and the engine power losses. We make only the assumption that the performance data can be calculated separately from the balance calculation at some average (for a given centering of the helicopter) value of deflection of the automatic pitch control $\varkappa_{av}$. This leads to an error in determining the angle of attack of the fuselage and wing; therefore, at great differences between $\varkappa$ and $\varkappa_{av}$ for a helicopter with a large wing ($S_w/F > 0.05 - 0.07$), the assumption is

no longer valid.

A shortcoming of this method is its relatively great expenditure of time. Consequently, it ranges among methods of final aerodynamic design. However, whenever graphs of the aerodynamic characteristics of the lifting system are available, the calculation of the performance data is not excessively laborious and the method can be used also for preliminary calculations.

In the calculation, auxiliary graphs suitable for all craft with similar lifting systems and equal parasite drag coefficients are constructed. By means of these graphs, plotted once and for all, numerous aerodynamic design calculations of versions of a craft can be performed, including calculations for different conditions of helicopter use (variations in flying weight, rotor rpm, or atmospheric conditions).

1. Construction of Auxiliary Graphs for Helicopter Performance Data

In this Subsection, we present a method of constructing auxiliary graphs for calculating helicopter performance data. Strictly speaking, these graphs, constructed for a helicopter with a specific lifting system and specific dependence $\bar{c}_x$ on α_f, are applicable only to this type or to other helicopters with similar lifting systems and identical dependences of $\bar{c}_x$ on α_f. However, the graphs can be used with sufficient accuracy for all helicopters of the same configuration having identical values of σ, $\bar{c}_{x_{(\alpha=0)}}$ and other dimensionless characteristics (for example, ε_w, $\bar{S}_w$ for a helicopter with wing) and M_0 not greater than 0.55 - 0.6, when the blade shape does not excessively influence the aerodynamic rotor characteristics. Therefore, at $M_0 \leq 0.55 - 0.6$, the auxiliary graphs are universal. Characterizing the parasite drag of the helicopter only by its magnitude at $\alpha_f = 0$, $\bar{c}_{x_{(\alpha=0)}}$, it will be assumed that the increment of $\bar{c}_x$ upon a variation in α_f can be considered identical for helicopters of the same configuration. We will disregard the lifting force of the nonlifting elements.

For helicopters with a narrow variation range of M_0 (flight at constant rotor rpm; dynamic ceiling less than 5000 - 6000 m) and with a maximum M_0 less than 0.6 - 0.65, the auxiliary graphs are constructed for a mean value of M_0. For helicopters with higher M_0, determination of the performance data for the mean value of M_0 leads to noticeable errors, as a result of which the auxiliary graphs lose their universality and can be used only for one value of M_0.

The method of employing the graphs for determining performance data of a helicopter is presented in Subsection 2.

Auxiliary graphs for required helicopter power. In horizontal flight /303
of a rotary wing aircraft ($\theta_{f1.p} = 0$), the equations of motion (1.6) and (1.7) take the form

$$\bar{c}_x \frac{\bar{V}^2}{\sigma} = -t_{x v_{h.f}}; \qquad (3.1)$$

$$\frac{G}{1/2\varrho\sigma\pi R^2(\omega R)^2} = t_{y\Sigma_{h.f}}. \tag{3.2}$$

In eqs.(3.1) and (3.2), the index "Σ" means that the coefficients t_y and t_x are total coefficients of the lifting system of a helicopter.

If the characteristics of the lifting system are calculated with consideration of $\bar{c}_x$ of the helicopter, then $\bar{c}_x$ in the first equation is assumed as equal to zero.

Below, we will omit the index "Σ". For simplicity, we will use the term rotor instead of lifting system and helicopter instead of rotary wing aircraft. The geometric rotor characteristics will be labeled by the solidity ratio σ.

It follows from eq.(3.1) that, for a given value of $\bar{V}$ in helicopters with identical rotors (equal σ) and equal drag coefficients, the coefficient t_x has an identical value. Since the aerodynamic rotor characteristics, i.e., the interrelations of the quantities t_y, t_x, m_t, $\bar{V}$, and M_0 are known (see Figs.2.142 to 2.145), it is possible to construct auxiliary graphs valid for all flight conditions of a given helicopter and for all helicopters with equal σ, $\bar{c}_x$, and M_0, by means of which - for any value of t_y as a function of $\bar{V}$ - we can find the torque coefficient $m_{t_{h.f}}$, angle of attack $\alpha_{h.f}$, and angle of rotor setting $\theta_{0_{h.f}}$ required for horizontal flight.

The sequence of constructing the auxiliary graphs for calculating horizontal flight regimes will be described for the Mi-4 helicopter with rectangular metal blades (σ = 0.063, $\bar{c}_{x_{(\alpha=0)}}$ = 0.009 with consideration of the rotor hub, or $\bar{c}_{x_{(\alpha=0)}}$ = 0.0075 without it). The calculation is made on the basis of experimental aerodynamic characteristics of a rotor with rectangular metal blades, σ = 0.0525. When using these characteristics for the rotor of the Mi-4, the conversion formulas are utilized (see Sect.6, Chapt.II). In this case, the conversion is required because of differences in the rotors with respect to their solidity ratio, and the difference in M_0 must be allowed for. No differences exist in profile or quality of blade manufacture, and both blade mass characteristic and flapping compensator are practically identical. The parasite drag of the helicopter is taken without the rotor hub (the influence of the hub is taken into account in the experimental characteristics of the rotor).

Thus, conversion of the rotor characteristics is performed by the formulas:

$$t_x = t_{x_1} - \frac{(\sigma_1 - \sigma)\, t_y^2}{4B^2\bar{V}^2}; \tag{3.3}$$

$$\alpha = \alpha_1 - \frac{(\sigma_1 - \sigma)\, t_y}{4B^2\bar{V}^2}; \tag{3.4}$$

$$m_t = m_{t_1} + \delta m_{co}; \tag{3.5}$$

$$\theta_0 = \theta_{0_1}, \tag{3.6}$$

where t_{x_1}, α_1, m_{t_1}, θ_{0_1} are characteristics of the tested rotor.

The coefficients and angles without the subscript pertain to the Mi-4 rotor. /304

The parasite drag coefficient of the Mi-4 helicopter entering eq.(3.1) was determined from the curve of $\bar{c}_x = f(\alpha_f)$ obtained from full-scale wind-tunnel tests of a helicopter without rotor (Fig.3.25). If the angle of attack α at zero deflection of the automatic pitch control is indicated on the aerodynamic characteristics of the rotor, then the angle of attack of the fuselage is related with the angle of attack of the rotor by the approximate expression (Fig.3.26):

$$\alpha_f = \alpha + \varepsilon_f - D_1 \varkappa_{av}. \tag{3.7}$$

Here, ε_f is the angle of advance of the fuselage axis to the plane of rotation, and $D_1\varkappa_{av}$ is the difference in the angles of attack of the rotor at $\varkappa \neq 0$ and $\varkappa = 0$. For the Mi-4 helicopter, $\varepsilon_f = 5^\circ$ and the quantity $D_1\varkappa_{av}$ is taken to be equal to -3°.

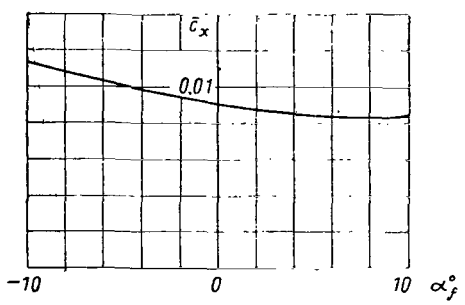

Fig.3.25 Parasite Drag Coefficient of Mi-4 Helicopter vs. Fuselage Angle of Attack.

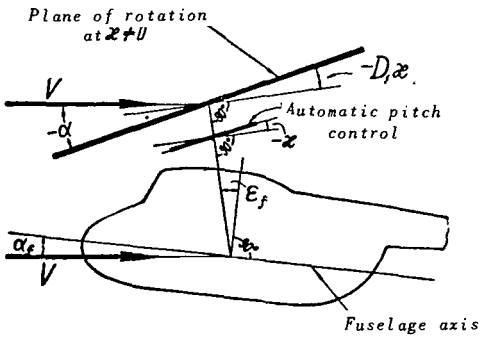

Fig.3.26 For Determining the Fuselage Angle of Attack.

Equations (3.3) - (3.7) are used in the following sequence: For the selected values of t_y and $\bar{V}$, prescribe the angle of attack of the rotor α and find α_f, $\bar{c}_x$, and $t_{x_{h.f}}$. Using eqs.(3.3) and (3.4) for determining t_{x_1} and α_1 from the graph of the aerodynamic characteristics, check whether the values of t_{x_1} and α_1 correspond. If not, assign a new value of α and again find t_{x_1} and α_1. Selection of the value of α can be done rapidly in practice. After determining the final value of t_{x_1}, use the graphs of the aerodynamic characteristics to find m_{t_1} and θ_{0_1}, and determine $\delta_{m_{co}}$ from eq.(6.18) of Chapter II by means of the graphs in Figs.2.80 - 2.88. In this case, again make use of eq.(3.3) to find the value of t'_{x_1} corresponding to $\sigma = 0.091$, for which the graphs of Δm_{co} are constructed:

$$t'_{x_1}=t_x+\frac{(\sigma_0-\sigma)\,t_y^2}{4B^2\bar{V}^2}=t_x+\frac{(0.091-0.063)\,t_y^2}{4\cdot 0.96\bar{V}^2}.$$

The calculation is carried out in Table 3.1.

In hovering flight, m_t was determined also from the experimental curve (Fig.2.141) with conversion to $\sigma = 0.063$ by the formulas:

$$\left.\begin{aligned} m_t&=(m_{t_1}-m_{pr_1})\left(\frac{B_1}{B}\right)^3\sqrt{\frac{\sigma}{\sigma_1}}+m_{pr_1},\\ \theta_0&=\theta_{0_1}+\frac{3}{4B^2}\sqrt{t}\,(\sqrt{\sigma}-\sqrt{\sigma_1}).\end{aligned}\right\} \qquad (3.8)$$

TABLE 3.1 /305

$t_y=0.14$; $\sigma=0.063$; $M_0=0.6$

$\bar{V}$	0.15	0.20	0.25	0.30
$\alpha°$	—3.5	—5.25	—8.0	—11.0
α_f°	4.5	2.75	0	—3
$\bar{c}_x$	0.007	0.0072	0.0077	0.0081
$t_{x_{h.f}}$	—0.0025	—0.00457	—0.00765	—0.01155
$\frac{(\sigma_1-\sigma)\,t_y^2}{4B^2\bar{V}^2}$	—0.00239	—0.00134	—0.00086	—0.0006
t_{x_1}	—0.00489	—0.00591	—0.00851	—0.01215
$57.3\,\frac{(\sigma_1-\sigma)\,t_y}{4B^2\bar{V}^2}$	—0.98	—0.55	—0.35	—0.25
α_1°	—4.5	—5.8	—8.35	—11.25
m_{t_1}	0.0055	0.00545	0.00645	0.00875
$\theta_{0_1}^\circ$	7.6	7.9	9.0	10.2
δm_{c0}	0.00008	0.0001	0.00015	0.0002
$m_{t_{h.f}}$	0.00558	0.00555	0.0066	0.00895

Having made similar calculations for a large range of t_y, we construct universal auxiliary graphs for determining the characteristics of the horizontal flight of helicopters with $\sigma = 0.063$, $\bar{c}_{x(\alpha=0)} = 0.0075$ (without a rotor hub), and $M_0 = 0.6$. These graphs are shown in Figs.3.27 - 3.29.

Some simplification in the use of the auxiliary graph of $m_{t_{h.f}}$, shown in Fig.3.27, changing from physical quantities to dimensionless and vice versa is possible by constructing a graph in which the ordinate does not give $m_{t_{h.f}}$ but

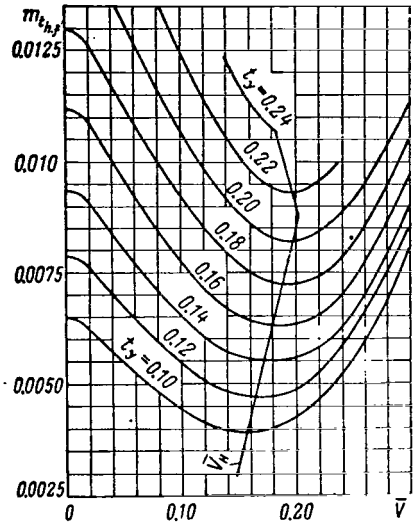

Fig.3.27 Auxiliary Graph for Calculating Horizontal Flight Regimes: Required Power Coefficient as a Function of $\bar{V}$, t_y (M_o = 0.6; σ = 0.063; $\bar{c}_{x(\alpha=0)}$ = 0.0075 without rotor hub).

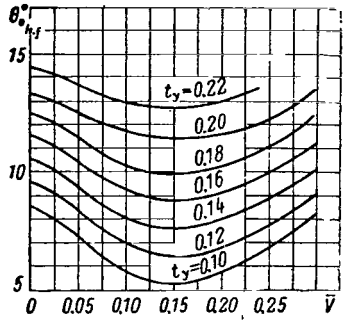

Fig.3.28 Auxiliary Graph for Calculating Horizontal Flight Regimes: Setting Angle of Rotor (at $\underline{k}$ = 0.55; γ = 4.85) as a Function of $\bar{V}$ and t_y (M_o = 0.6; σ = 0.063; $\bar{c}_{x(\alpha=0)}$ = 0.0075 without Rotor Hub).

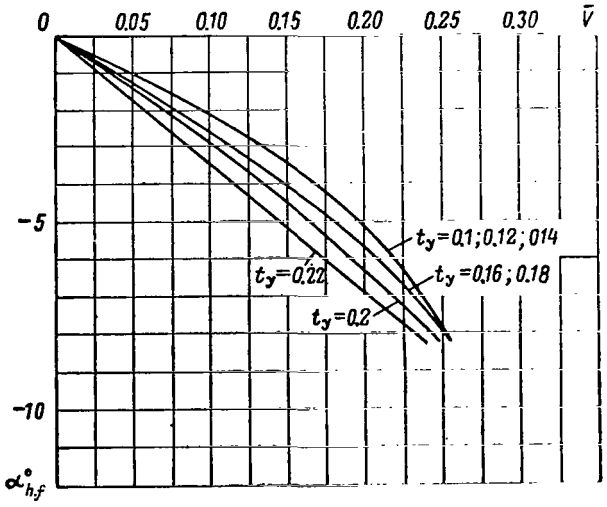

Fig.3.29 Auxiliary Graph for Calculating Horizontal Flight Regimes: Rotor Angle of Attack as a Function of $\bar{V}$ and t_y (M_o = 0.6; σ = 0.063; $\bar{c}_{x(\alpha=0)}$ = 0.0075 without Rotor Hub).

the quantity $\frac{m_{t_{h.f}}}{t_y}$ which is connected with the physical quantities by a relation having a simpler form than eq.(1.6):

$$\frac{m_{t_{h.f}}}{t_y} = \frac{75N_{h.f}\,\xi}{G\omega R}. \tag{3.9}$$

Such a graph is shown in Fig.3.30.

In Figs.3.27 - 3.30 the curves are plotted to values of $\bar{V}$ permissible for the condition of flow separation at the rotor blades (see Figs.2.120 and 2.121). The curves corresponding to $t_y = 0.24$ were obtained by extrapolation of the experimental graphs.

At large M_0, when the compressibility effect is appreciable and the auxiliary graphs become applicable only to the value of M_0 for which they were constructed, it is expedient to plot, for helicopters with a turboprop engine, a graph for determining $N_{h.f}$ in reduced parameters: $N_{h.f_r} = f(V_r)$ with the parameter G_r for $M_0 = \text{const}$ ($\omega_r = \text{const}$). The reduced parameters are determined by the formulas: /307

$$\left.\begin{aligned}
N_{h.f_r} &= N_{h.f}\frac{p_0}{p}\sqrt{\frac{T_0}{T}} = \frac{1}{75}\frac{\varrho_0}{2}\left(0{,}379\frac{p}{T}\right)\sigma F(20{,}1\sqrt{T})^3\times \\
&\quad\times M_0^3 m_{t_{h.f}}\frac{p_0}{p}\sqrt{\frac{T_0}{T}} = \text{const}_1\, m_{t_{h.f}}; \\
V_{r_r} &= V\sqrt{\frac{T_0}{T}} = 20{,}1\sqrt{T_0}\,\frac{V}{a} = \text{const}_2 M_{t_{h.f}} = \text{const}_2 M_0 \bar{V}; \\
G_r &= G\frac{p_0}{p} = \frac{\varrho_0}{2}\left(0{,}379\frac{p}{T}\right)\sigma F(20{,}1\sqrt{T})^2 M_0^2 t_y\frac{p_0}{p} = \text{const}_3 t_y.
\end{aligned}\right\} \tag{3.10}$$

Since, in the case of a turboprop engine, N_r determines the reduced fuel consumption per hour $G_{hr_r} = G_{hr}\frac{p_0}{p}\sqrt{\frac{T_0}{T}}$, it is possible to construct auxiliary graphs for determining G_{hr_r} and the relative fuel consumption per kilometer $\frac{q_r}{G_r} = \frac{q}{G}$ in the case of helicopters with turboprop engines.

Auxiliary graph for the helicopter dynamic ceiling. From the minima of the curves of the required torque coefficients (broken curve in Fig.3.27, designated by $\bar{V}_H$) we can construct a graph of $(m_{t_{h.f}})_{min} = f(t_y)$. This graph, shown in Fig.3.31, can be used for determining the minimum required power at any flight altitude (at any t_y) and for finding the theoretical dynamic ceiling of the helicopter H_{dyn_t}, i.e., the heights at which the available power is equal to the minimum required power. The graph can also be used for determining the altitude up to which horizontal flight is possible upon failure of some of the engines /308 of a multiengine helicopter.

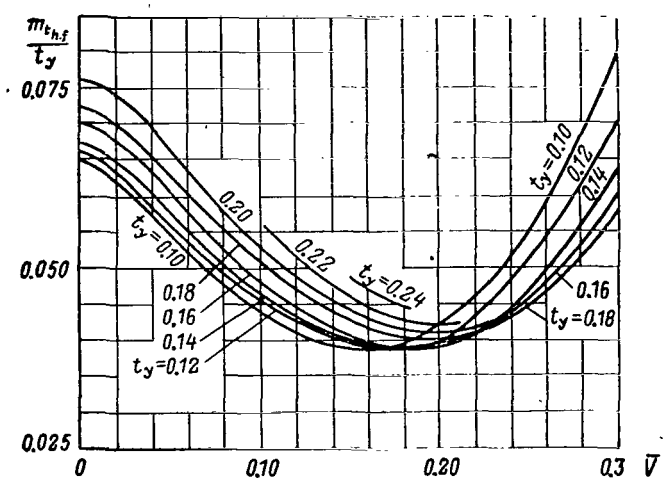

Fig.3.30 Auxiliary Graph for Calculating Horizontal Flight Regimes: Ratio $\frac{m_{t_{h.f}}}{t_y}$ as a Function of $\bar{V}$ and t_y (M_o = 0.6; σ = 0.063; $\bar{c}_{x_{(\alpha=0)}}$ = 0.0075 without Rotor Hub).

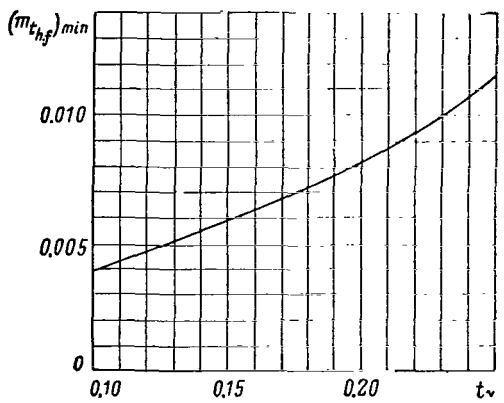

Fig.3.31 Coefficient of Minimum Required Power of Helicopter as a Function of t_y (M_o = 0.6; σ = 0.063; $\bar{c}_{x_{(\alpha=0)}}$ = 0.0075 without Rotor Hub).

Auxiliary graph for maximum rate of climb. To calculate flight regimes of a helicopter in which the flight-path angle $\theta_{fl.p}$ is not equal to zero, eqs.(1.6) and (1.7) must be solved for $\theta_{fl.p}$ after determining the value of m_t with respect to the available engine power for optimum rate of climb and after setting m_t = 0 for gliding in autorotation of the rotor. This problem is solved either with the assumption of a small value of the angle $\theta_{fl.p}$ ($\cos\theta_{fl.p}$ = 1), or by successive approximations; however, it is more convenient to construct a universal auxiliary graph.

First we determined the flying speed at which the vertical speed is maximum, i.e., the optimum rate of climb V_H. Calculations show that, for a helicopter, the optimum rate of climb practically coincides with the rate of horizontal flight at which the required power is minimum. This is explained by the fact that the excess of rotor shaft horsepower used for climbing is maximum in this regime (since the available shaft horsepower of the rotor depends little on the flying speed) and that the propulsive efficiency of the rotor (see Sect.7, Chapt.II), i.e., the efficiency of converting the excess rotor shaft horsepower to an excess of propulsive power creating vertical speed, depends very little on the flying speed (with the exception of near-separation regimes). Therefore, the optimum rate of climb for all values of t_y is found in Fig.3.27 from the curve connecting the minima of the required torque coefficients.

It is obvious that, for all values of t_y, the regime of optimum climb corresponds to $\bar{V}$ = 0.15 - 0.2.

Therefore, the auxiliary graph for determining the vertical speed of a

helicopter is constructed for two values of $\overline{V}$: $\overline{V}$ = 0.15 and $\overline{V}$ = 0.2; for intermediate values the vertical speed can be determined by interpolation. The auxiliary graph is constructed in the following sequence:

Assign several values of $\theta_{fl.p}$ (both positive and negative).

From eq.(1.6), find t_{x_θ}, and determine $\overline{c}_x$ as a function of α_f:

$$\alpha_f = \alpha_{f_{h.f}} - \theta_{fl.p}; \tag{3.11}$$

Assign a number of values of t_y and find t_{y_θ}:

$$t_{y_\theta} = t_y \cos \theta_{fl.p}; \tag{3.12}$$

From the graph of aerodynamic rotor characteristics with respect to t_{x_θ} and t_{y_θ}, determine m_t for all values of t_y.

Then, determine Δm_t (see Fig.3.32): /309

$$\Delta m_t = m_t - m_{t_{h.f}}; \tag{3.13}$$

Determine the vertical component of flying speed

$$\overline{V}_y = \frac{V_y}{\omega R} = \frac{V \sin \theta_{fl.p}}{\omega R} = \overline{V} \sin \theta_{fl.p}; \tag{3.14}$$

Construct the graph of $\overline{V}_y = f(\Delta m_t)$ with the parameter t_y; such a graph is shown in Fig.3.33.

It should be noted that, because of the linearity of the aerodynamic rotor characteristics and because of the equidistant translation of the curves of t_x upon a variation in σ, the auxiliary graph shown in Fig.3.33 is applicable for calculating helicopters with any $\overline{c}_x$ and σ (for M_0 less than 0.6).

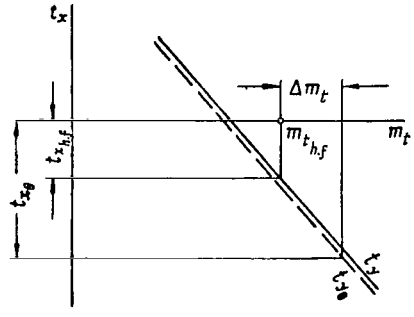

Fig.3.32 For Determining the Increment in Power Coefficient in Flight along an Inclined Path.

If the graph is constructed for large negative values of Δm_t, then the vertical rate of descent of the helicopter during gliding in an autorotation regime at a given peripheral rotor speed can be determined.

To determine the static ceiling of a helicopter and the rate of climb in vertical ascent, let us use the graph shown in Fig.3.34 which is a reconstructed graph of the aerodynamic rotor characteristics for V = 0.

2. Determination of Helicopter Performance Data

The sequence of determining the performance data of a helicopter from

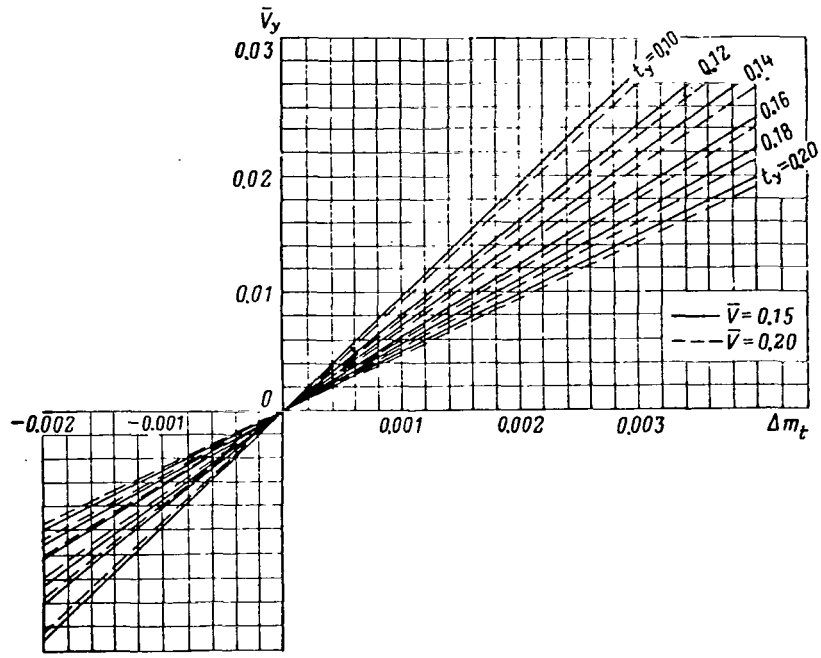

Fig.3.33 Auxiliary Graph for Determining Maximum Rate of Climb.

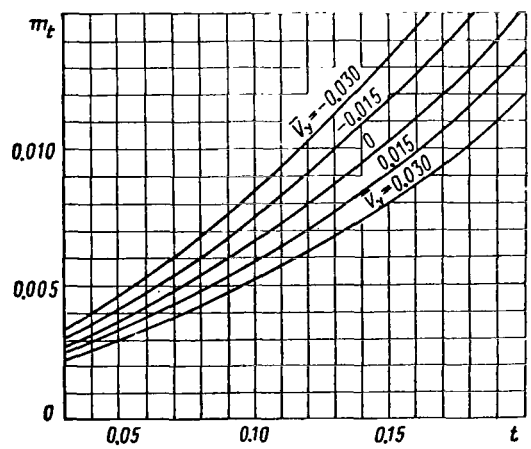

Fig.3.34 Torque Coefficient as a Function of t and $\bar{V}_y$ for V = 0 (M_0 = 0.6; σ = 0.063).

auxiliary graphs is as follows:

Select the design flight altitudes and calculate, for each altitude, the lift coefficient in horizontal flight and the available power coefficient of the rotor:

$$t_y = \frac{G}{\frac{1}{2}\varrho_0 \Delta \sigma F (\omega R)^2} = \frac{16G}{\sigma F (\omega R)^2} \frac{1}{\Delta} = t_{y_0} \frac{1}{\Delta}; \tag{3.15}$$

$$m_{t_{dis}} = \frac{75N\xi}{\frac{1}{2}\varrho \sigma F (\omega R)^3}. \tag{3.16}$$

The design flight altitudes are selected at intervals of 1000 - 1500 m. The design altitudes should include the critical altitude and other salient points of the altitude characteristics of the engine.

The torque coefficient $m_{t_{h.f}}$, angle of attack $\alpha_{h.f}$, and angle of setting $\theta_{0_{h.f}}$ required for horizontal flight of the helicopter are found for calculated t_y by interpolation from the auxiliary graphs in Figs.3.27 - 3.30.

Maximum and minimum flying speeds. These are determined from the intersection points of the curves of $m_{t_{h.f}}$ and $m_{t_{dis}}$. There is no need to construct a special graph of $m_{t_{h.f}}$ and $m_{t_{dis}}$, and $\overline{V}_{max}$ and $\overline{V}_{min}$ can be found by direct /311 interpolation from Figs.3.27 - 3.30. If the curves of $m_{t_{h.f}}$ and $m_{t_{dis}}$ at large $\overline{V}$ do not intersect (at the limit of separation $m_{t_{h.f}} < m_{t_{dis}}$), then the maximum flying speed at this altitude is not limited by the available engine power but by the separation of flow.

Maximum vertical rate of climb. This is determined from the auxiliary graph in Fig.3.33. Here, $\overline{V}_H$ and $(m_{t_{h.f}})$ are found from Fig.3.27 for all calculated flight altitudes, calculating

$$\Delta m_{t_{max}} = m_{t_{dis}} - (m_{t_{h.f}})_{min}. \tag{3.17}$$

After determining $\overline{V}_y$ from the graph in Fig.3.33, we find

$$V_{y_{max}} = \overline{V}_{y} \omega R. \tag{3.18}$$

As a typical example, let us determine maximum and minimum speed, optimum rate of climb, and maximum vertical speed of the Mi-4 helicopter with an all-up weight of G = 7200 kg, ωR = 196 m/sec, and R = 10.5 m. All calculations are given in Table 3.2, and the results are plotted in Fig.3.35.

Practical and theoretical dynamic ceilings. These can be found from /312

TABLE 3.2

H, m	0	1000	1860	3500	5000	5500
t_y	0.138	0.152	0.166	0.195	0.229	0.243
$N_{eng_{nom}}$, hp	1430	1500	1550	1315	1380	1300
$\xi_{(V=0)}$			0.80			
$m_{t_{dis}}$ $(V=0)$	0.00836	0.00966	0.0109	0.01085	0.0134	0.0134
$\xi_{(V_H \div V_{max})}$			0.84			
$m_{t_{dis}}$	0.008775	0.01015	0.0115	0,01145	0.0141	0.0141
$\overline{V}_{max}$	0.297	0.312	0.325	0.305	—	—
V_{max}, km/hr	210	220	230	215	—	—
$\overline{V}_{min}$	0.035	0.033	0.03	0,09	0.103	0.122
V_{min}, km/hr	25	23	21	63	72	85
$\overline{V}_H$	0.170	0.18	0.18	0.20	0.19	0.18
V_H, km/hr	120	127	127	141	134	127
$m_{h.f\,min}$	0.00537	0.00595	0.00665	0.00795	0.010	0.0109
Δm_t	0.0034	0.0042	0.00485	0.0035	0.0041	0.0032
$\overline{V}_y$	0.024	0.0277	0.0292	0.0179	0.0179	0.0132
$V_{y_{max}}$, m/sec	4.7	5.4	5.7	3.5	3.5	2.6

Fig.3.35: The former is the altitude at which $V_{y_{max}} = 0.5$ m/sec and the latter, the altitude at which $V_{y_{max}} = 0$. From Fig.3.35 we can determine, by extrapolation, that the ceilings of the Mi-4 helicopter are equal to: $H_{dyn} = 6400$ m and $H_{dyn_T} = 6550$ m. These data can be found without constructing a graph of $V_{y_{max}}$, using instead the graph shown in Fig.3.31. For this, the data in Table 3.2 are used for plotting, in Fig.3.31, the curves of $m_{t_{dis}}$ and $m_{t_{dis}} - \frac{t_y \overline{V}_y}{\eta} = m_{t_{dis}} - t_y \frac{0.51}{\omega R \eta}$ against t_y (the propulsive efficiency of the rotor η is determined from the graphs in Sect.7, Chapt.II). The values of t_y at which these curves intersect with the curve of $(m_{t_{h.f}})_{min}$ correspond to the theoretical and practical dynamic ceilings. Such constructions are performed in Fig.3.36 from where we find that, at the practical dynamic ceiling, we have $t_y = 0.268$ and, at the theoretical dynamic ceiling, $t_y = 0.274$. After determining, by means of eq.(3.19), the relative air density

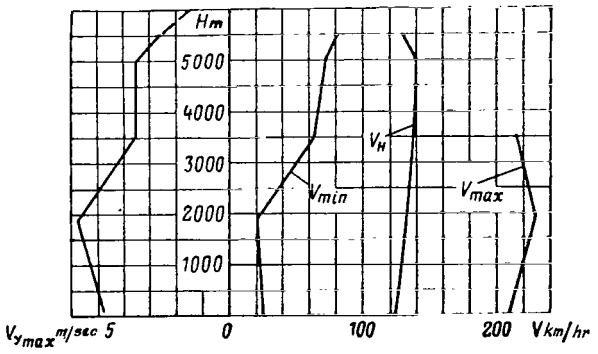

Fig.3.35 Flight Characteristics of Helicopter.

$$\Delta = \frac{t_{y_0}}{t_y}, \qquad (3.19)$$

from the standard atmosphere table or from the formula

$$\Delta = \frac{20 - H\,[\text{km}]}{20 + H\,[\text{km}]},$$

the ceilings are determined. In our example we have

$$\Delta_1 = \frac{0.138}{0.268} = 0{,}515;\ H_{dyn} = 6400\,m \text{ and } \Delta_2 = \frac{0{,}138}{0{,}274} = 0{,}505;\ H_{dyn} = 6550\,m,$$

which coincides with the values obtained above.

Static ceiling of helicopter and rate of climb in vertical ascent. These /313 are found from the auxiliary graph in Fig.3.34, for which purpose the curve of $m_{t_{dis}} = f(t_y)$ was plotted there.

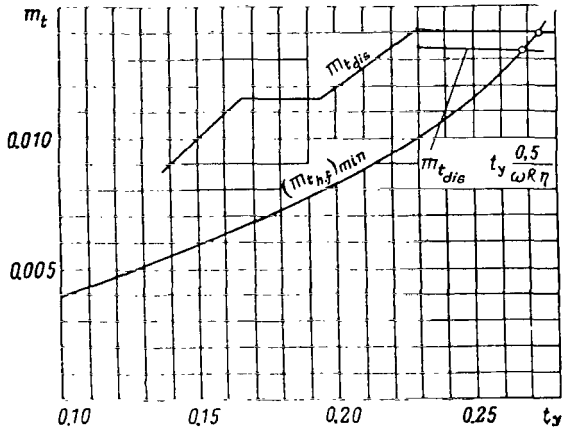

Fig.3.36 Determination of Practical and Theoretical Dynamic Ceilings of a Helicopter ($M_0 = 0.6$; $\sigma = 0.063$; $\overline{c}_{x_{(\alpha=0)}} = 0.0075$ without Rotor Hub).

The static ceiling of a helicopter is determined under maximum engine operating conditions, since transport helicopters are generally not intended for prolonged hovering and usually hover briefly during takeoff and landing, closely above the field in the zone of influence of the air cushion.

As a typical example, let us determine the static ceiling and vertical rate of ascent of a helicopter at takeoff power, with $\omega R = 212$ m/sec. The calculations, made by means of the graph shown in Fig.3.34, are given in Table 3.3.

From the intersection of the curve of $m_{t_{dis}}$ with the curve m_t for $\overline{V} = 0$, we find t_y corresponding to the static ceiling, and the static ceiling itself: $t_y = 0.128$; $\Delta = \frac{0.1175}{0.128} = 0.917$; $H_{st} = 890$ m.

For a more complete study of helicopter data in hovering, a graph of maximum rotor thrust should be plotted as a function of flight altitude, for different temperature conditions t_{rot} with and without consideration of the ground effect (the latter is required for estimating the possibility of takeoff and landing of a helicopter in mountainous terrain). The calculation (Table 3.3) is

TABLE 3.3

H, m	0	750	1000	1500	1860
t_y	0.1175	0.126	0.13	0.136	0.141
$N_{eng_{t.o}}$, hp	1700	1720	1685	1600	1560
ξ			0.8		
$m_{t_{dis}}$	0.00784	0.00854	0.00858	0.00857	0.00865
$\bar{V}_y$	0.001	0.002	—0.0005	—	—
V, m/sec	0.2	0.4	—0.1	—	—
t	0.119	0.1285	0.129	0.129	0.130
T_{max}, kg	7287	7320	7170	6820	6630

performed by means of the graph in Fig.3.34 in terms of the curve for $V_y = 0$: Here, m_t is determined from the available engine power, t is found from the graph, and the maximum rotor thrust T_{max} is then defined. The graph of T_{max} for the Mi-4 helicopter at takeoff power of the engine is shown in Fig.3.37. Consideration of the ground effect on the rotor thrust is accomplished by means of the coefficient K_h which, for a given rotor, depends on the relative distance to the ground h/R. Thrust with consideration of the ground effect $T_{g.e}$ is equal to

$$T_{g.e} = K_h T. \tag{3.20}$$

In Fig.3.37, $T_{g.e}$ is determined during hovering of the helicopter at a distance of 2 m from the ground, when $K_h \approx 1.12$; this distance enables a helicopter of the size of the Mi-4 to take off vertically and to change to forward flight without touching the ground (ground contact may take place during the takeoff run when the pilot deflects the helicopter and it drops slightly).

The maximum range of horizontal flight $L_{h.f_{max}}$ and maximum duration of /314
horizontal flight $\tau_{h.f_{max}}$ are determined by the expressions:

$$L_{h.f_{max}} = \frac{G_{f_{h.f}}}{q_{min}} [km]; \tag{3.21}$$

$$\tau_{h.f_{max}} = \frac{G_{f_{h.f}}}{G_{hr_{min}}}. \tag{3.22}$$

In these expressions, we denote:

$G_{f_{h.f}}$ = weight of the fuel consumed in horizontal flight of the helicopter;

G_h = hourly fuel consumption in horizontal flight of a helicopter;

q = fuel consumption per kilometer in horizontal flight of the helicopter:

$$q = \frac{G_{hr}}{V}. \tag{3.23}$$

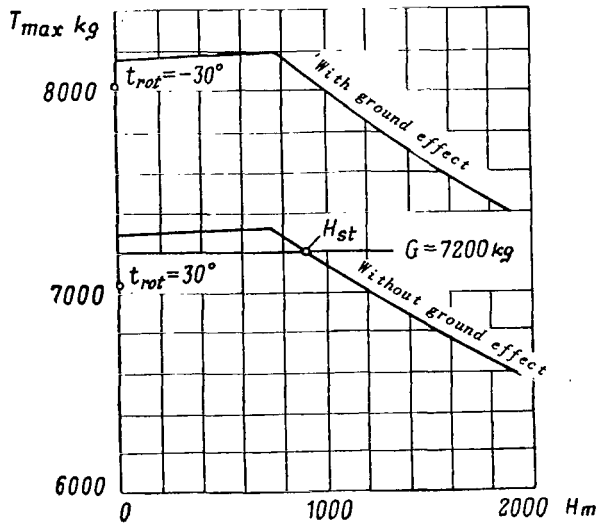

Fig.3.37 Maximum Rotor Thrust of Helicopter in Hovering Flight.

To determine the minimum fuel consumption per kilometer, the minimum fuel consumption per hour, and the economic and cruising speeds, we construct a graph of the fuel consumption per hour and kilometer as a function of flying speed. To construct the graph, we first use Figs.3.27 or 3.30 to find the engine power required for horizontal flight, and the engine characteristics to find the fuel consumption per hour.

The rotor rpm at cruising and economic speeds should be established beforehand. Usually these are equal to the minimum permissible rpm selected by the helicopter designer, on the basis of flight safety and design considerations; they should be combined with the cruising regime of the engine. For the Mi-4 helicopter, the peripheral rotor speed in cruising and economic regimes is equal to ωR = 180 m/sec. Calculation of the graph shown in Fig.3.38 is accomplished in Table 3.4 for an average gross weight of $G_{av} \approx G - \frac{1}{2} G_f$ = 6900 kg.

TABLE 3.4 /315

H=1000 m; ωR=180 m/sec; G_{av}=6900 kg ; t_y=0.172

$\bar{V}$	0.10	0.15	0.20	0.225	0.25	0.30
V, km/hr	65	97	130	146	162	194
$m_{t_{h.f}}$	0.0086	0.00725	0.00685	0.00715	0.0078	0.01015
$N_{h.f}$, hp	985	830	785	819	893	1162
G_{hr}, kg/hr	230	175	163	170	195	308
q, kg/m	3.54	1.8	1.25	1.164	1.203	1.587

It follows from the graph that the minimum fuel consumption per hour and kilometer and their corresponding cruising and economic speeds are equal to

$$q_{min} = 1{,}16 \frac{kg}{km} \quad at \quad V_{cru} = 149 \frac{km}{hr};$$

$$G_{hr.min} = 163 \frac{kg}{hr} \quad at \quad V_{ec} = 125 \frac{km}{hr}.$$

The normal fuel load of the Mi-4 helicopter is 600 kg. From this amount, we must subtract the fuel consumed for starting and ground testing of the engine, for taxiing before takeoff, for test hovering, climbing, descending, and landing, and also amount of fuel needed for maneuvering in the air. The remainder of the unconsumed fuel is incorporated into the empty weight of the helicopter and is disregarded in defining the fuel load.

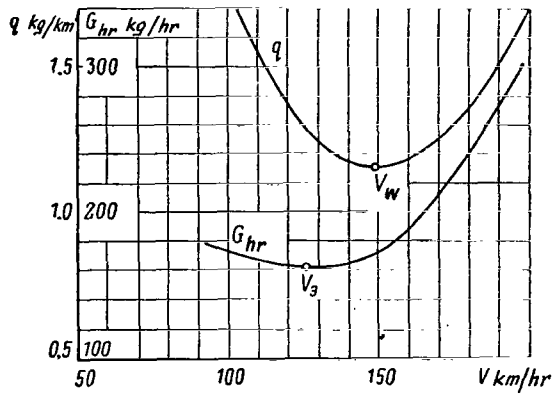

Fig.3.38 Fuel Consumption per Hour and Kilometer of Helicopter.

In determining the above fuel consumption values, it is assumed that engine testing takes 5 min at low speed, taxiing at an engine power of 0.3 of the rated power takes 2 min (distance 0.3 - 0.5 km), test hovering and landing at takeoff power takes 2 - 3 min, climbing at the optimum rate takes place at rated power, descent proceeds at the most advantageous speed of V_y = = 4 - 5 m/sec at 0.3 - 0.5 of the rated power. For transport helicopters, the fuel needed for navigation is assumed as equal to 5% of the total fuel supply.

For the Mi-4 helicopter in long-distance flight at an altitude of 1000 m, the sum of all fuel expenditures, together with the navigation supply, amounts to 100 - 115 kg, i.e., to about 15 - 20% of the total fuel load. The path and flying time consumed in climbing and descending are, respectively, equal to 20 km and 0.2 hr. /316

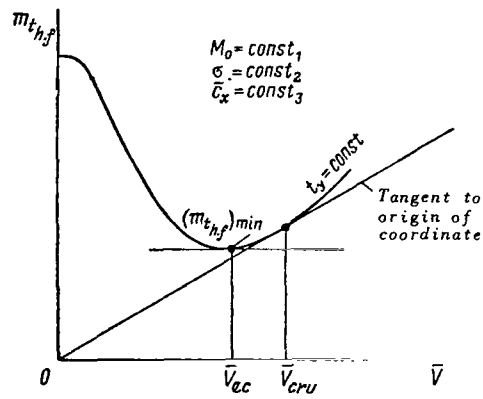

Fig.3.39 For Determining Cruising and Economic Speeds.

Thus, the Mi-4 helicopter consumes 600 - 115 = 485 kg of fuel in horizontal flight; the maximum range and endurance of the helicopter are $L_{h.f_{max}}$ = $= \frac{485}{1.16} = 418$ km, $\tau_{h.f_{max}} = \frac{485}{163} \approx$ $\approx$ 3 hr, while the technical range and endurance are L_{max} = 418 + 20 = 438 km, τ_{max} = 3.2 hr.

On the assumption that the specific fuel consumption is independent of engine power and that the power utilization coefficient is independent of flying speed, the regimes corresponding to maximum range and endurance can be determined directly from the graphs in Fig.3.27 in the manner shown in Fig.3.39.

Usually the optimum rpm in cruising and economic regimes is below that

selected by the helicopter designer. However, if the optimum rpm is to be determined, calculation of $N_{h.f}$ and G_{h_r} is performed for several values of ωR and the optimum rpm is selected from this. On the assumption that the specific fuel consumption is independent of both engine power and engine rpm and if the power utilization factor does not depend on the flying speed, the maximum range and duration can be determined from the following expressions:

$$L_{hf\max} = \frac{270 G_{f_{h.f}}}{C_e G}\xi \frac{1}{\left(\frac{m_{t_{h.f}}}{t_y \overline{V}}\right)_{\min}} [\text{km}]; \tag{3.24}$$

$$\tau_{hf\max} = \frac{33{,}3 G_{f_{h.f}}}{C_e G^{3/2}} \xi R \sqrt{\Delta}\sqrt{\sigma} \frac{1}{\left(\frac{m_{t_{h.f.}}}{t_y^{3/2}}\right)_{\min}} [\text{hr}]. \tag{3.25}$$

The flying speeds and the corresponding rotor rpm (or $\overline{V}$ and t_y) at which $\frac{m_{t_{h.f}}}{t_y \overline{V}}$ and $\frac{m_{t_{h.f}}}{t_y^{3/2}}$ reach a minimum can be found from the graphs of these quantities plotted on the basis of the graphs shown in Fig. 3.27.

It should be noted that the quantity $1/\frac{m_{t_{h.f}}}{t_y \overline{V}}$ is equal to the product of helicopter performance and propulsive efficiency of the rotor $K_h \eta$ [see eq.(7.10) in Chapt. II]; consequently,

$$L_{hf} = \frac{270 G_{f_{h.f}}}{C_e G} K_h \eta \xi [\text{km}]. \tag{3.24'}$$

Minimum vertical rate of descent. This rate, in gliding in an autorotation regime at a given peripheral rotor speed is determined from the auxiliary graph shown in Fig. 3.33. For this, eq.(3.2) is used for calculating $t_{y_{h.f}}$; for $\Delta m_t = -(m_{t_{h.f}})_{\min}$ and $\overline{V}_a$, Fig. 3.33 is used for determining $\overline{V}_y$ and then $V_y = \overline{V}_y \omega R$. /317

However, in autorotation the vertical rates of descent are determined in the entire range of flying speeds, both at constant rotor rpm and at constant pitch θ_{0_c}. To solve these problems, the graphs of rotor characteristics in autorotation, shown in Fig. 2.110, are used [if necessary, these characteristics are converted by eqs.(3.3) - (3.6)].

For constant rotor rpm, the calculation is performed by the method of successive approximations. As first approximation, we use $\cos \theta_{f1.p_1} = 0.97$; after calculating $(t_{y_c})_1$ by means of eq.(1.5), the quantities $(t_{x_c})_1$, α_{c_1}, α_{f_1}, $\overline{c}_{x_1}$ for a series of V are determined from the graphs of the rotor characteristics, and the equations of motion of the helicopter are used for finding the angle $\theta_{f1.p_2}$

$$-\tan\theta_{fl.p_2}=\frac{(t_{x_c})_1+\bar{c}_x\frac{\overline{V}^2}{\sigma}}{(t_{y_c})_1}. \tag{3.26}$$

After repeating the calculations until the values of the angle $\theta_{fl.p}$ coincide, we find the flight-path speed and its vertical and horizontal components

$$V=\overline{V}\omega R; \tag{3.27}$$

$$V_y=V\sin\theta_{fl.p}; \tag{3.28}$$

$$V_x=V\cos\theta_{fl.p}. \tag{3.29}$$

We note that $-\tan\theta_{fl.p}$ is equal to the inverse helicopter performance during gliding in autorotation:

$$-\tan\theta_{fl.p}=\frac{1}{K_{h_c}}. \tag{3.30}$$

In calculating the autorotation regime with a selected rotor setting (usually θ_{0_c} = 3 - 5°), the quantities t_{y_c}, t_{x_c}, and α_c are determined for several $\overline{V}$ from the rotor characteristics. Then, $\theta_{fl.p}$, ωR, and M_0 are obtained from the expressions:

$$\tan\theta_{fl.p}=-\frac{t_{x_c}+c_x\frac{\overline{V}^2}{\sigma}}{t_{y_c}};$$

$$\omega R=\sqrt{\frac{G\cos\theta_{fl.p}}{\frac{1}{2}\rho\sigma F t_{y_c}}};$$

$$M_0=\frac{\omega R}{a}.$$

If M_0 is less than 0.6, the solution is considered valid since, in this case, the effect of M_0 on the rotor characteristics can be disregarded.

If $M_0 > 0.6$, the calculations must be repeated, determining t_{y_c}, t_{x_c}, and /318 α_c for M_0 obtained in the preceding approximation. The successive approximations are carried out rapidly and present no difficulties. After final determination of ωR, we determine V, V_y, and V_x by means of eqs.(3.27) - (3.29).

As a typical example, let us calculate gliding in autorotation of the Mi-4 helicopter with a gross weight of 7200 kg at an altitude of H = 0 for ωR = = 196 m/sec. The experimental characteristics of the rotor converted to the solidity ratio $\sigma \approx 0.063$ are shown in Figs.3.40 and 3.41.

The calculation is made in Table 3.5, and the dependence of V_y and $\theta_{fl.p}$ on

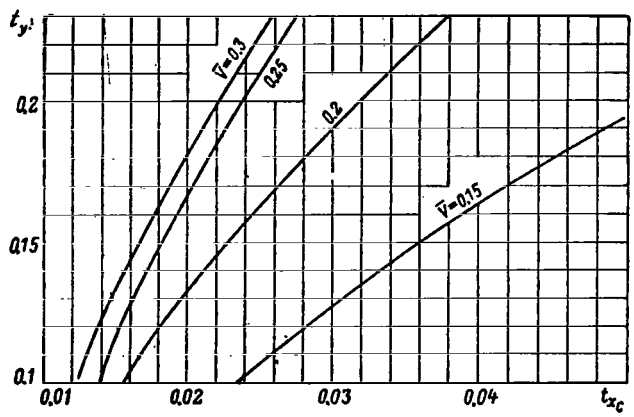

Fig.3.40 Polars of Rotor in Autorotation Regime (M_o = 0.6; σ = 0.063).

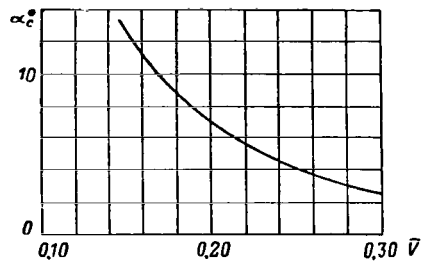

Fig.3.41 Angle of Attack of Rotor in Autorotation Regime (M_o = 0.6; σ = 0.063).

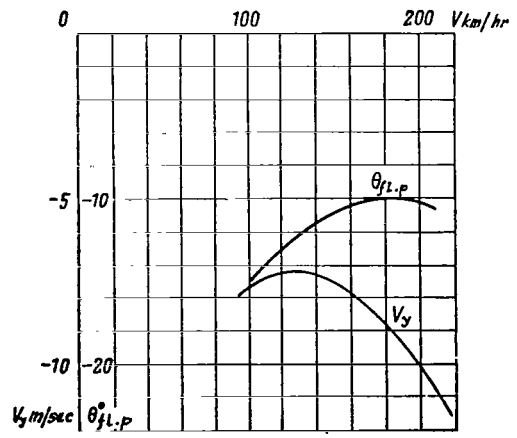

Fig.3.42 Rate of Descent and Gliding Angle of Helicopter in Autorotation Regime.

V is plotted in Fig.3.42. This diagram indicates that the minimum vertical rate of descent of the helicopter is 7.2 m/sec at V = 130 km/hr, while the maximum gliding range, equal to

$$L_{gl}=\frac{H}{|tan\theta_{fl.p}|}=HK_{h_c}, \tag{3.31}$$

is obtained for $\theta_{fl.p_{min}}$ = -10°; $(K_{h_c})_{max}$ = 5.7; V = 180 km/hr.

TABLE 3.5

$H=0$; $\omega R=196\ m/sec$; $t_y=0{,}138$

$\bar{V}$	0.15	0.20	0.25	0.30
V, km/hr	106	141	176	211
$(t_{y_c})_1$	0.1338			
$(t_{x_c})_1$	0.0315	0.0202	0.0166	0.0150
α_{c_1}	13	7	4.2	2.6
$\alpha_{f_1}=\alpha_{c_1}+8°$	21	15	12.2	10.6
$\bar{c}_x$	0.0067			
$\frac{\bar{c}_x\bar{V}^2}{\sigma}$	0.00239	0.00425	0.00664	0.00957
$\sin\theta_{fl.p}$	—0.253	—0.183	—0.174	—0.183
$\theta_{fl.p}$	—14°40′	—10°35′	—10°	—10°35′
$\cos\theta_{fl.p}$	0.967	0.983	0.9845	0.983
t_{y_c}	0.1334	0.1356	0.1358	0.1356
t_{x_c}	0.0315	0.0206	0.0168	0.0152
$\sin\theta_{fl.p}$	—0.254	—0.183	—0.1726	—0.1826
$\theta_{fl.p}$	—14°42′	—10°35′	—10°	—10°30′
$V_y=V\sin\theta_{fl.p}$, m/sec	—7.5	—7.2	—8.45	—10.7

3. Graphs for Determining Optimum Helicopter Aerodynamic Parameters

/320

The described method of aerodynamic design and the graphs of rotor characteristics used in it are convenient for a check calculation of a helicopter with known parameters, since sufficient data are available for determining the coeffi-

cients $t_{y_{h.f}}$ and $t_{x_{h.f}}$ in calculating horizontal flight regimes and the coefficient $m_{t_{dis}}$ in calculating climbing regimes.

In designing a helicopter, a preliminary version of the parameters is selected on the basis of practical experience with previous models and on the basis of applicable values of peripheral speed, thrust coefficient, load per square meter of rotor disk, etc. The next step is to refine the helicopter parameters. To study the effect of parameters on the performance data of a helicopter, special graphs should be constructed. Such graphs are necessary also in investigating the maximum possibilities of helicopters for improving the flight characteristics.

Calculations for aerodynamic parameter selection should be accompanied by weight calculations and by investigations of the variation of parameters in a limited range within which the helicopter has a sufficient useful load.

In this Subsection, a graph is described to be used for defining the rotor parameters ensuring the minimum required power (minimum fuel consumption per hour and kilometer) at given weight, $\Sigma c_x S$, speed, and altitude. From this graph, the optimum diameter, solidity ratio, and peripheral speed of the rotor can be determined.

The equations for calculating horizontal flight regimes are transformed in such a manner that, in all equations, the smallest number of sought parameters will correlate dimensionless coefficients with the prescribed quantities. Equations (3.1) and (3.2) can be reduced to the form

$$\frac{\sum c_x S}{F} = \frac{-t_x \sigma M_0^2}{M_{fl}^2}; \tag{3.32}$$

$$G = \frac{1}{2} \varrho (\omega R)^2 \sigma F t_y = \frac{1}{2} \varrho (a M_0)^2 \sigma \left(\frac{M_{fl}^2 \sum c_x S}{-t_x \sigma M_0^2} \right) t_y;$$

$$\frac{G}{\sum c_x S} = \frac{1}{2} \varrho a^2 \left(\frac{t_y M_{fl}^2}{-t_x} \right). \tag{3.33}$$

In like manner, we transform the equation for determining the required power

$$N_{rot} = \frac{1}{150} \varrho (\omega R)^3 \sigma F m_t = \frac{1}{150} \varrho (a M_0)^3 \sigma \left(\frac{M_{fl}^2 \sum c_x S}{-t_x \sigma M_0^2} \right) m_t;$$

$$\frac{N_{rot}}{\sum c_x S} = \frac{1}{150} \varrho a^3 \frac{m_t M_0 M_{fl}^2}{-t_x}. \tag{3.34}$$

It should be noted that the quantities M_0, M_{fl}, $\frac{G}{\rho a^2}$, $\frac{N_{rot}}{\rho a^3}$ are proportional to the reduced parameters of the helicopter: ω_r, V_r, G_r, N_{rot_r}.

It is obvious that the required power will be lowest at a minimum of the

TABLE 3.6

	M_0	0.61				0,655			
	t_y	0,12	0.14	0.16	0,18	0.12	0,14	0,16	0,18
	t_x	−0.00853	−0,00995	−0,01138	−0,0128	−0,00853	−0,00995	−0,01138	−0,0128
σ=0,091	m_t	0,00825	0,00957	0,01157	0,0146	0,0086	0,0098	0,01165	0,0143
	$\frac{m_t M_0 M_{fl}^2}{-t_x}$	0,03056	0,03039	0,03214	0,0360	0,0342	0,0334	0,0347	0,0379
	$\frac{-t_x \sigma M_0^2}{M_{fl}^2}$	0,00558	0,00651	0,00744	0,00837	0,00643	0,0075	0,00857	0,00965
σ=0,1	Δt_x	0,00024	0,00033	0,00043	0,00055	0,00028	0,00038	0,00050	0,00063
	$t_{x\,(\sigma=0,091)}$	−0,00877	−0,01028	−0,01181	−0,01335	−0,00881	−0,01033	−0,01188	−0,01343
	m_t	0,0084	0,00972	0,01178	0,01483	0,00872	0,00993	0,01188	0,0146
	$\frac{m_t M_0 M_{fl}^2}{-t_x}$	0,0312	0,03085	0,0327	0,0366	0,03465	0,0338	0,0354	0,0387
	$\frac{-t_x \sigma M_0^2}{M_{fl}^2}$	0,00614	0,00715	0,00817	0,0092	0,00706	0,00824	0,00942	0,0106

ratio $\frac{m_t M_0 M_{f1}^2}{-t_x}$. To find it, a graph in coordinates $\frac{m_t M_0 M_{f1}^2}{-t_x} = f\left(\frac{-t_x \sigma M_0^2}{M_{f1}^2}\right)$ is plotted for a value of the ratio $\frac{t_y M_{f1}^2}{-t_x}$ given by eq.(3.33) at $M_{f1} = V/a =$ /322
$=$ const.

The sequence of constructing the graph is as follows: For the value of M_{f1} selected for the investigation, define the aerodynamic characteristics of the rotor in the form of a dependence, shown in Figs.2.105 - 2.109, for several values of M_0. After assigning several values to the coefficient t_y and the quantity $\frac{G}{\Sigma c_x S} \cdot \frac{1}{1/2\,\rho a^2}$, determine t_x from eq.(3.33) and find m_t for each M_0 from the graphs of the aerodynamic characteristics. Then, calculate the ratio of the coefficients entering eqs.(3.32) and (3.34). When using the solidity ratio of the rotor, the quantity t_x is converted by eq.(3.3) or by the formula

$$t_{x_2} = t_{x_1} - \frac{(\sigma_1 - \sigma_2)\, t_y M_0^2}{4B^2 M_{f1}^2}.$$

In Table 3.6 a calculation is made for a flying speed of V = 275 km/hr at an altitude of H = 1000 m (a = 336.1 m/sec, $\frac{1}{2}\rho a^2$ = 6400 kg/m^2) for $\frac{G}{\Sigma c_x S}$ = $=$ 4670 kg/m^2. For these data, we have

$$M_{f1} = 0.227;$$

$$-t_x = t_y \frac{0.227^2 \cdot 6400}{4670} = 0.0711 t_y.$$

TABLE 3.7

Assigned Parameter	Optimum Parameter	$\left(\frac{150 N_{rot}}{\rho a^3 \sum c_x S}\right)_{min}$	$\frac{N_{rot\,min}}{hp}$
σ=0.091; ωR=212 *m/sec*; M_0=0.63 (*point a*)	$\left(\frac{\sum c_x S}{F}\right)_{opt}$=0.00682; D_{opt}=37.43 *m*	0.0317	6816
D=34.56 *m*; $\frac{\sum c_x S}{F}$ = 0.008; σ=0.091 (*point b*)	$M_{0_{opt}}$=0.63; ωR_{opt}= =212 *m/sec*	0.0331	7117
D=34.56 *m*; $\frac{\sum c_x S}{F}$ = 0.008; ωR=220 *m/sec*; M_0=0.655 (*point c*)	σ_{opt}=0.095	0.0336	7224

The graph for determining the optimum aerodynamic parameters is shown in Fig.3.43. Curve 1 connects the minima of the curves with identical σ. From

curve 1 we find the optimum rotor diameter at a given rpm (M_0) and σ. Curve 2 is the envelope of the curves with identical σ, from which we find the optimum rpm at given diameter and σ. Curve 3 is the envelope of the curves with identical M_0, from which we find the optimum solidity ratio at given diameter and M_0.

As an example, Table 3.7 gives the optimum parameters of a helicopter for G = 35,000 kg and $\Sigma c_x S = 7.5$ m^2.

/323

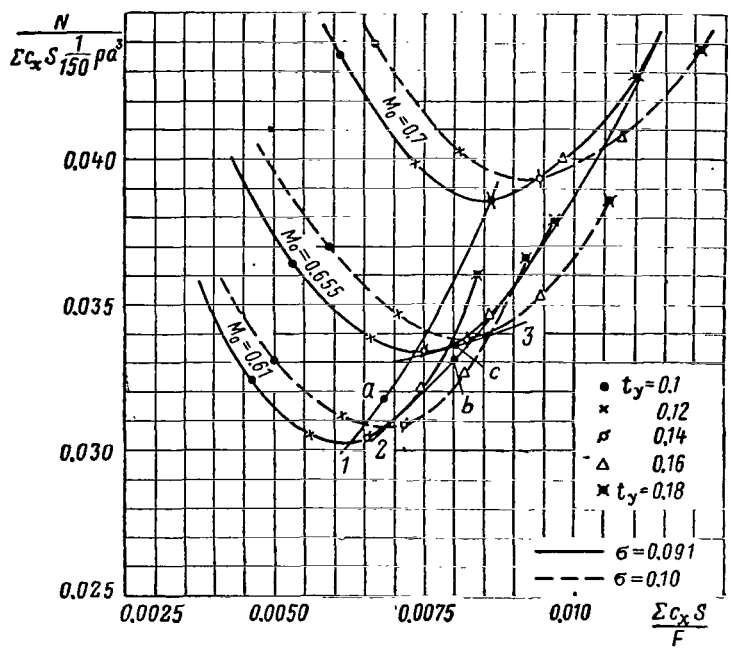

Fig.3.43 Graph for Determining the Optimum Aerodynamic Parameters of a Helicopter ($M_{f1} = 0.227$; $\frac{G}{\frac{1}{2}\rho a^2 \Sigma c_x S} = 0.73$).

The above method can be used for finding the optimum aerodynamic parameters of a helicopter with a tractor propeller and wing; however, in this case, it is necessary to first determine the parameters of the propeller and wing ($m_{t_{t.p}}$, t_{y_w}/t_{y_Σ}, etc.) at which the dependence $t_{x_\Sigma} = f(m_{t_\Sigma})$ is optimum, i.e., at which the smallest values of t_{x_Σ} for all m_{t_Σ} and t_{y_Σ} are obtained.

Section 4. Aerodynamic Design of a Helicopter Based on Concepts of Rotor Performance and Efficiency

The concepts of performance K and propulsive efficiency η of a rotor are given in Chapter II, Section 7. There graphs are presented, obtained from experiment and calculation and useful for finding the values of K and η.

In this Section, we present a method of aerodynamic design of a helicopter

with the use of the concepts of performance K and efficiency η. The design formulas for determining required power and vertical speed of a helicopter are completely analogous to the formulas for calculating airplanes.

This is a very simple method of calculation, easily extended to helicopters of any configuration with a wing and tractor propeller or cruise jet engine. In a general form, it permits making various estimate calculations in a simple manner: estimating the expediency of installing a wing and tractor propellers on a helicopter, finding the power/weight ratio N/G required for producing a given maximum speed, and determining then the amount by which to reduce the required power when reducing the parasite drag of the helicopter. /324

Since the performance and efficiency yield an approximate description of the aerodynamic characteristics of the rotor, this method of calculation ranges high among the approximate methods of aerodynamic design.

1. Helicopter Performance

The helicopter performance in horizontal flight regime is determined by eq.(7.9) of Chapter II

$$K_h = \frac{t_y}{t_{x_c} - t_{x_{hf}}} = \frac{t_y}{t_{x_c} + \bar{c}_x \frac{\bar{V}^2}{\sigma}} = \frac{C_Y}{C_{X_c} + \bar{c}_x \bar{V}^2}. \tag{4.1}$$

In calculations it is more convenient to use the inverse quantity, namely the inverse performance of the helicopter:

$$\frac{1}{K_h} = \frac{t_{x_c}}{t_y} + \frac{\bar{c}_x \bar{V}^2}{t_y \sigma} = \frac{1}{K} + \frac{\bar{c}_x \bar{V}^2}{t_y \sigma}. \tag{4.2}$$

Changing to dimensional quantities, Y = G and Q_{par}, we obtain

$$\frac{1}{K_h} = \frac{1}{K} + \frac{Q_{par}}{G}, \tag{4.3}$$

where the parasite drag of the helicopter is

$$Q_{par} = \frac{1}{2} \rho V^2 \sum c_x S. \tag{4.4}$$

When using the conversion formulas for determining the performance of a rotor with differing parameters (see Chapt.II, Sect.7.6), the helicopter performance is found from the expression

$$\frac{1}{K_h} = \frac{1}{K} + \frac{(\sigma - \sigma_1) t_y}{4B^2 \bar{V}^2} + \frac{\Delta m_{pr} \eta}{t_y \bar{V}} + \frac{Q_{par}}{G}. \tag{4.5}$$

2. Performance of Multirotor and Composite Helicopters

In the general case, the inverse performance of the craft is

$$\frac{1}{K_h}=\frac{\sum X+Q_{par}}{\sum Y}=\frac{\sum X}{G}+\frac{Q_{par}}{G}, \tag{4.6}$$

where $\sum Y$ and $\sum X$ are the sums of lifts and drag of all lifting elements of the helicopter.

Let us derive the expressions of ΣY and ΣX, for two types of helicopters.

Single-rotor helicopter with wing. The lift of the helicopter lifting system consists of the sum of lifts of the rotor and wing

$$\sum Y=Y_{rot}+Y_w\ . \tag{4.7}$$

We represent $\sum y$ in the form $\Sigma Y = G(\overline{Y}_{rot} + \overline{Y}_w)$ having designated: $\overline{Y}_{rot} = \frac{Y_{rot}}{\Sigma Y}$ and $\overline{Y}_w = \frac{Y_w}{\Sigma Y}$.

In horizontal flight, we have /325

$$\left.\begin{aligned}&\sum Y=G;\\&t_{y_\Sigma}=t_{y_{rot}}+t_{y_w};\\&\bar{Y}_{rot}+\bar{Y}_w=1;\end{aligned}\right\} \tag{4.8}$$

$$\left.\begin{aligned}&\bar{Y}_{rot}=\frac{Y_{rot}}{G}=\frac{t_{y_{rot}}}{t_{y_\Sigma}};\\&\bar{Y}_w=\frac{Y_w}{G}=\frac{t_{y_w}}{t_{y_\Sigma}}=\frac{c_{y_w}}{t_{y_\Sigma}}\frac{S_w}{Fa}\bar{V}^2.\end{aligned}\right\} \tag{4.9}$$

The drag is made up of the drags of the isolated rotor and wing and of projections of the rotor and wing lifts onto the direction of motion (see Fig.3.11)

$$\sum X=X_{rot}+X_w+Y_{rot}\,\Delta\alpha_{rot}+Y_w\,\Delta\alpha_w, \tag{4.10}$$

where $\Delta\alpha_{rot}$ and $\Delta\alpha_w$ are the averaged downwash angles of the rotor and wing.

On substituting eqs.(4.8) and (4.10) into eq.(4.6), we obtain

$$\frac{1}{K_h}=\bar{Y}_{rot}\left(\frac{1}{K}+\Delta\alpha_{rot}\right)+\bar{Y}_w\left(\frac{1}{K_w}+\Delta\alpha_w\right)+\frac{Q_{par}}{G}. \tag{4.11}$$

The downwash angles are determined, as described in Section 1, by the expressions

$$\left.\begin{aligned}\Delta\alpha_{rot}&=\varkappa_{rot}\frac{c_{y_W}}{\pi\lambda_W};\\ \Delta\alpha_W&=0.26\varkappa_W\frac{t_{y\sigma}}{\bar{V}^2}.\end{aligned}\right\}\qquad(4.12)$$

Two-rotor helicopter with wing. After performing similar calculations, we find

$$\frac{1}{K_h}=\bar{Y}_{rot_1}\left(\frac{1}{K_1}+\Delta\alpha_{rot_1}\right)+\bar{Y}_{rot_2}\left(\frac{1}{K_2}+\Delta\alpha_{rot_2}\right)+\bar{Y}_W\left(\frac{1}{K_W}+\Delta\alpha_W\right)+\frac{Q_{par}}{G},\qquad(4.13)$$

where the subscripts "1" and "2" denote quantities pertaining to each of the rotors.

The total downwash angles due to the other two elements of the lifting system of the helicopter are equal to

$$\left.\begin{aligned}\Delta\alpha_{rot_1}&=\varkappa_{rot_1}\frac{c_{y_W}}{\pi\lambda_W}+0.26\varkappa_1\frac{\sigma t_{y_1}}{\bar{V}^2},\\ \Delta\alpha_{rot_2}&=\varkappa_{rot_2}\frac{c_{y_W}}{\pi\lambda_W}+0.26\varkappa_2\frac{\sigma t_{y_2}}{\bar{V}^2},\\ \Delta\alpha_W&=0.26\varkappa_{W_1}\frac{\sigma t_{y_1}}{\bar{V}^2}+0.26\varkappa_{W_2}\frac{\sigma t_{y_2}}{\bar{V}^2}.\end{aligned}\right\}\qquad(4.14)$$

For a helicopter of side-by-side configuration, both rotors operate under equal conditions (all quantities with the subscripts "1" and "2" are equal to each other), and $\varkappa_1 = \varkappa_2 = \varkappa_{s.s}$. Therefore, for a helicopter of side-by-side configuration we obtain the following expressions:

$$2\bar{Y}_{rot}=1-\bar{Y}_W;\qquad(4.15)$$

/326

$$\frac{1}{K_h}=2\bar{Y}_{rot}\left(\frac{1}{K}+\Delta\alpha_{rot}\right)+\bar{Y}_W\left(\frac{1}{K_W}+\Delta\alpha_W\right)+\frac{Q_{par}}{G};\qquad(4.16)$$

$$\left.\begin{aligned}\Delta\alpha_{rot}&=\varkappa_{rot}\frac{c_{y_W}}{\pi\lambda_W}+0.26\varkappa_{ss}\frac{\sigma t_{y_{rot}}}{\bar{V}^2};\\ \Delta\alpha_W&=2\cdot0.26\varkappa_W\frac{\sigma t_{y_{rot}}}{\bar{V}^2}.\end{aligned}\right\}\qquad(4.17)$$

For a helicopter of fore-and-aft configuration with a wing between the rotors, the front rotor is virtually outside the influence of the tail rotor and wing, and the wing is outside the influence of the tail rotor. However, the induction coefficients $\varkappa$ for the tail rotor and for the wing should be doubled

$$\left.\begin{aligned} \varkappa_{rot_1} = \varkappa_1 = \Delta\sigma_{rot_1} = 0; \\ \varkappa_{w_1} = 0; \\ \varkappa_{rot_2} = 2\varkappa_{rot}; \\ \varkappa_2 = 2\varkappa_{c0}; \\ \varkappa_{w_1} = 2\varkappa_w. \end{aligned}\right\} \qquad (4.18)$$

The total required power of rotors of a fore-and-aft helicopter depends little on the relation of rotor lifts. This is explained by the fact that, in conformity with the general theory of induced drag, this power does not depend on the lift distribution between individual elements of the lifting system, and the profile power of the rotors does not greatly depend on the lifting force of the rotors (in regimes not close to flow separation). Therefore, to determine the total required power of two rotors we can set $Y_1 = Y_2$. Actually, the lifts of both rotors are close in value with respect to balancing conditions of the helicopter.

After setting $\overline{Y}_{rot_1} = \overline{Y}_{rot_2} = \overline{Y}_{rot}$ and $K_1 = K_2 = K$ in eqs.(4.13) and (4.14), we find that the quantity K_h can be determined by eqs.(4.16) and (4.17), with the induction coefficients not doubled. The physical meaning of this expression is that, to determine the total power, it is possible to replace two rotors by one with a double lifting force inserted between the rotors. The downwash of this rotor is equal to the half-sum of the downwashes of the front and tail rotors, i.e., equal to half of the downwash of the tail rotor.

The sequence of calculation of helicopter performance is as follows: In a check calculation of a helicopter the gross weight, diameter, solidity ratio, rotor rpm, and parasite drag coefficient are known. After assigning the flying speed and altitude, find the following dimensionless coefficients:

$$t_{y\Sigma} = \frac{G}{\frac{1}{2}\rho\sigma F(\omega R)^2};$$

$$\overline{V} = \frac{V}{\omega R};$$

$$M_0 = \frac{\omega R}{a},$$

on the basis of which, using the graphs in Section 7, Chapter II, find the rotor performance. Then, calculate Q_{par} from eq.(4.5) and determine K_h.

In calculating the performance of composite helicopters, it is necessary /327 to know the lift distribution between individual elements of the lifting system, i.e., $\overline{Y}_{rot_1}$, $\overline{Y}_{rot_2}$, $\overline{Y}_w$. For estimate calculations, we can assign $\overline{Y}_w$ and c_{y_w} for some flight regime, bearing in mind that these quantities can be obtained by an appropriate selection of the setting angle and the wing area. Then, using eqs.(4.8) and (4.9), we find $\overline{Y}_{rot}$, $t_{y_{rot}}$; from the rotor and wing characteristics we determine K, K_w. After calculating the downwash angles by eqs.(4.17), we

find K_h.

When the geometric characteristics and the setting angle of the wing are given, the following method can be used for determining rotor and wing lift in horizontal flight.

The angle of pitch of a two-rotor helicopter, measured from the plane of rotation of the rotor (front rotor for a helicopter of fore-and-aft configuration), is determined by the following expression:

$$\vartheta = \frac{Q_{par}}{2\bar{Y}_{rot}\, G} - \frac{\bar{Y}_w}{2\bar{Y}_{rot}}\left(\frac{1}{K_w} + \Delta\alpha_w\right) - 0.35\bar{V} - D_1\varkappa - \frac{\Delta\varepsilon_{rot_e}}{2}. \qquad (4.19)$$

Equation (4.19) is obtained from the condition of equating to zero the sum of projections of all forces onto the direction of motion, on the assumption that the angle $\vartheta = \alpha_h = \alpha_1$ is small, $T_1 = T_2$, $H_1 = H_2 = H_e + TD_1\varkappa$, $H_e \approx 0.35\ \bar{V}T$, $\bar{Y}_{rot} = T$, $X_{rot} = T\vartheta + H{:}T_1\vartheta + T_2\ (\vartheta + \varepsilon_{rot}) + H_1 + H_2 + Q_{par} + X_w \approx \Sigma X = 0$.

From the angle of pitch of the helicopter, we can find the angle of attack of the wing

$$\alpha_w = \vartheta + \varepsilon_w - \Delta\alpha_w, \qquad (4.20)$$

where ε_w is the setting angle of the wing relative to the plane of rotation of the rotor.

For known $\bar{V}$, t_{y_Σ}, $\frac{S_w}{F\sigma}$, $\bar{l}_w$, $\frac{Q_{par}}{G}$, ε_w, ε_{rot_e}, $D_1\varkappa$ (the desired value of $D_1\varkappa$ is obtained by selecting the angle of stabilizer setting), using eqs.(4.19) and (4.20), as well as (4.9), (4.14), and (4.15), all quantities entering these formulas are found by successive approximations: α_w, ϑ, c_{y_w}, $t_{y_{rot}}$, $\bar{Y}_w$, $\bar{Y}_{rot}$.

We recommend the following sequence of calculation: After assigning α_w, find c_{y_w}, $\bar{Y}_w$, K_w; by means of eq.(4.15) determine $2\bar{Y}_{rot}$, and then $t_{y_{rot}}$, $\Delta\alpha_w$; find ϑ and, from eq.(4.20), determine α_w of the second approximation.

Two or three approximations must be performed. In this manner all quantities for calculating K_h can be obtained.

As an example, Table 3.8 gives a calculation of the reciprocal performance of the Mi-4 helicopter. The initial data of this helicopter are given in Section 3. Performance and efficiency of the rotor were determined from the graphs in Figs.2.159 and 2.160, with conversion to the difference in solidity ratio. The difference in blade profiles for $M_0 = 0.6$ can be disregarded.

The results of calculating $\frac{1}{K_h}$ for the entire range of t_y are plotted in Fig.3.44, indicating that the inverse performance of the helicopter is minimal at $\bar{V} = 0.25 - 0.3$ and at a lift coefficient close to the maximum permissible owing to flow separation.

The maximum performance is $K_{h_{max}} = 6.0$. At small $\bar{V}$, the reciprocal performance of a helicopter increases owing to a decrease in rotor performance and at large $\bar{V}$, owing to an increase in helicopter drag.

TABLE 3.8 /328

$$\frac{1}{K_h} = \frac{1}{K_{a_1}} + \frac{(0.063-0.091)t_y}{4\cdot 0.96\bar{V}^2} + \frac{\bar{c}_x\bar{V}^2}{0.063 t_y}\ ;\quad t_y = 0.14$$

$\bar{V}$	0.15	0.20	0.25	0.30	0.35
K_{a_1}	3.5	5.4	6.95	8.5	9.25
η	1.011	0.980	0.972	0.964	0.947
$1/K_{a_1}$	0.286	0.1854	0.144	0.1176	0.108
$\frac{0.063-0.091}{4\cdot 0,96\bar{V}^2} t_y$	−0.0462	−0.0261	−0.0167	−0.0116	−0.0085
$1/K$	0.2398	0.1593	0.1273	0.106	0.0995
$\bar{c}_x$	0.009	0.009	0.009	0.0095	0.01
$\frac{\bar{c}_x\bar{V}^2}{0.063 t_y}$	0.023	0.0408	0.0638	0.0980	0.139
$1/K_h$	0.2628	0.2001	0.1911	0.204	0.2385

A second example of calculation is that of the performance of helicopters of different configurations: single-rotor, fore-and-aft, tandem, single-rotor with wing, and tandem with wing.

The calculations were made under the following conditions: For helicopters without a wing, the lift coefficient of the rotor is equal to $t_{y_{rot}} = 0.13$, and for helicopters with a wing to $t_{y_\Sigma} = 0.16$ and 0.32. The larger value of t_{y_Σ} for helicopters with a wing corresponds to two cases: a decrease in rotor diameter when a wing is installed and a decrease in peripheral speed without a change in rotor diameter. The solidity ratio of the rotor is $\sigma = 0.091$, $M_0 = 0.65$, and $M_0 = 0.65\sqrt{\frac{0.13}{0.16}} = 0.587$ in the latter case. The angle of wing setting was selected so that relief of the rotor load was equal to at least 20% at $M_{f1} > 0.2$. The performance and efficiency of the rotor were determined /329 from the graphs in Figs.2.159 and 2.160 and both c_y and wing performance, from Fig.3.45. The parasite drag coefficient of the single-rotor helicopter, referred to rotor area, is equal to 0.0075 and, on a decrease in diameter, becomes $0.0075\ \frac{0.16}{0.13} = 0.00925$; for two-rotor helicopters, the magnitude of $\Sigma c_x S$ is twice that of the single-rotor helicopter. The wing area of the single-rotor helicopter, referred to rotor area, is equal to 0.0325; on a decrease in rotor diameter, the wing area did not change and in relative values was equal to

$0.0325 \frac{0.16}{0.13} = 0.04$. The relative wing span t_w/R is equal to 0.85 and 0.95, respectively. For tandem helicopters, the wing area is determined by the rotor dimensions and is assumed as 0.16 of the area of one rotor. The aspect ratio of the wings is equal to $\lambda_w = 7.2$.

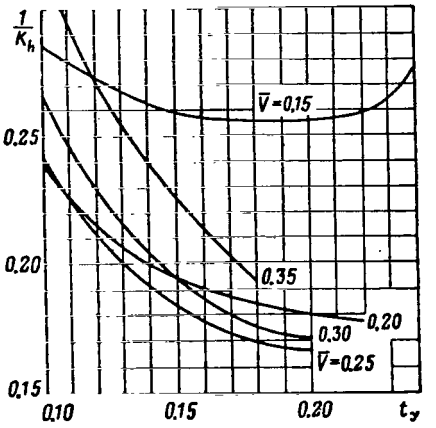

Fig.3.44 Reciprocal Performance of Helicopter as a Function of Lift Coefficient and Relative Flying Speed.

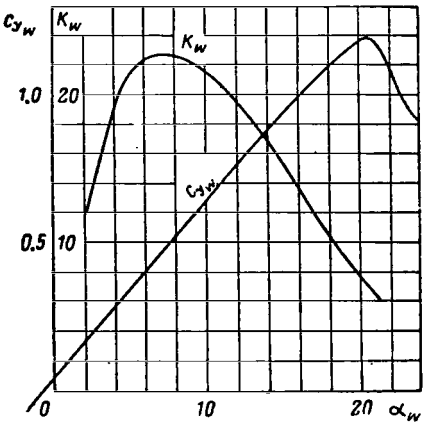

Fig.3.45 Lift Coefficient and Wing Performance as a Function of Angle of Attack.

Calculation of the performance of helicopters without a wing is made in Table 3.9, while the performance of helicopters with a wing in a version with a decreased rotor diameter is given in Table 3.10.

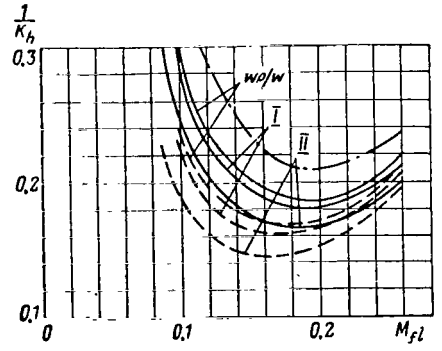

Fig.3.46 Reciprocal Performance of Helicopters of Different Configurations with and without a Wing as a Function of M_{fl}.

Legend:

—— Single-rotor configuration;
- - - - Side-by-side configuration;
-·-·- Fore-and-aft configuration;
wo/w, helicopter without wing;
I, helicopter with wing and reduced diameter;
II, helicopter with wing and reduced peripheral speed.

TABLE 3.9

HELICOPTERS WITHOUT WING

	$\bar{V}$	0.15	0.20	0.30	0.40
	K	3.5	5.2	7.85	8.42
	η	1.00	0.977	0.962	0.936
	$\frac{\bar{c}_x \bar{V}^2}{\sigma t_{y_\Pi}}$	0.0142	0.0253	0.057	0.1014
Single-rotor configuration	$\frac{1}{K_{rot}}$	0.286	0.1925	0.127	0.119
	$\frac{1}{K_h}$	0.300	0.2178	0.184	0.220
Fore-and-aft configuration	$\frac{\bar{Y}_{rot}}{K}$	0.143	0.0962	0.0635	0.0595
$x_{co} = 0.65$	α_{rot_s}	0.181	0.102	0.0454	0.0255
$t_{y_\Pi} = 0.26$	$\bar{Y}_{rot_s}\left(\frac{1}{K} + \Delta\alpha_{rot_s}\right)$	0.2335	0.1472	0.0862	0.0722
	$\frac{1}{K_h}$	0.3907	0.2687	0.2092	0.2373
Side-by-side configuration	$\Delta\alpha_{rot}$	—0.0558	—0.0314	—0.01395	—0.00785
$x_{s.s} = -0.4$	$\frac{1}{K} + \Delta\alpha_{rot}$	0.2302	0.1611	0.11305	0.11075
$t_{y_\Pi} = 0.26$	$\frac{1}{K_h}$	0.2444	0.1864	0.17005	0.21215

The results of the calculations are plotted in Fig.3.46, which shows that, in the entire speed range, the reciprocal performance of the helicopter of side-by-side configuration has a lower value and that of the fore-and-aft configuration, a higher value. The maximum performance is equal to: 6 for a side-by-side helicopter at $\bar{V} = 0.27$; 5.5 for a single-rotor helicopter at $\bar{V} = 0.29$; 4.8 for a fore-and-aft helicopter at $\bar{V} = 0.3$. At $M_{f_1} = 0.26$ ($\bar{V} = 0.4$), the performance of the helicopters is, respectively, equal to: 4.7; 4.55; and 4.23. /331

The wing, relieving 20 - 30% of the rotor load at high flying speeds, changes the helicopter performance in the following manner: If, on installation of a wing, the rotor diameter was decreased, the helicopter performance increases very little (curve I). If the rotor diameter was not decreased but its rpm was raised (curve II), the maximum performance of the helicopter increases by 0.5 - 0.9 (by 10 - 15%) and, at maximum speed ($M_{f_1} = 0.26$), increases by 0.4 (approximately 9%). Calculations showed that if, on installing a wing, the rotor parameters are not changed so that the rotor at high speeds has a very low

TABLE 3.10

Single-Rotor Helicopter with Wing $t_{y_2}=0.16$; $\bar{c}_x=0.00925$; $M_0=0.65$; $\bar{S}_w=0.04$; $\bar{l}_w=0.95$; $\varkappa_{rot}=0.2$; $\varkappa_w=0.69$; $\varepsilon_w=21.97°$					Tandem Helicopter with Wing $t_{y_2}=0.32$; $\bar{c}_x=0.0185$; $M_0=0.65$; $\bar{S}_w=0.16$; $\bar{z}=\bar{l}_w=1.9$; $\varkappa_{s.s}=-0.4$; $\varkappa_{rot}=0.12$; $\varkappa_w=0.4$; $\hat{\varepsilon}_w=16.3°$			
$\bar{V}$	0.15	0.20	0.30	0.40	0.15	0.20	0.30	0.40
$\vartheta°$	−0.45	−2.48	−7.10	−12.66	−0.6	−2.9	−7.62	−12.5
α_w^0	12.36	14.63	12.7	8.23	8.4	9.7	7.22	2.95
c_{y_w}	0.795	0.915	0.810	0.545	0.548	0.63	0.48	0.22
K_w	19	15.8	18.4	23.8	22.5	21.8	22.8	15.9
$\Delta\alpha_w$, radian	0.112	0.0595	0.0235	0.0126	0.1276	0.066	0.0262	0.0155
$\bar{Y}_w$	0.049	0.10	0.200	0.24	0.068	0.139	0.237	0.195
$\bar{Y}_{rot}$	0.951	0.90	0.80	0.76	0.932	0.861	0.763	0.805
$t_{y_{rot}}$	0.152	0.144	0.128	0.122	0.149	0.1376	0.122	0.1286
K_{rot}	3.45	5.3	7.8	8.05	3.5	5.23	7.6	8.3
$\Delta\alpha_{rot}$ (from wing)	0.0065	0.0075	0.0066	0.0045	0.00145	0.00167	0.00126	0.00058
$\Delta\alpha_{rot}$ (from interference)	—	—	—	—	−0.0640	−0.0332	−0.0131	−0.00777
$\Delta\alpha_{rot}$	0.0065	0.0075	0.0066	0.0045	−0.06255	−0.03153	−0.01184	−0.00719
$\frac{1}{K_{rot}}+\Delta\alpha_{rot}$	0.2963	0.1961	0.1348	0.1287	0.2274	0.1595	0.1198	0.1134
$\frac{1}{K_w}+\Delta\alpha_w$	0.1644	0.1228	0.0778	0.0546	0.172	0.1119	0.0701	0.0783
$\bar{Y}_{rot}\left(\frac{1}{K_{rot}}+\Delta\alpha_{rot}\right)$	0.282	0.176	0.1078	0.0979	0.212	0.1373	0.0915	0.0913
$\bar{Y}_w\left(\frac{1}{K_w}+\Delta\alpha_w\right)$	0.00809	0.0123	0.0156	0.031	0.0117	0.0156	0.0166	0.0153
$\bar{c}_x\bar{V}^2/t_{y_2}{}^a$	0.0143	0.0254	0.0571	0.1015	0.0143	0.0254	0.0571	0.1015
$1/K_h$	0.304	0.214	0.180	0.212	0.238	0.1813	0.1652	0.2081

thrust coefficient, then installation of a wing will not result in a decrease in required power.

It should be noted that an increase in thrust coefficient $t_{y\Sigma}$ for a helicopter with a wing leads to a decrease in its dynamic ceiling. This is so since, at the optimum rate of climb $\overline{V}_c \approx 0.2$, the wing only insignificantly relieves the rotor load, and t_y acquires the maximum permissible (in view of flow separation) value at a lower altitude. Furthermore, at large $t_{y\Sigma}$, flow separation at the rotor may occur at low flying speeds when t_{y_w} is still small. To reduce $t_{y_{rot}}$ at these altitudes, a 5 - 8% increase in rotor rpm can be advantageous.

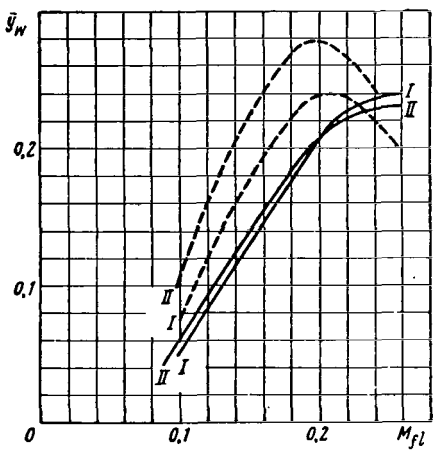

Fig.3.47 Relative Lift of Wing for Helicopters of Different Configurations.
Legend:
——— Single-rotor configuration;
– – – – Side-by-side configuration;
I - Helicopter with wing and decreased diameter;
II - Helicopter with wing and decreased peripheral speed.

It follows from Table 3.10 that the wing performance with consideration of downwash by the rotor $\left(\frac{1}{K'_w} = \frac{1}{K_w} + \Delta\alpha_w\right)$ decreases by several units at high flying speed and even more at low speed. The wing, producing downwash near the rotor, somewhat reduces its performance. This explains the slight change in helicopter performance when a wing is installed.

On a helicopter without a tractor propeller, a wing without a fixed angle of setting has a maximum angle of attack α_w in horizontal flight at $\overline{V} = 0.2 - 0.15$. At smaller $\overline{V}$, this angle decreases owing to an increase in downwash from the rotor; at larger values, it decreases due to an increase in pitch angle of the helicopter. Therefore, when a wing has a small area and large angles of attack, its lift increases at high speed despite a decrease in α_w, but insignificantly (Fig.3.47, single-rotor configuration). Conversely, if the wing has a large area and small α_w (side-by-side configuration), then at large speeds c_{y_w} markedly decreases and the lift becomes less than at average speeds. /332

Thus, on helicopters without a tractor propeller or other propeller, the wing should have a small area and large α_w or be provided with mechanization for controlling the amount of c_{y_w}.

In a climbing regime, the angle of attack of the wing decreases, while it increases in gliding. At a fixed angle of wing setting in an autorotation regime, flow separation from the wing is inevitable, which can be tolerated in the presence of a small wing lift (small wing area and reduction in c_{y_w} by

mechanization of the wing).

3. Determination of Helicopter Flight Data

If both helicopter performance and rotor efficiency are known, the required power of a helicopter is determined by the expression (see Sect.7, Chapt.II):

$$N_{h.f} = \frac{GV\,[m/sec]}{75\xi}\ \frac{1}{K_h\eta} \tag{4.21}$$

or

$$N_{h.f} = \frac{GV\,[km/hr]}{270\xi}\ \frac{1}{K_h\eta}. \tag{4.22}$$

The sequence of calculation for helicopters of various configurations is described in Subsection 2. The rotor efficiency is determined from the graphs given in Section 7, Chapter II. Consequently, on assigning the flying speed and altitude, a graph of the required power of the helicopter can be plotted. In hovering flight, the required power is determined from aerodynamic characteristics of the rotor in a hovering regime: $N_{h.f}$ is calculated at all flight altitudes under the condition T = G. /333

The maximum and minimum flying speeds are determined from the points of intersection of the curves of required and disposable power. At all flight altitudes we must find the maximum permissible speed V_{per} with respect to flow separation conditions; if $V_{max} > V_{per}$, then the flying speed of the helicopter is limited by the value of V_{per}.

Having plotted the curves of required power and knowing the engine characteristics with respect to fuel consumption, the fuel consumption of the helicopter per hour and kilometer can be plotted as a function of flying speed (see Fig.3.38) and, as described in Section 3, the maximum range and endurance, cruising and economic flying speeds can be determined.

If the helicopter flight path is inclined, the propulsive force of the rotor should balance the projection of helicopter weight onto the direction of flight, which is equal to G sin $\theta_{fl.p}$ or $G\frac{V_y}{V}$ (see Fig.3.1). Therefore, the expression for engine power takes the form

$$N = \frac{GV}{75\xi\eta}\left(\frac{1}{K} + \frac{Q_{par}}{G} + \frac{V_y}{V}\right) = N_{h.f} + \frac{GV_y}{75\xi\eta}. \tag{4.23}$$

It follows from eq.(4.23) that the maximum rate of climb of a helicopter is determined by the formula

$$V_{y_{max}} = \frac{75\,(N_{dis} - N_{h.f\ min})\xi\eta}{G}. \tag{4.24}$$

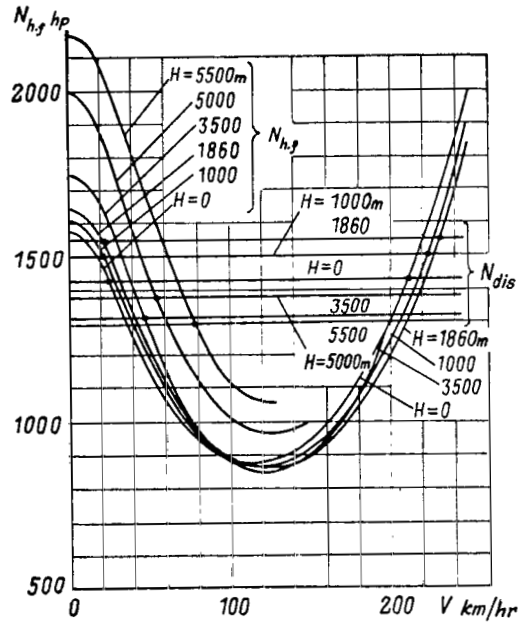

Fig.3.48 Required and Available Horsepower of Helicopter.

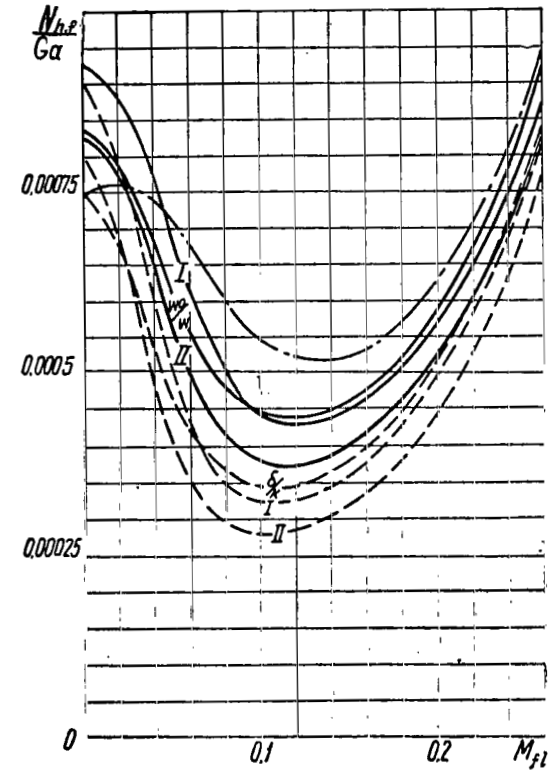

Fig.3.49 Ratio $N_{h.f}/Ga$ for Helicopters of Different Configurations with and without Wing, as a Function of M_{fl}.

Legend:

——— Single-rotor configuration;

– – – – – Side-by-side configuration;

—·— Fore-and-aft configuration;

w_0/w - Helicopter without wing;

I - Helicopter with wing and decreased diameter;

II - Helicopter with wing and decreased peripheral speed.

The optimum rate of climb and minimum power consumption $N_{h.f_{min}}$ are found from the graph of required powers. After determining $V_{y_{max}}$ at all altitudes and constructing the graph $V_{y_{max}} = f(H)$, the dynamic ceiling of the helicopter is determined by graphical means (see Fig.3.35).

From eq.(4.24) for $N_{dis} = 0$, the minimum rate of descent of a helicopter in an autorotation regime of the rotor $(V_{y_c})_{min}$ is derived.

To determine the angles of attack α and angles of setting θ_0 of the rotor it is necessary to calculate the coefficient of propulsive force of the rotor

$$t_x = -\frac{Q_{par} + G\frac{V_y}{V}}{\frac{1}{2}\rho\sigma(\omega R)^2 F} \tag{4.25}$$

and, knowing t_y and t_x, the angles α and θ_0 must be determined from the graphs (see Figs.2.63 - 2.70 and 2.105 - 2.109) or from eq.(3.95) given in Section 3, Chapter II.

As an example, let us carry out an aerodynamic calculation of the Mi-4 helicopter with rectangular metal blades. The graph of helicopter performance is given in Fig.3.44. The graph of the required and disposable powers is shown in Fig.3.48 for six flight altitudes.

At $\bar{V} = 0$, $N_{h.f}$ is determined by the expression:

$$N_{hf} = \frac{G\omega R}{75\xi}\frac{m_t}{t}, \tag{4.26}$$

where m_t is found from the graphs shown in Fig.3.34 for $\bar{V}_y = 0$.

The maximum vertical rates of climb and minimum rates of descent in an autorotation regime are calculated in Table 3.11. /335

Determination of the other flight data is accomplished by means of the graph in Fig.3.48.

A comparison of $N_{h.f}$ calculated by the auxiliary graph in Fig.3.27 with $N_{h.f}$ found from helicopter performance and efficiency shows satisfactory agreement; $V_{y_{max}}$ is also close in magnitude.

Figure 3.49 shows a graph of required power based on Ga for helicopters of various configurations. The graph is calculated by means of the helicopter performance graph given in Fig.3.46. The ratio $\frac{N_{h.f}}{Ga}$ is determined by the formulas:

$$\frac{N_{hf}}{Ga} = \frac{M_{fl}}{75\xi K_h \eta} \tag{4.27}$$

in forward flight, and by

$$\frac{N_{h.f}}{Ga} = \frac{1}{75\xi} \frac{1}{\frac{t}{m_t M_0}} \tag{4.28}$$

in hovering flight.

TABLE 3.11

H	0	1000	1860	3500	5000	5500
N_{dis}, hp	1430	1500	1550	1315	1380	1300
V_H, km/hr	115	115	120	125	125	115
$\overline{V}_H$	0.163	0.163	0.170	0.177	0.177	0.163
t_y	0.138	0.152	0.165	0.195	0.229	0.242
η	1.010	1.002	0.989	0.953	0.850	0.850
$N_{h.f\,min}$, hp	880	865	857	865	970	1060
ΔN, hp	550	635	693	450	410	240
$V_{y_{max}}$, m/sec	4.86	5.57	6.0	3.75	3.05	1.83
$(V_{y_c})_{min}$, m/sec	—7.8	—7.6	—7.4	—7.2	—7.2	—7.9

The power utilization factor ξ was taken as equal to 0.93 for two-rotor helicopters, and as $\xi = 0.88$ for a single-rotor helicopter at $\overline{V} \geq 0.15$ and as $\xi = 0.83$ at $V = 0$. In hovering flight, the helicopter wing is swept by the rotor and creates a negative lift; therefore, at $V = 0$ the lift coefficient of the rotor increases by 2% for the single-rotor helicopter with a wing and by 8% for the helicopter of side-by-side configuration with a wing; the value found from eq.(4.28) increases accordingly.

We see from the graph that, because of a difference in ξ in hovering regime, the ratio N/G is lower for two-rotor helicopters than for single-rotor versions.

The largest value of N/G refers to helicopters with a wing and with a reduced rotor diameter, while the smallest value refers to helicopters with a wing and with reduced rpm for the single-rotor helicopter and for the side-by-side helicopter without a wing.

Thus, to ensure the possibility of hovering, the helicopters in question should have a different engine power per kilogram of gross weight. Correspondingly, they will have different flight data in forward flight. Table 3.12 gives some flight characteristics of helicopters which were obtained in our example /336 at a flying altitude $H = 0$ for the following characteristics of the engine: $N_{t.o} = N_{hov}$; $N_{nom} = 0.85\ N_{t.o}$; $N_{cru} = 0.7\ N_{t.o}$.

The maximum vertical speed of the helicopter was determined by the formula

$$V_{y_{max}} = 75\xi\eta a\left(\frac{N_{dis}}{Ga} - \frac{N_{h.f\ min}}{Ga}\right). \qquad (4.29)$$

The minimum rate of descent in an autorotation regime $(V_{y_c})_{min}$ was determined for $N_{dis} = 0$.

TABLE 3.12

Helicopter Configuration	$N_{t.o}/G$ hp/hr	V_{max} at $N_{t.o}$ km/hr	V_{min} km/hr	$\frac{N_{h.f\ min}}{N_{t.o}}$	$V_{y_{max}}$ at N_{nom} m/sec	$(V_{y_c})_{min}$ m/sec	V_{cru} km/hr	$\bar{G}_f$
Side-by-side	0.253	301	0	0.456	6.6	— 7.66	246	0.127
Single-rotor	0.284	304	0	0.527	5.76	— 9.38	244	0.144
Fore-and-aft	0.253	280	0(47.7)	0.694	2.61	—11.65	185	0.169
Side-by-side with wing and reduced diameter	0.306	332	0	0.356	10.03	— 7.21	280	0.134
Side-by-side with wing and reduced peripheral speed	0.271	321	0	0.348	9.02	— 6.24	275	0.121
Single-rotor with wing and reduced diameter	0.315	325	0	0.465	7.59	— 9.17	268	0.145
Single-rotor with wing and reduced peripheral speed	0.281	317	0	0.448	7.06	— 7.89	261	0.133
	$\left(\frac{N}{Ga}\right)_{hov}$ for helicopters is identical							
Side-by-side	0.264	306	0	0.439	7.19	— 7.66	252	0.129
Single-rotor	0.264	292	29.4	0.568	4.67	— 9.38	230	0.141
Fore-and-aft	0.264	287	0	0.667	3.20	—11.65	203	0.160
Side-by-side with wing and reduced diameter	0.264	310	28.2	0.413	7.64	— 7.21	258	0.126
Side-by-side with wing and reduced peripheral speed	0.264	317	8.6	0.357	8.61	— 6.24	272	0.119
Single-rotor with wing and reduced diameter	0.264	300	47.7	0.555	4.88	— 9.17	235	0.138
Single-rotor with wing and reduced peripheral speed	0.264	309	23.3	0.477	6.16	— 7.89	251	0.129

The fuel supply required for flight over a given range at the cruising power of the engine was found by the formula /337

$$\bar{G}_f = \frac{G_f}{G} = \frac{1{,}1LC_e \frac{N_{cru}}{G}}{V_{cru}} = \frac{1{,}1LC_e \frac{N_{cru}}{Ga}}{3{,}6M_{fl_{cru}}}. \qquad (4.30)$$

The coefficient 1.1 is introduced to account for the fuel supply for navigation and fuel consumption in transitional regimes for a height of H = 0. Here, $\bar{G}_f = \frac{G_f}{G}$ was calculated for L = 500 km at C_e = 0.32 kg/hp hr.

Table 3.12 indicates that, under equal conditions in hovering flight ($N_{t.o} = N_{hov}$), the fore-and-aft helicopter has the worst flying qualities in forward flight: The rate of climb and cruising speed are appreciably smaller, the fuel requirement is greater, the rate of descent in an autorotation regime is greater, and $\frac{N_{h.f}}{N_{t.o}} = 0.69$, i.e., continuation of horizontal flight is possible only if not more than one of the three engines fails.

To improve the flight characteristics, the fore-and-aft helicopter should have a more powerful engine: $N_{t.o} > N_{hov}$.

The side-by-side helicopter has the best flight data.

The qualitative difference in flight data of helicopters of different configurations in forward flight also remains for helicopters of equal available horsepower per unit weight (see the second part of Table 3.12), and also if we take into account that helicopters of different configurations have a somewhat differing flying weight at an identical lift capacity. At equal available power per unit weight for single-rotor and two-rotor helicopters, the former can hover only on a ground cushion, with its minimum speed outside the ground cushion being about 30 km/hr.

By installing a wing on a single-rotor helicopter to reduce the rotor diameter by 11% and increasing the engine power also by 11% to ensure hovering outside the ground effect, the flight characteristics of a helicopter in forward flight are improved: The maximum and cruising speeds increase by 20 km/hr and the rate of climb by about 2 m/sec. Without an increase in engine power, the characteristics of a helicopter in hovering flight deteriorate, but in forward flight they change negligibly: The maximum and cruising speeds increase by 5 - 8 km/hr and the relative fuel feed decreases by 3%. When a wing is installed without changing the rotor diameter but with decreasing the peripheral speed, the flight characteristics of the helicopter improve both in hovering and in forward flight: The maximum and cruising speeds increase by 15 - 20 km/hr, and the relative fuel feed decreases by 8 - 9%.

As noted above, the dynamic ceiling of a helicopter with a wing decreases.

4. Calculation of a Helicopter with a Tractor Propeller

When calculating a helicopter with a tractor propeller (jet engine) developing a thrust $P_{t.p}$, the drag of the helicopter must be reduced by the quantity $P_{t.p}$, i.e., the drag will be equal to $\frac{G}{K} + Q_{par} - P_{t.p}$.

The tractor propeller requires an amount of power determinable by the expression

$$N_{t.p} = \frac{P_{t.p} V}{270 \xi_{t.p} \eta_{t.p}}. \tag{4.31}$$

Therefore, the required power of a helicopter with a tractor propeller /338 is equal to

$$N_{h.f} = N_{rot} + N_{t.p} = \frac{V}{270 \xi \eta} \left(\frac{G}{K} + Q_{par} - P_{t.p} \right) + \frac{P_{t.p} V}{270 \xi_{t.p} \eta_{t.p}} \tag{4.32}$$

or

$$N_{h.f} = \frac{GV}{270 \xi \eta} \left[\frac{1}{K} + \frac{Q_{par}}{G} - \frac{P_{t.p}}{G} \left(1 - \frac{\xi \eta}{\xi_{t.p} \eta_{t.p}} \right) \right]. \tag{4.33}$$

In calculations using eqs.(4.32) or (4.33) we must assign the value of $P_{t.p}$ or $N_{t.p}$; in so doing we must bear in mind that in steady horizontal flight the drag of the helicopter cannot be negative; consequently, the following condition should be satisfied:

$$\frac{P_{t.p}}{G} \leqslant \frac{1}{K} + \frac{Q_{par}}{G}. \tag{4.34}$$

Accordingly, in a climbing or descending regime this condition takes the form

$$\frac{P_{t.p}}{G} \leqslant \frac{1}{K} + \frac{Q_{par}}{G} + \frac{V_y}{V}. \tag{4.35}$$

Such an additional term in formulas for $N_{h.f}$ as in eq.(4.33) appears whenever tractor propellers are installed on helicopters of any configuration.

The flight data of a helicopter with a tractor propeller are determined in the same sequence as one without tractor propellers.

Let us estimate how much the required power and maximum rate of climb may vary when a tractor propeller is installed on a helicopter.

For $M_0 = 0.60$ and average values of t_y at high flying speeds ($\bar{V} \approx 0.35$), the efficiency η of the rotor can be considered equal to 0.87. Having taken $\xi = 0.91$ for a two-rotor helicopter and $\eta_{t.p} = 0.78$, $\xi_{t.p} = 0.97$ for the tractor propeller, we find the value in parentheses in eq.(4.33): $1 - \frac{0.91 \times 0.87}{0.97 \times 0.78} = -0.05$.

If the tractor propeller completely overcomes the helicopter drag, i.e., if

$$\frac{P_{t.p}}{G} = \frac{1}{K} + \frac{Q_{par}}{G}, \qquad (4.36)$$

then the increase in required power amounts to 5%, but if it overcomes this drag only by half, then the increase in required power amounts to 2.5%. Consequently, the losses are small.

For $M_\theta = 0.7$ and $\bar{V} = 0.35 - 0.4$, when $\eta \approx 0.85 - 0.8$, there can be a 1 - 3% gain in required power when a tractor propeller is used.

In a maximum rate-of-climb regime for $M_\theta \simeq 0.6 - 0.7$, $\bar{V} = 0.2$, and at average values of t_y, the efficiency can be considered equal to at least $\eta = 0.87$. Consequently, if it is possible to obtain a very high value of tractor propeller efficiency ($\eta_{t.p} = 0.78$) in a maximum rate-of-climb regime, then the value in parentheses in eq.(4.33) is equal to -0.05. For a side-by-side helicopter, more than half of the available helicopter power is consumed in a maximum rate-of-climb regime for producing vertical speed. Consequently, when all power is delivered to the tractor propeller, the total thrust of the helicopter decreases by 5%, whereas the excess of thrust used for climbing decreases by 10%. The rate-of-climb loss will be about 1 m/sec. At $\eta = 0.9$, we have $\eta_{t.p} = 0.7$, and when half of the available power is supplied to tractor propellers /339 the rate-of-climb loss will amount to 20%, or about 2 m/sec. General considerations on when the installation of a tractor propeller or other propeller on a helicopter is expedient or necessary are given at the end of Section 7, Chapter II.

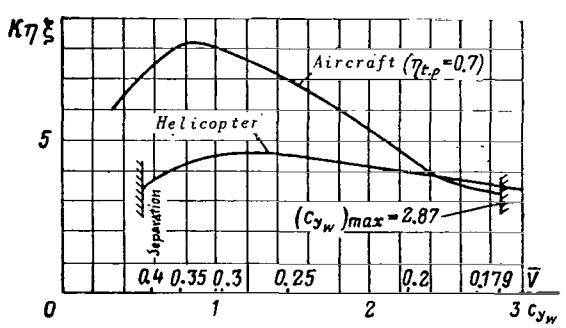

Fig.3.50 Comparison of the Product of Aircraft Performance and Efficiency for Regular Aircraft and Helicopter.

5. Comparison of Helicopter and Airplane

At identical flying weight of helicopter and airplane, the relation $D = L_w$ is approximately satisfied; this relationship is determined by design advisability of the size of wings and rotors. A comparison of the parameters of regular aircraft and helicopters shows that a wing has an aspect ratio larger by a factor of 7 - 9 and an equally larger load per square meter of area. Consequently, $\left(\frac{G}{L_w^2}\right)_{airc} = \left(\frac{G}{D^2}\right)_h = \frac{p}{\lambda} = \text{const}$. This means that a given aircraft and helicopter have an approximately equal induced drag at the same flying speed.

Provided that $D = L_w$, the dimensionless coefficients of an airplane and helicopter are connected by the relation

$$G = c_{y_w} \frac{\varrho}{2} V^2 S_w = t_y \sigma \frac{\varrho}{2} (\omega R)^2 F,$$
$$c_{y_w} = \frac{t_y \sigma}{\bar{V}^2} \frac{\pi \lambda_w}{4}. \qquad (4.37)$$

For a comparison, let us take the following data of a helicopter and an airplane. For a helicopter, $\sigma = 0.091$; $t_y = 0.15$, $\bar{c}_x = 0.0075$. For an airplane, the wing characteristics are taken from data of wing exposure to propeller slipstream of a modern low-speed transport aircraft. A rectangular wing with a slat and double slotted flap was tested. The wing aspect ratio was $\lambda_w = 9$. The parasite drag coefficient $c_{x_{airc}}$ of the airplane, based on wing area, was taken to be equal to 0.025 [$\Sigma c_x S$ of the airplane is approximately one half that of a helicopter: $\frac{(\Sigma c_x S)_{airc}}{F_{rot}} = c_{x_{airc}} \frac{S_{airc}}{F_{rot}} = \frac{0.025}{\pi \frac{\lambda_w}{4}} = 0.0036$ and for the helicopter, $\bar{c}_x = 0.0075$].

TABLE 3.13 /340

	Slat	Retracted							Moved Forward
	Slot	Overlapped				Open			Open
	Deflection of Flap	0	0	0	0	20	40	50	50
Airplane	c_{y_w}	0.4	0.8	1.2	1.45	2	2.4	2.55	2.87
	c_{x_w}	0.0185	0.0439	0.0873	0.1175	0.232	0.417	0.451	0.582
	K_w	21.6	18.25	13.75	12.35	8.63	5.77	5.6	4.93
	$K_{airc.}$	9.2	11.6	10.65	10.2	7.8	5.44	5.36	4.72
	$K_{airc.}\eta_{t.p}$ ($\eta_{t.p}=0.7$)	6.44	8.12	7.45	7.15	5.46	3.8	3.75	3.31
	$K_{airc.}\eta_{t.p}$ ($\eta_{t.p}=0.85$)	7.82	9.86	9.05	8.67	6.62	4.62	4.55	4.02
Helicopter	$\bar{V}$	0.479	0.34	0.277	0.252	0.214	0.196	0.19	0.179
	K	—	9.3	8.2	7.3	5.9	5.12	4.19	4.45
	η	—	0.875	0.915	0.93	0.965	0.975	0.98	1.0
	K_h	—	5.75	6.03	5.77	5.1	4.66	4.5	4.11
	$K_h \eta \xi$	—	4.43	4.85	4.72	4.33	4.00	3.88	3.62

For the selected values of c_{y_w} we find, in Table 3.13, c_{x_w}, K_w, K_{airc}, $K_{airc}\eta_{t.p}$. For these same values of c_{y_w}, the values of $\bar{V}$, K, η, K_h, and $K_h\eta$ are

determined for the helicopter. Since the helicopter has additional engine power losses, the product $K_h\eta\xi$, where $\xi = 0.88$, is calculated for a single-rotor helicopter with a tail rotor. The graph in Fig.3.50 is constructed from the data of Table 3.13.

A comparison of wing and rotor performance shows that, in the examined example, the wing without mechanization, at all c_{y_w}, has a performance greater by a factor of 2 - 1.7 than the rotor. The wing with mechanization has a 46% greater performance at $c_{y_w} = 2.0$ (at this c_w, the minimum flying speed corresponds to $\overline{V}_{min} = 0.214$), whereas at $(c_{y_w})_{max} = 2.87$ ($\overline{V}_{min} = 0.18$), the wing performance is only 10% higher than that of the rotor.

It follows from Table 3.13 and Fig.3.50 that the maximum value of $K_{airc}\eta_{t.p}$ at $\eta_{t.p} = 0.7$ is by a factor of 1.75 greater than $K_h\eta\xi$. The fuel consumption of the airplane per kilometer is less by the same factor than that of the helicopter (at equal specific consumptions of the engine). The speeds corresponding to maxima of the product of the craft performance and efficiency is by a factor of 1.2 greater for the airplane (actually, airplanes fly the range at a greater speed and with a performance less than maximum).

On comparing a helicopter and an airplane at equal flying speeds, it will be found that at speeds reached by an airplane without the use of wing mechanization ($\overline{V} \geq 0.3 - 0.25$), $(K\eta)_{airc}$ is by a factor of 1.5 - 2 greater than $(K\eta\xi)_h$. At $\overline{V} > 0.43$, flow separation from the rotor blade begins at the helicopter. At low flying speeds, reached by an airplane with the use of powerful mechanization, $(K\eta)_{airc}$ is less than $(K\eta\xi)_h$ owing to the large profile drag of the wing. Thus, it is aerodynamically less expedient to use such an airplane with its low attainable speed for long flights; a helicopter is then preferable.

Table 3.13 shows that, at equal flying weight and at $D = L_w$, the minimum /341
speed of the airplane, determined by the quantity $(c_{y_w})_{max} = 2.87$, will be $\overline{V} = 0.18$. A low flying speed can correspond to this value of $\overline{V}$ only if the airplane has a small wing loading. The minimum speed of the helicopter is determined by the available engine power and is usually equal to zero, whereas when the helicopter is overloaded it will not exceed a value corresponding to $\overline{V} = 0.05$.

6. Power of Front and Tail Rotors in a Helicopter of Fore-and-Aft Configuration

An expression was derived in Subsection 2 for determining helicopter performance and total required power of both rotors. However, the tail rotor usually requires substantially greater power than the front rotor (by a factor of 1.5 and more). Let us derive an expression for determining the power required by each rotor separately.

First, let us find the propulsive forces of the rotors. They are not identical, since various rotors may have different lifts and different angles of attack.

According to eq.(4.8), the relation between α_1 and α_2 is equal to

$$\alpha_2=\alpha_1-\Delta\alpha_{rot_2}+\Delta\varepsilon_{rot_e},$$

where $\Delta\alpha_{rot_2}$ is determined by eq.(4.14) with consideration of eq.(4.18).

Proceeding from the approximate expression for X:X = Y(α + a_1), we find

$$\begin{gathered}X_1=Y_1(\alpha_1+a_{1_1});\\ X_2=Y_2(\alpha_2+a_{1_2})=\frac{Y_2}{Y_1}Y_1(\alpha_1+a_{1_2})+\\ +Y_2(\Delta\varepsilon_{rot_e}-\Delta\alpha_{rot_2})\approx\frac{Y_2}{Y_1}X_1+Y_2(\Delta\varepsilon_{rot_e}-\Delta\alpha_{rot_2}).\end{gathered}\tag{4.38}$$

From the condition of equilibrium of forces acting in the direction of motion (Fig.3.4), we obtain the following equality:

$$X_1+X_2+Y_2\Delta\alpha_{rot_2}+Q_{par}=0.\tag{4.39}$$

In eq.(4.39), Q_{par} for a helicopter with a wing and tractor propeller represents the sum Q_{par} + X_w + $Y_w\Delta\alpha_w$ - $P_{t.p}$.

From eqs.(4.38) and (4.39), we obtain

$$X_1=-\frac{1}{1+\frac{Y_2}{Y_1}}Q_{par}-\frac{Y_2}{1+\frac{Y_2}{Y_1}}\Delta\varepsilon_{rot_e};\tag{4.40}$$

$$X_2=-\frac{\frac{Y_2}{Y_1}}{1+\frac{Y_2}{Y_1}}Q_{par}+\frac{Y_2}{1+\frac{Y_2}{Y_1}}\Delta\varepsilon_{rot_e}-Y_2\Delta\alpha_{rot_2}.\tag{4.41}$$

Equations (4.40) and (4.41) indicate that vee-ing of the rotors by an angle $\Delta\varepsilon_{rot_e}$ redistributes the propulsive forces of the rotors, thus influencing the power required by the rotors. Owing to downwash of the tail rotor, its propulsive force is greater (more negative) by an amount of $Y_2\Delta\alpha_{rot_2}$. At $Y_1 \neq Y_2$, the front and tail rotors do not furnish an equal share of parasite drag.

Substituting X_1 and X_2 into the expression for calculating the required power /342

$$N_{h.f_1}=\frac{Y_1V}{270\eta_1\xi}\left(\frac{1}{K_1}-\frac{X_1}{Y_1}\right)=\frac{GV}{270\eta_1\xi}\left(\frac{\overline{Y}_1}{K_1}-\frac{X_1}{G}\right),\tag{4.42}$$

we obtain

$$N_{h.f_1}=\frac{GV}{270\eta_1\xi}\left(\frac{\overline{Y}_1}{K_1}+\frac{1}{1+\frac{Y_2}{Y_1}}\frac{Q_{par}}{G}+\frac{\overline{Y}_2}{1+\frac{Y_2}{Y_1}}\Delta\varepsilon_{rot_e}\right); \tag{4.43}$$

$$N_{h.f_2}=\frac{GV}{270\eta_2\xi}\left(\frac{\overline{Y}_2}{K_2}+\frac{\frac{Y_2}{Y_1}}{1+\frac{Y_2}{Y_1}}\frac{Q_{par}}{G}-\frac{\overline{Y}_2}{1+\frac{Y_2}{Y_1}}\Delta\varepsilon_{rot_e}+\overline{Y}_2\Delta\alpha_{rot_2}\right). \tag{4.44}$$

It is easy to demonstrate that, on adding the expressions in parentheses in eqs.(4.43) and (4.44), the sum will coincide with eq.(4.13) for the case of a fore-and-aft helicopter. The angle of vee-ing of the rotors $\Delta\varepsilon_{rot_e}$ and the ratio $\frac{Y_1}{Y_2}$ at $\eta_1 = \eta_2$ will not influence the total power of the helicopter. At $Y_1 = Y_2$ and $\Delta\varepsilon_{rot_e} = \Delta\alpha_{rot_2}$, the power of both rotors is identical. It is necessary to note, however, that the longitudinal stability of the helicopter deteriorates when $\varepsilon_{rot_e} > 0$.

7. Retraction of Landing Gear on Helicopters

It is known that helicopters have a parasite drag about twice that of regular aircraft.

This can be attributed to the specific configuration of a helicopter, the presence of a cabane and large hub of the rotor, tail boom with a tail rotor placed high, and also to the necessity of loading and unloading in hovering flight and maintenance without the use of an airdrome. Therefore, various hoisting devices, numerous railings and hatches, movable doors, blisters, etc. are often installed on the outside of a helicopter. On the other hand, the weight coefficient which is lower than that of a regular aircraft necessitates a careful approach to any measures that reduce the parasite drag but increase the structural weight.

Below, we will estimate the expediency of installing a retractable landing gear on a helicopter from the viewpoint of its load-carrying capacity.

Retraction of the landing gear reduces the parasite drag of a helicopter by 20 - 25%. Figure 3.51 shows the graph of the ratio $\frac{N_{h.f}}{Ga}$ for two values of $\overline{c}_x$: 0.0075 and (by 25% less) 0.0056. The graph also contains the quantity $\frac{N_{cru}}{Ga} \approx 0.7\,\frac{N_{hov}}{Ga}$. It is obvious that, with retraction of the landing gear, the cruising speed of the helicopter increases from $V_{cru} = 253$ km/hr ($M_{f1} = 0.207$) to $V_{cru} = 269$ km/hr ($M_{f1} = 0.22$), i.e., by 6%. The required fuel supply will decrease by this same amount, while the range will remain unchanged. If the cruising speed is retained, then the required power diminishes by 9%

$\left(\frac{N}{Ga} = 0.000555 \text{ in place of } 0.000605\right)$. Since the specific fuel consumption of turboprop engines greatly increases upon a decrease in engine power, a change in power - as shown by calculations - will result in a change in fuel consumption smaller by a factor of about 1.5. Consequently, we arrive at the same figure: The required fuel supply decreases by 6%.

Now we can calculate that portion of the structural weight increase by retraction of the landing gear which is compensated by a decrease in fuel requirement. Thus, an increase in structural weight by 1% of the takeoff weight will be compensated at a fuel requirement equal to 17% of the takeoff weight, i.e., $\bar{G}_f = 0.17$, since 6% of 17% is 1%. A 1.5% increase in structural weight will be compensated when $\bar{G}_f = 0.25$. /343

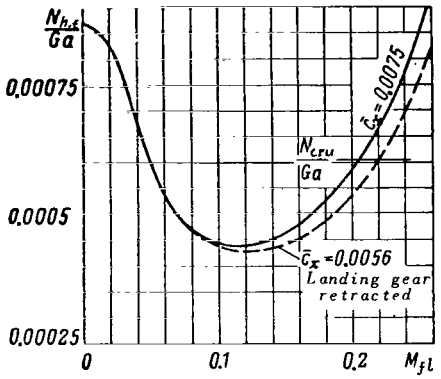

Fig.3.51 Ratio $N_{h.f}/Ga$ of Helicopter for Two Values of Parasite Drag Coefficient, as a Function of M_{fl}.

The normal fuel supply of modern turboprop helicopters is about 15% of the takeoff weight, with a maximum of 20-25%. It is obvious that installation of a retractable landing gear on modern helicopters is expedient if the increase in structural weight does not exceed 1 - 1.5% of the takeoff weight. In so doing, however, the maximum load-lifting capacity of the helicopter decreases in flights with a smaller fuel supply.

A 6% decrease of fuel supply and an equal increase in cruising speed lead to cheaper hauling on helicopters, which should also be taken into account by the designer when attacking the problem of landing-gear retraction.

It should be pointed out that, on airplanes with a higher performance of the lifting system, a decrease in parasite drag will lead to a greater decrease in fuel consumption. Furthermore, regular aircraft have greater relative fuel supplies $\bar{G}_f$, for which reason retraction of the landing gear on airplanes has become advantageous at cruising speeds lower than those presently used for helicopters.

Section 5. Aerodynamic Calculation of a Helicopter by the Power Method

In an aerodynamic design of a helicopter by the power method, the condition of power balance in steady helicopter flight is used: The power supplied to the rotor is equal to the sum of all power losses. Thus, having determined all losses of power - both of the profile and induced type - produced in overcoming the parasite drag of the nonlifting parts as well as the helicopter weight component in climbing, we find the power which must be supplied to the rotor.

The formulas for determining the torque coefficient of a rotor, derived in

Section 3, Chapter II, express the condition of the power balance. The same Section contains formulas and graphs for calculating the profile and induced power losses for a rotor.

It is general practice to determine all power losses approximately so as /344 to simplify the calculations; therefore, the aerodynamic calculations of a helicopter by the power method constitutes an approximate method.

1. Determination of Required Power in Horizontal Helicopter Flight

The required power of a helicopter is equal to the sum of the profile and induced losses at the rotor and the loss due to overcoming the parasite drag of nonlifting parts of the helicopter

$$N_{hf} = N_{pr} + N_{ind} + N_{par}. \tag{5.1}$$

The profile power loss coefficient m_{pr} is determined from special graphs, or by the approximate formula (3.75) from Chapter II:

$$m_{pr} = \frac{1}{4} c_{xp_{av}} (1 + 5\bar{V}^2) P + \Delta m_{co}. \tag{5.2}$$

In dimensional form, the profile losses of a rotor are calculated by the formula

$$N_{pr} = \frac{1}{75\xi} \frac{\varrho}{2} m_{pr} \sigma (\omega R)^3 F, \tag{5.3}$$

where ξ is the engine power utilization factor.

The induced power loss coefficient is determined by means of eq.(3.83) from Chapter II

$$m_{ind} = \frac{\Phi}{4B^4} \frac{t_y^2 \sigma}{\bar{V}} = 0.285 \frac{t_y^2 \sigma}{\bar{V}}, \tag{5.4}$$

while, in dimensional form, the induced losses of a rotor are determined by

$$N_{ind} = \frac{1}{75\xi} \frac{\varrho}{2} m_{ind} \sigma (\omega R)^3 F = \frac{\Phi}{16 \cdot 75 \pi B^4 \xi} \frac{G^2}{V \Delta D^2} = \frac{1}{3300} \frac{G^2}{\xi D^2 V \Delta}. \tag{5.5}$$

The induced losses can also be represented as the product of the force of the induced drag of the rotor and the flying speed, or as the product of rotor lift and average downwash angle in the rotor plane and flying speed

$$N_{ind} = \frac{\Phi}{B^2} \frac{X_{ind} V}{75\xi} = \frac{\Phi}{B^2} \frac{Y (\Delta\alpha) V}{75\xi}. \tag{5.6}$$

The average downwash angle in the rotor plane is determined by the average

induced velocity of the rotor

$$v \approx \frac{Y}{2FB^2\varrho V} = \frac{G}{2FB^2\varrho V}, \tag{5.7}$$

$$\Delta\alpha = \frac{v}{V} = \frac{G}{2FB^2\varrho V^2}. \tag{5.8}$$

It is obvious that eq.(5.5) is also obtained from eqs.(5.6) and (5.8).

It follows from eq.(5.5) that the induced power losses are directly proportional to the square of flying weight, referred to the effective linear dimension BD (i.e., the span of the lifting system determines the volume of air flowing through the rotor). The induced losses are inversely proportional to flying speed and air density.

Consequently, upon an increase in helicopter weight without a proportional increase in rotor diameter, the induced losses increase with respect to a /345 quadratic relation. If the load per unit rotor disk area $p = \frac{G}{F}$ is retained, then the induced losses will be directly proportional to the flying weight and the ratio $\frac{N_{ind}}{G}$ will remain unchanged. However, since increasing the helicopter tonnage causes p to increase (for decreasing the relative weight of the rotor), the ratio $\frac{N_{ind}}{G}$ is greater for heavy helicopters than for light ones.

For multirotor helicopters, the induced power losses are determined as the sum of the product of the type of eq.(5.6), taken for all elements of the lifting system:

$$N_{ind} = \frac{V}{75\xi} \sum \frac{\Phi}{B^2} Y \Delta\alpha. \tag{5.9}$$

In eq.(5.9), the downwash angles $\Delta\alpha$ are equal to the sum of all downwash angles for each element of the lifting system: the downwash angle due to self-induction defined by eq.(5.8) and the downwash angles due to interference*, whose expressions are given in Sections 1 and 4.

As a typical example, let us develop eq.(5.9) for a fore-and-aft helicopter, using eqs.(4.14) and (4.18) for the downwash angle due to interference:

$$N_{ind} = \frac{V}{75\xi} \frac{\Phi}{B^2} (Y_1 \Delta\alpha_1 + Y_2 \Delta\alpha_2);$$

$$\Delta\alpha_1 = \frac{Y_1}{2FB^2\varrho V^2};$$

* For the terms containing the downwash angles due to interference, we can take $\Phi/B^2 = 1$.

$$\Delta\alpha_2 = \frac{Y_2}{2FB^2\varrho V^2} + 2\varkappa_{co}\frac{Y_1}{2FB^2\varrho V^2}.$$

Having substituted $\Delta\alpha_1$ and $\Delta\alpha_2$ into the expression for N_{ind}, we obtain

$$N_{ind} = \frac{\Phi}{75\xi 2B^4\varrho VF}(Y_1^2 + Y_2^2 + 2\varkappa_{co}Y_1Y_2).$$

If the rotors have no excess, then the graph of $\varkappa_{co}$ in Fig.3.8 furnishes $\varkappa_{co} = 1$ and

$$N_{ind} = \frac{\Phi}{75\xi 2B^4\varrho VF}(Y_1 + Y_2)^2 = \frac{16\Phi}{75\pi B^4\xi}\frac{G^2}{V\Delta D^2}.$$

The expression for N_{ind} shows that, at $\varkappa_{co} = 1$, the quantity N_{ind} does not depend on the distribution of helicopter weight between the front and tail rotors and is determined only by the sum of lifts $Y_1 + Y_2 = G$. Displacement of the lifting elements along the direction of flight does not influence the quantity N_{ind}, so that the expressions for N_{ind} coincide for single-rotor and fore-and-aft helicopters.

However, it must be borne in mind that, for a two-rotor helicopter of fore-and-aft configuration, the flying weight is equal to the thrust of the two rotors and that, at identical load on the rotor disk area p, the ratio G/D is twice that of a single-rotor helicopter. Therefore, as already indicated in Chapter I, N_{ind} is by a factor of 4 greater for a fore-and-aft helicopter than for a single-rotor type, and the ratio $\frac{N_{ind}}{G}$ is twice as large. This explains why fore-and-aft helicopters have poorer flying characteristics in horizontal flight and why the flying characteristics deteriorate more noticeably upon an increase in flying weight. /346

If $\varkappa_{co} \neq 1$, then $N_{ind} = \frac{16\Phi}{75\pi B^4\xi} - \frac{G^2}{V\Delta D^2}\frac{1+\varkappa_{co}}{2}$.

For the side-by-side helicopter, the effective transverse dimension, i.e., the span of the system, increases with increasing flying weight, which is expressed by the fact that $\varkappa_{s.s} < 0$. At $\varkappa_{s.s} = 0$ (with the rotors spaced far apart), $\frac{N_{ind}}{G}$ is the same for the side-by-side helicopter as for the single-rotor helicopter; at $\varkappa_{s.s} < 0$, the ratio $\frac{N_{ind}}{G}$ of the former is lower.

Losses for overcoming the parasite drag of the nonlifting parts of a helicopter are determined by the formula

$$N_{par} = \frac{Q_{par}V}{75\xi} = \frac{\sum c_x S}{16\cdot 75\xi}V^3\Delta = \frac{\sum c_x S}{1200\xi}V^3\Delta \qquad (5.10)$$

or, in dimensionless form,

$$m_{par} = -t_{x_{h.f}} \overline{V}, \tag{5.11}$$

where

$$t_{x_{h.f}} = -\bar{c}_x \frac{\overline{V}^2}{\sigma}. \tag{5.12}$$

When calculating a helicopter with a wing, we will refer the wing drag to the parasite drag of the helicopter, i.e.,

$$\sum c_x S = \left(\sum c_x S\right)_{par} + \left(c_{x_w} + c_{y_w} \Delta\alpha_w\right) S_w, \tag{5.13}$$

where c_{x_w} is the parasite drag coefficient of an isolated wing; $\Delta\alpha_w$ is the downwash angle of the wing due to interference of the rotors.

The interference of the wing with the rotors should be taken into account when determining the total rotor downwash angles for calculating N_{ind} by eq.(5.9).

Thus, the required engine power of a helicopter, in conformity with eqs.(5.1), (5.3), (5.5), and (5.10), is equal to

$$N_{h.f} = N_{pr} + \frac{1}{3300} \frac{G^2}{\xi D^2 V \Delta} + \frac{\sum c_x S}{1200\,\xi} V^3 \Delta. \tag{5.14}$$

If the helicopter has a propeller, then the power balance is expressed in the form

$$N_{h.f} + \frac{N_{t.p}}{\xi} = N_{pr} + N_{ind} + N_{par}.$$

The aerodynamic calculations can be performed in dimensionless form. In this case, the coefficient of required torque is determined, in conformity with eqs.(5.4) and (5.11), by the expression

$$m_{t_{h.f}} = m_{pr} + 0.285 \frac{t_y^2 \sigma}{\overline{V}} - t_{x_{h.f}} \overline{V}. \tag{5.15}$$

As a dimensionless form of calculation, convenient - for example - for comparative calculations, we can determine the ratio $\frac{N_{h.f}}{Ga}$ which, when using the method of powers, is equal to

$$\frac{N_{h.f}}{Ga} = \frac{1}{75\xi\left(t_y \sigma M_0^2\right)} m_{t_{h.f}} \sigma M_0^3, \tag{5.16}$$

where

$$t_y \sigma M_0^2 = \frac{p}{\frac{1}{2} \varrho a^2}; \tag{5.17}$$

/347

$$m_{t_{h.f}}\sigma M_0^3 = \frac{\Phi\left(t_{y\sigma}M_0^2\right)^2}{4B^4 M_{fl}} - \left(t_{x_{hf}}\sigma M_0^2\right) M_{fl} + m_{pr}\sigma M_0^3; \tag{5.18}$$

$$t_{x_{h.f}}\sigma M_0^2 = -\bar{c}_x M_{fl}^2 . \tag{5.19}$$

At given $p = \frac{G}{F}$, $\bar{c}_x = \frac{\sum c_x S}{F}$, height, and speed, the value of the products $t_y \sigma M_0^2$ and $t_{x_{h.f}}\sigma M_0^2$ does not change upon a change in the rotor parameters ωR and σ. Consequently, when studying the effect of rotor parameters on the magnitude of required power of the helicopter, eqs.(5.16) and (5.18) are transformed into

$$\frac{N_{h.f}}{Ga} = \text{const}_1 m_{t_{h.f}}\sigma M_0^3;$$

$$m_{t_{h.f}}\sigma M_0^3 = \text{const}_2 + m_{pr}\sigma M_0^3.$$

As an example of the aerodynamic calculation by the power method, let us determine the required power of the Mi-4 helicopter. The helicopter data were given in Section 3. The calculation is performed by means of eq.(5.14) in Table 3.14. For simplicity, the profile losses were determined from the graphs in Figs.2.63 - 2.66, using eq.(6.10) of Chapter II for converting t_x; we can disregard the differences in blade profiles for $M_0 = 0.6$.

TABLE 3.14

$G = 7200\ kg$; $\sigma = 0{,}063$; $\omega R = 196\ m/sec$; $\xi = 0.84$;

$F = 346\ m^2$; $M_0 = 0.6$; $t_y = 0.138\frac{1}{\Delta}$; $N_{pr} = 163 \cdot 10^3\ m_{pr}\Delta$;

$N_{ind} = 9000\frac{1}{V\Delta}$; $N_{par} = \frac{\Sigma c_x S}{1010} V^3 \Delta$;

$H = 1000\ m$; $t_y = 0.152$; $\Delta = 0{,}907$

$\bar{V}$	0.15	0.20	0.25	0.30
V, *km/hr*	106	141	176	212
V, *m/sec*	29.4	39.2	49	58.8
α_f°	4.5	2.75	0	—3
$\bar{c}_x$	0.0088	0.0089	0.0092	0.0096
$\Sigma c_x S$	3.04	3.08	3.18	3.32
$t_{x_{hf}}$	—0.00314	—0.00565	—0.00915	—0.0137
$t_{x(\sigma=0.091)}$	0.0046	—0.00135	—0.0063	—0.0117
m_{pr}	0.00286	0.00306	0.0034	0.0037
N_{pr}	420	450	500	545
N_{ind}	338	253	203	168
N_{par}	70	165	340	610
$N_{h.f}$	828	868	1043	1323

The dependence of required power on flying speed is found by means of the formulas given in Subsection 1. Maximum and minimum speeds, maximum range and endurance, cruising and economic speeds are then determined by the method described in Section 3.

During ascent, the propulsive force of the rotor increases by an amount equal to the projection of the helicopter weight onto the flight direction $G \sin \theta_{fl.p}$. Consequently, the engine power of the helicopter increases by an amount of

$$N_{asc} = \frac{1}{75\xi} G \sin \theta_{fl.p} V = \frac{1}{75\xi} G V_y \tag{5.20}$$

while the total power of the engine is equal to

$$N = N_{pr} + N_{ind} + N_{par} + N_{asc}. \tag{5.21}$$

Here, N_{asc} represents the variation in potential energy of the helicopter upon a change in its flight altitude.

The components N_{pr}, N_{ind}, and N_{par} on vertical ascent and in horizontal flight differ somewhat in magnitude. However, for approximate calculations we can disregard this, and under this assumption eq.(5.21) can be represented in the form

$$N = N_{h.f} + N_{asc} = N_{h.f} + \frac{1}{75\xi} G V_y. \tag{5.22}$$

It is obvious that the maximum vertical rate of ascent of the helicopter is

$$V_{y_{max}} = \frac{75 (N_{dis} - N_{h.f\,min}) \xi}{G}. \tag{5.23}$$

The discrepancy between eqs.(5.23) and (4.24) can be explained by the assumption that N_{ind} and N_{pr} are equal in horizontal flight and vertical ascent. Equation (4.24) gives a more correct result. At flight altitudes where the rotor lift coefficient is less than the maximum value permissible with respect to flow separation, we can take, in conformity with the graphs in Figs.2.166 and 2.167, the average value of the propulsive efficiency as equal to 0.95 and determine $V_{y_{max}}$ by the formula:

$$V_{y_{max}} = \frac{0.95 \cdot 75 (N_{dis} - N_{h.f\,min}) \xi}{G}. \tag{5.24}$$

At high flight altitudes in a climbing regime, where $t_y \approx t_{y_{cr}}$, the speed $V_{y_{max}}$ should be determined from eq.(4.24).

3. Relation between N_{pr}, N_{ind}, and N_{par} during Horizontal Flight of a Single-Rotor Helicopter

It is of interest to examine the relation between individual components of the required power of a helicopter. Since the helicopter parameters determining N_{pr}, N_{ind}, and N_{par} depend on the gross weight of the helicopter, we will give data for helicopters of different weight classes.

Helicopters of different weight classes have a maximum weight coefficient at a different load per square meter of rotor disk area p and correspondingly have different peripheral speeds and solidity ratios, since the lift coefficient t_y limited in value by flow separation should be within 0.23 - 0.27 at the dynamic ceiling and 0.13 - 0.17 near the ground. Let us assume that the characteristic parameters for a light helicopter with an all-up weight to G = 3000 kg are: $M_0 = 0.55$, $\sigma = 0.05$; for a medium helicopter G = 7000 - 14,000 kg; $M_0 = 0.6$, $\sigma = 0.07$; for a heavy helicopter: $M_0 = 0.65 - 0.7$, $\sigma = 0.09$. /349

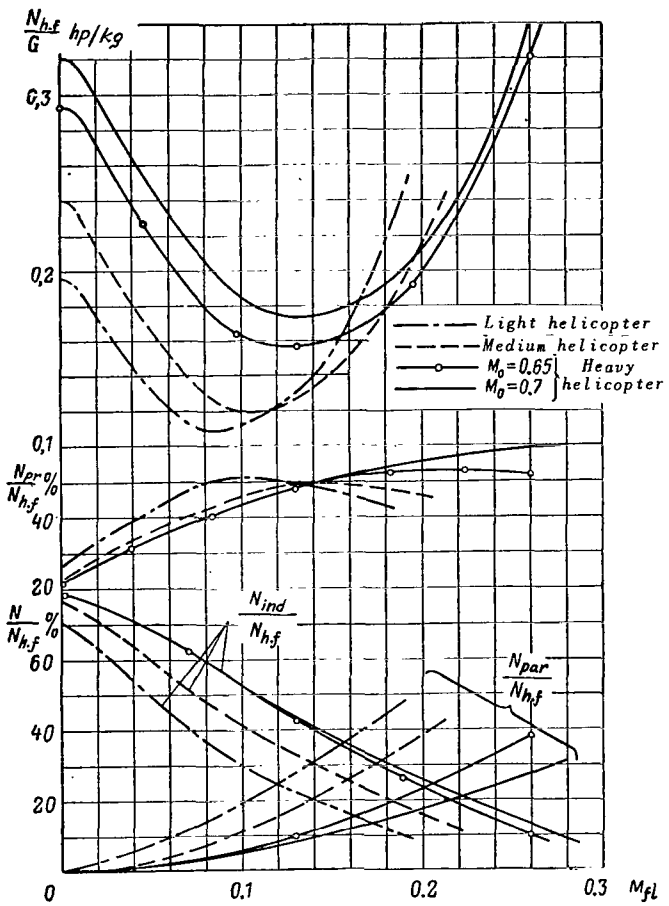

Fig.3.52 Quantity $N_{h.f}/G$ and Relation between Components of Required Power of Helicopters of Different Weight Classes.

The quantity $\Sigma c_x S$ of the helicopter referred to gross weight decreases upon an increase in weight owing to the relative decrease in the overall size of the helicopter (so-called "scale effect"). However, with an increase in G of a helicopter the value of p will increase, while the parasite drag coefficient referred to the rotor area, $\bar{c}_x = \frac{\Sigma c_x S}{G} p$, will change little for helicopters of different weight classes. Let us take it to be equal to 0.0085 for light and medium helicopters and 0.0075 for heavy helicopters.

For calculations at $\bar{V} \neq 0$, we use eqs.(5.4), (5.11), (5.12), and (5.16). The coefficient m_{pr} is found from the graph in Figs.2.63 - 2.70 as a function of the coefficients t_y and t_x. At V = 0, we use eq.(8.27) and the graph in Fig.2.174.

The calculation results are shown in Fig.3.52. Owing to an increase in p, σ, M_0, the quantity $\frac{N_{h.f}}{G}$ in hovering flight is much greater for heavy helicopters than for light helicopters.

In forward flight, eq.(5.16) can be written in the form /350

$$\frac{N_{h.f}}{G} = \frac{a}{75\xi}\left(\frac{m_{pr} M_0}{t_y} + 0.285 \frac{p}{\frac{1}{2}\varrho a^2 M_{fl}} + \frac{\sum c_x S}{G}\frac{1}{2}\varrho a^2 M_{fl}^3\right). \qquad (5.25)$$

This expression indicates that, at high flying speeds, the value of $\frac{N_{h.f}}{G}$, despite the increase in p and M_0, is lower for heavy helicopters than for light ones owing to a decrease in the ratio $\frac{\Sigma c_x S}{G}$.

If the available power of helicopters is equal to the required power in hovering flight, then the average value of the maximum speeds of helicopters of different weight classes is equal to 210 km/hr ($M_{fl} = 0.17$), 260 km/hr ($M_{fl} = 0.21$), and 310 km/hr ($M_{fl} = 0.25$).

The graph shows that the profile power losses, in percentage of the power of horizontal flight, are 22 - 27% at $\bar{V} = 0$ and 50% at average flying speeds, while they are 45% for light and medium helicopters and 55% and more for heavy helicopters at $\bar{V}_{max}$. It will be recalled that the graphs of m_{pr} in Figs.2.63 - 2.70 pertain to a rotor of average blade manufacturing quality and that c_{xp} of the profile increased by $\Delta c_{xp} = 0.002$.

The induced power losses amount to 73 - 78% in hovering flight, 40% at average flying speeds, and only 13% at maximum speed.

Losses due to parasite drag amount to 15 - 10% at average flying speeds and to 40 - 35% at maximum speed.

Thus, it turns out that, although helicopters of different weight classes differ in speed range, in load per square meter of rotor disk area, in peripheral speed, and in relative parasite drag, the power losses in fractions of the required power show a distribution that is practically the same at corresponding speeds.

The above data permit an approximate estimate as to the degree of variation in required power of a helicopter on introduction of various modifications in the helicopter design. For example, an improvement in blade finish may cause its profile drag to decrease by 20%; consequently, the required power of the helicopter will decrease by 10% at medium and high speeds. In hovering flight, the required power diminishes by 5%, which is very substantial since, in this case, the relative efficiency of the rotor increases by a like quantity while the maximum thrust of the rotor increases by $\frac{2}{3} \times 5 = 3.3\%$ [the coefficient $\frac{2}{3}$ is

obtained in accordance with eq.(8.34) of Chapt.II].

Upon a change in blade shape, the induced losses of the rotor may vary within several percent. It is obvious that this substantially affects the maximum thrust of the rotor in hovering flight but practically causes no change in the required power at high flying speeds. The change in blade shape at large M_0 significantly changes the rotor profile losses (see Sect.3, Chapt.II).

A 25% decrease in parasite drag of a helicopter leads to a 3% decrease in required power at medium flying speeds and to a 10% decrease close to maximum speed; this yields an increase in maximum speed by 15 - 20 km/hr.

CHAPTER IV /351

ROTOR FLUTTER

The phenomenon of rotor flutter has been a persistent companion of the development of helicopter construction. Numerous cases are known of the occurrence of flutter in experimental helicopters during their first ground test or during flight tests. Cases of the appearance of flutter have been observed also during operation of helicopters that had already undergone all test stages. Rotor flutter has been the cause of a number of accidents.

The greatest number of cases of flutter was observed at a time when this phenomenon had not yet been adequately studied and due attention had not yet been given to its investigation. At present, flutter has been studied in great detail, and there are numerous means for completely preventing its appearance. However, the helicopter designer must keep constant track of the rotor parameters and hold them to limits that ensure the necessary safety margin before onset of flutter. However, these parameters vary constantly with design and technological modifications made in designing and plant testing of a helicopter and during its series production. Such variations continue even when the helicopter has been placed in service. This is due to various circumstances. The most common case is deterioration of the individual blade balance, either due to penetration of moisture into the blade or due to its increase in weight during repair.

Experience shows that even the slightest letting up in control of the rotor parameters will immediately cause appearance of flutter. This is primarily explained by the fact that the designer strives to reduce the margin before onset of flutter to a minimum since the expenditures produced by an increase in rotor weight are generally proportional to the magnitude of this margin. Its increase requires a corresponding increase in blade weight or in weight of the structural elements of the rotor control system.

As a result, the most economic design of a helicopter keeps these parameters at the minimum level allowable by the flutter limits. Even their slightest variation produced by some unforeseen happening may lead to flutter. The blade parameters, at all times, are kept close to the flutter limit.

This circumstance necessitated taking reliable measures to keep the flutter characteristics of a rotor within limits that would ensure prescribed margins /352
before onset of flutter, which, as a rule, are rigorously standardized. These measures should be enforced both during production and service of the helicopter. In addition, each helicopter must be subjected to special ground tests to check for flutter in the final inspection. Experience gained in mass use of helicopters confirms the reliability of this inspection system. We can consider that, at present, conditions have been created that preclude the possibility of accidents owing to flutter. Actually, cases of unforeseen occurrence of flutter have almost completely stopped.

The achievement of the present favorable state as regards flutter was preceded by extensive theoretical and experimental investigations.

Valuable contributions to the development of the theory of flutter were made by P.M.Riz, L.N.Grodko, V.D.Il'ichev, M.S.Galkin, A.I.Pozhalostin, F.L. Zarzhevskaya, M.E.Lipskaya, V.M.Pchelkin, and many other engineers. Numerous papers by foreign authors are also well known [see (Ref.39 - 42)].

Results of great importance for the development of the theory were obtained in flight tests on flutter carried out by S.B.Bren and A.A.Dokuchayev and performed by the pilot V.V.Vinitskiy.

Many highly useful results were obtained by L.S.Popov, B.A.Kirshteyn, N.V.Lebedev, and B.B.Martynov in tests of dynamically similar models.

All this work led to rather clear and distinct concepts concerning the phenomenon of flutter which permitted developing new blades with the necessary parameter margins, without additional modifications after tests, as had often been necessary before. However, for this it was necessary, in designing the blade, to perform numerous rather laborious calculations. This Chapter will be devoted mainly to an account of the method of these calculations.

In writing this Chapter F.L.Zarzhevskaya was of considerable help to the author, for which the author extends his gratitute.

Section 1. Basic Assumptions and Characteristics of an Approach to Flutter Calculation

1. Bending and Torsional Vibrations of the Blade. Possible Cases of Stability Loss

The theory of rotor flutter is developed on the basis of an investigation of bending and torsional vibrations of blades during their rotation in air.

When solving the problem of bending and torsional vibrations of blades in air, the designer is interested primarily in two qualitatively different problems. The first of them reduces to a determination of steady bending and torsional vibrations of the blade, occurring in all helicopter flight regimes. This problem requires the development of special calculation methods which are a further development of calculation methods for forced vibrations of a blade and should, in particular, answer the problem of the effect of torsional deformations of a blade on its bending vibrations and, accordingly, on the magnitude of variable stresses from blade bending. The second question is associated with a determination of the stability of blade motion. Usually, purely bending vibrations of blades are stable. Loss of their stability occurs only in flow-separation regimes.

In studying bending and torsional vibrations we find that, at certain rotor parameters, there is a loss of stability of motion of blades which leads to flutter or divergence. The phenomenon in which blades undergo oscillatory instability is called flutter, whereas the phenomenon of aperiodic instability of

blade motion is called divergence. The most common of these two phenomena /353
in practice is rotor flutter. Therefore, when examining bending and torsional vibrations of a blade, the designer is more interested in the conditions leading to flutter.

2. Effect of Blade Attachment to Hub and the Possibility of Theoretical Investigation of Flutter of an Isolated Blade

The results of calculating flutter largely depend on the design configuration of the rotor and primarily on the conditions of blade attachment to the root, i.e., on hub design and rotor control system. The characteristics of blade attachment influence the boundary conditions of the problem and hence the design formulas for determining flutter parameters.

The most common type of rotor with individual hinge attachment of each blade to the hub, with the control exercised over an automatic pitch control mechanism, will be examined below when presenting the method of calculating flutter. For rotors with a rigid and universal joint attachment of the blade to the hub or with some other type of control, the approach to flutter calculation remains the same. However, the conditions under which flutter occurs may change extensively.

Flutter is greatly influenced by the design of the system controlling the angle of blade setting and, primarily, by the design of the automatic pitch control. The automatic pitch control couples the oscillations of the different rotor blades. Thus, as soon as this couple becomes sufficiently strong - and this generally takes place on real helicopters - it is impossible to investigate the flutter of an isolated blade. It is then necessary to study the flutter of the entire rotor as a whole.

In all practical cases, there occurs only flutter of the entire rotor as a whole, when each advancing blade of the rotor duplicates the motion of the retreating blade with some lag. Flutter of a single blade has never been noted.

However, in many cases the investigation of flutter of a rotor as a whole can be reduced to calculation of the vibrations of an isolated blade. Therefore, calculation of the flutter of an isolated blade often furnishes a sufficiently comprehensive answer so that we can frequently restrict ourselves to this result in practice. In so doing, however, it is important to properly prescribe the stiffness of the isolated blade control. This question will be taken up in greater detail in Section 4.

3. Different Types of Flutter Differing with Respect to Blade Vibration. Flapping and Bending Flutter

The problem of determining the conditions for occurrence of flutter is solved usually by means of differential equations of bending and torsional (binary) vibrations of the blade (see Sect.6). These equations permit obtaining the parameters of different types of flutter which differ by the blade vibration

modes. The critical rpm and other parameters of flutter obtained from solving these equations are quite complex functions of the initial rotor parameters. Therefore, an analysis of these relations is conveniently begun with the simplest particular case. In fact, flutter in which blade vibration in the flapping plane occurs mainly with the fundamental vibration mode of the blade is most widespread in practice. Bending strains of the blade in this case have the character of an admixture to the vibration mode and do not determine the phenomenon. /354 Therefore, in this case all relations of interest to the designer can be obtained from examination of a rotor model with blades that have absolute flexural rigidity and execute flapping vibrations about the flapping hinges. This type of flutter will henceforth be called "flapping flutter" in contrast to "bending flutter", whose characteristics cannot be determined without regard for the flexural deformations of the blade.

4. Characteristics of the Torsional Vibration Modes of a Blade and Possible Correlated Assumptions

The relation between torsional rigidity of the blade and the rotor control system in most modern helicopters is such that, in torsional vibrations, the blade turns mainly as a consequence of deformations of the controls (Fig.4.1). In this case, the setting angle φ of the blade element over its length, especially at the most effective portion from $\bar{r} = 0.5$ to the blade tip, vary so insignificantly that in flutter calculations we can set, with a sufficient degree of accuracy,

$$\varphi = \text{const.} \qquad (1.1)$$

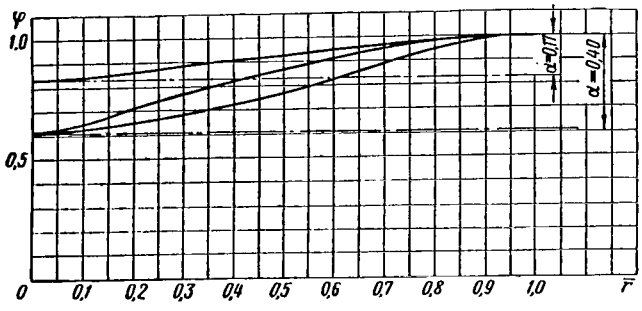

Fig.4.1 Typical Natural Vibration Modes of a Blade in Torsion (the Curves Refer to Three Different Helicopters).

The acceptance of this law of angle distribution φ is equivalent to the assumption that the blade is absolutely rigid in torsion and executes torsional vibrations only as a consequence of deformations of the control. To have this assumption lead to the smallest possible error, we will introduce into the calculations the equivalent value of the hinge stiffness of the controls which takes into account the elasticity of the blade itself.

Calculations made to substantiate this assumption show that it can be successfully used for all rotors for which the values of the angle $\alpha < 0.4 - 0.5$ (see Fig.4.1), which probably encompasses almost all existing helicopters.

It should also be noted that the described character of the relation between torsional rigidity of the blade and its attachment causes the axis about which the blade elements in torsional vibrations are turning to come close to the axis of the axial hinge. Hence, the position of the axis of blade stiffness in the examined cross section loses its significance. This circumstance permits

the approximate assumption that, in torsional vibrations, the blade elements turn about the axial hinge.

5. Assumptions on Blade Oscillations in the Plane of Rotation /355

There exists a definite coupling between blade vibrations in the flapping plane and in the plane of rotation. This coupling is due to two types of forces. The stronger is the coupling created by Coriolis forces. The weaker is the coupling due to aerodynamic forces.

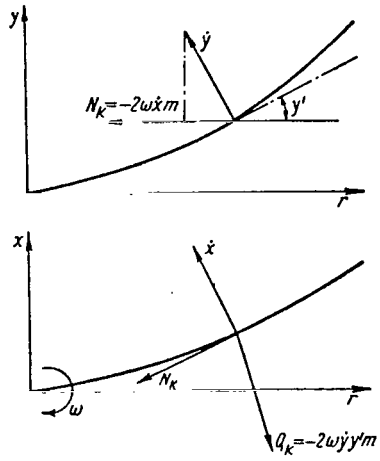

Fig.4.2 Coriolis Forces Acting on a Vibrating Blade.

Let us examine in some detail the forces coupling vibrations in the flapping plane and in the plane of rotation.

During vibrations in the flapping plane, Coriolis forces arise which act in the plane of rotation

$$Q_K = -2\omega\dot{y}y'm, \tag{1.2}$$

where

$\dot{y}$ = rate of displacement of the blade elements in the flapping plane (Fig.4.2);
y' = angle of inclination of the blade axis upon deflection of the blade from the plane of rotation;
m = mass of the blade element.

During blade vibration in the plane of rotation, variable Coriolis forces are set up which act in a direction close to the direction of centrifugal forces. These forces stretch the blade and therefore should be taken into account in differential equations of blade vibrations, along with centrifugal forces.

The Coriolis forces acting in the direction of the blade axis can be determined by the formula

$$N_K = -2\omega\dot{x}m, \tag{1.3}$$

where $\dot{x}$ is the rate of displacement of the blade elements during vibrations of the blade in the plane of rotation (Fig.4.2).

The Coriolis forces determined by eqs.(1.2) and (1.3) relate the blade vibrations in the flapping plane and plane of rotation.

The aerodynamic forces create an analogous coupling.

If, in the flapping plane, variable aerodynamic forces associated with a change in the value c_y act on the blade, then the component of these forces

$$Q=\Phi T \tag{1.4}$$

will cause blade vibration in the plane of rotation [the value of Φ entering eq.(1.4) determines the angle of inflow].

During blade vibration in the plane of rotation, the aerodynamic forces acting in the flapping plane will vary as a function of any variation in the relative velocity U.

Thus, the presence of the described couples requires that blade vibrations in the plane of rotation be taken into account also in flutter calculations. However, calculations and experiments show that blade vibrations in the plane of rotation have an insignificant effect on the critical numbers of revolution of flutter. Therefore, in all calculations of flutter, blade vibration in the plane of rotation can be disregarded. We must also take into account that, in the absence of thrust at the blade, when the angle of inflow Φ is equal to zero (such a position is possible for an untwisted flat blade) and the blade is not deflected from the plane of rotation so that $y' = 0$, the terms of the coupling /356 determined by eqs.(1.2) and (1.4) are absent. Thus, in this case there is no coupling between vibrations in the indicated plane.

6. Determination of Aerodynamic Forces Acting on a Vibrating Profile

The occurrence of diverging vibrations in flutter is caused by aerodynamic forces acting on the blade profile. Therefore, the basis on which these aerodynamic forces are determined is very important.

In performing practical calculations of flutter, the method of determining aerodynamic forces based on the "steady-state hypothesis" is widely employed. In this hypothesis, it is assumed that, during vibrations of the profile, it is acted on by loads that are the same as those created if the flow pattern formed at a given instant of time were to be time-invariant. The use of the "steady-state hypothesis" for calculating rotor flutter yields quite satisfactory results which are in good agreement with experiments. Therefore, our entire account will be based on the results obtained under application of the "steady-state hypothesis". Refinements that can be made by taking unsteady flow into consideration will not be examined here.

The use of the "steady-state hypothesis" leads to the following well-known formulas [see for example (Ref.29, 32, 33)] for determining aerodynamic loads acting on a vibrating profile of unit length:

$$\left.\begin{aligned} T&=-\frac{1}{2}c_y^a\varrho bU^2\left[\varphi-\frac{1}{U}\dot{y}+\left(\frac{3}{4}-\frac{x_0}{b}\right)\frac{b}{U}\dot{\varphi}\right];\\ \mathfrak{M}_{aer}&=\frac{1}{2}\varrho bU^2\left\{-\frac{\pi}{8}\frac{b^2}{U}\dot{\varphi}-c_y^a\sigma_f\times\right.\\ &\left.\times\left[\varphi-\frac{1}{U}\dot{y}+\left(\frac{3}{4}-\frac{x_0}{b}\right)\frac{b}{U}\dot{\varphi}\right]\right\}, \end{aligned}\right\} \tag{1.5}$$

where

T = aerodynamic force per unit length acting on the vibrating profile in a direction perpendicular to the relative flow velocity U;

$\mathfrak{M}_{aer}$ = torsional moment per unit length of aerodynamic forces acting relative to the axis passing at a distance x_0 from the profile leading edge;

φ = angle of blade profile setting in the examined sections;

$\dot{y}$ = rate of displacement of the blade elements in the flapping plane;

x_0 = distance between profile leading edge and flexural axis, i.e., up to the point where the elements of the blade start twisting under application of a torque;

σ_f = distance between profile focus or a.c. and flexural axis of the blade; in some formulas below [see eqs.(2.13) and (5.2)] we will also use the designation $\sigma_f \simeq \frac{\sigma_f}{R}$.

Equations (1.5) are obtained for a plane-parallel flow. Therefore, their use for determining the helicopter blade loading is approximate also in this sense, since the flow past the blade markedly differs from plane-parallel.

It is convenient to make a slight transformation of eqs.(1.5) when using /357 them for the helicopter blade, by introducing certain additional simplifications and refinements. The relative velocity U of the flow past the profile can be approximately equated to its component U_x parallel to the plane of rotation of the rotor. It must also be considered that the other component of this velocity U_y directed perpendicular to the velocity U_x differs from $\dot{y}$ by the amount of the velocity of the air stream flowing through the rotor. Therefore, for a helicopter blade, these formulas are generally used in the following form:

$$\left.\begin{aligned} T &= \frac{1}{2} c_y^{\alpha} \varrho b \left[\varphi U_x^2 + U_x U_y + \left(\frac{3}{4} - \frac{x_0}{b}\right) b U_x \dot{\varphi}\right]; \\ \mathfrak{M}_{aer} &= -\frac{\pi}{16} \varrho b^3 U_x \dot{\varphi} - \sigma_f T. \end{aligned}\right\} \quad (1.6)$$

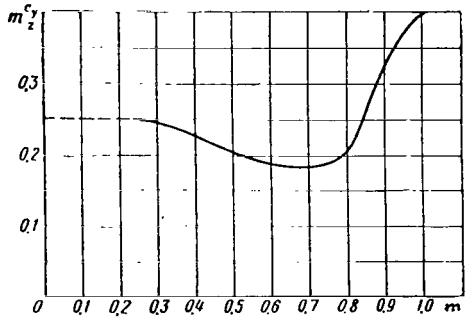

Fig.4.3 Position of the Aerodynamic Center on the Mach Number, for a NACA 230 Profile.

The last term in the first equation in the systems (1.5) and (1.6) ordinarily has little influence on the calculation results. Therefore, it can be neglected without resulting in substantial errors.

In calculations of flutter under conditions of axial flow past the rotor in hovering flight or in operation of the rotor under ground conditions, the aerodynamic loads can be determined on the basis of the linear dependence of the aerodynamic coefficient on the angle of attack. This assumption is also included in eqs.(1.5) and (.16). However, under conditions of forward flight, especially in regimes close to stalling, this assumption becomes quite inaccurate. Therefore, a method permitting rejection of this assumption will be discussed below in Section 7. Refined formulas for calculating aerodynamic loads for this case will also be derived in the same Section.

As is known, the Mach number M has a strong influence on the aerodynamic characteristics of a profile. To calculate flutter of a helicopter rotor it is especially important that M have a substantial effect on the position of the profile focus which, as will be shown below, greatly affects the critical revolutions of flutter. Therefore, in calculations for each blade radius, we must take the position of the aerodynamic center corresponding to the local value of M at this radius. Figure 4.3 gives the position of the a.c. as a function of the Mach number, for a NACA 230 profile.

When calculating flutter in forward flight it must be taken into account that the local Mach number varies relative to the rotor azimuth. This, in turn, leads to fluctuations of the position of the profile focus during each revolution of the blade. In approximate calculations, this circumstance can be disregarded.

When using the calculation method presented in Section 7, fluctuations of the a.c. relative to azimuth can be accounted for without difficulty, which is one of the important advantages of this method.

Section 2. Flapping Flutter of an Isolated Blade with Axial Flow past the Rotor /358

1. Blade Model

The parameters of flapping flutter can be determined with sufficient reliability from a calculation based on the following assumptions:

1) The blade is absolutely rigid in bending and vibrates in the flapping plane like a solid body as a consequence of turning about the flapping hinge.

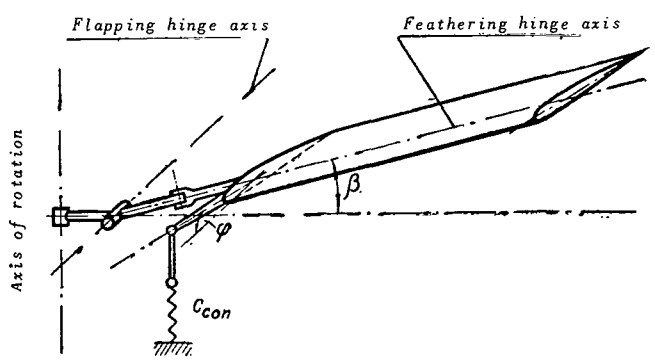

Fig.4.4 Blade Model Used in the Calculation.

2) The blade is absolutely rigid also in torsion and executes torsional vibrations, rotating like a solid body about the feathering hinge of the hub as a consequence of deformation of the control, presence of an automatic pitch control mechanism, and installation of a flapping compensator.

These assumptions lead to the possibility of calculating a blade model with two degrees of freedom, determined by the variables β and φ (Fig.4.4). This model is usually called "semirigid".

2. Derivation of Differential Equations of Flutter

In this Subsection we will derive the differential equations of flutter for a model of an isolated blade. It will be shown below, in Section 4, that in many cases the theoretical investigations of flutter of a rotor as a whole can be reduced to an examination of the flutter of an isolated blade. Therefore, it is expedient to evaluate first the effect of various factors on the flutter of an isolated blade and to determine later (in Sect.4) in what manner and in what cases these results can be extrapolated to a rotor as a whole.

Let us construct the differential equations of torsional-flapping vibrations of an isolated blade. These equations can be derived by equating to zero the sum of the moment of all forces acting on the blade during its vibrations relative to the flapping and feathering hinges of the hub. As usual, we will examine small vibrations for which all terms of the second order relative to small displacements of the blade can be neglected.

To avoid needless complication of the equations, let us assume that the distance from the axis of rotation to the flapping hinge is equal to zero ($r_0 = 0$). Then, the condition of equilibrium of the moments of all forces relative to the flapping hinge can be written as

$$\int_0^R m(r\ddot{\beta} - \sigma\ddot{\varphi})\,r\,dr + \omega^2 \int_0^R m(r\beta - \sigma\varphi)\,r\,dr = \int_0^R T\,r\,dr, \tag{2.1}$$

where /359

β = angle of rotation of the blade relative to the flapping hinge;
φ = angle of rotation of the blade relative to the feathering hinge;
m = mass per unit length of the blade element;
σ = distance from the axis of the feathering hinge to the center of gravity of the blade element;
T = aerodynamic load per unit length determined by eq.(1.6).

The integrals entering the left-hand side of eq.(2.1) can be expressed in terms of the moments of inertia of the blade relative to the horizontal hinge $I_{h.h}$ and the centrifugal moment of inertia of the blade I_{cf}:

$$\left.\begin{aligned} I_{h.h} &= \int_0^R mr^2 dr, \\ I_{cf} &= \int_0^R mr\sigma dr. \end{aligned}\right\} \tag{2.2}$$

On introducing these designations into eq.(2.1) and referring all terms of this equation to $I_{h.h}$, the expression can be rewritten in the form

$$\ddot{\beta} + \omega^2\beta - \frac{I_{cf}}{I_{h.h}}(\ddot{\varphi} + \omega^2\varphi) = \frac{1}{I_{h.h}}\int_0^R T\,r\,dr. \tag{2.3}$$

For the regime of axial flow past the rotor, the velocities entering

eq.(1.6) can be equated to

$$\left.\begin{aligned} U_x &= \omega r, \\ U_y &= \omega R\lambda - r\dot{\beta}, \end{aligned}\right\} \tag{2.4}$$

where λ is the relative rate of flow through the rotor.

Substituting eqs.(2.4) into eq.(1.6), and then eq.(1.6) into eq.(2.3), we obtain

$$\ddot{\beta} + d_{11}\omega\dot{\beta} + \omega^2\beta + c_{12}\ddot{\varphi} + d_{12}\omega\dot{\varphi} + b_{12}\omega^2\varphi = \omega^2\gamma_0 \int_0^1 \bar{b}\lambda\bar{r}^2 d\bar{r}, \tag{2.5}$$

where γ_0 is the mass characteristic of the rigid blade [see eq.(2.14)].

The values of the coefficients b_{12}, c_{12}, d_{11}, and d_{12} will be given below [see eq.(2.14)].

The moment of external forces, relative to the feathering hinge, loading the system that controls the angle of blade setting, can be written as

$$\begin{aligned} M_{con} = -(\ddot{\varphi} + \omega^2\varphi) I_{a.h} + (\ddot{\beta} + \omega^2\beta) I_{cf} - M_{fr} + \\ + \omega^2 \int_0^R I_m \Delta\varphi_{geom}\, dr + \int_0^R \mathfrak{M}_{aer} dr, \end{aligned} \tag{2.6}$$

where

$I_{a.h}$ = moment of inertia of the blade relative to the feathering or axial hinge;

I_m = moment of inertia of the blade per unit length relative to this axis;

$\mathfrak{M}_{aer}$ = moment of aerodynamic forces per unit length relative to the axial hinge with this moment being determined by eqs.(1.6):

M_{fr} = moment due to friction forces in the axial hinge of the hub.

The moment acting on the control system, M_{con} can be expressed in terms of rigidity or stiffness and deformation of the control system: /360

$$M_{con} = c_{con}\gamma, \tag{2.7}$$

where

γ = angle of rotation of the blade relative to the feathering hinge due to deformations of the control system;

c_{con} = stiffness of the control system.

In order to express the value of γ in terms of the setting angle of the blade sections, we put

$$\varphi = \theta - \varkappa\beta + \gamma, \tag{2.8}$$

where

θ = angle of setting of the blade sections prescribed by the control system;

$\varkappa$ = flapping compensator.

The angle θ is determined from the expression

$$\theta=\theta_0-\theta_1\sin\psi-\theta_2\cos\psi, \tag{2.9}$$

where

θ_0 = angle of blade setting at the root for $\beta = 0$;

θ_1 and θ_2 = angles of cyclic pitch control.

It follows from eq.(2.8) that

$$\gamma=\varphi+\varkappa\beta-\theta. \tag{2.10}$$

Substituting γ into eq.(2.7) and then eq.(2.7) into eq.(2.6) and referring all terms of eq.(2.6) to the moment of inertia of the blade relative to the axial hinge $I_{a.h}$, we obtain

$$\begin{aligned}\ddot{\varphi}+(p_{tw}^2+\omega^2)\varphi+c_{21}(\ddot{\beta}+\omega^2\beta)+\varkappa p_{tw}^2\beta+\frac{M_{fr}}{I_{a.h}}-\\ -\frac{1}{I_{a.h}}\int_0^R \mathfrak{M}_{aer}dr=p_{tw}^2\theta+\omega^2\frac{1}{I_{a.h}}\int_0^R I_m\Delta\varphi_{geom}dr.\end{aligned} \tag{2.11}$$

Here p_{tw} is the frequency of natural vibrations in twist or torsion of an absolutely rigid blade in compliant control:

$$p_{tw}=\sqrt{\frac{c_{y_{pr}}}{I_{a.h}}}. \tag{2.12}$$

Substituting into eq.(2.11) the value of $\mathfrak{M}_{aer}$ from eq.(1.6) and taking the resultant equation together with eq.(2.5), we obtain a system of differential equations of binary vibrations of a rigid blade:

$$\left.\begin{aligned}\ddot{\beta}+d_{11}\omega\dot{\beta}+\omega^2\beta+c_{12}\ddot{\varphi}+d_{12}\omega\dot{\varphi}+b_{12}\omega^2\varphi=\omega^2\gamma_0\int_0^1\bar{b}\lambda\bar{r}^2d\bar{r},\\ \ddot{\varphi}+d_{22}\omega\dot{\varphi}+(p_{tw}^2+b_{22}\omega^2)\varphi+c_{21}\ddot{\beta}+d_{21}\omega\dot{\beta}+\\ +(\varkappa p_{tw}^2+c_{21}\omega^2)\beta=p_{tw}^2\theta+\omega^2\frac{1}{I_{a.h}}\int_0^R I_m\Delta\varphi_{geom}dr-\\ -\omega^2\frac{1}{i_0}\gamma_0\int_0^R\bar{b}\lambda\tilde{\sigma}_f\bar{r}d\bar{r}.\end{aligned}\right\} \tag{2.13}$$

The coefficients entering eqs.(2.13) can be determined by the following formulas: /361

$$
\left.
\begin{aligned}
c_{12} &= -\frac{1}{I_{h.h}}\int_0^R mr\sigma dr = i_0 c_{21},\\
c_{21} &= -\frac{1}{I_{a.h}}\int_0^R mr\sigma dr,\\
d_{11} &= \frac{1}{2}c_y^\alpha \frac{\varrho}{I_{h.h}}\int_0^R br^3 dr,\\
d_{12} &= -\frac{1}{2}c_y^\alpha \frac{\varrho}{I_{h.h}}\int_0^R b^2 r^2\left(\frac{3}{4}-\frac{x_0}{b}\right)dr,\\
d_{21} &= -\frac{1}{2}c_y^\alpha \frac{\varrho}{I_{a.h}}\int_0^R br^2\sigma_f dr,\\
d_{22} &= \frac{1}{I_{a.h}}\left[\frac{\pi}{16}\varrho\int_0^R b^3 r dr+\frac{1}{2}c_y^\alpha\varrho\times\right.\\
&\quad\left.\times\int_0^R b^2 r\sigma_f\left(\frac{3}{4}-\frac{x_0}{b}\right)dr\right]+d_{fr},\\
b_{12} &= -\frac{1}{2}c_y^\alpha \frac{\varrho}{I_{h.h}}\int_0^R br^3 dr + i_0 c_{21},\\
b_{22} &= 1+\frac{1}{2}c_y^\alpha \frac{\varrho}{I_{a.h}}\int_0^R br^2\sigma_f dr,\\
\gamma_0 &= \frac{c_y^\alpha \varrho b_{0.7}R^4}{2I_{h.h}},\\
i_0 &= \frac{I_{a.h}}{I_{h.h}}.
\end{aligned}
\right\} \qquad (2.14)
$$

The coefficients of eq.(2.14) entering the differential equation completely determine the behavior of the blade in vibration. Certain comments are necessary relative to these coefficients.

The damping factor d_{11} of flapping vibration of the blade is determined only by aerodynamic forces since the moment of friction forces in the flapping hinge is relatively small. A quite substantial addition d_{fr} due to friction in the feathering hinge enters the damping coefficient of the torsional vibrations of the blade d_{22}, in addition to aerodynamic damping. The effect of friction in the feathering hinge will be discussed in greater detail in Section 3 of this Chapter.

The coefficient d_{12} entering the equation is small and not essential for

the final results of the calculation. Therefore, it can be disregarded in practical calculations.

If the ratio of the moments of inertia $i_\Phi = \frac{I_{a.h}}{I_{h.h}} < \frac{1}{1000}$, then we can /362 also neglect the coefficient c_{12}. In so doing, the system of equations (2.13) is simplified even more.

It is important to note that the effect of the position of the center of gravity of the blade element will appear in the calculation only upon a change in the coefficient

$$c_{21} = -\frac{1}{I_{a.h}} \int_0^R mr\sigma\, dr. \tag{2.15}$$

3. Particular Solution of the Differential Equation

It is not difficult to demonstrate that the expressions

$$\left.\begin{aligned} \beta^* &= a_0 - a_1 \cos\psi - b_1 \sin\psi, \\ \varphi^* &= \varphi_0 - \bar{\varphi}_1 \cos\psi - \bar{\bar{\varphi}}_1 \sin\psi \end{aligned}\right\} \tag{2.16}$$

are a particular solution of the system of differential equations (2.13) and determine the undisturbed motion of the blade. If the swashplate of the automatic pitch control is set in a neutral position and if $\theta_1 = \theta_2 = 0$, then the particular solution of these equations is constituted by the expressions

$$\left.\begin{aligned} \beta^* &= a_0, \\ \varphi^* &= \varphi_0. \end{aligned}\right\} \tag{2.17}$$

4. Differential Equation of Disturbed Motion

Let us substitute into eq.(2.13)

$$\left.\begin{aligned} \beta &= \beta^* + \beta_d, \\ \varphi &= \varphi^* + \varphi_d, \end{aligned}\right\} \tag{2.18}$$

where β_d and φ_d are the angles of deflection of the blade from a position corresponding to its undisturbed motion.

Then, bearing in mind that β^* and φ^* represent the particular solution of eqs.(2.13), we obtain a system of differential equations of disturbed motion of the blade:

$$\left.\begin{aligned} &\ddot{\beta} + d_{11}\omega\dot{\beta} + \omega^2\beta + c_{12}\ddot{\varphi} + d_{12}\omega\dot{\varphi} + b_{12}\omega^2\varphi = 0; \\ &\ddot{\varphi} + d_{22}\omega^2\dot{\varphi} + (p_{tw}^2 + b_{22}\omega^2)\varphi + c_{21}\ddot{\beta} + d_{21}\omega\dot{\beta} + (\varkappa p_{tw}^2 + c_{21}\omega^2)\beta = 0. \end{aligned}\right\} \tag{2.19}$$

In these equations, the subscript of the variables β and φ, designating that these variables refer only to disturbed motion, is dropped for simplicity.

5. Notation of Differential Equations in Matrix Form

It is convenient to write differential equation (2.19) in the following matrix form:

$$C\ddot{X}+D\omega\dot{X}+(A+\omega^2B)X=0. \tag{2.20}$$

Here, C is the inertia matrix:

$$C=\begin{pmatrix}1 & c_{12}\\ c_{21} & 1\end{pmatrix};$$

D is the damping matrix: /363

$$D=\begin{pmatrix}d_{11} & d_{12}\\ d_{21} & d_{22}\end{pmatrix};$$

A is the stiffness matrix:

$$A=\begin{pmatrix}0 & 0\\ \varkappa p_{t_W}^2 & p_{t_W}^2\end{pmatrix};$$

B is the matrix of centrifugal and aerodynamic forces:

$$B=\begin{pmatrix}1 & b_{12}\\ b_{21} & b_{22}\end{pmatrix},$$

where $b_{21} = c_{21}$.

X is the vector function:

$$X=\begin{pmatrix}\beta\\ \varphi\end{pmatrix}.$$

6. Solution of Differential Equations of Blade Vibrations

Setting, in the system of equations (2.19),

$$\left.\begin{aligned}\beta&=\beta_0e^{\lambda t};\\ \varphi&=\varphi_0e^{\lambda t},\end{aligned}\right\} \tag{2.21}$$

we obtain the following characteristic equation:

$$\bar{\lambda}^4+A_1\bar{\omega}\bar{\lambda}^3+(B_1\bar{\omega}^2+B^2)\bar{\lambda}^2+(C_1\bar{\omega}^2+C_2)\bar{\omega}\bar{\lambda}+D_1\bar{\omega}^4+D_2\bar{\omega}^2=0. \tag{2.22}$$

Here for simplifying the calculations, the values of λ and ω are referred to the frequency of natural torsional vibrations of the blade p_{tw}, i.e.,

$$\left.\begin{aligned}\bar{\lambda}&=\frac{\lambda}{p_{tw}};\\ \bar{\omega}&=\frac{\omega}{p_{tw}}.\end{aligned}\right\} \tag{2.23}$$

The coefficients entering the characteristic equation (2.22) have the following form:

$$\left.\begin{aligned}A_1&=\frac{1}{1-i_0c_{21}^2}(d_{11}+d_{22}-c_{12}d_{21}-c_{21}d_{12}),\\ B_1&=\frac{1}{1-i_0c_{21}^2}(1+b_{22}+d_{11}d_{22}-b_{12}c_{21}-d_{12}d_{21}-c_{12}c_{21}),\\ B_2&=\frac{1}{1-i_0c_{21}^2}(1-\varkappa c_{12}),\\ C_1&=\frac{1}{1-i_0c_{21}^2}(d_{22}+d_{11}b_{22}-b_{12}d_{21}-c_{21}d_{12}),\\ C_2&=\frac{1}{1-i_0c_{21}^2}(d_{11}-\varkappa d_{12}),\\ D_1&=\frac{1}{1-i_0c_{21}^2}(b_{22}-b_{12}c_{21}),\\ D_2&=\frac{1}{1-i_0c_{21}^2}(1-\varkappa b_{12}).\end{aligned}\right\} \tag{2.24}$$

Let us examine the behavior of the roots of the characteristic equation (2.22) for different rotor parameters. /364

In the major portion of the rpm range of practical interest, the motion of the blade is determined by two pairs of roots:

$$\bar{\lambda}_I=\bar{q}_1\pm i\bar{p}_1 \text{ and } \bar{\lambda}_{II}=\bar{q}_2\mp i\bar{p}_2. \tag{2.25}$$

Figures 4.5 and 4.6 show the dependence of the real and imaginary parts of these roots on the rotor rpm and on the blade balancing. In both graphs, we plotted, on the abscissa, the rotor rpm $\bar{n}$ related to the frequency of natural vibrations of the blade in torsion p_{tw}, expressed in oscillations per minute:

$$\bar{n}=n/p_{tw}.$$

The values of $\bar{n}$ coincide in magnitude with the values of the relative angular velocity

$$\bar{\omega}=\omega/p_{tw},$$

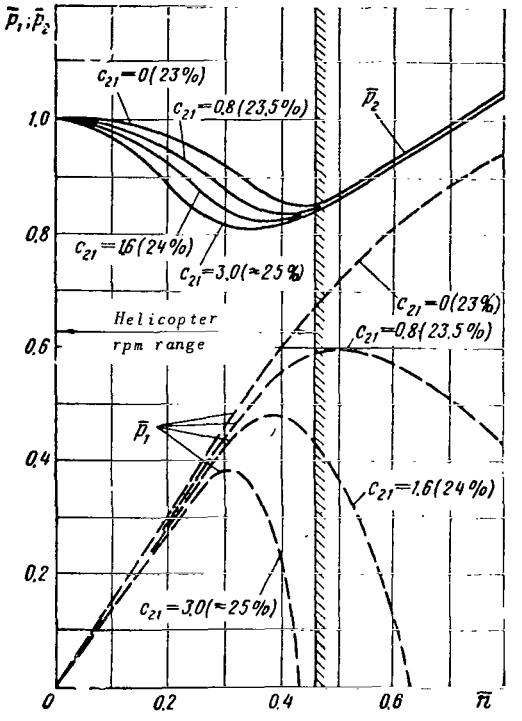

Fig.4.5 Imaginary Part of the Roots of the Characteristic Equation as a Function of Angular Velocity, for Different Values of the Coefficient c_{21}. [In this diagram, as well as in Fig.4.6, we indicate the absolute value of c_{21} (without the minus sign).]

where p_{tw} is expressed in rad/sec.

Therefore, we will henceforth use the designations $\bar{n}$ and $\bar{\omega}$ on an equal footing.

The roots of the characteristic equation determine the law governing the motion of the blade after some extraneous action (in practice, this may be - for example - a gust of wind) unbalances the blade. In this case, the value of the real part of the root $\bar{q}$ determines the rate at which the amplitude of the vibrations varies, whereas the imaginary part $\bar{p}$ determines their frequency. The negative real part of the root corresponds to damping oscillations of the blade. When this quantity is positive, vibrations of an amplitude increasing in time will be generated.

The first pair $\bar{\lambda}_I$, shown in Figs.4.5 and 4.6 by broken curves, determines the motion in which deflection of the blade relative to the flapping hinge is predominant. The second pair of roots $\bar{\lambda}_{II}$, shown by solid curves, determines the motion with an appreciable rotation of the blade relative to the feathering hinge which is due to deformation of the controls.

This second motion is of greatest interest since, at certain blade balancing, the real part of the root $\bar{q}_2$ passes into the area of positive values (see Fig.4.6), which corresponds to vibrations of increasing amplitude, which are known as flutter. /365

The values of the rotor rpm at which $\bar{q}_2 = 0$ are usually called "critical rpm of flutter".

When $\bar{q}_2 < 0$, the blade executes damping oscillations. In this case, the value of $\bar{q}_2$ determines the magnitude of forces that produce damping of the blade vibrations and constitutes a criterion for their stability. It follows from Fig.4.6 that the damping forces begin to decrease long before the critical flutter rpm. This decrease is observed even when flutter cannot arise no matter what the rotor rpm but the margin for blade balance is insufficiently narrow. A decrease in aerodynamic damping, and hence of stability of blade vibrations, is undesirable and may have an adverse effect on the characteristics of helicopter controllability.

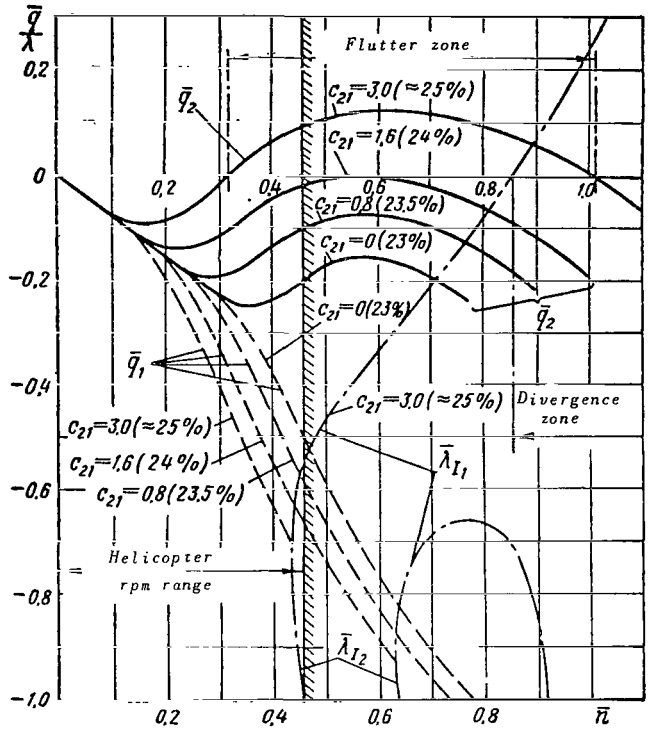

Fig.4.6 Real Part of the Roots of the Characteristic Equation as a Function of Angular Velocity, for Different Values of the Coefficient c_{21}.

The peculiarities of the behavior of the first pair of roots $\bar{\lambda}_I$ will be examined below in Subsection 8.

7. Determination of the Critical Flutter Rpm

To determine the critical flutter rpm, it is possible to derive an analytical expression if, in the characteristic equation, we set

$$\left.\begin{aligned}\bar{\lambda}=i\bar{p}_2=i\bar{p}_{flu};\quad(\bar{q}_2=0)\\ \bar{\omega}=\bar{\omega}_{flu}.\end{aligned}\right\} \tag{2.26}$$

Then, the characteristic equation (2.22) reduces to a biquadratic equation: /366

$$\bar{\omega}_{flu}^4-2L\bar{\omega}_{flu}^2+M=0, \tag{2.27}$$

where

$$\left.2L=\frac{C_1(2C_2-A_1B_2)+A_1(A_1D_2-B_1C_2)}{C_1^2+A_1(A_1D_1-B_1C_1)},\right| \tag{2.28}$$

$$M=\frac{C_2(C_2-A_1B_2)}{C_1^2+A_1(A_1D_1-B_1C_1)}\Bigg\}$$

from which we can determine the critical flutter rpm

$$\bar{\omega}_{flu}=\sqrt{L\mp\sqrt{L^2-M}}. \tag{2.29}$$

The vibration frequency in flutter is determined from the expression

$$\bar{p}_{flu}=\sqrt{\frac{C_1\bar{\omega}_{flu}^2+C_2}{A_1}}. \tag{2.30}$$

8. Blade Divergence

A study of the graphs in Fig.4.6 indicates the behavior of the first pair of roots $\bar{\lambda}_I$.

Beginning with a certain rotor rpm, the imaginary part of this pair vanishes and two real roots appear. The presence of real roots indicates aperiodic motion of the blade.

With a further increase in rpm, one of these roots $\bar{\lambda}_{I_1}$ passes into the region of positive values, which characterizes the appearance of aperiodic instability at this rpm, known as blade divergence.

The value of the rotor rpm at which $\bar{\lambda}_{I_1}=0$ is known as the "critical rpm of divergence" and can be determined by the formula

$$\bar{\omega}_{div}=\sqrt{-\frac{D_2}{D_1}}=\sqrt{\frac{\varkappa b_{12}-1}{b_{22}-b_{12}c_{21}}}. \tag{2.31}$$

Usually, the critical divergence rpm is higher than the critical flutter rpm and the maximum rotor rpm. However, in a number of special cases, blade divergence is a decisive factor. For example, the possibility of the occurrence of divergence does not permit using negative values for the flapping compensator. At $\varkappa = 0$, the possibility of occurrence of divergence is already quite real, and at small negative values of $\varkappa$ the blade becomes aperiodically unstable. This circumstance must be taken into account when designing the rotor hub, especially when deflection of the blade relative to the drag hinge kinematically leads to a decrease in the values of $\varkappa$ to below zero.

9. Parameters Characterizing Blade Balance (Effective Blade Balance)

To evaluate a blade from the point of view of possible flutter, it is convenient to introduce several concepts characterizing the position of the c.g. of blade elements over the blade length. The quantity

$$\bar{\sigma}=\frac{\sigma}{b} \tag{2.32}$$

is called blade balance in a given section.

If balancing of the sections is constant over the blade length, then the /367 value of the coefficient c_{21} entering the equations will be directly related with the magnitude of this balance. The flutter characteristics of a blade in this case can be characterized by the value of the balance of its sections.

In practice, however, balancing of blade sections lengthwise is always different. Therefore, it is convenient to evaluate its flutter characteristics by means of the so-called effective balancing.

The effective balancing of the blade in question is defined as the balancing of some equivalent blade with an identical rotation of the centers of gravity over the length and having the same value of the coefficient c_{21}. It is convenient to assume the planform and mass distribution over the length of the equivalent blade as being identical to those of the blade in question. In this case, the effective balancing of the examined blade can be determined by the expression

$$\bar{\sigma}_{eff}=\frac{\int_0^R m\sigma r\,dr}{\int_0^R mbr\,dr}=\frac{-c_{21}I_{a.h}}{\int_0^R mbr\,dr}. \tag{2.33}$$

For blades having the axis of the feathering hinge at a distance constant in percent of the chord from the leading edge $\bar{x}_0 = \frac{x_0}{b} = \text{const}$, it is convenient to characterize the effective balancing of the blade by the value of balancing of an equivalent blade relative to its leading edge

$$\bar{x}_{eff}=\bar{x}_0+\bar{\sigma}_{eff}. \tag{2.34}$$

Since the position of the axis of the feathering hinge has only a slight effect on the values of the critical flutter rpm, it is convenient to reckon effective balancing from the leading edge also in cases in which the condition $\frac{x_0}{b} = \text{const}$ is not satisfied. Then, the effective balancing can be determined by the expression

$$\bar{x}_{eff}=\frac{\int_0^R m\sigma r\,dr}{\int_0^R mbr\,dr}. \tag{2.35}$$

The effective balancing of manufactured blades can be determined only by

cutting the blade and experimentally determining the balancing of its individual segments.

10. Dependence of Critical Flutter Rpm on Blade Balancing and Values of the Flapping Compensator Coefficient

To illustrate the effect of various parameters on the critical flutter rpm, Figs.4.7, 4.8, and 4.9 give the results of calculations performed by eq.(2.29). The curves refer to different values of the flapping compensator coefficient $\varkappa$ and to three values of the position of the feathering hinge axis $\bar{x}_0$ at a constant position of the profile focus.

The graph shows that a shift of the c.g. toward the leading edge, just as a decrease in the flapping compensator, will improve the flutter characteristics of the blade, whereas a shift of the c.g. toward the trailing edge and an increase in the flapping compensator will lead to a decrease in the critical flutter rpm. These results coincide qualitatively with experimental data.

/368

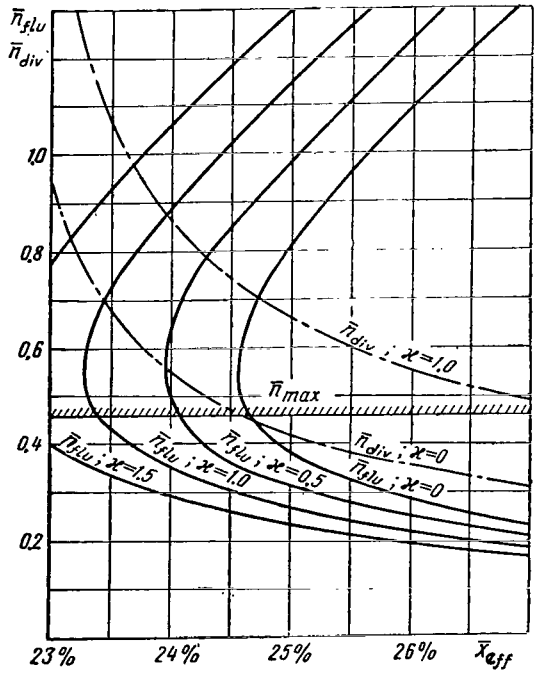

Fig.4.7 Critical Flutter and Divergence Rpm as a Function of Effective Blade Balancing, for $\bar{x}_0 = 0.18$.

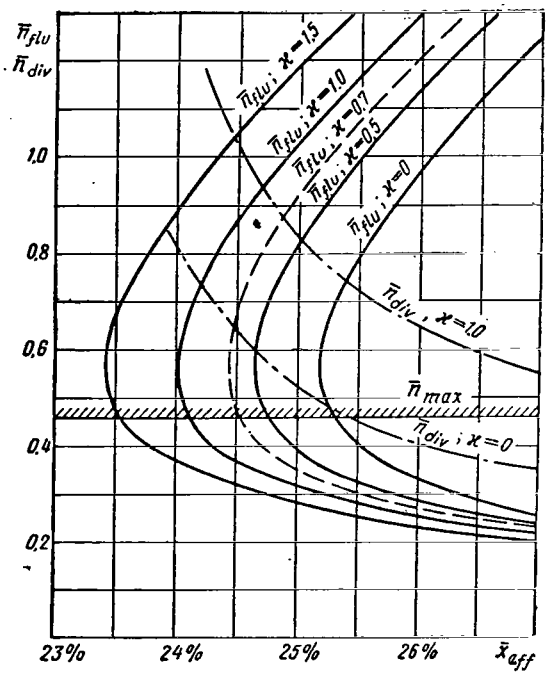

Fig.4.8 Critical Flutter and Divergence Rpm as a Function of Effective Blade Balancing, for $\bar{x}_0 = 0.23$.

A comparison of the results of calculations performed for three different /369 positions of the feathering hinge axis shows that the effect of this parameter on the critical flutter rpm is incomparably weaker than the effect of blade balancing. Consequently, the critical flutter rpm depends mainly on the mutual

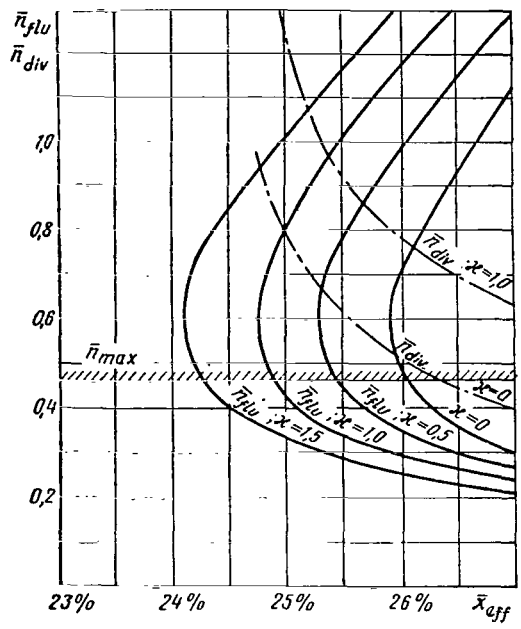

Fig.4.9 Critical Flutter and Divergence Rpm as a Function of Effective Blade Balancing, for $\bar{x}_0 = 0.28$.

position of the centers of gravity of the blade elements and of the profile focus. Therefore, a shift of the a.c. of the profile relative to the chord is just as effective as a shift of the blade balance.

11. Blade Arrangement

The presented dependences of the critical rpm on the balancing permit necessary conclusions with respect to blade arrangement. It follows from the above calculations that the best way to improve the flutter characteristics of a blade is to shift its centers of gravity as much as possible toward the leading edge and to use aerodynamic profiles which, in operating flight regimes, have their aerodynamic centers as far rearward as possible. This measure has a favorable effect even when the blade spar is shifted toward the leading edge to create forward balance, together with the feathering hinge axis which often is associated with the axis of the spar. The arrangement of the blade shown in Fig.4.10 is an example of such a solution.

However, it must be borne in mind that the statement as to the relatively /370 weak influence of the position of the feathering hinge axis on the flutter characteristics in comparison with blade balancing holds true only when the variation in these parameters is of the same order of magnitude. In practice, a shift in the position of the feathering hinge can be performed in appreciably wider limits than a shift in blade balancing. Therefore, this should be regarded as still another means of influencing the blade flutter characteristics.

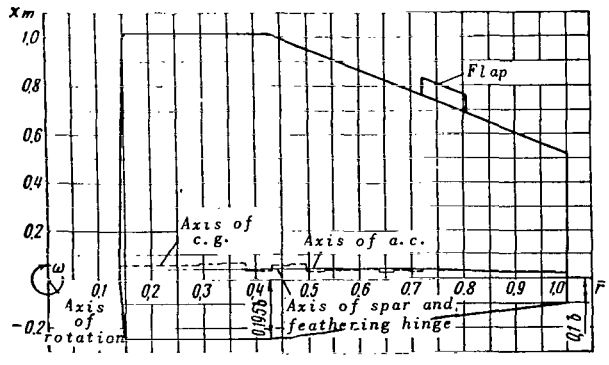

Fig.4.10 Blade Arrangement with Feathering Hinge Axis and Spar Shifted toward the Leading Edge.

The blade whose arrangement is shown in Fig.4.11 can serve as an example for the case in which a change of the position of the feathering hinge is used as a means of improving the flutter characteristics.

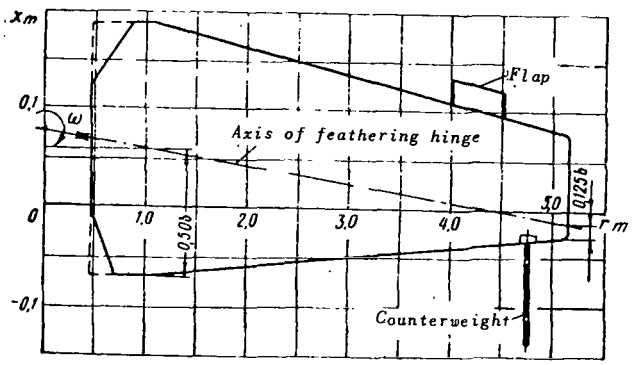

Fig.4.11 Arrangement of Blade with Turned Feathering Hinge Axis.

12. Effect of Control Rigidity

A highly important parameter greatly influencing the flutter speed is the magnitude of the frequency of natural blade vibration in torsion or twist p_{tw}. In the idealized blade scheme examined here, the magnitude of this frequency is completely determined by the hinge rigidity of the system controlling the angle of rotor setting c_{con}. In practice, however, the magnitude of this frequency is influenced also by torsional deformations of the blade itself. Therefore, to take into account the torsional rigidity of the blade it is proposed to use, in calculations by the approximate method proposed here, the value p_{tw} calculated with regard to deformation of both the controls and the blade.

We see from the differential equations of blade vibrations [eq.(2.19)] that the critical flutter rpm (flutter speed) and frequency of vibrations in flutter are directly proportional to the quantity p_{tw}. Therefore, in all calculations whose results are presented in the above graphs, the flutter speed is referred to p_{tw} and is characterized by the relative quantities

$$\bar{n}_{flu}=\frac{n_{flu}}{p_{tw}}. \qquad (2.36)$$

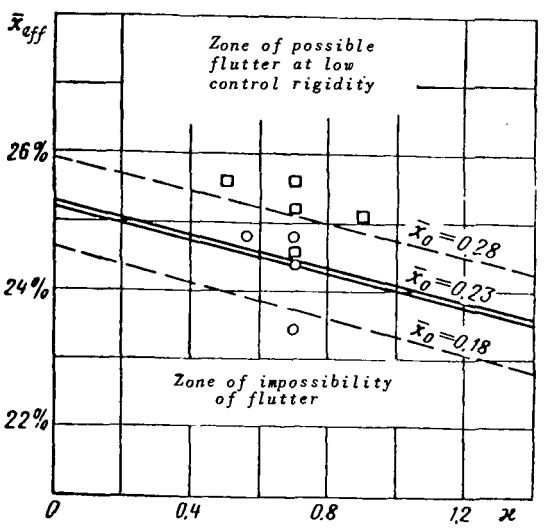

Fig.4.12 Boundaries between Zones in which Flutter is Impossible and the Zone in which it Arises at Small Control Rigidity.
o - Rotor blades for which no flutter was observed
□ - Rotor blades for which there was flutter.

13. Conditions for Absence of Flutter

The character of the dependence of flutter speed on various parameters shows that the creation of the necessary flutter characteristics does not require a simultaneous change of all parameters. Production of the necessary characteristics is possible upon satisfying even one of the two following conditions:

The first condition is the creation of a sufficiently high torsional rigidity of the blade and its attachment to the control system, so that /371

$$p_t > k_1 n_{max}. \qquad (2.37)$$

Here, n_{max} is the maximum possible rotor rpm. It is sufficient that $k_1 = 4 - 5$.

When the condition (2.37) is satisfied, there is no need to secure any specific transverse blade balancing. It can be arbitrary, and there is no need for introduction of special counterweights into the design.

The second condition is the creation of a sufficiently forward blade balancing so that

$$\bar{x}_{aff} < \bar{x}_{lim}. \qquad (2.38)$$

Here, $\bar{x}_{lim}$ is some limiting blade balancing at which flutter is impossible no matter how small, say, the torsional rigidity of the blade attachment to the control.

Figure 4.12 gives the calculated value of the limit balancing $\bar{x}_{lim}$ as a function of the value of the flapping compensator and position of the feathering hinge axis $\bar{x}_0$. This balancing divides the entire area of parameters into two zones, in one of which flutter cannot occur even at very low control rigidity.

The available statistics on full-scale flutter tests of rotors with blades whose effective balancing after the test was determined by cutting, satisfactorily agree with the described limit (see Fig.4.12).

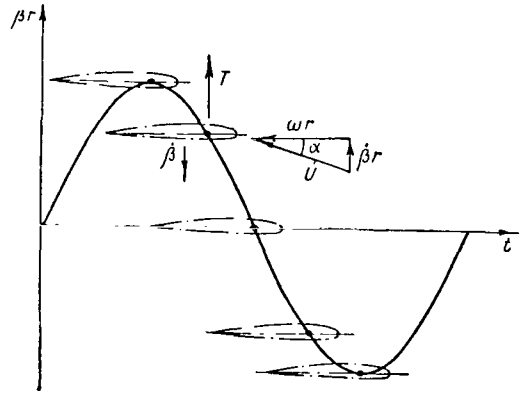

Fig.4.13 Damping Forces Acting on a Vibrating Profile without Torsional Vibrations of the Blade.

Experience has shown that, in practice, only one of the indicated conditions is more readily met.

14. Mechanism of Generation of Forces Exciting Flutter

The calculation methods that reduce to a determination of flutter parameters are left without an explanation of the mechanism of action of aerodynamic forces leading to the generation of divergent vibrations. A detailed study of the nature of the aerodynamic forces acting in flutter yields no new data for flutter investigations. However, in certain cases it does promote better understanding of this phenomenon.

Let us examine the blade model which was described in Subsection 1 of this Section. For simplification of the problem, we will limit ourselves to the

particular case where the aerodynamic center coincides with the axis of the feathering hinge and where $\sigma_f = 0$. We can also disregard the dependence of the force T on $\dot{\varphi}$, which does not have any particular meaning. Then, the aerodynamic forces acting on the profile can be represented in the form /372

$$T = \frac{1}{2} c_y^{\alpha} \varrho b U^2 \alpha; \tag{2.39}$$

$$\mathfrak{M}_{aer} = -\frac{\pi}{16} \varrho b^3 U \dot{\varphi}, \tag{2.40}$$

where α is the angle of attack of the blade element.

The moment of the aerodynamic forces T acting relative to the flapping hinge can be written as

$$M_{h.h} = k\alpha, \tag{2.41}$$

where

$$k = \frac{1}{2} c_y^{\alpha} \varrho \omega^2 \int_0^R b r^3 dr. \tag{2.42}$$

We will assume that the blade executes vibrations relative to the flapping hinge according to the law

$$\beta = \beta_0 \sin pt. \tag{2.43}$$

In this notation, the time reference point is taken from the instant at which $\beta = 0$.

First, we will examine the case in which the blade does not execute torsional vibrations. The angle of setting of its elements will be considered as equal to zero and constant in time. In this case, the angle of attack of the blade elements will vary according to the law (Fig.4.13)

$$\alpha = \bar{\alpha} \cos pt, \tag{2.44}$$

where

$$\bar{\alpha} = -\beta_0 \frac{p}{\omega}. \tag{2.45}$$

The moment of the aerodynamic forces relative to the flapping hinge will vary by the same law

$$M_{h.h} = \bar{M} \cos pt. \tag{2.46}$$

In accordance with eq.(2.41), the sign of M will coincide with the sign of $\bar{\alpha}$.

If $\bar{\alpha} < 0$, as occurs in the case in question, then the moment relative to the flapping hinge always acts opposite to the angular velocity of blade vibrations $\dot{\beta}$ (see Fig.4.13) and does negative work in blade displacements.

The magnitude of this work during the vibration period can be calculated by the formula

$$A=\int_0^T M_{h.h}\dot{\beta}\,dt=\int_0^{\frac{2\pi}{p}}\bar{M}\beta_0 p\cos^2 pt\,dt=\pi\beta_0\bar{M}, \qquad (2.47)$$

where $T=\frac{2\pi}{p}$ is the period of blade vibration.

The sign of the work A coincides with the sign of $\bar{M}$ which, in turn, coincides with the sign of $\bar{\alpha}$. In the examined case, $A<0$. /373

This means that the air stream flowing past the blade absorbs the work expended to maintain blade vibrations. Thus, in the presence of aerodynamic forces the blade will vibrate with a constant amplitude β_0 only if energy equal to the magnitude of work calculated by eq.(2.47) is furnished to it from without. Otherwise the kinetic energy of the blade and, together with it, the amplitude of oscillations β_0, will diminish and the oscillations will decay.

A different picture may be produced in the presence of torsional blade vibrations. Torsional vibrations of the blade arise as a consequence of deformations of the control system and kinematic coupling across the flapping compensator. Deformations of the control system arise from aerodynamic and inertia forces acting on the blade during its flapping vibrations.

Centrifugal and inertia forces arising during flapping vibrations of the blade create a moment relative to the feathering hinge due to the presence of an arm between the centers of gravity of the blade element and this axis

$$m_{inert}=-(p^2-\omega^2)\beta_0\int_0^R mar\,dr\sin pt. \qquad (2.48)$$

The aerodynamic forces create a moment on the arm between the profile focus and the feathering hinge axis σ_f

$$m_{aer}=-\frac{1}{2}c_y^{\alpha}\varrho\omega p\beta_0\int_0^R br^2\sigma_f\,dr\cos pt. \qquad (2.49)$$

At $\sigma_f=0$, this moment is equal to zero. Therefore, as a consequence of flapping vibrations only the moment m_{inert} will act on the blade. Under the effect of this moment, the blade pitch control is deformed and the blade begins to execute torsional vibrations. However, the phase of the torsional vibrations will not coincide with the phase of the flapping vibrations. Phase shift of the torsional vibrations is caused by damping forces acting in the control system directed opposite to the vibrations. These forces are caused by forces of aerodynamic damping determined by eq.(2.40) and by the moment of friction acting in the feathering hinge of the blade. The direction of phase shift of the torsional vibrations depends on the sign of the external moment m_{inert}.

The law according to which the blade executes torsional vibrations

(Fig.4.14) can be written as

$$\varphi=\bar{\varphi}\cos pt+\bar{\bar{\varphi}}\sin pt. \tag{2.50}$$

Here, it is assumed that the initial setting of the blade elements is equal to zero.

The angle of attack in this case will vary according to the law

$$\alpha=\bar{\alpha}\cos pt+\bar{\bar{\alpha}}\sin pt, \tag{2.51}$$

where

$$\bar{\alpha}=\bar{\varphi}-\beta_0\frac{p}{\omega};$$

$$\bar{\bar{\alpha}}=\bar{\bar{\varphi}}.$$

The appearance of a sinusoidal component in the law of change of the angle of attack $\bar{\bar{\alpha}}$ and, along with this, the sinusoidal component of the moment relative to the flapping hinge, does not influence the energy transfer during blade vibrations. Actually, a check on the work done by the sinusoidal component of the moment $\bar{\bar{M}}$ in blade displacements relative to the horizontal hinge will show that it is equal to zero: /374

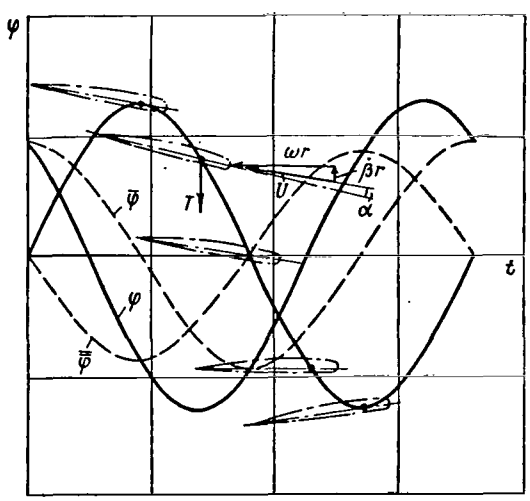

Fig.4.14 Damping Forces Acting on a Vibrating Profile in the Presence of Torsional Vibrations of the Blade.

$$A=\int_0^T \bar{\bar{M}}\sin pt\, p\beta_0\cos pt\, dt=0. \tag{2.52}$$

The magnitude of the cosinusoidal component of the angle of attack $\bar{\alpha}$, as follows from eq.(2.51), largely depends on the sign and magnitude of $\bar{\varphi}$.

When $\bar{\varphi}<0$, the work absorbed by the air stream flowing past the blade increases which causes a rise in the rate of damping of the free vibrations of the blade. Thus, when $\bar{\varphi}<0$, the stability of flapping vibrations of the blade increases. When $\bar{\varphi}>0$, the work absorbed by the stream past the blade decreases and when

$$\bar{\varphi}=\beta_0\frac{p}{\omega} \tag{2.53}$$

it becomes equal to zero, whereas when

$$\bar{\varphi}>\beta_0\frac{p}{\omega} \tag{2.54}$$

the cosinusoidal component of the horizontal hinge moment is directed along the

angular velocity of the flapping vibrations $\dot{\beta}$. This leads to "resonant build-up" of the blade. The kinetic energy of blade vibrations begins to increase, which leads to a rise in the vibration amplitude. Such a type of oscillation at amplitude build-up is known as flutter.

Thus, the occurrence of flutter is associated with the magnitude and sign of the component of torsional vibrations $\bar{\varphi}$.

Let us examine how the quantity $\bar{\varphi}$ changes under the effect of an external moment varying by the sine law in conformity with eq.(2.48). Figure 4.15 shows the dependence of $\bar{\varphi}$ and $\bar{\bar{\varphi}}$ on the vibration frequency p of the external moment m_{inert}. As usual during vibrations close to resonance, the component $\bar{\varphi}$ which is in 90° phase with the external forces first increases, whereas the vibration component coinciding in phase with the external forces changes its sign in resonance, passing through zero.

Thus, the value of $\bar{\varphi}$ increases especially upon approaching resonance with the frequency of natural blade vibration in torsion. Therefore, flutter always occurs with a frequency close to but slightly below the frequency of torsion. /375 Usually the frequency of flutter amounts to about 0.8 p_{tw}.

It follows from the foregoing that flutter occurs as a consequence of the following causes: The torsional moment due to inertia forces acting during flapping vibrations of the blade leads to the appearance of torsional blade vibrations. In so doing, the torsional vibrations with a 90° phase shift relative to the flapping vibrations increase especially strongly at frequencies close to the frequency of the natural vibrations of the blade in torsion. This component of the torsional vibrations leads to excitation of flapping vibrations of the blade. As soon as this excitation [first term in eq.(2.55)] becomes stronger than the forces damping the flapping vibrations [second term in eq.(2.55)], flutter will occur.

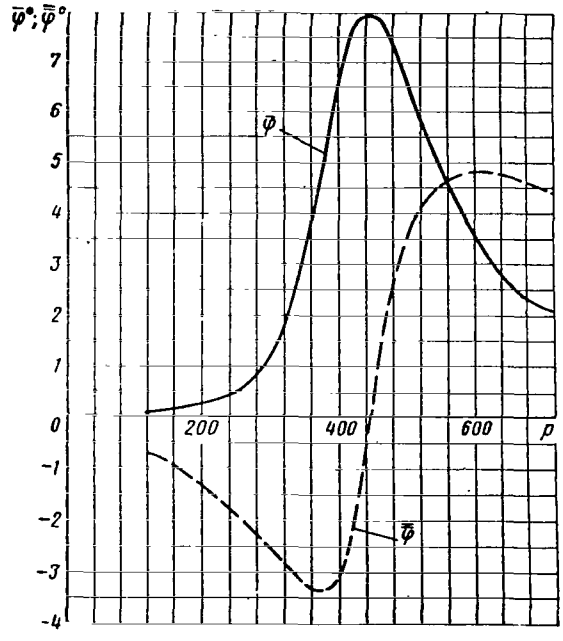

Fig.4.15 Variation in the Torsional Vibration Components $\bar{\varphi}$ and $\bar{\bar{\varphi}}$ during Blade Vibration Frequency.

From the expression for the cosinusoidal component of the angle of attack

$$\bar{\alpha} = \bar{\varphi} - \beta_0 \frac{p}{\omega} \qquad (2.55)$$

it is also possible to trace the effect of rotor rpm on flutter. Actually, the second term in this formula rapidly decreases with increasing rotor rpm, whereas $\bar{\varphi}$ does not greatly depend on

the rpm since the external torsional moment m_{inert} is determined mainly by the vibration frequency [see eq.(2.48)] because of the fact that, during flutter, p^2 usually is by a factor of 5 - 8 greater than ω^2. The variation in $\bar{\varphi}$ with respect to rotor rpm is related mainly with an increase in aerodynamic damping at increasing ω.

Thus, on tracing the mode of variation of the quantities entering eq.(2.55) with the rotor rpm, it will be found that, at some value of ω, the cosinusoidal component of the angle of attack $\bar{\alpha}$ changes in sign and becomes positive. This /376 leads to the appearance of flutter, beginning with some specified rotor rpm. A rearward shift of blade balancing leads to an increase in the absolute value of m_{inert} [eq.(2.49)] and hence to an increase on $\bar{\varphi}$. In this case, as follows from eq.(2.55), flutter arises at smaller ω.

In the same manner, it is possible to trace the effect of various other parameters on the flutter speed. However, there is no need for this since this has already been done above with sufficient detail.

Section 3. Consideration of Friction Forces during Flutter

1. Character of the Effect of Friction Forces during Flutter

The occurrence of flutter leads to the appearance of oscillatory motions in the hinges of the rotor hub and in the hinge control. Therefore, the friction forces acting in these hinges have a substantial effect on the critical rpm and on the nature of generation of flutter. Of primary importance in this case is friction in the feathering hinge of the blade loaded by a centrifugal force, in comparison with which the friction in all other hinges can be neglected.

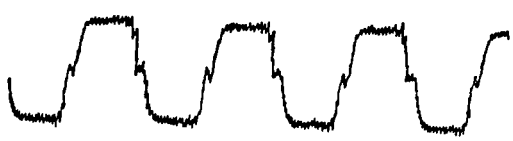

Fig.4.16 Recording of the Moment of Friction in the Feathering Hinge during Torsional Blade Vibrations.

Experiments show that forces acting in the feathering hinge are similar in character to forces of dry Coulomb friction [eq.(4.16)]. The introduction of these forces into the calculation makes the problem of flutter essentially nonlinear. Therefore, in simplified calculations it is natural to use any of the possible methods of linearization of friction forces. A more exact solution to this problem without such linearization will be given in Section 7 of this Chapter.

As is known, linearization of friction forces leads to the dependence of the damping coefficient on the amplitude of oscillations. Here the nature of flutter generation, described on the basis of the calculation changes at increasing amplitude, approaching that observed in experiments on helicopters. These results permit explaining numerous peculiarities in the development of flutter in full-scale experiments. The possibility of interpreting these characteristics appreciably facilitates the conduction of tests.

2. Linearization of Friction Forces

Let us use the energy method of linearization of friction forces. For this, we will replace the moment of friction acting in the feathering hinge of the blade by some equivalent moment whose magnitude is proportional to the rate of angular blade displacement

$$M_{eq} = -\gamma_{fr}\dot{\varphi}. \tag{3.1}$$

The value of the coefficient γ_{fr} is determined from the condition of equality of the work done during the vibration period by the moment of friction,

$$A_{fr} = 4M_{fr}\varphi_{flu} \tag{3.2}$$

and by an equivalent moment whose magnitude is proportional to the vibration rate /377

$$A_{eq} = \pi\gamma_{fr}\, p_{flu}\,\varphi^2_{flu}, \tag{3.3}$$

where

M_{fr} = constant (in magnitude) moment of friction acting in the feathering hinge, always opposite to the rate of relative displacement;
φ_{flu} = amplitude of torsional blade vibrations in the feathering hinge during flutter;
p_{flu} = frequency of blade vibrations during flutter.

The moment of friction acting in the feathering hinge can be considered proportional to ω^2, since its magnitude is determined mainly by the centrifugal force

$$M_{fr} = a_{fr}\omega^2. \tag{3.4}$$

In a number of cases, however, this dependence is disturbed as a consequence of the following circumstances:

1) The bearing is installed with appreciable prestressing. In this case, the load acting on the bearing is determined not only by centrifugal force but also by the initial tension.

2) The design of the packing glands is such that they have an appreciable moment of friction regardless of the magnitude of the effective centrifugal force.

3) The use of too heavy a lubricant in the bearing creates an appreciable additional moment due to the generation of viscous friction. The appearance of relatively large viscous friction forces is often observed at low negative temperatures of the ambient air.

All these facts have an influence on the flutter speed but introduce no fundamental features into the pattern of the phenomenon. Therefore, in the following account we will take eq.(3.4) as the basis.

The coefficient a_{fr} entering eq.(3.4) is determined from the expression

$$a_{fr} = f r_{be} S_{a.r}, \tag{3.5}$$

where

$S_{a.r}$ = static moment of the blade relative to the axis of rotation;
r_{be} = radius of the thrust bearing;
f = coefficient of friction in the bearing.

The values of the friction coefficients f are usually quite stable and amount to about 0.003 for ball and 0.006 for roller bearings.

After equating eqs.(3.2) and (3.3), we obtain the expression for determining the coefficient γ_{fr}:

$$\gamma_{fr} = \frac{4}{\pi} \frac{a_{fr}\omega^2}{p_{flu}\varphi_{flu}}. \tag{3.6}$$

With this method of linearization, consideration of the friction forces leads to only one change in the initial equations (2.19), namely of the coefficient d_{22} standing for the first derivative of the angle of rotation of the blade in the hinge, which is supplemented by some addition d_{fr}.

In an investigation of flapping flutter with a blade rigid in torsion, this supplement should be determined by the formula

$$d_{fr} = \frac{4a_{fr}\omega}{\pi I_{a.h} p_{flu}} \frac{1}{\varphi_{flu}}. \tag{3.7}$$

3. Determination of Flutter Speed with Consideration of Friction /378

Equation (3.7) derived above, which determines the magnitude of the addition term due to friction forces to one of the coefficients of the equations of blade vibration d_{22}, is distinguished by a highly important characteristic. This addition depends on the amplitude of blade vibration in the feathering hinge during flutter φ_{flu}. Consequently, the critical rpm at which the amplitude of oscillations theoretically remains constant in time depend on the amplitude of flutter oscillations.

Figure 4.17 shows such a dependence for three values of blade balancing obtained in a calculation of flapping flutter. Along the abscissa in this diagram is laid out the amplitude of angular blade vibrations in the feathering hinge φ_{flu}, and along the ordinate the critical flutter rpm referred to the frequency of natural vibrations of the blade in torsion $\bar{n}_{flu}$.

These curves determine the amplitude of the oscillatory regime, which forms the boundary between oscillations with amplitude build-up and damping oscillations.

For all practical purposes, this means that for flutter to occur some initial impetus is needed leading to deflection of the blade from a position of equilibrium by an angle determined by these curves, usually called the excita-

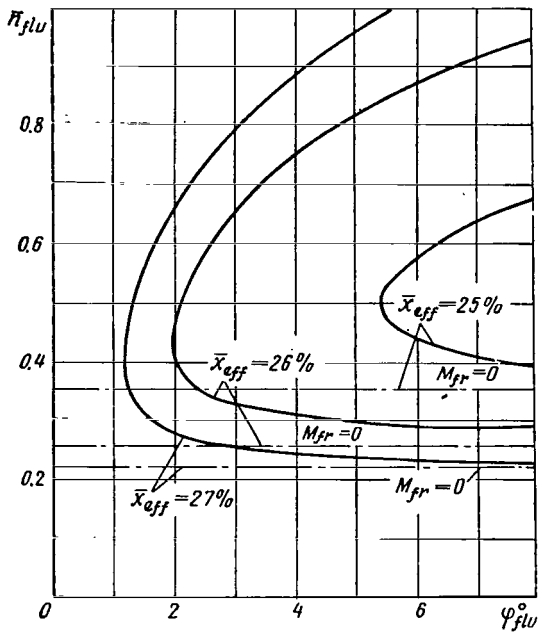

Fig.4.17 Critical Flutter Rpm as a Function of the Vibration Amplitude φ_{flu}.

tion threshold.

If there is no such impetus present, flutter will not occur at all no matter what the rotor rpm might be.

For a comparison, Fig.4.17 shows the critical rpm for the case in which the moment of friction in the feathering hinge is $M_{fr} = 0$.

4. Effect of Forced Motion in the Feathering Hinge

Quite a different picture of the occurrence of flutter is observed when forced motion is present in the feathering hinge of the hub caused by tilting of the swashplate of the automatic pitch control or by forced flapping vibrations of the blades arising in flight during oblique flow past the rotor. In this case, the vibrations in the feathering hinge following the occurrence of flutter are generated by a complex law consisting of two oscillatory motions with different frequencies.

Figure 4.18 shows, as an example, the pattern of this motion observed during flutter under conditions of ground tests when forced motion is present in the feathering hinge caused by tilting of the swashplate of the automatic pitch control (curve $\dot{\varphi}_{for}$) and the motion caused by flutter ($\dot{\varphi}_{flu}$). /379

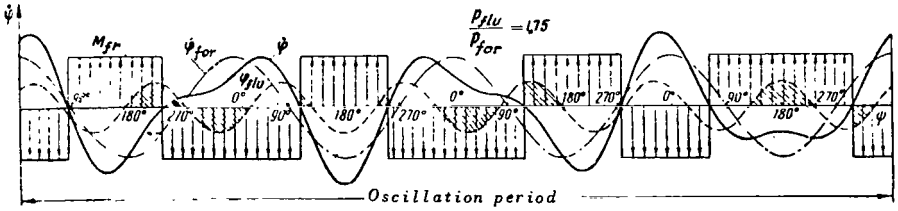

Fig.4.18 Character of Flutter in the Presence of Forced Motion in the Feathering Hinge.

For convenience of further discussion, we plotted the rate of vibration in the feathering hinge rather than the displacements.

The work of the friction forces acting in the feathering hinge can be

determined by the expression

$$A_{fr} = \int_0^t M_{fr}\dot{\varphi}\,dt, \tag{3.8}$$

where the moment of friction M_{fr} is always directed opposite to the rate of angular displacement of the blade $\dot{\varphi}$.

If the rate of angular motion $\dot{\varphi}$ is the sum of two oscillatory motions

$$\dot{\varphi} = \dot{\varphi}_{for} + \dot{\varphi}_{flu}, \tag{3.9}$$

then the work of the friction forces can always be represented as consisting of two works, in each of these motions

$$A_{fr} = A_{for} + A_{flu}, \tag{3.10}$$

where

$$A_{for} = \int_0^t M_{fr}\dot{\varphi}_{for}\,dt;$$

$$A_{flu} = \int_0^t M_{fr}\dot{\varphi}_{flu}\,dt.$$

Here, the moment of friction - as usual - is directed opposite to the rate of total motion $\dot{\varphi}$.

The simultaneous presence in the feathering hinge of two oscillatory motions of different frequency always leads to the appearance of time segments during which the friction force coincides in direction with the rate of one of these motions, in this case doing positive work. In Fig.4.18 the area segments corresponding to the positive work of friction forces in displacement of one of the composite motions of a frequency p_{flu} are hatched. As a result, the overall magnitude of work of the friction forces during the vibration period in displacement of each of the composite motions decreases in comparison with the case where there is no concomitant motion. As applied to our case, this means that the work expended for damping flutter vibrations markedly drops because an appreciable portion of the friction forces is expended by forced motion. This drop can be characterized by a special coefficient which represents the ratio /380

$$\overline{A}_{flu} = \frac{A_{flu}}{A_{fr}}, \tag{3.11}$$

where

A_{flu} = work of friction forces during the vibration period in displacements of the component of motion caused by flutter, which is of interest here;

A_{fr} = work of friction forces during the same period when there is no concomitant forced motion.

Figure 4.19 shows the dependence of the coefficient $\overline{A}_{flu}$ on the amplitude

ratio of the velocity components of oscillatory motion $\left(\frac{V_{flu}}{V_{for}}\right)$.

At the values of $\frac{p_{flu}}{p_{for}} = 1.5 - 2.5$ of interest to us, the coefficient $\bar{A}_{flu}$ depends little on the ratio of these frequencies.

If the value of the coefficient γ_{fr} is determined in this case, as was done above, from the condition of equality of work [see eq.(3.6)], then eq.(3.7) takes the following form:

$$d_{fr} = \frac{4a_{fr}\bar{A}_{flu}}{\pi I_{a.h.}} \frac{\omega}{p_{flw}} \frac{1}{\varphi_{flw}}. \qquad (3.12)$$

It follows from this expression that the critical flutter rpm depending on the coefficient d_{fr} is related with the amplitude of forced motion in the axial hinge φ_{for}, since d_{fr} depends on the quantity $\bar{A}_{flu}$. With consideration of the nonlinear dependence $\bar{A}_{flu} = f\left(\frac{V_{flu}}{V_{for}}\right)$ shown in Fig.4.19, this relation becomes rather complex. However, consideration of this dependence radically changes the character of the conditions necessary for the occurrence of flutter.

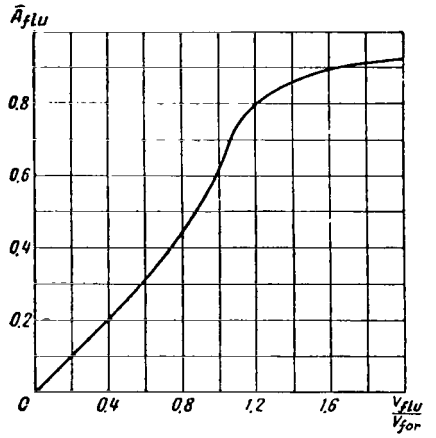

Fig.4.19 Dependence of the Coefficient $\bar{A}_{flu}$ on the Amplitude Ratio of the Velocity Components of Oscillatory Motion.

Figure 4.20 gives the values of critical flutter rpm at different magnitudes of the oscillatory blade motion in the feathering hinge φ_{for}, calculated with consideration of this nonlinear dependence as applied to flapping flutter. The calculation was made only for one value of blade balancing and different amplitudes of forced motion in the feathering hinge φ_{for}.

The curves plotted in Fig.4.20 permit a number of interesting conclusions.

First of all, it follows from these curves that, in the presence of forced motion in the feathering hinge, flutter occurs at certain revolutions of the rotor and its appearance is not due to the effect of any extraneous influence in the form of some initial impetus. In this case, the rpm of flutter onset is smaller, the greater the amplitude of forced motion in the feathering hinge φ_{for}. This fact is responsible for the dependence of the critical flutter rpm in flight on all parameters of the flight regime that determine the amplitude of φ_{for}, and primarily on the helicopter balancing and the flying speed. In ground tests, this leads to dependence of the critical rpm on the position of the control stick. /381

A second important characteristic of flutter, following from the curves

(see Fig.4.20), is the appearance of two different types of flutter which differ by the character of the increase in vibration amplitude upon any change in rotor rpm.

Upon an increase in rpm to values corresponding to the points a_1, a_2, a_3, flutter will set in with an amplitude smoothly increasing with increasing rotor rpm. If, after the occurrence of such oscillations, which are usually called "soft flutter", the rotor rpm remains unchanged, then their amplitude will remain constant for as long as desired.

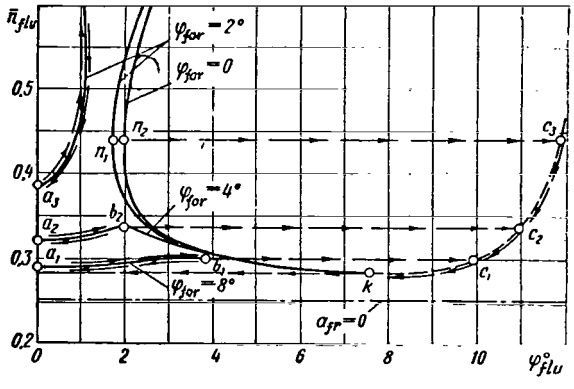

Fig.4.20 Variation in Critical Flutter Rpm with Vibration Amplitude in the Feathering Hinge φ_{flu}, at Different Magnitudes of Forced Motion.

Oscillations of this type have been repeatedly observed in ground and flight studies of flutter in helicopters. A decrease in rotor rpm after the occurrence of "soft flutter" leads to cessation of oscillations at the same rpm at which flutter began.

Upon an increase in rotor rpm to values determined by the points b_1 and b_2, oscillations are generated whose amplitude increases in time without an increase in rotor rpm. Oscillations of this type are called "hard flutter".

Probably, the limiting values of the vibration amplitudes obtainable in this case are determined by the nonlinear nature of the change in aerodynamic forces relative to the angle of attack. This branch of the curve in Fig.4.20 is shown approximately by a dashed line.

When "hard flutter" occurs during ground tests of a helicopter, the increase in blade vibrations can be stopped (to prevent an accident) only by a marked decrease in rotor rpm. The generation of such oscillations in flight may lead to serious consequences.

A decrease in rotor rpm after the onset of "hard flutter" leads to cessation of vibration at an rpm corresponding to the point k, which, as a rule, is smaller than the values corresponding to a_1 and a_2.

Thus, to stop "hard flutter" the rotor rpm should be decreased to values lower than those at which flutter began.

At small amplitudes of forced motion in the axial hinge, the occurrence of "hard flutter" is possible only after some initial impetus, just as in the case when forced motion is absent.

The rpm corresponding to the point n_1 should be considered the most /382

probable rpm for the start of "hard flutter" since, in this case, the magnitude of the necessary impetus is minimal.

In calculating the critical rpm for the onset of flutter, corresponding to a_1, a_2, a_3 in Fig.4.20, additional simplifications can be made in eq.(3.12).

As follows from Fig.4.19, when $\frac{V_{flu}}{V_{for}} \leq 0.5$, the value of the coefficient $\overline{A}_{flu}$ can be determined by the formula:

$$\overline{A}_{flu} = \frac{1}{2} \frac{V_{flu}}{V_{for}}. \tag{3.13}$$

If the frequency of forced motion is $p_{for} = m\omega$ (m being the order of the harmonic of this motion with respect to rotor rpm), then we can write

$$V_{flu} = p_{flu}\varphi_{flu};$$
$$V_{for} = m\omega\varphi_{for}.$$

In this case, eq.(3.12) takes the following form:

$$d_{fr} = \frac{2a_{fr}}{\pi I_{a.h}\, m\varphi_{for}}. \tag{3.14}$$

The value of the equivalent moment of friction is here proportional to the rate of angular displacements and does not depend on the vibration amplitude of flutter φ_{flu}:

$$M_{eq} = -\frac{2M_{fr}}{\pi m\omega\varphi_{for}}\dot{\varphi}. \tag{3.15}$$

In other words, the moment of friction acting in the feathering hinge in the presence of forced motion in this hinge affects small oscillations of the blade in the same manner as a linear vibration damper, whose moment is proportional to the rate of relative displacement. This conclusion pertains not only to the feathering or axial hinge of the blade but is generally valid for all mechanisms with friction.

It also follows from Fig.4.20 that friction in the feathering hinge, even in the presence of forced motion, increases the critical flutter rpm in comparison with the case where $M_{fr} = 0$ and represents a useful factor from this point of view. Therefore, to improve the flutter characteristics of a rotor it is possible to use friction dampers in the feathering hinges. Of course, the use of such dampers is possible only when the helicopter has a sufficiently powerful and reliable booster control.

Section 4. Rotor Flutter with Consideration of Coupling of Blade Vibrations through the Automatic Pitch Control

1. Forms of Rotor Flutter Observed in Helicopter Experiments

As mentioned above, the occurrence of flutter in a helicopter sets up vibrations of all rotor blades. These oscillations begin simultaneously despite the fact that the parameters of individual blades making up the rotor generally differ somewhat. Consequently, the simultaneous occurrence of flutter cannot be explained by the coincidence of the critical rpm of individual blades. Furthermore, it has been noted in almost all experiments on helicopters that the vibrations of all blades are strictly synchronized so that each advancing /383 blade duplicates the motion of the retreating blade with some lag in time. The vibration amplitudes of different blades increase simultaneously so that their magnitude on the different blades is approximately identical. Flutter of one individual blade of the rotor of a given helicopter is practically never observed.

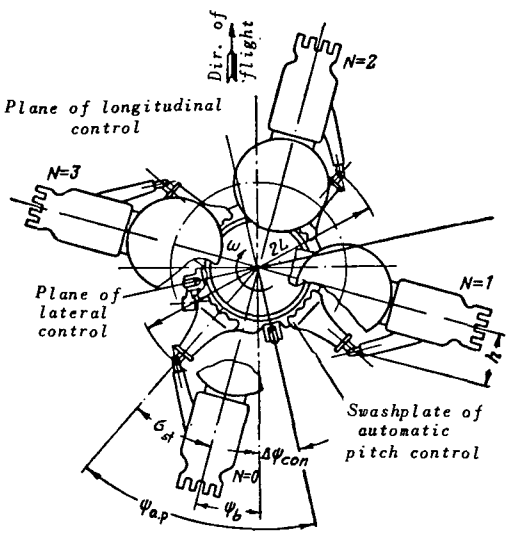

Fig.4.21 Diagram of Rotor Hub.

This type of vibrations in flutter is ascribable primarily to the coupling of individual rotor blades through the automatic pitch control (Fig.4.21).

The vibration mode of the rotor in which each advancing blade duplicates the motion of the retreating blade with some lag in time is usually called cyclic vibration mode. Such modes are very often encountered in studies of helicopter rotor vibrations. Therefore, they should be examined in greater detail.

2. Analytical Expression for Cyclic Modes of Rotor Vibration

For cyclic modes of flutter, distinguished by the fact that each advancing blade duplicates the motion of the retreating one, we can construct an analytical expression determining the law of variation of the blade motion parameters in time.

If we fix the point of reference in time such that for t = 0 we have $\beta_{N=0} = 0$, then this expression can be written in the following manner:

$$\beta_N = \beta_0 e^{qt} \sin(pt - N\Delta\psi_m), \tag{4.1}$$

where

β_N = flapping angle of the n-th blade;

β_0 = angle determining the magnitude of blade deflection at the initial reference time, for t = 0;
q = exponent determining the time rate of change of vibration amplitude;
p = frequency of oscillations in flutter;
$\Delta\psi_m$ = phase shift of vibrations for two successive blades.

Equation (4.1) is used for determining the motion of blades with numbered N = 0, 1, 2, ..., z_b - 1 (z_b being the number of blades of the rotor).

For a blade with N = z_b, the law of change of variables should coincide with the law of motion of the blade having N = 0. Proceeding from this assumption, the phase shift $\Delta\psi_m$ should be a multiple of the azimuth angle between /384
the blades, i.e.,

$$\Delta\psi_m = m\frac{2\pi}{z_b}. \tag{4.2}$$

At critical flutter rpm, for q = 0, the vibrations of all blades take place at constant and identical amplitude but with different vibration phases. The analytical expression for the law of change of variables at critical flutter rpm can be obtained by substituting eq.(4.2) into eq.(4.1) and setting q = 0:

$$\beta_N = \beta_0 \sin\left(pt - Nm\frac{2\pi}{z_b}\right). \tag{4.3}$$

It follows from eq.(4.3) that the vibration phase distribution for blades in cyclic modes may differ depending on the quantity m. The quantity m is called the order of the vibration mode and may vary from m = 0 to m = z_b - 1. At m - z_b, the vibration mode of the rotor, as follows from eq.(4.3), will coincide with the mode having the order m = 0. In like manner, for m > z_b all modes will be repeated. Thus, for any rotor there can be z_b different vibration modes corresponding to different orders m varying from m = 0 to m = z_b - 1.

Equations (4.1) and (4.3), derived above for determining the modes of rotor vibration, were constructed only for the variable β_N. However, all other parameters characterizing blade motion vary in the same manner. Nevertheless, a certain vibration phase usually exists between them and the variable β_N. Therefore, in many cases it will be convenient to represent the law of change of variables in a complex form. With respect to the variable β_N, this can be written as

$$\beta_N = \beta_0 e^{\lambda t - iN\Delta\psi_m}, \tag{4.4}$$

where

$$\lambda = q \mp ip.$$

It should be noted that, in forward flight of a helicopter, the blade executes also forced vibrations of cyclic modes since, in flight, each advancing blade duplicates the motion of the retreating blade. However, unlike vibrations in flutter, the forced blade vibrations in flight are strictly synchronized relative to the rotor rpm, so that each harmonic of vibrations of an order m

will correspond to the vibration mode having the same order:

$$\beta_N = \beta_m \sin m\left(\omega t - N\frac{2\pi}{z_b}\right). \qquad (4.5)$$

Here, m corresponds to the order of the harmonic of forced vibrations.

3. Cyclic Vibration Modes in Specific Cases and Control Loads

The division of vibrations into cyclic modes is convenient in that only certain rotor control loops are loaded in the presence of each such mode. Therefore, the critical flutter rpm is determined by the rigidity of that control loop which is loaded in the presence of the particular vibration mode under consideration. Of practical interest are only those rotor vibration modes /385 that correspond to the smallest control rigidity and hence to the lowest critical flutter rpm.

Let us study the manner of generation of cyclic vibration modes during flutter, in a specific case - for example - for a four-blade rotor.

With a vibration mode of zero order (m = 0), all four blades vibrate with identical phases and load only the collective pitch control. This form of flutter is called in-phase flutter. The control rigidity referred to the axial hinge, and hence the critical in-phase flutter rpm, depend only on the rigidity of the collective pitch control loop.

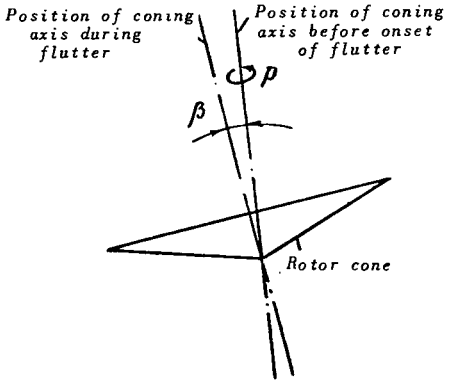

Fig.4.22 Position of Coning Axis in Antiphase Flutter.

The vibration mode of the first order (m = 1), just as that of the third (m = 3), is of greatest interest since on helicopters it corresponds usually to the smallest control rigidity and hence to the lowest values of critical flutter rpm. Vibrations of these modes are characterized by the fact that only the moment loading the lateral and longitudinal control loops is applied to the swashplate of the automatic pitch control.

The opposite blades in modes of the first and third order oscillate in opposite phases. Therefore, this mode of flutter is usually called antiphase flutter.

The coning angle of the rotor in antiphase modes of flutter does not change. Therefore, the motion of the blades in these modes is conveniently characterized by the motion of the coning axis (Fig.4.22). In vibrations of the first-order mode, the cone of the rotor is deflected relative to the original axis through an angle β and rotates about it with an angular velocity $p_1 = p_{f1u} - \omega$ opposite to the rotor rotation.

Both the direction and magnitude of this angular velocity vary in the third-order mode: $p_3 = p_{flu} + \omega$.

The vibration frequency of the variable forces in nonrotating parts of the control system, just as the vibration frequency of the fuselage during flutter, coincides in magnitude with the angular velocity of rotation of the coning axis, which constitutes the basic difference between these modes.

If the dynamic rigidity of the nonrotating parts of the control did not depend on the frequency of forces applied to it, then the values of the critical flutter rpm corresponding to modes of the first and third order would be identical. However, in all experimental investigations of flutter, only vibrations of one of these modes, most often of the third-order (m = 3), are usually encountered. In several cases, in particular when the control system includes inertia dampers, the first-order vibration (m = 1) is observed in flutter. This is explained by the fact that the dynamic rigidity of the nonrotating part of the control, operated by the inertia inherent to its components, depends on the vibration frequency. Consequently, the hinge control rigidities corresponding to modes of the first and third order on a helicopter differ somewhat in magnitude. Accordingly, the critical flutter rpm also differs. These considerations will be supplemented in Section 8.6. /386

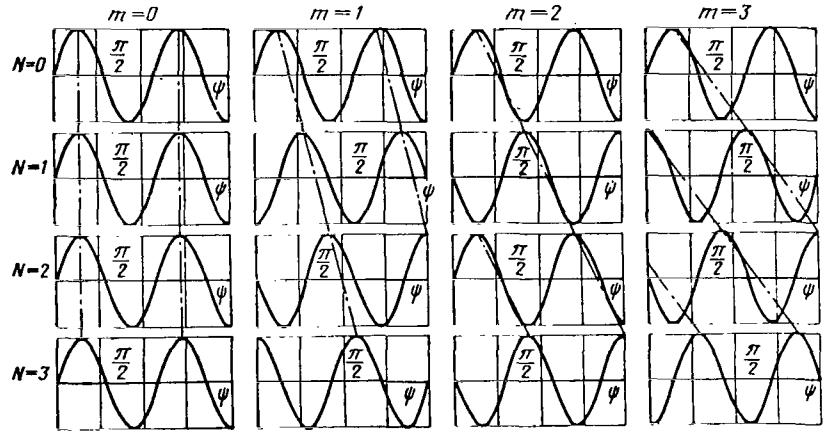

Fig.4.23 Vibration Phase Distribution in Different Modes of Flutter, for a Four-Blade Rotor at $\frac{p}{\omega} = 1.75$.

During second-order vibration modes (m = 2), the opposite blades in each pair have an identical phase, and the phases of these pairs differ by half a period. The forces applied to the control during vibrations of this mode are locked on the swashplate of the automatic pitch control whose rigidity mainly determines the hinge control rigidity for this case. Since this rigidity is usually sufficiently high, the possibility of flutter with this mode, which is usually called the plate mode of flutter, is improbable within the operating rpm of the rotor.

The curves (Fig.4.23) plotted on the basis of eq.(4.3) permit judging the character of the phase distribution by blades in all these modes for a four-blade rotor.

4. Differential Equations of Rotor Flutter with Consideration of Coupling of Blade Vibrations through the Automatic Pitch Control

Each rotor blade, during vibration, generates a moment acting on the blade pitch control system. The magnitude of this moment, taken relative to the feathering hinge axis of the hub, can be written in conformity with eqs.(2.19) as

$$M_{con}^{(N)} = -I_{a.h}\left[\ddot{\varphi}_N + d_{22}\omega\dot{\varphi}_N + b_{22}\omega^2\varphi_N + c_{21}\ddot{\beta}_N + d_{21}\omega\dot{\beta}_N + b_{21}\omega^2\beta_N\right], \tag{4.6}$$

where N = 0, 1, 2, ..., z_b - 1 is the numeral of the blade.

Here we have used the same notations as those given in Section 2 in deriving the differential equations of flapping flutter of an isolated blade with axial flow past the rotor. Now, the number of equations has increased z_b times, i.e., as many times as there are blades in the rotor.

If oscillations of individual rotor blades are in no way related and if each blade is attached to the hub as an isolated entity, then, after substitution of /387

$$M_{con}^{(N)} = c_{con}(\varphi_N + \varkappa\beta_N), \tag{4.7}$$

into eq.(4.6), we obtain equations coinciding with eqs.(2.19).

However, helicopters usually do not have such rotor designs.

Generally, as a consequence of interference, the elastic angle of rotation of each blade in the feathering hinge

$$\gamma_N = \varphi_N + \varkappa\beta_N \tag{4.8}$$

follows the deformations of individual rotor control loops, which in turn are determined by the totality of forces arising from all rotor blades.

For the conventional rotor control system, this relation can be represented in the form

$$\gamma_N = \gamma_{c.p} + \gamma_x \sin\psi_{a.p}^{(N)} + \gamma_z \cos\psi_{a.p}^{(N)} + \gamma_{a.p}^{(N)}, \tag{4.9}$$

where, as before, N = 0, 1, 2, ..., z_b - 1.

Here,

$\gamma_{c.p}$ = angle of rotation of the blade according to deformations of the collective pitch control;

γ_x and γ_z = amplitude values of the angles of blade twist as a consequence of deformations of the lateral and longitudinal controls respectively;

$\gamma_{a.p}^{(N)}$ = angle of rotation of the n-th rotor blade as a consequence of deformation of the swashplate of the automatic pitch control under the effect of forces completely balanced on the plate; it is assumed that, if all external forces are balanced on the swashplate, its deformation obeys the condition

$$\sum_N \gamma_{a.p}^{(N)} = 0; \tag{4.10}$$

where $\psi_{a.p}^{(N)}$ is the azimuth of the N-th blade reckoned from the plane of the longitudinal control with respect to the swashplate spider (see Fig.4.21); this azimuth is related with the blade azimuth by the expression

$$\psi_{a.p}^{(N)} = \psi_b^{(N)} + \sigma_{st} + \Delta\psi_{con} + \xi, \tag{4.11}$$

where

σ_{st} = angle of stagger of the rotor hub spider;

$\Delta\psi_{con}$ = control angle of advance;

ξ = blade angle of lag during rotation about the drag hinge; in Fig.4.21 the blades are shown in a position where $\xi = 0$;

$$\psi_b^{(N)} = \psi_b^{(0)} + N\frac{2\pi}{z_b}.$$

If the rotor has three or less blades, then the quantity $\gamma_{a.p}^{(N)}$ should be set equal to zero, since in this case there is no combination of forces which could be balanced completely on the swashplate.

For a four-blade rotor, all values of $\gamma_{a.p}^{(N)}$ are equal in modulus, i.e., when N = 0, 1, 2, 3

$$|\gamma_{a.p}^{(N)}| = \text{const.} \tag{4.12}$$

This equality is not observed for a greater number of blades. /388

If we introduce the concepts of rigidity of various control loops referred to the axial hinge of the blade, then the hinge moment acting on the blade due to the control can be expressed in terms of these rigidities and deformations of the corresponding control runs:

$$M_{con}^{(N)} = c_{c.p}\gamma_{c.p} + c_x\gamma_x \sin\psi_{a.p}^{(N)} + c_z\gamma_z \cos\psi_{a.p}^{(N)} + c_{a.p}\gamma_{a.p}^{(N)}, \tag{4.13}$$

where $c_{c.p}$, c_x, c_z, and $c_{a.p}$ are the rigidities of the collective pitch control, lateral and longitudinal controls, and swashplate respectively, referred to the feathering hinge of the blade.

The form of notation of eq.(4.13) assumes that the rigidity $c_{c.p}$ remains constant regardless of the type of combinations of forces locked on the swash-plate.

The values of the deformations of different control loops referred to the feathering hinge can be expressed in terms of the angles of rotation of individual blades γ_N if we represent eqs.(4.9) as a system of equations relative to the unknowns $\gamma_{c.p}$, γ_x, γ_z, and $\gamma_{a.p}$. The solution of the system (4.9) yields the following expressions for deformations of individual control loops:

$$\left.\begin{aligned}\gamma_{c.p}&=\frac{1}{z_b}\sum_N \gamma_N,\\ \gamma_x&=\frac{2}{z_b}\sum_N \gamma_N \sin\psi_{a.p}^{(N)},\\ \gamma_z&=\frac{2}{z_b}\sum_N \gamma_N \cos\psi_{a.p}^{(N)}.\end{aligned}\right\} \tag{4.14}$$

When

$$z_b<4$$
$$\gamma_{a.p}^{(N)}=0.$$

For a four-blade rotor, $\gamma_{a.p}^{(N)}$ can be determined by the formula

$$\gamma_{a.p}^{(N)}=\frac{1}{4}\cos\pi N\sum_N \gamma_N\cos\pi N. \tag{4.15}$$

For a number of blades $z_b > 4$, the quantity $\gamma_{a.p}^{(N)}$ is determined by the expression

$$\gamma_{a.p}^{(N)}=\frac{1}{z_b}\sum_{m=2}^{m=z_b-2}\cos\frac{2\pi m}{z_b}N\sum_N \gamma_N\cos\frac{2\pi m}{z_b}N. \tag{4.16}$$

Substituting eqs.(4.14) and (4.16) into eq.(4.13), we obtain the expressions for the hinge moment from the control for a blade with the numeral N:

$$\begin{aligned}M_{con}^{(N)}=&\frac{1}{z_b}c_{c.p}\sum_N\gamma_N+\frac{2}{z_b}c_x\sin\psi_{a.p}^{(N)}\sum_N\gamma_N\sin\psi_{a.p}^{(N)}+\\ &+\frac{2}{z_b}c_z\cos\psi_{a.p}^{(N)}\sum_N\gamma_N\cos\psi_{a.p}^{(N)}+\\ &+\frac{c_{a.p}}{z_b}\sum_{m=2}^{m=z_b-2}\cos\frac{2\pi m}{z_b}N\sum_N\gamma_N\cos\frac{2\pi m}{z_b}N.\end{aligned} \tag{4.17}$$

Substituting eq.(4.17) into eq.(4.6) and examining this equation together with the first equation of the system (2.19), we obtain a system of differential equations of coupled blade vibrations at axial flow past the rotor: /389

$$
\left.
\begin{aligned}
&\ddot{\beta}_N + d_{11}\omega\dot{\beta}_N + \omega^2\beta_N + c_{12}\ddot{\varphi}_N + d_{12}\omega\dot{\varphi}_N + b_{12}\omega^2\varphi_N = 0,\\
&\ddot{\varphi}_N + d_{22}\omega\dot{\varphi}_N + b_{22}\omega^2\varphi_N + c_{21}\ddot{\beta}_N + d_{21}\omega\dot{\beta}_N + \\
&\quad + b_{21}\omega^2\beta_N + \frac{1}{z_b}\,p_{c.p}^2 \sum_N (\varphi_N + \varkappa\beta_N) + \\
&\quad + \frac{2}{z_b}\,p_x^2 \sin\psi_{a.p}^{(N)} \sum_N (\varphi_N + \varkappa\beta_N)\sin\psi_{a.p}^{(N)} + \\
&\quad + \frac{2}{z_b}\,p_z^2 \cos\psi_{a.p}^{(N)} \sum_N (\varphi_N + \varkappa\beta_N)\cos\psi_{a.p}^{(N)} + \\
&+ \frac{1}{z_b}\,p_{a.p}^2 \sum_{m=2}^{m=z_b-2} \cos\frac{2\pi m}{z_b} N \sum_N (\varphi_N + \varkappa\beta_N)\cos\frac{2\pi m}{z_b} N = 0,
\end{aligned}
\right\} \qquad (4.18)
$$

where

$$
\left.
\begin{aligned}
p_{a.h} &= \sqrt{\frac{c_{a.h}}{I_{a.h}}},\\
p_x &= \sqrt{\frac{c_x}{I_{a.h}}},\\
p_z &= \sqrt{\frac{c_z}{I_{a.h}}},\\
p_{a.p} &= \sqrt{\frac{c_{a.p}}{I_{a.h}}}.
\end{aligned}
\right\} \qquad (4.19)
$$

The system of equations (4.18) is a system of ordinary differential equations relative to the unknown functions β_N and φ_N, with periodic time-variant coefficients together with the variable

$$
\psi_{a.p}^{(N)} = \omega t - N\Delta\psi_b, \qquad (4.20)
$$

where

$$
\Delta\psi_b = \frac{2\pi}{z_b}.
$$

5. Transformation of Eqs.(4.18) in Particular Cases where Cyclic Modes are the Solution of the Differential Equations of Rotor Flutter

Let us check whether cyclic vibration modes are the solution to the differential equations (4.18) of rotor flutter written with consideration of coupling between blade vibrations through the swashplate.

In the general case, the relation between variables in cyclic vibration modes of a rotor can be represented in the form

$$
\left.
\begin{aligned}
\beta_N &= \beta_0 e^{iN\Delta\psi_m},\\
\varphi_N &= \varphi_0 e^{iN\Delta\psi_m},
\end{aligned}
\right\} \qquad (4.21)
$$

where /390

β_0 and φ_0 = angles of rotation of the blade with the numeral N = 0 relative to the flapping and feathering hinges, which are unknown functions of time;

$\Delta\psi_m = \frac{2\pi m}{z_b}$ = phase angle characterizing the vibration mode of the order m.

Substituting eqs.(4.21) into the differential equations (4.18) and successively varying the values of m from 0 to $z_b - 1$, we find that cyclic vibration modes are the solution to eqs.(4.18) only for values of m = 0 (in-phase flutter) and $z - 2 \geq m \geq 2$ (plate mode of flutter). At these values, the differential equations (4.18) are transformed into equations exactly coinciding with the equations of flutter of an isolated blade [eq.(2.19)]. Only the value of the frequency of natural vibrations of a blade in torsion entering the second equation of system (2.19) becomes equal to

$$p_{tw} = p_{c.p} \tag{4.22}$$

during in-phase flutter (m = 0) and

$$p_{tw} = p_{a.p} \tag{4.23}$$

during plate flutter ($z_b - 2 \geq m \geq 2$), when all forces due to the blades close to the swashplate and the lateral and longitudinal controls and collective pitch control are not loaded.

At the same time, cyclic vibration modes at m = 1 and $m = z_b - 1$ are the solution to the differential equations (4.18) only in one particular case, when $c_x = c_z$. In this particular case, the differential equations (4.18) are transformed into equations coinciding with eq.(2.19) for an isolated blade. Only the value of p_{tw} in this case should be equal to

$$p_{tw} = p_x = p_z. \tag{4.24}$$

Thus, flutter of a rotor as a whole can be studied on the model of an isolated blade having a rigidity of attachment equal to the rigidity of the collective pitch control $c_{c.p}$, with the cyclic pitch control $c_x = c_z$ and swashplate $c_{a.p}$ taken separately.

6. Rotor Flutter in the Presence of Different Rigidity of Longitudinal and Lateral Controls

To solve the differential equations (4.18) in the case of $c_x \neq c_z$, we can use the following method. Let us introduce the new variables:

$$\left.\begin{aligned} \xi_\varphi &= \sum_N \varphi_N \sin \psi_{a.p}^{(N)}, \\ \eta_\varphi &= \sum_N \varphi_N \cos \psi_{a.p}^{(N)}, \end{aligned}\right\} \tag{4.25}$$

$$\left.\begin{aligned}\xi_\beta &= \sum_N \beta_N \sin\psi_{a.p}^{(N)},\\ \eta_\beta &= \sum_N \beta_N \cos\psi_{a.p}^{(N)}.\end{aligned}\right\}$$

Successively multiplying all terms of eqs.(4.18) by $\sin\psi_{a.p}^{(N)}$ and by $\cos\psi_{a.p}^{(N)}$ and summing them with respect to N, we obtain a system of ordinary differential equations relative to the new variables of the following form: /391

$$\left.\begin{aligned}
&\ddot{\xi}_\beta + d_{11}\omega\dot{\xi}_\beta - 2\omega\dot{\eta}_\beta - d_{11}\omega^2\eta_\beta + c_{12}\ddot{\xi}_\varphi + d_{12}\omega\dot{\xi}_\varphi + \\
&\quad + \omega^2(b_{12}-c_{12})\xi_\varphi - 2c_{12}\omega\dot{\eta}_\varphi - d_{12}\omega^2\eta_\varphi = 0,\\
&\ddot{\eta}_\beta + d_{11}\omega\dot{\eta}_\beta + 2\omega\dot{\xi}_\beta + d_{11}\omega^2\xi_\beta + c_{12}\ddot{\eta}_\varphi + d_{12}\omega\dot{\eta}_\varphi + \\
&\quad + \omega^2(b_{12}-c_{12})\eta_\varphi + 2c_{12}\omega\dot{\xi}_\varphi + d_{12}\omega^2\xi_\varphi = 0,\\
&\ddot{\xi}_\varphi + d_{22}\omega\dot{\xi}_\varphi + [(b_{22}-1)\omega^2 + p_x^2]\xi_\varphi - 2\omega\dot{\eta}_\varphi - d_{22}\omega^2\eta_\varphi + \\
&\quad + c_{21}\ddot{\xi}_\beta + d_{21}\omega\dot{\xi}_\beta + p_x^2\varkappa\xi_\beta - 2c_{21}\omega\dot{\eta}_\beta - d_{21}\omega^2\eta_\beta = 0,\\
&\ddot{\eta}_\varphi + d_{22}\omega\dot{\eta}_\varphi + [(b_{22}-1)\omega^2 + p_z^2]\eta_\varphi + 2\omega\dot{\xi}_\varphi + d_{22}\omega^2\xi_\varphi + \\
&\quad + c_{21}\ddot{\eta}_\beta + d_{21}\omega\dot{\eta}_\beta + p_z^2\varkappa\eta_\beta + 2c_{21}\omega\dot{\xi}_\beta + d_{21}\omega^2\xi_\beta = 0.
\end{aligned}\right\} \qquad (4.26)$$

The system of equations (4.26) can be solved by the conventional method for solving a system of differential equations with constant coefficients.

A similar method of reducing the problem to a system of equations with constant coefficients was used by Coleman and B.Ya.Zherebtsov in investigating the ground resonance of helicopters.

We can show that the variables (4.25) can be expressed by the variables proposed by A.P.Proskuryakov for investigating helicopter stability.

In his works, A.P.Proskuryakov expressed the angle of rotation of the blade relative to the flapping hinge in the form

$$\beta_N = a_0(t) + a_1(t)\cos\psi_N + b_1(t)\sin\psi_N. \qquad (4.27)$$

On alternately multiplying eq.(4.27) by $\cos\psi_N$ and $\sin\psi_N$ and summing with respect to N, it will be found that

$$\left.\begin{aligned}a_1(t) &= \frac{2}{z_b}\sum_N \beta_N\cos\psi_N,\\ b_1(t) &= \frac{2}{z_b}\sum_N \beta_N\sin\psi_N,\end{aligned}\right\} \qquad (4.28)$$

i.e., the variables $a_1(t)$ and $b_1(t)$ virtually coincide with the variables η_β and ξ_β.

The use of the above method for solving equations of helicopter flutter at $c_x \neq c_z$ and $\mu \neq 0$ was proposed by L.N.Grodko. It was also used by V.D.Il'ichev for obtaining practical results.

Section 5. Flapping Flutter of a Rotor in Forward Flight

1. Preliminary Statements

Experiments carried out on various helicopters showed that, in forward flight, flutter might set in earlier than under conditions of axial flow past the rotor, for example, in ground-testing. Therefore, a determination of the critical flutter rpm in flight is of appreciable practical interest. The basic problem requiring solution in this case is the degree to which the critical flutter rpm is lower in flight than on the ground. /392

A variety of other important practical problems arises in this connection. For example, what parametric margin prior to flutter should be secured under ground-testing conditions so as to preclude the possibility of the occurrence of flutter in flight.

All these problems can be solved if there is an opportunity to calculate flutter in forward flight, which permits determining, in particular, the dependence of critical rpm on the flying speed.

Furthermore, difficulties arise in calculating the flutter in flight. These refer primarily to substantial complication of the differential equations describing blade vibration. Therefore, in examining the problem, one should begin with these.

2. Differential Equations of Blade Oscillations in Forward Flight

The differential equations of torsional and flapping vibrations of a blade in forward flight are derived in the same manner as for the regime with axial flow past the rotor. Only the values of the relative velocities of the stream flowing past the profile should be calculated with consideration of the addition term due to forward velocity. These velocities can be written in the form

$$\left.\begin{aligned} U_x &= \omega R(\bar{r} + \mu \sin\psi), \\ U_y &= \omega R\left(\lambda - \bar{r}\frac{\dot{\beta}}{\omega} - \mu\cos\psi\,\beta\right), \end{aligned}\right\} \tag{5.1}$$

where $\mu = \dfrac{V\cos\alpha}{\omega R}$.

Substituting eqs.(5.1) into eqs.(1.6) and then eq.(1.6) into eqs.(2.3) and (2.11), we obtain the differential equations of blade vibration in forward flight:

$$
\left.
\begin{aligned}
&\ddot{\beta}+(d_{11}+\mu b_{11}^{I}\sin\psi)\omega\dot{\beta}+\left(1+\mu b_{11}^{I}\cos\psi+\frac{1}{2}\mu^2 b_{11}^{II}\sin 2\psi\right)\omega^2\beta+\\
&+c_{12}\ddot{\varphi}+(d_{12}+\mu d_{12}^{I}\sin\psi)\omega\dot{\varphi}+\left[b_{12}-\frac{1}{2}\mu b_{11}^{I}\sin\psi-\right.\\
&\left.-\frac{1}{2}\mu^2 b_{11}^{II}(1-\cos 2\psi)\right]\omega^2\varphi=\omega^2\gamma_0\int_0^R b\bar{r}\lambda(\bar{r}+\mu\sin\psi)\,d\bar{r},\\
&\ddot{\varphi}+(d_{22}+\mu d_{22}^{I}\sin\psi)\omega\dot{\varphi}+\left\{\left[b_{22}+\frac{1}{2}\mu b_{22}^{I}\sin\psi+\frac{1}{2}\mu^2 b_{22}^{II}(1-\right.\right.\\
&\left.\left.-\cos 2\psi)\right]\omega^2+p_t^2\right\}\varphi+c_{21}\ddot{\beta}+(d_{21}-\mu b_{22}^{I}\sin\psi)\omega\dot{\beta}+\\
&+\left\{\left[b_{21}-\mu b_{22}^{I}\cos\psi-\frac{1}{2}\mu^2 b_{22}^{II}\sin 2\psi\right]\omega^2+\varkappa p_t^2\right\}\beta=p_t^2\,\theta+\\
&+\frac{\omega^2}{I_{a.h}}\int_0^R I_m\Delta\varphi_{geom}\,dr-\omega^2\frac{\gamma_0}{i_0}\int_0^R\bar{b}\tilde{\sigma}_f\lambda(\bar{r}+\mu\sin\psi)\,d\bar{r}.
\end{aligned}
\right\}
\tag{5.2}
$$

Here, the coefficients c_{12}, c_{21}, d_{11}, d_{21}, d_{22}, b_{21}, b_{22} are the same as in eqs.(2.14); furthermore, we introduce the following additional coefficients: /393

$$
\left.
\begin{aligned}
d_{12}^{I}&=-\frac{1}{2}c_{y}^{\alpha}\frac{\varrho}{I_{h.h}}\int_0^R b^2 r\left(\frac{3}{4}-\frac{x_0}{b}\right)dr,\\
d_{22}^{I}&=\frac{\pi}{16}\frac{\varrho}{I_{a.h}}\int_0^R b^3\,dr+\frac{1}{2}c_{y}^{\alpha}\frac{\varrho}{I_{a.h}}\int_0^R b^2\sigma_f\left(\frac{3}{4}-\frac{x_0}{b}\right)dr,\\
b_{11}^{I}&=\frac{1}{2}c_{y}^{\alpha}\frac{I}{I_{h.h}}\int_0^R br^2\,dr,\\
b_{11}^{II}&=\frac{1}{2}c_{y}^{\alpha}\frac{\varrho}{I_{h.h}}\int_0^R br\,dr,\\
b_{22}^{I}&=\frac{1}{2}c_{y}^{\alpha}\frac{\varrho}{I_{a.h}}\int_0^R br\sigma_f\,dr,\\
b_{22}^{II}&=\frac{1}{2}c_{y}^{\alpha}\frac{\varrho}{I_{a.h}}\int_0^R b\sigma_f\,dr.
\end{aligned}
\right\}
\tag{5.3}
$$

Assuming that the particular solution β^* and φ^* of eqs.(5.2) is found, we set, as before (see Sect.2.4)

$$\beta=\beta^*+\beta_d;$$

$$\varphi=\varphi^*+\varphi_d,$$

where β_d and φ_d are the angles of deflection of the blade from a position

corresponding to its steady motion, determinable by the particular solution.

Substituting these expressions into eqs.(5.2), we obtain the following differential equations of disturbed motion of the blade in forward flight:

$$\left.\begin{aligned}
&\ddot{\beta}+(d_{11}+\mu b^{I}_{11}\sin\psi)\,\omega\dot{\beta}+(1+\mu b^{I}_{11}\cos\psi+\frac{1}{2}\mu^2 b^{II}_{11}\sin 2\psi)\,\omega^2\beta+\\
&+c_{12}\ddot{\varphi}+(d_{12}+\mu d^{I}_{12}\sin\psi)\,\omega\dot{\varphi}+\\
&+\left[b_{12}-\frac{1}{2}\mu b^{I}_{11}\sin\psi-\frac{1}{2}\mu^2 b^{II}_{11}(1-\cos 2\psi)\right]\omega^2\varphi=0,\\
&\ddot{\varphi}+(d_{22}+\mu d^{I}_{22}\sin\psi)\,\omega\dot{\varphi}+\left\{\left[b_{22}+\frac{1}{2}\mu b^{I}_{22}\sin\psi+\right.\right.\\
&\left.\left.+\frac{1}{2}\mu^2 b^{II}_{22}(1-\cos 2\psi)\right]\omega^2+p_t^2\right\}\varphi+c_{21}\ddot{\beta}+(d_{21}-\mu b^{I}_{22}\sin\psi)\,\omega\dot{\beta}+\\
&+\left\{\left[b_{21}-\mu b^{I}_{22}\cos\psi-\frac{1}{2}\mu^2 b^{II}_{22}\sin 2\psi\right]\omega^2+\varkappa p_t^2\right\}\beta=0.
\end{aligned}\right\} \qquad (5.4)$$

Here, the subscripts of the variables β_d and φ_d, which indicate that they refer to disturbed motion, are omitted for simplicity.

3. Solution of Differential Equations

/394

Equations (5.4) represent a system of differential equations with periodic coefficients. The solution of such a system can be written in the form

$$\left.\begin{aligned}
\beta&=\beta_0 e^{\lambda t}(1+T_\beta);\\
\varphi&=\varphi_0 e^{\lambda t}(1+T_\varphi),
\end{aligned}\right\} \qquad (5.5)$$

where the functions T_β and T_φ determine the content of the harmonic components of blade vibration in flutter.

These functions can be written as

$$\left.\begin{aligned}
T_\beta&=\sum_n(\bar{\beta}_n\cos n\psi+\bar{\bar{\beta}}_n\sin n\psi);\\
T_\varphi&=\sum_n(\bar{\varphi}_n\cos n\psi+\bar{\bar{\varphi}}_n\sin n\psi),
\end{aligned}\right\} \qquad (5.6)$$

where n = 1, 2, 3, ... are constant coefficients determining the order of the corresponding harmonics.

The critical flutter rpm in this case can be determined if eqs.(5.5), with consideration of eqs.(5.6), are substituted into the differential equations (5.4) and if the coefficients of like harmonic components are equated. This operation results in the formation of a system of algebraic equations relative to the unknown coefficients β_0, φ_0, $\bar{\beta}_n$, $\bar{\bar{\beta}}_n$, $\bar{\varphi}_n$, and $\bar{\bar{\varphi}}_n$. To solve this system, it is necessary to determine the roots of the characteristic equation whose order

depends on the number of harmonic components n retained in the solution.

The solution of eqs.(5.4), with consideration of the harmonics, greatly complicates the calculation and at the same time - at the values of $\mu < 0.4$ actually used - introduces no essential refinements into the calculation results. Therefore, in practical calculations we usually employ either the approximate method without consideration of the harmonic components or else the method of calculation with numerical integration of the equations of blade motion with respect to time. One of the versions of this method will be given in Section 7 of this Chapter.

4. Determination of Critical Flutter Rpm without Consideration of Harmonic Components of Blade Motion

If the effect of harmonic components on the critical rpm is disregarded, the calculation of flutter in forward flight is no more complex than under conditions of axial flow past the rotor. An approximate solution, neglecting the effect of harmonic components can be obtained, if the periodic coefficients in the differential equations (5.4) are omitted*. In this case, the forward flying speed is taken into account by introducing, into eqs.(1.6), the constant part of the functions depending on U_x. For this it suffices to set

$$\left.\begin{aligned} U_x &= \omega r, \\ U_x^2 &= \omega^2 R^2 \left(\bar{r}^2 + \frac{1}{2}\mu^2\right). \end{aligned}\right\} \qquad (5.7)$$

Then, the system of differential equations of disturbed motion can be written in the following manner: /395

$$\left.\begin{aligned} &\ddot{\beta} + d_{11}\omega\dot{\beta} + \omega^2\beta + c_{12}\ddot{\varphi} + d_{12}\omega\dot{\varphi} + b_{12}\left(1 - \frac{1}{2}\mu^2 b_{12}^*\right)\omega^2\varphi = 0, \\ &\ddot{\varphi} + d_{22}\omega\dot{\varphi} + \left[(p_t^2 + \omega^2) + b_{22}\left(1 - \frac{1}{2}\mu^2 b_{22}^*\right)\omega^2\right]\varphi + \\ &\quad + c_{21}\ddot{\beta} + d_{21}\omega\dot{\beta} + (b_{21}\omega^2 + \varkappa p_t^2)\beta = 0, \end{aligned}\right\} \qquad (5.8)$$

where

$$b_{12}^* = \frac{b_{11}^{II}}{b_{12}};$$

$$b_{22}^* = \frac{b_{22}^{II}}{b_{22}}.$$

For a blade of rectangular planform, the coefficient b_{12}^* can be considered as approximately equal to -2. The coefficient b_{22}^* is small in magnitude and has no substantial effect on the results.

Equations (5.8) differ from eqs.(2.19) for a regime with axial flow past the rotor only by terms of the type of $\left(1 - \frac{1}{2}\mu^2 b_{12}^*\right)$. This permits determining

* This method was proposed by V.D.Il'ichev.

the critical flutter rpm in forward flight by eq.(2.27); however, in the expressions of certain coefficients of eq.(2.24) entering this formula there appears an additional term of the type $\left(1 - \frac{1}{2}\mu^2 b_{12}^*\right)$:

$$
\left.
\begin{aligned}
B_1 &= \frac{1}{1 - i_0 c_{21}^2}\left[1 + b_{22}\left(1 - \frac{1}{2}\mu^2 b_{22}^*\right) + d_{11}d_{22} - \right. \\
&\quad \left. - b_{12}c_{21}\left(1 - \frac{1}{2}\mu^2 b_{12}^*\right) - d_{12}d_{21} - c_{12}c_{21}\right], \\
C_1 &= \frac{1}{1 - i_0 c_{21}^2}\left[d_{22} + d_{11}b_{22}\left(1 - \frac{1}{2}\mu^2 b_{22}^*\right) - \right. \\
&\quad \left. - b_{12}d_{21}\left(1 - \frac{1}{2}\mu^2 b_{12}^*\right) - c_{21}d_{12}\right], \\
D_1 &= \frac{1}{1 - i_0 c_{21}^2}\left[b_{22}\left(1 - \frac{1}{2}\mu^2 b_{22}^*\right) - b_{12}c_{21}\left(1 - \frac{1}{2}\mu^2 b_{12}^*\right)\right], \\
D_2 &= \frac{1}{1 - i_0 c_{21}^2}\left[1 - \varkappa b_{12}\left(1 - \frac{1}{2}\mu^2 b_{12}^*\right)\right].
\end{aligned}
\right\} \qquad (5.9)
$$

Thus, disregarding all harmonic components of blade motion, the problem of determining the critical flutter rpm in forward flight can be reduced to solving the system of differential equations (5.8) with constant coefficients.

5. Effect of Flying Speed on Critical Flutter Rpm

The effect of flying speed, definable by the term $\left(1 - \frac{1}{2}\mu^2 b_{12}^*\right)$ in eqs.(5.8) proves to be quite weak. Figure 4.24 shows the dependence of the critical rpm on the flying speed, determined by the value of μ, for three different values of blade balancing.

If follows from the graph (see Fig.4.24) that the critical flutter rpm drops by about 5 - 10% with an increase in flying speed to values of μ = 0.25 - 0.3. /396

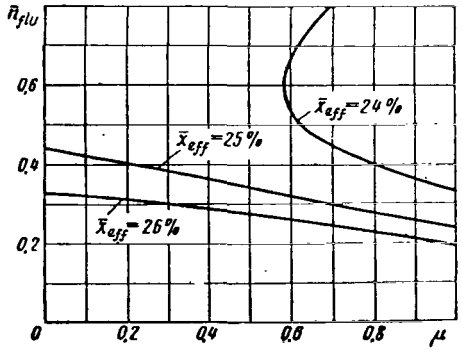

Fig.4.24 Critical Flutter Rpm as a Function of Flying Speed.

In experiments carried out on helicopters, the effect of speed is somewhat stronger. This can be explained by the effect of the following factors:

It is shown above in Section 3 that, for small blade oscillations during flutter, the axial hinge with friction can be regarded as a linear damper whose efficiency is smaller, the higher the angular velocity of relative displacements in this hinge during forced vibrations of the blade. Therefore, the critical flutter rpm in flight decreases with increasing relative

displacements in the axial hinge and hence with flying speed, since relative displacements usually increase with speed. Hence it follows that all factors on which the helicopter balancing depends may affect the flutter, since balancing determines the vibration amplitude in the axial hinge with respect to the first harmonic of rotor rpm.

Displacements of the blade in the axial hinge, with harmonics higher than the first, may also have a strong effect. These harmonic components usually have smaller amplitudes of displacement but relatively high angular velocity, leading to an appreciable reduction of the effectiveness of the damping action of dry friction in the axial hinge of the blade.

Thus, in many cases the severe drop in critical flutter rpm in forward flight is explained by a decrease in the damping action of friction in the axial hinge.

A no less important factor capable of substantially influencing critical revolutions of flutter is the variation in the aerodynamic characteristics of the blade profile in connection with fluctuations of the value of the Mach number under forward flight conditions. As mentioned above, a change in M in the range from 0.5 to 0.9 causes a marked change in the aerodynamic characteristics and, what is especially important for flutter, a distinct shift in the position of the profile focus.

Only the method employing numerical integration of the differential equations of blade motion with respect to time (see Sect.7) permits taking into account these factors with sufficient accuracy.

Section 6. Calculation of Flutter with Consideration of Bending and Torsion of the Blade

1. Bending and Torsion of Blade during Flutter

It was pointed out above that, in the overwhelming majority of cases, vibrations of the blade as a solid body predominate in the mode of blade vibration in the flapping plane during flutter. The blade executes these oscillations, rotating about the flapping hinge. Torsional vibrations of the blade occur mainly as a consequence of its rotation about the feathering hinge. In this /397
hinge, the blade rotates owing to the kinematic action of the swashplate of the automatic pitch control and flapping compensator as well as deformations of the control cables. Flexural and torsional deformations of the blade itself generally have no significant effect on the critical flutter rpm. Nevertheless, the flexural and torsional deformations of the blade during flutter of this type are usually quite pronounced. They lead to smaller displacements of the blade elements in comparison with displacements during vibration of the blade as a solid body, but these displacements are of the same order. Therefore, it is impossible to neglect deformations of the blade itself or to show no interest in them.

In individual cases, the flexural deformations of the blade increase and begin to have a noticeable effect on the critical flutter rpm. It is especially important to take into account blade bending in determining the effect of con-

centrated balancers installed on the blade to eliminate flutter.

Also known are individual cases where the blade during flutter executes flexural vibrations in which the share of the flapping mode is quite small. It should be emphasized that such cases are very rare. However, for jet helicopters with blade-tip engines, such flutter - usually called "bending flutter" - constitutes a serious danger. Subsection 8 of this Section will be devoted to an examination of this type of flutter.

As stated above, the effect of torsional vibrations of the blade during flutter can be disregarded at a value of the coefficient $\alpha < 0.4 - 0.5$ (see Sect.1.4). In the remaining cases, in particular when the pitch control system has relatively great rigidity, blade torsion cannot be disregarded. This may result in a very large error.

However, most of the presently constructed helicopters have a coefficient $\alpha < 0.4$. Therefore, in Subsection 6, we will specifically study flutter with consideration of bending but without consideration of torsional deformations of the blade. Such an approach leads to a considerable simplification of the differential equations.

2. Determination of the Torque from Bending Forces on the Blade

In calculating torsional strains of a blade it is important what method is used for determining the torque due to bending forces on the blade. If the blade is bent in the flapping plane, then the force Q applied to the blade in the plane of rotation creates torque on the arm Δy relative to the section, at a radius r closer to its root (Fig.4.25). Likewise, when the blade is bent in the plane of rotation a similar torque on the arm Δx is created by the force T acting in the flapping plane.

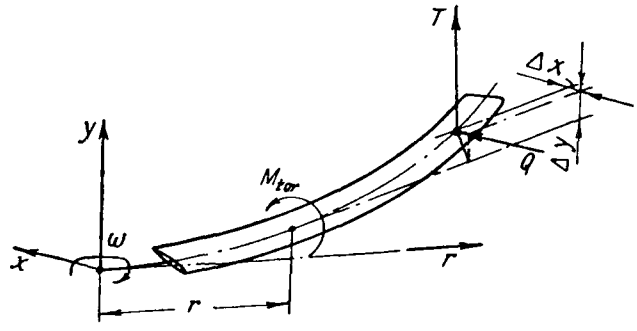

Fig.4.25 Diagram of the Occurrence of Twisting Moments due to Bending Forces on the Blade.

In calculating the twisting moments due to bending forces on the blade, it is important to recall the fact that the components of the centrifugal forces relieving the blade in bending also participate in the generation of twisting moments. If we calculate only the torque due to external bending forces on the blade, the value will be much larger than the actual torque, just as the moment due only to the external forces bending the blade will be many times greater than the bending moment in the blade section.

Let us examine a blade element of length dr, bent in two mutually perpendic-

ular planes (Fig.4.26). Equating to zero the sum of the moments of all external forces relative to the tangent to the blade axis in a section at the radius r /398 and discarding all terms of higher orders of smallness relative to dr, we obtain

$$-M_{tor}+M_{tor}+dM_{tor}-M_y x''dr+M_x y''dr=0 \tag{6.1}$$

or

$$\frac{\partial M_{tor}}{\partial r}=M_y x''-M_x y''. \tag{6.2}$$

If, for simplicity, we assume that the planes of maximum and minimum blade rigidity coincide with the planes of rotation and flapping, then, having set

$$x''=\frac{M_x}{EI_x} \tag{6.3}$$

and

$$y''=\frac{M_y}{EI_y}, \tag{6.4}$$

we obtain

$$\frac{\partial M_{tor}}{\partial r}=M_x M_y\left(\frac{1}{EI_x}-\frac{1}{EI_y}\right), \tag{6.5}$$

where I_x and I_y are the elastic moments of inertia of the blade section during bending in the plane of rotation and flapping plane.

Equation (6.5) was first proposed for calculations of a blade by V.N.Novak.

It follows primarily from an examination of this formula that the torque $\frac{\partial M_{tor}}{\partial r}$ per unit length due to the bending forces on the blade is always equal to zero if

$$I_x=I_y, \tag{6.6}$$

i.e., if the rigidity of the blade in the plane of rotation and in the flapping plane is identical.

Furthermore, by virtue of the smallness of the bending moments M_x and M_y (as a consequence of load relieving by centrifugal forces, these moments are by a factor of 8 - 12 less than the moments due to the external forces acting on the blade), the torque $\frac{\partial M_{tor}}{\partial r}$ per unit length will be quite small in all cases even if $I_x \neq I_y$. This conclusion is highly important and results in a general approach to calculating torques and torsional deformations of a blade, as follows:

In each section of the blade, we must determine the torque relative to /399 the flexural axis of the blade in the examined section due to forces acting only in this section. Then, these local twisting moments should be summed with

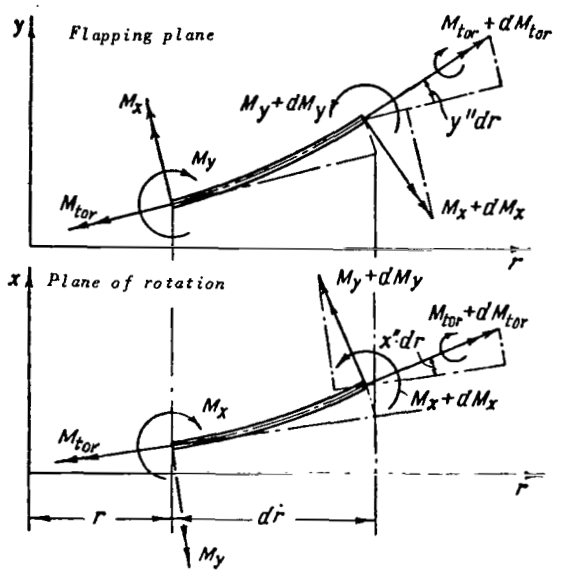

Fig.4.26 Diagram of Loading the Blade Element with Stresses in Two Mutually Perpendicular Planes.

respect to the blade length. Hence it follows in particular that the arms of the forces causing the twisting moments of the blade must remain constant regardless of whether or not the blade is bent.

With regard to flutter calculations, it follows from this conclusion that the torque per unit length of the blade from centrifugal forces should be calculated by the formula

$$\frac{\partial M_{tor_{c.f}}}{\partial r}=\omega^2 mr\sigma y', \qquad (6.7)$$

rather than by the frequently used formulas of the type

$$\frac{\partial M_{tor_{c.f}}}{\partial r}=\omega^2\left[y'\int_r^R mr\sigma\,dr\right]' \qquad (6.8)$$

or

$$\frac{\partial M_{tor_{c.f}}}{\partial r}=\omega^2 r\left[y'\int_r^R m\sigma\,dr\right]', \qquad (6.9)$$

which holds true only for a blade with an infinitely great rigidity in the plane of rotation.

3. Differential Equations of Binary Blade Vibration

Binary blade vibrations in vacuum are examined in Section 5, Chaoter I of Vol.II. In studying binary vibrations in air, we must additionally take into account aerodynamic forces. Using the differential equations of flexural [eq.(1.9)] and torsional vibrations [eq.(5.6)] of a blade (see Chapt.I of Vol.II) and supplementing these with inertia terms of the couple and with aerodynamic forces expressed by eqs.(1.6) of this Chapter, we obtain a set of differential equations of torsional blade vibrations in air: /400

$$\left.\begin{aligned} &m\ddot{y}+[EIy'']''-[Ny']'-m\sigma\ddot{\varphi}-\\ &-\frac{1}{2}c_y^{\alpha}\varrho b\left[U^2\varphi+\left(\frac{3}{4}b-x_0\right)U\dot{\varphi}-U\dot{y}\right]=0;\\ &I_m\ddot{\varphi}-[GT\varphi']'+\omega^2 I_m\varphi+\frac{\pi}{16}\varrho b^3U\dot{\varphi}+\\ &+\frac{1}{2}c_y^{\alpha}\varrho b\sigma_f\left[U^2\varphi+\left(\frac{3}{4}b-x_0\right)U\dot{\varphi}-U\dot{y}\right]-\omega^2 m\sigma ry'-m\sigma\ddot{y}=0. \end{aligned}\right\} \qquad (6.10)$$

These equations are written in a form pertaining only to disturbed motion of the blade. The particular solution describing undisturbed steady motion of a blade will not be discussed here.

In eqs.(6.10), we use the following designations:

y = displacement of the blade element in the flapping plane during disturbed motion of the blade;
φ = angle of rotation of the blade element in the same motion;
m = mass of the blade element per unit length;
I_m = moment of inertia of the blade element per unit length relative to the feathering hinge axis;
GT = torsional rigidity of the blade;
N = centrifugal force in the blade section:

$$N=\omega^2\int_r^R mrdr;$$

σ = distance from the center of gravity of the section to the feathering hinge axis, with the direction from this axis to the trailing edge of the blade considered positive;
σ_c = distance from the profile aerodynamic center to the feathering hinge axis.

Differentiation with respect to the blade radius is denoted by a prime and with respect to time by a dot.

To solve this set of equations it is convenient to change from the variable φ, which determines the total angle of rotation of the blade element in disturbed motion, to the variable ϑ representing only the elastic angle of rotation of the blade and correlated with φ by the relation

$$\varphi=\vartheta-\varkappa y_0',$$

where

y_0' = angle of rotation of the blade in the flapping hinge;
$\varkappa$ = flapping compensator.

Let us substitute the expression for the angle φ into the differential equations of binary blade vibration [eq.(6.10)]. This makes it possible to rewrite them in a form more convenient for further transformation: /401

$$\left.\begin{aligned}
&m\ddot{y}+[EIy'']''-[Ny']'+m\sigma\varkappa\ddot{y}_0'+\\
&+\frac{1}{2}c_y^{\alpha}\rho b\varkappa\left[U^2y_0'+\left(\frac{3}{4}b-x_0\right)U\dot{y}_0'\right]-\\
&-m\sigma\ddot{\vartheta}-\frac{1}{2}c_y^{\alpha}\rho b\left[U^2\vartheta+\left(\frac{3}{4}b-x_0\right)U\dot{\vartheta}-U\dot{y}\right]=0;\\
&I_m\ddot{\vartheta}-[GT\vartheta']'+\omega^2I_m\vartheta+\frac{\pi}{16}\rho b^3U\dot{\vartheta}+
\end{aligned}\right\}\qquad(6.11)$$

$$+\frac{1}{2}c_y^{\alpha}\varrho b\sigma_f\left[U^2\vartheta+\left(\frac{3}{4}b-x_0\right)U\dot{\vartheta}-U\dot{y}\right]-\omega^2 m\sigma r y'-$$
$$-m\sigma\ddot{y}-I_{mx}\dddot{y}_0'-\omega^2 I_{mx}\dot{y}_0'-\frac{\pi}{16}\varrho b^3 U_x\dot{y}_0'-$$
$$-\frac{1}{2}c_y^{\alpha}\varrho b x_{\sigma_f}\left[Uy_0'+\left(\frac{3}{4}b-x_0\right)U\dot{y}_0'\right]=0.$$

In the presence of a horizontal flying speed of the helicopter, the relative velocity of the flow past the profile will be a periodic function of time and radius. This velocity can be set approximately equal to the velocity U_x:

$$U_x=\omega r+V\sin\omega t. \tag{6.12}$$

Therefore, eqs.(6.11) represent a system of partial differential equations with coefficients periodically varying in time.

When the flying speed of the helicopter V equals zero, the periodic coefficients of the system (6.11) become constant, independent of time.

For the examined type of rotors system, eq.(6.11) has the following boundary conditions:

$$\left.\begin{aligned}M_0&=[EIy'']_0=\varkappa(M_b+M_{fr}),\\ M_b&=[GT\vartheta']_0=c_{con}\vartheta_0-M_{fr},\end{aligned}\right\} \tag{6.13}$$

where

M_0 = bending moment in the blade root;
M_b = twisting moment in the blade root;
M_{fr} = moment of friction in the axial hinge of the hub;
c_{con} = rigidity of the control system;
ϑ_0 = angle of rotation of the blade root due to deformations of the control system.

4. Solution of Differential Equations

The solution of the system of differential equations (6.11) can be obtained by using B.G.Galerkin's method. We set

$$\left.\begin{aligned}y&=\sum_j \delta_j y^{(j)};\\ \vartheta&=\sum_k \gamma_k \vartheta^{(k)},\end{aligned}\right\} \tag{6.14}$$

where

$y^{(j)}$ and $\vartheta^{(k)}$ = modes of the natural flexural and torsional vibrations of the blade in vacuum;
δ_j and γ_k = coefficients of flexural and torsional deformations of the

blade with respect to the j-th flexural and k-th torsional harmonic of natural vibration.

The coefficients δ_j and γ_k are certain functions of time. Since eqs.(6.11) are differential equations with periodic coefficients, the coefficients δ_j and γ_k should be functions of time of the type /402

$$\delta_j = \delta_{j_0} e^{\lambda t}(1+T) \tag{6.15}$$

where the function T determines the content of harmonic oscillations during flutter.

If, as before in Section 5.4, we seek the solution with an accuracy limited only by the fundamental frequency and disregard the effect of harmonic components, then we can omit the periodic coefficients in eq.(6.11).

Applying B.G.Galerkin's method to this simplified system of equations, we obtain a system of ordinary differential equations relative to the variables δ_j and γ_k. In matrix form, this system can be written as before (Sect.2.5) as the equation

$$C\ddot{X} + D\omega\dot{X} + (A + \omega^2 B)X = 0. \tag{6.16}$$

Here the variable X is the vector function with projections δ_j and γ_k, i.e.,

$$X = \begin{pmatrix} \delta_0 \\ \gamma_1 \\ \delta_1 \\ \gamma_2 \\ \delta_2 \\ \cdots \end{pmatrix}, \tag{6.17}$$

while A, B, C, and D are rectangular matrices of the order z, where z is the sum of the number of flexural and torsional harmonics accounted for in the calculation.

Setting $X = X_0 e^{\lambda t}$ in eq.(6.16), we obtain a system of algebraic equations of the form

$$|C\lambda^2 + D\omega\lambda + A + \omega^2 B| X_0 = 0. \tag{6.18}$$

Let us then equate the determinant of this system to zero. The resultant algebraic equation relative to the unknown parameter λ is the characteristic equation of the system (6.16). The roots of this equation completely characterize the blade motion described by the system (6.11).

To determine the boundaries of flutter, we should set $\lambda = ip$ in the characteristic equation and find the corresponding values of ω and p. These values will determine the parameters of the limits of the flutter zone.

An analysis of the results obtained from calculations shows that, in the general case, each combination of torsional and flexural harmonics of blade vibrations may correspond to a zone of instability with oscillations having a mode in which the content of the harmonics of this combination predominate. However, with actually used blade parameters, a given flutter zone by no means corresponds to each combination of harmonics. Thus, the number of flutter zones is always smaller than the number of combinations of flexural and torsional harmonics and can never be greater than the number of these combinations.

For practical purposes, an important point is the direct dependence of the critical flutter rpm on the frequency of the natural vibrations of the torsional harmonic of the blade entering into the combination in question. Therefore, combinations involving only the first harmonic of torsional blade vibration /403 give the lowest values of critical flutter rpm. All other combinations based on higher torsional harmonics of the blade are of no practical interest since the critical flutter rpm corresponding to these zones is always higher than the operating range of interest here.

All forms of flutter, corresponding to combinations of different flexural harmonics of the blade with the first harmonic of torsional vibrations of the blade, will be called the principal modes of flutter. Below, we will be interested only in the principal vibration modes since these modes of flutter have the lowest critical rpm and therefore are the only ones encountered in practice.

5. Calculation of Flutter with Consideration of Three Degrees of Freedom

To illustrate the above method, let us examine in greater detail the computational formulas for the case where the vibration mode during flutter is represented as combinations of the zero r and the first y flexural and first torsional harmonics.

The matrices entering eq.(6.16) will be of the third order in this case, and the vector function X will have only three projections:

$$X=\begin{pmatrix}\delta_0\\ \gamma_1\\ \delta_1\end{pmatrix}. \tag{6.19}$$

The coefficients of the matrices A, B, C, and D will be referred, as above, to the values of the coefficients $I_{h.h}$, L_1, and I_1 standing for the higher derivative of the variables:

$$L_1=\int_0^R I_m\vartheta^2 dr;$$

$$I_1=\int_0^R my^2 dr.$$

Let us write out the expressions for the coefficients of the matrices:

a) Inertia matrix C:

$$C=\begin{pmatrix} c_{11} & c_{12} & c_{13} \\ c_{21} & c_{22} & c_{23} \\ c_{31} & c_{32} & c_{33} \end{pmatrix}; \tag{6.20}$$

where

$$\left.\begin{aligned} c_{11} &= 1+\frac{\varkappa}{I_{h.h}}\int_0^R m\sigma r\,dr, \\ c_{12} &= -\frac{1}{I_{h.h}}\int_0^R m\sigma r\vartheta\,dr, \\ c_{13} &= \varkappa\beta_0\frac{1}{I_{h.h}}\int_0^R m\sigma r\,dr, \\ c_{21} &= -\frac{1}{L_1}\left[\int_0^R m\sigma r\vartheta\,dr+\varkappa\int_0^R I_m\vartheta\,dr\right], \\ c_{22} &= 1, \\ c_{23} &= -\frac{1}{L_1}\left[\int_0^R m\sigma y\vartheta\,dr+\varkappa\beta_0\int_0^R I_m\vartheta\,dr\right], \\ c_{31} &= \frac{\varkappa}{I_1}\int_0^R m\sigma y\,dr, \\ c_{32} &= -\frac{1}{I_1}\int_0^R m\sigma y\vartheta\,dr, \\ c_{33} &= 1+\frac{\varkappa}{I_1}\beta_0\int_0^R m\sigma y\,dr; \end{aligned}\right\} \tag{6.21}$$

/404

b) Damping coefficient matrix D:

$$D=\begin{pmatrix} d_{11} & d_{12} & d_{13} \\ d_{21} & d_{22} & d_{23} \\ d_{31} & d_{32} & d_{33} \end{pmatrix}, \tag{6.22}$$

where

$$\left.\begin{aligned} d_{11} &= \frac{1}{2}c_y^{\alpha}\frac{\varrho}{I_{h.h}}\left[\int_0^R br^3\,dr+\varkappa\int_0^R b^2r^2\left(\frac{3}{4}-\frac{x_0}{b}\right)dr\right]; \\ d_{12} &= -\frac{1}{2}c_y^{\alpha}\frac{\varrho}{I_{h.h}}\int_0^R b^2r^2\left(\frac{3}{4}-\frac{x_0}{b}\right)\vartheta\,dr, \end{aligned}\right\} \tag{6.23}$$

$$
\left.
\begin{aligned}
d_{13} &= \frac{1}{2} c_y^{\alpha} \frac{\varrho}{I_{h.h}} \left[\int_0^R br^2 y\, dr + \varkappa \beta_0 \int_0^R b^2 r^2 \left(\frac{3}{4} - \frac{x_0}{b} \right) \right] dr, \\
d_{21} &= -\frac{1}{2} c_y^{\alpha} \frac{\varrho}{L_1} \left[\int_0^R b \sigma_f r^2 \vartheta\, dr + \varkappa \int_0^R b^2 \sigma_f \left(\frac{3}{4} - \frac{x_0}{b} \right) r \vartheta\, dr \right] - \\
&\quad - \frac{\pi}{16} \varrho \frac{\varkappa}{L_1} \int_0^R b^3 r \vartheta\, dr - \varkappa \vartheta_0^2 d_{fr}, \\
d_{22} &= \frac{1}{L_1} \left[\frac{\pi}{16} \varrho \int_0^R b^3 r \vartheta^2 dr + \frac{1}{2} c_y^{\alpha} \varrho \int_0^R b^2 \sigma_f \left(\frac{3}{4} - \frac{x_0}{b} \right) r \vartheta^2 dr + \right. \\
&\quad \left. + \vartheta_0^2 d_{fr}, \right. \\
d_{23} &= -\frac{1}{2} c_y^{\alpha} \frac{\varrho}{L_1} \left[\int_0^R b \sigma_f r y \vartheta\, dr + \varkappa \beta_0 \int_0^R b^2 \sigma_f \left(\frac{3}{4} - \frac{x_0}{b} \right) r \vartheta\, dr \right] - \\
&\quad - \frac{\pi}{16} \varrho \frac{\varkappa}{L_1} \beta_0 \int_0^R b^3 r \vartheta\, dr - \varkappa \beta_0 \vartheta_0 d_{fr}, \\
d_{31} &= -\frac{1}{2} c_y^{\alpha} \frac{\varrho}{I_1} \left[\int_0^R br^2 y\, dr + \varkappa \int_0^R b^2 \left(\frac{3}{4} - \frac{x_0}{b} \right) r y\, dr \right], \\
d_{32} &= -\frac{1}{2} c_y^{\alpha} \frac{\varrho}{I_1} \int_0^R b^2 \left(\frac{3}{4} - \frac{x_0}{b} \right) r y \vartheta\, dr, \\
d_{33} &= \frac{1}{2} c_y^{\alpha} \frac{\varrho}{I_1} \left[\int_0^R br\, y^2 dr + \varkappa \beta_0 \int_0^R b^2 \left(\frac{3}{4} - \frac{x_0}{b} \right) r y dr \right],
\end{aligned}
\right\} \qquad (6.23)
$$

/405

if $d_{fr} = \frac{2a_{fr}}{\pi L_1 m \varphi_{pr}}$ [see eq.(3.14)].

c) Stiffness matrix A:

$$
A = \begin{pmatrix} 0 & 0 & 0 \\ 0 & a_{22} & 0 \\ 0 & 0 & a_{33} \end{pmatrix}, \qquad (6.24)
$$

where

$$
\left.
\begin{aligned}
a_{22} &= p_{tw}^2 = \frac{c_{con} \vartheta_0^2 + \int_0^R GT (\vartheta')^2 dr}{L_1}; \\
a_{33} &= p_{0_1}^2.
\end{aligned}
\right\} \qquad (6.25)
$$

Here, p_{0_1} is the frequency of natural flexural vibrations of the first harmonic of a nonrotating blade.

d) Centrifugal and aerodynamic stiffness matrix B:

$$B=\begin{pmatrix} b_{11} & b_{12} & b_{13} \\ b_{21} & b_{22} & b_{23} \\ b_{31} & b_{32} & b_{33} \end{pmatrix}, \tag{6.26}$$

where

$$\left.\begin{aligned}
b_{11} &= 1+\frac{1}{2}c_y^{\alpha}\varrho\frac{\varkappa}{I_{h.h}}\left[\int_0^R br^3\,dr+\frac{1}{2}\mu^2R^2\int_0^R br\,dr\right],\\
b_{12} &= -\frac{1}{2}c_y^{\alpha}\frac{\varrho}{I_{h.h}}\left[\int_0^R br^3\vartheta\,dr+\frac{1}{2}\mu^2R^2\int_0^R br\vartheta\,dr\right],\\
b_{13} &= \frac{1}{2}c_y^{\alpha}\varrho\frac{\varkappa}{I_{h.h}}\beta_0\left[\int_0^R br^3\,dr+\frac{1}{2}\mu^2R^2\int_0^R br\,dr\right],\\
b_{21} &= -\frac{1}{L_1}\left\{\int_0^R m\sigma r\vartheta\,dr+\varkappa\int_0^R I_m\vartheta\,dr+\right.\\
&\left.+\frac{1}{2}c_y^{\alpha}\varrho\varkappa\left[\int_0^R b\sigma_f r^2\vartheta dr+\frac{1}{2}\mu^2R^2\int_0^R b\sigma_f\vartheta\,dr\right]\right\},\\
b_{22} &= 1+\frac{1}{2}c_y^{\alpha}\frac{\varrho}{L_1}\left[\int_0^R b\sigma_f r^2\vartheta^2dr+\frac{1}{2}\mu^2R^2\int_0^R b\sigma_f\vartheta^2\,dr\right],\\
b_{23} &= -\frac{1}{L_1}\left\{\frac{1}{2}c_y^{\alpha}\varrho\varkappa\beta_0\left[\int_0^R b\sigma_f r^2\vartheta\,dr+\frac{1}{2}\mu^2R^2\int_0^R b\sigma_f\vartheta\,dr\right]+\right.\\
&\left.+\int_0^R m\sigma r\beta\vartheta\,dr+\varkappa\beta_0\int_0^R I_m\vartheta\,dr\right\},\\
b_{31} &= \frac{1}{2}c_y^{\alpha}\varrho\frac{\varkappa}{I_1}\left[\int_0^R br^2y dr+\frac{1}{2}\mu^2R^2\int_0^R by\,dr\right],\\
b_{32} &= -\frac{1}{2}c_y^{\alpha}\frac{\varrho}{I_1}\left[\int_0^R br^2y\vartheta\,dr+\frac{1}{2}\mu^2R^2\int_0^R by\vartheta\,dr\right],\\
b_{33} &= k+\frac{1}{2}c_y^{\alpha}\varrho\frac{\varkappa}{I_1}\beta_0\left[\int_0^R br^2y dr+\frac{1}{2}\mu^2R^2\int_0^R by\,dr\right];
\end{aligned}\right\} \tag{6.27}$$

/406

Here, $k=\frac{1}{I_1}\int_0^R\beta^2\int_r^R mr\,dr$ where $\beta = y'$.

The characteristic equation for this case will have the following form:

$$\lambda^6A_0+\lambda^5\omega A_1+\lambda^4(B_1\omega^2+B_2)+\lambda^3\omega(\omega^2C_1+C_2)+\lambda^2(\omega^4D_1+\omega^2D_2+D_3)+ \tag{6.28}$$

$$+\lambda\omega(\omega^4E_1+\omega^2E_2+E_3)+\omega^2(\omega^4F_1+\omega^2F_2+F_3)=0.$$

Hence,

$$\left.\begin{aligned}
A_0&=c_{11}S_0+c_{13}R_0+c_{12}T_0;\\
A_1&=d_{11}S_0+c_{11}S_1+d_{13}R_0+c_{13}R_1+d_{12}T_0+c_{12}T_1;\\
B_1&=b_{11}S_0+d_{11}S_1+c_{11}S_2+b_{13}R_0+d_{13}R_1+c_{13}R_2+\\
&\quad+b_{12}T_0+d_{12}T_1+c_{12}T_2;\\
B_2&=c_{11}S_3+c_{13}R_3+c_{12}T_3;\\
C_1&=b_{11}S_1+d_{11}S_2+c_{11}S_4+b_{13}R_1+d_{13}R_2+c_{13}R_4+\\
&\quad+b_{12}T_1+d_{12}T_2+c_{12}T_4;\\
C_2&=d_{11}S_3+c_{11}S_5+d_{13}R_3+c_{13}R_5+d_{12}T_3+c_{12}T_5;\\
D_1&=b_{11}S_2+d_{11}S_4+c_{11}S_6+b_{13}R_2+d_{13}R_4+c_{13}R_6+\\
&\quad+b_{12}T_2+d_{12}T_4+c_{12}T_6;\\
D_2&=b_{11}S_3+d_{11}S_5+c_{11}S_7+b_{13}R_3+d_{13}R_5+c_{13}R_7+\\
&\quad+b_{12}T_3+d_{12}T_5+c_{12}T_7;\\
D_3&=c_{11}S_8;\\
E_1&=b_{11}S_4+d_{11}S_6+b_{13}R_4+d_{13}R_6+b_{12}T_4+d_{12}T_6;\\
E_2&=b_{11}S_5+d_{11}S_7+b_{13}R_5+d_{13}R_7+b_{12}T_5+d_{12}T_7;\\
E_3&=d_{11}S_8;\\
F_1&=b_{11}S_6+b_{13}R_6+b_{12}T_6;\\
F_2&=b_{11}S_7+b_{13}R_7+b_{12}T_7;\\
F_3&=b_{11}S_8,
\end{aligned}\right\}\qquad(6.29)$$

/407

where

$$\left.\begin{aligned}
S_0&=c_{22}c_{33}-c_{23}c_{32};\\
S_1&=c_{22}d_{33}+c_{33}d_{22}-c_{23}d_{32}-c_{32}d_{23};\\
S_2&=b_{22}c_{33}+b_{33}c_{22}+d_{22}d_{33}-b_{23}c_{32}-b_{32}c_{23}-d_{23}d_{32};\\
S_3&=a_{22}c_{33}+a_{33}c_{22};\\
S_4&=b_{22}d_{33}+b_{33}d_{22}-b_{23}d_{32}-b_{32}d_{23};\\
S_5&=a_{22}d_{33}+a_{33}d_{22};\\
S_6&=b_{22}b_{33}-b_{23}b_{32};\\
S_7&=a_{22}b_{33}+a_{33}b_{22};\\
S_8&=a_{22}a_{33};\\
R_0&=c_{21}c_{32}-c_{22}c_{31};\\
R_1&=c_{21}d_{32}+c_{32}d_{21}-c_{22}d_{31}-c_{31}d_{22};\\
R_2&=b_{21}c_{32}+b_{32}c_{21}+d_{21}d_{32}-b_{22}c_{31}-b_{31}c_{22}-d_{22}d_{31};\\
R_3&=-a_{22}a_{31};\\
R_4&=b_{21}d_{32}+b_{32}d_{21}-b_{22}d_{31}-b_{31}d_{22};\\
R_5&=-a_{22}d_{31};\\
R_6&=b_{21}b_{32}-b_{22}b_{31};
\end{aligned}\right\}\qquad(6.30)$$

$$
\left.
\begin{aligned}
R_7 &= -a_{22}b_{31};\\
T_0 &= c_{23}c_{31} - c_{21}c_{33};\\
T_1 &= c_{23}d_{31} + c_{31}d_{23} - c_{21}d_{33} - c_{33}d_{21};\\
T_2 &= b_{23}c_{31} + b_{31}c_{23} + d_{23}d_{31} - b_{21}c_{33} - b_{33}c_{21} - d_{21}d_{33};\\
T_3 &= -a_{33}c_{21};\\
T_4 &= b_{23}d_{31} + b_{31}d_{23} - b_{21}d_{33} - b_{33}d_{21};\\
T_5 &= -a_{33}d_{21};\\
T_6 &= b_{23}b_{31} - b_{21}b_{33};\\
T_7 &= -a_{33}b_{21}
\end{aligned}
\right\}
$$

The roots of the characteristic equation (6.28) can be determined by means of any standard program available for digital computers of any type. Such a program can include the operation of computing the coefficients of the characteristic equation directly from the coefficients of eq.(6.16). In this case, eqs.(6.29) need not be used.

The values of the angular velocity ω corresponding to the limits of flutter can be obtained also directly if, in the characteristic equation (6.28), we set $\lambda = ip$ and equate to zero the real and imaginary parts of the equation separately.

The equations thus obtained will have the following form:

$$L_1(\omega, p) = p^6 A_0 - p^4(\omega^2 B_1 + B_2) + p^2(\omega^4 D_1 + \omega^2 D_2 + D_3) - \\ - \omega^2(\omega^4 F_1 + \omega^2 F_2 + F_3) = 0; \tag{6.31}$$

$$L_2(\omega, p) = p^4 A_1 - p^2(\omega^2 C_1 + C_2) + \omega^4 E_1 + \omega^2 E_2 + E_3 = 0. \tag{6.32}$$

If, from the equation $L_2(\omega, p) = 0$, we determine $p = f(\omega)$ and substitute into the equation $L_1(\omega, p) = 0$, then the points of intersection of the obtained curve $L_1(\omega) = 0$ with the abscissa will correspond to the limits of flutter.

6. Calculation of Flutter with Three Degrees of Freedom Disregarding Blade Torsion

/408

All the formulas presented above are appreciably simplified if we assume that the rotor blade is absolutely rigid in torsion. It was noted above that this assumption is valid for all rotors for which the torsional rigidity of the blade is appreciably higher than the rigidity of the blade pitch control system. In this case, during torsional vibrations the blade elements rotate mainly as a consequence of deformations of the control system and, to a lesser degree, owing to deformations of the blade itself.

Consideration of a variation in the angle of rotation of the blade with respect to length leads to a minor change of certain coefficients of eq.(6.18) [see eqs.(6.21), (6.23), and (6.27)]. This is explained by the fact that the magnitudes of the integrals entering the expressions of these coefficients are determined mainly by the blade tip which is subject to large aerodynamic forces,

while the change in the angle of rotation ϑ over the length of only the blade tip is insignificant. Therefore, the assumption of constancy of the angles of rotation of the blade cross sections over its length, in many cases, will not lead to substantial errors. At the same time, this assumption appreciably simplifies all computations, since $\vartheta = 1$ and there is no need to decompose the angle of rotation of each blade section into ϑ and $\varkappa y_0'$.

The differential equations of motion for this case can be written in the following manner:

$$\left.\begin{aligned} &m\ddot{y}+[EIy'']''-[Ny']'-m\sigma\ddot{\varphi}- \\ &-\frac{1}{2}c_y^{\alpha}\rho b\left[U^2\varphi+\left(\frac{3}{4}b-x_0\right)U\dot{\varphi}+U\dot{y}\right]=0, \\ &I_{a.h}\ddot{\varphi}+\omega^2 I_{a.h}\varphi+c_{con}(\varphi+\varkappa y_0')+M_{fr}+ \\ &+\int_0^R\left\{\frac{\pi}{16}\rho b^3U\dot{\varphi}+\frac{1}{2}c_y^{\alpha}\rho b\sigma_f\left[U^2\varphi+\right.\right. \\ &\left.\left.+\left(\frac{3}{4}b-x_0\right)U\dot{\varphi}-U\dot{y}\right]-m\sigma\ddot{y}\right\}dr- \\ &-\omega^2\int_0^R mr\sigma y'dr=0. \end{aligned}\right\} \qquad (6.33)$$

The variable φ here represents the total angle of rotation of the blade relative to the feathering hinge as a consequence of deformations of the control and as a result of the kinematic action of the flapping compensator.

The solution to this system of equations, just as for the system (6.10), can be obtained by means of B.G.Galerkin's method, if we put

$$y=\sum_j \delta_j y^{(j)};$$

$$\varphi=\varphi_0,$$

where φ_0 is a function only of time and does not depend on the blade radius.

Let us write out the computational formulas for the case where the vibration mode in the flapping plane is represented by means of only the zero r and the first y harmonics of the natural blade vibrations. In this case, the coefficients of the matrices entering the equation of the form of eq.(6.16) can be determined by the following expressions: /409

a) Inertia coefficient matrix C:

$$C=\begin{bmatrix} c_{11} & c_{12} & 0 \\ c_{21} & c_{22} & c_{23} \\ 0 & c_{32} & c_{33} \end{bmatrix}, \qquad (6.34)$$

where

$$\left.\begin{aligned} c_{11}&=1;\\ c_{12}&=-\frac{1}{I_{h.h}}\int_0^R m\sigma r dr;\\ c_{21}&=-\frac{1}{I_{a.h}}\int_0^R m\sigma\, r dr;\\ c_{22}&=1;\\ c_{23}&=-\frac{1}{I_{a.h}}\int_0^R m\sigma y\, dr;\\ c_{32}&=-\frac{1}{I_1}\int_0^R m\sigma y\, dr;\\ c_{33}&=1; \end{aligned}\right\} \qquad (6.35)$$

b) Damping coefficient matrix D:

$$D=\begin{bmatrix} d_{11} & d_{12} & d_{13}\\ d_{21} & d_{22} & d_{23}\\ d_{31} & d_{32} & d_{33} \end{bmatrix}, \qquad (6.36)$$

where

$$\left.\begin{aligned} d_{11}&=\frac{1}{2}c_y^{\alpha}\varrho\frac{1}{I_{h.h}}\int_0^R br^3dr;\\ d_{12}&=-\frac{1}{2}c_y^{\alpha}\varrho\frac{1}{I_{h.h}}\int_0^R b^2\left(\frac{3}{4}-\frac{x_0}{b}\right)r^2dr;\\ d_{13}&=\frac{1}{2}c_y^{\alpha}\frac{\varrho}{I_{h.h}}\int_0^R br^2y\, dr;\\ d_{21}&=-\frac{1}{2}c_y^{\alpha}\frac{\varrho}{I_{a.h}}\int_0^R b\sigma_f r^2dr;\\ d_{22}&=\frac{1}{I_{a.h}}\left[\frac{\pi}{16}\varrho\int_0^R b^3rdr+\frac{1}{2}c_y^{\alpha}\varrho\times\right.\\ &\left.\times\int_0^R b^2\sigma_f r\left(\frac{3}{4}-\frac{x_0}{b}\right)dr\right]+d_{fr};\\ d_{23}&=-\frac{1}{2}c_y^{\alpha}\frac{\varrho}{I_{a.h}}\int_0^R b\sigma_f ry dr; \end{aligned}\right\} \qquad (6.37)$$

/410

$$
\left.
\begin{aligned}
d_{31} &= \frac{1}{2} c_y^{\alpha} \frac{\varrho}{I_1} \int_0^R br^2 y \, dr; \\
d_{32} &= -\frac{1}{2} c_y^{\alpha} \frac{\varrho}{I_1} \int_0^R b^2 \left(\frac{3}{4} - \frac{x_0}{b} \right) ry \, dr; \\
d_{33} &= \frac{1}{2} c_y^{\alpha} \frac{\varrho}{I_1} \int_0^R br \, y^2 dr;
\end{aligned}
\right\}
$$

c) Stiffness matrix A:

$$
A = \begin{bmatrix} 0 & 0 & 0 \\ a_{21} & a_{22} & a_{23} \\ 0 & 0 & a_{33} \end{bmatrix}, \tag{6.38}
$$

where

$$
\left.
\begin{aligned}
a_{21} &= \varkappa p_{tw}^{\prime 2}; \\
a_{22} &= p_{tw}^{\prime 2} = \frac{c_{con}}{I_{a.h}}; \\
a_{23} &= \varkappa \beta_0 p_{tw}^2; \\
a_{33} &= p_{0_1}^2;
\end{aligned}
\right\} \tag{6.39}
$$

d) Centrifugal and aerodynamic stiffness matrix B:

$$
B = \begin{bmatrix} b_{11} & b_{12} & 0 \\ b_{21} & b_{22} & b_{23} \\ 0 & b_{32} & b_{33} \end{bmatrix}, \tag{6.40}
$$

where

$$
\left.
\begin{aligned}
b_{11} &= 1; \\
b_{12} &= -\frac{1}{2} c_y^{\alpha} \frac{\varrho}{I_{h.h}} \left[\int_0^R br^3 dr + \frac{1}{2} \mu^2 R^2 \int_0^R br dr \right]; \\
b_{21} &= -\frac{1}{I_{a.h}} \int_0^R m\sigma r dr; \\
b_{22} &= 1 + \frac{1}{2} c_y^{\alpha} \frac{\varrho}{I_{a.h}} \left[\int_0^R b\sigma_f r^2 \, dr + \frac{1}{2} \mu^2 R^2 \int_0^R b\sigma_f \, dr \right]; \\
b_{23} &= -\frac{1}{I_{a.h}} \int_0^R m\sigma r^3 dr; \\
b_{32} &= -\frac{1}{2} c_y^{\alpha} \frac{\varrho}{I_1} \left[\int_0^R br^2 y \, dr + \frac{1}{2} \mu^2 R^2 \int_0^R by \, dr \right];
\end{aligned}
\right\} \tag{6.41}
$$

$$b_{33}=k=\frac{\int_0^R \beta^2 \int_r^R mrdr}{I_1}.$$

The characteristic equations for this case will have the same form as in the preceding case [see eq.(6.28)]: /411

$$\lambda^6 A_0+\lambda^5\omega A_1+\lambda^4(\omega^2 B_1+B_2)+\lambda^3\omega(\omega^2 C_1+C_2)+\lambda^2(\omega^4 D_1+\omega^2 D_2+D_3)+ \\ +\lambda\omega(\omega^4 E_1+\omega^2 E_2+E_3)+\omega^2(\omega^4 F_1+\omega^2 F_2+F_3)=0. \tag{6.42}$$

Here,

$$\begin{aligned}
A_0&=c_{11}S_0+c_{12}T_0;\\
A_1&=d_{11}S_0+c_{11}S_1+d_{13}R_0+d_{12}T_0+c_{12}T_1;\\
B_1&=b_{11}S_0+d_{11}S_1+c_{11}S_2+d_{13}R_1+b_{12}T_0+d_{12}T_1+c_{12}T_2;\\
B_2&=c_{11}S_3+c_{12}T_3;\\
C_1&=b_{11}S_1+d_{11}S_2+c_{11}S_4+d_{13}R_2+b_{12}T_1+d_{12}T_2+c_{12}T_4;\\
C_2&=d_{11}S_3+c_{11}S_5+d_{13}R_3+d_{12}T_3+c_{12}T_5;\\
D_1&=b_{11}S_2+d_{11}S_4+c_{11}S_6+d_{13}R_4+b_{12}T_2+d_{12}T_4+c_{12}T_6;\\
D_2&=b_{11}S_3+d_{11}S_5+c_{11}S_7+d_{13}R_5+b_{12}T_3+d_{12}T_5+c_{12}T_7;\\
D_3&=c_{11}S_8+c_{12}T_8;\\
E_1&=b_{11}S_4+d_{11}S_6+d_{13}R_6+b_{12}T_4+d_{12}T_6;\\
E_2&=b_{11}S_5+d_{11}S_7+d_{13}R_7+b_{12}T_5+d_{12}T_7;\\
E_3&=d_{11}S_8+d_{12}T_8;\\
F_1&=b_{11}S_6+b_{12}T_6;\\
F_2&=b_{11}S_7+b_{12}T_7;\\
F_3&=b_{11}S_8+b_{12}T_8,
\end{aligned} \tag{6.43}$$

where

$$\begin{aligned}
S_0&=c_{22}c_{33}-c_{23}c_{32};\\
S_1&=c_{22}d_{33}+c_{33}d_{22}-c_{23}d_{32}-c_{32}d_{23};\\
S_2&=b_{22}c_{33}+b_{33}c_{22}+d_{22}d_{33}-d_{23}d_{32}-b_{23}c_{32}-b_{32}c_{23};\\
S_3&=a_{22}c_{33}+a_{33}c_{22}-a_{23}c_{32};\\
S_4&=b_{22}d_{33}+b_{33}d_{22}-b_{23}d_{32}-b_{32}d_{23};\\
S_5&=a_{22}d_{33}+a_{33}d_{22}-a_{23}d_{32};\\
S_6&=b_{22}b_{33}-b_{23}b_{32};\\
S_7&=a_{22}b_{33}+a_{33}b_{22}-a_{23}b_{32};\\
S_8&=a_{22}a_{33};\\
R_0&=c_{21}c_{32};\\
R_1&=c_{21}d_{32}+c_{32}d_{21}-c_{22}d_{31};\\
R_2&=b_{21}c_{32}+b_{32}c_{21}+d_{21}d_{32}-d_{22}d_{31};
\end{aligned} \tag{6.44}$$

$$R_3 = a_{21}c_{32};$$
$$R_4 = b_{21}d_{32} + b_{32}d_{21} - b_{22}d_{31};$$
$$R_5 = a_{21}d_{32} - a_{22}d_{31};$$
$$R_6 = b_{21}b_{32};$$
$$R_7 = a_{21}b_{32};$$

/412

$$T_0 = -c_{21}c_{33};$$
$$T_1 = c_{23}d_{31} - c_{21}d_{33} - c_{33}d_{21};$$
$$T_2 = d_{23}d_{21} - b_{21}c_{33} - b_{33}c_{21} - d_{21}d_{33};$$
$$T_3 = -a_{21}c_{33} - a_{33}c_{21};$$
$$T_4 = b_{23}d_{31} - b_{21}d_{33} - b_{33}d_{21};$$
$$T_5 = a_{23}d_{31} - a_{21}d_{33} - a_{33}d_{21};$$
$$T_6 = -b_{21}b_{33};$$
$$T_7 = -a_{21}b_{33} - a_{33}b_{21};$$
$$T_8 = -a_{21}a_{33}.$$

The values of the critical angular velocities of a given case are determined by simultaneous solution of two equations obtained from eq.(6.42) if we set $\lambda = ip$, as in the case of the blade elastic in torsion.

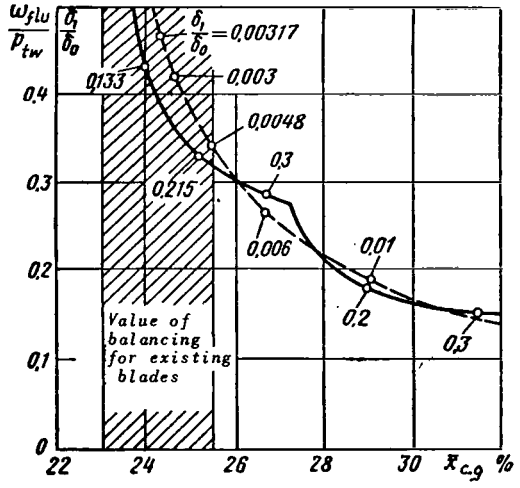

Fig.4.27 Critical Flutter Rpm as a Function of Blade Balancing, for Two Values of its Flexural Rigidity.

7. Calculation Results

To illustrate the effect of flexural rigidity of a blade, Fig.4.27 gives the critical flutter rpm as a function of $\bar{x}_{c.g}$ for a blade of mass constant over its length and with balancing. The curves are plotted for two values of flexural rigidity of the blade. The degree of rigidity is characterized by the values of the frequency of natural bending vibrations of the first harmonic of a nonrotating blade p_{o_1}. The cases investigated are those of blades with the usual magnitude of flexural rigidity, at $p_{o_1}/p_{tw} = 0.3$ (solid curve) and of $p_{o_1}/p_{tw} = 3.0$ which corresponds to a very rigid blade (broken curve).

The share of bending in the mode of blade vibrations during flutter can be estimated from the ratios δ_1/δ_0 plotted for a number of points on the same graph. The quantity δ_1/δ_0 is equal to the ratio of the blade tip deflection in bending relative to the shape of the first harmonic to the displacement of the /413

tip during vibration of the blade as a solid body (shape of the zero harmonic).

It follows from these data that for a blade with constant mass and balancing over its length, consideration of flexural deformations with respect to the first harmonic does not greatly refine the calculation results.

8. Bending Flutter

The results presented above cannot be extended to all designs of rotor blades. In individual cases, vibrations with primarily bending of the blade occur during flutter. This type of flutter is usually called "bending flutter".

In bending flutter, the blade vibrates in the flapping plane with a mode close to some harmonic of the natural vibration of the blade in bending and is twisted with respect to a mode close to that of the first harmonic of the natural vibrations in torsion. As already noted, flutter with modes of subsequent harmonics of natural vibrations of the blade in torsion is theoretically also possible. However, the critical rpm of such flutter is several times greater than the maximum rotor rpm.

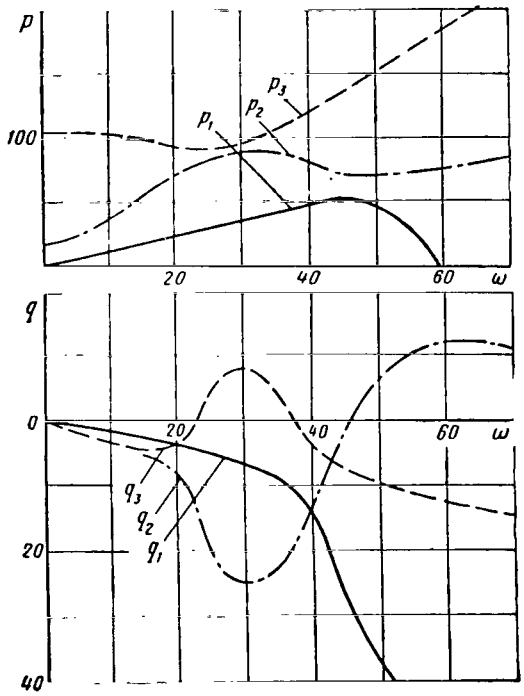

Fig.4.28 Variation of the Real and Imaginary Parts of the Roots of the Characteristic Equation as a Function of Rotor Rpm.

The previously examined flapping flutter can be regarded as a particular case of bending flutter in which the blade vibrates with a mode close to that of the zero harmonic of natural vibrations of the blade in the flapping plane.

To each harmonic of bending vibrations of the blade there corresponds a separate flutter zone in which the vibrations are characterized by specific parameters inherent only to this zone. Blade vibrations with different modes of flutter may occur quite independently. The mode of flutter having the lowest critical rpm is practically the first to be detected. Most often, this form is the flapping mode of flutter. However, we can mention a number of particular cases in which the critical rpm of some bending mode of flutter proved to be below the critical rpm of the flapping mode.

As an example, let us discuss flutter of a blade with tip loading. This case is of practical interest for jet helicopters with an engine installed at the blade tip*.

* For footnote see next page.

Figure 4.28 shows the change of the real and imaginary part of the roots of the characteristic equation (6.42) with respect to rotor rpm. The roots of the characteristic equation (6.42) were calculated for a blade with a tip loading approximately equal to the weight of the blade itself.

Figure 4.28 indicates that, in this case, there are two flutter zones; the flutter zone appearing first relative to rotor rpm is distinguished by a vibration mode having a high content of blade bending. Therefore, this zone is usually called the zone of bending flutter.

It is possible to trace the manner in which the zone with the vibration /414
mode having an increasing share of bending with increasing tip loading begins to separate from the zone of flapping flutter as the blade-tip loading gradually increases. At certain loading, these zones may separate into two different flutter zones.

Figure 4.29 shows the flutter zone at a relatively small tip loading, equal approximately to 1/5 of the blade weight. In this case, the characteristic form of the zone of flapping flutter is distorted and the second zone begins to separate from it.

Figures 4.30 and 4.31 show the flutter zones for a blade with a tip loading equal to 42% of the blade weight $\left(\frac{G_{to}}{G_b} = 0.42\right)$ and approximately equal to the blade weight $\left(\frac{G_{to}}{G_b} = 1.1\right)$. In the latter case, the flutter zone separates into two different zones of flapping and bending flutter.

Figures 4.29, 4.30, and 4.31 give the values of $\bar{\delta} = \frac{\delta_1}{\delta_0}$ characterizing the vibration mode on flutter and the quantities $\bar{p}$ representing the ratios of flutter frequency to rotor rpm:

$$\bar{p} = \frac{p_{flu}}{n_{flu}}.$$

It is of interest that the share of the flapping mode of vibration in /416
the bending flutter remains rather large in all cases, whereas the share of bending in the flapping flutter may be almost completely absent in certain cases.

It should be emphasized that, for blades with tip loading, the critical rpm of bending flutter is appreciably below the critical rpm of flapping flutter, and that there is a weak dependence of critical rpm on the blade balancing. This fact greatly complicates the problem of developing blades for jet helicopters.

---

* The results of the calculations given here (in Subsects.7 and 8) were obtained by V.M.Pchelkin.

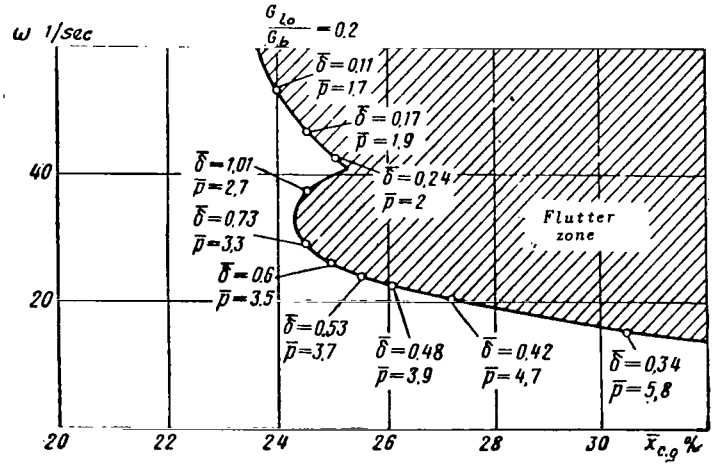

Fig.4.29 Flutter Zones with Blade Tip Loading Referred to Blade Weight $\frac{G_{1o}}{G_b}$ = 0.20

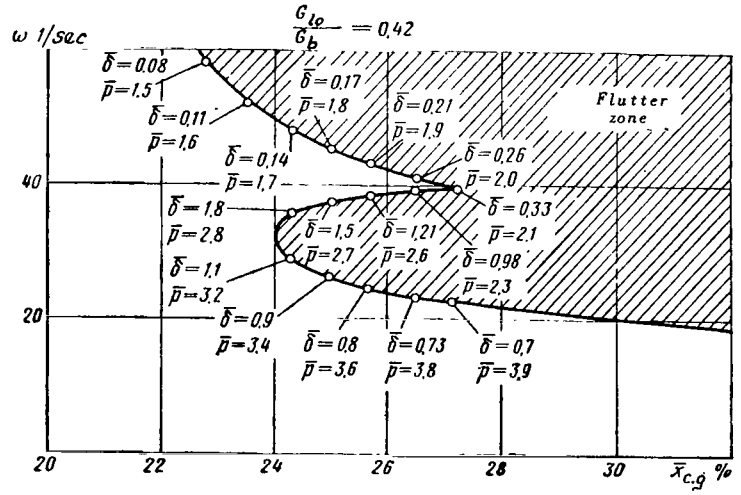

Fig.4.30 Flutter Zones with Blade Tip Loading Referred to Blade Weight $\frac{G_{1o}}{G_b}$ = 0.42.

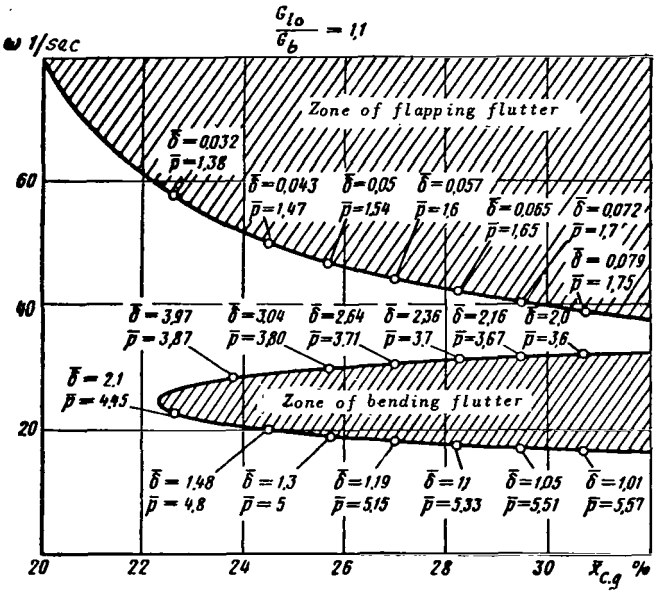

Fig.4.31 Flutter Zones with Blade Tip Loading Referred to Blade Weight $\frac{G_{lo}}{G_b} = 1.1$.

9. Approximate Method of Determining the Mode of Bending Vibrations in Flutter

If, in the first equation of the system (6.33), we discard terms of blade vibration damping as well as the small term $m\omega\ddot{\varphi}$, then we can write this equation in the form

$$m\ddot{y} + [EIy'']'' - [Ny']' = \frac{1}{2} c_y^{\alpha} \rho b U^2 \varphi. \qquad (6.45)$$

Setting approximately $U \cong \omega r$, we can represent the solution in the form

$$\left.\begin{aligned} \varphi &= \sin p_{flu} t, \\ y &= y_{ben} \sin p_{flu} t, \end{aligned}\right\} \qquad (6.46)$$

where p_{flu} is the vibration frequency of flutter.

The calculations of bending flutter show that the frequency p_{flu} can be approximately set equal to the frequency of natural vibration of the blade in torsion and twist, i.e., $p_{flu} \cong p_{tw}$.

We assume that /417

$$y_{ben} = \sum_j \delta_j y^{(j)}, \qquad (6.47)$$

where

δ_j = coefficients of deformations;

$\bar{y}^{(j)}$ = mode of the j-th harmonic of the natural blade vibration.

Substituting eq.(6.47) into eq.(6.45) and applying B.G.Galerkin's method, we obtain expressions for determining the coefficients of deformation δ_j:

$$\frac{\delta_j}{R} = \frac{\gamma_j A_j}{\left(\frac{p_j}{\omega}\right)^2 - \left(\frac{p_{flu}}{\omega}\right)^2}. \tag{6.48}$$

Here,

$$A_j = \int_0^1 \bar{b}_r \bar{r}^2 \bar{y}^{(j)} d\bar{r}; \tag{6.49}$$

$$\gamma_j = \frac{\frac{1}{2} c_y^{\alpha} \varrho b_{0,7} R^2}{m_j^{eq}}, \tag{6.50}$$

where

$$m_j^{eq} = \int_0^R m \left[\bar{y}^{(j)}\right]^2 dr \tag{6.51}$$

is called the equivalent mass of the blade during its vibration relative to the shape of the j-th harmonic.

γ_j = mass characteristic of the blade during vibration relative to the same harmonic;

p_j = frequency of the j-th harmonic of natural vibration of the blade in bending; for the zero harmonic $y^{(0)}$, we can set $p_j = \omega$.

It follows from eq.(6.48) that the share of one or another harmonic of bending vibrations in the mode of flutter depends primarily on two parameters: relation of flutter frequency and frequency of natural vibration of the corresponding harmonic, and magnitude of the integral A_j.

For example, the share of the flapping vibration mode (j = 0) in the mode of flutter is smaller, the higher the "harmonic" of flutter, i.e., the ratio of flutter frequency to rotor rpm. Here, we should note that since A_0 is always greater than zero, i.e.,

$$A_0 \cong \int_0^1 \bar{b}_r \bar{r}^3 d\bar{r} > 0,$$

then the flapping mode will always be present in the vibration mode during flutter. This conclusion is rather important and indicates, in particular, that it would be incorrect to calculate flutter of some vibration mode without consideration of the flapping mode.

The content of the first-harmonic natural vibration mode in bending increases as the frequencies of the natural vibrations in bending p_1 and the frequency of flutter p_{flu} close to the frequency of natural blade vibrations in

torsion are approached.

However, in this case the magnitude of the integral A_1 is very substantial:

$$A_1 = \int_0^1 \bar{b}\bar{r}^2 y^{(1)} d\bar{r}.$$

The calculation of this integral shows that, for the vast majority of blades, this integral is close to zero so that the content of the first-harmonic natural vibration mode in the vibration mode with the frequency p_{flu} is quite small. This explains the relatively rare appearance of bending flutter. /418

A quite different picture arises when concentrated loads are mounted to the blade tip. The node of the shape of the first harmonic in this case shifts toward the blade tip and the absolute value of the integral A_1 begins to increase. Correspondingly, this causes an increase in the content of the first harmonic in the vibration mode with a frequency p_{flu}.

Having assumed approximately that the vibration mode during flutter can be calculated in a form of eq.(6.47) where the coefficients are calculated by means of eq.(6.48), we can develop a simplified calculation method for bending flutter.

Section 7. General Method of Calculation of Flutter and Bending Stresses in the Rotor Blade during Flight

1. Calculation Method and its Possibilities

All methods presented above for the calculation of flutter were based on a number of assumptions which, in many cases, it would be desirable to discard. These assumptions include the following:

1) In the calculation of aerodynamic forces, the nonlinear dependence of the aerodynamic coefficients on the profile angle of attack was disregarded. Consideration of this dependence may have a substantial effect on the critical rpm and especially on the character of amplitude build-up of oscillations in flutter.

2) In calculating the aerodynamic forces under conditions of forward flight, the flow compressibility was accounted for by introducing only values of c_y^{α} and x_f averaged with respect to the rotor azimuth. Under conditions of forward flight these quantities periodically change with respect to rotor azimuth, which may have a noticeable effect on the critical flutter rpm.

3) Consideration of the forces of friction in the feathering hinge, which - as is known - have a strong effect on the critical flutter rpm, was quite arbitrarily done, by linearization of these forces.

In this Section, we will derive a method for calculating the bending and twisting (binary) blade vibrations of a helicopter in flight, which permits discarding these assumptions. This method makes it possible to determine the

bending stresses acting on the blade in the absence of rotor flutter and at stable blade vibrations. If flutter is possible in the operating regime of the rotor under consideration, then calculation by this method permits determining the process of divergent blade vibrations and thus investigating the phenomenon of flutter.

The calculation method is based on the approximate solution of differential equations of blade vibration. In this case, B.G.Galerkin's method is used for determining the form of blade deformations at some instant of time, while the method of numerical integration of differential equations is applied for determining the overall process of blade motion with respect to time. B.G.Galerkin's method permits transforming the system of partial differential equations into a system of ordinary differential equations and to use numerical integration for solving this transformed system.

As applied to stress analysis, the method permits accounting for torsional deformations of the blade in calculating the bending stresses in the flapping plane. Under the effect of constant and variable external forces in flight, the helicopter blade is twisted through some angle ϑ which is time-variant and differs with respect to blade length. Torsional deformations of the blade change the angle of attack of its sections, which in turn leads to the generation of additional constant and variable aerodynamic forces. These auxiliary forces must be taken into consideration when calculating the bending stresses of the blade. If this is not done, good agreement between calculation and experimental data is quite impossible. /419

When applied to flutter calculations, the proposed method is not too convenient in practical application, since it does not permit an exact numerical determination of the parameters characterizing the limit of flutter. The flutter limit can be established only in first approximation by visual inspection of curves describing the blade motion for parameters close to this limit; similarly, it is impossible to determine, with the required accuracy, the margins of flutter based on parameters used in practice for evaluating the rotor from the safety angle. The described method basically permits only a determination whether or not flutter occurs in the flight regime under consideration and a description of its evolution.

Nevertheless, the method has a number of important advantages in comparison with methods that use the roots of the characteristic equation and generally investigate flutter only in a linear array. It is difficult to imagine any other method which would permit such a complete and accurate consideration of all nonlinear dependences, both in the magnitudes of aerodynamic forces and in determining friction forces, as is offered by this method in combination with numerical integration of the equations with respect to time. Consideration of these dependences is highly important for flutter calculations. Therefore, it is preferably used in control tests and check calculations, after determining the flutter parameters by means of the roots of the characteristic equation.

Of great importance for practical use is the fact that this method, without excessive complication of the calculation, permits considering the elastic couple between blades through the automatic pitch control, even at different rigidity of the longitudinal and lateral controls. Without consideration of

this couple, a calculation of torsional deformations of the blade cannot lay claim to accuracy.

2. Basic Assumptions and Suggestions

To derive the differential equations of motion of the blade, let us examine the conventional type of rotor with individual hinge attachment of each blade to the hub and with control through the swashplate. In determining the angles of twist of the blades as a consequence of deformation of the control system, we will consider that the rigidity of the longitudinal and lateral control loops differ. We will consider deformations of all control loops of both cyclic and collective pitch control including deformation of the swashplate, which is necessary when external forces generated by the rotor blades are locked on the plate.

The motion of an individual rotor blade will be considered to consist of flapping and bending vibrations in the thrust plane and of torsional vibrations, both due to deformation of the blade and of the control system and to the kinematic action of the swashplate and flapping compensator. As above, we will disregard blade vibrations in the plane of rotation.

With respect to blade design, let us use the following stipulations: Let us consider that the flexural axis of the blade is rectilinear and coincides with the feathering hinge axis. The plane of least rigidity of the blade will be assumed to coincide with the flapping plane, i.e., with the plane going through the axis of rotation of the rotor and perpendicular to the axis of the flapping hinge. The flexural deformations of the blade will be determined in /420
this plane.

The rotor blade will be considered as a beam with the parameters continuously distributed over its length.

3. Differential Equations

With consideration of the above stipulations, the differential equations of blade vibration can be written in the following form:

$$\left.\begin{aligned} m\ddot{y}+[EIy'']''-[Ny']'-m\sigma\varphi+\omega^2[m\sigma r\varphi]^{\sim}{}'=T,\\ I_m\ddot{\varphi}-[GT_{tw}\varphi']'+\omega^2 I_m\varphi-m\sigma\ddot{y}-\omega^2 m\sigma r y'=\mathfrak{M}_{aer}, \end{aligned}\right\} \qquad (7.1)$$

where

y = displacement of points of the elastic axis of the blade relative to the plane of rotation of the rotors;
φ = angle between the profile chord and plane of rotation of the rotor;
m = mass of the blade per unit length;
I_m = moment of inertia of the blade per unit length relative to its flexural axis;
EI = flexural rigidity of the blade;
GT_{tw} = torsional rigidity or twist of the blade;

σ = distance from the flexural axis of the blade to the centers of gravity of its elements, with the shift of the c.g. toward the trailing edge of the blade considered as positive;
ω = angular velocity of rotation of the rotor;
r = distance from the axis of rotation to the examined blade element;
N = centrifugal force in the blade section:

$$N=\omega^2\int_r^R mrdr;$$

T = aerodynamic load per unit length in the flapping plane;
$\mathfrak{M}_{aer}$ = aerodynamic torque per unit length relative to the flexural axis.

The method of determining the aerodynamic loads will be described in Subsection 6.

The dots in eqs.(7.1) denote differentiation with respect to time and the primes, with respect to the blade radius. In differentiating the function φ with respect to the radius we should not introduce the geometric twist of the blade into the value of φ', assuming that $\varphi' = \vartheta'$ where ϑ is the elastic angle of twist of the blade.

4. Boundary Conditions of the Problem

For the type of rotors discussed here, the boundary conditions in the blade root can be written in the form

$$\left.\begin{aligned} M_0&=[EIy'']_0=\varkappa[M_b+M_{fr}],\\ m_h\ddot{y}_0&=-\sum_N[EIy'']'_0,\\ M_b&=[GT_{tw}\varphi']_0=c_{eq}\gamma-M_{fr}, \end{aligned}\right\} \qquad (7.2)$$

where

M_0 = bending moment in the blade root;
M_b = external torque relative to the feathering hinge axis due to forces acting on the blade, with the pitching moment considered as positive;
$\varkappa$ = flapping compensator;
m_h = mass of the helicopter without blades; /421
$\sum_N[EIy'']'_0$ = sum of forces striking the helicopter hub from all rotor blades (the index N denotes the blade numeral);
M_{fr} = moment of friction acting on the blade in the feathering hinge from the side of the rotor hub, with the pitching moment considered as positive;
c_{eq} = equivalent rigidity of the control system reduced to the axial hinge of the hub (the method of determining this rigidity will be given in Subsect.5);
γ = angle of rotation of the blade root in the axial hinge of the hub, as a consequence of deformations of the control system.

In deriving these boundary conditions, friction was taken into account only in the axial hinge of the hub loaded by centrifugal forces. Usually, we can disregard friction in the other hinges of the hub and of the control system.

With a sufficient degree of accuracy, the second boundary condition of eq.(7.2) can be replaced by the condition

$$y_0 = 0. \tag{7.3}$$

5. Determination of Equivalent Rigidity of the Control System

To use the third boundary condition, we must determine the magnitude of the equivalent rigidity of the control system c_{eq}. This value can be determined if the angles of twist γ_N of all z_b blades of the rotor in the axial hinge of the hub are known.

The angle of rotation of the N-th blade of the rotor γ_N is related with the deformations of the individual control loops by formulas derived previously [see eq.(4.9)]:

$$\gamma_N = \gamma_{c.p} + \gamma_x \sin\psi_{a.p}^{(N)} + \gamma_z \cos\psi_{a.p}^{(N)} + \gamma_{a.p}^{(N)}, \tag{7.4}$$

where N = 0, 1, 2, 3, ..., z_b - 1.

Solution of the system (7.4) yields the following expressions for its unknown $\gamma_{c.p}$, γ_x, γ_z, and $\gamma_{a.p}^{(N)}$:

$$\left.\begin{aligned}
\gamma_{c.p} &= \frac{1}{z_b}\sum_N \gamma_N, \\
\gamma_x &= \frac{2}{z_b}\sum_N \gamma_N \sin\psi_{a.p}^{(N)}, \\
\gamma_z &= \frac{2}{z_b}\sum_N \gamma_N \cos\psi_{a.p}^{(N)}, \\
\gamma_{a.p}^{(N)} &= \gamma_N - \gamma_{c.p} - \gamma_x \sin\psi_{a.p}^{(N)} - \gamma_z \cos\psi_{a.p}^{(N)}.
\end{aligned}\right\} \tag{7.5}$$

The magnitude of the hinge moment acting on the blade from the control can be expressed in terms of rigidity and deformations of the corresponding control cables

$$M_{con} = c_{c.p}\,\gamma_{c.p} + c_x\gamma_x \sin\psi_{a.p}^{(N)} + c_z\gamma_z \cos\psi_{a.p}^{(N)} + c_{a.p}\gamma_{a.p}^{(N)}, \tag{7.6}$$

where $c_{c.p}$, c_x, c_z, and $c_{a.p}$ are the rigidities of the collective pitch control, lateral and longitudinal controls, and swashplate, respectively, reduced to the axial hinge of the blade.

If we represent the magnitude of the hinge moment due to the control in /422

the form

$$M_{con}^{(N)} = c_{eq}^{(N)} \gamma_N, \tag{7.7}$$

then the equivalent control rigidity can be determined by the formula

$$c_{eq}^{(N)} = c_{c.p}\,\bar{\gamma}_{c.p} + c_x \bar{\gamma}_x \sin\psi_{a.p}^{(N)} + c_z \bar{\gamma}_z \cos\psi_{a.p}^{(N)} + c_{a.p}\bar{\gamma}_{a.p}^{(N)}, \tag{7.8}$$

where the vinculum denotes that the given magnitude of twist pertains to the value γ_N.

6. Determination of Aerodynamic Forces

To solve a system of differential equations (7.1), it is necessary to determine the aerodynamic forces and torque entering the equation.

It is known that, during flow past the blade profile in flight, the angles of attack of its sections may vary within wide limits, even to the extent that - on the retreating blade - the flow passes over its root parts from the side of the trailing edge. Flow-separation conditions occur at the blade tip in certain regimes. At high flying speeds and at appreciable peripheral rate of rotation of the rotor, the effect of flow compressibility has a considerable influence on the magnitude of the aerodynamic forces. Therefore, a determination of aerodynamic forces acting on the helicopter blade should take into account the nonlinear dependence of the aerodynamic coefficients on the angle of attack α and the Mach number. Correspondingly, the expressions for determining the aerodynamic forces should be written with consideration of the possibility of a wide change in the angles of attack. At the same time, we can make use of the generally employed assumption of smallness of the displacements y and angles of rotation of the blade sections φ. Therefore, to determine the aerodynamic forces the following expressions can be used:

$$\begin{aligned} T &= \frac{1}{2}\varrho b (c_y U_x + c_x U_y) U + \pi \varrho b \left(\frac{3}{4} b - x_0\right) U\dot{\varphi}, \\ \mathfrak{M}_{aer} &= x_0 T + \frac{1}{2}\varrho b \left(m_z b U - \frac{\pi}{8} b^2 \dot{\varphi}\right) U, \end{aligned} \tag{7.9}$$

where

c_y and c_x = aerodynamic lift and drag coefficients;
m_z = torque coefficient of the profile, with c_y, c_x, and m_z determined from the results of downwash exposure as a function of the section angle of attack α and M;
ρ = air density;
b = blade chord in the examined section;
x_0 = distance from the leading edge to the flexural axis of the blade;
U_x and U_y = mutually perpendicular relative velocity components of the flow in a plane normal to the elastic axis of the blades, with U_x being parallel to the plane of rotation of the rotor and U_y perpendicular to U_x;

U = total magnitude of the relative velocity of flow past a profile in a plane normal to the elastic axis of the blade.

The magnitude of the relative velocity U can be determined in terms of its components /423

$$U=\sqrt{U_x^2+U_y^2}, \tag{7.10}$$

where

$$U_x=\omega r+V\cos\alpha_h\sin\psi_b; \tag{7.11}$$

$$U_y=\omega R\lambda-\dot{y}-V\cos\alpha_h\cos\psi_b\beta. \tag{7.12}$$

Here,

ωR = tip speed of the blade;
V = flying speed of the helicopter;
α_h = angle of attack of the helicopter rotor in the shaft axes, i.e., angle between direction of flight and plane of rotation of the rotor;
ψ_b = azimuth angle of the blade;
$\beta = y'$ = angle of inclination of the elastic axis of the blade in the flapping plane;
λ = velocity of flow through the rotor referred to the peripheral blade tip speed ωR, with the direction of λ coinciding with the axis of the rotor shaft; when the flow passes through the rotor from the bottom up, λ is considered positive.

The relative velocity of flow is determined by the formula

$$\lambda=\mu tan\alpha_h+v_{ind}, \tag{7.13}$$

where

$$\mu=\frac{V\cos\alpha_h}{\omega R}.$$

Here, v_{ind} is the induced part of the velocity of flow, also referred to ωR.

The induced velocity v_{ind} is a variable with respect to the rotor disk area and to time.

In a number of flight regimes, the variable part of the induced velocity increases so much as to lead to the occurrence of appreciable variable stresses in the blade (see Sect.8, Chapt.I of Vol.II). To determine stresses in the blade with consideration of the variable field of induced velocities, it is suggested to use the calculation method which involves calculation of the induced velocities. If we limit ourselves to a consideration of only the constant component of the induced velocity, then its value can be determined from the formula

$$v_{oav}=-\frac{C_T}{4\sqrt{\mu^2+(\lambda_{oav})^2}}, \tag{7.14}$$

where

v_{0av} and λ_{0av} = components of the induced velocity and flow-through velocity, constant with respect to the azimuth and average with respect to the radius of the blade;

C_T = thrust coefficient of the rotor:

$$C_T = \frac{T_{rot}}{\frac{1}{2}\varrho F(\omega R)^2}. \tag{7.15}$$

Here,

T_{rot} = rotor thrust;

F = rotor area.

The angle of attack of the blade sections, needed to determine the aerodynamic coefficients, can be calculated as

$$\alpha = \varphi + \Phi, \tag{7.16}$$

where

φ = angle of setting of the blade profile;

Φ = angle of inflow: /424

$$\Phi = tan^{-1}\frac{U_y}{U_x}. \tag{7.17}$$

The angle of setting φ is a variable with respect to both blade radius and time. It consists of two parts:

$$\varphi = \eta + \vartheta, \tag{7.18}$$

where

η = angle of rotation of the blade in the feathering hinge as a consequence of the kinematic action of the swashplate and the flapping compensator, including also the geometric twist of the blades;

ϑ = angle of elastic twist of the blade, with the angle ϑ determined by solving the system of differential equations (7.1).

The angle η is determined by the expression:

$$\eta = \theta_0 + \Delta\varphi_{geom} - \theta_1 \sin\psi_b - \theta_2 \cos\psi_b - \kappa\beta_0. \tag{7.19}$$

Here,

θ_0 = angle of setting of some blade section taken as the point of reference at $\beta_0 = 0$; this angle is usually called the "indicator" angle of setting since its value is often given on the instrument panel of the pilot;

$\Delta\varphi_{geom}$ = geometric twist of the blade;

θ_1 and θ_2 = angles of cyclic pitch control caused by tilting of the swashplate;

β_0 = angle of rotation of the blade in the flapping hinge.

The Mach number, also needed for determining the aerodynamic coefficients,

is calculated by the formula

$$M=\frac{U}{a_{so}}, \tag{7.20}$$

where $a_{s\,o}$ is the speed of sound.

Thus, eqs.(7.1) together with eq.(7.9) make up a set of partial differential equations with coefficients representing complex nonlinear functions of variables.

7. Method of Solving the Differential Equations

The method of solving eqs.(7.1) most convenient for practical use at the present state of the art of computer technology is the method of numerical integration of the equations of blade motion with respect to time, in which the blade deformations are determined by B.G.Galerkin's method. In the formulation of the problem adopted here, this method permits obtaining the most accurate results.

In determining the bending strain of a blade, it is natural to represent the solution by means of functions which are natural vibration modes of the hinged blade in vacuum. The peculiarities in the distribution of rigidity and mass characteristics over the blade length and the boundary conditions of the problem have already been covered by such functions. We set

$$y=\sum_j \delta_j y^{(j)}, \tag{7.21}$$

where

$y^{(j)}$ = mode of the j-th harmonic of natural blade bending vibrations;
δ_j = coefficients of blade deformation with respect to the j-th harmonic.

In determining the torsional strain, certain difficulties are produced /425
by the fact that the deformations of the controls vary substantially, depending on the direction of the moment of friction in the axial feathering hinge and on forces generated at the swashplate by the totality of rotor blades. The relations between the twist of the blade root and of all its longitudinal sections also vary, depending on the conditions of the effect of these factors. To take this into account, we must introduce some additional variable into the calculation.

Let us study this problem in greater detail. To determine torsional deformations by the Galerkin method, just as in determining bending deformations, it is logical to use the modes of natural torsional vibrations of the blade in vacuum. Here we can use various systems of eigenfunctions, differing by the boundary conditions in the attachment of the blade at the root.

The solution to eqs.(7.1) is simplest if we assign the blade twist by means of natural torsional vibration modes, determined for a blade represented as a beam with a fixed value of torsional stiffness at the point of attachment (Fig.4.32a). This method of solution is quite common in practice. However,

here the problem basically reduces to a calculation of the vibrations of an isolated blade, since the use of the indicated modes precludes the possibility of accounting for the elastic couple between the blades through the swashplate. The effect of the moment of friction in the axial hinge of the hub cannot be fully covered. Actually, the elastic twist of the blade root is determined by the magnitudes of the moments $M_{con}^{(N)}$ acting on the control system; furthermore, the magnitude of these moments at known moments due to the blade M_b^N depends on the direction and magnitude of the moment of friction:

$$M_{con}^{(N)} = M_b^{(N)} + M_{fr}^{(N)}. \tag{7.22}$$

Therefore, blade twist at the root, and consequently the connection between the twist of all sections of the blade length, are related with the magnitude of the moment of friction. This effect cannot be accounted for if the indicated connection between the twists is fixed by vibration modes used in the calculation.

It follows from the foregoing that this calculation method should be considered invalid as applied to real helicopters. It can be used only in individual - rarely encountered - particular cases.

To take into account the couple between blades through the swashplate and the effect of the moment of friction in the feathering hinge, we could use a system of functions representing the modes of natural torsional vibrations of the blade in the form of a free beam unattached at the root (see Fig.4.32b). However, owing to the discrepancy of boundary conditions, the use of such functions might lead to a solution of only an approximate type. Actually, the modes of torsional deformations thus obtained will substantially differ from the real modes. This difference will be especially pronounced in twist of the root portions of the blade where, for a free beam, the torque diagram drops to zero.

All these considerations necessitate applying a nonorthogonal system of functions to this problem, as shown in Fig.4.32c. In this case, the twist of the blade can be represented in the form

$$\varphi = \eta + \gamma_0 + \sum_k \gamma_{tw} \vartheta^{(k)}, \tag{7.23}$$

where k = 1, 2, ...

Here,

γ_0 = angle of twist of the blade as a consequence of deformation of the control system; /426

$\vartheta^{(k)}$ = mutually orthogonal modes of natural torsional vibrations of a blade rigidly fixed at the root;

γ_{tw} = unknown coefficients of the torsional deformations of the blade.

Thus, the blade twist is represented by a system of orthogonal functions $\vartheta^{(k)}$, supplemented by a function $\vartheta^{(0)} = 1$ nonorthogonal to this system.

Equation (7.23) can be written in the form

$$\varphi=\eta+\sum_k \gamma_{tw}\vartheta^{(k)}, \tag{7.24}$$

where k = 0, 1, 2.

This form of representing the blade twist creates certain complications in the calculation, produced by the nonorthogonality of the functions $\vartheta^{(k)}$. Nevertheless, we must put up with these complications in order to account for all of the above highly important factors.

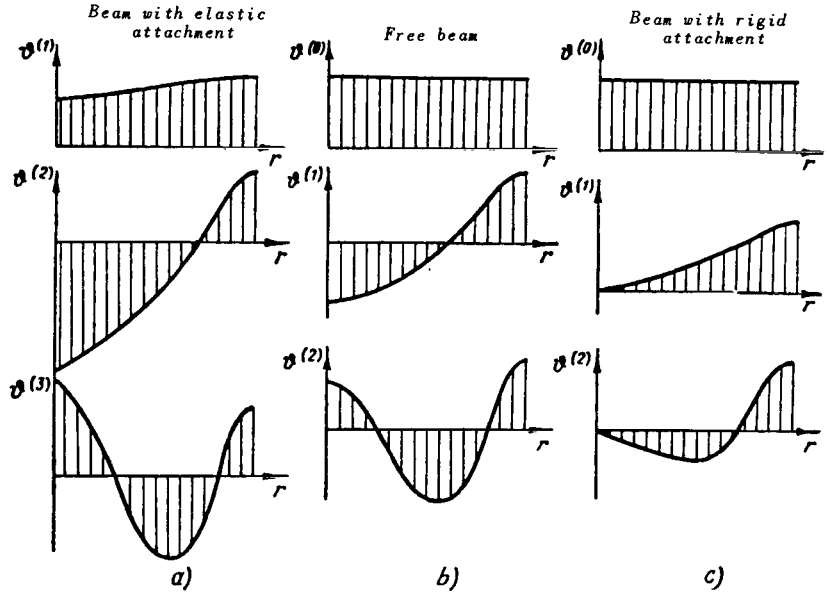

Fig.4.32 Modes of Natural Torsional Vibrations of a Beam with Various Attachments.

8. Transformation of Partial Differential Equations into Ordinary Differential Equations

Having represented the solution of system of differential equations (7.1) in the form of eqs.(7.21) and (7.24), let us apply the Galerkin method. For this, let us twice differentiate eqs.(7.21) and (7.24) and substitute them, together with their second derivatives, into eqs.(7.1).

The second derivatives from eqs.(7.21) and (7.24) will have the following form:

$$\left.\begin{aligned}\ddot{y}&=\sum_j \ddot{\delta}_j y^{(j)};\\ \ddot{\varphi}&=\ddot{\eta}+\sum_k \ddot{\gamma}_{tw}\vartheta^{(k)}.\end{aligned}\right\} \tag{7.25}$$

TABLE 4.1

	$j=0$	$j=1$	$j=2$	$j=3$	$k=0$	$k=1$	$k=2$	$j=0$	$j=1$	$j=2$	$j=3$	$k=0$	$k=1$	$k=2$	
	$\ddot{\delta}_0$	$\ddot{\delta}_1$	$\ddot{\delta}_2$	$\ddot{\delta}_3$	$\ddot{\gamma}_0$	$\ddot{\gamma}_1$	$\ddot{\gamma}_2$	δ_0	δ_1	δ_2	δ_3	γ_0	γ_1	γ_2	
$i=0$	k_{00}	k_{01}	k_{02}	k_{03}	c_{00}	c_{01}	c_{02}	a_{00}	a_{01}	a_{02}	a_{03}	b_{00}	b_{01}	b_{02}	$=A_0$
$i=1$	k_{10}	k_{11}	k_{12}	k_{13}	c_{10}	c_{11}	c_{12}	a_{10}	a_{11}	a_{12}	a_{13}	b_{10}	b_{11}	b_{12}	$=A_1$
$i=2$	k_{20}	k_{21}	k_{22}	k_{23}	c_{20}	c_{21}	c_{22}	a_{20}	a_{21}	a_{22}	a_{23}	b_{20}	b_{21}	b_{22}	$=A_2$
$i=3$	k_{30}	k_{31}	k_{32}	k_{33}	c_{30}	c_{31}	c_{32}	a_{30}	a_{31}	a_{32}	a_{33}	b_{30}	b_{31}	b_{32}	$=A_3$
$k=0$	c_{00}	c_{01}	c_{02}	c_{03}	I_0	I_1	I_2	b_{00}	b_{01}	b_{02}	b_{03}	$\omega^2 I_0+c_{eq}$	$\omega^2 I_1$	$\omega^2 I_2$	$=B_0+M_{fr}$
$k=1$	c_{10}	c_{11}	c_{12}	c_{13}	I_1	L_1		b_{10}	b_{11}	b_{12}	b_{13}	$\omega^2 I_1$	$\nu_1^2 L_1$		$=B_1$
$k=2$	c_{20}	c_{21}	c_{22}	c_{23}	I_2		L_2	b_{20}	b_{21}	b_{22}	b_{23}	$\omega^2 I_2$		$\nu_2^2 L_2$	$=B_2$

We then multiply the first equation of the system (7.1) by $y^{(j)}$ and the second by $\vartheta^{(k)}$ and integrate all terms with respect to the blade radius. The boundary conditions (7.2) should be accounted for in the integration. This operation transforms the system of partial differential equations into a system of ordinary differential equations relative to the new variables δ_j and γ_{tw} /428

For practical purposes, it is highly important what number of variables δ_j and γ_{tw} is used in the calculation. Experience has shown that a sufficiently complete answer can be obtained if the bending strains are represented by means of the first four harmonics of the natural blade vibration and the torsional strains by two or - in the extreme case - by three harmonics. Thus, the problem of bending and twisting vibrations of a helicopter blade can be solved with the use, in any case, of seven independent variables. We will restrict the further calculation to this number of variables.

The system of ordinary differential equations obtained from application of the Galerkin method is written out in the form of a table (see Table.4.1).

All equations of this system represent the sum of the products of certain constant coefficients and the unknown functions δ_j and γ_{tw} and their second derivatives. In Table 4.1, the coefficients pertaining to one equation occupy one row. The known constants that do not change during the calculation are written out in the squares of the table.

The independent variables δ_j and γ_{tw} and their second derivatives, entering simultaneously all equations of the system, are extended with respect to the vertical in a special row in the upper part of Table 4.1. The right-hand sides of the equations are extended in a special column next to the table of constants.

The coefficients of the left-hand side of the equations of the system (see Table 4.1) are determined after calculating the modes and frequencies of the natural blade vibrations in bending and torsion. As stated above, in calculating the torsional frequencies a blade rigidly fixed at the root is used.

A number of coefficients are determined directly during this calculation. This concerns primarily the frequencies of the natural vibration of a rotating blade in bending p_j and in torsion ν_k, and also the coefficients into which the mass characteristics of the blade enter:

$$\left.\begin{aligned} I_{tw} &= \int_0^R I_m \vartheta^{(k)} dr; \\ L_{tw} &= \int_0^R I_m [\vartheta^{(k)}]^2 dr. \end{aligned}\right\} \qquad (7.26)$$

After calculating the modes and frequencies, we determine the coefficients into which simultaneously enter the data obtained from calculating the blade in bending and in torsion. These are the following coefficients:

$$
\left.
\begin{aligned}
k_{ij} &= \int_0^R m y^{(i)} y^{(j)} dr + \varkappa^2 \beta_0^{(i)} \beta_0^{(j)} I_0 + \varkappa \beta_0^{(i)} \int_0^R m \sigma y^{(j)} dr + \\
&+ \varkappa \beta_0^{(j)} \int_0^R m \sigma y^{(i)} dr, \\
a_{ij} &= p_j^2 \int_0^R m y^{(i)} y^{(j)} dr + \varkappa^2 \omega^2 \beta_0^{(i)} \beta_0^{(j)} I_0 + \\
&+ \varkappa \omega^2 \left[\beta_0^{(i)} \int_0^R m \sigma r \beta^{(j)} dr + \beta_0^{(j)} \int_0^R m \sigma r \beta^{(i)} dr \right].
\end{aligned}
\right\} \qquad (7.27)
$$

/429

The second, third, and fourth terms in these expressions are small in comparison with the first and can be neglected. At $i \neq j$, the first terms of eqs.(7.27) vanish by virtue of the orthogonality of the functions $y^{(i)}$ and $y^{(j)}$, and the coefficients k_{ij} and a_{ij} can be assumed as approximately equal to zero, i.e.,

$$k_{ij} \cong 0;$$
$$a_{ij} \cong 0.$$

Next, the coupling coefficients are determined whose value depends mainly on the blade balancing.

At j = 1, we have

$$
\left.
\begin{aligned}
c_{kj} &= c_{lk} = -\varkappa \beta_0^{(i)} I_k - \int_0^R m \sigma y^{(j)} \vartheta^{(k)} dr, \\
b_{kj} &= b_{lk} = -\varkappa \omega^2 \beta_0^{(j)} I_k - \omega^2 \int_0^R m \sigma r \beta^{(j)} \vartheta^{(k)} dr.
\end{aligned}
\right\} \qquad (7.28)
$$

The terms on the right-hand side of the system of equations (see Table 4.1) are determined by means of the following expressions:

$$
\left.
\begin{aligned}
A_i &= \int_0^R T y^{(i)} dr - \varkappa \beta_0^{(i)} [M_{fr} + B_0] + \\
&+ \omega^2 \int_0^R m \sigma r \beta^{(i)} (\theta_0 + \Delta \varphi_{geom}) dr + \\
&+ \omega^2 (\theta_1 \sin \psi + \theta_2 \cos \psi) \left[\int_0^R m \sigma y^{(i)} dr - \int_0^R m \sigma r \beta^{(i)} dr \right], \\
B_k &= \int_0^R \mathfrak{M}_{aer} \vartheta^{(k)} dr - \omega^2 I_k^{\varphi}.
\end{aligned}
\right\} \qquad (7.29)
$$

Here, $I_k^{\varphi} = \theta_0 I_k + \int_0^R I_m \Delta\varphi_{geom} \vartheta^{(k)} dr$.

The first terms of eqs.(7.29) are those determining the value of the coefficients A_i and B_k. The following terms are small and can be neglected.

9. Determination of the Magnitude of the Moment of Friction in the Feathering Hinge of the Hub

During the numerical integration of the equations (Table 4.1), the magnitude of the moment of friction can be obtained from the values of the torsional deformations of the blade determining the external torque in the feathering hinge and from the direction of blade rotation in this hinge. In so doing, the magnitude of the moment of friction should be determined by a different method, depending on which is greater in absolute value: the external torque in the feathering hinge M_{hi} or the maximum possible moment of friction M_{fr}.

The external torque in the feathering hinge is determined by the formula /430

$$M_{hi} = M_b - M_{con} = \sum_k \nu_{tw} M_b^{(k)}, \qquad (7.30)$$

where k = 0, 1, 2, 3, ...

Here,

M_b = hinge moment due to forces acting on the blade;

$M_{con} = c_{eq}\gamma_0$ = moment relative to the feathering hinge due to the control system; in conformity with this notation the pitching moment due to the control is considered as positive just as in eqs.(7.6), (7.7), and (7.22);

$M_b^{(k)}$ = magnitude of the hinge moment in blade deformations with respect to the mode of the k-th harmonic of natural vibrations of the blade in torsion.

Modes of natural vibration normalized in some manner, for example, by the quantity $\vartheta_R^{(k)} = 1$, will now be discussed. Here, we assume that

$$M_b^{(0)} = -c_{eq}.$$

The magnitude of the maximum possible moment of friction M_{fr}^{max} is usually determined experimentally in the laboratory. If the coefficient of friction in the bearing f is known, then this magnitude can be determined by the formula

$$M_{fr}^{max} = f N_0 r_{be},$$

where

N_0 = centrifugal force acting on the bearing of the axial hinge;

r_{be} = radius of this bearing.

If $|M_{hi}| < |M_{fr}^{max}|$, then $M_{fr} = -M_{hi}$. In this case, the blade in the feathering hinge does not turn, and $\dot{\varphi}_0 = \ddot{\varphi}_0 = 0$. This condition permits determining immediately $\dot{\gamma}_0$ and $\ddot{\gamma}_0$.

If $|M_{hi}| > |M_{fr}^{max}|$, then

$$\left.\begin{aligned} M_{fr} &= -M_{fr}^{max}, \quad if \quad \dot{\varphi} > 0; \\ M_{fr} &= M_{fr}^{max}, \quad if \quad \dot{\varphi} < 0. \end{aligned}\right\} \tag{7.31}$$

10. Sequence of Performing the Calculation

The system of differential equations (see Table 4.1) is written here in a form such that its solution is conveniently found by numerical integration with respect to time. During this integration, mainly the right-hand sides of the equations will change. All coefficients on the left-hand side of the equations remain unchanged during the calculation, with the exception of the coefficient c_{eq} whose magnitude is recalculated at each integration step.

The numerical solution of the system (see Table 4.1) also represents the basic part of the method of calculating binary blade vibrations presented here.

The calculation of blade vibration by this method is carried out in the following sequence:

1) Calculate the modes and frequencies of natural blade vibrations in vacuum. For calculation by this method, it is necessary to determine the first four harmonics of flexural vibrations of the blade, including the so-called zero harmonic of vibration of the blade as a solid body, and the first two harmonics of the torsional vibrations of a blade rigidly fixed at the root. From resultant vibration modes, determine the constant coefficients of the system of differential equations (see Table 4.1). In the numerical integration of the equations, all these coefficients remain unchanged with the exception of the coefficient c_{eq} whose determination is described in Subsection 5. /431

2) Select the parameters of the flight regime ρ, ω, μ, α_h, θ_0, θ_1, θ_2 in which the bending and twisting vibrations must be calculated.

Usually, these parameters are taken from an aerodynamic calculation of the rotor and from calculation of the balancing characteristics of the helicopter. However, another more natural method can be used. The calculation method presented here can be used as a method of aerodynamic calculation and calculation of balancing, by adding a number of simple operations. The values of α_h and θ_0 can be obtained from the calculation if the values of thrust and propulsive force of the rotor and the angles θ_1 and θ_2 necessary for fulfilling the flight regime are prescribed and if the moments on the hub necessary for balancing of the helicopter are determined.

3) At the initial instant of time, which is usually related with the azimuth angle $\psi_b = 0$, assign arbitrary values of the variables and their first derivatives δ_j, γ_{tw}, $\dot{\delta}_j$ and $\dot{\gamma}_{tw}$. To account for the coupling between the blades through the swashplate, these values are assigned for all z_b blades of the rotor.

4) Determine the magnitudes of the aerodynamic forces necessary for calculation:

$$\left.\begin{aligned} \dot{y} &= \sum_j \dot{\delta}_j y^{(j)}, \\ \dot{\varphi} &= \dot{\eta} + \sum_k \dot{\gamma}_{tw} \vartheta^{(k)}, \\ \beta &= \sum_j \delta_j \beta^{(j)}, \end{aligned}\right\} \qquad (7.32)$$

where the value of $\dot{\eta}$ is determined by differentiation of eq.(7.19):

$$\dot{\eta} = -\omega\theta_1 \cos\psi_b + \omega\theta_2 \sin\psi_b - \varkappa\dot{\beta}_0. \qquad (7.33)$$

Here, $\dot{\beta}_0 = \sum_j \dot{\delta}_j \beta_0^{(j)}$.

5) From eqs.(7.10), (7.11), and (7.12), determine the velocity of flow past the profile and its components, and derive the angles of attack of the sections from eq.(7.16). Use eq.(7.20) for determining the Mach number.

6) From the polars of the profile fed into the computer together with the initial data, determine the values of c_x, c_y, and m_z. After this, making use of eqs.(7.9), calculate the aerodynamic forces per unit length T and the torsional moments $\mathfrak{M}_{aer}$.

7) From the known values of T and $\mathfrak{M}_{aer}$, determine the terms A_i and B_k entering the right-hand side of the differential equations (see Table 4.1).

8) To determine the value of c_{eq}, it is necessary to know the values of blade twist in the feathering hinge $\gamma_0^{(N)}$ for all z_b blades of the rotor. In this case, c_{eq} is determined by the method presented in Subsection 5.

9) Determine the value and sign of the moment of friction M_{fr} in the feathering hinge (see Subsect.9).

After this, derive all coefficients of the equations (see Table 4.1) and start with the solution.

10) The system of equations (see Table 4.1) permits determining all values of $\ddot{\delta}_j$ and $\ddot{\gamma}_{tw}$ if δ_j, γ_{tw} and the right-hand sides of the equations A_i and B_k are known at the azimuth ψ_b in question. This fact permits its use in the calculation program in the form of some operator of the type /432

$$\ddot{\delta}_j, \ \ddot{\gamma}_{tw} = P(\delta_j, \gamma_{tw}, \psi_b). \qquad (7.34)$$

After applying this operator, determine the values $\ddot{\delta}_j$ and $\ddot{\gamma}_{tw}$ at the initial instant of time.

11) The change to the next instant of time can be accomplished by means of various methods of numerical integration of differential equations.

Good results are obtained by a system of formulas in which the transition from the instant of time t to the time t + Δt is accomplished by two checks. This system of formulas is illustrated for the example of determining the values of the variable δ_j. The index pertaining to the number of the harmonic is omitted for simplicity.

First check:

$$\delta^{I}_{t+\Delta t}=\delta_t+\Delta t\dot{\delta}_t+\frac{1}{2}\Delta t^2\ddot{\delta}_t;$$

$$\dot{\delta}^{I}_{t+\Delta t}=\dot{\delta}_t+\Delta t\ddot{\delta}_t;$$

$$\ddot{\delta}^{I}_{t+\Delta t}=P\left(\delta^{I}_{t+\Delta t},\ \gamma^{I}_{t+\Delta t},\ \psi_{t+\Delta t}\right).$$

Determination of $\ddot{\delta}_{av}$:

$$\ddot{\delta}_{av}=\frac{\ddot{\delta}_t+\ddot{\delta}_{t+\Delta t}}{2}. \tag{7.35}$$

Second check:

$$\delta^{II}_{t+\Delta t}=\delta_t+\Delta t\dot{\delta}_t+\frac{1}{2}\Delta t^2\ddot{\delta}_{av};$$

$$\dot{\delta}^{II}_{t+\Delta t}=\dot{\delta}_t+\Delta t\ddot{\delta}_{av};$$

$$\ddot{\delta}^{II}_{t+\Delta t}=P\left(\delta^{II}_{t+\Delta t},\ \gamma^{II}_{t+\Delta t},\ \psi_{t+\Delta t}\right).$$

The values of $\delta^{II}_{t+\Delta t}$, $\dot{\delta}^{II}_{t+\Delta t}$, $\ddot{\delta}^{II}_{t+\Delta t}$ obtained as a result of recalculation are considered final for the instant of time t + Δt.

Operations analogous to eq.(7.35) are performed on the coefficients of torsional deformations. The change-over to the next instant of time is thus accurately accomplished.

A simpler method of numerical integration can be proposed. This will be presented in greater detail in Vol.II.

12) The type of problem investigated is important for the sequence of calculation. If it is a question of determining the possibility of rotor flutter, then the process of numerical integration must be carried out simultaneously for all rotor blades and the value of c_{eq} must be determined at each instant of time. The coupling between blades through the swashplate is taken into account by calculating the quantity c_{eq}. If the question of investigating flutter is not raised and only stresses in the blade are being determined, the problem is greatly simplified. In this case we can introduce into the calculation the assumption that all blades of the rotor duplicate the motion of the blade in question, and the process of numerical integration is performed for only one blade.

When determining c_{eq} in this case it is assumed that /433

$$\gamma_N(\psi_b^{(0)}) = \gamma_0\left(\psi_b^{(0)} - \frac{2\pi N}{z_b}\right), \tag{7.36}$$

where

$\psi_b^{(0)}$ = azimuth angle of the blade with the number N = 0 whose motion is determined in the calculation;

$\gamma_0\left(\psi_b^{(0)} - \frac{2\pi N}{z_b}\right)$ = coefficient of deformation of the blade with the number N = 0, not at the azimuth $\psi_b^{(0)}$ in question but at the azimuth $\left(\psi_b^{(0)} - \frac{2\pi N}{z_b}\right)$;

$\gamma_N(\psi_b^{(0)})$ = coefficient of deformation of the blade with the number N, when the blade with N = 0 is at the azimuth $\psi_b^{(0)}$.

13) In determining the stresses, the numerical integration is performed for several rpm of the rotor until all values of δ_j and γ_{tw} at two successively calculated rpm differ less than the prescribed accuracy of calculation. This will indicate that the process has converged. After this, the bending stresses at each azimuth can be determined by the formula

$$\sigma_\psi = \sum_j \delta_j \sigma^{(j)}, \tag{7.37}$$

where $\sigma^{(j)}$ are the bending stresses of the blade with respect to a normed mode of natural vibrations of the j-th harmonic.

Further reduction of the obtained data can be performed in any form, depending on the purpose of the calculation. Usually, the amplitude of the stresses is determined and the variation in stresses with respect to azimuth is decomposed into harmonics.

14) In the investigation of flutter, the results can be evaluated after studying the entire process of variation in the deformation coefficients during several rotor rpm. This is not very convenient in practice since it requires considerable graphic work for plotting the dependences $\delta_j = f(\psi)$ and $\gamma_{tw} = f(\psi)$. Nevertheless, these drawbacks are compensated by the advantages of this calculation method.

The method presented here involves a large amount of work, but it is known from practical experience in design shops that, if modern digital computers are used, this method best meets the requirements in designing and perfecting blades and permits introducing additional refinements into the results of the calculation based on an analysis of the roots of the characteristic equation.

Section 8. Experimental Investigations of Flutter

1. Ground Tests for Flutter

The features of helicopter design permit the performance of flutter analysis

of the rotor under safe conditions, with the helicopter on the ground. This constitutes a distinct advantage of the helicopter over regular aircraft.

Ground tests for flutter are carried out for different purposes. Often these purposes are purely of a research nature. In many cases, it is necessary to check or refine - under full-scale conditions - the effect of various parameters on flutter characteristics, to evaluate the peculiarities of the development and cessation of flutter and, finally, to simply refine individual moments in the procedure of conducting such tests.

Nevertheless, in the overwhelming majority of cases these tests are /434 carried out for inspection purposes. Recently, it has become the rule that each experimental helicopter must undergo flutter tests before the start of flight tests. The actual margins to the onset of flutter are established in these tests. If they prove to be too large, the designer can reduce them, for example, by decreasing the weight of the counterbalance in the blade and thus lightening it. In the case of insufficient margins, it is necessary to make some design modifications and recheck them in tests.

The finally established flutter margins on an experimental helicopter will later serve as criteria for evaluating the characteristics of other helicopters of the same design in production at a series-production plant or in actual service.

Usually, in developing a new helicopter it is possible to restrict the testing to ground tests without the need for additional flight tests. In exceptional cases in the past, it had been necessary to also conduct flight tests. As a rule, there is no need for these.

Ground flutter tests are usually carried out in the following manner:

The helicopter is made fast on a special platform so that the possible occurrence of flutter and consequent failure of a part will not cause the helicopter to roll over. As is known, roll-over of a helicopter will cause the blades to strike the ground and almost completely wreck the craft. In some cases, there might be casualties. Generally, such does not happen in ground tests for flutter, but the experimenter must always be prepared for any eventuality.

To begin the tests, the rotor should be revved to the maximum rpm at which flutter cannot yet occur. Then the rpm is gradually increased. Usually, this increase is accomplished in steps of a certain quantity Δn, so that $n_2 = n_1 + \Delta n$. Here n_1 is the initial value of the rpm and n_2 the new value. The quantity Δn is generally taken as about 2% of the operating rpm of the rotor.

At the new rpm n_2, the rotor is held for some time (usually 1 - 2 min) so that vibrations can proceed up to noticeable intensities; if flutter does not occur, the rpm is again increased by the quantity Δn until flutter does develop.

Flutter tests are usually greatly simplified if, to cause flutter, it is not necessary to create initial disturbances as it is required in hard flutter with an excitation threshold (see Sects.3.3 and 3.4). Therefore, an attempt

should be made in the tests to create conditions favorable for the occurrence of soft flutter. Such conditions usually are present if a sufficiently large forced motion is generated in the feathering hinge. For this, the control lever, and along with it the swashplate, are deflected forward as far as possible. Usually, this is limited by the fact that the blades begin to strike the supports of the vertical overhang guard.

When a forced motion is created in the feathering hinge, flutter sets in earlier with respect to the rotor rpm. Thus, pulling the control stick, in a way, is a means of generating flutter. Here, the start of flutter tests is as follows: The increase in rotor rpm by Δn is carried out at neutral position of /435 the swashplate, after which the control stick is pulled forward and the regime is maintained with the stick deflected. If flutter does not occur, the control stick is returned to the neutral position and the rotor rpm is again increased, and so on, until flutter occurs.

Upon the appearance of flutter, if the oscillations build up rapidly, it is first necessary to reduce the engine power sharply so as to cause a rapid drop in rotor rpm. An additional means of stopping flutter is to return the control stick to the neutral position.

In flutter tests, it is of great importance to achieve the maximum possible rotor rpm. To prevent the rpm from being limited by the engine power, the rotor is usually lightened meaning that the angle of blade setting is reduced. Experiments have shown that the overall angle of blade setting has only a slight influence on the critical rpm of flutter and thus can be reduced without risk. However, one definite limitation does exist. The lower the angle of rotor setting, the sooner will the blade begin to strike the supports where the control stick is deflected. Furthermore, severe lightening of the rotor is unwarranted so that the maximum rpm in the tests is limited not so much by the power as by the mechanical strength of the engine. Therefore, the angle of blade setting is selected as maximum in the tests but is kept at a value preventing the blades from striking the supports when the control stick is deflected while maintaining sufficient engine power for maximum possible rpm allowable for mechanical strength reasons.

Flutter tests under ground conditions obviously are possible only if the rotor characteristics are such that flutter will take place under these conditions. On helicopters rated for service, flutter cannot occur under ground conditions. Therefore, to conduct ground tests for flutter, the rotor parameters must be disturbed somehow. This is usually accomplished in the simplest way by disturbing the blade balance, which can be achieved by attaching small weights to the trailing edge of the blade. Occasionally, the balance is shifted by coating the surface of the blade close to the trailing edge with some kind of material whose weight will shift the blade balance rearward. It is also possible to introduce some elastic elements into the control loop. Thus, in conducting flutter tests, the rotor parameters must first be changed so as to make occurrence of flutter possible.

When conducting the tests, it is necessary to provide for the recording of various parameters to permit an accurate determination of critical rpm, frequency, vibration mode, and deflection of the control stick at which flutter began.

Without a determination of these parameters it is impossible to make a sufficiently accurate evaluation of the flutter margin and to indicate what parameters should be changed to increase this margin.

When conducting the tests, the onset of flutter is detected by the pilot from the disturbance of the blade coning angle and from the increase in fuselage vibrations and, in the case of reversible control, also from vibrations of the control stick. However, all these signs are sufficiently distinct only after the vibration amplitudes reach extremely high values and conduction of the test becomes dangerous. Consequently, it is desirable to stop flutter tests earlier, before oscillations have time to develop. In this case, the pilot may easily /436 confuse flutter with the usually present distortion of the blade coning angle. This is promoted by vibrations which, as a rule, arise in such tests owing to wind and lack of controllability of the rotor.

In this case, the occurrence of flutter can be judged only by recordings of various factors that are characteristic for vibration. To determine the onset of flutter and its parameters, the type of recordings made in the tests is of great importance. It has been shown that it is not always easy to determine the onset of flutter from a recording of the flapping motion of the blade in the hub hinges, since flutter vibrations in these hinges lead only to a distortion of the recording of the flapping motion caused by deflection of the control stick.

This is illustrated in Figs.4.33 and 4.34 which show a recording of blade motion in the flapping hinge (angle β), with the recording of weak flutter shown in Fig.4.33 and of stronger flutter in Fig.4.34. As follows from Fig.4.33, a determination of the onset of low-amplitude flutter would be difficult from a recording of the angle β. The same is true with respect to recording the hinge moment M_b.

The onset of flutter is best reflected in the recording of forces in the nonrotating control loops. The recording of forces in the longitudinal control P_{long} is shown in the oscillograms (Figs.4.33 and 4.34). It is easy to define the onset of flutter from these recordings.

It should be mentioned that Figs.4.33 and 4.34 show the recordings of antiphase flutter with an order m = 3 for a four-blade rotor. Consequently, the frequency of the variable forces in the longitudinal control is governed by the relation

$$p_{long} = p_{flu} + n_{flu}, \tag{8.1}$$

where

$$p_{flu} \cong 330 \ osc/min$$

$$n_{flu} \cong 184 \ rpm$$

$$p_{long} \cong 514 \ osc/min.$$

When the control stick is deflected from the neutral position by even the slightest amount x_p, the vibration frequency of the blade in flutter p_{flu} can no longer be determined from recording the angle β (see Figs.4.33 and 4.34), but can easily be calculated from eq.(8.1) since the value of the frequency p_{long} is

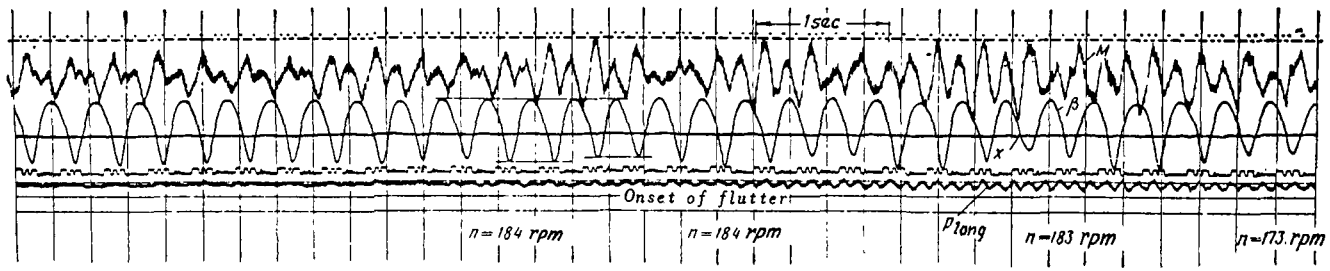

Fig.4.33 Oscillogram of Hinge Moment M_b, Blade Flapping Angle β, Position of Control Stick x_p, and Forces in Longitudinal Control P_{long} in the Presence of Weak Flutter.

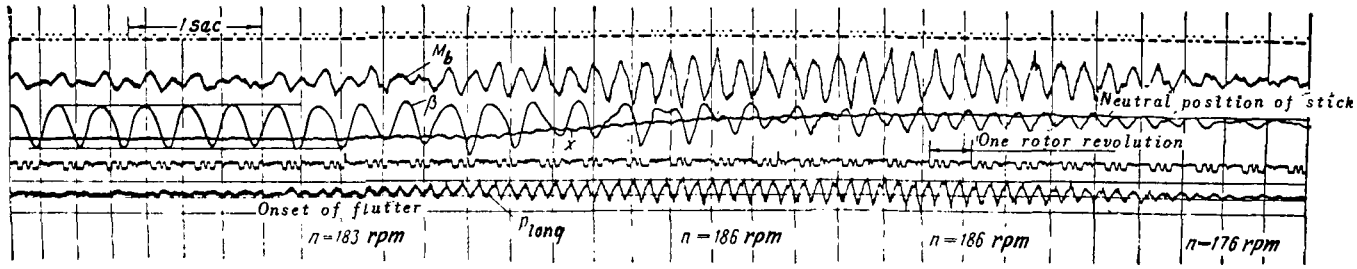

Fig.4.34 Oscillogram of Hinge Moment M_b, Blade Flapping Angle β, Position of Control Stick x_p, and Forces in Longitudinal Control P_{long} in the Presence of Stronger Flutter.

readily determined from the oscillograms.

If, after occurrence of flutter, the control stick is returned to neutral, the flapping motion caused by tilting of the swashplate will stop and the only motion in the flapping hinge will be that due to flutter (see Fig.4.34). In this case, the frequency of flutter can be determined also from the recording of β.

In the tests whose recordings are shown in Figs.4.33 and 4.34, flutter was caused by an increase in rotor rpm and by deflection of the control stick by an amount x_p.

In the first case (see Fig.4.33), the rpm was raised to $n_{flu} = 184$ and, as soon as weak flutter set in, it was stopped again by decreasing the rotor rpm. The position of the control stick x_p had not been changed.

In the second case (see Fig.4.34), the rpm was raised somewhat more, up to n = 186, causing stronger flutter to occur. At the start, the control stick was returned to neutral without a change in rpm; this caused the increase in vibration to stop, after which the rpm was lowered and the flutter disappeared. /438

It should be mentioned that the recordings shown in Fig.4.33 and 4.34 correspond to rather weak flutter with a slowly increasing amplitude. Such flutter is not always observed; often, the vibration amplitude increases much more rapidly and the manipulation of the control stick, described above, becomes impossible.

As an example of such abruptly developing flutter, Fig.4.35 shows an oscillogram of blade motion about the flapping hinge for another helicopter with a three-blade rotor. To stop flutter on this helicopter it was necessary to reduce the rpm as rapidly as possible.

The flutter vibration mode whose recording is shown in Fig.4.35, is of the in-phase type which means that the collective pitch control is loaded during the vibration. This makes the recording of the swashplate slide vibrations, shown in Fig.4.36, quite interesting. This recording was made with a CV-11 automatic recorder.

The recordings shown in Figs.4.33 - 4.36 are given only as an example and in no way exhaust all possible types of flutter observed on helicopters. These types may differ in modes of blade vibration, phase distribution of vibrations over the blades (different values of m), frequencies, rate and character (soft and hard flutter) of build-up of vibrations, and in numerous other features. All these peculiarities must be taken into account in flutter tests and in processing the obtained recordings.

2. Flutter Tests in Flight

Flutter tests in flight became necessary when it was found that, during mass service of helicopters, there were individual cases of flutter in flight when such flutter should not have been possible according to concepts held at that time.

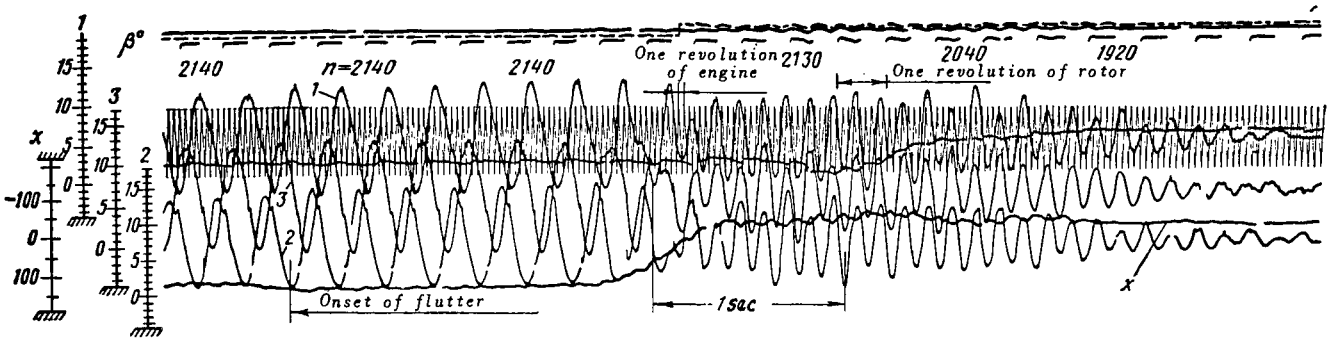

Fig.4.35 Oscillogram of Blade Flapping Motion during Violent Flutter.

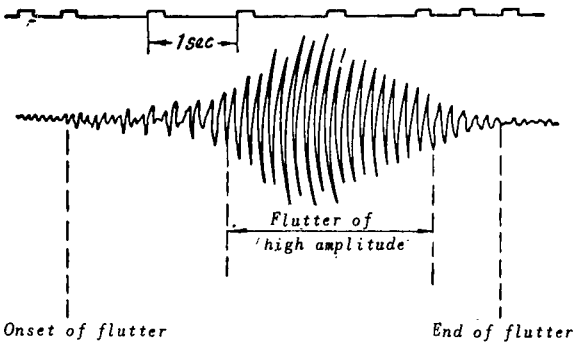

Fig.4.36 Recording of Forces in Collective Pitch Control during Violent Flutter.

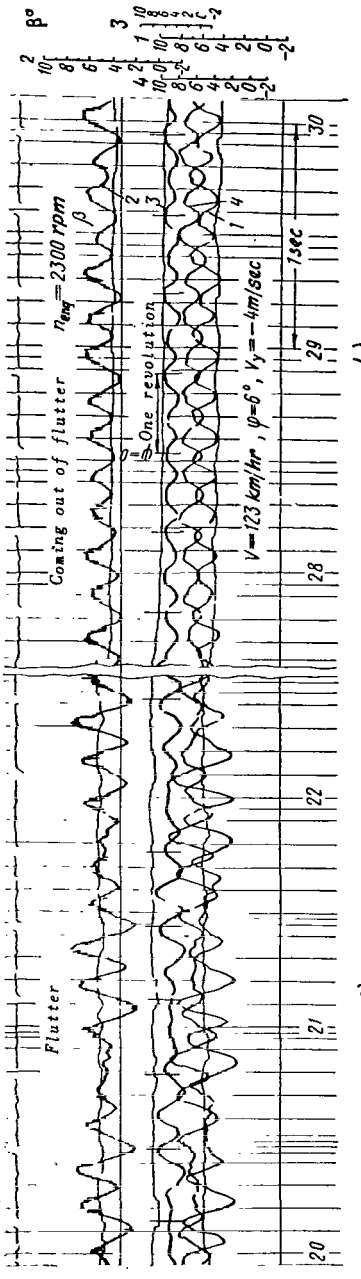

Fig.4.37 Oscillogram of Flapping during Flutter in Flight.

Tests were carried out, which showed that the critical flutter rpm in flight is appreciably lower than in ground tests.

The relation between the critical rpm in flight and on the ground was calculated and it became possible to define the characteristics, checked in ground tests, that were needed for prevention of flutter in flight. The obtained conclusions can be used in developing new helicopter, making flutter tests in flight for each type of helicopter unnecessary. It should be borne in mind that tests with excitation of flutter in flight are extremely dangerous. Such tests should be performed only if absolutely necessary and should be organized with maximum safety for the crew.

Primarily, before starting the tests the researchers should collect data ensuring that abrupt development of flutter will not occur in flight and that, if it does start, it can be stopped again. Such data can be obtained in cases in which unscheduled flutter sets in during flight tests or during service on some helicopter of the type in question. This occasionally occurs as a consequence of some operating error, for example, if the rotor is revved to an rpm by far exceeding the permissible maximum.

Ground tests can be used as an indirect criterion for the degree of abruptness of flutter. Experience has shown that the rate of build-up of vibration on the ground and /440 in flight is determined to some extent by the overall parameters. Therefore, in some cases data of ground tests can be used as basis.

The only reliable measure for stopping flutter in flight is a sharp reduction in rpm. Therefore, to ensure definite stopping of flutter it is necessary to have a large rpm excess in a regime where flutter begins in comparison with the minimum rpm at which flight is possible. During the tests, the pilot should induce flutter by raising the rpm and stop flutter by sharply reducing the rpm to the minimum possible for continuation of the flight.

All considerations referring to recording in ground tests hold also for flight tests. However, we should point out one peculiarity of vibrations during

flutter in flight, which distinguishes these vibrations from those observed in ground tests.

In ground tests, forced flapping motion in the hinges caused by tilting of the swashplate takes place almost exclusively at the frequency of the first harmonic of the rotor rpm. In flight, the flapping motion contains also the second and higher harmonics. Therefore, blade vibration in flapping flutter usually generated at frequencies close to the second harmonic but generally not equal to it, will lead to beats between the second harmonic of flapping and flutter vibration. Therefore, flutter in flight is often perceived as beats.

As a typical example, Fig.4.37 shows the recording of flutter in flight in a regime where flapping in the axes of the shaft consists almost exclusively of the second harmonic (see Fig.4.37b). This is explained by the fact that attachment of the shaft was selected such that vibrations of the first harmonic are eliminated in cruising flight.

The vibrations during flutter in this regime have well-defined beats (see Fig.4.37a).

In all other cases, if the lower critical rpm is disregarded, flutter in flight will not differ from that observed on the ground. /441

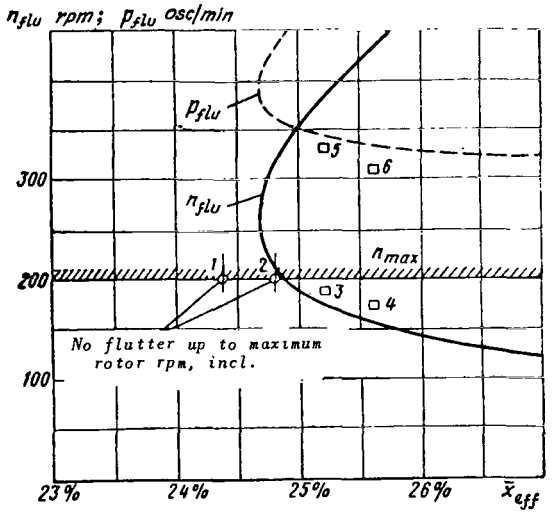

Fig.4.38 Comparison of Experimental and Calculated Values of Vibration Frequency and Critical Flutter Rpm.

3. Comparison of Calculation and Experiment under Conditions of Axial Flow past the Rotor

In comparing calculation and experiment, the initial rotor parameters used in the calculation are of prime importance, along with type of blade balancing, rigidity of the control system, and magnitude of friction in the feathering hinge of the hub, as well as reliability with which the location of the profile focus is known. Errors in determining the initial data naturally affect the accuracy of determining the flutter parameters. Therefore, in comparing calculation and experiment it is desirable to eliminate errors in determining the initial parameters. For this, the parameters should be checked experimentally. Balancing should be determined by weighing individual segments of the blade obtained after cutting it.

To determine the control rigidity a special method of measuring dynamic rigidity should be used, which will be taken up in greater detail in Section 6. The use of other methods generally leads to misunderstandings and fallacies and

therefore should be discarded.

To check the position of the profile a.c. a segment of a full-scale blade should be exposed to the air stream in a wind tunnel. In this case, it can be expected that deviations in the aerodynamic characteristics due to design errors of the blade profile and deformation in work will be refined to some extent.

Figure 4.38 gives the results of a comparison of calculation and experiment for the Mi-4 helicopter. The solid curve shows the theoretically obtained dependence of the critical flutter rpm on the effective blade balancing. The circles mark the experimental results. Circle 1 with the forwardmost blade balancing corresponds to the maximum rpm obtainable with a helicopter engine. There was no flutter in this case. After attaching 0.46-kg weights to the blade flaps, the experiment was repeated. There again was no flutter (circle 2).

Attachment of weights of 0.86 and 1.3 kg to the blade flap caused flutter at rotor rpm of n = 187 and n = 173 respectively (squares 3 and 4 in Fig.4.38).

The frequency of blade vibration during flutter is indicated in the diagram by squares 5 and 6, which should be compared with the theoretically determined frequency values shown by the dashed curve. /442

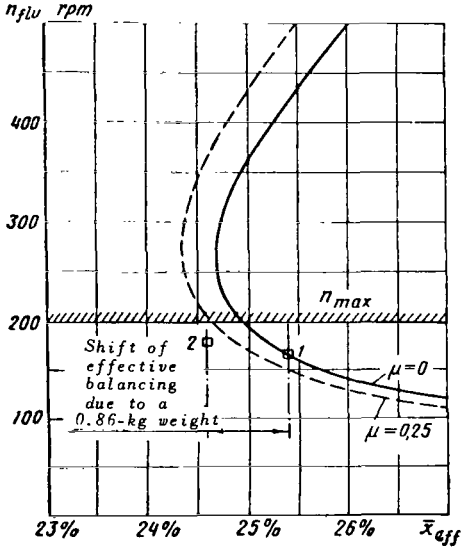

Fig.4.39 Comparison of Experimental and Calculated Data in Flight.

After the experiments, the blades were cut into segments and their effective balancing was determined, which is noted on the graph in Fig.4.38. The dynamic rigidity of the control system was determined on the same helicopter. The magnitude of friction in the feathering hinge, which was highly stable, was measured in the laboratory on another hub of the same design.

These data indicate satisfactory (with an accuracy to within 0.5% of the chord for the value of effective balancing) agreement of calculation and experiment. We note that such a good agreement was observed in all other experiments carried out on other helicopters. This creates confidence in the reliability of the results obtained from calculation and in the validity of the initial assumptions, including that of the permissibility of determining aerodynamic forces by formulas based on the "steady-state hypothesis".

It should be added that the flutter calculation pertains to a case quite rare in rotor calculations when good agreement with experiment is observed. Probably, this is due primarily to the fact that even substantial errors in determining the magnitudes of aerodynamic forces have no great effect on the final results of calculation at critical flutter rpm.

4. Comparison of Calculation and Experiment in Flight

Comparisons of calculation and experiment in flight do not show such good agreement as in similar comparisons of results obtained under conditions of axial flow past the rotor in ground tests. In flight, the decrease in critical flutter rpm is felt more strongly than on the basis of calculation. Figure 4.39 gives two curves obtained by calculation for a regime with axial flow ($\mu = 0$) and for horizontal flight with $\mu = 0.25$. The curves do not differ greatly. Conversely, the experimental results differ substantially. In Fig.4.39 point 1 marks the critical rpm obtained in a ground test with a 0.86-kg weight attached to the flaps while point 2 refers to the critical flutter rpm obtained on the same helicopter in flight but without weights on the flaps. The test points in Fig.4.39 were obtained in tests laid out by S.B.Bren and A.A.Dokuchayev and performed by the pilot V.V.Vinitskiy.

The diagram indicates that the difference between the flight and ground tests is appreciably greater than that obtained by calculation. The cause for the difference lies in the fact that, in calculations, the amplitude of the /443
forced motion in the feathering hinge was taken to be the same on the ground and in flight, i.e., it was assumed that in ground tests the amplitude of the angular velocities of blade vibration in the feathering hinge, as a result of deflecting the control stick, was the same as in flight as a consequence of ordinary flapping motion. Here, it was disregarded that, in flight, the different vibrations and oscillations with harmonics of higher orders may noticeably reduce the effectiveness of damping of oscillations due to friction in the feathering hinge. This assumption is usually made to explain the more abrupt drop in critical flutter rpm in flight in comparison with the calculation.

5. Check for Flutter

It has been noted above that, for a reliable elimination of the possibility of flutter under service conditions, the helicopter rotor should have a well-defined flutter margin. This margin should be checked on the ground and, if the margin is below some standard value, the helicopter should not be allowed to fly. In this approach, the required margin before flutter, checked on the ground, should take into account a decrease in critical rpm in flight, possible deterioration in flutter characteristics due to moisture penetrating into the blade, and other factors, and should secure the necessary stability of blade vibration at maximum approach to this margin.

The idea of flutter checking was first expressed by M.L.Mil' who proposed to excite rotor oscillations by installing an eccentric in the cyclic pitch control system and to measure the stability margin in terms of the amplitude of the obtained resonance vibrations, which should be greater the smaller the flutter margin. Such experiments were carried out and yielded interesting results.

Figure 4.40 shows the experimentally obtained dependence of the amplitude of the hinge moment on the excitation frequency of the eccentric for various rotor rpm. The diagram shows that the higher the rotor rpm and hence the closer to flutter, the greater will be the amplitude of the hinge moment. The same dependence is obtained for blade balancing. During experiments on the Mi-4 heli-

copter with a four-blade rotor, we noted the occurrence of two modes of resonance vibrations of frequencies $p_1 = p_{ecc} + n$ and $p_2 = p_{ecc} - n$ (p_{ecc} is the frequency of excitation from the eccentric), which agrees nicely with the theoretical notions presented in Section 4. The experiments confirm the possibility of using the described method for checking the stability margin of the rotor.

However, some time later a simpler method for checking the necessary margin in terms of blade balancing was developed. This method provides for checking the helicopter on the ground with blades whose balancing is shifted rearward by a certain predetermined quantity. The balance is shifted by means of special weights placed on the trailing edges of the blade during the check. If, on raising the rpm to a prescribed maximum, flutter does not set in, the weights are removed and the helicopter is admitted to service.

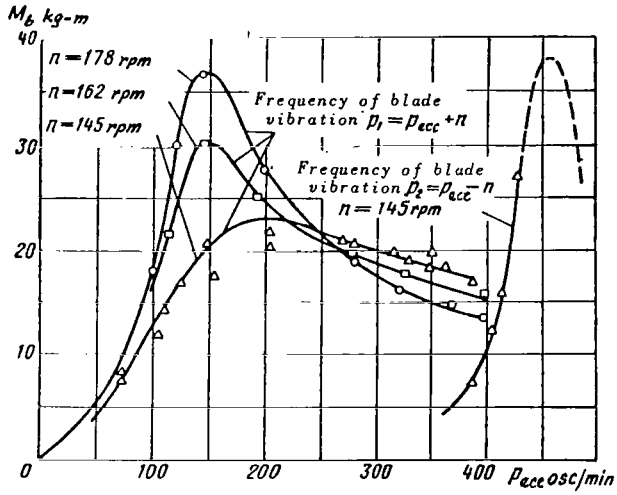

Fig.4.40 Hinge Moment Amplitude as a Function of Vibration Frequency of the Eccentric.

The weights were originally selected on the basis of calculations and later corrected for different experiments and service conditions. Two magnitudes of the required margins are usually established. When the helicopter is released from the plant, an increased margin is established which can be partially expended in service. Therefore, in a number of cases flutter check is also introduced in service, but then a smaller required margin is established. /444

The introduction of a flutter check has proved a useful measure, after which cases of the development of flutter in service completely stopped.

6. Experimental Determination of Control System Rigidity

It was already pointed out above that the critical flutter rpm greatly depends on the magnitude of the control system rigidity. It can be approximately assumed that the critical flutter rpm is directly proportional to $\sqrt{c_{con}}$. Hence it is obvious that it is important to determine control rigidity as accurately as possible for a successful calculation. How does one determine the magnitude of this rigidity? When performing the first calculations for flutter, control rigidity is often calculated theoretically by summing the design rigidities of all components entering the control loop. First measurements of this rigidity showed that the calculated values are much higher than the experimental values. Therefore, it was necessary to reject the calculation of control rigidity.

However, the problem of the manner of experimental determination of control rigidity also proved difficult. At first, the control rigidity was determined statically, i.e., by the slope of the dependence of the magnitude of deformations on the external load. However, this method did not clarify the mode of accounting for play in the control system, friction, and inertia of the components entering this system. Therefore, the so-called dynamic method of determining control rigidity was used, in which the external forces exerted at the control by the blades were applied dynamically, at a frequency equal or close to the frequency of flutter. With this method of measurement, the control rigidity /445 was by a factor of 2 - 2.5 less than with the static method.

It is natural that the results obtained in static analysis cannot be used for the flutter calculations.

What is the simplest way of determining the dynamic rigidity of the control system? For this, we used the following method:

On a helicopter with a nonrotating rotor we replaced the blades by special weights whose moments of inertia relative to the feathering hinge were equal to the moments of inertia of the removed blades. By measuring the natural vibration frequency of this system, the magnitude of the corresponding hinge control rigidity can be completely defined. These rigidities can obviously be calculated by means of the formula

$$c_{con} = p^2 I_{c.p}, \tag{8.2}$$

where

p = one of the natural vibration frequencies of this system, which should be considered equivalent to a rotor with blades absolutely rigid in torsion;

c_{con} = hinge control rigidity corresponding to the vibration mode for which the frequency p is determined.

The necessary values of the natural vibration frequencies can be determined by the usual method of forced vibrations with excitation by a vibrator or eccentric.

Since the rigidity of the longitudinal and lateral controls on a helicopter is usually not the same, two different values of the natural vibration frequency will correspond to loading of these controls [see eq.(4.19)].

Let us present the values of the frequencies corresponding to loading of different control loops obtained on the Mi-4 helicopter with a nonrotating rotor:

$$p_x = 400 \div 420 \ osc/min$$
$$p_z = 440 \div 450 \ osc/min$$
$$p_{a.h} = 590 \div 620 \ osc/min$$
$$p_{a.p} = 920 \div 940 \ osc/min.$$

The notations used here are the same as those used in eqs.(4.19).

This raises the question whether the control rigidity thus measured depends on the amplitude of external forces acting on the control system. To check this, we carried out experiments with the maximum permissible (in terms of strength) magnitudes of hinge moments acting on the control, approximately the same as those which act at the maximum flying speed, and with moments lower by a factor of 10. There was no substantial difference in the value of the obtained frequencies.

Dynamic control rigidity may depend on the frequency of the forces acting in the control cables. By changing the moments of inertia of the weights installed in place of the blades and measuring the new natural vibration frequencies of the system, it becomes possible to define the mode of variation of rigidity with variation of the vibration frequency. Figure 4.41 shows the results of such measurements. The abscissa gives the natural vibration frequency for the control system which varies as a function of the magnitude of the moment of inertia of the weights, while the ordinate gives the dynamic rigidity expressed in terms of the corresponding natural vibration frequency in agreement with eqs.(4.19).

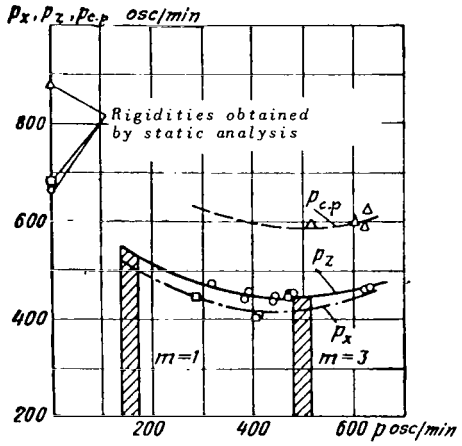

Fig.4.41 Control Rigidity as a Function of Vibration Frequency.

Figure 4.41 indicates the approximate values of the frequencies of variable /446 forces acting in the nonrotating parts of the lateral and longitudinal controls during flutter with modes of the first (m = 1) and third order (m = 3). These results illustrate the above assumption (see Sect.4.3) that the magnitude of control rigidity may depend on the frequency of the forces acting in it.

For comparison, Fig.4.41 also gives the values of the static control rigidity obtained from the slope of the dependence of control deformations on the magnitude of effective forces.

The dynamic method described here for determining control rigidity has been sufficiently checked and can be recommended for practical use.

7. Experiments on Dynamically Similar Models

For conducting experiments on full-scale helicopters, the researcher usually runs into many difficulties having to do with observance of safety rules, since full-scale experiments are usually carried out by a pilot or mechanic in the helicopter. This imposes certain restrictions, especially for flutter tests in flight where, for safety considerations, flutter is usually generated only once in some regime or, in the extreme case, three to four times but never more

often. It is impossible to obtain any dependences for the parameter.

Furthermore, there are limitations to the possibility of investigating various flight regimes, due to the characteristics of the helicopter on which the experiment is carried out. The engineer is almost always interested in the flutter margin with respect to rpm. However, the maximum rpm achievable in experiments is limited by the capabilities of the engine. For example, the maximum flying speed is limited. Therefore, the researcher naturally will attempt to make wind-tunnel tests on dynamically similar models. Such tests often yield interesting results. However, their wide use is restricted by a number of basic shortcomings. To estimate the need for such tests in each individual case, let us discuss the basic principles underlying the simulation in greater detail.

In producing a reduced-scale rotor model, geometric similitude of the external blade shape and the characteristic linear dimensions of rotor blade and hub are of prime importance. We are thinking here of linear dimensions determining the planform of the blade; distribution of profiles and their setting angles over the blade length; dimensions of its components determining, for example, the position of the feathering hinge axis along the blade length; /447
relative position of other hub hinges; and many other dimensions. Next, it is necessary that all relations between aerodynamic, inertia, and elastic forces remain constant. In this case, the variable aerodynamic loads set up at the model blade lead to the same relative deformations as on the original blade.

Let us examine this in greater detail for the example of bending vibrations of a blade in the flapping plane. It can be demonstrated that bending deformations of a blade with respect to some natural vibration harmonic are determined by the coefficients of deformation calculated by the formula (see Vol.II)

$$\delta^{(j)}=\frac{\omega^2}{p_j^2}\gamma_j\alpha_j, \tag{8.3}$$

where

p_j = frequency of the j-th harmonic of natural blade bending vibration;
γ_j = mass characteristic of the blade in vibrations of the j-th harmonic [see eq.(7.55) of Chapt.I in Vol.II]

$$\gamma_j=\frac{\frac{1}{2}c_y^a\varrho b_{0,7}R^2}{m_j}; \tag{8.4}$$

α_j = dimensionless coefficient, characterizing the magnitude of work done by the aerodynamic forces in displacements of the blade during deformation with respect to the j-th harmonic:

$$\alpha_j=\int_0^1 P\bar{y}^{(j)}d\bar{r}. \tag{8.5}$$

Let us define the mode of variation in the relative coefficients of blade bending deformations $\delta^{(j)}$ upon a similar change in all its geometric dimensions.

The relation between aerodynamic and inertia parameters of the blade is determined by the values of the mass characteristics of the blade γ_j. If all geometric dimensions of the blade change the same number of times, namely, K_L times, then, as follows from eq.(8.4), the mass characteristics of the blade do not change.

However, we see from eq.(8.3) that, to retain similitude in bending deformations, the relation between the natural vibration frequency p_j and the angular velocity of rotation of the rotor ω must be retained. This requirement is equivalent to keeping the Strouhal number constant:

$$\mathrm{Sh} = \frac{pb}{U}, \tag{8.6}$$

where

p = vibration frequency;
U = velocity of flow.

The natural vibration frequency p_j is determined by the formula

$$p_j^2 = \frac{1}{m_j}\left[\int_0^R EI(\bar{y}'')^2 dr + \int_0^R N(y')^2 dr\right]. \tag{8.7}$$

Upon a similar change in all geometric dimensions of the blade, the quantity of the elastic moment of inertia of its section I changes K_L^4 times. In this case, as easily seen from eq.(8.7), the magnitude of the natural vibration frequency of the nonrotating blade p_{0j} changes K_L times. Consequently, the relation between this frequency and the angular velocity of rotation remains constant if the angular velocity changes the same number of times. /448

Thus, to retain similitude in aerodynamic, inertia, and elastic forces, all geometric blade dimensions must change the same number of times (K_L) and the peripheral blade speeds must remain constant. Such dynamically similar models are called Mach-similar models since similarity with respect to the Mach number is retained in all blade sections.

The requirement of changing all geometric dimensions the same number of times is easiest to meet by keeping the blade design unchanged. Therefore, the development of such models actually reduces to the development of models similar in design. This is a difficult problem, requiring the solution of many highly complex technical problems and the organization of a special production of small-dimension designs. A sufficiently high accuracy is necessary in their manufacture. Considerable difficulties also arise in developing hub hinges. It is necessary to state that such models are also under considerable stress relative to mechanical strength and do not permit much widening of the regimes in which investigations can be carried out, in comparison with those on full-scale helicopters.

Upon a reduction of the geometric blade dimensions, the relation between the blade weight and its aerodynamic and elastic characteristics drops by K_L times. This leads to a reduction of the influence of the blade weight parameters in comparison with the value for a full-scale helicopter. In particular,

the relative overhang of the blade of a nonrotating rotor decreases by K_L times. The blade, so to speak, becomes more rigid "to the eye". However, this disturbance of similitude is observed only when the rotor is not rotating. Upon rotation of the rotor the effect of the weight forces is generally negligible. Therefore, a disturbance of their similitude has practically no effect on the behavior of the blades.

The difficulties in developing Mach-similar and design-similar blades resulted in their being used infrequently. Most often, dynamically similar blades are developed with disturbance in similitude relative to the Mach number. The peripheral blade speeds on a model are reduced in comparison with the full-scale blade by several times. In so doing, to retain the ratio of natural blade vibration frequency p_j to angular velocity of rotation ω, the blade rigidities are reduced not by K_L^4 times, as is required by geometric similitude, but by a greater number of times, most often by K_L^5. In this case, the necessary ratio of natural vibration p_j to angular velocity is achieved at peripheral speeds $\sqrt{K_L}$ smaller than those on a full-scale helicopter. Presumably, the results of tests on such models can be extrapolated in totality to full-scale units only at $M < 0.4$ (see Fig.4.3). At $M = 0.5 - 0.9$, the test results of such models can be used only for qualitative estimates. In this connection, non-Mach-similar models are used in only a limited volume for practical purposes.

REFERENCES

1. Zhukovskiy, N.Ye.: Theoretical Determination of the Effect of Wind Blowing in the Plane of a Helicopter Rotor (1909) [Opyt teoreticheskogo opredeleniya effekta vetra, duyushchego v ploskosti gelikopternogo vinta (1909)]. Collected Works (Sobr. soch.), Vol.VI, p.68, 1937; Vol.IV, p.388, 1949.
2. Yur'yev, B.N.: Aeroldnamic Calculation of Helicopters (Aerodinamicheskiy raschet vertoletov). Oborongiz, 1956.
3. Yur'yev, B.N.: Investigation of the Flight Characteristics of Helicopters (Issledovaniye letnykh svoystv gelikopterov). Tr. VVIA im. Zhukovskogo, No.49, 1939.
4. Mil', M.L.: Takeoff Run of an Autogiro (O razbege avtozhira). Tekhnika Vozdushnogo Flota, No.5, 1934.
5. Mil', M.L.: Autogiro Balancing and Stability (Balansirovka i ustoychivost' avtozhira). Tekhnika Vozdushnogo Flota, No.10, 1934.
6. Mil', M.L.: Dynamic Twisting of an Autogiro Rotor Blade in Flight (O dinamicheskom zakruchivanii lopasti rotora avtozhira v polete). Tekhnika Vozdushnogo Flota, No.2, 1937.
7. Mil', M.L.: The Aerodynamics of an Autogiro Rotor in Curvilinear Flight (Aerodinamika rotora avtozhira pri krivolineynom dvizhenii). Tekhnika Vozdushnogo Flota, No.1, 1939.
8. Mil', M.L.: Aerodynamics of a Rotor with a Hinged Blade in Curvilinear Flight (Aerodinamika nesushchego vinta s sharnirnym krepleniyem lopastey pri krivolineynom dvizhenii). Tr. Tsentr. Aero-Gidrodinam. Inst., No.465, 1940.
9. Mil', M.L. and Yaroshenko, V.N.: Aerodynamic Calculation of a Helicopter (Aerodinamicheskiy raschet gelikoptera). Tekhnika Vozdushnogo Flota, No.11, 1946.
10. Mil', M.L.: Helicopters (Vertolety). Izd. Znaniye, 1957.
11. Bratukhin, I.P.: Autogiros (Avtozhiry). Gosmashmetizdat, 1934.
12. Bratukhin, I.P.: Design and Structure of Helicopters (Proyektirovaniye i konstruktsiya vertoletov). Oborongiz, 1956.
13. Proskuryakov, A.P.: Effect of Unsteady Flow on the Aerodynamics of the Autogiro Blade (Vliyaniye nestatsionarnosti potoka na aerodinamiky lopasti avtozhira). Tr. Tsentr. Aero-Gidrodinam. Inst., No.460, 1939.
14. Proskuryakov, A.P.: Aerodynamic Calculation of a Rotor with a Blade Pitch Variable in Azimuth (Aerodinamicheskiy raschet nesushchego vinta s peremennym po azimutu uglom ustanovki lopastey). Tr. LII, No.16, 1946.
15. Mikhaylov, A.N.: Theory of the Autogiro Rotor with a Variable Setting Angle (Teoriya rotora avtozhira s peremennym uglom ustanovki). Tekhnika Vozdushnogo Flota, No.3, 1940.
16. Baskin, V.E.: Induced Velocities of a Propeller Exposed to Flow at an Angle to its Axis (Induktivnyye skorosti vozdushnogo vinta, obduvayemogo pod uglom k yego osi). Report at the All-Union Congress on Theoretical and Applied Mechanics, Moscow, 1960 (Doklad na Vsesoyuznom s"yezde po teoreticheskoy i prikladnoy mekhanike, Moskva, 1960).
17. Baskin, V.E., D'yachenko, A.S., Maykopar, G.I., and Martynov, A.I.: Investigation of Airflow and Loads on the Helicopter Rotor Blade in Horizontal Flight (Issledovaniye techeniya vozdukha i nagruzok lopasti vinta verto-

leta v gorizontal'nom polete). Inzh. Zh., Vol.III, No.3, Akad. Nauk SSSR, 1963.
18. Maykopar, G.I.: Application of the Vortex Rotor Theory (Prilozheniye vikhrevoy teorii vinta). Tr. Tsentr. Aero-Gidrodinam. Inst., No.613, 1947.
19. Maykopar, G.I.: Vortex Rotor Theory (Vikhrevaya teoriya nesushchego vinta). Collection of Works on Propeller Theory (Sbornik rabot po teorii vozdushnykh vintov). BNI Tsentr. Aero-Gidrodinam. Inst., 1958.
20. Vil'dgrube, L.S.: Determination of the Flight Characteristics of a Helicopter in all Regimes and at all Altitudes and Selection of its Design Parameters (Opredeleniye letnykh kharakteristik gelikoptera na vsekh rezhimakh i vysotakh i vybor yego parametrov pri proyektirovanii). Tekhnika Vozdushnogo Flota, No.6, 1947.
21. Braverman, A.S.: Theory of an Ideal Helicopter Rotor (Teoriya ideal'nogo nesushchego vinta vertoleta). Izv. Akad. Nauk SSSR, Otd. Tekhn. Nauk, Mekhan. i Mashinostr., No.2, 1959.
22. Wan Shi-Tsun: Generalized Vortex Rotor Theory. Problems of Helicopter Rotor Aerodynamics (Obobshchennaya vikhrevaya teoriya nesushchego vinta. Voprosy aerodinamiki nesushchego vinta vertoletov). Oborongiz, 1961.
23. Durend, V.F.: Aerodynamics (Aerodinamika). Vol.IV, Oborongiz, 1939.
24. Hessow and Meyers: Aerodynamics of the Helicopter (Aerodinamika vertoleta). Oborongiz, 1954. /450
25. Peyn, P.R.: Dynamics and Aerodynamics of the Helicopter (Dinamika i aerodinamika vertoleta). Oborongiz, 1963.
26. Tinyakov, G.A.: Piloting the Helicopter (Pilotirovaniye vertoleta). Voyenizdat, 1960.
27. Izakson, A.M.: Soviet Helicopter Engineering (Sovetskoye vertoletostroyeniye). Oborongiz, 1954.
28. Golubev, V.V.: Lecture on Airfoil Theory (Lektsii po teorii kryla). Izd. Tekhn.-Teoret. Lit., 1949.
29. Keldysh, M.V.: Hydrodynamic Derivation of Rauscher's Formula (Gidrodinamicheskiy vyvod formuly Raushera). Tekhn. Zametki, No.52, Part 2, Tsentr. Aero-Gidrodinam. Inst., 1935.
30. Nekrasov, A.I.: Airfoil Theory in Unsteady Flow (Teoriya kryla v nestatsionarnom potoke). Akad. Nauk SSSR, 1947.
31. Lamb, G.: Hydrodynamics (Gidrodinamika). OGIZ-Gostekhizdat, 1947.
32. Grossman, Ye.P.: A Course on Vibrations of Aircraft Components (Kurs vibratsiy chastey samoleta). Oborongiz, 1940.
33. Riz, P.M. and Pozhalostin, A.I.: Vibrations and Dynamic Strength of Propellers (Vibratsii i dinamicheskaya prochnost' vozdushnykh vintov). Tr. Tsentr. Aero-Gidrodinam. Inst., No.609, 1947.
34. Ryzhik, I.M. and Gradshteyn, M.S.: Tables of Integrals, Schemes, Series, and Products (Tablitsy integralov, skhem, ryadov i proizvedeniy). GITTL, 1951.
35. Watson, G.N.: Theory of Bessel Functions. Izd. Inostr. Lit., 1949.
36. Glauert, H.A.: General Theory of the Autogiro. R & M, No.1111, Nov. 1926.
37. Lock: Further Development of the Autogiro Theory. R & M, No.1127.
38. Shapiro, Jacob: Principles of Helicopter Engineering. Temple Press Ltd., Bowling Green Lane, London, E.C.I.
39. Coleman, R.P.: A Preliminary Theoretical Study of Helicopter Blade Flutter Involving Dependence upon Coning Angle and Pitch Setting. NACA Rept., No.408, 1946.
40. Miller, R.H. and Ellis, C.W.: Blade Vibration and Flutter. J. Am. Heli-

copter Soc., Vol.1, pp.19-38, July 1956.
41. Daughaday, H., DuWaldt, F., and Gates, C.: Investigation of Helicopter Blade Flutter and Load Amplification Problems. Inst. Aeron. Sci., Preprint, No.705, Jan. 1957; J. Am. Helicopter Soc., Vol.2, No.3, July 1957.
42. Hooper, M.S.: The Theoretical Approach to some Rotor Blade Flutter and Forced Vibrations Problems. J. Helicopter Assoc. Great Britain, Vol.12, 1958.

Translated for the National Aeronautics and Space Administration by the O.W.Leibiger Research Laboratories, Inc.

"The aeronautical and space activities of the United States shall be conducted so as to contribute . . . to the expansion of human knowledge of phenomena in the atmosphere and space. The Administration shall provide for the widest practicable and appropriate dissemination of information concerning its activities and the results thereof."

—NATIONAL AERONAUTICS AND SPACE ACT OF 1958

NASA SCIENTIFIC AND TECHNICAL PUBLICATIONS

TECHNICAL REPORTS: Scientific and technical information considered important, complete, and a lasting contribution to existing knowledge.

TECHNICAL NOTES: Information less broad in scope but nevertheless of importance as a contribution to existing knowledge.

TECHNICAL MEMORANDUMS: Information receiving limited distribution because of preliminary data, security classification, or other reasons.

CONTRACTOR REPORTS: Scientific and technical information generated under a NASA contract or grant and considered an important contribution to existing knowledge.

TECHNICAL TRANSLATIONS: Information published in a foreign language considered to merit NASA distribution in English.

SPECIAL PUBLICATIONS: Information derived from or of value to NASA activities. Publications include conference proceedings, monographs, data compilations, handbooks, sourcebooks, and special bibliographies.

TECHNOLOGY UTILIZATION PUBLICATIONS: Information on technology used by NASA that may be of particular interest in commercial and other non-aerospace applications. Publications include Tech Briefs, Technology Utilization Reports and Notes, and Technology Surveys.

Details on the availability of these publications may be obtained from:

SCIENTIFIC AND TECHNICAL INFORMATION DIVISION

NATIONAL AERONAUTICS AND SPACE ADMINISTRATION

Washington, D.C. 20546